Sequence stratigraphy using wireline logs from the Upper Jurassic of England

Ziad M. Ahmadi, B.Sc. (Wales), M.Sc. (Dublin)

Department of Geological Sciences
University of Durham

A thesis submitted to the University of Durham
for the degree of Doctor of Philosophy
1997

Declaration

I declare that this thesis, which I submit for the degree of Doctor of Philosophy at the University of Durham, UK is my own work and is not substantially the same as any which has previously been submitted for a degree at this or any other university.

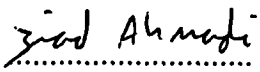

Ziad M Ahmadi
University of Durham
November 1997

Abstract

Sequence stratigraphy using wireline logs from the Upper Jurassic of England

Wireline logs have been interpreted interms of sequence stratigraphy to produce detailed stratigraphic wireline correlations for the Oxfordian and Kimmeridgian successions in the Wessex Basin, southern England. The recognition and interpretation of trends seen on the wireline logs, rather than absolute values or specific lithologies, have proved to be vital in the sequence stratigraphic interpretation of the wireline logs.

Field gamma-ray and density logs were constructed to extend the known sequence stratigraphic interpretation of the Upper Jurassic outcrops to the wireline logs. Both the field gamma-ray and density logs have been constructed to have comparable amplitudes and resolution to wireline logs, although the absolute values do not match precisely. The field gamma-ray logs were measured on the outcrops at intervals of 30-45 cm. The field density logs were produced by measuring volume and grain density of 376 rock samples, followed by interpolation and filtering.

The wireline logs over the Oxfordian succession cannot be correlated peak for peak across the Wessex Basin because major facies changes occur; nevertheless they can be correlated using trends that relate to the sequence stratigraphic interpretation. The Kimmeridgian succession is correlated at a high resolution using wireline logs across the Wessex Basin and into Yorkshire. Unlike the Oxfordian, the Kimmeridgian succession could be correlated virtually peak for peak.

Total gamma-ray and spectral gamma-ray wireline log trends match a detailed relative sea-level curve constructed in this study which is based on the sequence stratigraphic interpretation of the British outcrops. The two sequence stratigraphic scales of cyclicity recognized in the wireline logs are short-term sequence cycles and long-term transgressive-regressive cycles.

For the Oxfordian, the gamma-ray logs show a funnel trend followed by a bell trend. This is interpreted to reflect long-term regression followed by transgression, as has previously been interpreted from the outcrops. At a smaller scale there are eight cycles of funnel - bell - funnel and/or irregular trends, which each correspond to a progradation, retrogradation and finally progradation and/or aggradation pattern and are interpreted to represent the eight Oxfordian sequence cycles.

The Kimmeridgian gamma-ray logs show an irregular trend for the lower three quarters of the Kimmeridgian followed by a funnel trend which continues into the Portlandian. This is interpreted to represent the long-term transgression followed by regression characteristic of the outcrop. Superimposed on the longer term wireline trend are eight smaller scale wireline cycles; these represent the shorter term third-order sequence stratigraphic cycles, and are particularly well-expressed in the upper part of the Kimmeridgian.

Contents

Title i
Declaration ii
Abstract iii
Contents iv
List of Tables & Figures ix
Acknowledgements xx

CHAPTER 1 1
Introduction 1
1.1 Introduction 1
1.2 Aims of the thesis 1
1.3 Database 2
1.4 Structure of the thesis 4
1.5 Regional setting 5
1.5.1 Introduction 5
1.5.2 Wessex Basin 5
1.5.2.1 General structure of the Wessex Basin 5
1.6 Sequence stratigraphy 9
1.6.1 Introduction to sequence stratigraphy 9
1.6.2 Sequence stratigraphy of the Upper Jurassic outcrops of the Wessex Basin 11
1.6.3 Key sequence stratigraphic definitions 13
1.7 Geological interpretation of wireline logs 15
1.7.1 Gamma-ray logs 15
1.7.2 Spontaneous potential log 17
1.7.3 Resistivity and conductivity logs 18
1.7.4 Density log 19
1.7.5 Neutron logs 19
1.7.6 Sonic logs 19
1.8 Wireline logs and sequence stratigraphy 20

CHAPTER 2 23
Surface - Subsurface Correlation 23
2.1 Introduction 23
2.2 Field gamma-ray logs 25
2.2.1 Introduction 25
2.2.2 Gamma-ray theory 27
2.2.3 Portable gamma-ray spectrometers 29
2.2.3.1 geoMetrics GR310 30
2.2.3.2 Exploranium GR320 32
2.2.4 Field procedures 33
2.2.5 Tool and data calibration 35

2.3 Previous field spectral gamma-ray studies 39
2.4 Correlation of field gamma-ray logs with wireline gamma-ray data 43
2.4.1 Upper Jurassic composite field gamma-ray log 43
2.4.2 Comparison of the geoMetrics GR310 and the Exploranium GR320 45
2.4.3 Correlation of field and wireline gamma-ray logs 49
2.4.3.1 Upper Oxford Clay and Corallian Beds 49
2.4.3.2 Kimmeridge Clay Formation 49
2.5 Field density logs 53
2.5.1 Introduction 53
2.5.1.1 Wireline density tools 53
2.5.2 Field and laboratory procedures 53
2.3.2.1 Ruska Universal Porometer 54
2.3.2.2 Density calculations 57
2.3.2.3 Errors in density measurement 58
2.5.3 Computer program to generate field density log 59
2.5.4 Porosity data correction 62
2.6 Correlation of field density logs with wireline density data 62
2.6.1 Upper Oxford Clay and Corallian Beds 62
2.6.2 Kimmeridge Clay Formation. 64
2.7 Discussion 66
2.8 Conclusions 67

CHAPTER 3 68
Wireline Correlation Methods and Techniques 68
3.1 Introduction 68
3.2 Quality control of the wireline data set 68
3.3 Wireline log manipulation 72
3.3.1 Introduction 72
3.3.2 Change of scale 72
3.3.3 Simple mathematical transforms to enhance wireline log trends 74
3.3.4 Filtering logs 77
3.3.5 Normalising curves and adding them together 78
3.4 Wireline log correlation techniques 78
3.4.1 Introduction 78
3.4.2 The most useful wireline log for correlation of the Upper Jurassic succession 80
3.4.3 Manual correlation 83
3.4.4 Automatic computer correlation programs 86
3.4.5 Graphical correlation 87
3.5 Biostratigraphic data and wireline correlation 90
3.6 Lithology determination from wireline logs 91
3.7 Discussion 93
3.8 Conclusions 94

CHAPTER 4 96
Upper Jurassic Wireline Log Trends 96
4.1 Introduction 96
4.2 Wireline log trends 96
4.2.1 Sequence stratigraphical interpretation of the wireline log trends 99
4.3 Upper Jurassic long-term trends 102
4.3.1 Introduction 102
4.3.2 Oxfordian 102
4.3.3 Kimmeridgian 104
4.3.4 Portlandian 106
4.4 Upper Jurassic sea-level changes 106
4.5 Spectral gamma-ray curves as sea-level indicators 110
4.6 Discussion 112
4.7 Conclusions 112

CHAPTER 5 114
Oxfordian 114
5.1 Introduction 114
5.1.1 Upper Oxford Clay Formation 114
5.1.2 Corallian Group 116
5.1.2.1 Dorset Coast 117
5.1.2.2 North Dorset 118
5.1.2.3 Wiltshire and Oxfordshire 120
5.2 Oxfordian palaeogeography of the Wessex Basin 121
5.3 Sequence stratigraphy of Oxfordian exposures 124
5.3.1 Introduction 124
5.3.2 Oxfordian sequence stratigraphy 124
5.3.3 Other sequence stratigraphic interpretations 125
5.4 Sequence stratigraphical interpretation of the wireline logs 127
5.4.1 Introduction 127
5.4.2 Field gamma-ray and density logs 127
5.4.3 Boreholes with biostratigraphical control 130
5.4.4 Lithostratigraphy 135
5.4.5 Wessex Basin 139
5.4.5.1 Central Channel Sub-basin 148
5.4.5.2 Dorset Sub-basin & South Dorset High 148
5.4.5.3 Mere Sub-basin 149
5.4.5.4 Hampshire - Dieppe High 150
5.4.5.5 Vale of Pewsey Sub-basin 150
5.4.5.6 Weald Sub-basin 151
5.5 Previous wireline correlations 154
5.6 Discussion 156
5.7 Conclusions 162

CHAPTER 6 163
Kimmeridgian 163
6.1 Introduction 163
6.2 Sequence stratigraphy of Kimmeridgian exposures 166
6.2.1 Introduction 166
6.2.2 Lower Kimmeridge Clay 166
6.2.3 Upper Kimmeridge Clay 169
6.2.4 Other sequence stratigraphic interpretations 170
6.3 Sequence stratigraphy as seen on the field gamma-ray and density logs 171
6.3.1 Field gamma-ray and density logs 171
6.3.2 Spectral gamma-ray logs 173
6.3.2.1 Introduction 173
6.3.2.2 Interpretation principles 175
6.3.2.2.1 Potassium 175
6.3.2.2.2 Uranium 175
6.3.2.2.3 Thorium 176
6.3.2.2.4 Shales 176
6.3.2.3 Potassium content of the Kimmeridge Clay Formation 177
6.3.2.4 Uranium content of the Kimmeridge Clay Formation 180
6.3.2.5 Thorium content of the Kimmeridge Clay Formation 180
6.3.2.6 Th/K 183
6.3.2.7 Th/U 188
6.3.2.8 Previous work 188
6.3.2.9 Discussion 190
6.4 Sequence stratigraphical interpretation of the wireline logs 191
6.4.1 Introduction 191
6.4.2 Boreholes with biostratigraphical control 193
6.4.2.1 Wessex Basin 193
6.4.2.2 The Wash and Yorkshire 199
6.4.3 Wessex Basin 202
6.4.3.1 Weald Sub-basin 202
6.4.3.2 Central Channel Sub-basin 210
6.4.3.3 Dorset Sub-basin & South Dorset High 213
6.4.3.4 Mere Sub-basin 213
6.4.3.5 Vale of Pewsey Sub-basin 214
6.4.3.6 Hampshire - Dieppe High 214
6.4.4 The Wash and Yorkshire 215
6.5 Previous wireline correlations 219
6.6 Depositional models for the Kimmeridge Clay Formation 221
6.7 Discussion 224
6.8 Conclusions 227

CHAPTER 7 229
Conclusions 229
7.1 Introduction 229
7.2 Conclusions 230
7.2.1 Surface - Subsurface Correlation 230
7.2.2 Wireline Correlation Methods and Techniques 231
7.2.3 Upper Jurassic Wireline Log Trends 231
7.2.4 Oxfordian 233
7.2.5 Kimmeridgian 235
7.3 Further work 238

REFERENCES 240

APPENDIX A 256
List of boreholes used in this study 256

APPENDIX B 261
Stratigraphic logs showing location of the field gamma-ray and density measurements 261
B.1 Introduction 262
B.2 Oxfordian 263
B.3 Kimmeridgian 269
B.4 Portlandian 287
B.5 geoMetrics GR310 field log 290
B.6 Exploranium GR320 field log 296
B.7 Density data 310

APPENDIX C 328
'DEN' FORTRAN program 328

APPENDIX D 332
GMT C-shell scripts 332

List of Tables & Figures

CHAPTER 1: Introduction

Figure 1.1 Map showing the location of the boreholes used in this thesis..... 3

Figure 1.2 Map of England showing the location of the sub-basins within the Wessex Basin. The Kimmeridgian and Corallian outcrops and the principal faults are also shown. 6

Figure 1.3 Representative cross sections across the Wessex Basin. 8

Figure 1.4 Chadwick's (1986) tectonic model for the western Wessex Basin. 9

Figure 1.5 Hierarchy of stratigraphic cycles..... 10

Figure 1.6 (a) Gamma-ray log showing that the natural radiation decreases as the Oxford Clay grades into the coarser Corallian beds. (b) Increasing gamma-ray does not always indicate decreasing grain size and decreasing gamma-ray does not always indicate an increase in grain size. 16

Figure 1.7 Diagram showing that the spontaneous potential log does not have much character over the Kimmeridge Clay Formation. 17

Figure 1.8 Diagram showing that the micro resistivity log (MSFL) has the best vertical resolution. 18

Figure 1.9 Model wireline log patterns for systems tracts. 21

Figure 1.10 Schematic log-motif characteristics for interpretation of wireline log sequence stratigraphic patterns. 22

CHAPTER 2: Surface - Subsurface Correlation

Table 2.1 Background radiation values for NW Europe. 38

Table 2.2 Background radiation values recorded for this study. 38

Figure 2.1 Maps showing the main structural features of the Wessex Basin and the location of boreholes and Upper Jurassic exposures..... 25

Figure 2.2 Composite field gamma-ray log of the Upper Jurassic of Dorset, constructed using a geoMetrics GR310. 26

Figure 2.3 Gamma-ray emission spectra of radioactive minerals..... 27

Figure 2.4 Regions of dominance of the three principal gamma-ray scattering mechanisms..... 28

Figure 2.5 The continuos spectrum recorded with the Exploranium GR320, showing the diagnostic peaks of potassium, uranium and thorium. 29

Figure 2.6 Gamma-ray spectrum for the barium (133 Ba) reference isotope in the geoMetrics GR310. 30

Figure 2.7 Gamma-ray spectra for cesium, the reference isotope in the Exploranium GR320. The automatic stabilization ensures that the cesium peak (662 KeV) is always in channel 55, which in turn ensures that the diagnostic peaks for K, U and Th always fall in the correct channels. 33

Figure 2.8 Effective sampling area of a portable gamma-ray spectrometer compared to a wireline gamma-ray sonde 34

Figure 2.9 Spectral gamma-ray data recorded with the Exploranium GR320, over part of the Kimmeridge Clay Formation between Hobarrow Bay and Chapman's Pool. 36

Figure 2.10 Scintillation spectra of potassium, uranium, and thorium gamma radiation from the ground 37

Figure 2.11 Comparison of field gamma-ray log produced by Talwar *et al.* (1992) and the part of the field log produced in this study, using the geoMetrics GR310, over part of the Oxfordian at Bran Point. 41

Figure 2.12 Comparison of field gamma-ray log produced by Myers (1987) and the two field gamma-ray logs produced in this study over part of the Kimmeridge Clay Formation. Also shown are the gamma-ray logs from Encombe 1 and 98/11-4 boreholes. 42

Figure 2.13 Composite field gamma-ray log for the Upper Jurassic succession exposed on the Dorset coast, plotted along side the wireline gamma-ray log from 98/11-4 borehole located in the Central Channel Sub-basin. 44

Figure 2.14 Comparison of the field gamma-ray logs measured using the Exploranium GR320 and the geoMetrics GR310 portable gamma-ray spectrometers, for that part of the Kimmeridge Clay Formation exposed between Hobarrow Bay and Chapman's Pool. 46

Figure 2.15 The correlation coefficient, calculated using the CORPAC program, over the part of the Kimmeridge Clay Formation. 47

Figure 2.16 Detailed comparison of the field gamma-ray logs for the Oxfordian produced using the geoMetrics GR310 spectrometer with the wireline gamma-ray logs from boreholes 98/11-4 and 98/11-3 in the Central Channel Sub-basin 48

Figure 2.17 Detailed comparison of the field gamma-ray logs for part of the Kimmeridge Clay Formation produced using the two portable field gamma-ray spectrometers and the wireline gamma-ray log from the nearby Encombe 1 borehole. 50

Figure 2.18 The correlation coefficient between the two field gamma-ray logs and the wireline gamma-ray from the Encombe 1 borehole calculated using the CORPAC program..... 51

Figure 2.19 Comparison of the field gamma-ray log produced using the geoMetrics GR310 spectrometer with wireline logs from three boreholes from the Central Channel Sub-basin and the Weald Sub-basin..... 52

Figure 2.20 Density curve constructed using Oxfordian age rock samples from six exposures on the Dorset coast..... 55

Figure 2.21 Density curve constructed using rock samples from that part of the Kimmeridge Clay Formation exposed between Kimmeridge Bay and Chapman's Pool. 56

Figure 2.22 The volume scale and dial reading (V'f) read off the porometer is plotted on this graph to obtain the grain volume of the sample..... 57

Figure 2.23 Fourteen lithology types were used in the construction of the field density log for the Kimmeridge Clay section shown in Fig. 2.21. The average density value for each lithology, which was used to represent the density of the beds from which no sample was taken, is shown on each of the graphs..... 60

Figure 2.24 Flow chart for the FORTRAN program 'DEN'..... 61

Figure 2.25 Atlas Wireline Services field acquisition (CLS) filter. 62

Figure 2.26 Porosity and lithology determination, from the Formation Density and Compensated Neutron Logs, for the Oxfordian strata in borehole 98/11-1..... 63

Figure 2.27 Detailed comparison of the density log for part of the Kimmeridge Clay Formation produced from rock specimens and wireline density logs from the nearby Encombe 1 borehole and Bletchingly 1 and Detention 1 boreholes in the Weald Sub-basin..... 64

Figure 2.28 The correlation coefficient between the outcrop density log and the wireline density log from the nearby Encombe 1 borehole, calculated using the CORPAC program..... 65

Plate 2.1 The geoMetrics GR310 portable gamma-ray spectrometer. 31

Plate 2.2 The Exploranium GR320 portable gamma-ray spectrometer. 31

CHAPTER 3: Wireline Correlation Methods and Techniques

Figure 3.1 Comparison of wireline gamma-ray logs recorded in 1952 (Arreton 1) and 1974 (Arreton 2). 69

Figure 3.2 Diagram showing features looked for during the quality control of the wireline data set. 70

Figure 3.3 Diagram showing artefacts seen on the wireline data in some cases when two logging runs are spliced together. 71

Figure 3.4 Diagram showing that just by changing the gamma-ray scale and by extending the horizontal thickness of the plot the trends seen on the gamma-ray log, for the whole of the Upper Jurassic in the Ashdown 1 borehole, can be significantly enhanced. 72

Figure 3.5 The same induction curve plotted on different scales. The induction resistivity is the reciprocal of the induction conductivity. 73

Figure 3.6 Effect of simple mathematical transforms (power and root) on the shape of the gamma-ray log 75

Figure 3.7 Figure showing the 1st and 2nd derivative of the total gamma-ray log and two filtered gamma-ray logs. 76

Figure 3.8 Low-pass filtering of the wireline gamma-ray log from Ashdown 1 borehole. 77

Figure 3.9 The gamma-ray, neutron and density logs from the Marchwood 1 borehole have been normalized (put of a scale of 0 to 1) and then added together. 79

Figure 3.10 The full suite of wireline logs from the 98/11-1 borehole. The gamma-ray log has proved to be the most suitable log for the correlation of the Upper Jurassic of the Wessex Basin. 81

Figure 3.11 Diagram showing the wireline logs for the Oxfordian succession in Henfield 1, drilled in 1936, and Collendean Farm 1, drilled in 1964. The diagram clearly shows that correlating this Oxfordian succession using the SP or resistivity logs is difficult. 82

Figure 3.12 Diagram showing that shading the wireline logs can enhance visual correlation. Subtle changes are easier to see on the shaded wireline logs than on the unshaded wireline logs. 84

Figure 3.13 The shading of the wireline logs can be done using any log. 85

Figure 3.14 Diagram showing the comparison of the same part of the Kimmeridge Clay Formation as seen on the gamma-ray logs from 98/11-4, which is located in the Central Channel Sub-basin, and 98/11-1, which is located on the south Dorset High. 86

Figure 3.15 Diagram showing the information gained from graphical correlation.(a) Plot showing a fault. (b) Plot showing a fault and an unconformity, and a possible error in the correlation. (c) Plot showing that even though condensed successions seen on palaeohighs are significantly thinner than successions encountered in the sub-basins the line of correlation is still fairly straight. 89

Figure 3.16 Lithology calculated using the Petra module of the Terrastation II computer package, for the interval which encompasses the Oxfordian succession in the 98/11-1 borehole. 92

Figure 3.17 Flow chart showing the steps involved in the sequence stratigraphical interpretation of the wireline data set. 94

CHAPTER 4: Upper Jurassic Wireline Log Trends

Figure 4.1 Wireline log trends, illustrated using the wireline gamma-ray log from 98/11-4 borehole. 97

Figure 4.2 Use of wireline log trends in sequence stratigraphy. 100

Figure 4.3 Wireline log trends seen on the full suit of logs for borehole 98/11-4 . 101

Figure 4.4 Map showing the main structural features of the Wessex Basin and the location of boreholes discussed in this chapter 103

Figure 4.5 Wireline trends on the full suit of logs from the Marchwood 1 borehole, which is representative of condensed Upper Jurassic successions. 104

Figure 4.6 Typical wireline log trends for the Upper Jurassic succession in the Weald Sub-basin. 105

Figure 4.7 Sea-level curve based on the sequence stratigraphic field interpretation of the Upper Jurassic exposures of the UK by A. L. Coe. 107

Figure 4.8 Comparison of Upper Jurassic sea-level curve and trends seen on the wireline gamma-ray logs. 108

Figure 4.9 Sea-level curve for the Kimmeridgian has been stretched and squeezed so that the key sequence stratigraphical surfaces line up with the key sequence stratigraphical surfaces which have been picked on the gamma-ray curve from borehole 98/11-4 110

Figure 4.10 Spectral gamma-ray data recorded over part of the Kimmeridge Clay Formation plotted against sea-level curve. 111

Figure 4.11 Sea-level curve constructed in this study plotted alongside the sea-level curve constructed by Haq et al. (1987, 1988) 113

CHAPTER 5: Oxfordian

Table 5.1 Correlation of the Sub Mediterranean, north-west European and Boreal zonal schemes for the Oxfordian 116

Table 5.2 Lithostratigraphic nomenclature for the Oxfordian of the Wessex Basin. 117

Table 5.3 Corallian Group terminology in north Dorset. 120

Table 5.4 Comparison of the different sequence stratigraphic interpretations of the Oxfordian succession exposed on the Dorset coast. 126

Table 5.5 List of boreholes, in the Wessex Basin, with references containing biostratigraphical data for the Oxfordian. 134

Figure 5.1 Map of England showing the Corallian Group outcrop and the principal faults. Insert shows location of the main Corallian Group exposures on the Dorset coast together with Furzy Cliff where part of the Upper Oxford Clay is exposed..... 115

Figure 5.2 Palaeogeographic map for the Oxfordian. 123

Figure 5.3 Composite field gamma-ray and density field logs for the Oxfordian succession exposed on the Dorset coast, showing the key sequence stratigraphic surfaces. 128

Figure 5.4 Comparison of the composite field gamma-ray log over the Osmington Oolite Formation at Bran Point and Black Head on the Dorset coast.. 129

Figure 5.5 Gamma-ray trends seen in each of the systems tracts on the composite field gamma-ray log for the Oxfordian succession exposed on the Dorset coast..... 131

Figure 5.6 Biostratigraphic information obtained from fossils found in core and cuttings from Ashdown 1 borehole. 132

Figure 5.7 Diagram showing the biostratigraphic information obtained from the Warlingham borehole core by Worssam & Ivimey-Cook (1971). 133

Figure 5.8 Lithology calculated using the Petra module of the Terrastation II computer package, for the interval which encompasses the Oxfordian succession in the 98/11-1 borehole. 136

Figure 5.9 Lithology calculated using the Petra module of the Terrastation II computer package, for the Oxfordian succession typical of the Weald Sub-basin. 137

Figure 5.10 Lithostratigraphic subdivision of the Oxfordian successions in the 98/11-3 and 98/11- 4 boreholes, based on the available biostratigraphic data, calculation of lithology using Petra and comparison with exposures on the Dorset coast using the field gamma-ray and density logs. 138

Figure 5.11 Comparison of two interpretations of the Oxfordian succession encountered in the Winterbourne Kingston 1 Borehole..... 139

Figure 5.12 Sequence stratigraphical wireline correlation of the Oxfordian succession in the Wessex Basin. 141

Figure 5.13 Sequence stratigraphical wireline correlation of the Oxfordian succession in the Wessex Basin. 142

Figure 5.14 Sequence stratigraphical wireline correlation of the Oxfordian succession in the Wessex Basin. 143

Figure 5.15 Sequence stratigraphical wireline correlation of the Oxfordian succession in the Wessex Basin. 144

Figure 5.16 Sequence stratigraphical wireline correlation of the Oxfordian succession inthe Wessex Basin. 145

Figure 5.17 Sequence stratigraphical wireline correlation of the Oxfordian succession in the Wessex Basin. 146

Figure 5.18 Sequence stratigraphical wireline correlation of the Oxfordian succession in the Wessex Basin. 147

Figure 5.19 Diagram showing the typical Oxfordian succession in the Weald Sub-basin. (a) Three boreholes in the Weald Sub-basin showing the typical wireline signature of the Oxfordian succession. (b) Simplified sketch of the reef, located on the northern margin of the sub-basin. The relative location of the three boreholes in a) have been plotted to show how the different intervals in unit 1 relate to each other. 152

Figure 5.20 Corallian succession in the Weald Sub-basin. The shading shows that the mudstone of unit 2 in the Corallian has a different wireline character from the mudstones in the overlying Kimmeridge Clay Formation and the underlying Oxford Clay Formation. 155

Figure 5.21 Isopach maps of parts of the Oxfordian succession.. 161

CHAPTER 6: Kimmeridgian

Table 6.1 Potassium in clay minerals. 177

Table 6.2 Bulk chemistry of the Kimmeridge Clay lithologies. 186

Table 6.3 List of boreholes, in the Wessex Basin, with references containing biostratigraphical data for the Kimmeridgian. 199

Figure 6.1 Map of England showing the Kimmeridgian outcrop and the main structural features of the Wessex Basin. 164

Figure 6.2 Outcrop section exposed between Kimmeridge Bay and Chapman's Pool, showing the prominent 'Stone Band' marker horizons..... 165

Figure 6.3 Composite field gamma-ray log, for part of the Lower Kimmeridge Clay Formation, showing the location of the key sequence stratigraphic surfaces. 167

Figure 6.4 Composite field gamma-ray and density logs, for the part of the Kimmeridge Clay Formation exposed between Hobarrow Bay and Chapman's Pool, showing the location of the key sequence stratigraphic surfaces. 168

Figure 6.5 Diagram showing the differences between the various sequence stratigraphic interpretations of Kimmeridgian strata. 172

Figure 6.6 Spectral gamma-ray data recorded over part of the Kimmeridge Clay Formation between Hobarrow Bay and Chapman's Pool, showing the location of the key sequence stratigraphic surfaces. 174

Figure 6.7 Potassium content of the various lithologies in the Kimmeridge Clay Formation plotted against the distance to the closest bed boundary 178

Figure 6.8 Potassium content of the calcareous mudstones plotted against distance along cliff, bed thickness and distance to closest bed boundary. 179

Figure 6.9 Uranium content of the various lithologies in the Kimmeridge Clay Formation plotted against the distance to the closest bed boundary 181

Figure 6.10 Thorium content of the various lithologies in the Kimmeridge Clay Formation plotted against the distance to the closest bed boundary 182

Figure 6.11 Th/K cross-plots for the individual ammonite zones. 184

Figure 6.12 Spectral gamma-ray data recorded over part of the Kimmeridge Clay Formation, plotted on the Th/K plot for the identification of clay minerals developed by Quirein *et al.* (1982). 185

Figure 6.13 Spectral gamma-ray data recorded over part of the Kimmeridge Clay Formation, plotted on the Th/K plot for the identification of clay minerals from Western Atlas (1992). 185

Figure 6.14 Th/K, Th/U and U/K ratios for the part of the Kimmeridge Clay Formation exposed between Hobarrow Bay and Chapman's Pool, showing the key sequence stratigraphical surfaces. 187

Figure 6.15 Spectral gamma-ray data plotted up with the kaolinite/illite ratio from Wignall & Ruffell (1990). 188

Figure 6.16 Kimmeridge Clay spectral gamma-ray data plotted on the spectral gamma-ray KUT ratio plot. 189

Figure 6.17 Spectral gamma-ray data recorded in this study plotted alongside the spectral data recorded by Myers (1987). 190

Figure 6.18 Map showing the location of the boreholes used in this chapter. 192

Figure 6.19 Diagram showing the Warlingham borehole with the key sequence stratigraphic surfaces picked. 194

Figure 6.20 Hartwell borehole showing the location of the key sequence stratigraphic surfaces. 195

Figure 6.21 Brill borehole showing the key sequence stratigraphic surfaces. 196

Figure 6.22 Brightling 1 borehole showing the key sequence stratigraphic surfaces. 198

Figure 6.23 North Wootton borehole showing the location of the key sequence stratigraphic surfaces. 200

Figure 6.24 Denver Sluice borehole showing the location of the key sequence stratigraphic surfaces. 201

Figure 6.25 Wireline correlation of boreholes in the Wessex Basin showing the key sequence stratigraphic surfaces and ammonite zones. 203

Figure 6.26 Wireline correlation of boreholes in the Wessex Basin showing the key sequence stratigraphic surfaces and ammonite zones. 204

Figure 6.27 Wireline correlation of boreholes in the Wessex Basin showing the key sequence stratigraphic surfaces and ammonite zones. 205

Figure 6.28 Wireline correlation of boreholes in the Wessex Basin showing the key sequence stratigraphic surfaces and ammonite zones. 206

Figure 6.29 Wireline correlation of boreholes in the Wessex Basin showing the key sequence stratigraphic surfaces and ammonite zones. 207

Figure 6.30 Wireline correlation of boreholes in the Wessex Basin showing the key sequence stratigraphic surfaces and ammonite zones. 208

Figure 6.31 Isopach maps of two sequences in the Wessex Basin. (a) Isopach of the Ki sequence. (b) Isopach of the K1 sequence 209

Figure 6.32 Comparison of the Kimmeridgian succession in the Weald Sub-basin (Cowden 1) and the Kimmeridgian exposures on the Dorset coast 211

Figure 6.33 Comparison of the Kimmeridgian succession in the Weald Sub-basin (Cowden 1) and the Kimmeridgian succession in the Central Channel Sub-basin (98/11-4). 212

Figure 6.34 Comparison of the Kimmeridgian succession in the Weald Sub-basin (Cowden 1) and the Kimmeridgian succession on the Hampshire - Dieppe High (Marchwood) 214

Figure 6.35 Wireline correlation, of boreholes around the Wash and Yorkshire, showing the key sequence stratigraphic surfaces and ammonite zones. 216

Figure 6.36 Wireline correlation, of boreholes around the Wash and Yorkshire, showing the key sequence stratigraphic surfaces and ammonite zones. 217

Figure 6.37 Comparison of the Kimmeridgian succession in the Weald Sub-basin (Cowden 1) and the Kimmeridgian succession in the Wash (Ulceby Cross)..... 218

Figure 6.38 Late Kimmeridgian paleogeography. Note the southward flow of the water currents from the Boreal Ocean. 218

Figure 6.39 Comparison of synthetic gamma-ray log of Melnyk *et al.* (1995) and field gamma-ray logs constructed in this study. 220

Figure 6.40 Diagram showing the main points from the depositional model of Myers & Wignall (1987), for the Upper Kimmeridge Clay Formation. 223

Figure 6.41 Spectral gamma-ray data, recorded over part of the Kimmeridge Clay Formation, plotted against sea-level curve. 226

CHAPTER 7: Conclusions

Figure 7.1 Sea-level curve for the Oxfordian and Kimmeridgian plotted with the gamma-ray curve from borehole 98/11-4..... 232

Figure 7.2 Map of the Wessex Basin showing the location of the carbonate reef and the O6 sequence in the Weald Sub-basin. The map also shows the area where part of the Upper Corallian is not present..... 234

Figure 7.3 Graphical correlation plot of the Oxfordian succession in 98/11-4, located in the Central Channel Sub-basin, and 98/11-3, located on the South Dorset High... .. 234

Figure 7.4 Map of the Wessex Basin showing the extent the base Cretaceous unconformity, the location of the offshore sand bodies which have been interpreted as being the lowermost systems tract of the Ki sequence is also indicated.. 235

Figure 7.5 Graphical correlation plots showing that the lowermost systems tract is generally lower gradient than the transgressive and highstand systems tracts. 237

Figure 7.6 Synthetic seismic for 98/11-4. 239

APPENDIX A: List of Boreholes Used in This Study

Table A.1 List of all the boreholes used in this study which contained wireline data. 257

Table A.2 List of the boreholes which penetrate Upper Jurassic strata but contain no wireline data. 258

Table A.3 List of boreholes in the Wessex Basin which do not penetrate any Upper Jurassic strata. 259

APPENDIX B: Stratigraphic Logs Showing Location of The Field Gamma-ray and Density Measurements

Table B.5.1 Upper Jurassic composite field gamma-ray log data..... 291

Table B.6.1 Spectral gamma-ray data..... 298

Table B.7.1 Density of the Oxfordian specimens. 311

Table B.7.2 Box curve and final filtered density data for the Oxfordian. 312

Table B.7.3 Density of the Kimmeridgian specimens. 317

Table B.7.4 Box curve and final filtered density data for the Kimmeridgian. 318

Figure B.1 Map showing the location of the Upper Jurassic exposures on the Dorset coast..... 262

Acknowledgements

I would especially like to thank Angela Coe for the supervision and encouragement she has provided during the last 3 years. My other supervisors Neil Goulty and Maurice Tucker are also thanked for there help.

I would like to thank the University of Durham for providing me with a University of Durham Research Studentship, and the Department of Geological Sciences at Durham for funding some of my field work and conference expenses. The PESGB and AAPG are thanked for awarding me a field work grant from the 1996 Grant-in-Aid Award program.

I would like to thank the following companies/organisations and there employees for access to their digital wireline data and biostratigraphic reports: British Geological Survey, Heather Baily and Phil Roberts; British Gas Exploration and Production, M. J. Oates; Conoco, Ian Lisseter; Elf, Stuart Harker; Department of Trade and Industry, Mike Hurley.

Atlas Wireline Services, in particular Mike Overton, is thanked for providing me and the department with the Atlas Wireline 'Well Data System' computer software package. Ricardo Olea, from Kansas Geological Survey is thanked for providing me with a copy of his automatic wireline correlation program 'Correlator'. Doug Martinson and Rich Iannuzzi are thanked for providing me with their wireline correlation program 'Corpac'.

The technical staff in the department are also thanked, in particular George Ruth and Dave Stevenson for keeping the computer system up and running (most of the time!). Rich and Berny, engineering geology technicians, are thanked for showing me how to use the Porometer, even though they convinced me that I had broken it for a while!.

I would like to thank Ismail Che Mat Zin, my office mate for two years, for the long chats about our research and life in general (and for selling me his Polo). Alwyn and Maureen Ross are also thanked for making the office an interesting place to be for the few months they shared the office with me.

Charlotte Martin and Toby Harrold are thanked for providing me with some company during parts of my field work. Brain Turner and Angela Coe are thanked for lending me their portable gamma-ray spectrometers.

I would like to take this opportunity to thank all the past and present research students and post doctorates for making my stay in Durham a pleasurable one. In particular I would like to thank: Alun Price, Adam Styles, Wayne Bailey (and big bird), Jo Garland, Gail Radcliffe, Jonney Imber, the four Simon's (Grant, Russell, Molyneux, Williams), Ian Turner, Mark Osbourne, Neil Mitchell, Daneil Grunberger and Matt Pritchard.

My parents and grandmother are also thanked for their support and encouragement during these last three years. Lastly and most importantly I would like to thank Charlotte Martin for her continued support during the last three years, even though she nagged me about my diagrams!

CHAPTER 1

Introduction

1.1 Introduction

Sequence stratigraphy has proven to be a powerful method of sub-dividing the stratigraphical record. The technique is now widely used to interpret the sedimentary record and to develop high-resolution correlation over wide geographical areas. Most sequence stratigraphy has been carried out using seismic or outcrop data. Wireline logs provide the obvious means to extend sequence stratigraphical interpretation from outcrop into the subsurface and to link through to seismic data.

The Upper Jurassic of the United Kingdom was chosen for this study because it is represented by a wide range of sediment types from deep-marine mudstones and sandstones to non-marine carbonates, and therefore provides a variety of wireline signals suitable for developing interpretation techniques. In addition, the sequence stratigraphy of the Upper Jurassic of the United Kingdom outcrops has been established and thus provides the framework for the detailed correlation of the large subsurface data set.

1.2 Aims of the thesis

The main objective of this thesis was to extend the established sequence stratigraphic interpretation of the Upper Jurassic outcrops of the United Kingdom to the subsurface using wireline logs. The aims of the thesis may be summarised as follows:

- To construct 'synthetic' wireline logs (field logs) from outcrops which could be directly compared with the wireline logs obtained by oil companies by measuring the natural gamma-ray response at outcrop and the density of fresh rock samples in the laboratory.

- To develop simple mathematical techniques which enhance the wireline logs making them more suitable for sequence stratigraphical interpretations.

- To establish a technique for the sequence stratigraphic interpretation of the full suite of wireline logs.

- To establish whether the trends seen on the wireline logs relate to relative sea-level changes.

- To correlate the wireline logs, from boreholes across the Wessex Basin, in a sequence stratigraphic manner for the Oxfordian and Kimmeridgian successions. To extend the correlation from the Wessex Basin to Yorkshire for the Kimmeridgian succession.

1.3 Database

The main database for this thesis comprises wireline logs from 83 boreholes. The full suite of logs (gamma-ray, sonic, density, neutron, resistivity, self potential and caliper) was available for some of the boreholes, while others only had one log. Appendix A contains a list of all the boreholes, showing which wireline logs were available for each borehole, and Figure 1.1 shows the location of all 83 boreholes for which wireline data were available in this study. Some biostratigraphical and lithostratigraphic data for these boreholes were obtained from the National Geosciences Database well files, which are held at the British Geological Survey offices at Keyworth and Exeter. Unpublished biostratigraphical reports were available for the following boreholes: 98/11-1 (Jacovides *et al.* 1983), 98/11-2 (Jacovides & Woollam 1994), 98/11-3 (King & Allen 1987), 98/11-4 (King *et al.* 1987), 98/23-1 (King & Jacovides 1983) and Detention 1 (Perkins 1982).

A literature search resulted in the location of another 83 boreholes without wireline log data but which did contain stratigraphical and biostratigraphical data. This resulted in a total of 166 boreholes which were used in this study (Fig. 1.1).

Fieldwork carried out during the project resulted in the measurement of 1124 total gamma-ray measurements over 503 m of the Upper Jurassic succession, and 824 spectral gamma-ray measurements over 251 m of the Kimmeridge Clay Formation. Density measurements were made on 116 samples collected over 90 m of the Oxfordian succession and 260 samples collected from 280 m of the Kimmeridge Clay Formation.

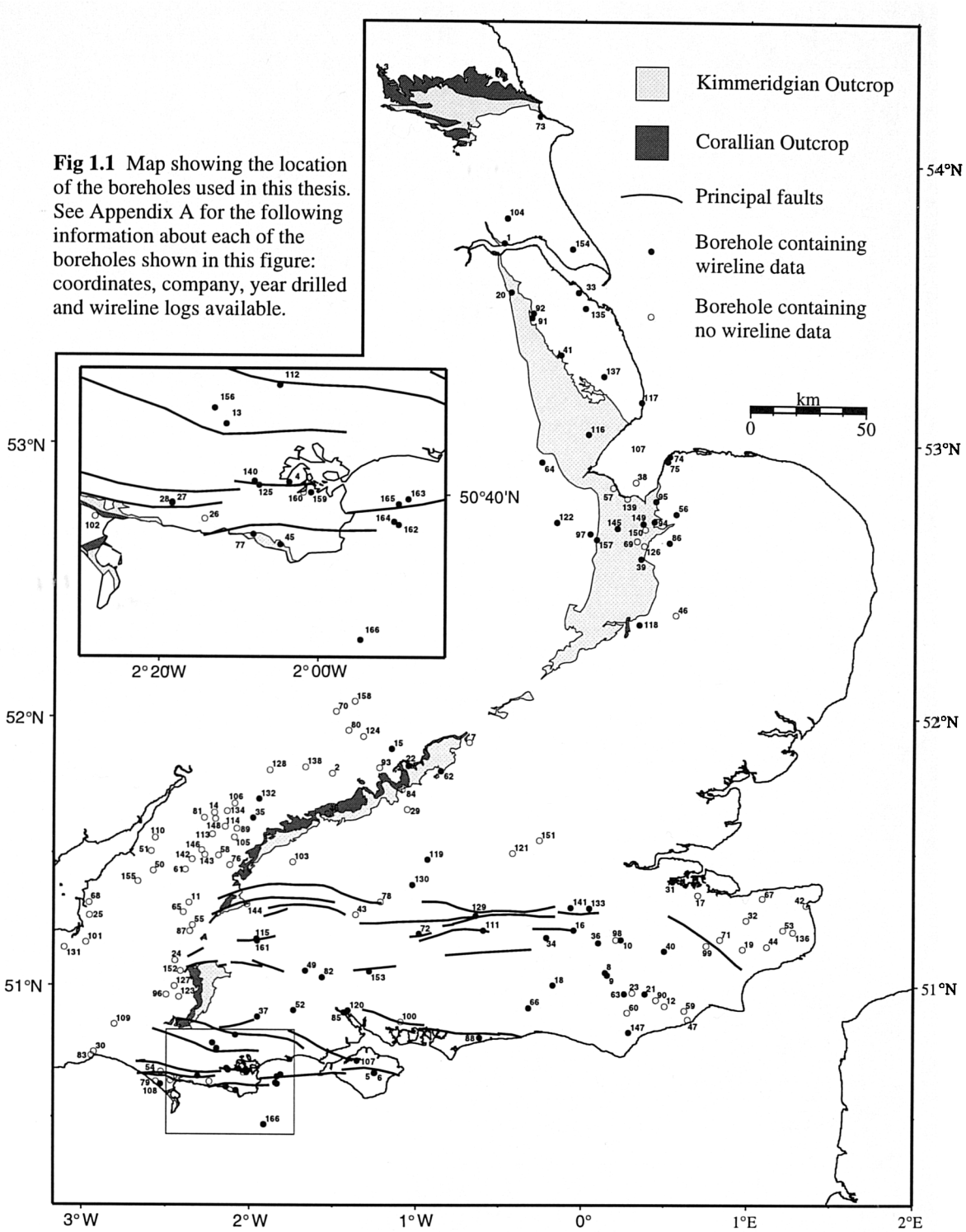

Fig 1.1 Map showing the location of the boreholes used in this thesis. See Appendix A for the following information about each of the boreholes shown in this figure: coordinates, company, year drilled and wireline logs available.

1 Alandale
2 Apley Barn
3 Arden Moor
4 Arne G1
5 Arreton 1
6 Arreton 2
7 Ascott Farm
8 Ashdown 1
9 Ashdown 2
10 Ashour 1
11 Baggridge 1
12 Battle
13 Bere Regis 1
14 Beverston
15 Bicester 1
16 Blechingley 1
17 Bobbing
18 Bolney 1
19 Branbourne
20 Brigg 1
21 Brightling 1
22 Brill
23 Broadoak
24 Burton
25 Burton Row
26 Chaldon Herring G2
27 Chaldon Herring 1
28 Chaldon Herring G3
29 Chalgrove
30 Charmouth
31 Chatham
32 Chilham
33 Cleethorpes
34 Collendean farm
35 Cooles Farm
36 Cowden 1
37 Cranbourne 1
38 Daseley's Sand
39 Denver Sluice 1
40 Detention 1
41 Donington on Bain
42 Ebbsfleet
43 Egbury
44 Elham
45 Encombe
46 Eriswell
47 Fairlight
48 Faringdon 1
49 Farley South 1
50 Filton 1
51 Filton 2
52 Fordingbridge 1
53 Freville
54 Friar Waddon
55 Frome
56 Gayton
57 Gedney Drove End
58 Grittleton
59 Guestling
60 H. Grove Hill 1
61 Hamswell
62 Hartwell
63 Heathfield 7
64 Helpringham 1
65 Henington
66 Henfield 1
67 Herne
68 Hill Lane
69 Hook Drian
70 Hook Norton
71 Hothfield
72 Humbly Grove
73 Hunmanby 1
74 Hunstanton 1
75 Hunstanton IGS
76 Ivyfields 3
77 Kimmeridge K5
78 Kingsclere
79 Langton Herring 1
80 Ledwell
81 Leighterton
82 Lockerley 1
83 Lyme Regis
84 M40 site 9
85 Marchwood 1
86 Marham
87 Marston
88 Middleton 1
89 Milbourne 1
90 Mountfield 1
91 Nettleton
92 Nettleton Bottom
93 Noke Hill
94 North Runcton 1
95 North Wootton 1
96 Oborne
97 Parson Drove 1
98 Penhurst 1
99 Pluckley
100 Portsdown 2
101 Puriton
102 Radipole
103 Richmond
104 Risby 1
105 Rodbourne 1
106 Rodmarton A
107 Sandhills 1
108 Seaburn Farm
109 Seaborough
110 Severn Bridge Tunnel
111 Shalford 1
112 Shapwick 1
113 Sherston
114 Shipton Moyne 5A
115 Shrewton 1
116 Sibsey 1
117 Skegness
118 Soham 1
119 Sonning eye 1
120 Southhampton 1
121 Southhall
122 Spalding 1
123 Stalbridge
124 Steeple Aston
125 Stoborough 1
126 Stowbridge
127 Stowell
128 Stowell Park
129 Strat A1
130 Strat B1
131 Swang Farm 1
132 Swindon BH 2
133 Tatsfield 1
134 Tetbury
135 Tetney Lock
136 Tilmanstone
137 Ulceby Cross
138 Upton
139 Walkers Marsh
140 Wareham 3
141 Warlingham 1
142 West Farm
143 West Kington
144 West Lavington
145 West Walton Highway
146 Westfield Farm
147 Westham 1
148 Westonbirt
149 Wiggenhall 1
150 Wiggenhall St. Peter
151 Willesden
152 Wincanton
153 Winchester 1
154 Winestead 1
155 Winford
156 Winterbourne Kingston
157 Wisbech
158 Withycombe Farm
159 Wytch Farm 2
160 Wytch Farm D5
161 Yarnbury 1
162 98/11-4
163 98/11-3
164 98/11-2
165 98/11-1
166 98/16-1

1.4 Structure of the thesis

The thesis is comprised of seven chapters. The first part of this chapter introduces the study and outlines the aims. The rest of this chapter briefly describes the structural geology of the study area, the concepts of sequence stratigraphy, the geological information available from wireline logs, and the sequence stratigraphical interpretation of wireline logs. The contents of the succeeding chapters are outlined below.

Chapter 2: Within this chapter the techniques used to produce field gamma-ray and density logs are described. The results of correlating the field gamma-ray and density logs with wireline gamma-ray and density logs from across the Wessex Basin are also discussed.

Chapter 3: This chapter describes the techniques used to enhance the wireline logs to make them more suitable for sequence stratigraphical interpretation. The technique established for the sequence stratigraphic interpretation of the full suite of wireline logs is also discussed.

Chapter 4: Long-term wireline log trends are discussed in this chapter, paying particular attention to whether these trends are related to relative sea-level changes.

Chapters 5 and 6: These two chapters detail the sequence stratigraphic interpretation of the wireline data set for the Oxfordian and Kimmeridgian successions, respectively.

Chapter 7: This chapter lists the main conclusions of this study.

Appendix A: This appendix contains a list of the boreholes used in this study.

Appendix B: This appendix contains stratigraphic logs showing the location of the field gamma-ray and density measurements, and the raw field spectral gamma-ray and density data.

Appendix C: FORTRAN program 'DEN' which converts the raw density values into a box curve which when filtered has the same resolution and character as wireline density logs.

Appendix D: Examples of GMT C-shell scripts written to display the digital wireline data.

1.5 Regional setting

1.5.1 Introduction

The Upper Jurassic strata (Oxfordian, Kimmeridgian and Portlandian) outcrop onshore in England from Dorset to Yorkshire (Fig. 1.2), and subcrop to the east of the outcrop. The thickest Upper Jurassic succession is found in the Wessex Basin; hence it is the main region dealt with in this study. The Kimmeridgian deposited on the Eastern England Shelf (Fig. 1.2) has also been examined in this study and compared to that deposited in the Wessex Basin.

Detailed palaeogeographic maps for the Oxfordian, Kimmeridgian and Portlandian of England can be found in Cope *et al.* (1992) and Whittaker (1985). More general palaeogeographic maps of Europe can be found in Zeigler (1982).

1.5.2 Wessex Basin

Kent (1949) proposed that a large depocentre existed across parts of, or all of, Devon, Somerset, Dorset, Wiltshire, Isle of Wight, Hampshire, Surrey, Sussex and Kent. He named this depocentre the Wessex Basin. Even though the area has subsequently been shown to consist of several sub-basins, the term Wessex Basin has survived. The Wessex Basin extends southwards into the English Channel and the Paris Basin, and is bounded to the north and east by the London-Brabant Massif and to the west and south-west by the Welsh and Cornubian Massifs (Fig. 1.2).

Hydrocarbon exploration began in the Wessex Basin in the 1930's (Terris & Bullerwell 1965, Butler & Pullan 1990) and has continued to the present day. The exploration has resulted in the discovery of several oil and gas fields, the most notable being: Wytch Farm (Dranfied *et al.* 1987, Colter & Harvard 1981), Humbly Grove (Hancock & Mithen 1987), and Palmers Wood (Butler & Pullan 1990). This exploration has also resulted in a large subsurface data set, making the Wessex Basin an ideal location for a study of this type.

1.5.2.1 General structure of the Wessex Basin

A number of detailed studies on the structure of the Wessex Basin have been carried out (Smith 1985, Whittaker *et al.* 1985, Chadwick 1986, Lake & Karner 1987, Karner *et al.* 1987, Hamblin *et al.* 1992). A summary of the structural history of the Wessex Basin based on these studies now follows.

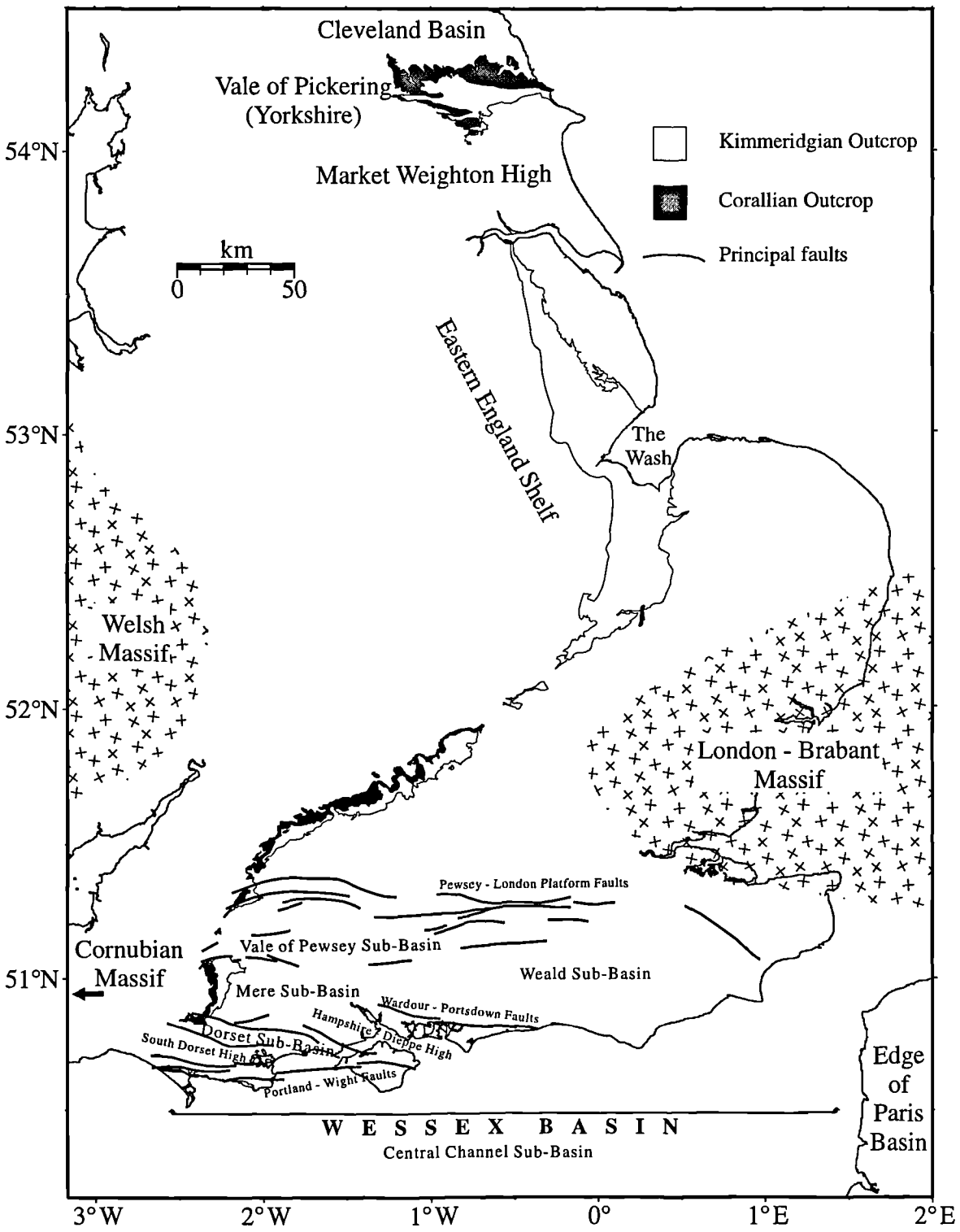

Fig. 1.2 Map of England showing the location of the sub-basins within the Wessex Basin. The Kimmeridgian and Corallian outcrops and the principal faults are also shown. The faults are after Whittaker (1985) and Hamblin *et al.* (1992). Position of the Welsh and London massifs from Ziegler (1982).

The Wessex Basin is an E-W trending Late Palaeozoic to Tertiary extensional basin which formed during the widespread post-Carboniferous subsidence of the northwest

European Shelf. The basin formed on Palaeozoic crust consisting mainly of Cambrian to Carboniferous sediments which were deformed into imbricated thrust sheets during the Late Carboniferous (Variscan) orogeny. An extensional tectonic regime dominated the evolution of the Wessex Basin during Late Carboniferous to Early Cretaceous times. During the extensional phases, reactivation of the Variscan thrusts took place resulting in compartmentalization of the basin. Differential subsidence led to the formation of a number of depocentres or sub-basins: Weald, Vale of Pewsey, Mere, Dorset (also known as Winterborne-Kingston Trough) and Central Channel (Fig. 1.2). These are flanked or separated by intervening 'highs': South Dorset High, Hampshire-Dieppe High and the London platform (Fig. 1.2). Figure 1.3 shows six representative cross-sections across the onshore part of the Wessex Basin.

By Callovian and early Oxfordian times, a tectonic regime of regional thermal subsidence had become established, with only minor contemporaneous fault activity that increased gradually with time. During this time the Oxford Clay was deposited overlapping earlier formations. This was followed by an extensional phase which resulted in the deposition of the Corallian Formation. Carbonates, coarse-grained siliciclastics and mudrocks were deposited during Corallian times. Extension then ceased and thermal subsidence took place once again, this time resulting in the widespread deposition of the Kimmeridge Clay Formation. Towards the end of the Jurassic, a marked fall in relative sea level led to a shrinkage of the depositional area and re-emergence of the structural highs. This trend continued into the Early Cretaceous. Rapid crustal extension accompanied by major normal faulting allowed thick siliciclastic successions to accumulate in the restricted Weald and Central Channel sub-basins, where sedimentation was probably continuous. In contrast, surrounding areas were uplifted and severely eroded. This extreme structural demarcation was accomplished by considerable movement along the major fault zones. Erosion was particularly severe in the western part of the area, where thick successions of Permo-Triassic and Jurassic strata were removed to uncover Palaeozoic basement rocks. Similar, though less severe, uplift affected the London Platform, where Jurassic strata were removed to reveal the basement. The Hampshire-Dieppe and South Dorset highs were also eroded, in places down to the level of middle Jurassic strata. This important period of erosion lasted from end-Jurassic to end-Barremian times, and resulted in the late-Cimmerian Unconformity.

Chadwick (1986) and Karner *et al.* (1987) proposed models which dealt with the extensional development of the Wessex Basin. Chadwick (1986) proposed that the Wessex Basin experienced episodic extensional tectonics producing a series of grabens and fault block highs. Chadwick presented McKenzie's (1978) model of rifting, followed by thermal subsidence, to explain the repeated pattern of shallow-water deposition being followed by laterally widespread deeper-water sedimentation (Fig. 1.4).

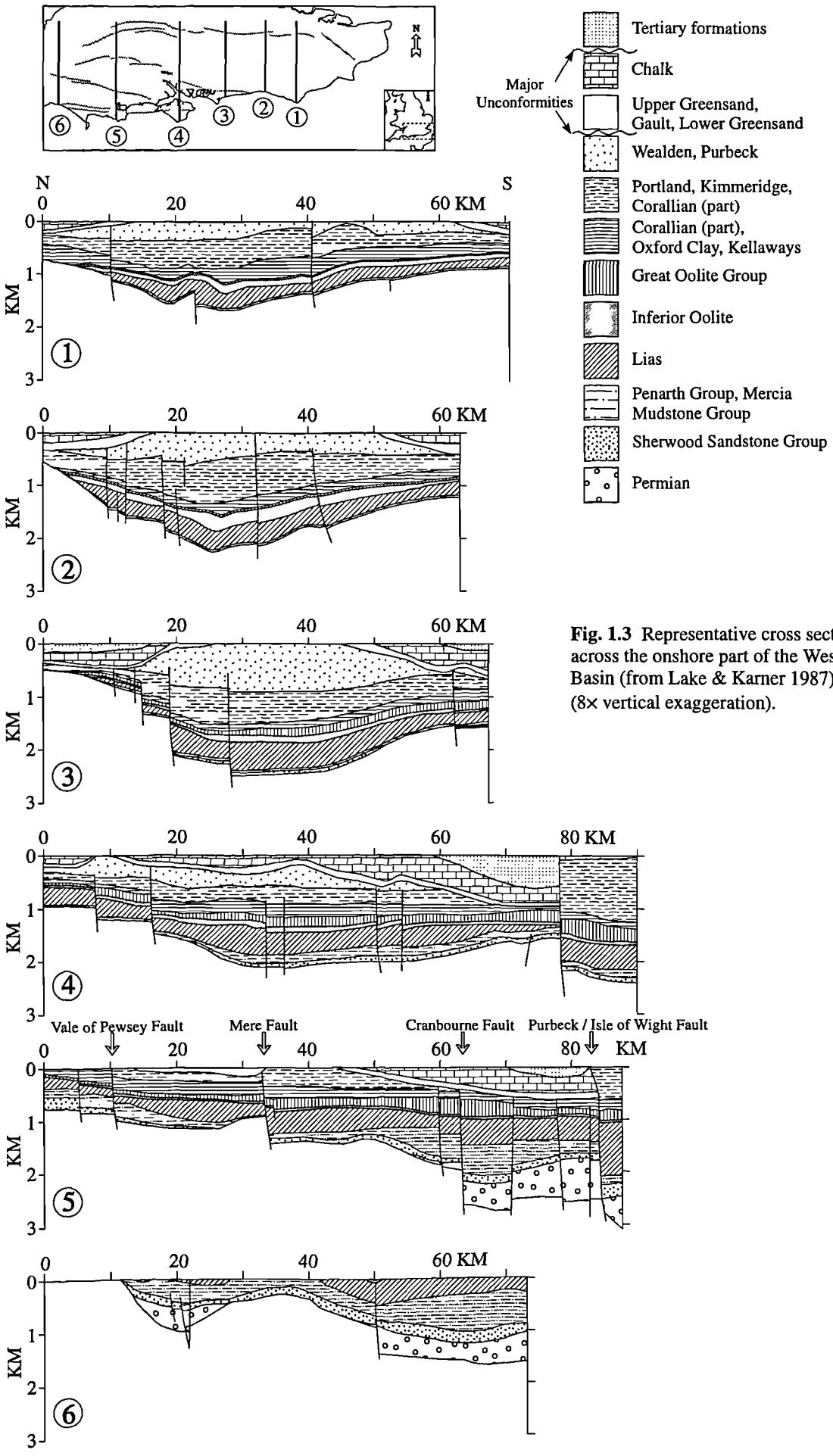

Fig. 1.3 Representative cross sections across the onshore part of the Wessex Basin (from Lake & Karner 1987). (8× vertical exaggeration).

Karner *et al.* (1987) used the back-stripping technique to isolate the driving tectonic subsidence responsible for the formation of the Wessex Basin. They proposed that the resultant driving subsidence was characterized by a gentle, sometimes negative, exponential form with superimposed rapid discrete subsidence events. They suggested that the basin is comprised of an upper crustal layer (above a crustal detachment) which fails in a brittle fashion, and a lower layer below the detachment which fails in a predominantly ductile and continuous manner.

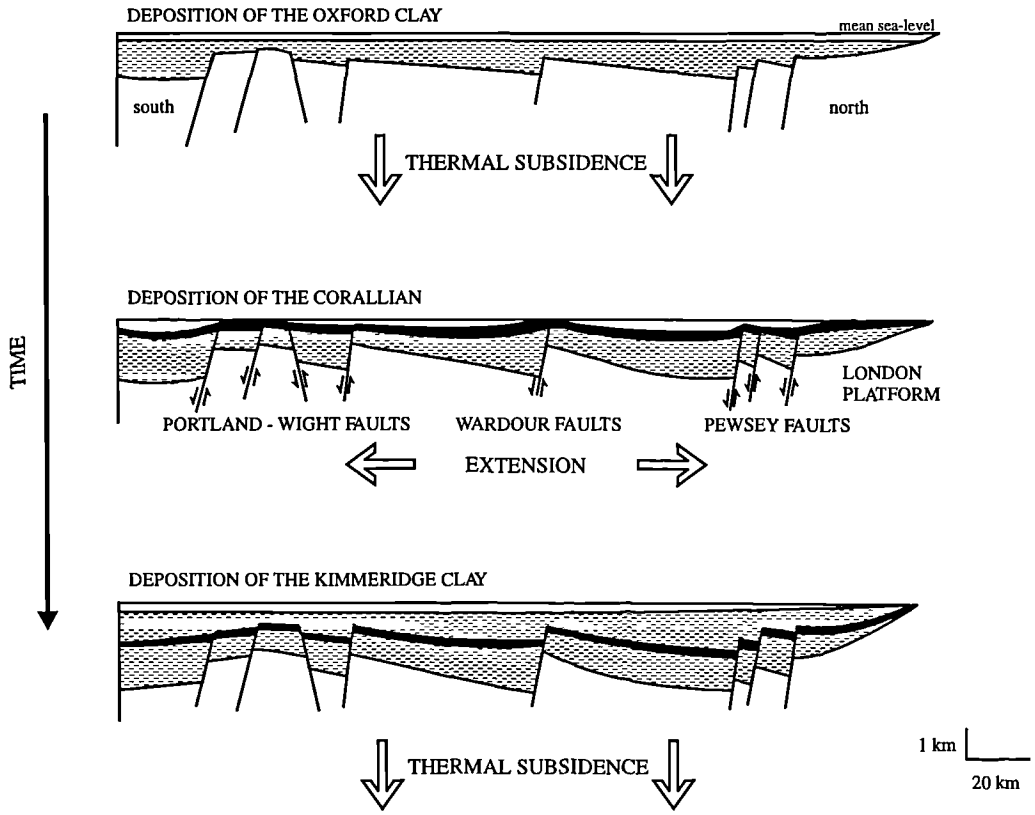

Fig. 1.4 Chadwick's (1986) tectonic model for the western Wessex Basin. The Corallian Beds (black layer) are bounded by the Oxford and Kimmeridge Clay Formations (after de Wet 1987).

1.6 Sequence stratigraphy

1.6.1 Introduction to sequence stratigraphy

Sequence stratigraphy is "the study of genetically related facies within a framework of chronostratigraphically significant surfaces" (Van Wagoner *et al.* 1990). It explains the vertical and lateral variations of sedimentary successions in terms of relative sea-level changes. Sequence cycles, third-order cycles of 0.5 - 3 Ma in duration (Fig. 1.5), are the building blocks of sequence stratigraphy.

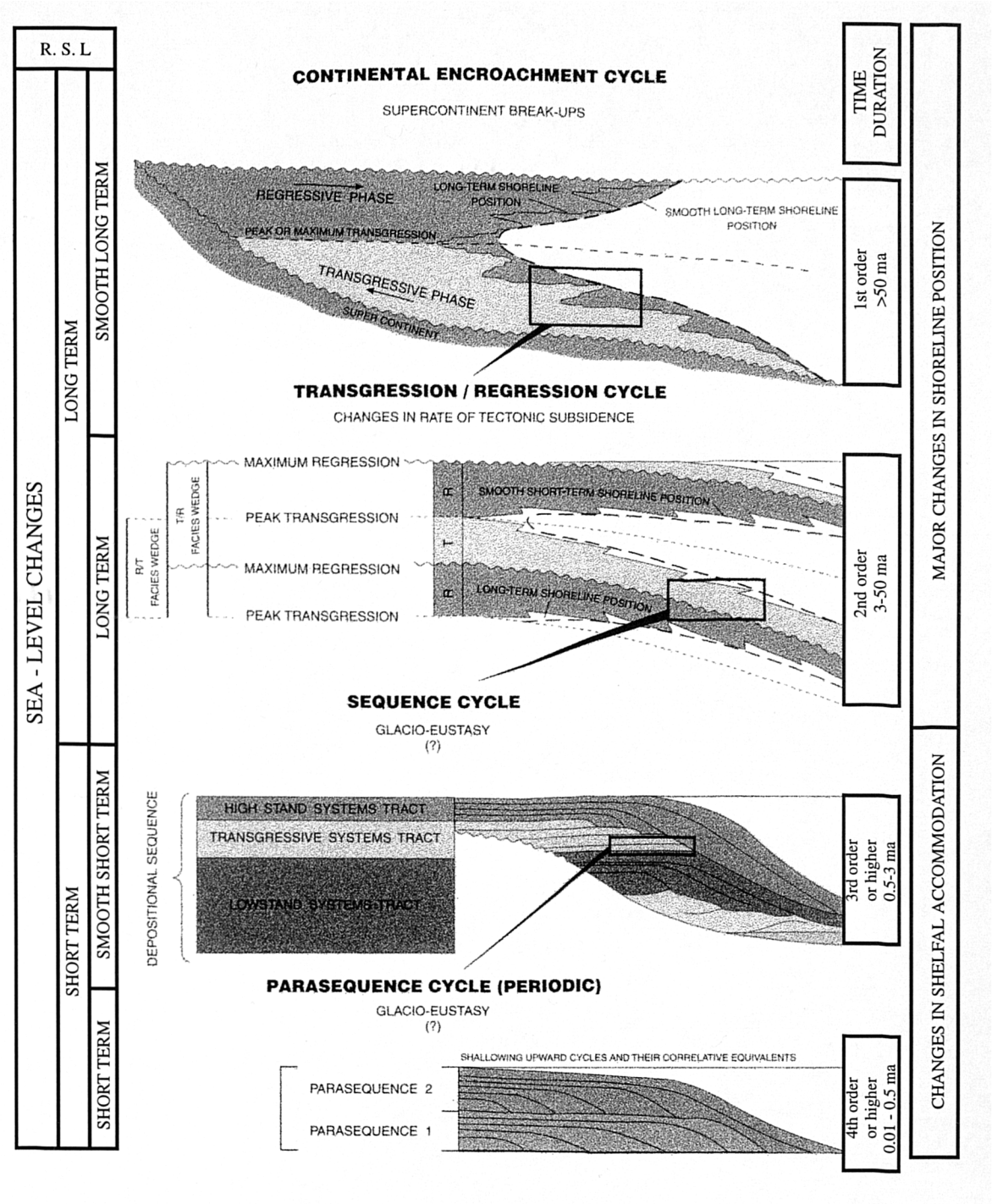

Fig 1.5 Hierarchy of stratigraphic cycles (after Duval *et al.* 1992).

These sequences are stratigraphic units comprising of relatively conformable successions of genetically related strata bounded by unconformities or their correlative conformities (Mitchum 1977). The bounding unconformities (sequence boundaries) and the other key sequence stratigraphic surfaces (transgressive surface and maximum flooding surface) are all believed to be caused by relative sea-level changes.

Some sequence stratigraphic workers believe that all major sea-level changes are eustatic, and therefore that all the unconformities (sequence boundaries) have absolute

geological ages which can be correlated on both regional and global scales (Vail 1992). Cloetingh (1988) suggested that intra-plate stresses which cause vertical motions of the lithosphere may provide an explanation for third-order cycles. Hardenbol (1992) proposes that Milankovitch cycles can affect sequences in such a manner as to make them uncorrelatable on a global scale. On the other hand, some workers believe that regional tectonic events and local variations in sediment supply enhance or subdue the sequences, but do not change the age when dated at the correlative conformity (Coe *et al.* 1989, Coe 1992, Vail 1992).

Sequence stratigraphy is an important development in stratigraphy because it forces the geologist to think in three dimensions; it changes the way in which successions are correlated and it is predictive (Prosser & Howell 1994).

There have been numerous publications on sequence stratigraphy which describe the various models, as well as Galloway's (1989) "genetic sequence stratigraphic sequences" where the bounding surfaces of the genetic sequences are maximum flooding surfaces. For a detailed explanation and discussion on all aspects of sequence stratigraphy, the reader is referred to Emery & Myers (1996) and Miall (1997) and the references therein.

The most detailed sequence stratigraphic interpretation of the Upper Jurassic outcrops of the United Kingdom to date has been carried out by Coe (1992, 1995, 1996). It is her interpretation, therefore, which forms the basis for the subsurface sequence stratigraphic wireline correlations produced in this study. A brief introduction to her interpretation follows in Section 1.6.2, and detailed discussions of her interpretation for the Oxfordian and Kimmeridgian successions are given in Chapters 5 and 6, respectively. Section 1.6.3 lists the definitions of the key sequence stratigraphic terms used in this study.

1.6.2 Sequence stratigraphy of the Upper Jurassic outcrops of the Wessex Basin

In the sequence stratigraphical interpretation of the Upper Jurassic, Coe (1992) concentrated on the recognition and documentation of unconformity surfaces and their lateral correlation in more complete successions. Her conclusions are as follows: the Upper Jurassic succession of the Wessex Basin was deposited during two and a half regressive-transgressive-regressive cycles (Coe 1994). The Oxfordian succession was deposited during a second-order regression-transgression cycle which was punctuated by eight unconformities, or their correlative conformities, which corresponded to the base of eight small-scale cycles (seqeunces) of relative sea-level change. She informally denoted these unconformities O1 to O8, and interpreted them to be sequence boundaries. The Kimmeridgian succession was interpreted to have been deposited during a minor

regression followed by an overall transgression which ended towards the end of the Kimmeridgian. The succession consists of eight third-order sequence cycles: four in the Lower Kimmeridge Clay (Ki to Kiv) and four in the Upper Kimmeridge Clay (K1 to K4). The Portlandian succession was deposited during a long-term regression, which started towards the end of the Kimmeridgian, on which are superimposed four shorter term relative sea-level changes (Coe 1996).

Coe (1992) noted several problems with applying sequence stratigraphy to the Upper Jurassic sediments of the Wessex Basin. The first problem was the discontinuous nature of the exposures which did not allow the geometry of parasequences and parasequence sets to be easily identified. This lack of continuous exposure also made it difficult to ascertain with certainty type 1 and type 2 sequence boundaries. Another problem was the fact that the Upper Jurassic of the Wessex Basin was deposited in an epeiric sea setting where there is no marked depositional slope and no structurally marked depositional shoreline break or offlap break. The final problem was that the sediment supply was low and intermittent which resulted in the superposition of different surfaces within the depositional succession over large areas of the basin.

In response to these problems, Coe (1992) concentrated on detecting all the key sequence stratigraphic surfaces: sequence boundaries, maximum flooding surfaces and transgressive surfaces. Because a succession of sediments cannot be put into a sequence stratigraphic context without, first of all, identifying the key surfaces (Baum & Vail 1988), Coe interpreted all the major unconformities and their correlative conformities found during her field study as sequence boundaries. She stated that maximum flooding surfaces were well-developed in the Kimmeridge Clay, but were poorly developed in the Corallian Group because the water depth was insufficient for sediment starvation. However, she did recognise significant flooding events within the Corallian Group. She also suggested that the transgressive surface or first major flooding surface is well-marked in shallow-marine sediments of the Upper Jurassic and that the transgressive surfaces may be expressed as minor unconformities which are laterally discontinuous. Coe noted that towards, and on the margins of, the basin the transgressive surface was often amalgamated with the sequence boundary and in some instances they may be amalgamated across the whole basin. She suggested that this was due to a low rate of sediment supply in the Wessex Basin and overall rapid transgression allowing erosive processes to dominate.

Another modification Coe (1992) made to the general sequence stratigraphic model was in the nomenclature for systems tracts, which she only used where it was informative. By definition, the sequence boundary, maximum flooding surface and transgressive surface divide the depositional sequence into constituent systems tracts. The geological setting and discontinuous nature of the exposure within the Wessex Basin meant that features which define each of the systems tracts (e.g. stacking pattern of

parasequences and parasequence sets) could not usually be recognised. Therefore, she used systems tracts in their widest definition.

The lowermost systems tract is divided into different parts according to whether or not it overlies a type 1 or type 2 sequence boundary (Van Wagoner et al. 1988). Because of the reasons outlined above, Coe (1992) did not interpret sequence boundaries as type 1 or type 2, so that in her work and in this thesis the lowermost systems tract is defined as the first systems tract which immediately overlies the sequence boundary (Coe 1992).

The following are Coe's (1992) observations about the individual systems tracts within the Wessex basin. The lowermost systems tracts are mainly confined to the central channel basin (Dorset coast section), where sediment supply and sediment-accommodation space versus level of erosion are great enough to preserve sediment. There are a few exceptions to this where sediment appears to have been sourced locally from along the basins margins, e.g. Lower Calcareous Grit Formation (Oxfordian). The lowermost systems tract usually comprises one particular lithology which was typically fairly rapidly deposited.

The transgressive systems tract is well-developed in the Upper Jurassic of the Wessex Basin and invariably comprises highly variable faunal-rich lithologies. The transgressive systems tract may be finer grained than the underlying lowermost systems tract, but reworking and erosion immediately subsequent to the transgressive surface commonly masks this change. In the shallow-marine sediments the basal part of the transgressive systems tract commonly has a mixture of clast types. In mudstone successions anoxia commonly developed during transgression due to increased water-depth and circulation of nutrients as the marginal areas are flooded. Organic-rich shales are thus deposited during transgressive systems tracts.

During deposition of the highstand systems tract conditions appear to have been more stable, resulting in carbonate production in the absence of siliciclastics or fairly uniform deposition of fine-grained siliciclastics. Towards the top of the highstand systems tract there is commonly a slight change in the lithology; siliciclastic successions coarsen slightly and in carbonates there may be a temporary deposition of grains characteristic of the next depositional sequence. Within the Upper Jurassic of the marginal areas of the Wessex Basin sediments of the highstand systems tracts have commonly been partially removed by erosion during formation of the subsequent sequence boundary, and in some instances they have been removed entirely.

1.6.3 Key sequence stratigraphic definitions

Accommodation space - The space (volume) made available for potential sediment accumulation (Jervey 1988).

Aggradation - Accumulation of a facies or group of facies within a depositional system, with no significant lateral migration of the facies belt or facies belts towards either the land or basin (Van Wagoner *et al.* 1988).

Condensed section - Condensed sections are thin marine stratigraphic units consisting of pelagic to hemipelagic sediments characterised by very low sedimentation rates. They are most areally extensive at the time of maximum regional transgression of the shoreline (Loutit *et al.* 1988).

Highstand systems tract - The highstand systems tract is the upper system tract in either a type 1 or a type 2 sequence (Van Wagoner *et al.* 1988).

Lowermost systems tract - This is the first systems tract which immediately overlies the sequence boundary, without any inference as to whether it is a type 1 or type 2 sequence boundary (Coe 1992).

Marine flooding surface - A surface separating younger from older strata across which is evidence of abrupt increase in water depth. This deepening commonly is accompanied by minor submarine erosion or non-deposition, with a minor hiatus indicated (Van Wagoner *et al.* 1990).

Maximum flooding surface - The surface corresponding to the time of maximum flooding is called the downlap surface or maximum flooding surface (Posamentier *et al.* 1988). It marks the boundary between the transgressive systems tract and the highstand systems tract (Coe 1992).

Progradation - The basinward migration of a facies belt or facies belts within a depositional system (Van Wagoner *et al.* 1988).

Retrogradation - Landward migration of a facies belt or facies belts within a depositional system (Van Wagoner *et al.* 1988).

Sequence - A stratigraphic unit composed of a relatively conformable succession of genetically related strata bounded at its top and base by unconformities or their correlative conformities (Mitchum 1977).

Sequence boundary - A sequence boundary is an unconformity or its correlative conformity (Mitchum 1977).

Systems tracts - A linkage of contemporaneous depositional systems (Brown & Fisher 1977).

Transgressive surface - The first significant marine-flooding surface across the shelf within a sequence (Van Wagoner *et al.* 1988). It marks the boundary between the lowermost systems tract and the transgressive systems tract (Coe 1992).

Transgressive systems tract - The transgressive systems tract is the middle systems tract of both type 1 and type 2 sequences. It is characterized by one or more retrogradational parasequence sets (Van Wagoner *et al.* 1988).

Unconformity - A surface separating younger from older strata at which there is evidence of a significant omission of strata (Coe 1992).

1.7 Geological interpretation of wireline logs

This section contains a brief explanation of the principles behind each of the different types of wireline log used in this study, and discusses the geological information which can be obtained from each log. For more detailed information on the principles and physics behind each of the tools the reader is referred to the following: Atlas Wireline Services (1992), Ellis (1987), Frank (1986), Schlumberger (1989), Serra (1984), Foster & Beaumont (1990a, 1990b) and Rider (1996). For more detailed information about the geological interpretation of wireline logs, the reader is referred to Serra (1984), Doveton (1994a) and Rider (1996).

1.7.1 Gamma-ray logs

Gamma-ray sondes measure the natural radioactivity of the rock. Gamma-rays are spontaneously emitted by a few elements, the most common in sedimentary rocks being potassium, uranium and thorium. Two types of wireline gamma-ray sondes exist, the conventional gamma-ray which records the total natural radiation, and the spectral gamma-ray which records gamma-rays emitted from potassium, uranium and thorium.

In general, the gamma-ray (GR) log reflects the mudstone content of sedimentary formations. Clean sandstones and carbonates normally exhibit a low level of natural radioactivity, whereas the clay minerals and fine-grained particles in mudstones show

higher levels of radioactivity due to adsorption of potassium, uranium and thorium, and the potassium content of the clay minerals themselves. Because natural radioactivity generally comes from the clay minerals and other fine-grained particles, gamma-ray logs have been used to infer grain-size changes, i.e. decreasing radioactivity reflects increasing grain-size (Rider 1996, Emery & Myers 1996). In some instances the presence of minerals, such as glauconite, which contain large amounts of potassium, uranium or thorium produces anomalously high gamma-ray values.

In the Upper Jurassic of the Wessex Basin the correlation of gamma-ray log response with mudstone content has also been observed. For example, the gamma-ray log shows a decrease in radioactivity from the fine grained Upper Oxford Clay to the coarser grained sandstones of the lower Corallian beds (Fig. 1.6a). However, there are exceptions where the correlation breaks down in the Upper Jurassic. For example, in parts of the Kimmeridge Clay Formation uranium has been precipitated from solution in anoxic depositional environments, resulting in organic-rich shales with have anomalously high gamma readings (Fig. 1.6b). Also not all gamma-ray lows are due to an increase in grain size. For example, in the Kimmeridge Clay Formation diagenetic limestone 'Stone Bands' have low gamma-ray values because they contain little potassium, uranium and thorium due to their low organic matter and clay content (Fig. 1.6b).

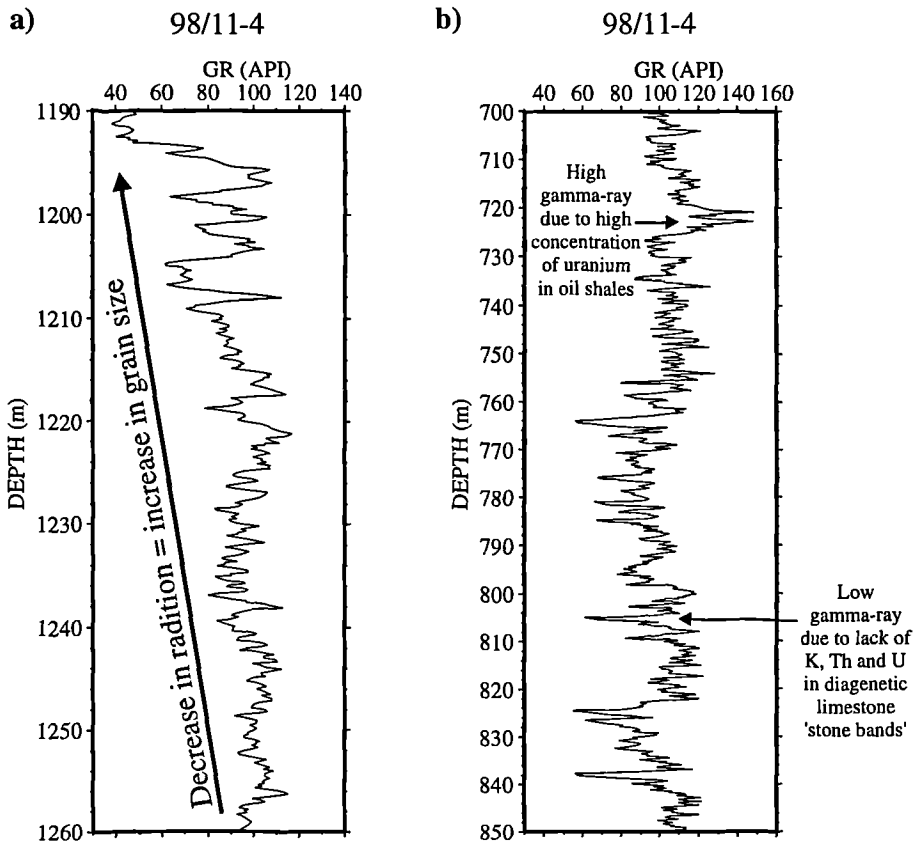

Fig. 1.6 **(a)** Gamma-ray log showing that the natural radiation decreases as the Oxford Clay grades into the coarser Corallian beds. **(b)** Increasing gamma-ray does not always indicate decreasing grain-size and decreasing gamma-ray does not always indicate increase in grain-size.

1.7.2 Spontaneous potential log

The spontaneous potential (SP) log measures the difference in electrical potential between a surface electrode and an electrode in the borehole. The spontaneous potential is produced by electrochemical effects at the contacts between permeable beds and shales / and across the transition zone between mud filtrate and formation water within the permeable beds.

The spontaneous potential curve usually shows a more-or-less straight line with little character compared to other logs through the impermeable shales of the Kimmeridge Clay and the Oxford Clay Formations (Fig. 1.7). Deflections, either to the left or the right of this line, usually occur opposite permeable formations, for example parts of the Corallian Beds and the thick sandstones at the base of the Kimmeridge Clay Formation seen in the Weald Sub-basin (Fig. 1.7). The direction of the deflection depends on the relative salinities of the formation water and of the mud filtrate.

The spontaneous potential log is of limited use in this study because the majority of the Upper Jurassic succession of the Wessex Basin is comprised of impermeable shales.

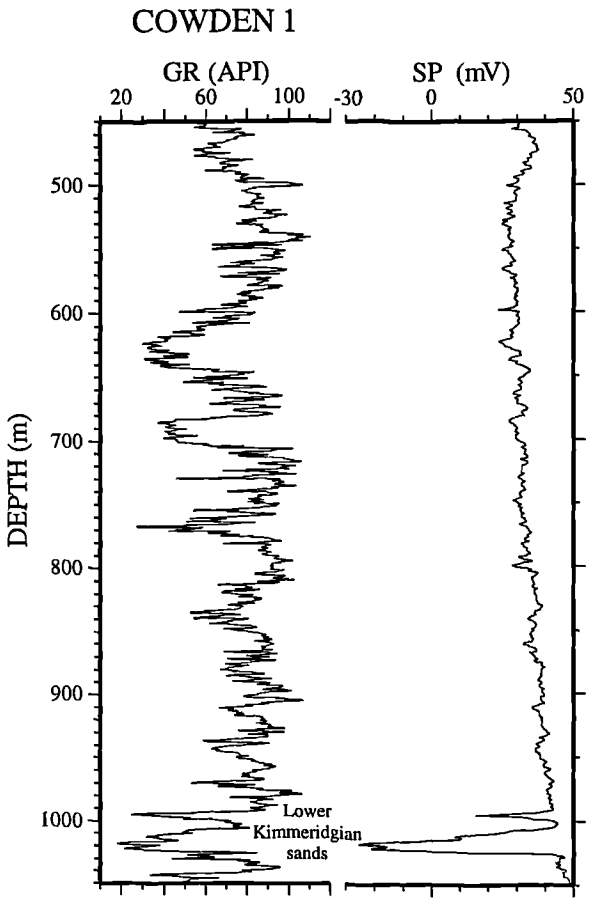

Fig. 1.7 Diagram showing that the spontaneous potenial log does not have much character over the Kimmeridge Clay Formation.

1.7.3 Resistivity and conductivity logs

Resistivity tools measure the electrical resistivity of rocks, whilst conductivity tools measure its reciprocal, the electrical conductivity (i.e., they measure the ability to conduct an electric current). In general the rock matrix is non-conductive and formation waters are conductive. When the porosity decreases the resistivity increases, so resistivity logs are good indicators of changes in porosity.

Resistivity logs do not allow direct identification of common lithologies because the rock matrix is non-conductive. However, they are very sensitive to subtle changes in lithologies where these are associated with small changes in porosity.

Micro-resistivity tools are capable of very fine bed resolution, as may be clearly seen in Figure 1.8.

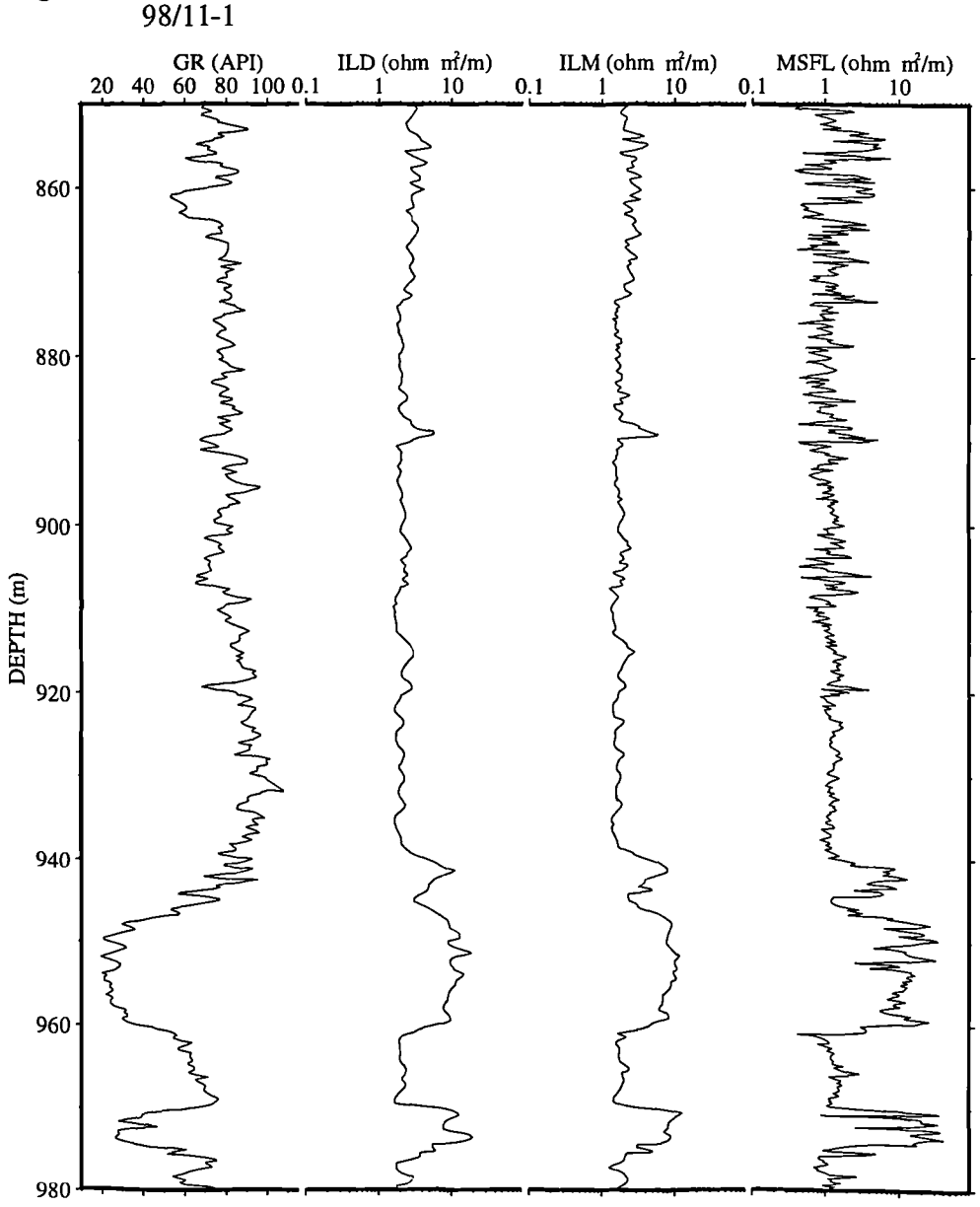

Fig. 1.8 Diagram showing that the micro resistivity log (MSFL) has the best vertical resolution.

1.7.4 Density log

The density log is a record of the formation's bulk density (i.e., density of the solid matrix of the rock plus the density of pore fluids). The density sonde contains a source of gamma-rays which invades the formation. The gamma-rays interact with the electrons in the formation by Compton scattering, and the flux of back-scattered gamma-rays is measured on near and far detectors at two fixed distances from the gamma-ray source. The measurement is directly related to the density of electrons in the formation, which is approximately related to the bulk density of the formation. The approximation is because the ratio of atomic mass to atomic number varies between different elements and isotopes. Thus, the density tool is calibrated with reference to a limestone matrix saturated with fresh water.

Density logs are primarily used to calculate porosity, but can also be used for mineral identification. Therefore they are very useful in sequence stratigraphical interpretations because they show changes in lithology. However, they only detect changes in lithology if the adjacent lithologies have different densities, so they have to be used in conjunction with other logs.

1.7.5 Neutron logs

Neutron logs emit neutrons into the rock and measure the flux of epithermal neutrons which are back-scattered to detectors in the sonde. Scattering takes place due to collisions with atomic nuclei in the rock, and the amount of energy lost per collision depends on the relative mass of the nucleus with which the neutron collides. Greater energy loss occurs when the neutron strikes a nucleus of comparable mass. Collisions with heavy nuclei do not slow the neutron very much but just cause scattering. The hydrogen nucleus has a mass equal to that of the neutron, so the slowing of neutrons depends largely on the amount of hydrogen in the formation.

Like the density log, the neutron log is mainly used to estimate porosity but it is also used for lithology determination. The density/neutron combination is a good indicator of lithology and thus is very useful in interpreting depositional trends.

1.7.6 Sonic logs

Sonic logs measure the sonic transit time through the formation. In its simplest form, a sonic tool consists of a transmitter that emits a sound pulse and two receivers that pick up and record the pulse as it passes each receiver. The difference in arrival times is the transit time which is related to porosity and lithology.

Shales will have a higher transit time (lower velocity) than sandstones of a similar porosity, which sometimes allows the sonic log to be used as a grain size indicator. The high concentrations of organic matter seen in the oil shales of the Kimmeridge Clay Formation result in long travel times which are seen as sonic spikes in the log. The sonic log is affected by post-depositional cementation and compaction, and by the presence of fractures. These factors have to be taken into account when correlating sonic logs across different parts of the Wessex Basin.

1.8 Wireline logs and sequence stratigraphy

One of the first pieces of work involving the application of wireline logs to sequence stratigraphy was that of Van Wagoner *et al.* (1990). Since then, a number of other studies have been published on the subject (Vail & Wornardt 1990, Armentrout *et al.* 1993, Bowen *et al.* 1993). Rider (1996) in his latest edition of "The geological interpretation of well logs" has included a chapter on sequence stratigraphy, in which he states "the use of wireline logs as a tool in sequence stratigraphy has so far been seriously underdeveloped".

Vail & Wornardt (1990) and Armentrout *et al.* (1993) integrated biostratigraphic, palaeobathymetric and wireline log data with seismic reflection profiles. Both these studies have resulted in the development of schematic wireline log characteristics for the sequence stratigraphic interpretation of wireline logs (Figs 1.9 & 1.10), either using Vail's (1987) sequence stratigraphy model or a slight adaptation to this model. It was shown in the previous section that this model cannot be used in this Upper Jurassic succession because the succession was deposited in an epeiric sea setting where there was no marked depositional slope and no structurally marked depositional shoreline break or offlap break. For this reason, these schematic wireline log models were of limited use in this study.

The studies of Vail & Wornardt (1990) and Armentrout *et al.* (1993) did show that the key sequence stratigraphic surfaces (sequence boundary, maximum flooding surface and transgressive surface) could be located by interpreting the trends seen on the wireline logs. This study also shows that the interpretation of trends on the full suite of wireline logs is needed to interpret successfully the logs in a sequence stratigraphic manner (see Chapter 4).

Sequence stratigraphy aims to use the vertical and lateral variations in sedimentary successions to divide the strata into cycles which are thought to be controlled by relative sea-level changes. Trends seen on the wireline logs are therefore important because they

indicate patterns of progradation, retrogradation and aggradation which in turn can be related to changes in sea-level (see Chapter 4).

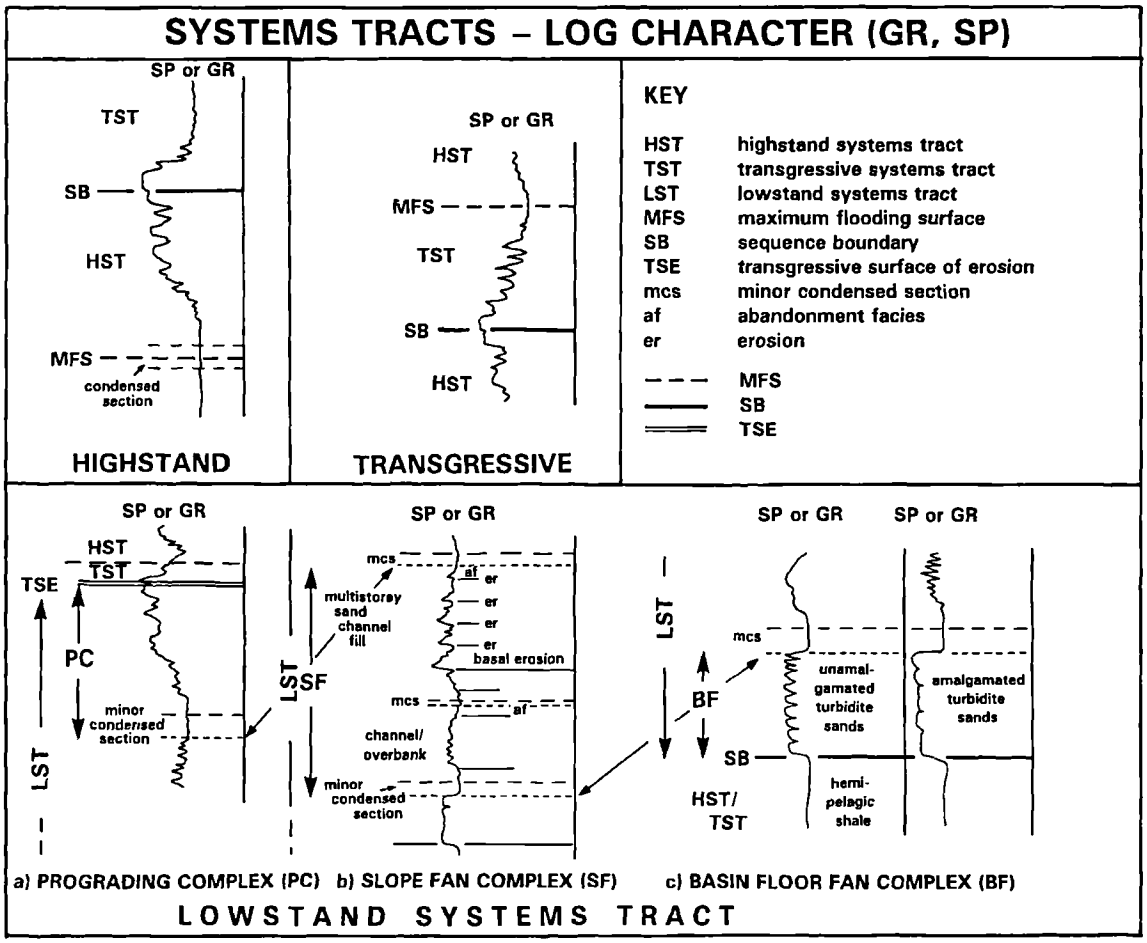

Fig. 1.9 Model wireline log patterns for systems tracts (from Rider 1996, originally after Vail & Wornardt 1990).

Davies & Elliott (1996) stated that the key sequence stratigraphic surfaces and systems tracts can be characterized more comprehensively and recognized with greater confidence if the spectral gamma-ray data are used in conjunction with traditional total gamma-ray data. This point is backed up by the work done in this study (see Chapters 2 & 6). However, Davies & Elliott (1996) also stated that maximum flooding surfaces can be distinguished from minor flooding surfaces by a distinctive uranium peak and low thorium/uranium ratio, without any mention of underlying or overlying trends. This study will show that the interpretation of the gamma-ray log alone can be inaccurate, and maximum flooding surfaces should not be picked on the basis of gamma-ray or uranium peaks alone but that it is better to look at the trends.

Biostratigraphic data are vital for any sequence stratigraphical interpretation. This is particularly true for sequence stratigraphical interpretations based on wireline logs because the key sequence stratigraphic surfaces are significantly harder to locate on

wireline logs than at outcrop. The manner in which biostratigraphic data have been used in this study is discussed further in Chapter 3, and more detailed information about the biostratigraphic data for the Oxfordian and Kimmeridgian can be found in Chapter 5 and 6, respectively.

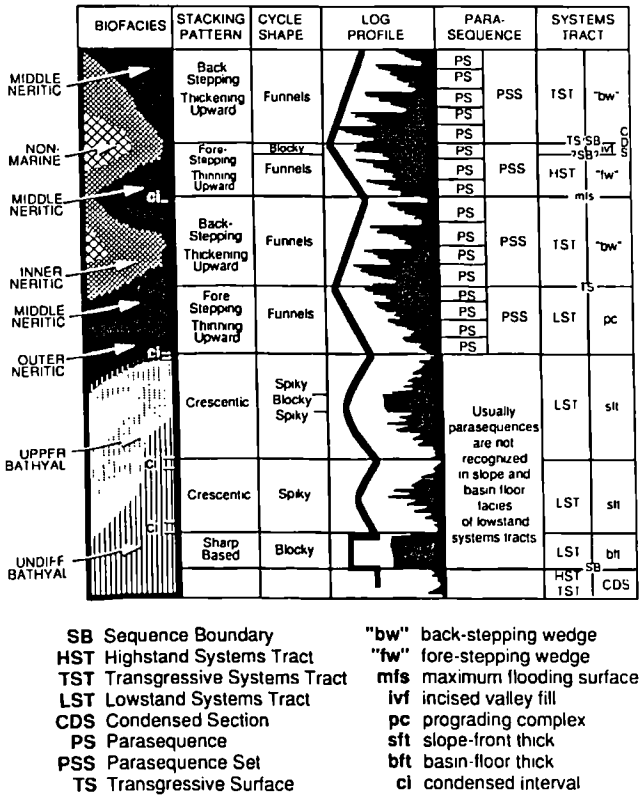

Fig. 1.10 Schematic log-motif characteristics for interpretation of wireline log sequence stratigraphic patterns (from Armentrout *et. al.* 1993).

SB Sequence Boundary
HST Highstand Systems Tract
TST Transgressive Systems Tract
LST Lowstand Systems Tract
CDS Condensed Section
PS Parasequence
PSS Parasequence Set
TS Transgressive Surface

"bw" back-stepping wedge
"fw" fore-stepping wedge
mfs maximum flooding surface
ivf incised valley fill
pc prograding complex
sft slope-front thick
bft basin-floor thick
ci condensed interval

CHAPTER 2

Surface - Subsurface Correlation

2.1 Introduction

Wireline logs provide an intermediate link between the small-scale, high-resolution sedimentological and stratigraphical features visible at outcrop and the large-scale data available from seismic sections. Simple, but accurate techniques have been developed in this study for producing natural gamma-ray and density wireline log trends from measurements on rock exposures and small samples. Emphasis has been placed, whilst constructing the field gamma-ray and density logs, on producing log trends which are at the same resolution and of similar character to typical downhole wireline logs rather than on obtaining absolute values to match those expected downhole. This approach thus concentrates on reproducing patterns of cyclicity, together with general decreasing and increasing trends, which in turn can be interpreted in terms of cyclostratigraphy, for example, transgression and regression, sequence stratigraphical and Milankovitch cycles.

The choice of which wireline measurement techniques were to be adopted for outcrop measurements was influenced by the fact that the physical phenomena being measured had to be easily comparable, whether the rocks were at the surface or a couple of kilometres deep. For example, gamma-ray tools measure the natural radioactivity emanating from rocks, which is roughly the same whether the rocks are at the surface or in the subsurface. The main difference between the surface and the subsurface measurements is the volume of rock from which the gamma-rays are recorded; the wireline sonde records gamma-rays from a sphere around the detector crystal whilst, the portable gamma-ray spectrometer records gamma-rays from a hemispherical volume. This results in a difference between the actual measurements at the surface and subsurface but the relative changes between successive measurements at the surface and subsurface are comparable.

The density of rock samples from a particular laterally extensive stratigraphic horizon, which has undergone the same cementation and diagenetic processes, will be the same whether they are at the surface or subsurface; therefore the density measurement is another physical measurement which could be used to correlate outcrops with subsurface data. One slight problem is that wireline density logs measure the formation's bulk density which is a function of the matrix density, pore fluid density and porosity. The fluids

contained in the rocks at the surface and in the rocks in the subsurface are very different. This can be easily corrected for by incorporating the product of the density of the formation fluids (which can be obtained from production test data) and the porosity of the rock from field studies in the calculation of the bulk density of the outcrop samples.

Wireline logs which measure physical parameters unique to the borehole environment obviously cannot be reproduced at outcrop. For example the SP log measures the electrochemical potential which occur at the contacts between drilling mud, the formation waters of permeable beds and shales. Resistivity and conductivity logs measure the formation's ability to conduct electricity, which is primarily a function of the pore fluids. However, as the pore fluids at depth are variable and different from those at the surface, construction of a field resistivity or conductivity log is complex. Similarly the wireline neutron tool measurement is related to the amount of hydrogen in the formation, which in turn is related to the type of fluid in the pore spaces.

Besides the gamma-ray and density measurements, the sonic measurement is the only other common wireline tool response which might be reproduced using outcrop samples. The sonic wireline tool measures the sonic transit time through the formation. At the surface sonic travel times can be measured though cylindrical samples, as small as a few centimetres in length, in a laboratory using ultrasonic measuring instruments. However, there are several problems with this method as sonic transit times are related to lithology, porosity and fluid content. The porosity of small rock samples at the surface is greater than the porosity of the same rock in the subsurface because of the overburden pressure. Therefore each sample in the laboratory would have to be placed under similar confining pressure to the rocks in the subsurface, with similar pore fluid and pore fluid pressure, prior to the sonic transit time measurement being taken. Another problem is that most of the Upper Jurassic rocks are shales and it is very hard in practice to get cylindrical shaped samples from shales without them breaking apart. Even though these problems could probably be overcome, it was decided that the gamma-ray and density field logs would be sufficient for the purpose of correlating outcrop with subsurface data.

The first part of this chapter (Sections 2.2 to 2.4) discusses the principles and procedures involved in the construction of a field gamma-ray log. The second part of the chapter (Sections 2.5 & 2.6) discusses the construction of the field density log. The location of the Upper Jurassic exposures and the boreholes mentioned in this chapter are shown in Figure 2.1.

The content of this chapter has been accepted for publication in the forthcoming 'Core-Log Integration' Special Publication of the Geological Society. The title of the paper is 'Methods for simulating natural gamma-ray and density wireline logs from measurements on outcrop exposures and samples: examples from the Upper Jurassic, England'.

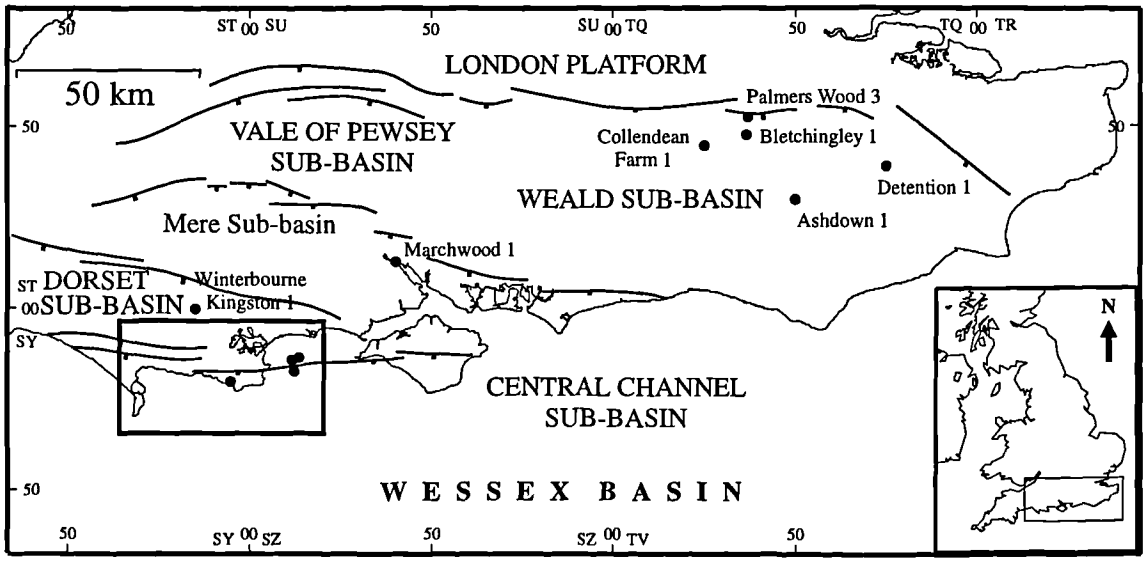

a)

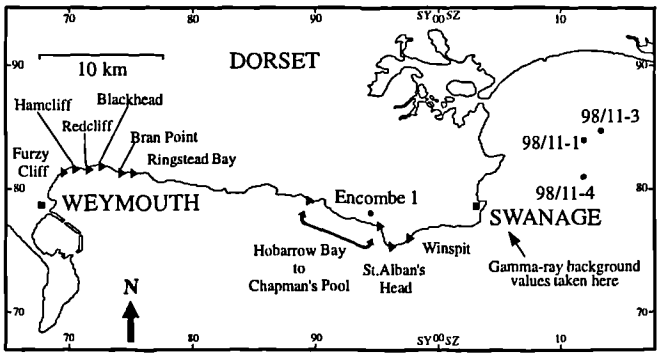

b)

Fig. 2.1 Maps showing the main structural features of the Wessex Basin (after Whittaker 1985) and the location of boreholes and Upper Jurassic exposures. **(a)** Boreholes in the Weald Sub-basin and the position of Fig. 2.1(b). **(b)** Details of the location of boreholes and outcrops in the Dorset area.

2.2 Field gamma-ray logs

2.2.1 Introduction

A composite field gamma-ray log has been constructed for the Upper Jurassic succession on the Dorset coast (Fig. 2.2). The purpose of the composite field gamma-ray log is to correlate the Upper Jurassic outcrops with the subsurface wireline data with the aim of extending the sequence stratigraphic boundaries found in the outcrops by Coe (1992, 1996) and seeing if further sequences could be found over the Upper Jurassic successions which do not outcrop in Southern England or are badly exposed, such as the Lower Kimmeridge Clay.

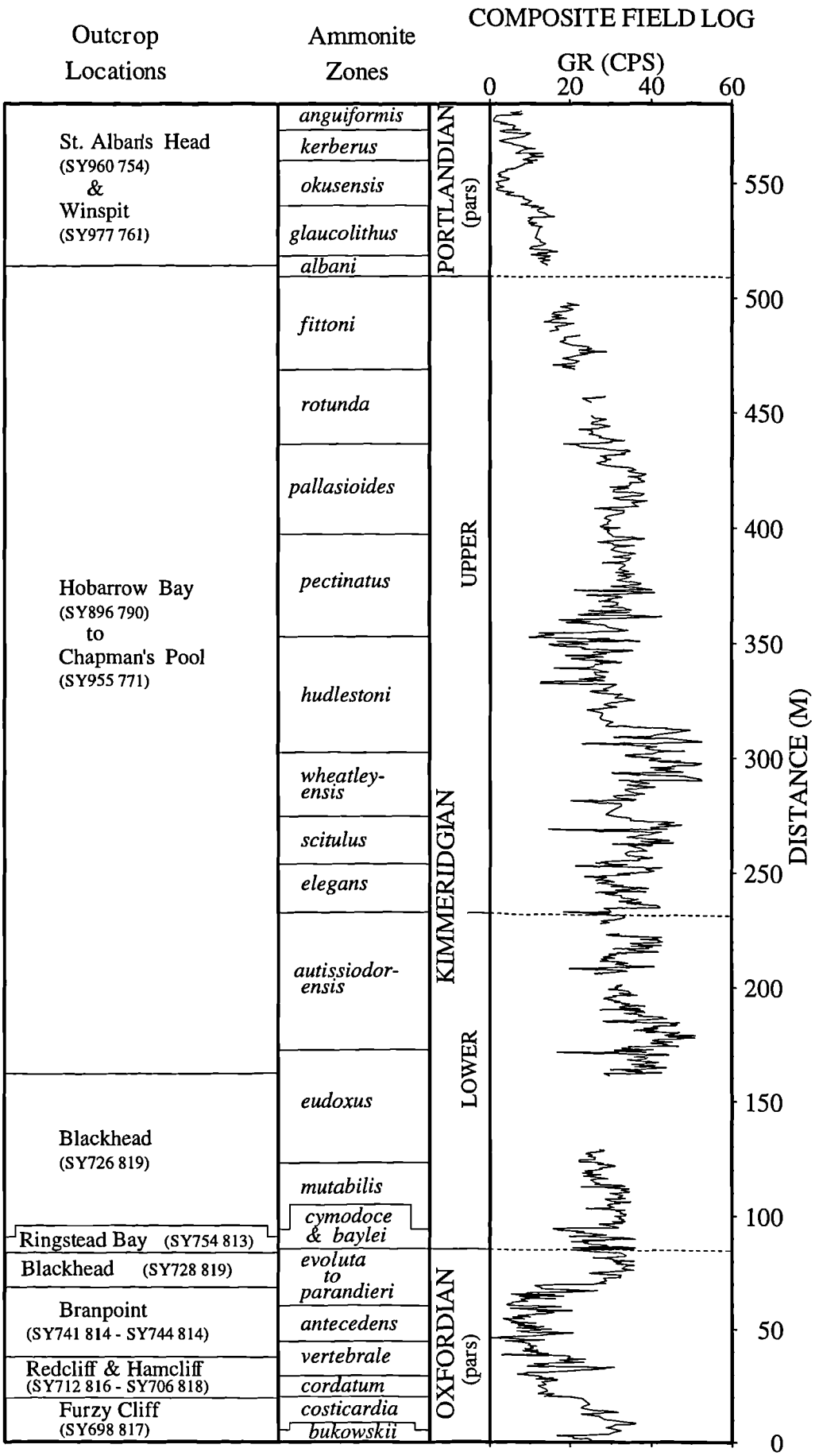

Fig. 2.2 Composite field gamma-ray log of the Upper Jurassic of Dorset, constructed using a geoMetrics GR310. The gaps in the data are due to a lack of exposure or non-accessibility of the section with the gamma-ray tool. See Fig. 2.1 for the location of the outcrops on the Dorset coast.

The aims of Sections 2.2.2 and 2.2.3 are to describe briefly the principles behind gamma-ray theory and how the portable spectral gamma-ray tools work. It is important that the basic principles of portable gamma-ray logging are understood for the purposes of carrying out correct field procedures and interpretation of the data. The field procedures used in this study will be discussed (Section 2.2.4) as well as tool and data calibration (Section 2.2.5). Section 2.3 reviews previous field gamma-ray studies over sections of the Upper Jurassic outcrops on the Dorset coast and Section 2.4 describes the results of correlating the composite field gamma-ray log produced in this study with wireline data from the Wessex Basin.

2.2.2 Gamma-ray theory

Gamma-rays are quanta of high-energy electromagnetic waves, which are also referred to as photons, that are emitted spontaneously by some radioactive elements while its nucleus is attaining stability. There are approximately 65 known unstable nuclides (Dresser Atlas 1982), the majority of which are so rare in nature that it is fair to say that most of the natural radiation from rocks comes mainly from the radioactive potassium isotope and the radioactive isotopes in the uranium and thorium series.

The gamma-rays emitted by potassium, uranium and thorium are distinctive both in the numbers emitted and in their energy. One gram of potassium (K^{40}) emits an average of 3.4 photons per second at a fixed 1.46 MeV (million electron volts) energy. However, an equal weight of either uranium or thorium produces respectively 26,000 or 12,000 gamma-rays per second with a spectrum of energies that average 0.5 MeV (Dresser Atlas 1982). Even though uranium and thorium produce a spectrum of energies, each has a distinctive energy peak, at 1.76 and 2.62 MeV respectively (Fig. 2.3).

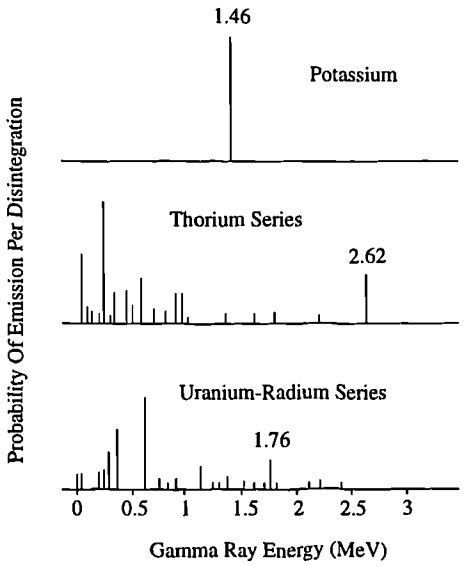

Fig. 2.3 Gamma-ray emission spectra of radioactive minerals (after Tittman 1956, redrawn from Schlumberger 1989)

As gamma-rays pass through matter they collide with atoms and lose energy with each collision. There are three principal gamma-ray scattering mechanisms: photoelectric effect, Compton effect and pair production. The scattering mechanism is dependent on the initial energy of the gamma-rays (Fig. 2.4). The energy of the naturally occurring gamma-rays are less than 3 MeV so the photoelectric effect and Compton effect are the only two mechanisms in operation. The photoelectric effect results from the interaction of gamma-rays with atoms in the material. In this process the incident gamma-ray disappears and transfers its energy to a bound electron (Ellis 1987). If the incident gamma-ray energy is large enough, the electron is ejected from the atom and begins interacting with the adjacent material. Normally the ejected electron is replaced by another less tightly bound electron with the accompanying emission of a characteristic fluorescence X ray, which has a significantly lower energy. Compton scattering involves interactions of gamma-rays and individual electrons. It is a process in which only part of the gamma-ray energy is imparted to the electron; the scattered gamma-ray is of reduced energy.

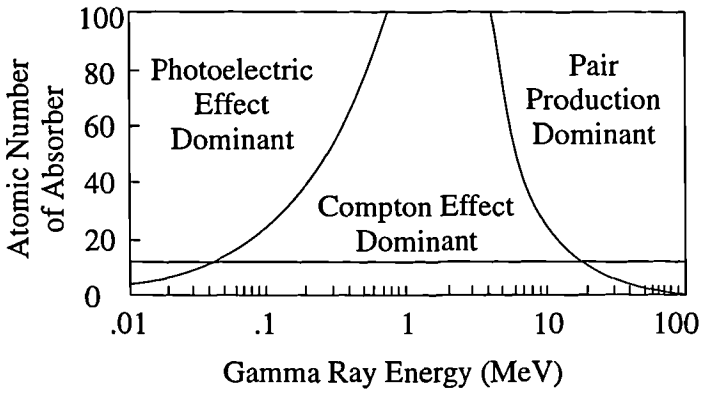

Fig 2.4 Regions of dominance of the three principal gamma-ray scattering mechanisms (after Ellis 1987)

In passing through matter, therefore, gamma-rays experience successive Compton-scattering collisions with atoms, losing energy with each collision. After the gamma-ray has lost enough energy it is absorbed by means of the photoelectric effect. Thus, natural gamma-rays are gradually absorbed and their energies reduced as they pass through the formation. The rate of absorption varies with formation density. Two formations having the same amount of radioactive material per unit volume, but having different densities, will show different radioactivity levels: the less dense formations will appear to be slightly more radioactive (Schlumberger 1989).

In both borehole logging and field measurement of natural radiation, the gamma-rays pass through rocks and fluids and the discrete energy levels (Fig. 2.3) at which the gamma-rays are emitted from potassium, uranium and thorium are degraded and a continuous spectrum of values is recorded (Fig. 2.5). This continuous spectrum shows the diagnostic peaks of potassium (1.46 MeV), uranium (1.76 MeV) and thorium (2.62 MeV) and can be used to calculate the amount of the original source of the radiation.

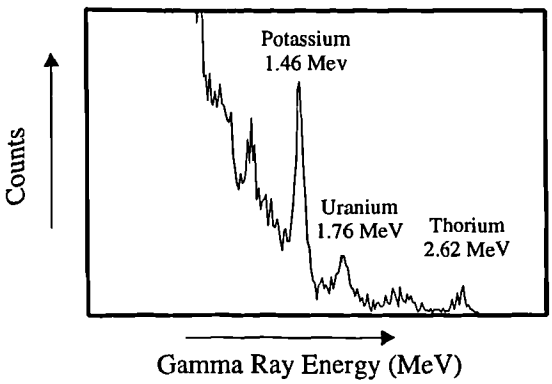

Fig. 2.5 The contineous spectrum recorded with the Exploranium GR320, showing the diagnostic peaks of Potassium, Uranium & Thorium.

The most common gamma-ray detector in both wireline tools and portable gamma-ray spectrometers is the sodium iodide scintillation crystal. Photoelectric cells are used to convert the flash of light produced when gamma-rays penetrate the crystal into electric pulses which are then counted.

2.2.3 Portable gamma-ray spectrometers

Portable gamma-ray spectrometers were originally developed and used for uranium ore exploration (Adams & Gasperini 1970). However, following the work of Ettensohn *et al.* (1979) total gamma-ray logs have also been used for surface to subsurface correlation of sedimentary strata (Chamberlain 1984; Cowan & Myers 1988; Slatt *et al.* 1992; Talwar *et al.* 1992; Van Buchem *et al.* 1992). More recently portable gamma-ray spectrometers have been used to study the distribution of K, U and Th in sedimentary rocks, and as a tool for stratigraphical correlation between rock exposures (Bessa & Hesselbo in press; Davies & Elliott 1996; Hesselbo 1996; Myers 1987; Myers & Bristow 1989; Myers & Wignall 1987; Parkinson 1996).

A natural gamma-ray field log was constructed from field measurements in a preliminary study during 1995. Total gamma-ray counts were recorded every 40 cm over most of the Upper Jurassic outcrop using a 15-year-old geoMetrics GR310 gamma-ray spectrometer. Spectral gamma-ray data were not recorded with this geoMetrics tool because of the long measuring time required; the tool only allows the measurement of gamma-rays in one of four windows (total counts, K, U or Th) during a particular measurement period; therefore four measurements at each location would have been needed. The total gamma-ray results were very encouraging, and showed that the long and short term sequence stratigraphical cycles observed at outcrop (Coe 1992) could be detected. However, it was apparent that more detailed spectral gamma-ray data were required to determine the relative abundances of K, Th and U, which could then be used to infer variations in sediment supply and climate during deposition. Therefore when a new state of the art gamma-ray spectrometer (Exploranium GR320) was made available, it was

decided that it would be worthwhile recording spectral gamma-ray data over part of the Kimmeridge Clay Formation. The Exploranium GR320, unlike the geoMetrics GR310, records the total gamma-ray counts and the counts in the K, U and Th windows simultaneously, thus reducing the time taken for recording spectral gamma-ray data by three quarters. The availability of the new gamma-ray spectrometer also gave an opportunity to compare the results from two different tools.

2.2.3.1 geoMetrics GR310

The source, detector, recorder and battery pack of the geoMetrics GR310 are all housed in one unit of dimensions 9 cm x 18 cm x 28 cm which weighs 3.4 kg (Plate 2.1). The detector is a thallium-doped sodium iodide crystal, 5.1 cm diameter and 5.1 cm thick (crystal volume 104 cm^3). The crystal is optically coupled and hermetically sealed to a high gain photo-multiplier. Power for approximately fifty hours of operation is provided by the battery pack.

The geoMetrics GR310 can record total gamma-ray counts (TC - all gamma-ray energy between 0.4 and 3 MeV) or counts in the energy windows for either potassium (K40 - window peak 1.46 MeV, window width 200 KeV), or uranium (Bi 214 - window peak 1.76 MeV, window width 200 KeV), or thorium (Tl208 - window peak 2.62 MeV, window width 400 KeV). The tool allows a count time of 1, 10, 100 and 1000 seconds to be chosen.

The reference source used in the geoMetrics GR310 is barium (^{133}Ba). The isotope has a half-life of about seven years and emits a variety of gamma-ray photons (Fig. 2.6). The calibration window is set to count gamma-ray photons with energies in the interval of 0.34 to 0.37 MeV. The reference photo peak is relatively free from spectral interference of the ^{232}Th and ^{233}U decay series, except for ^{214} Pb, which emits at 0.350 MeV.

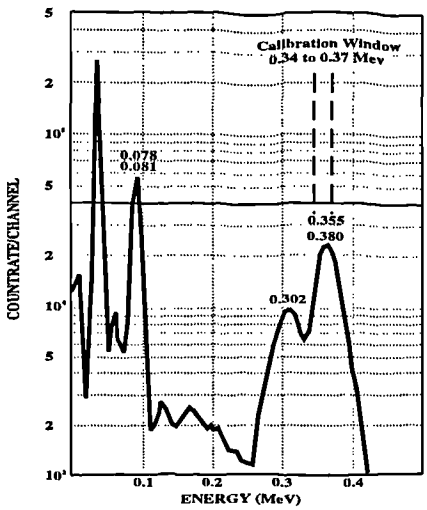

Fig. 2.6 Gamma-ray spectrum for the barium (133Ba) reference isotope in the geoMetrics GR310 (after geoMetrics Model GR310 manual).

Plate 2.1 The geoMetrics GR310 portable gamma-ray spectrometer.

Plate 2.2 The Exploranium GR320 portable gamma-ray spectrometer.

In gamma-ray spectrometry an important fact to note is that emitted gamma-rays absorbed in the detector all have a known position in the spectrum. The reference source, in this case barium, emits a distinctive peak at 0.34-0.37 MeV and must occur in a specific channel in the spectrum if the spectrometer is set correctly. However, although the barium peak always emits at 0.34-0.37 MeV, it may occur in a different channel in the spectrum due to electronic and thermal errors (tool drift). This is why the tool has to be calibrated at least several times a day and is very susceptible to changing weather conditions. The barium photo peak is subject to interference from the Compton effect and back scatter, so if calibration is attempted in the presence of high activity, Compton radiation from the ^{238}U-decay series will cause some interference (geoMetrics GR310 manual). Therefore it is recommended that when high activity (>500 counts per second total count) is suspected of interfering with calibration, the GR310 should be removed to a region of low background.

Due to the age of the tool, it was decided that prior to use in the field it should be serviced. The service report showed that the tool was in very good condition and the only thing wrong with it was that the counts expected during calibration were low. This was due to the fact that reference isotope, Barium, has a half life of about 7 years and because the tool was approximately 15 years old the reference isotope was not as active as it used to be.

2.2.3.2 Exploranium GR320

This spectrometer comprises two parts; a cylindrical detector (11.4 cm diameter x 39.4 cm long), and a recording / processing unit (24 cm x 10 cm x 25 cm) which have a combined weight of 8.4 kg (Plate 2.2). The detector is the same as that in the geoMetrics GR310 (thallium-doped sodium iodide crystal) but bigger, being 75 mm in diameter by 75 mm in length. The recording processing unit houses the maintenance-free rechargeable battery, which gives an operating time of typically 12 hours of measurement.

Total counts and counts in the K, U and Th fields are all recorded during one recording period which can be set by the user. The count time is variable from 1 to 9999 seconds. The inbuilt computer chip allows the spectra to be displayed and the amount of K, U and Th to be calculated directly and the internal memory (capacity 384K bytes) will hold full spectrum data for about 600 measurements. This data can then be downloaded to a personal computer. The system is also capable of having a GPS receiver connected to it, which would allow the latitude, longitude and altitude to be saved with each measurement.

Unlike the geoMetrics GR310, which has to be manually stabilised, the Exploranium GR320 carries out automatic gain stabilisation every 60 seconds. Automatic gain stabilisation is important because portable spectrometers are prone to tool drift due to

changes in temperature and moisture content. The fact that the Exploranium GR320 stabilises itself at regular intervals saves time and reduces the risk of errors due to incorrect manual stabilisation. The reference source is Cesium 137, which is better than Barium which is used in the geoMetrics GR310 because Cesium only emits gamma-ray photons at 622 keV (Fig. 2.7), unlike the range of energies emitted by Barium (Fig. 2.6).

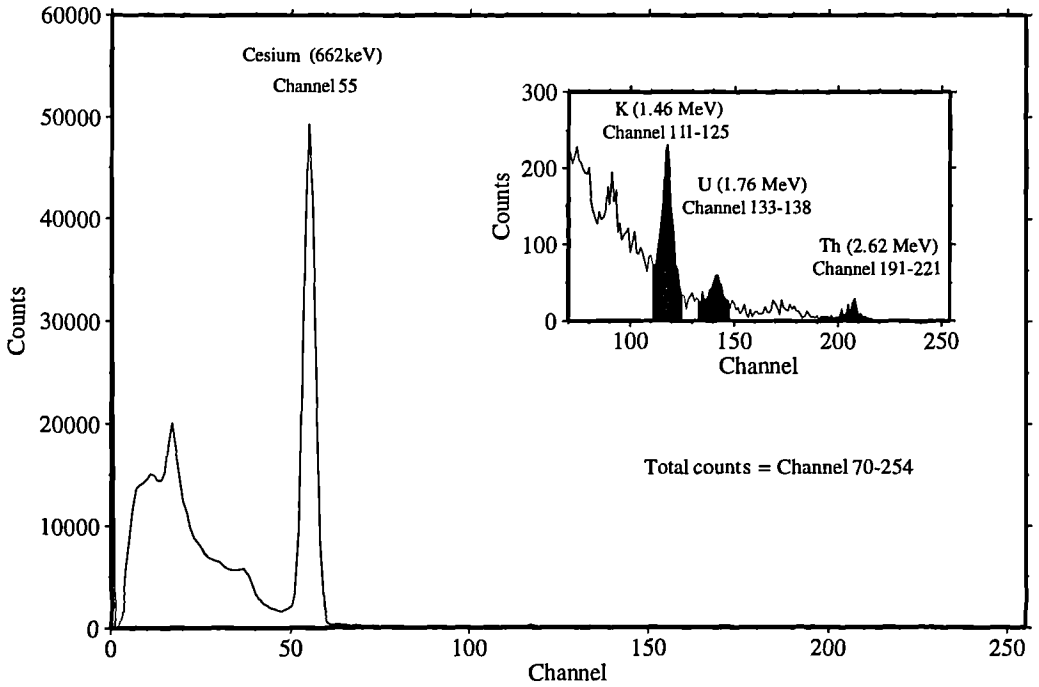

Fig. 2.7 Gamma-ray spectra for cesium, the reference isotope in the Exploranium GR320. The automatic stabilization ensures that the cesium peak (662 KeV) is always in channel 55, which in turn ensures that the diagnostic peaks for K, U and Th always fall in the correct channels. The insert shows the channel ranges for K, U and Th.

The user may set up to 8 regions of interest. These are windows in the spectrum used to select a data set centred around a specific peak for analysis. Since the sodium iodide crystal detector has fairly poor detector resolution, even though an isotope is emitting at a specific energy level the detector will display this peak as a Gaussian shape spread over a few channels. To improve count statistics and data quality, the International Atomic Energy Agency (IAEA 1976) has specified a spread of channels around each peak as the "range" of this peak. For example potassium only emits photons at 1.46 MeV, but all gamma-ray counts in channels 111-125 are grouped together as the potassium counts (Fig. 2.7).

2.2.4 Field procedures

The effective sample size of portable gamma-ray spectrometers is shown in Figure 2.8a. The distances shown in the figure are only estimates because they depend on the

density of the sample used. In this particular example Løvborg *et al.* (1971) used 2.8 g/cm^3 to calculate these values, which is slightly higher than most sedimentary rocks. Rocks with lower density and the same amount of natural radiation would result in a slightly larger effective sample size.

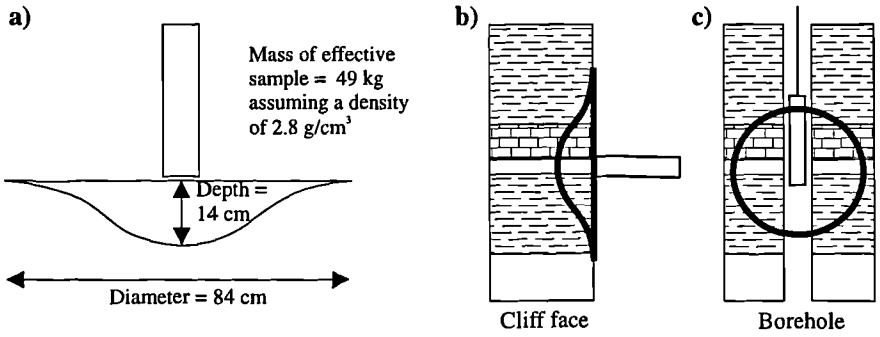

Fig. 2.8 Effective sampling area of a portable gamma-ray spectrometer compared to a wireline gamma-ray sonde. (a) Dimensions of the sample area for a portable spectrometer (modified from Løvborg *et al.* 1971). (b) Typical orientation and position of the effective sample area of the portable gamma-ray spectrometer as used in this study. (c) Position of wireline gamma-ray sonde and effective sample area in a borehole. The effective sample area depends on the speed at which the tool is drawn up the hole and the density of the rocks. In fact the sample area will tend more to an elliptical shape the faster the tool is drawn up the hole. Typical sample area assuming a spherical sampling area is about 30 cm radius (Rider 1986).

The most accurate *absolute* values for a particular bed of greater than about 14 cm in thickness are obtained by placing the tool on top of a flat bedding surface of at least 1 m diameter. Myers (1987) suggested wavecut platforms are ideal. Similar measurements made on beds with a thickness of less than 14 cm will obviously include some component of the underlying bed or beds. The aim of this study, however, was to correlate the general trends of field gamma-ray logs with wireline data. Therefore, the detector was placed perpendicular to bedding (Fig. 2.8b) so that the gamma-ray measurements made on all beds of less than approximately 84 cm thick would be influenced to some extent by gamma-ray radiation from adjacent beds, as is the case in wireline logging (Fig 2.8c). All readings, where ever possible, were taken on a relatively flat section of the cliff face, avoiding irregularities such as overhangs and corners so as to ensure that roughly the same volume of rock contributed to each reading. Readings were only taken where the tool could be used at least 1 m above the base of the cliff, thus avoiding errors due to gamma-ray contribution from rocks on the beach.

Count times of 100 seconds for the geoMetrics GR310 and 200 seconds for the Exploranium GR320 were used in this study. This resulted in tool precision errors of <2.5% and <1.5%, respectively, for the total count reading (see Section 2.2.5 for further details on data precision).

The measurement procedure used for both spectrometers was to take a reading once in every bed of less than 50 cm thick and every 30 - 50 cm in beds greater than 50 cm thick. The Oxfordian sedimentological field logs used in this study were from Coe (1995), the part of the Kimmeridgian from *mutabilis* to *autissiodorensis* zones were from Cox & Gallois (1981), the rest of the Kimmeridgian from *elegans* to *fittoni* zones were from Coe (1992), and finally the Portlandian sedimentological field logs were from Coe (1996). The geoMetrics GR310 was used to record total gamma-ray readings throughout the best Upper Jurassic exposures in Dorset, resulting in 1124 total gamma-ray readings with an average sample interval of 45 cm over 503 m (Fig. 2.2). Part of the Kimmeridge Clay Formation was selected to compare the results from the two spectrometers. Full spectral gamma-ray data were thus recorded with the Exploranium GR320 at 824 sample points over 251 m of the Kimmeridge Clay Formation (average sample interval 30 cm; Fig. 2.9). The average sampling distance of 30 – 45 cm is within the limits of the effective sampling size of the spectrometers (84 cm; Fig. 2.8a; Løvborg *et al.* 1971) and each consecutive reading overlaps the previous reading resulting in a moving average, thus making it comparable with the wireline gamma-ray tool as it is pulled slowly up the borehole.

Appendix B contains sedimentological logs of the Upper Jurassic succession exposed on the Dorset coast showing the location of all the gamma-ray measurements made in this study.

2.2.5 Tool and data calibration

The accepted unit for wireline gamma-ray logging is the API (American Petroleum Institute) which was introduced in 1958 (Frank 1986). The API unit is defined in a reference well, which is composed of concrete blocks of known radioactivity, at the University of Houston, Texas (Bateman 1985). Prior to 1958 the various logging companies used different units. For example; "radium-equivalent" per ton or counts per second (CPS). Eleven wells in this data set were drilled prior to 1958.

Portable gamma-ray spectrometers record the total gamma-rays counts in CPS (counts per second) or CPM (counts per minute). Since these units are wholly dependent on the detector crystal being used and the particular tool, the results from one study could not be directly compared with another so in 1976 the International Atomic Energy Agency recommended a new unit, the 'Ur' or 'unit of radioelement concentration' (IAEA 1976). The description of a Ur is "A geological source with 1 unit of radioelement concentration produces the same instrument response (e.g. count rate) as an identical source containing 1 ppm uranium in radioactive equilibrium". The counts in the potassium window are usually displayed as percent potassium (K%) and the abundances of U and Th are displayed as parts per million (U ppm & Th ppm; IAEA 1976).

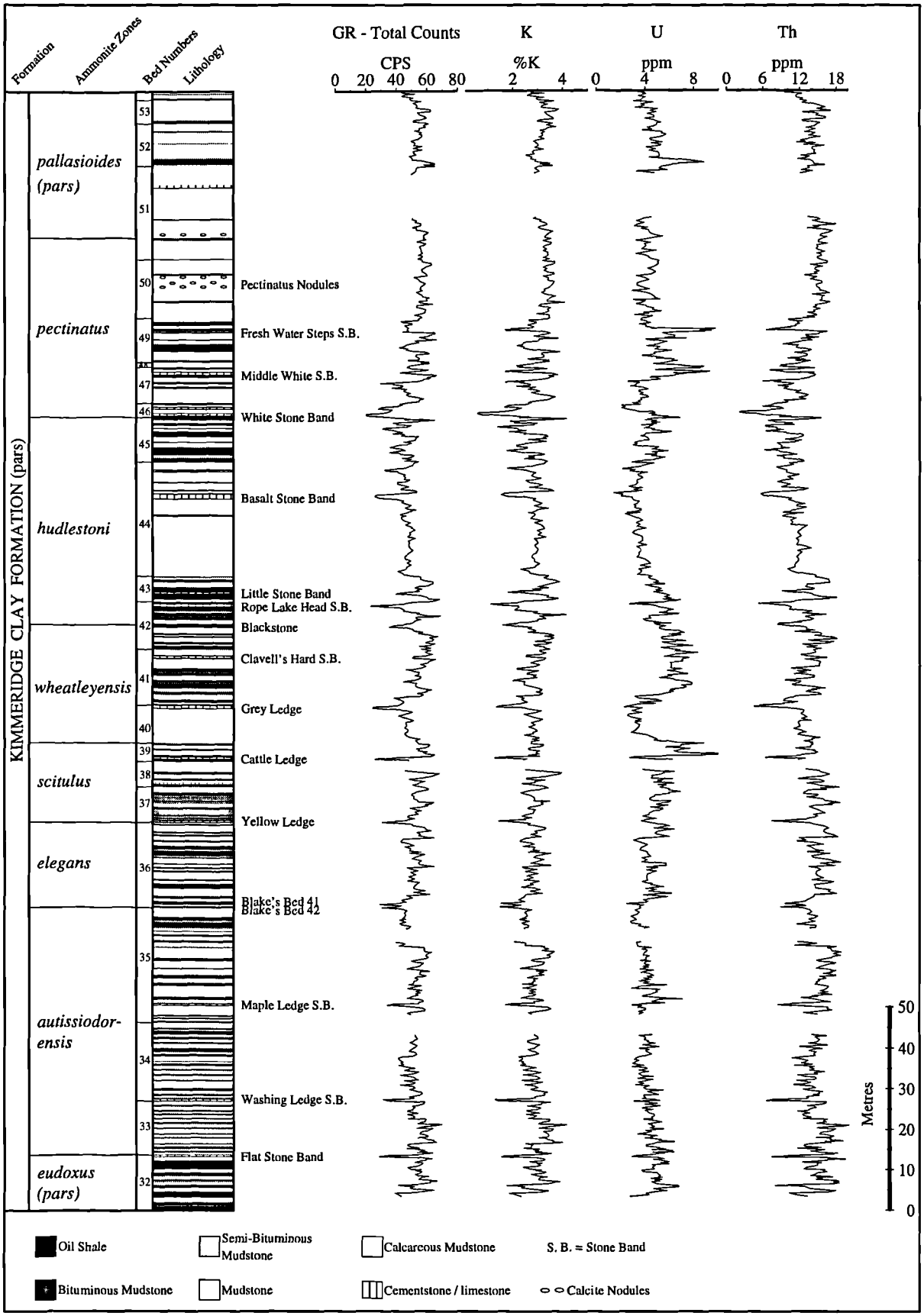

Fig. 2.9 Spectral gamma-ray data recorded with the Exploranium GR320, over part of the Kimmeridge Clay Formation between Hobarrow Bay and Chapman's Pool (see Fig. 2.1 for location of outcrops). The gaps in the data are due to non-accessiblity of the section with gamma-ray tool.

As we have just seen, the generally accepted units for the wireline and portable spectral gamma-ray data are different. So the actual values on the field gamma-ray log and the wireline gamma-ray data cannot be directly compared. This is not a problem in this study because, as we have already mentioned, the purpose of constructing the composite field gamma-ray log is to correlate the outcrops with the wireline data; so it is the trends we are interested in, not the actual values.

Tool calibration is only required to convert the gamma-rays detected in the potassium, uranium and thorium windows to concentrations of the three radioelements in the ground. The Exploranium GR320 was calibrated in Toronto by Exploranium Ltd. (Canada) and the geoMetrics GR310 was calibrated on the calibration pads at the British Geological Survey, Keyworth. The calibration procedure is as follows. The portable spectrometer is placed on various concrete pads with known concentration of potassium, uranium and thorium. Figure 2.10 shows that the counts on the potassium window are made up of counts from the potassium, uranium and thorium spectrum, while counts in the uranium and thorium windows are made up of counts from the uranium and thorium spectrum. Knowing the actual concentration of potassium, uranium and thorium in the various concrete pads and having recorded the counts on each pad, the radioelement assay values for potassium (%K), uranium (U ppm) and thorium (Th ppm) can be calculated. For more detailed information about portable spectrometer calibration see Løvborg (1984), Løvborg & Mose (1987) & Grasty *et al.* (1991).

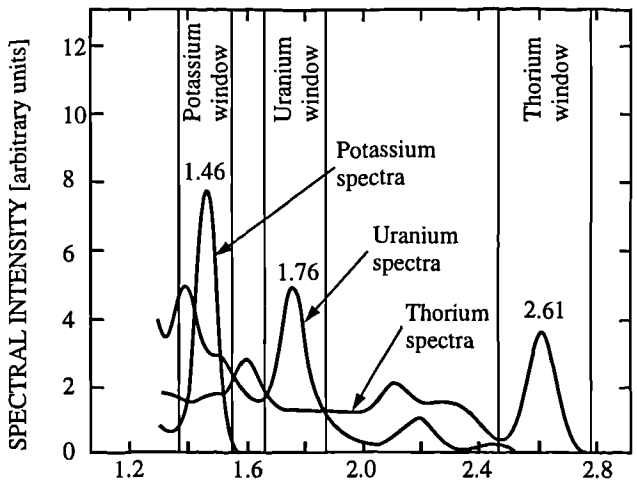

Fig. 2.10 Scintillation spectra of potassium, uranium, and thorium gamma radiation from the ground. The three energy windows shown are used for recording counts with a portable spectrometer in an assay locality (Løvborg & Mose 1987).

A very important feature of the tool calibration is the removal of the background radiation from all the raw data prior to the assay values being calculated. Background radiation is composed of gamma-rays from other sources, primarily cosmic rays, 214Bi from atmospheric radon and traces of radioactivity in the materials of the glass envelope of the photomultiplier tube (Løvborg & Mose 1987). The ideal place to record background

values for total counts and counts in the potassium, uranium and thorium windows is over a large body of water.

Løvborg (1984) published background values for the NW European environment (Table 2.1). He used a geoMetrics 410A with a 3"x3" detector crystal and recorded gamma-rays over large bodies of water for 0.5 to 2 hours.

Løvborg (1984)	K cpm	U cpm	Th cpm
Denmark	32.8	9.6	6.5
Hornavan Lake, N Sweden	22.7	11.9	8.2
St. Umevattnet, N Sweden	26.1	12.1	8.3
Finland	25.2	14.0	8.3
Average adopted by Løvborg & Mose (1987)	25.1±1.5	11.3±1.9	7.5±1

TABLE 2.1: Background values for NW Europe (from Løvborg 1984)

Myers (1987), who recorded spectral gamma-ray data over part of the Kimmeridge Clay Formation, used Løvborg's average background values for North West Europe instead of recording his own because he used the same model spectrometer as Løvborg, a geoMetrics 410A. It was decided to measure background values for both tools in this study and not use Løvborg's background values, because different spectrometers were used. Also it was thought that a background value measured close to the field area would be more accurate. Values for background radiation were thus recorded, for this study, 2 km offshore Swanage, Dorset (Fig. 2.1) on a small fishing boat, for each tool at the same time (Table 2.2). For comparison, a background value was also recorded for the geoMetrics tool over Lake Keilder, Northumberland in a rowing boat. At both locations the tools were held over the water while the background value was being measured.

Location	Tool	Recording Time	Total counts cpm	K cpm	U cpm	Th cpm
2 km off Swanage	Exploranium GR320	11.6 min (700 s)	314.4	28.6	12	5.8
2 km off Swanage	Exploranium GR320	8.3 min (500 s)	311.4	29.04	12.84	5.76
2 km off Swanage	geoMetrics GR310	16.6 min (1000 s)	857.4	-	-	-
Lake Keilder	geoMetrics GR310	16.6 min (1000 s)	913.8	-	-	-

TABLE 2.2: Background values recorded for this study.

All the data in this study have had the background values removed. The values used for the Exploranium GR320 can be seen in Table 2.2. The background used for the geoMetrics was the one recorded offshore from Swanage, because it was closer to the field area. The background value may vary during a field programme, but Løvborg & Mose (1987) suggest that this only becomes significant when measuring spectral data from low radioactivity rocks. The only spectral gamma-ray data recorded in this study were over part of the Kimmeridge Clay Formation, which are relatively high in radioactivity, so this fact can be ignored. In this study the total counts are displayed in counts per second (CPS) and the potassium, uranium and thorium in %K, U ppm and Th ppm respectively.

As was mentioned in the previous section, count times of 100 s for geoMetrics GR310 and 200 s for the Exploranium GR320 were used in this study. A longer count time was used for the Exploranium GR320 because spectral data were also recorded. Radioactive decay of natural elements is a random process; hence the gamma radiation released varies in intensity over any given time period. Generally, the shorter the sampling period the less gamma radiation is measured and the statistical error is greater. Specifically, the percentage of statistical error incurred varies with the number of counts collected, the higher the counts the more accurate the measurement. For typical needs, 1000 counts (3% error) is accurate enough (geoMetrics GR310 - Operating Manual). Therefore a longer count time was used for the Exploranium GR320 because it takes longer to record sufficient gamma-ray counts in the K, Th and U windows than it does for the total gamma-ray measurement. For a detailed account of counting statistics in radioelement assaying, the reader is referred to Løvborg & Mose (1987).

Parkinson (1996) showed that in practice for mudrocks, departures of measurement geometry from a true plane far outweigh instrument precision as a source of experimental error. Repeat readings taken in this study, along 20 m of bed, vary by up to 7% for both the geoMetrics GR310 and the Exploranium GR320. This is probably due to slight lithological variations, and differences in the volume of the effective sample size due to undulations in the cliff face.

2.3 Previous field spectral gamma-ray studies

Talwar *et al.* (1992) completed a short study of the gamma-ray spectrometry of the Corallian Beds (Oxfordian) at Bran Point, Dorset using a Scintrex Scintillation Counter (SCC) spectrometer. They too recorded gamma-ray measurements for the purpose of correlating outcrops with wireline data. There are two problems with the work of Talwar *et al.* (1992). Firstly, they appear to have used an exceedingly short sampling time of only

3-6 s which would result in significant errors; a count time of greater than 60 s for sedimentary rocks is usual. Secondly, their correlation with two boreholes from the North Dorset and Wiltshire area hardly show any similarity because the lower two thirds of the Oxfordian examined in the boreholes is older than any of the rocks which they illustrate from Bran Point, and they have not taken into account any of the unconformities in the Oxfordian succession (Coe 1992, 1995).

Figure 2.11 shows a comparison of the data recorded by Talwar *et al.* (1992) and the data recorded in this study. The field gamma-ray log constructed by Talwar *et al.* (1992) shows more character than the log constructed in this study, due to the fact that Talwar *et al.* (1992) used a 10 cm distance between measurements whilst a 35-45 cm distance between measurements was used in this study. A 10 cm sampling distance would have been impractical in this study because it would have taken 3 to 4 times longer to have constructed the two field gamma-ray logs. More importantly a 10 cm sampling distance is less than the wireline gamma-ray sonde sampling interval of 15 cm, so more data would be recorded than would be needed to correlate the field gamma-ray log with wireline gamma-ray data. The same general trends can be seen between the field gamma-ray data recorded by Talwar *et al.* (1992) and those recorded in this study.

A previous spectral gamma-ray study on part of the Upper Kimmeridge Clay in Dorset was completed by Myers (1987). Myers took spectral gamma-ray measurements using a geoMetrics GR410A on the wave-cut platforms, in order to achieve the best absolute assay values (K, Th & U) for individual beds. He utilised these data for a sedimentological and stratigraphical interpretation of organic-rich mudstones. The main differences between the data recorded in this study and the data recorded by Myers (1987) are the age of the portable spectrometer, the number of measurements taken and the orientation of the tool. Myers took his measurements on wave-cut platforms, so the number of measurements he could take was to a certain extent limited by the number of exposed wave-cut platforms. The measurements recorded in this study were taken on the cliff face at 35-45 cm intervals. Figure 2.12 shows a comparison between Myers's data set and the two recorded in this study. It is clear from this figure that gamma-ray measurements recorded for the purpose of correlating with wireline data should be taken on the cliff face rather than wave-cut platforms, because key features such as the gamma-ray lows seen at the base of the *wheatleyensis* Zone and the middle of the *hudlestoni* Zone are missing from Myers's log. These lows were recorded over calcareous mudstone units which do not form wave-cut platforms. Also, the longer the sample interval the smoother features become; for example, the gamma-ray data over bed group numbers 46 & 47 (Fig. 2.12) has significantly more character in the Exploranium log than that seen in Myers's log. Figure 2.12 also shows that the Exploranium log over bed group numbers 46 & 47 correlates better with the nearby Encombe 1 borehole than Myers's log.

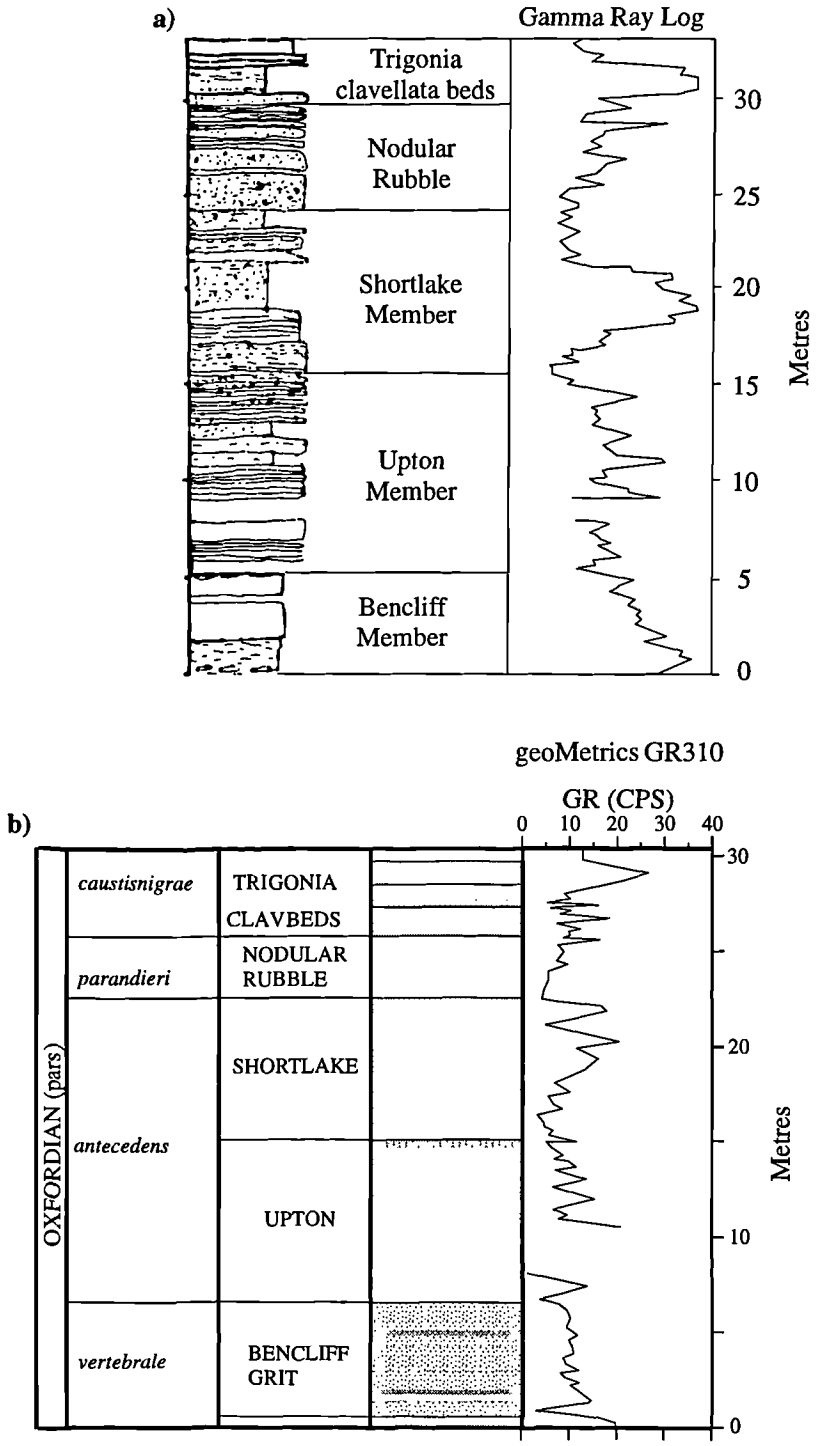

Fig. 2.11 Comparison of field gamma-ray log produced by Talwar *et al.* (1992) and the part of the field log produced in this study, using the geoMetrics GR310, over part of the Oxfordian at Bran Point. **(a)** Field gamma-ray log produced by Talwar *et al.* (1992). **(b)** Field gamma-ray log produced in this study. See Fig. 2.1 for location of Bran Point.

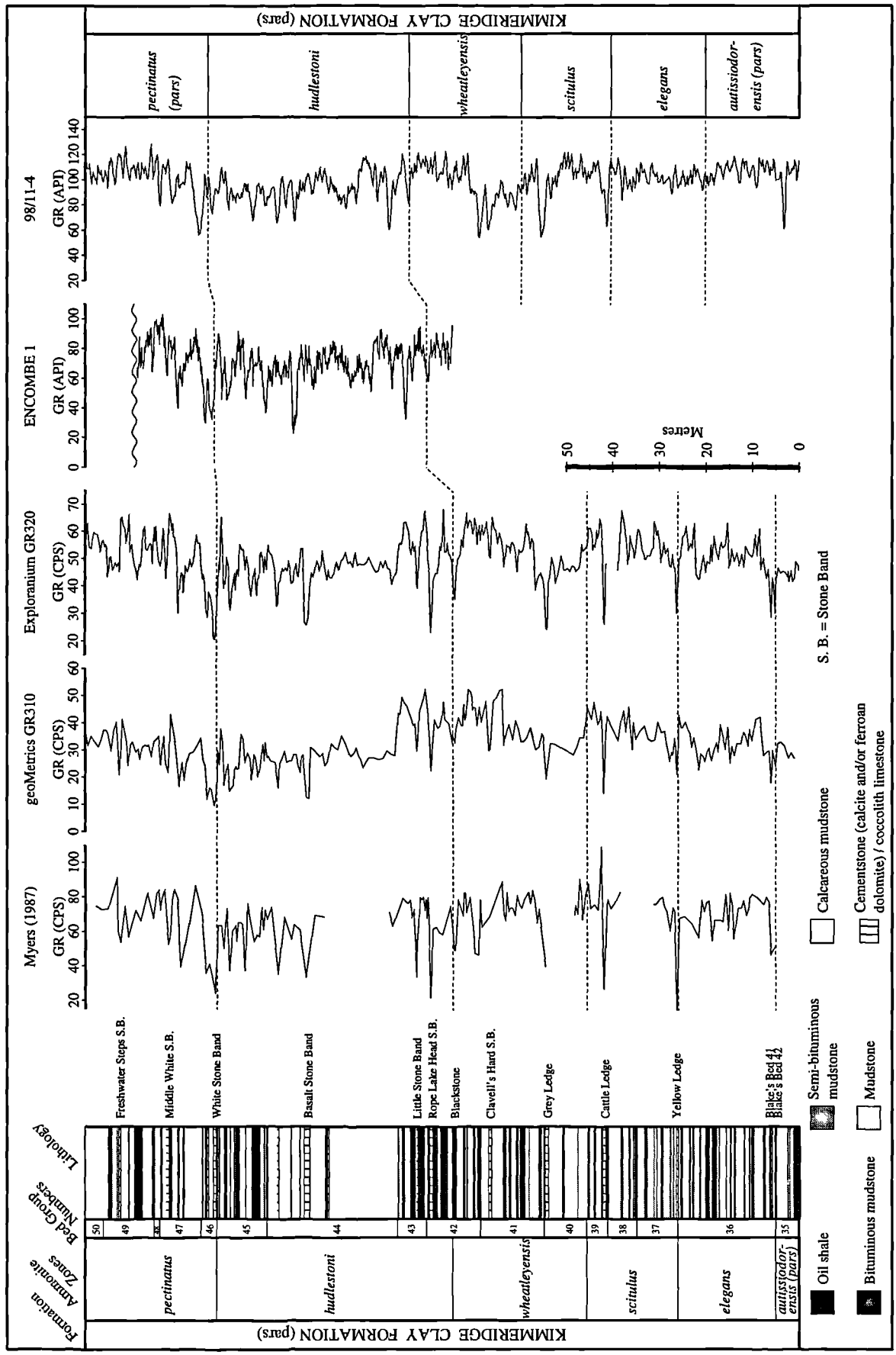

Fig. 2.12 Comparison of field gamma-ray log produced by Myers (1987) and the two field gamma-ray logs produced in this study over part of the Kimmeridge Clay Formation. Also shown are the gamma-ray logs from Encombe 1 and 98/11-4 boreholes (see Fig. 2.1 for location of boreholes).

Another disadvantage of measuring gamma-ray values on wave-cut platforms as opposed to measurements on the cliff face, for the purpose of correlating the field data with wireline data, can be seen by looking at the three field gamma-ray logs over the interval around bed group 39 (Fig. 2.12). Myers's data clearly show that the reading taken above Cattle Ledge Stone Band has an extremely high total gamma-ray value, which does not appear in either of the two field logs constructed in this study or in the wireline data from 98/11-4. On Myers's original log (Myers 1987) he stated that the oil shale above Cattle Ledge Stone Band contains the highest uranium content, and the data recorded in this study are in agreement (see U curve on Fig. 2.9). The reason for the very high total gamma-ray value on Myers's log is because the measurement was taken on top of the highly radioactive bed, where most of the radioactivity measured with the spectral gamma-ray tool would be from the bed itself. The measurements taken in this study were perpendicular to bedding, so even though the detector was placed on the highly radioactive bed, most of the gamma-rays would have been coming from the less radioactive beds above and below it. This example clearly shows that to obtain the best possible spectral gamma-ray values for individual beds the tool orientation used by Myers is better than that used for this study, but on the other hand for the purposes of correlating the field gamma-ray data with wireline gamma-ray data the tool orientation as described in this study is better than that described by Myers.

2.4 Correlation of field gamma-ray logs with wireline gamma-ray data

2.4.1 Upper Jurassic composite field gamma-ray log

All the field gamma-ray data from nine different locations along the Dorset coast (Fig. 2.1) were combined to produce a composite field gamma-ray log for the Upper Jurassic strata of Dorset (Fig. 2.2). Comparison with the wireline gamma-ray data from borehole 98/11-4 (Fig. 2.13), which is plotted at the same scale, shows that the same general trends and wireline log patterns are present in both sets of data throughout the Upper Jurassic interval. Clearly distinguishable in both log signatures are the low frequency trends which are interpreted to be related to the long-term facies changes controlled by relative changes in sea-level (Coe 1992 and pers. comm.). For instance, the overall decrease in gamma-ray values for the *pallasioides* Zone of the Kimmeridgian to the *anguiformis* Zone in the Portlandian reflects the change from marine mudstones to carbonates, interpreted as a long-term lowering of relative sea-level (Coe 1992, 1996).

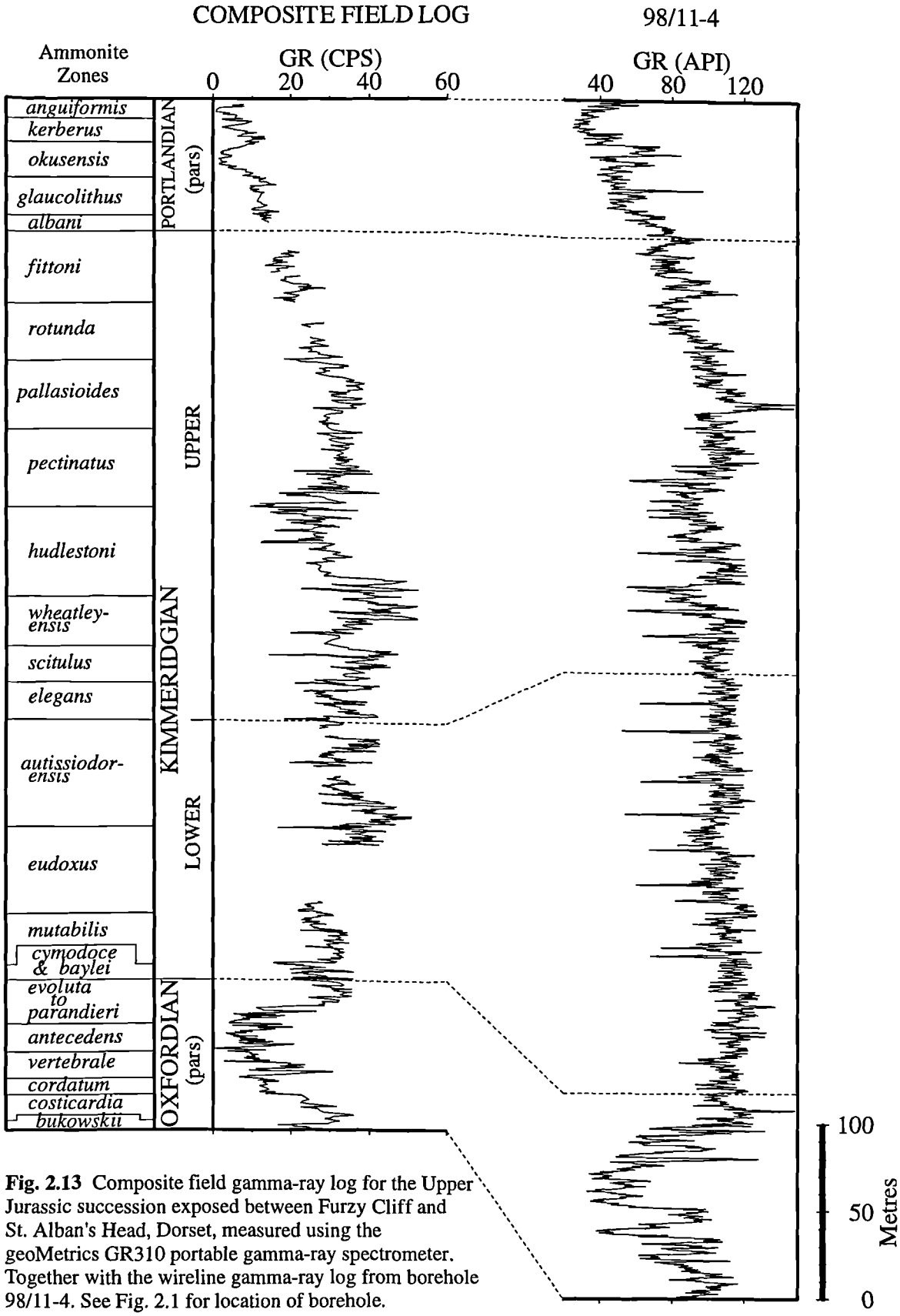

Fig. 2.13 Composite field gamma-ray log for the Upper Jurassic succession exposed between Furzy Cliff and St. Alban's Head, Dorset, measured using the geoMetrics GR310 portable gamma-ray spectrometer. Together with the wireline gamma-ray log from borehole 98/11-4. See Fig. 2.1 for location of borehole.

The one notable difference is that the Lower Kimmeridge Clay (*baylei* to *autissiodorensis* zones) is thicker in borehole 98/11-4 than in the outcrop section. This is due to the fact that the measurements for the Lower Kimmeridge Clay were made on the only available exposures, situated on the footwall close to the Isle of Purbeck fault which bounds the north side of the Central Channel Sub-basin, where the succession is apparently complete but thinner.

2.4.2 Comparison of the geoMetrics GR310 and the Exploranium GR320

Figure 2.14 shows a comparison of the total gamma-ray measurements taken with the two spectrometers over part of the Kimmeridge Clay Formation. The decreasing and increasing trends, amplitude of variation, and the shape of the peaks and troughs show a positive correlation. The main difference between the two signatures is the higher resolution of the Exploranium GR320 log; this is the result of the 30 cm average sampling interval as opposed to the 45 cm average sample interval for the geoMetrics GR310.

The correlation coefficient between the two field gamma-ray logs over the part of Kimmeridge Clay Formation shown in Figure 2.14 is 0.7 (Fig. 2.15). This was calculated using Corpac, which is a signal correlation computer program (Globex Consulting Services, Ltd. 1992). Corpac's automatic correlation method is designed to maximise the correlation between two signals, accommodating any nonlinear differences between them. The technique, which was adapted and modified from Martinson *et al.* (1982, 1984), works as follows: the program initially assumes that the two signals to be correlated are identical except that one has undergone distortion (stretching and/or squeezing) of its independent variable axis (in this case depth) relative to the other. This distortion is then described by a mapping function which relates correlative features between the signals. The mapping function is parameterized as a linear trend modified by a Fourier sine series with unknown coefficients. Since the coefficient values determine the shape of the mapping function, the program seeks to find those coefficient values that produce a mapping function whose shape maximises a correlation coefficient describing the degree of similarity between the two signals.

The reasons the correlation coefficient (0.7) is not higher are that the Exploranium GR320 log has higher resolution than the geoMetrics log and, probably more importantly, that there are gaps in the data. Figure 2.15c shows that the areas which do not correlate well are areas where no data were measured or where the distance between measurements was at its longest. Better correlation coefficients are obtained if these two logs are correlated over shorter intervals which contain no gaps in the data (Fig. 2.18b).

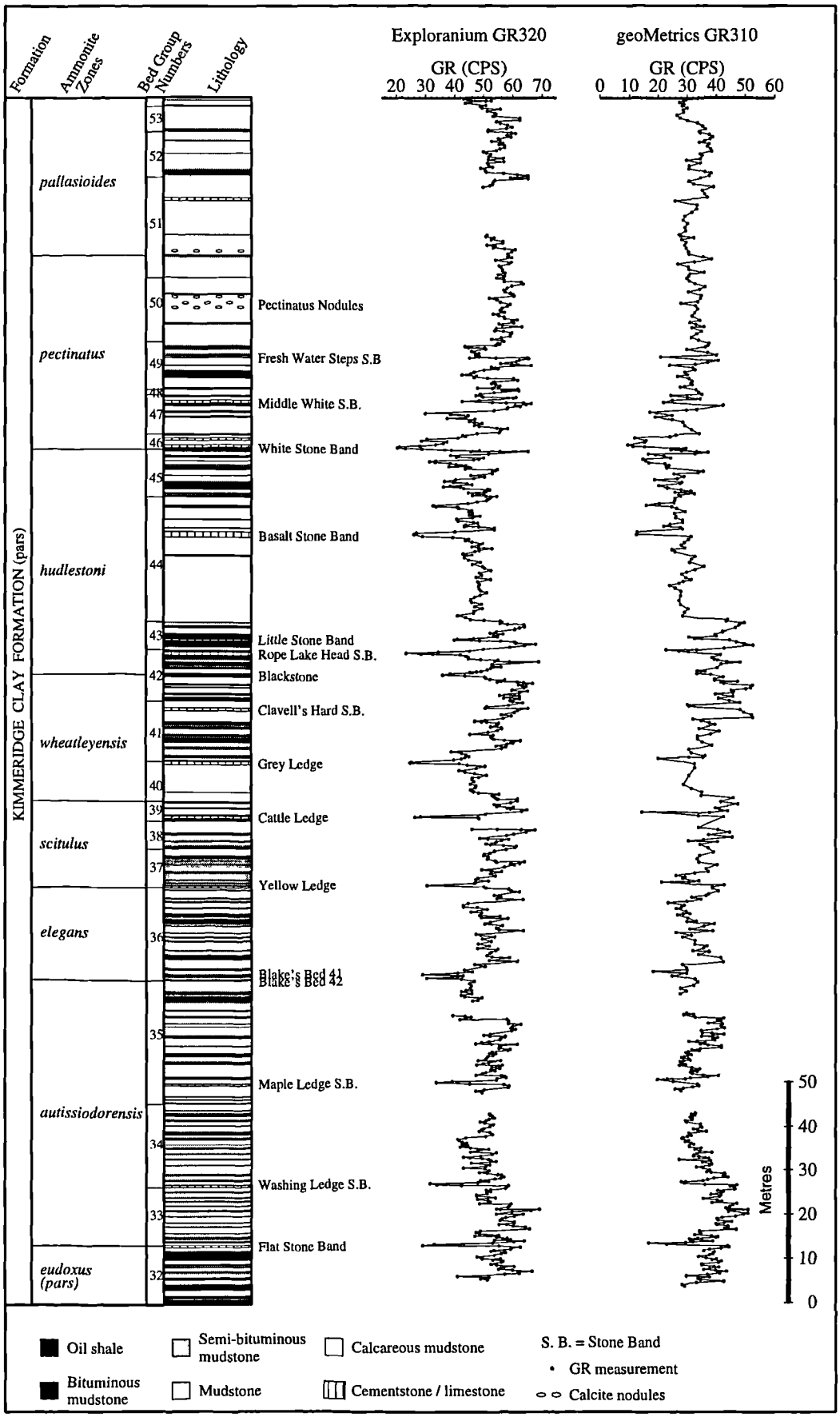

Fig. 2.14 Comparison of the field gamma-ray logs measured using the Exploranium GR320 and the geoMetrics GR310 portable gamma-ray spectrometers, for that part of the Kimmeridge Clay Formation exposed between Hobarrow Bay and Chapman's Pool, Dorset. See Fig. 2.1 for location of outcrop sections.

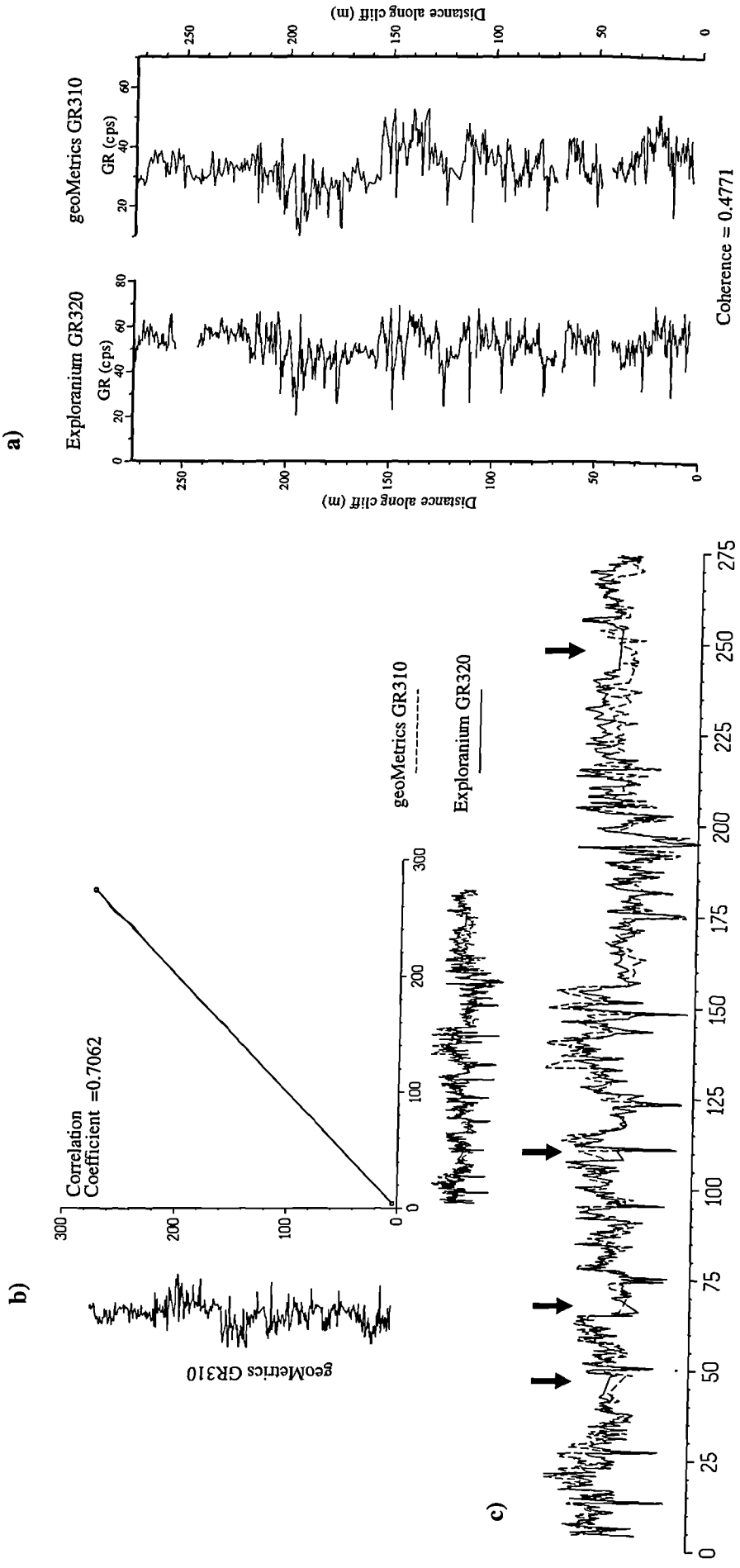

Fig. 2.15 The correlation coefficient, calculated using the CORPAC program, over the part of the Kimmeridge Clay Formation shown in Fig. 2.14. **(a)** The coherence of the two logs, using the COMPARE command. **(b)** The correlation coefficient of the two logs calculated using the CORRELATE command. **(c)** Close up of the x-axes of b), showing that the areas where no measurements were taken correspond to the areas where the two curves don't correlate well.

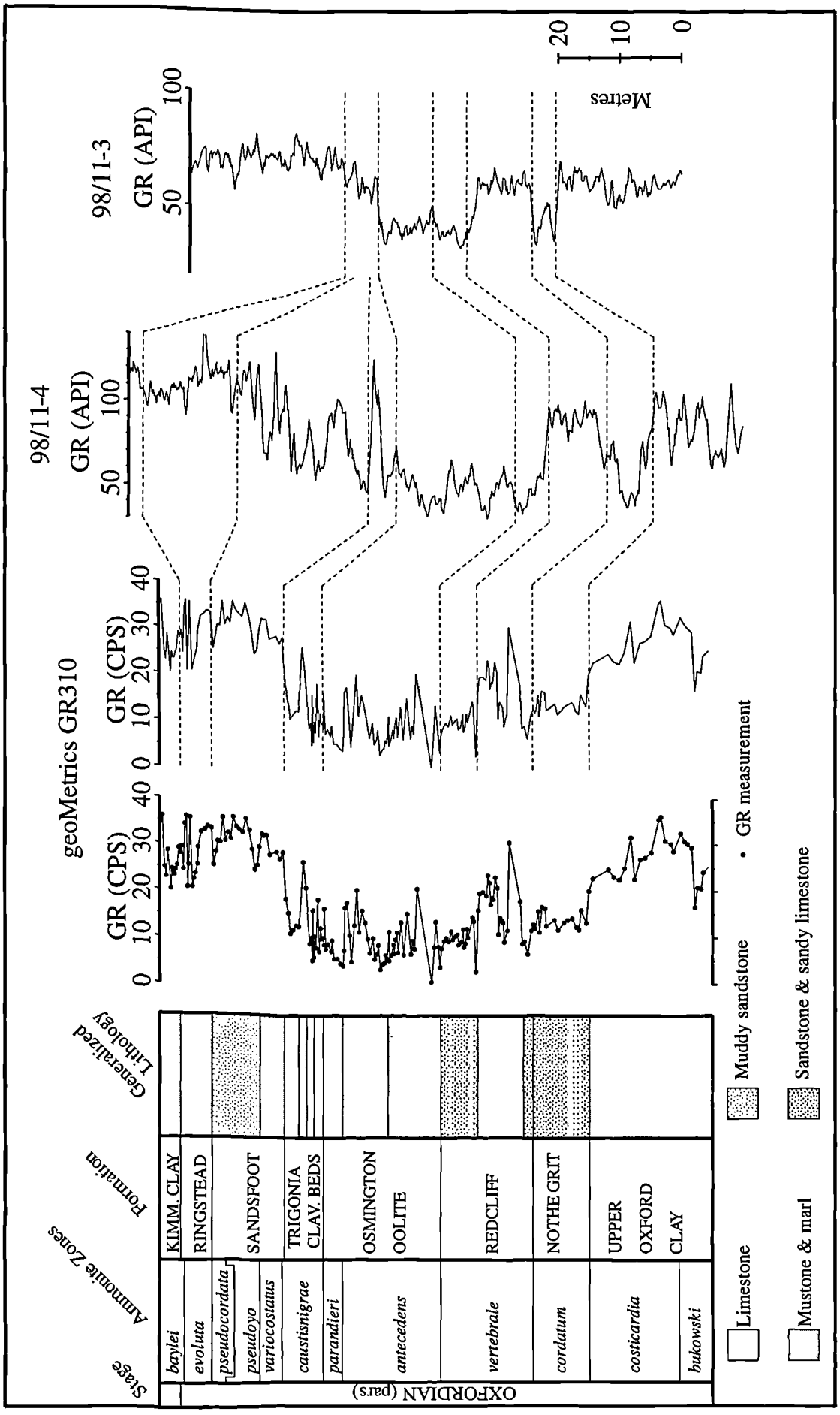

Fig. 2.16 Detailed comparison of the field gamma-ray log for the Oxfordian succession produced using the geoMetrics GR310 spectrometer with the wireline gamma-ray logs from boreholes 98/11-4 and 98/11-3 in the Central Channel Sub-basin. See Fig. 2.1 for location of boreholes and outcrop sections.

2.4.3 Correlation of field and wireline gamma-ray logs

2.4.3.1 Upper Oxford Clay and Corallian Beds

The field gamma-ray log shows an overall decreasing and then increasing trend in the gamma-ray values which is similarly shown in boreholes 98/11-4 and 98/11-3 reflecting the change in sediment type from mudstones, to sandstones and limestones, and then back to mudstones and iron-rich sandstones (Fig. 2.16). The Nothe Grit Formation is a better defined gamma-ray low in boreholes 98/11-4 and 98/11-3 than in the field gamma-ray log, probably because the sands are cleaner in the boreholes and the clays of the overlying Redcliff Formation contain a high percentage of limestone in the outcrop section. Three prominent gamma-ray peaks in the Osmington Oolite Formation can be seen on both field gamma-ray log and in 98/11-4. Over a wider geographical area the Corallian Beds are lithologically very variable, being represented by shallow-marine sandstones and limestones. Sequence stratigraphical interpretation of the wireline logs using the number and character of the cycles does permit a correlation to be made across the Wessex Basin (see Chapter 5); however, the lateral lithological variability makes correlation based purely on the wireline log character difficult.

2.4.3.2 Kimmeridge Clay Formation

The excellent positive correlation between field gamma-ray logs produced by the two different spectrometers and the wireline gamma-ray log from Encombe 1 borehole (approximately 1 km inland from the outcrops; Fig. 2.1) is shown in Figure 2.17. The higher resolution data produced by using a greater sampling frequency for the Exploranium GR320 spectrometer improves the correlation with the wireline data even further. Using the methodology for calculating correlation coefficients described above, the correlation coefficient for the Exploranium GR320 field gamma-ray log and the Encombe 1 borehole is 0.9193, whilst it is 0.8176 for the geoMetrics GR310 field gamma-ray log and the Encombe 1 borehole (Fig. 2.18).

Figure 2.19 shows the positive correlation between the geoMetrics GR310 field gamma-ray log and wireline gamma-ray logs from boreholes up to 170 km away (Fig. 2.1). There are several particularly prominent features, including the two gamma-ray low areas seen in Collendean Farm 1 and Ashdown 1 boreholes in the *hudlestoni* and *wheatleyensis* zones which are often referred to as the 'Kimmeridge limestones' (Hancock & Mithen 1987). In outcrop these two gamma-ray low zones are prominent thick homogeneous calcareous mudstone units (middle and upper part of bed 40 and the lower part of bed 44; Fig. 2.14). The two gamma-ray lows in Collendean Farm 1 and Ashdown 1 are probably

more enhanced than those in 98/11-4 and the field gamma-ray log because the sediments have an even higher calcium carbonate content. A higher quartz sand content is discounted because the lithology, over the same intervals in the nearby Warlingham borehole, is described as argillaceous limestones and calcareous mudstones by Worssam & Ivimey-Cook (1971). Prominent gamma-ray lows on the field gamma-ray log such as those in the middle of the *autissiodorensis* Zone, at the base of the *elegans* Zone and near the top of the *scitilus* Zone, are carbonate-rich cemented horizons. Similar sharp gamma-ray lows in 98/11-4 and Collendean Farm 1 probably also relate to calcareous cemented horizons.

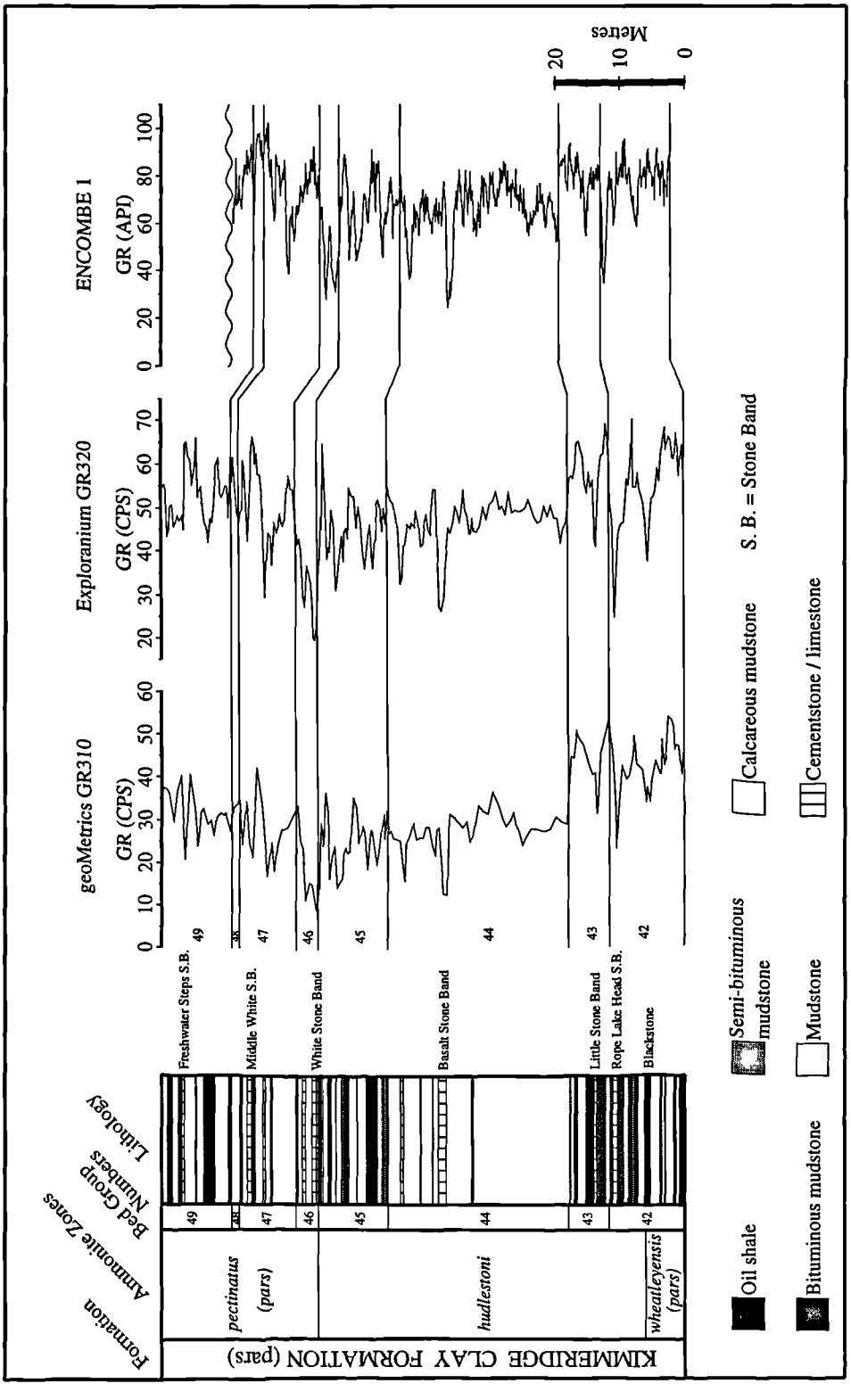

Fig. 2.17 Detailed comparison of the field gamma-ray logs for part of the Kimmeridge Clay Formation produced using the two protable field gamma-ray spectrometers and the wireline gamma-ray log from the nearby Encombe 1 borehole. See Fig. 2.1 for location of borehole.

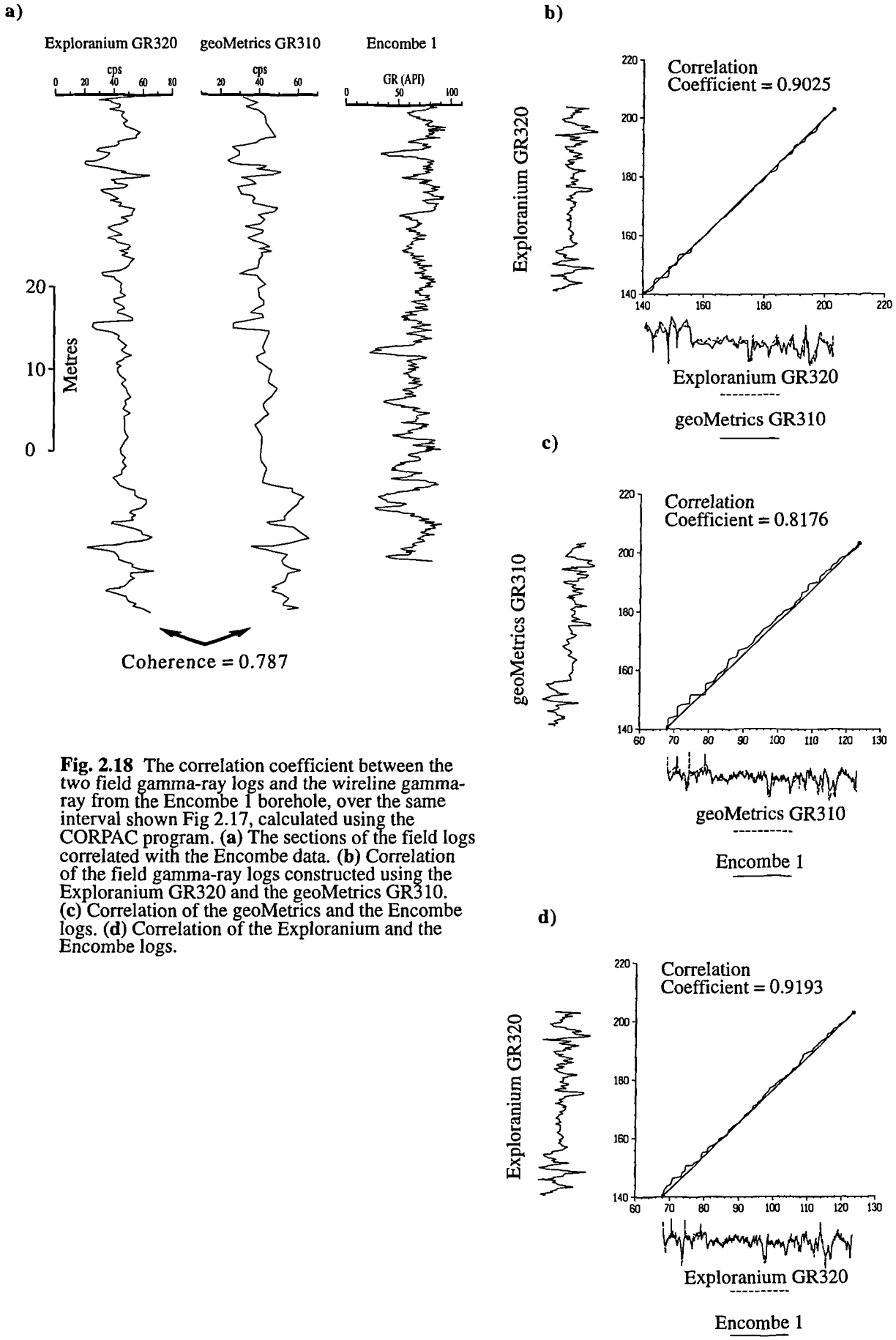

Fig. 2.18 The correlation coefficient between the two field gamma-ray logs and the wireline gamma-ray from the Encombe 1 borehole, over the same interval shown Fig 2.17, calculated using the CORPAC program. **(a)** The sections of the field logs correlated with the Encombe data. **(b)** Correlation of the field gamma-ray logs constructed using the Exploranium GR320 and the geoMetrics GR310. **(c)** Correlation of the geoMetrics and the Encombe logs. **(d)** Correlation of the Exploranium and the Encombe logs.

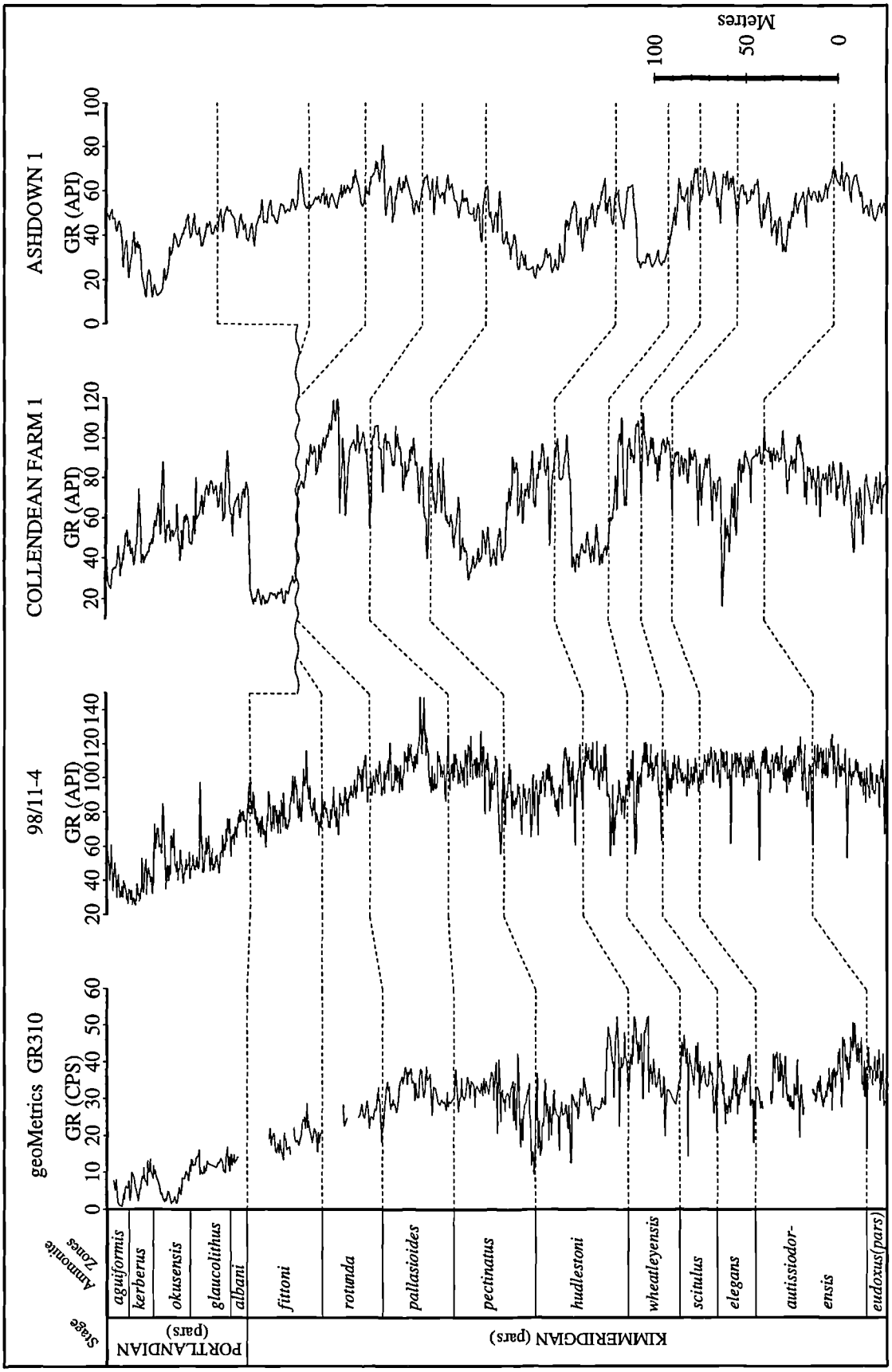

Fig. 2.19 Comparison of the field gamma-ray log produced using the geoMetrics GR310 spectrometer with wireline logs from three boreholes from the Central Channel Sub-basin and the Weald Sub-basin of the Wessex Basin. See Fig. 2.1 for location of the boreholes and outcrop sections.

2.5 Field density logs

2.5.1 Introduction

A field density log has been constructed for the upper parts of the Kimmeridgian and Oxfordian strata. As for the field gamma-ray log, the purpose of constructing the field density log was to correlate the Upper Jurassic outcrops with the subsurface wireline data with the aim of extending the sequence stratigraphic boundaries found in the outcrops by Coe (1992) to the subsurface. Another reason for constructing the field density log was to have two data sets which could be used to correlate the Upper Jurassic outcrops with the wireline data. The advantage of having two different data sets, from measurements of different physical parameters (natural radiation and density), is that in areas where there is no change in density there may well be a change in natural radiation (and visa versa). This makes the task of correlating the Upper Jurassic outcrops with the wireline data easier. To the author's knowledge this is the first time a field density log has been constructed for the purpose of correlating outcrops with wireline density data.

The aims of Section 2.5 are to describe the principles and procedures used to construct the field density log. The results of correlating the field density log with wireline density data are described in Section 2.6.

2.5.1.1 Wireline density tools

Wireline density logs record the rock's bulk density, by emitting gamma-rays into the formation and recording the number of scattered gamma-rays at a fixed distance from the source. The rock's bulk density is thus a function of the density of the rock and the density of the fluids in the pore space. The vertical resolution for older single-detector tools is 40 cm and for more modern two-detector tools is 25 cm (Serra 1984). Therefore any attempt to construct a field density log of the same character and resolution as the wireline density log has to take into account the density of the rocks and the density of the fluid in the pore space.

2.5.2 Field and laboratory procedures

Fresh rock samples of smaller than 3.1 cm x 3.1 cm x 3.7 cm representative of the majority of the beds in the Upper Oxford Clay Formation, Corallian Beds and Upper Kimmeridge Clay were collected for density analysis. Most of the Kimmeridgian hand samples were collected between 1988-1992 by A. L. Coe, but further sampling was

necessary to fill in the gaps. This amounted to 116 samples over 90 m of the Oxfordian (Fig. 2.20) and 260 samples over 280 m of the Kimmeridge Clay Formation (Fig. 2.21). The location of the samples from which density measurements were made can be seen in Appendix B. All the samples were dried for a couple of days in an oven at a temperature of less than 35°C prior to the measurements being taken.

2.3.2.1 Ruska Universal Porometer

A Ruska Universal Porometer (model number 1051-801) was then used to measure the volume and grain density of the samples. The porometer consists of a mercury pump, to which a pycnometer is attached. The chamber of the pycnometer has a volume of approximately 50 cc and admits samples up to 3.1 cm long and 3.8 cm in diameter. The movement of the pump metering plunger is indicated on a scale which is graduated to read the plunger displacement in cubic centimetres. The hand wheel dial is graduated in 0.01 cc subdivisions and permits estimation of plunger displacement to 0.005 cc (Ruska Instrument Corporation 1973).

The porometer was used to measure bulk volume and porosity, from which the bulk density could then be calculated. To determine bulk volume the sample is placed in the pycnometer and the pycnometer lid is locked in position, leaving the valve open. Mercury is injected into the pycnometer until a bead of mercury appears in the pycnometer valve seat. The appearance of the bead indicates the pycnometer is full, the void space being completely occupied by mercury and the sample. The volume of the sample is read directly on the volume scale and hand wheel dial numbers, in cubic centimetres.

Porosity can be measured by either the mercury injection method or the Kobe (Boyles' Law) method. The Kobe method was used for porosity measurements because accuracy rather than speed was the prime consideration. The Kobe method determines the grain or solids volume of a porous mass. If the bulk volume is known, the porosity is readily calculated from the grain volume measurement, since the difference between bulk and grain volumes is equal to the pore space. The Kobe method is based on Boyle's Law, which states that in a gaseous system the product of absolute pressure and volume is a constant at a given temperature.

The response of the porometer to various grain volumes is determined initially by means of a preliminary calibration. The outcome of this calibration is a graphical relationship (Fig. 2.22) which facilitates future grain volume measurements. This calibration process was carried out prior to each batch of samples being measured.

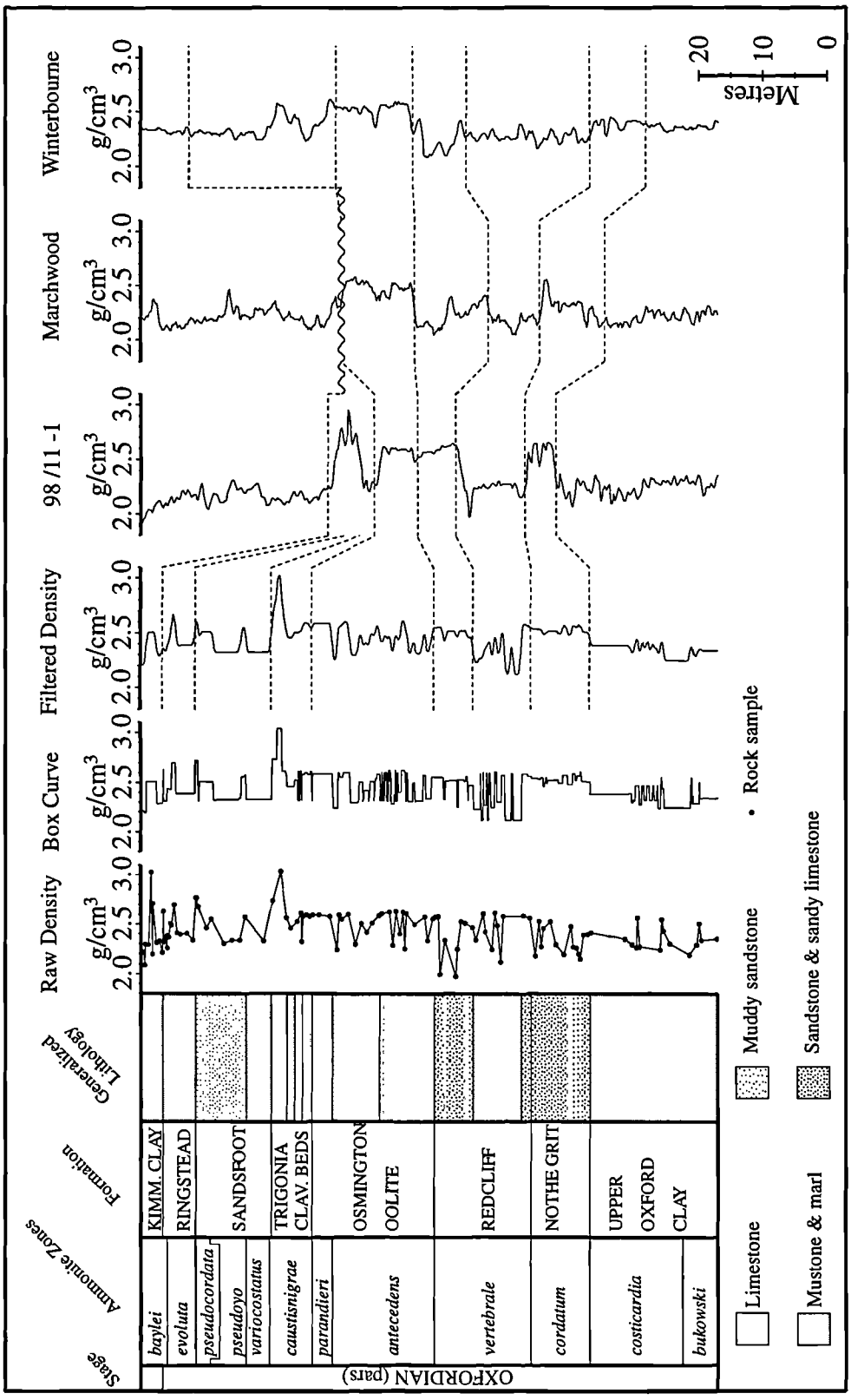

Fig. 2.20 Density curve constructed using Oxfordian age rock samples from 6 exposures on the Dorset coast. The raw density curve shows the raw data for individual samples. The box curve has been constructed by assigning the same density value for the whole bed, and where no samples were taken, assigning an average density value for the lithology of that particular bed. The density data were adjusted for the difference in porosity found between the surface exposures and subsurface strata over the Nothe Grit Formation and over the sandstone interval in the top third of the Redcliff Formation (see text for further explanation). The filtered density curve was constructed by filtering the box curve with a weighted moving average filter (see text for further explanation). See Fig. 2.1 for location of boreholes and outcrop sections.

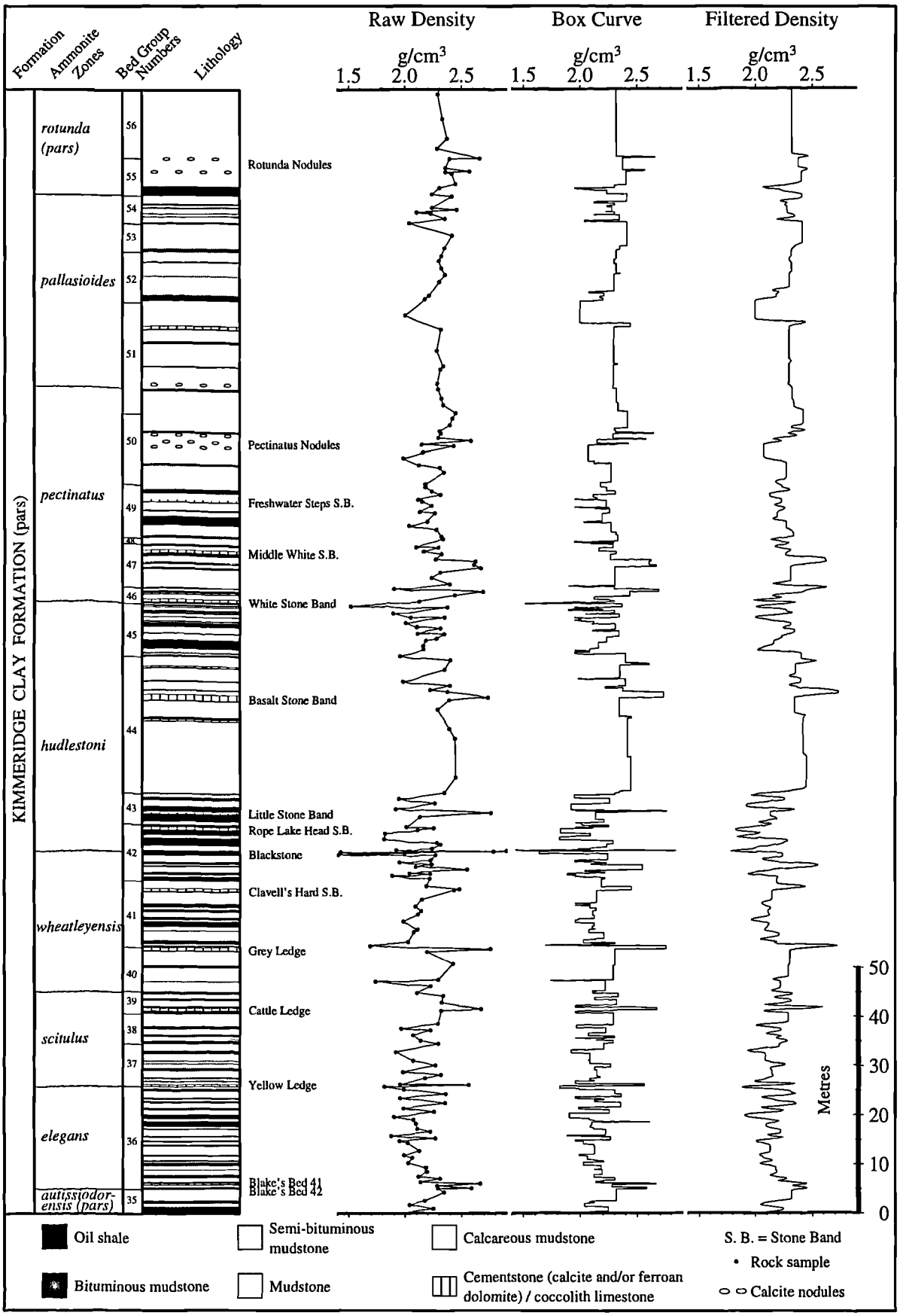

Fig. 2.21 Density curve constructed using rock samples from that part of the Kimmeridge Clay Formation exposed between Kimmeridge Bay and Chapman's Pool, Dorset.The raw density curve shows the raw data for individual samples. The box curve has been constructed by assigning the same density value for the whole bed, and for the 22% of beds where no sample was taken, an average density value for the lithology of that particular bed was assigned. The filtered density curve was constructed by filtering the box curve with a weighted moving average filter (see text for further explanation). See Fig. 2.1 for location of outcrop sections.

Assuming the porometer scale and dial have been calibrated, the procedure for determining the porosity of a sample is as follows. Using a reference pycnometer volume of 40.00 cc, a sample was enclosed in the pycnometer. Assuming operating thermal equilibrium exists, the system pressure increased to 30 psig and the final volume scale and dial reading (V'_f) is obtained. Using the graphical relationship in Figure 2.22, the grain volume (V_G) corresponding to the final volume reading (V'_f) obtained is determined.

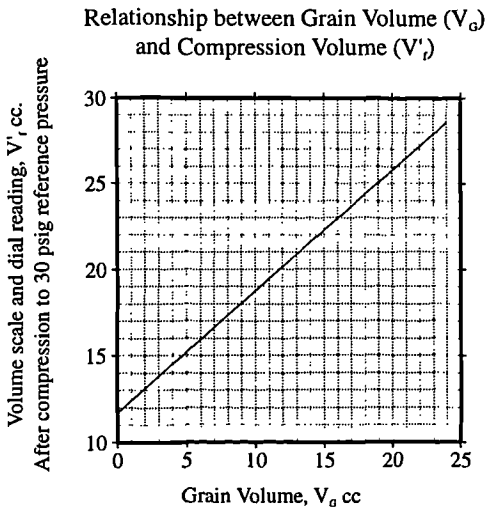

Fig. 2.22 The volume scale and dial reading (V'_f) read off the porometer is plotted on this graph to obtain the grain volume of the sample.

2.3.2.2 Density calculations

The bulk volume and grain volume of a sample are obtained directly from the Ruska Universal Porometer. The other values needed to calculate the density of the sample are the mass of the sample and the fluid density of the pore fluids. The mass of the samples was measured using a digital balance, which was accurate to four decimal places. A typical fluid density value for pore fluids in Upper Jurassic rocks of the Wessex Basin was obtained from production test data, recorded at Palmers Wood 3 borehole in the Weald Sub-basin (1.06 g/cm^3 pers. comm. P. Rowe).

The density of each sample was calculated using the following equations:

$$\text{Bulk Volume } (V_b) - \text{Grain Volume } (V_G) = \text{Pore Volume (Vp)}$$

$$\text{Pore Volume (Vp)} \times \text{Density of Fluid (Df)} = \text{Mass of Fluid (Mf)}$$

$$\text{Density} = (\text{Mass of Sample (Ms)} + \text{Mass of Fluid (Mf)}) \div \text{Bulk Volume } (V_b)$$

2.3.2.3 Errors in density measurement

As has already been stated, the hand wheel dial on the Ruska Universal Porometer is graduated in 0.01 cc subdivisions and permits estimation of plunger displacement to 0.005cc. The errors therefore for the measurements read off the porometer are:

$$\text{Bulk Volume} = V_b \quad \Rightarrow \quad \delta V_b = \pm 0.005 \text{ cm}^3$$

$$\text{Final Volume} = V_f \quad \Rightarrow \quad \delta V_f = \pm 0.005 \text{ cm}^3$$

The Grain Volume (V_G) is taken off the graph shown in Figure 2.22. The error in V_G was calculated as follows:

$$V'f = M V_G + C$$

$$\text{so} \quad V_G = \frac{V'f - C}{M}$$

$$\Rightarrow \delta V_G = \sqrt{\left(\frac{\sqrt{\delta V'f^2 + \delta C^2}}{V'f - C}\right)^2 + \left(\frac{\delta M}{M}\right)^2}$$

The error in the Pore Volume was calculated, using the errors in the Bulk Volume and Grain Volume, as follows:

$$Vp = Vb - V_G$$

$$\Rightarrow \delta Vp = \sqrt{\delta Vb^2 + \delta V_G{}^2}$$

The error in the Density of the Fluid (Df) was assumed to be = 1.06 ± 0.01 g/cm^3.
The error in the Mass of Fluid (Mf) = Vp x Df is:

$$\delta Mf = \sqrt{\left(\frac{\delta Vp}{Vp}\right)^2 + \left(\frac{\delta Df}{Df}\right)^2}$$

Finally the error in the Density measurements were calculated as follows:

$$\text{Density} = \frac{\text{Mass of sample (M)} + \text{Mass of fluid (Mf)}}{\text{Bulk volume (Vb)}}$$

$$\Rightarrow \delta\text{Density} = \sqrt{\left(\frac{\sqrt{\delta M^2 + \delta Mf^2}}{M + Mf}\right)^2 + \left(\frac{\delta Vb}{Vb}\right)^2}$$

As was already mentioned in the introduction to this chapter, emphasis has been placed on producing log trends which are at the same resolution and of similar character to typical downhole wireline logs rather than absolute values which might be expected downhole. Therefore the purpose of calculating the errors in the density measurements was simply for quality control reasons (i.e., to reduce experimental errors). Samples which showed high errors were re-measured. The reasons for the high errors in several of the sample measurements were attributed to the fact that small parts of sample broke off after the samples had been weighed prior to the measurements being taken with the porometer. The highest laboratory-based error calculated from all the density measurements made was $\pm$ 0.07 g/cm^3.

2.5.3 Computer program to generate field density log

The raw density curves on Figures 2.20 & 2.21 show the density values calculated from the actual samples measured. A FORTRAN program 'DEN' (Appendix C) was written to produce the box curves seen in Figures 2.20 & 2.21. To obtain the box curve the program carries out the following procedures; firstly, beds from which no sample was obtained were assigned an average density value typical of that particular lithology (Fig. 2.23) and calculated from the measured samples collected nearby stratigraphically. Secondly, the same density value was assigned to the whole thickness of the bed. The reason for producing the Box curve was so that a density value could be assigned to every 0.1m which would result in a curve with similar resolution to a wireline density log.

The flow chart shown in Figure 2.24 shows the main processing steps involved in the 'DEN' program. The program requires two input files, the first containing a distance in metres, the density of sample and the lithology number. The second file contains two distance measurements (the base and top of every bed) and the lithology number. The reason for having the lithology number in both input files was to spot any errors in the original data. For example, if the lithology of a sample at a particular distance did not match the lithology of the bed from which the sample was taken, the program would notify the user in which case the original raw input files would be checked and corrected.

The box curve was then filtered using the Atlas Wireline Services field acquisition filter (Fig. 2.25; Atlas Wireline Services 1994). This is an eleven point, Gaussian-like, weighted moving average filter. The total filter length used was 1.1 m. This resulted in a filtered field density curve with similar character and resolution to a wireline density log (Figs 2.20 & 2.21).

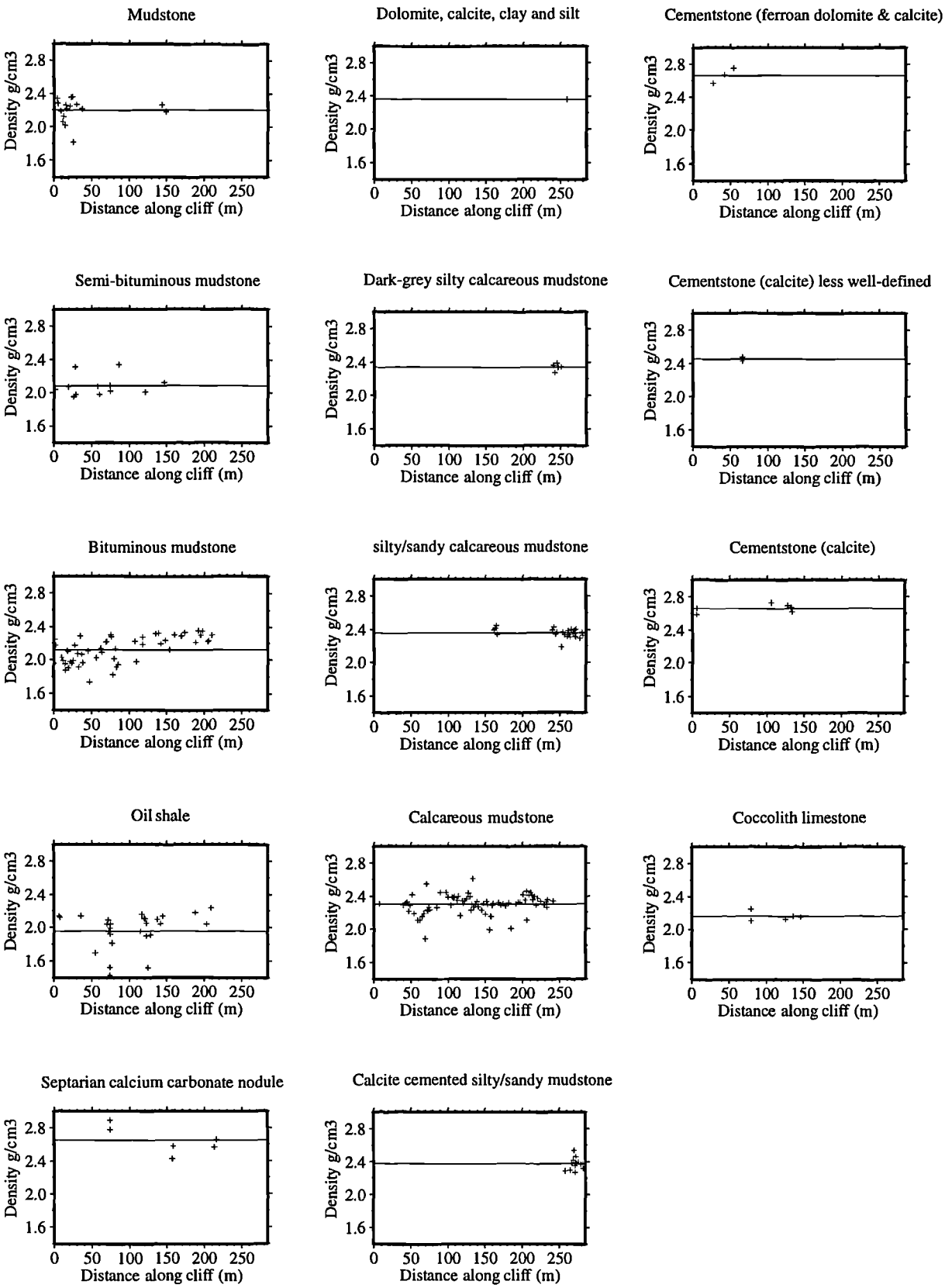

Fig. 2.23 Fourteen lithology types were used in the construction of the field density log for the Kimmeridge Clay section shown in Fig. 2.21. The average density value for each lithology, which was used to represent the density of beds from which no sample was taken, is shown on each of the graphs.

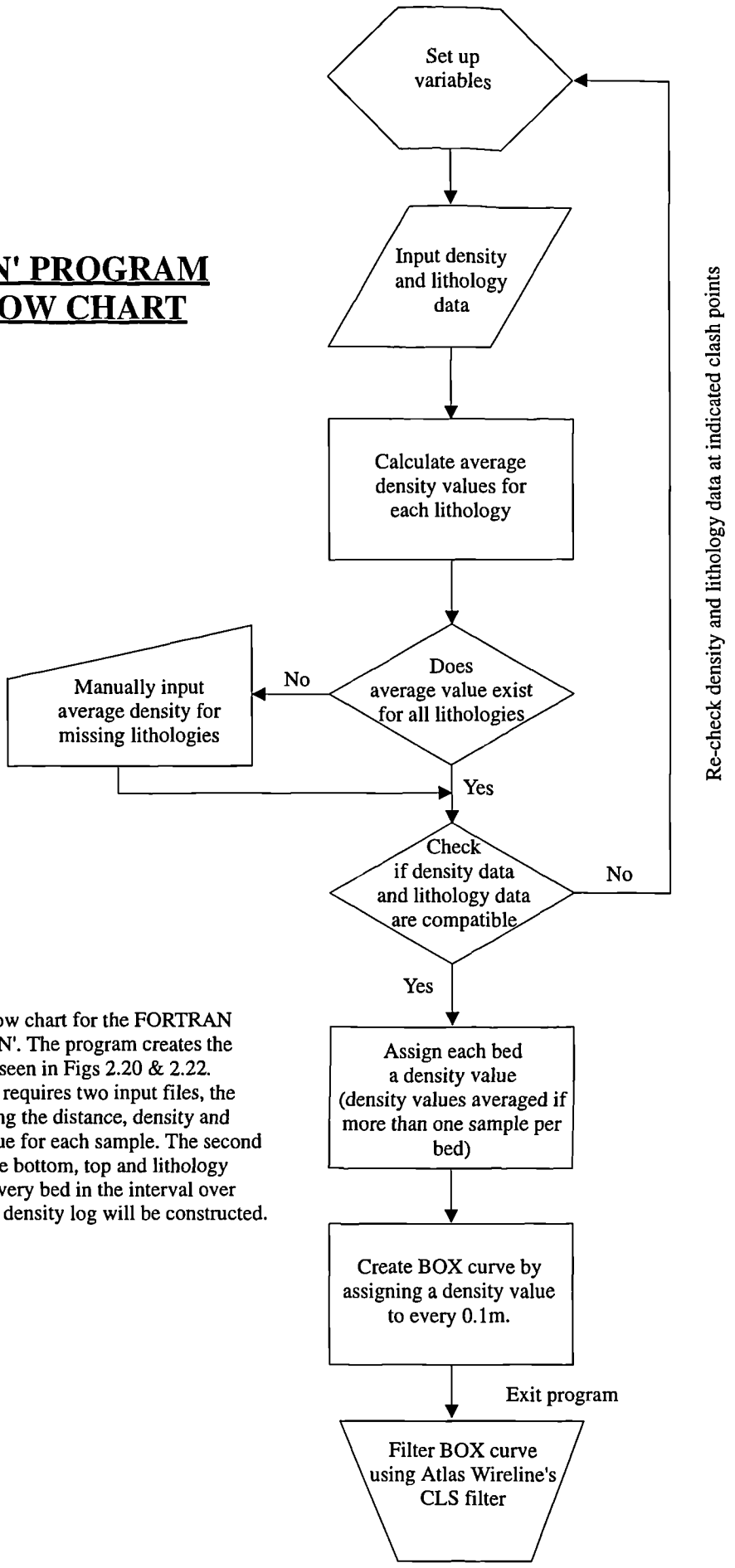

Fig. 2.24 Flow chart for the FORTRAN program 'DEN'. The program creates the BOX curves seen in Figs 2.20 & 2.22. The program requires two input files, the first containing the distance, density and lithology value for each sample. The second containing the bottom, top and lithology number for every bed in the interval over which a field density log will be constructed.

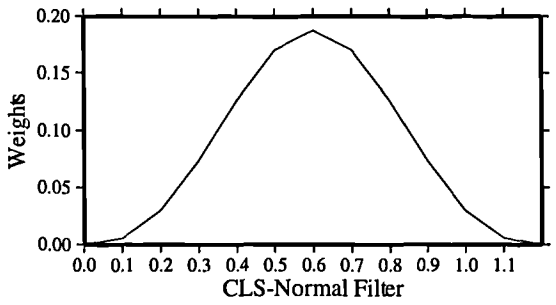

Fig. 2.25 Atlas Wireline Services field aquisition (CLS) filter, used to filter the BOX curves in Figs 2.20 & 2.21.

2.5.4 Porosity data correction

It was noted that the density of sandstones from the Nothe Grit and the Bencliff Grit (top of the Redcliff Formation; Fig. 2.20) had lower density values than those seen on the wireline density logs. This was interpreted to be due to the porosity of these rocks being higher at outcrop than in the subsurface because of dissolution of the calcite cement. The density values of these beds were therefore corrected by calculating the average porosity of these strata in the subsurface by plotting typical density, neutron and sonic values on porosity evaluation log interpretation charts (Fig 2.26; Atlas Wireline Services 1985; Schlumberger 1994) and then adding the density of calcite to the extra porosity found in the outcrop samples.

2.6 Correlation of field density logs with wireline density data

2.6.1 Upper Oxford Clay and Corallian Beds

Production of an outcrop density log over this interval of mixed siliciclastics and carbonates was more problematic than that for the Kimmeridge Clay Formation. Processing of the data in a similar manner to that of the Kimmeridge Clay Formation resulted in a filtered density curve with very little variation. However, further processing of the data to take into account dissolved carbonate cement at outcrop as described above resulted in a curve which is more comparable with the borehole density logs.

The general trends seen on the filtered density log (Fig. 2.20) show a positive correlation with the wireline density from Marchwood 1 borehole and to a certain extent with borehole 98/11-1. The Winterbourne Kingston 1 borehole density log is more difficult to correlate in the lower part due to the lack of variation on the large scale. Figure 2.20 also shows the marked lateral and vertical variation of the Oxfordian strata between the wireline logs of 98/11-1, Marchwood 1 and Winterbourne Kingston 1. One notable

example difference between the three wells is the change in density of both the Nothe Grit Formation (or its equivalent) and the Osmington Oolite Formation.

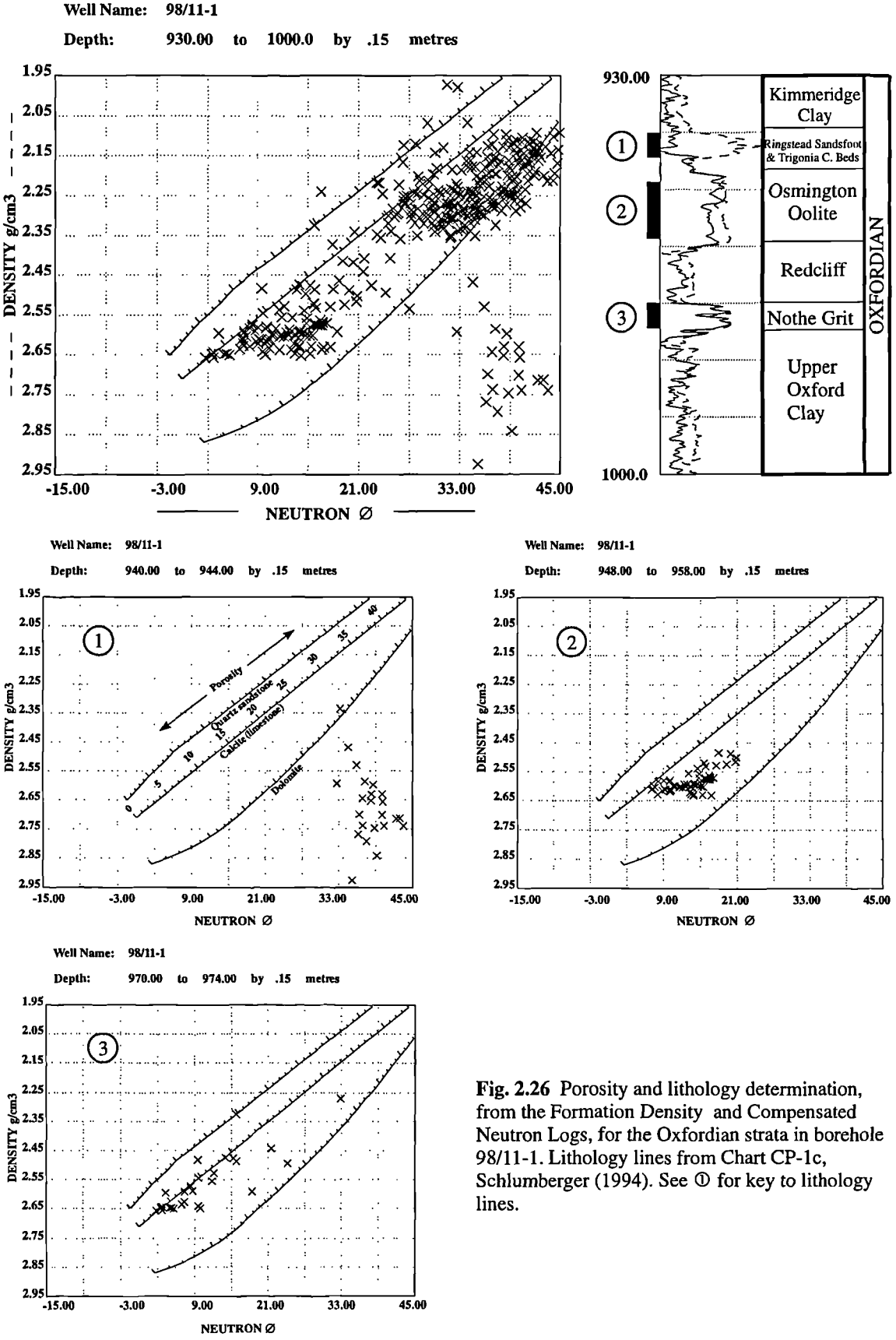

Fig. 2.26 Porosity and lithology determination, from the Formation Density and Compensated Neutron Logs, for the Oxfordian strata in borehole 98/11-1. Lithology lines from Chart CP-1c, Schlumberger (1994). See ① for key to lithology lines.

The Red Beds Member (part of the Trigonia Clavellata Beds Formation; Fig. 2.20) is composed of alternations of shelly oolite set in an argillaceous matrix, and sideritic limestones (Coe 1995). These sideritic limestones have a high density so show up as a high density peak which can clearly be seen in the field density log, the 98/11-1 borehole and the Winterbourne Kingston borehole (Fig. 2.20). The Red Bed member can also clearly be seen on a density/neutron cross plot (Fig. 2.26).

2.6.2 Kimmeridge Clay Formation.

Figure 2.27 shows the comparison between the processed field density log for the Dorset coast (filtered density log of Fig. 2.21) against the nearby Encombe 1 borehole, and the Bletchingley 1 and Detention 1 boreholes in the Weald Basin (Fig. 2.1). The general trends and the character of all of these logs is remarkably similar. The four high peaks which straddle the *pectinatus* to *hudlestoni* zonal boundary in both the outcrop density log and Encombe 1 log represent more carbonate-rich cementstone beds. The distinctive increase in density seen in all the logs at the top of the lower third of the *hudlestoni* Zone represents a change at outcrop from interbedded organic-rich and organic-poor mudstones to a thick calcareous mudstone. Similar lithological changes are interpreted to occur in the borehole sections.

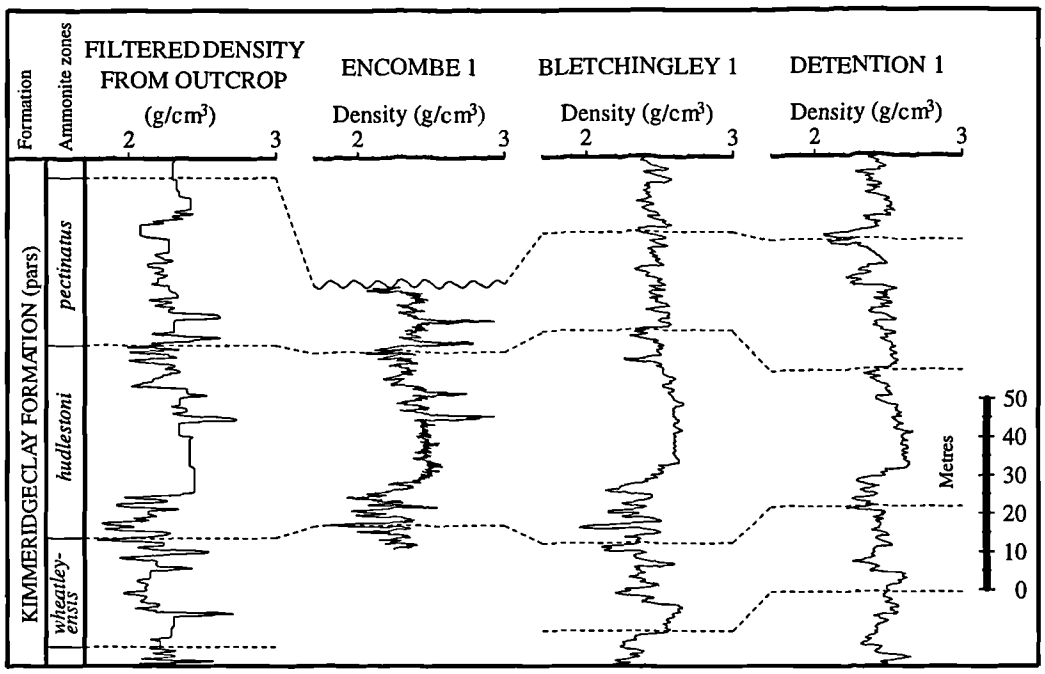

Fig. 2.27 Detailed comparison of the density log for part of the Kimmeridge Clay Formation produced from rock specimens (see Fig. 2.21) and wireline density logs from the nearby Encombe 1 borehole and Bletchingly 1 and Detention 1 boreholes in the Weald Sub-basin. See Fig. 2.1 for location of boreholes and outcrop sections.

Using the methodology described in Section 2.4.2 the correlation coefficient for the outcrop density log and the wireline density log from the Encombe 1 borehole is 0.93 (Fig. 2.28).

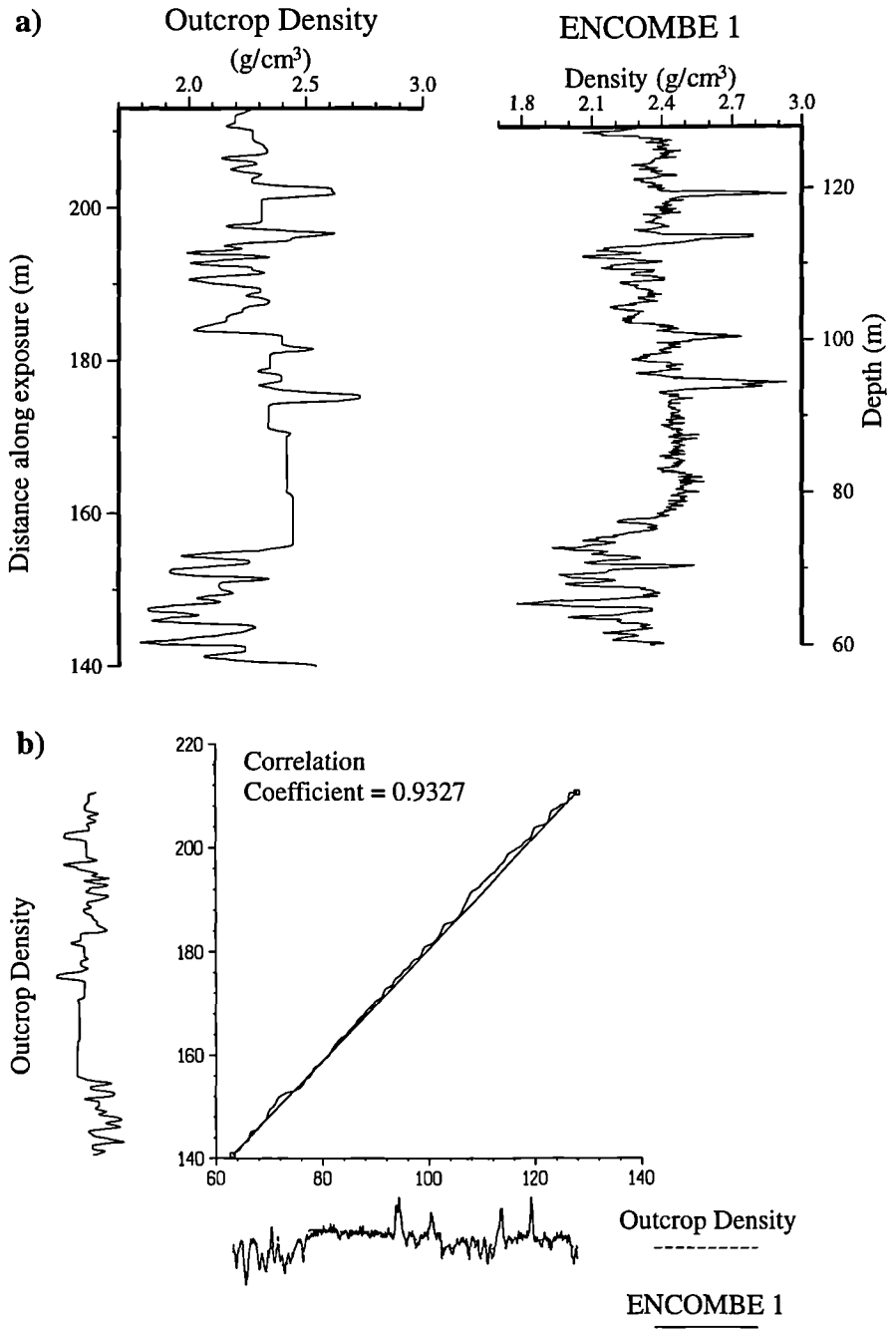

Fig. 2.28 The correlation coefficient between the outcrop density log and the wireline density log from the nearby Encombe 1 borehole, calculated using the CORPAC program. **(a)** The intervals of the field density log and the wireline density log from the nearby Encombe 1 borehole, over which the correlation coefficient was calculated. See Fig. 2.27 for ammonite zones. **(b)** The correlation coefficient of the two logs is 0.9327. See Fig. 2.1 for location of the Encombe 1 borehole.

2.7 Discussion

The results of this chapter clearly show that both techniques developed and used to correlate surface exposures with wireline data work very well. The gamma-ray data recorded at outcrop (in particular the spectral gamma-ray data), as will be seen in Chapter 6, can also be used to infer variations in sediment supply and climate during deposition as well as being used for surface to subsurface correlation.

The reason the spectral data were not used to correlate the surface exposures with wireline data in this study was simply due to the fact that no spectral data have been recorded over the Upper Jurassic interval in any of the wells available in this study. There are two reasons for this; firstly, wireline spectral sondes were not introduced until the early 1980's and most of the onshore wells in the study were drilled prior to this date. Secondly oil companies usually only run the full suite of logs over the reservoir interval (or suspected reservoir interval), whilst just running the standard suite of the logs (gamma-ray, density, sonic, resistivity) over the entire well interval. The spectral gamma-ray curves would be more useful than just the total gamma-ray for the correlation of outcrops with wireline data. If a particular bed showed a high concentration of either potassium, uranium or thorium, then that bed could be correlated more easily using the spectral curves than just the total gamma-ray curve because the high concentration of either potassium, uranium or thorium may well be masked in the total gamma-ray reading. For example, the high uranium peaks seen in Figure 2.9 above the Cattle Ledge (bed 39) and above Fresh Water Steps Stone Band (bed 49) are both masked in the total gamma-ray curve. Whilst it was unfortunate that spectral curves could not be fully utilised in this study it is hoped that the data (Appendix B) will be of use in the future when wireline spectral data are recorded over the Upper Jurassic interval.

It has been shown that the construction of the field density log is a quick and easy method of correlating surface exposures and wireline data. Because samples are usually routinely collected during sedimentological field studies for thin sections and/or geochemical analysis, the simple task of measuring the density of the samples makes this a viable technique for any surface to subsurface study. This technique could also be used to tie core and wireline data in boreholes.

Burst (1969) showed that the density of shales gradually increases with depth, particularly at depths greater than 5000m. Therefore if this method of producing a field density log was used to correlate shales which were at a depth greater than 5000 m, the field log would have to be corrected for this increase.

2.8 Conclusions

1. The geoMetrics GR310 and Exploranium GR320 gamma-ray spectrometers can both be used to produce field gamma-ray logs which are comparable with borehole gamma-ray wireline logs. Whilst the newer Exploranium GR320 is more accurate and can be used to gather spectral data more quickly the geoMetrics GR310, the older geoMetrics GR310 does produce excellent data with repeatable and comparable gamma-ray trends. The geoMetrics GR310 is more portable making it easier to use in the field. The most comparable signal between hand-held spectrometers and wireline log tools is produced by using the hand-held spectrometer perpendicular to the bedding and by using a sample spacing of 30 cm or less.

Field gamma-ray logs produced for the Kimmeridge Clay Formation can be used to positively correlate, down to at least bed group scale (typically 10 m), with wireline gamma-ray data from nearby boreholes. Larger features can also be correlated with boreholes as far as 170 km away in the Weald Sub-basin (see Chapter 6). Field gamma-ray and wireline gamma-ray data for the Oxfordian show similar trends but complex local variations in lithology may be misleading. An appreciation of the sequence stratigraphical interpretation (i.e. the metre scale cycles) considerably aids the correlation (see Chapter 5).

2. Small rock samples from outcrop or core can be used to produce a field density log. Some mathematical processing of the data is required to produce a signal which is directly comparable with the wireline tool.

Excellent results comparable with the wireline signature were obtained for a thick succession of interbedded organic-rich and organic-poor mudstones and cementstones (Kimmeridge Clay Formation). Where the lithology varies more widely and shallow-marine sandstones and limestones (e.g. Corallian Beds) are present, it is necessary to take into account the differences in porosity between the borehole and outcrop section and apply a further correction factor to the outcrop density data.

The measurement and processing of the physical characteristics of rock exposures to produce a wireline log signature is invaluable in the understanding of boreholes where core is not available. The data can be readily used to supplement and enhance conventional correlations between boreholes, and boreholes and outcrop.

CHAPTER 3

Wireline Correlation Methods and Techniques

3.1 Introduction

This chapter describes the methods and techniques used to produce the sequence stratigraphical wireline correlations seen in Chapters 5 and 6. It includes a discussion about the quality of the wireline data set (Section 3.2), methods of enhancing the wireline logs trends in order to make the sequence stratigraphical interpretation more accurate (Section 3.3) and the actual wireline correlation techniques used (Section 3.4).

The importance of biostratigraphical data in sequence stratigraphical interpretations of wireline logs is also discussed (Section 3.5), as well as the wireline lithology determination technique used in this study (Section 3.6).

3.2 Quality control of the wireline data set

The first stage in the interpretation of the wireline data for the full suite of logs from all the boreholes in this study was to examine them for artefacts in the data which might have an effect on the final interpretation of the data.

The oldest wireline data set came from Henfield 1 borehole which was drilled in 1936, and the newest data set was from 98/11-4 which was drilled in 1987. In general, the older the wireline data the poorer the resolution of the wireline curves. For example, Figure 3.1 shows the wireline gamma-ray logs from Arreton 1 and Arreton 2, which were drilled in 1952 and 1974, respectively. This figure clearly shows that the newer data have a much lower amplitude character which is probably due to the change in gamma-ray detector technology in the late 1950's when scintillation detectors were introduced. Early gamma-ray logs were made with very inefficient ionization chambers and Geiger-Mueller detectors (Frank 1986). This lack of low amplitude character makes picking bed boundaries less accurate on the older wireline logs. However, Figure 3.1 also shows that the increasing and decreasing gamma-ray trends seen on the older log are the same as

those seen on the newer log. Trends seen on the gamma-ray log are of more importance than accurate bed detection in sequence stratigraphical interpretations, so the older logs were used with confidence in this study. The importance of wireline log trends in wireline sequence stratigraphical interpretations is discussed in Chapter 4.

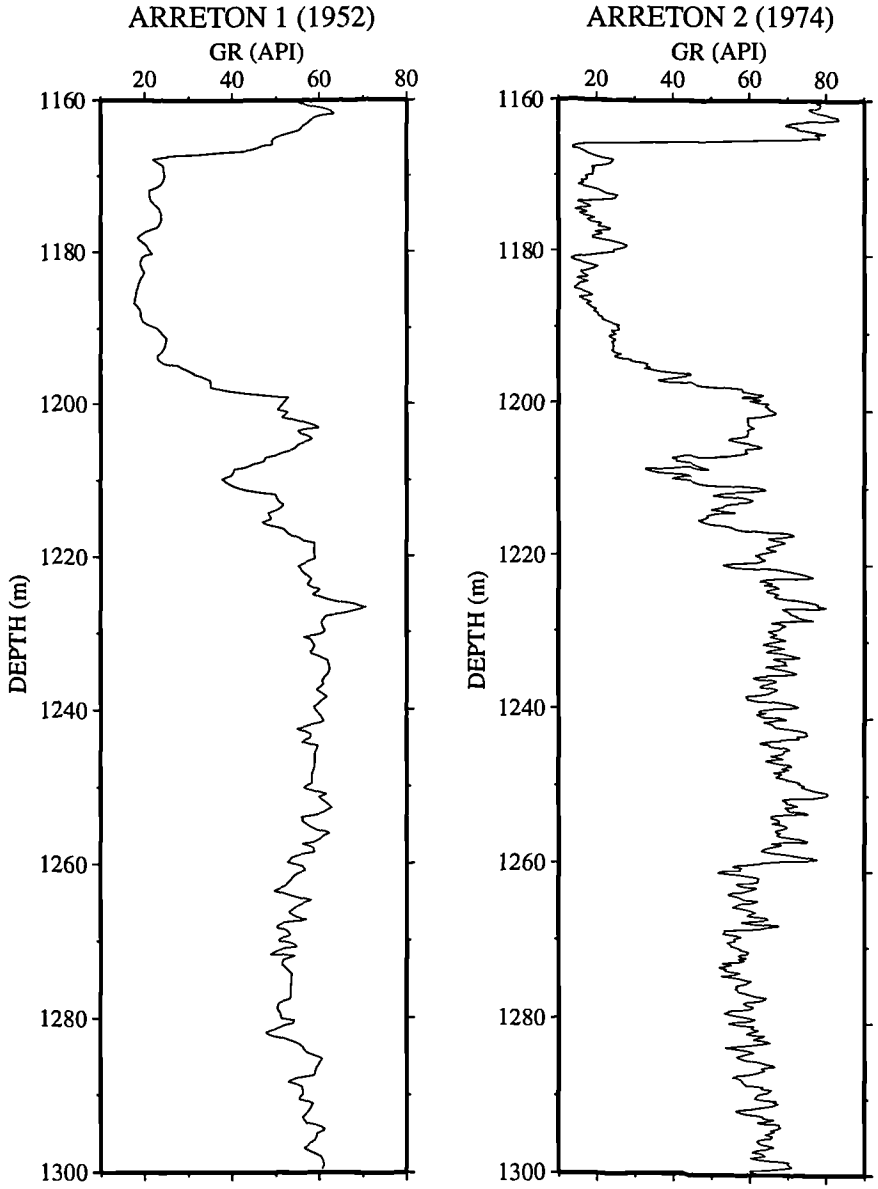

Fig. 3.1 Comparison of wireline gamma-ray logs recorded in 1952 (Arreton 1) and 1974 (Arreton 2).

A common logging artefact seen on some wireline logs is caused when the wireline sonde gets stuck in a borehole during recording, while the tool is being pulled up the hole. The tool is generally only stuck for a short time, being released when the tension in the logging cable becomes too great. At this point the tool shoots up the borehole until the tension in the logging cable is back to normal. Whilst the tool accelerates up the borehole very few, if any, data values are recorded, resulting in a straight line. In the wireline log

industry this is generally known as 'stick & pull', three examples of which can be seen in Figure 3.2. The wireline data from Detention 1 show 'stick & pull' in the gamma-ray and sonic logs at a depth of 400 - 410 m. However, this artefact is not seen on the density and neutron logs because the gamma-ray and sonic were recorded during a separate logging run, and obviously the tool string did not get stuck while the density and neutron were recorded.

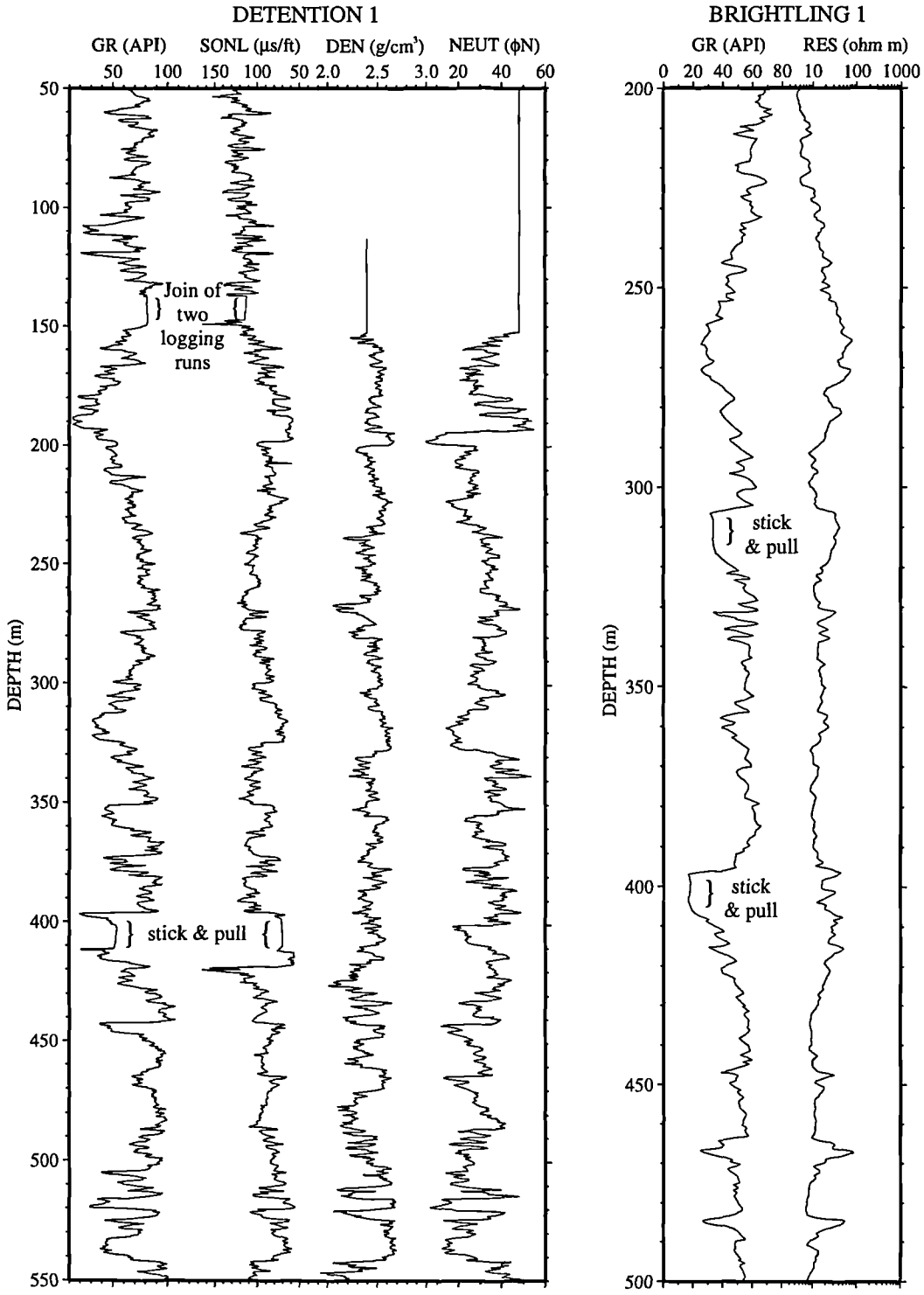

Fig. 3.2 Diagram showing features looked for during the quality control of the wireline data set.

Another common artefact which is seen on wireline data is caused when the wireline data from the various logging runs are spliced (combined) to form one composite wireline data set for the entire well. Logging runs are generally made in the open hole prior to casing the borehole. If there is not enough overlap between the first and second logging runs then gaps in the data occur, as can be clearly seen in Figure 3.2 in the Detention 1 borehole at a depth of 140 m. In some cases the effect of the casing shoe (the end of the casing pipe) can also be seen on the logs. Figure 3.3 shows the effect of the casing shoe on the calliper, gamma-ray and sonic logs from 98/11-3. The high calliper reading, indicating a large borehole, seen below the casing shoe is caused by the drilling muds scouring out the borehole as is comes out of the casing, know as 'washout'. In areas of large washout, whether they are below the casing or not, the wireline data from most wireline sondes will be poor, especially for pad devices (i.e. electrical tools) which make contact with the borehole wall.

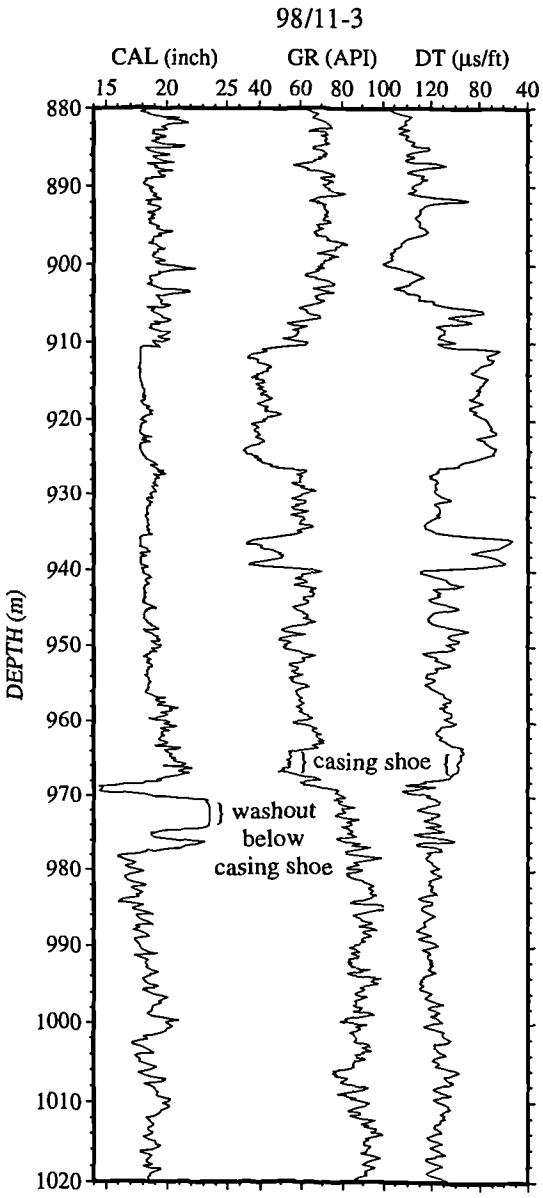

Fig. 3.3 Diagram showing artifacts caused on the wireline data in some cases when two logging runs are spliced together.

3.3 Wireline log manipulation

3.3.1 Introduction

The recognition of trends is important in sequence stratigraphic interpretations of wireline data (see Chapter 4), so various techniques have been developed which try to enhance the trends seen in the wireline data.

3.3.2 Change of scale

One of the simplest things which can be done to enhance the trends on the wireline data is to change the scale, and extend the horizontal axis of the plot in relation to the vertical axis. For example, the standard scale for gamma-ray logs is 0-100 or 0-150 API (Rider 1996). Just by changing the horizontal gamma-ray scale so that the range is defined by the minimum and maximum values has the effect of enhancing the trends seen on the curve. For example, in Figure 3.4 the first log shows the gamma-ray curve on a scale of 0-150 API, whereas in the second log the scale has been changed to 10-85 API. Figure 3.4 also shows that trends can be greatly enhanced by expanding the horizontal axis more than by just changing the scale.

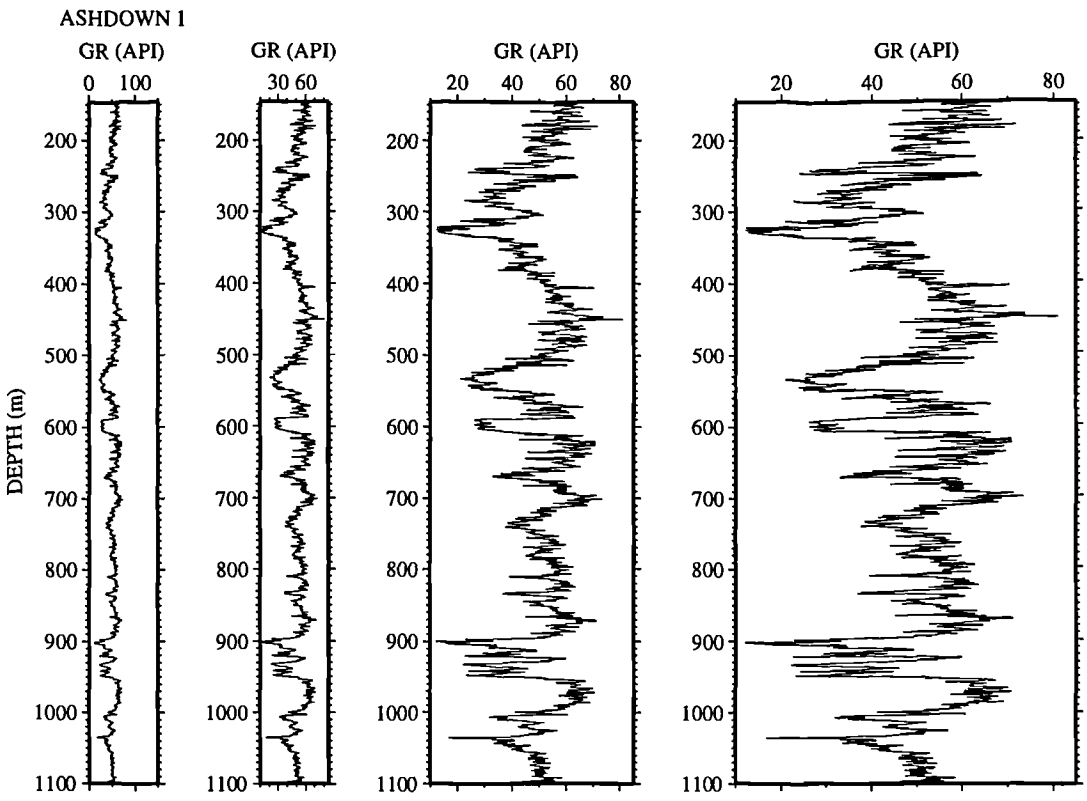

Fig. 3.4 Diagram showing that just by changing the gamma-ray scale and by extending horizontal thickness of the plot the trends seen on the gamma-ray log, for the whole of the Upper Jurassic in the Ashdown 1 borehole, can be significantly enhanced.

Doveton (1994b) showed that by plotting induction logs in both resistivity form and the original conductivity recording, the reciprocal relationship between resistivity and conductivity causes a marked contrast in the scaling of measurement units and emphasises the different bed types, even though the traces show the same physical measurement. Figure 3.5 shows the resistivity and conductivity for part of the Upper Jurassic succession in 98/11-1. The higher resistivity beds are subdued in the conductivity logs whilst the lower resistivity beds are enhanced in the conductivity log.

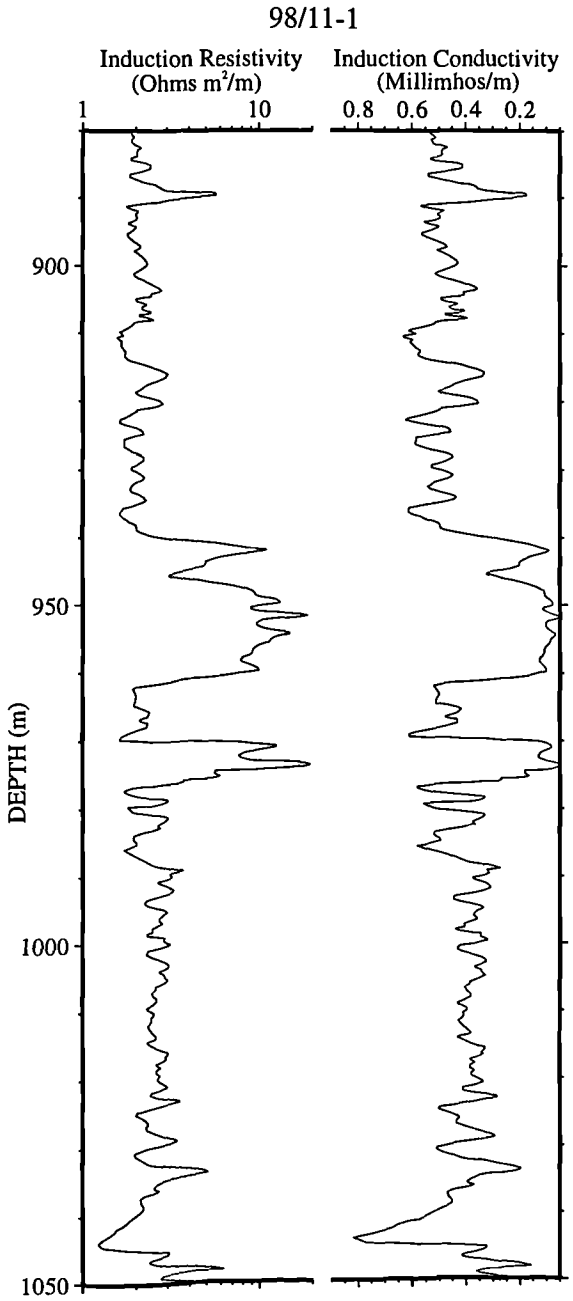

Fig. 3.5 The same induction curve plotted on different scales. The induction resistivity is the reciprocal of the induction conductivity.

3.3.3 Simple mathematical transforms to enhance wireline log trends

It was observed, in this study, that by raising the data values on logs by successive powers and re-scaling the plot, the trends seen on the logs were enhanced more than by just re-scaling the plot as described in the previous section. Power transforms tend to emphasise the higher than average values in the log, while suppressing the lower values (Fig. 3.6). Square roots and higher negative powers also enhance the trends. They are the opposite of power transforms in that they emphasise the lower than average log values, whilst suppressing the higher values (Fig. 3.6). Either of these two techniques can be used to good effect depending on what the analyser is looking for. For example, power transforms of the gamma-ray log are good for enhancing clay rich intervals whilst root transforms are good for intervals of low radioactivity such as limestones and sandstones. Although the example shown in Figure 3.6 only shows a gamma-ray log, this technique can be used for all the wireline logs.

Robinson (1975) also observed that power and root transforms were useful for wireline correlation. He suggested that the first derivative and second derivative of a log could be useful in correlation. Figure 3.7 shows the first and second derivative for the gamma-ray log from the Ashdown 1 borehole. The first derivative of a log with respect to depth is a continuous profile of log slope which oscillates between positive and negative values. The zero crossing of this profile marks positions at which the original log shows the extreme of either a peak or a trough feature (Doveton 1994b). The second derivative measures the rate of change of slope, and when plotted as a continuous function also varies between positive and negative values, with zero crossings at positions of curve inflection on the original log (Doveton 1994b). Normally, depth boundaries of subsurface zones are picked at inflection points on logs. The second derivative of a log therefore provides an automatic zonation device where the depths of zone boundaries are marked at zero crossing points. Both the first and second derivative curves produced in this study (Fig. 3.7) are very busy, so the original gamma-ray curve was smoothed using a low frequency bandpass filter (see Section 3.2.4) to remove variations at wavelengths of 6 and 10 metres, respectively (Fig. 3.7).

The second derivative curves for the filtered gamma-ray logs (Fig. 3.7) show a ringing effect at wavelengths just below the cutoff. Differentiation has the effect of multiplying the amplitude spectrum by the wave number k, so the second derivative curve has an amplitude spectrum multiplied by k^2 compared to the low-pass filtered log. This results in a peak in the amplitude spectrum just below the cutoff taper, which is manifested as ringing on the second derivative curve.

The derivative curves were not routinely used in this study because they remove the trends seen on the curves which are important in sequence stratigraphical interpretation of wireline logs. Doveton (1994b) described a colour image transformation technique

which uses the derivative curves to discern shapes and trends seen on the log. Doveton (1994b) also suggested that derivative logs can be useful in correlation as a measure of bed frequency, provided that the noise error of the nuclear logs is first suppressed by smoothing.

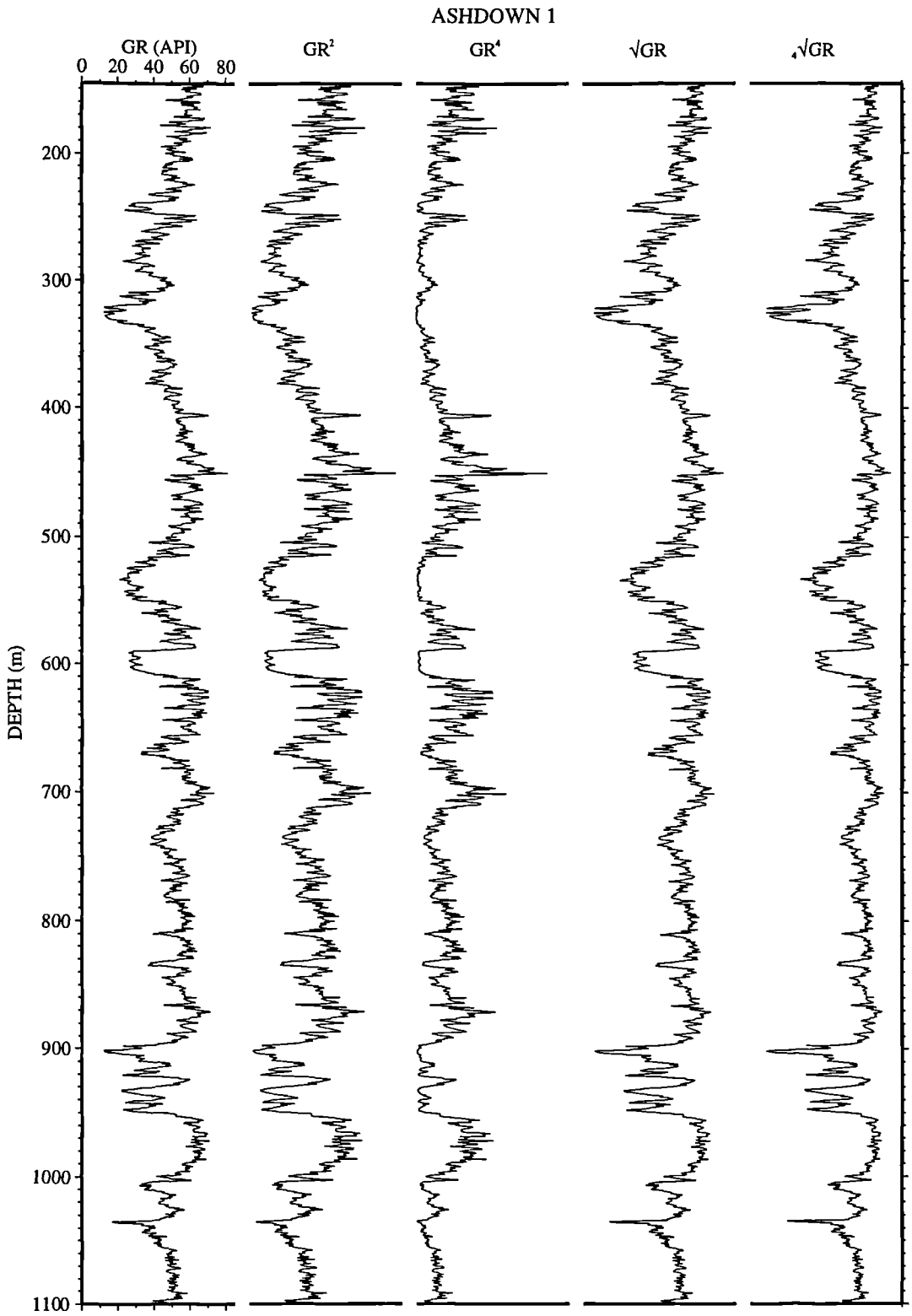

Fig. 3.6 Effect of simple mathematical transforms (power and root) on the shape of the gamma-ray log.

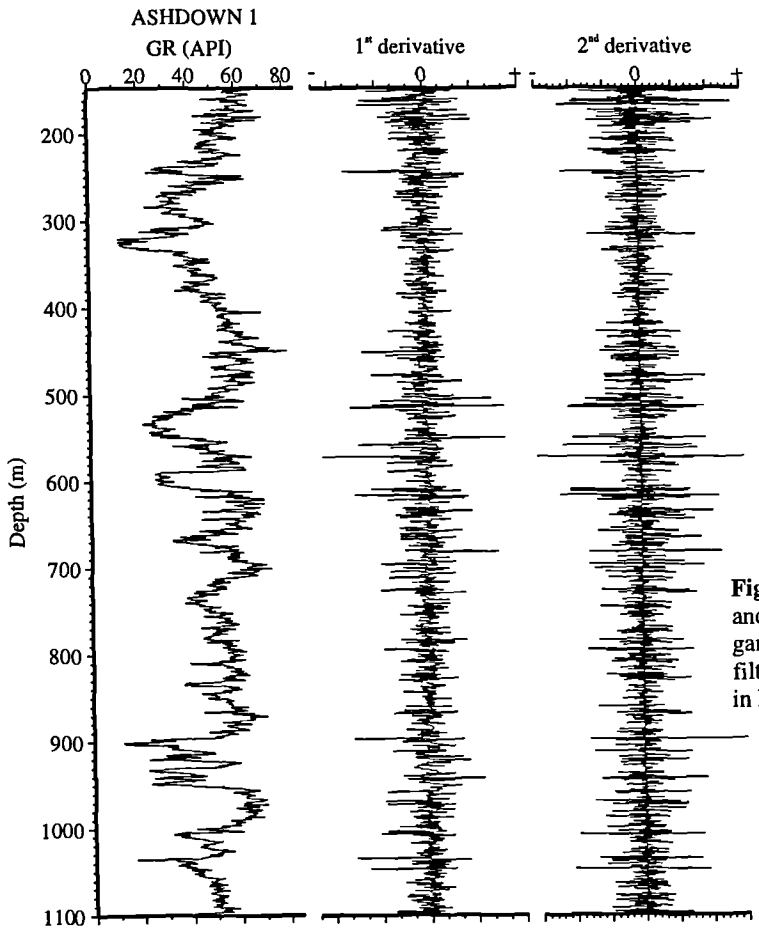

Fig. 3.7 Figure showing the 1st and 2nd derivative of the total gamma-ray log and two of the filtered gamma-ray logs shown in Figure 3.8.

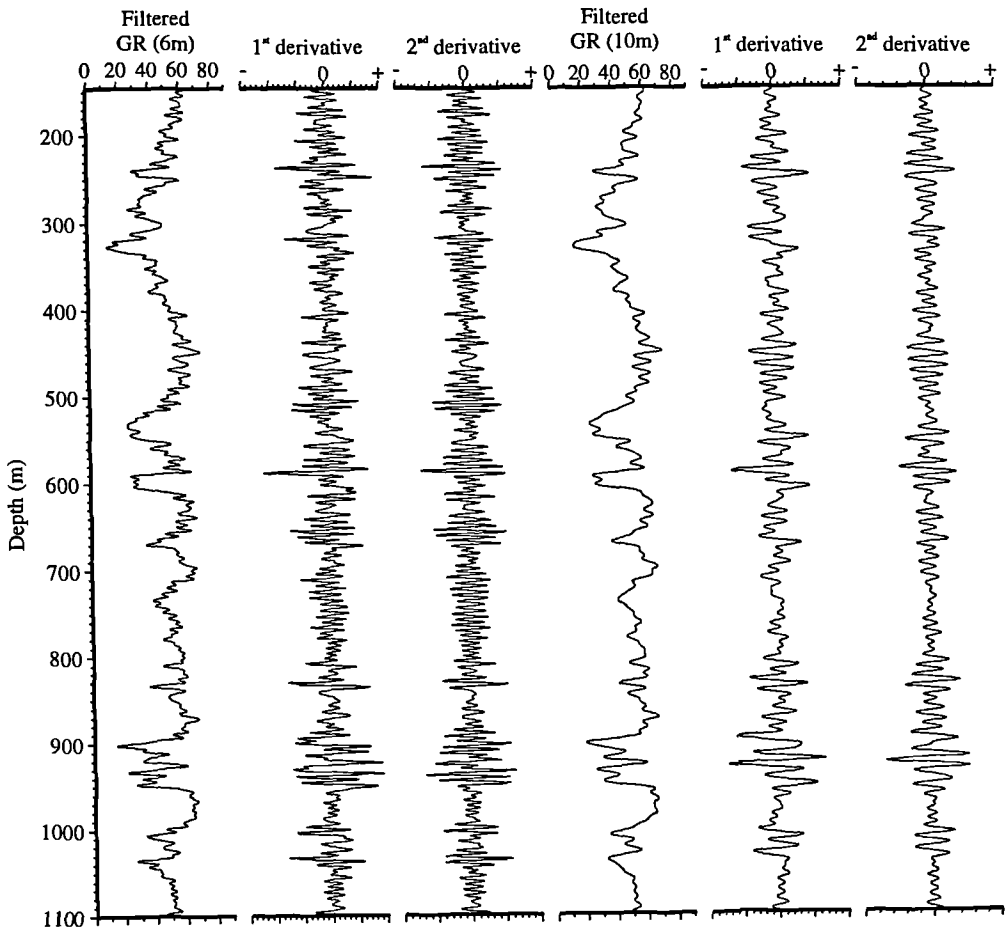

3.3.4 Filtering logs

Melnyk *et al.* (1994) showed that filtering wireline gamma-ray logs with a low-frequency bandpass filter enhanced the correlatability of low frequency cyclic components within the log. They suggested that the cyclicities were related to stratigraphic phenomena at the sequence and parasequence scale (>> 10 m in thickness and >> 100 ka in duration). Figure 3.8 shows six examples of low-frequency bandpass filters, each removing the variations at successive wavelengths of less than 2m, 4m, 6m, 10m, 15m, and 20m, respectively.

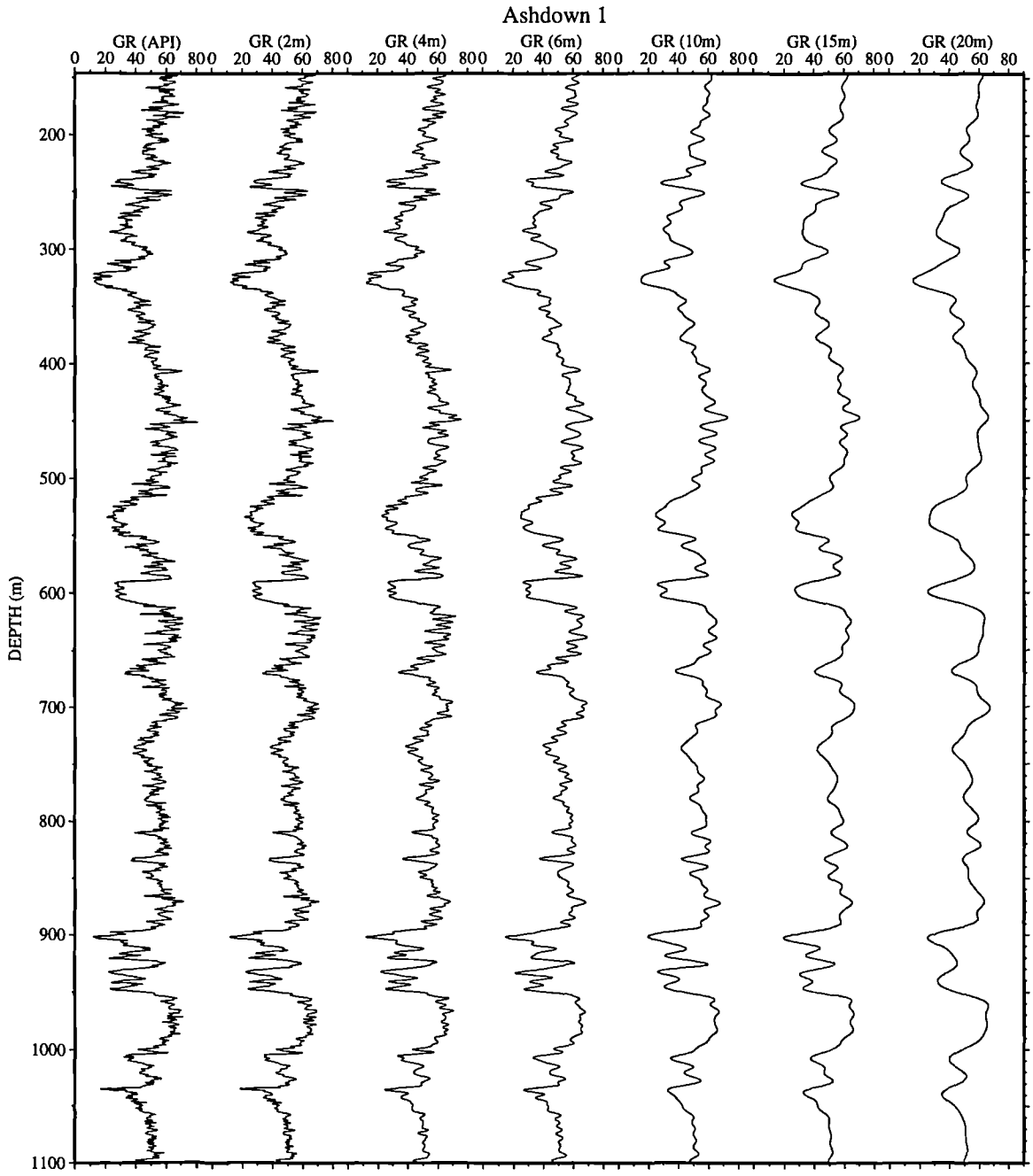

Fig. 3.8 Low-pass filtering of the wireline gamma-ray log from Ashdown 1 borehole. The filter removes variations at wavelengths of less than the cutoff value shown in header above each curve.

The low-pass filter clearly makes the curve less busy, by removing the short-wavelength fluctuations, making the log easier to correlate and to interpret the logs in terms of trends (Fig. 3.8). However, the filter does have the effect of reducing the vertical resolution of the curve, which results in less accurate detection of the key sequence stratigraphic surfaces or ammonite zones. Therefore routine filtering of the logs in this study was not carried out, but was used in several instances when correlating parts of the Upper Jurassic succession which have a busy wireline character and lack any distinctive wireline marker horizons, such as the Lower Kimmeridge Clay succession.

3.3.5 Normalising curves and adding them together

The various wireline logs measure different physical properties of the rocks in the subsurface, so no two wireline curves are the same because they measure different physical properties. Because of this, different wireline curves have been added together to see if the new curves were better for sequence stratigraphic interpretations. The scale of each log varies, so each curve was normalised (put on a scale of 0 to 1) prior to being added to other curves. Figure 3.9 shows the gamma-ray, neutron and density curves from the Marchwood 1 borehole and the new curves which have been generated by adding the original three curves together in different ways. These new curves do in some cases enhance certain features within the Upper Jurassic succession. However, this technique was not routinely used because it was hard to imagine what the curves were showing geologically.

3.4 Wireline log correlation techniques

3.4.1 Introduction

Wireline correlations are still generally done manually because stratigraphic correlation is full of ambiguities and requires pattern recognition skills with geological understanding. Because the correlation of wireline logs is usually a laborious manual process, and because correlations of a set of logs made by several geologists often differ substantially, automated correlation methods have been developed (Matuszak 1972; Rudman & Lankston 1973; Mann 1979; Shaw & Cubitt 1979; Martinson *et al.* 1982; Wu & Nyland 1987; Fang *et al.* 1992; Olea 1994). Doveton (1994b) suggested that the change over from manual to automated correlation is only a matter time, for much the same

reasons that automated contouring has made such substantial inroads into manual contouring.

In this section, a discussion on which wireline curves are the most useful for correlation of the Upper Jurassic succession is given (Section 3.4.2) as well as descriptions on the manual correlation techniques used in this study (Section 3.4.3) and the automatic computer correlation programs used (Section 3.4.4).

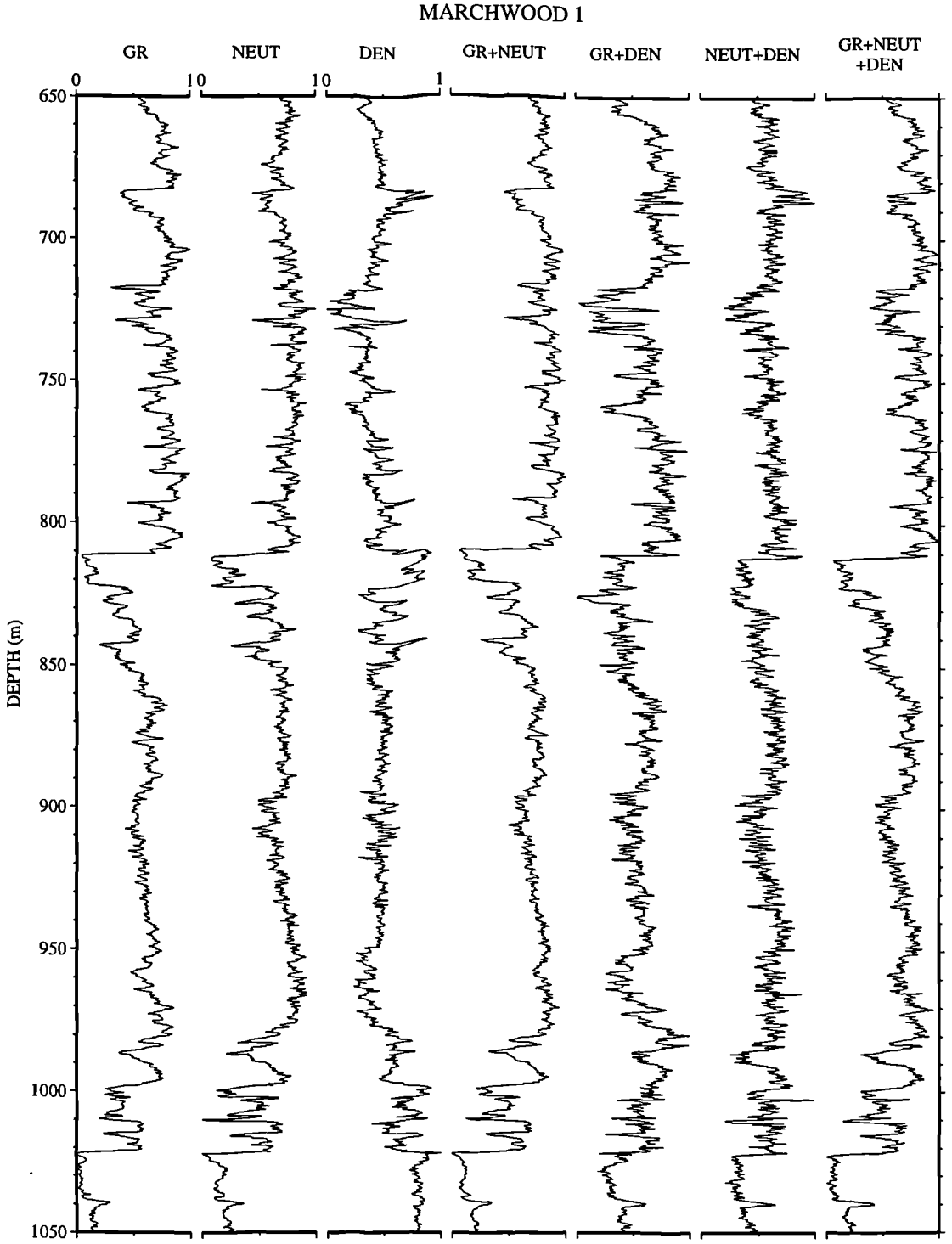

Fig. 3.9 The gamma-ray, neutron and density logs from the Marchwood 1 borehole have been normalized (put of a scale of 0 to 1) and the added together.

3.4.2 The most useful wireline log for correlation of the Upper Jurassic succession

The best wireline log for the correlation of the Upper Jurassic of the Wessex Basin is the gamma-ray log. This is so for several reasons. Firstly, out of all the digital wireline data sets from the boreholes used in this study only four did not contain a gamma-ray log, making it the most common wireline log in the whole data set. Secondly, the field gamma-ray log has more character than the field density log (see Chapter 2), so the field gamma-ray log was chiefly used to tie the surface outcrops to the sub-surface wireline data set. Thirdly, the gamma-ray log is a recording of the natural radiation emitted from rocks and is not generally affected by the fluids contained within the pores.

Even though the gamma-ray log was the main correlation log, all the wireline curves were used during the correlation procedure, because certain logs detect different physical properties. The full suite of logs from the 98/11-1 borehole can be seen in Figure 3.10. This figure shows two different beds, marked A and B, which are only detected on certain logs. For example, bed A is a siltstone layer within the Lower Kimmeridge Clay which shows up more clearly on the resistivity logs and sonic logs than on the other logs because it has higher porosity than the surrounding clays. Bed B is the Osmington Mills Ironstone Member which shows up clearly on the density log due to the presence of phosphatic nodules, iron ooids and siderite cement. However, it does not show up clearly on the gamma-ray log because its natural radioactivity lies between those of the underlying Osmington Oolite Formation and the overlying Lower Kimmeridge Clay.

Figure 3.10 also shows that the resistivity log (MSFL - micro-spherically focused log) has the best vertical resolution (i.e. can detect very thin beds), whilst the self potential log (SP) has the worst vertical resolution.

A good example showing why the SP and resistivity logs were not used as the main correlation logs can be seen in Figure 3.11. This figure shows that to make a correlation using the SP and resistivity logs between these two wells, which are both in the Weald Sub-basin, would be very hard because neither has much character over this Oxfordian interval. Another reason why the resistivity logs were not used as a the main correlation curve is because they are influenced by changes in formation pressure and interstitial water salinity (Rider 1996), both of which vary in different parts of the Wessex Basin.

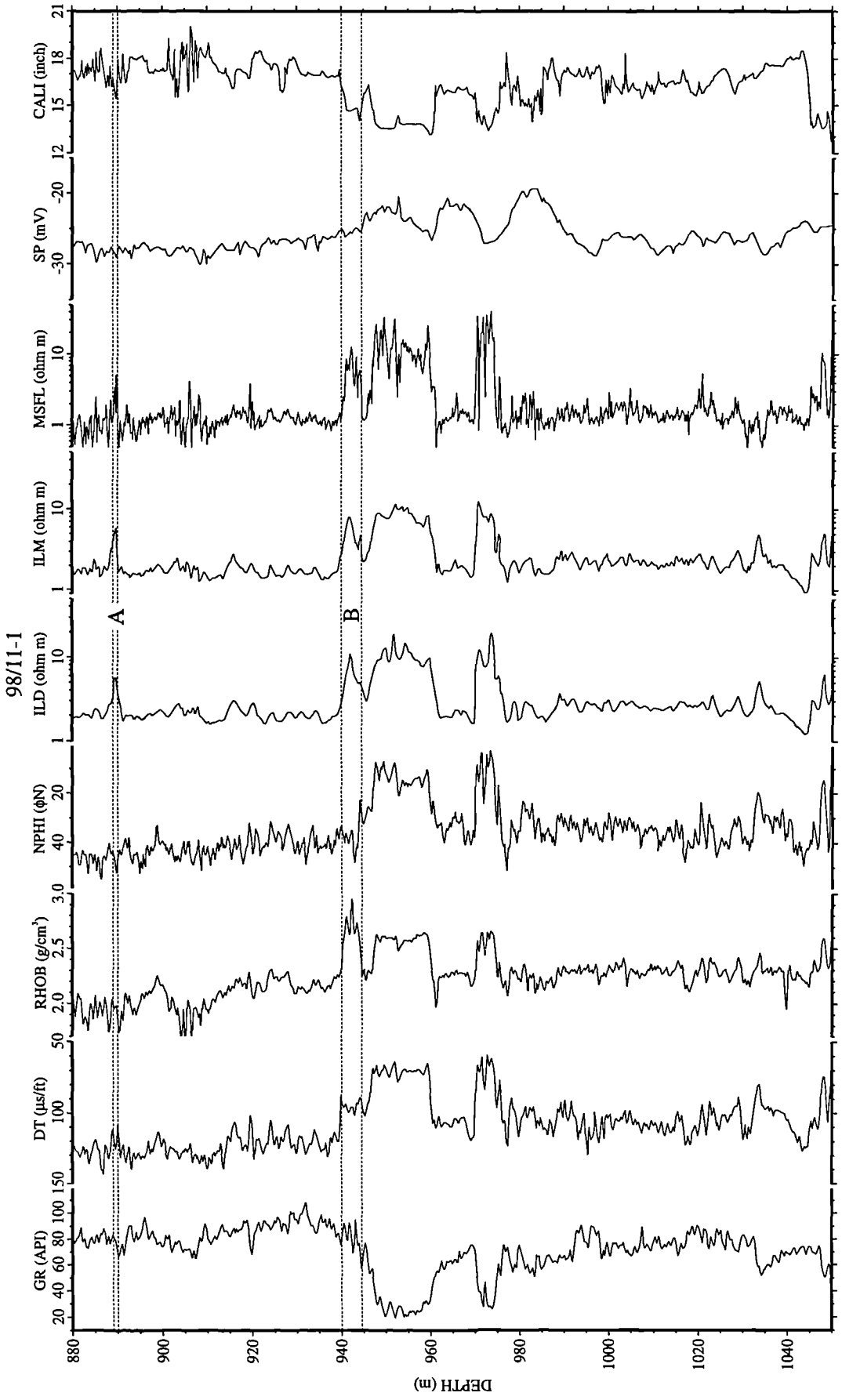

Fig. 3.10 The full suite of wireline logs from the 98/11-1 borehole. The gamma-ray log has proved to be the most suitable log for the correlation of the Upper Jurassic of the Wessex Basin. Bed A is only clearly seen on the resistivity logs (ILD & ILM). Bed B is not detected on the gamma-ray (GR), neutron (NPHI) or self potential (SP) logs but is seen on the rest of the logs even the caliper (CALI).

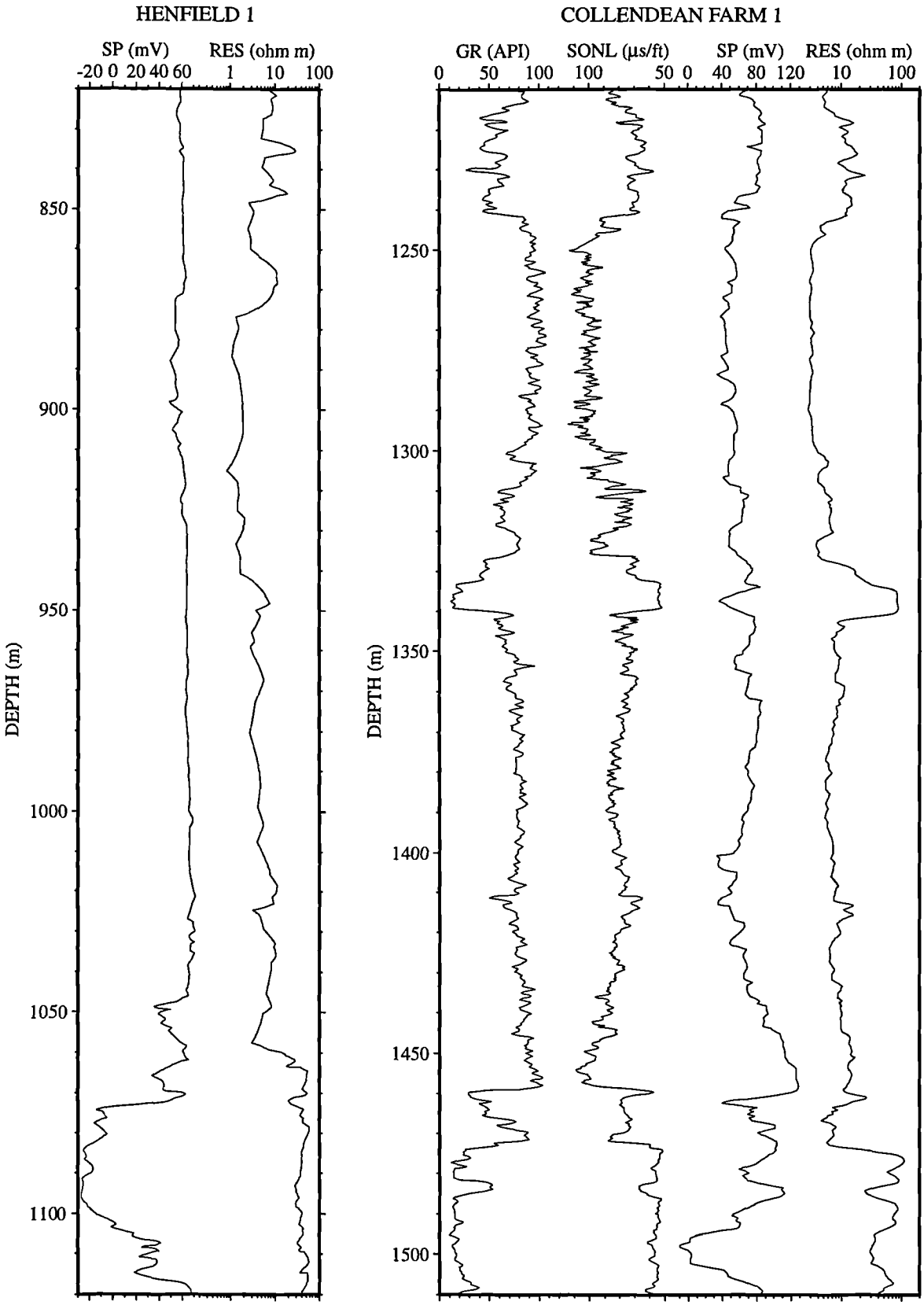

Fig. 3.11 Diagram showing the wireline logs for the Oxfordian succession in Henfield 1, drilled in 1936, and Collendean Farm 1, drilled in 1964. The diagram clearly shows that correlating this Oxfordian succession using the SP or resistivity logs is difficult.

3.4.3 Manual correlation

Manual wireline correlations can be done by hand on pre-selected wireline curves plotted alongside each other, or can be done using commercial oil industry wireline correlation programs. In this study the manual wireline correlations for the Oxfordian succession (Chapter 5) were done on paper correlations which were plotted using the Generic Mapping Tools (GMT) software package, whilst the manual correlations for the Kimmeridgian succession (Chapter 6) were done using the correlation module of the Terrastation II (Terrasciences Ltd.) computer package.

The Generic Mapping Tools (GMT) is a freely available software package which was designed to plot geophysical data (see Wessel & Smith (1991, 1995a) and the GMT world wide web internet site "http://www.soest.hawaii.edu/soest/gmt.html"). Most of the figures in this thesis, including all those showing wireline curves, were produced using GMT. The GMT technical reference and cookbook (Wessel & Smith 1995b) does not show any example UNIX shell scripts for plotting wireline logs, so some of shell scripts used to produce some of the figures in this thesis are given in Appendix D.

Certain techniques can be applied to the logs to make manual wireline correlations easier. For example, shading the logs on either a grey scale or a colour scale has been found to be useful in this study. Figure 3.12 shows two lines of correlation, one with and the other without shading. The human eye picks up the trends and subtle differences in wireline character better in the shaded correlation. The shading between the gamma-ray curve and the sonic curve in Figure 3.12 is based on the gamma-ray log for each of the wells in the correlation, where the highest gamma-ray reading in the interval is black and the lowest reading is white. The shading can be based on any wireline log or a combination of two of logs (Fig. 3.13). Figure 3.13a shows that the gamma-ray curve is shaded using the gamma-ray values and the sonic curve is shaded using the sonic values. The shading in Figure 3.13b on the other hand is based on the gamma-ray and sonic values (normalised gamma-ray + sonic value; see Section 3.2.5). The FORTRAN program, written as part of this study, to produce the GMT shell script which shades the logs is given in Appendix D.

Commercial oil industry wireline correlation programs contain features which are designed to aid manual correlations. For example, Terrastation II contains a wireline correlation module which allows the user to correlate wireline logs interactively, with complete control over display interval and scale. A very good feature of this module is the ability to pick up a log curve, move it over the top of another, and then stretch or compress the curve. This was very useful in this study, especially for correlating the Kimmeridgian successions found on palaeohighs and those found in the sub-basins (Fig. 3.14). Another major advantage of using the interactive wireline correlation programs is that every pick made is automatically added to a database, which makes calculating isopach thicknesses a very quick procedure.

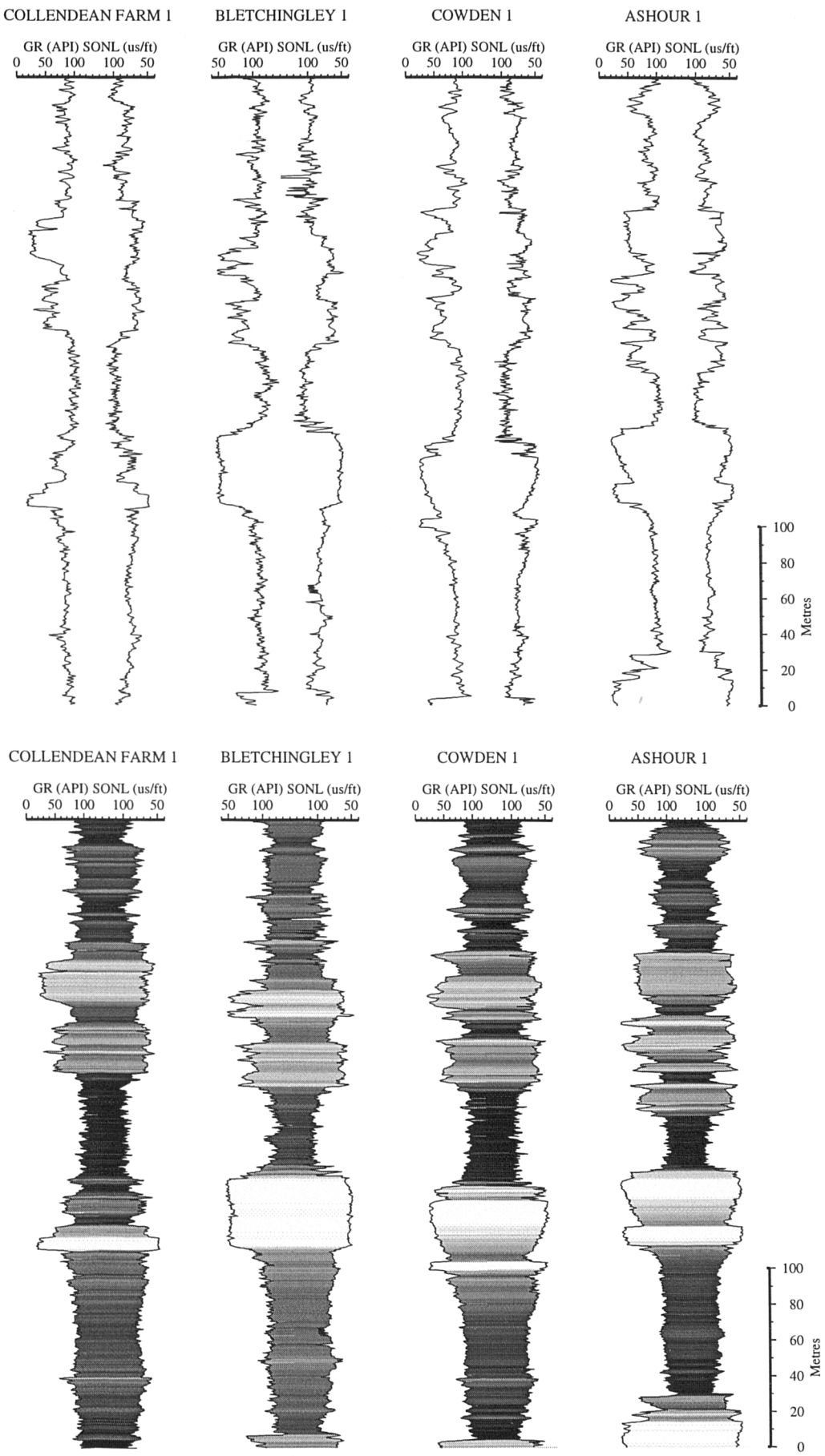

Fig. 3.12 Diagram showing that shading the wireline logs can enhance visual correlation. Subtle changes are easier to see on the shaded wireline logs than on the unshaded wireline logs.

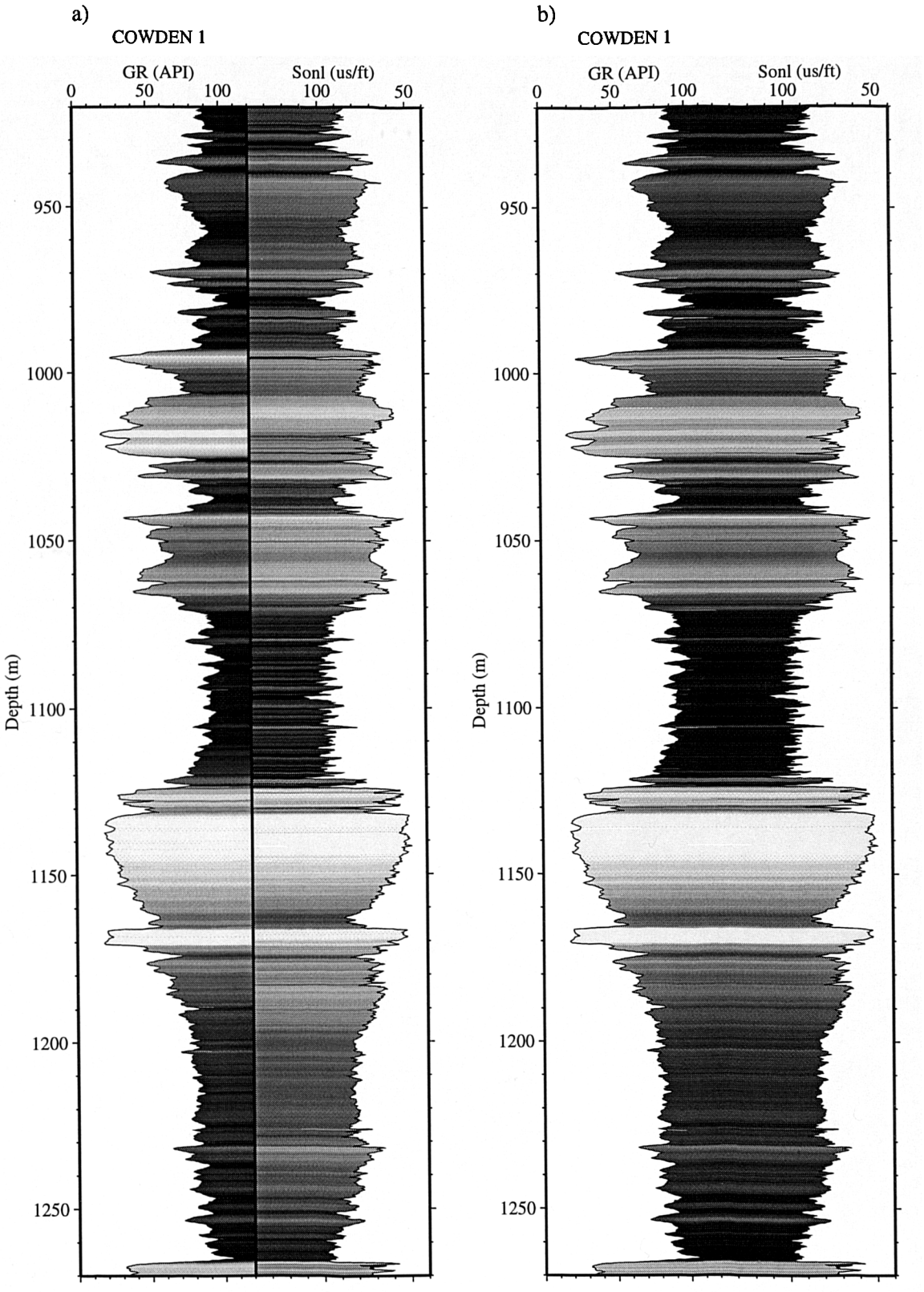

Fig. 3.13 The shading of the wireline logs can be done using any log. **(a)** The left hand side of the figure is shaded using the gamma-ray values whilst the right hand side is shaded using the sonic values. **(b)** The shading is based on the gamma-ray and the sonic curve.

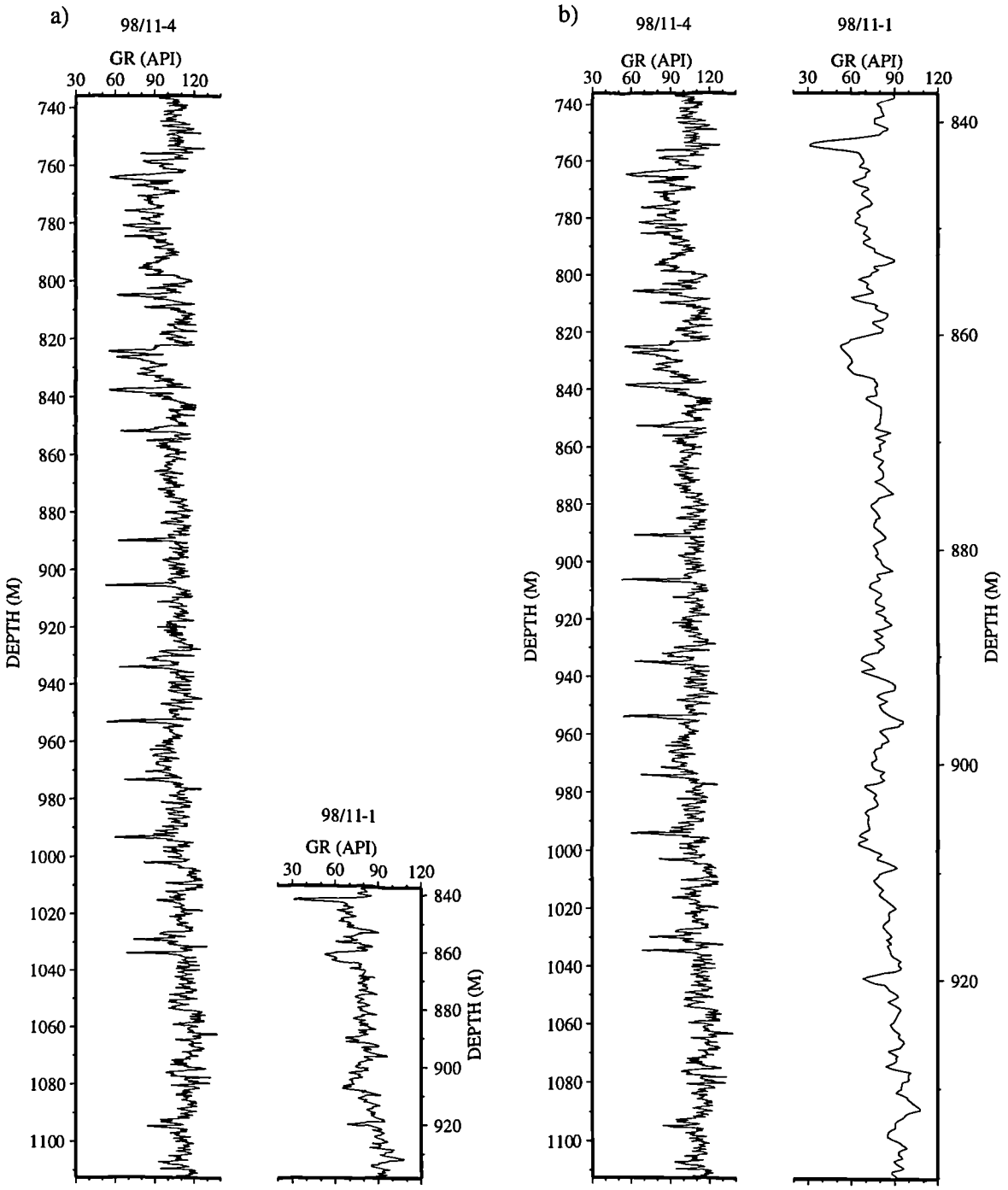

Fig. 3.14 Diagram showing the comparison of the same part of the Kimmeridge Clay Formation as seen on the gamma-ray logs from 98/11-4, which is located in the Central Channel Sub-basin, and 98/11-1, which is located on the south Dorset High. **(a)** Both logs plotted at the same scale, a correlation is difficult because the succession in the 98/11-4 borehole is over three time thicker than that in 98/11-1. **(b)** The gamma-ray log from 98/11-1 has been stretched making a correlation between the two logs easier.

3.4.4 Automatic computer correlation programs

The first automatic computer correlation programs were those used for dip log processing (Doveton 1994b). Moran *et al.* (1962) described a procedure for automatic correlation of dip curves and according to Bigelow (1987) computers were routinely used

to automatically process dip data by 1963. Dip log processing involves the correlation of four, six or eight curves recorded around the borehole wall. These curves tend to be very similar so are ideal for automatic correlation. However, the correlation of wireline log curves from different boreholes across a basin is much more complicated due to facies changes in sediments, laterally and vertically, unconformities and faults.

Doveton (1994b) described the role of computers in lateral correlation and interpolation of logs as well as describing in detail all the various automated correlation methods for wireline logs. For a very detailed bibliography of automated wireline correlation, the reader is referred to the 'Bibliography of Well-Log Applications' by Prensky (1996).

Two automatic wireline correlation computer programs were available to this study. The first was Correlator, developed and written by Ricardo Olea of the Kansas Geological Survey (Olea 1988, 1994). The second was Corpac, developed by Martinson *et al.* (1982, 1984) with software written by Globex Consulting Services, Ltd.

Correlator is an interactive program for lithostratigraphic correlation of wireline logs. The program is based on the maximization of a weighted correlation coefficient using two wireline logs per well. The results of the program presented by Olea (1988, 1994) and Doveton (1994b) look very good, but in practice the program is not very user friendly. The program was written by R. Olea for his own work in the Kansas Geological Survey and was not intended to be used by other people; hence the lack of instructions or on-line help in the program (pers. comm. R. Olea). This package was not therefore routinely used in this study. Another reason for not routinely using this software was because the version of software available would not allow output to a printer.

Corpac is a signal correlation computer program which was designed to maximize the correlation between two signals, accommodating any non-linear differences between them (see Chapter 2 for more information). Unlike Correlator, Corpac was not specifically designed for the correlation of wireline logs, so it was not routinely used in this study either. However, it was used on several occasions when manual correlation proved difficult.

3.4.5 Graphical correlation

Graphical correlation as proposed by Shaw (1964) has been modified in this study to use wireline logs instead of biostratigraphic data, for which it was intended. This simplified modification of graphical correlation which has been used for the Kimmeridgian succession (see Chapter 6) is described below. The reader is referred to the recent publication on graphic correlation edited by Mann *et al.* (1995) for more information about more conventional uses of the technique.

The Cowden borehole located in the Weald Sub-basin contains the thickest and therefore presumably the most complete, Kimmeridgian succession in the Wessex Basin and Cleveland Basin, Yorkshire. This Cowden succession was therefore chosen as the standard reference section. Boreholes from various locations around the Wessex Basin and Yorkshire have been plotted against this standard reference section in order to see visually how the Kimmeridgian succession varies across the study area.

Figure 3.15 shows three examples of how cross plotting the data aided in the correlation of the wireline logs. The line on the graphic correlation diagram represents the lines of correlation between the Cowden borehole and another borehole based on the final wireline correlation of all the curves from both boreholes. Changes of slope imply some change in relative sedimentation rates. In most cases these changes are subtle and are not readily perceived by visual comparison of the logs alone (Melnyk *et al.* 1992, 1995). A 45 degree line of correlation implies equal sedimentation rates between two sections, as can be seen in Figure 3.15a where the correlation line from the *autissiodorensis* to the top *fittoni* ammonite zones is very nearly a straight line at 45 degrees. The almost perfect correlation is possible between these two wells (Cowden and Ashour) because they lie close together in the Weald Sub-basin and are therefore very similar. The horizontal line from the *eudoxus* to the *autissiodorensis* zones, in this case, is due to the *eudoxus* Zone being cut out by a fault in the Ashour borehole (Fig. 3.15a). However, in other instances horizontal lines have been interpreted to being due to condensed sections or missing strata due to sediment starvation (Neal *et al.* 1995).

The example shown in Figure 3.15b shows the Cowden borehole plotted against the Warlingham borehole, which again lies in the Weald Sub-basin. This time the lower part of the Kimmeridgian succession has been cut out by a fault and the upper part has been eroded by an unconformity, resulting in two horizontal lines. Again the line of correlation is nearly a straight line at 45 degrees, although there is one point which is slightly off the main 45 degree line (the base of the *hudlestoni* Zone). If this is not due to any sedimentological variation between the two successions, then this would suggest that the original correlation was incorrect. In cases like this the cross-plotting technique was used to quality control the wireline correlations so the original correlation would be re-examined.

The third example in Figure 3.15 shows the thickest Kimmeridgian succession plotted against one of the thinnest full Kimmeridgian successions seen in the Marchwood borehole, which is located on a palaeohigh (Fig. 3.15c). This last example shows that the relative thickness of the ammonite zones in the Kimmeridge Clay Formation stays fairly uniform, because the line of correlation is close to a straight line. The slope of the line of correlation is less than 45 degrees which implies that the there is a lower sedimentation rate in the Marchwood succession. In general, lines of correlation tend to be straight

segments of constant gradient separated by dog-legs, implying that changes in sedimentation rate tend to be rapid. This could also be the case in this example where some dog-leg sections are evident, such as in the *elegans* Zone (Fig. 3.15c).

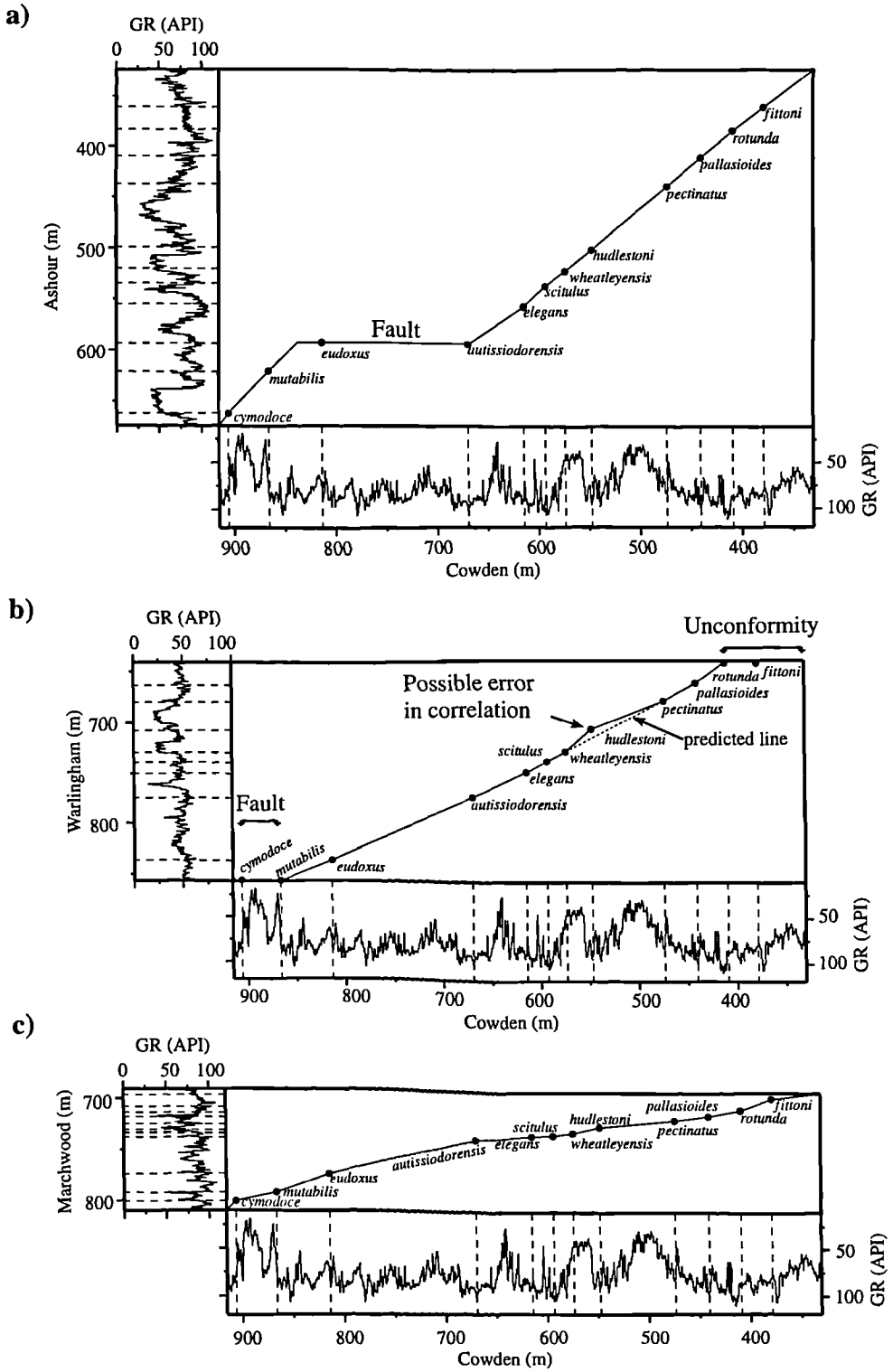

Fig. 3.15 Diagram showing the information gained from graphical correlation. **(a)** Plot showing a fault. **(b)** Plot showing a fault and an unconformity, and a possible error in the correlation. **(c)** Plot showing that even though condensed successions seen on palaeohighs are significantly thinner than successions encountered in the sub-basins the line of correlation is still fairly straight.

In Figure 3.15 only the ammonite zones have been plotted on the graphical correlations. However, in Chapter 6 the key sequence stratigraphic surfaces are plotted on the graphical correlations and the relationship between sequence stratigraphy and sedimentation rate is discussed.

A GMT C-Shell script used to generate the graphical correlation diagrams is given in Appendix D.

3.5 Biostratigraphic data and wireline correlation

Biostratigraphy and palaeoecology are very important in sequence stratigraphical interpretations because they constrain the age of stratigraphic sequences and indicate more about the nature of the environment. A number of studies have been done which show that biostratigraphic discontinuities and abundance/diversity peaks (palaeoecology) are indicators of sequence boundaries and condensed sections, respectively (Copestake 1993; Emery & Myers 1996). The use of biostratigraphy in sequence stratigraphical interpretations is out of the realm of this study so the reader is referred to Copestake (1993), Emery & Myers (1996) and references therein for more information.

Biostratigraphic data were important to this study because it formed a constraint to the sequence stratigraphic interpretation of the wireline data. Ammonites were used as the main source of biostratigraphic data because they form the basis of the primary chronostratigraphic standard for the Upper Jurassic outcrops of the United Kingdom (Cox 1990). A description of the nature and resolution of the Jurassic ammonite biozones can be found in Cox (1990) and Cope (1994). Details of the ammonite zones for the Oxfordian and Kimmeridgian can be found in Chapters 5 and 6, respectively.

The only source of ammonite biostratigraphic data from the boreholes used in this study came from core and drill cuttings. The most accurate biostratigraphic data are from boreholes which had been fully cored. The data obtained from drilled cuttings were also used in this study, but were not always adhered to because the depth associated with drill cuttings is exceedingly unreliable (North 1990). Drill cutting depths are unreliable for two reasons: firstly, cuttings are easily contaminated by material derived by caving from any part of the borehole between the drill bit and the bottom of the casing; and secondly, the journey from the bit to the shale shaker on the rig takes time, and the deeper the well, the longer the time, so the more inaccurate is the assignment of the cuttings to their proper depth (Rider 1996).

Due to the limitation of the sample size obtained from boreholes, smaller fossils, usually less than a few millimetres in diameter and as small as 4 μm, are the most widely

used in biostratigraphy (Emery & Myers 1996). Therefore, for practical and economic reasons, correlations between the ammonite zones with various microfossil groups have been developed (Cox 1990).

3.6 Lithology determination from wireline logs

The calculation of lithology from the so-called lithology logs (gamma-ray, density, neutron and sonic) was routinely done in this study in particular for the complex Oxfordian succession which consists of interbedded siliciclastic and carbonate sedimentary rocks (see Chapter 5). The wireline lithology was calculated using the Petra module of the TerraStation II software package. Petra, which stands for petrophysical analysis, calculates the relative proportions of mineral components and pore fractions of the borehole successions (Terrasciences 1996). Petra resolves the components by solving a set of linear equations defined by the input curves. For example, if density is an input curve, the following equation might be used:

$$(2.65 \times \text{Sandstone}) + (2.71 \times \text{Limestone}) + (2.5 \times \text{Shale} + 1.0) \times \text{Porosity} = \text{Bulk Density from log}$$

where the values 2.65, 2.71, 2.5 and 1.0 are the density coefficients for each component in gm cm^{-3}. Each curve used as an input generates a similar equation. One extra equation, the mass balance equation, defines the sum of the components to be unity:

$$\text{Sandstone} + \text{Limestone} + \text{Shale} + \text{Porosity} = 1$$

The log response coefficients for each component are adjusted to suit each well. This is done by looking at the lithology data available for each borehole, which are in the form of lithology descriptions from drill cuttings, side wall cores or core. Knowing for example, that a side wall core from a certain depth is limestone, cross plots are then used to find the average value for limestone from each of the wireline logs.

A reconstruction of the input curves is automatically done during the Petra operation. The reconstructed curves are created by multiplying the stored component fractions by the appropriate log response coefficients (Terrasciences 1996). The curves represent a log of the interpreted lithology according to the Petra solution. This is a good quality control feature which allows the comparison of the actual logging data and the Petra lithology solution (Fig. 3.16).

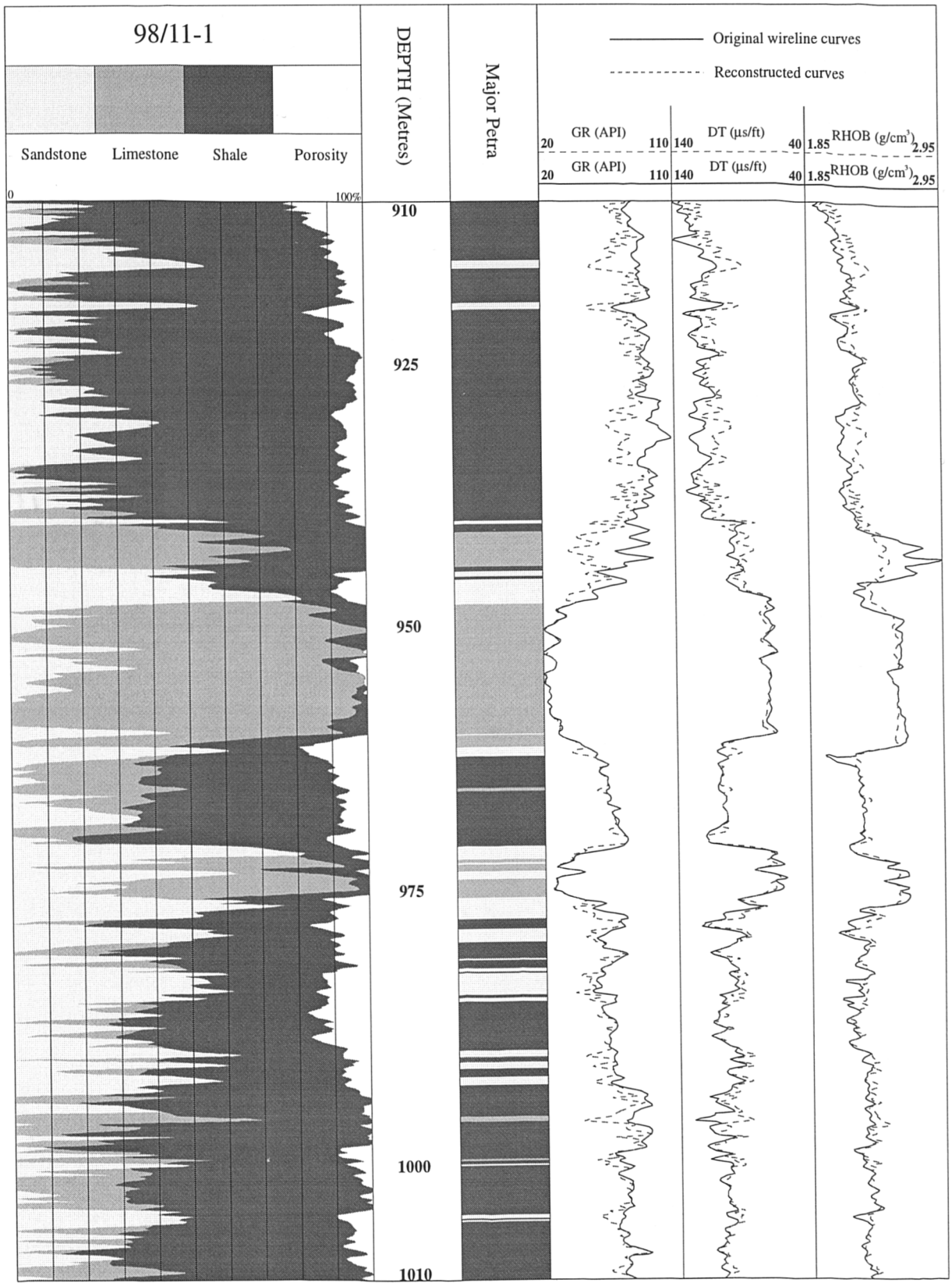

Fig. 3.16 Lithology calculated using the Petra module of the Terrastation II computer package, for the interval which encompasses the Oxfordian succession in the 98/11-1 borehole.

For a more detailed explanation of the Petra module the reader is referred to Terrasciences (1996). For more information about the algorithms employed in Petra the reader is referred to Burke *et al.* (1966) and Doveton & Cable (1979).

Figure 3.16 shows the results of the Petra calculation for the 98/11-1 borehole which is located in the Wessex Basin. This example shows that the gamma-ray, sonic and density logs were used to calculate the lithology by resolving four components which were entered into the program: sandstone, limestone, shale and porosity. These four components were chosen because for the majority of the Oxfordian succession these are the only components present in any significant quantity. In some beds, however, other lithologies such as phosphatic nodules, iron ooids and siderite cement are present so the Petra solution is not ideal. For example, in Figure 3.16 it is evident that the reconstructed Petra curves do not match the original gamma-ray and density wireline curves around the depth of about 940 m. It is believed that these beds at around 940 m represent a condensed section of the argillaceous upper part of the Corallian Beds (the Osmington Mills Ironstone Member) above the Osmington Oolite Formation, where phosphatic nodules, iron ooids and siderite cement are all found (see Chapter 5 and lithology logs in Appendix B).

In this study the lithology was calculated for the Oxfordian succession in all the boreholes which had at least two lithology logs. The calculated lithology for each well was then compared with the field gamma-ray and density logs, the nearest well with good biostratigraphic data, and the closest outcrop exposures, so that a final lithostratigraphic subdivision of the well could be undertaken. The procedure was not carried out routinely for the Kimmeridgian succession because it principally comprises the Kimmeridge Clay Formation which is more homogeneous than the Oxfordian succession

3.7 Discussion

The first stage in the sequence stratigraphical interpretation of the wireline data set was the quality control of the wireline logs. All the poor data were high lighted so that they was not used in the final interpretation. The second stage was to locate the ammonite zones on all the boreholes which had biostratigraphical data, and these boreholes were also correlated with the field gamma-ray and density logs. The next stage was to pick the ammonite zones on the whole wireline data set. This was done by manually correlating the boreholes with the biostratigraphically controlled boreholes and the field gamma-ray and density logs. The lithology of the Oxfordian succession was calculated using the Petra module of the Terrastation II software package. For areas with no distinctive wireline marker beds, such as the Lower Kimmeridge Clay, Corpac and/or Correlator were used to

aid in the location of the ammonite zonal boundaries. The correlation of the ammonite zones in the Kimmeridgian was then checked by plotting wells from different parts of the study against the Cowden succession in graphical correlation plots. The final stage in the sequence stratigraphical interpretation of the wireline data set was to manipulate the logs to enhance the trends before the logs were interpreted sequence stratigraphically using the ammonite zones as a constraint to the interpretation. The sequence stratigraphical interpretation of wireline logs trends is discussed in the next chapter. A flow chart showing the steps involved in the sequence stratigraphical interpretation of the wireline data set can be seen in Figure 3.17.

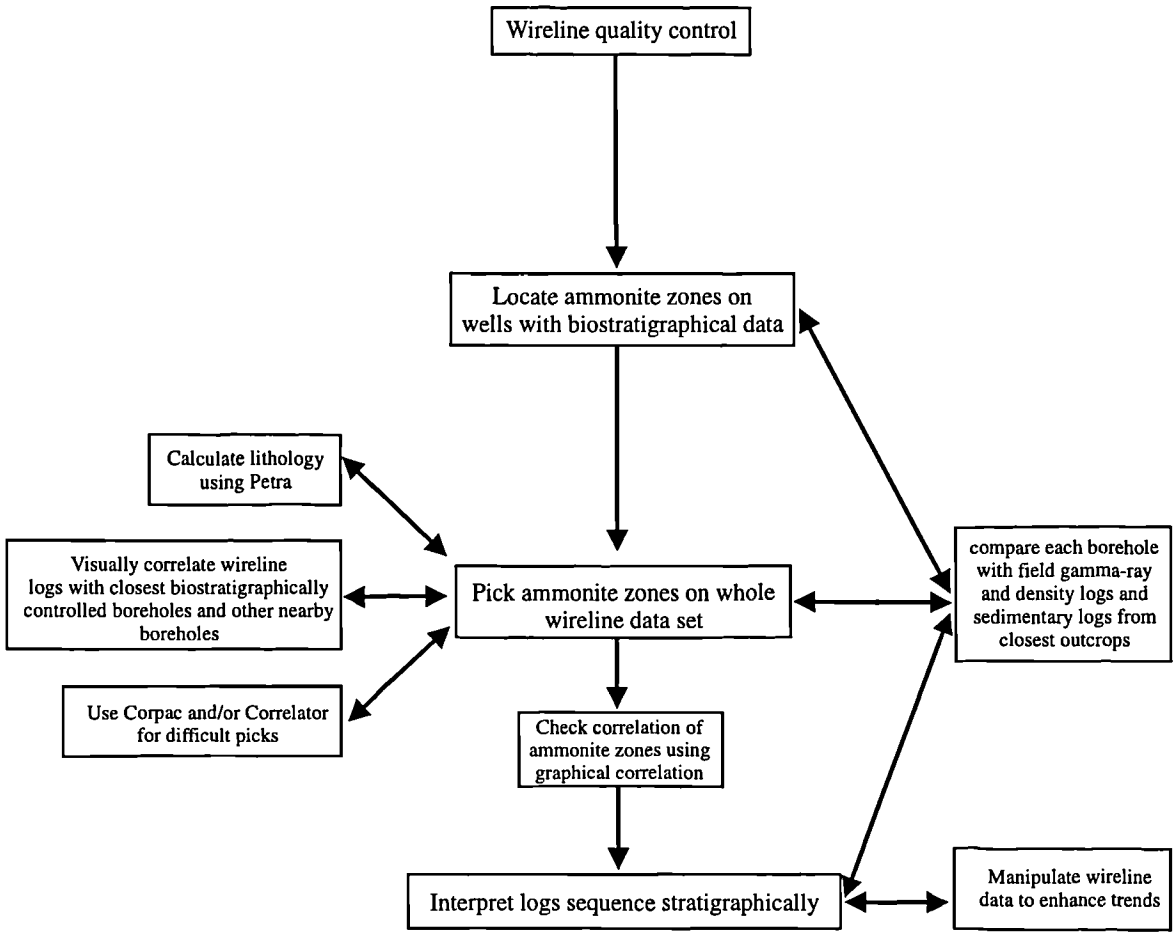

Fig. 3.17 Flow chart showing the steps involved in the sequence stratigraphical interpretation of the wireline data set.

3.8 Conclusions

(1) - Quality control is an important first stage of any study involving the interpretation of wireline logs.

(2) - The simplest wireline log manipulation techniques, such as changing the scale and power and root transforms, proved to be of most use.

(3) - Manual correlation is the best method to carry out a sequence stratigraphical wireline log interpretation.

(4) - Shading the wireline logs and the ability to stretch one log in relation to another log proved to be the best aid during the manual wireline correlation.

(5) - Graphical correlation can be used to check the wireline correlations and to locate subtle changes in relative sedimentation rates.

CHAPTER 4

Upper Jurassic Wireline Log Trends

4.1 Introduction

One of the most obvious and earliest geological uses of wireline logs, apart from the determination of lithology, was the interpretation of vertical successions of strata. The characteristic irregular trend, funnel trend (upward-coarsening), and bell trend (upward-fining), which are interpreted to show patterns of aggradational, progradational and retrogradational, are readily recognized on wireline logs (Galloway & Hobday 1983).

The interpretation of log trends in terms of relative sea-level changes is very important for wireline sequence stratigraphic interpretations. For example, a sequence boundary (i.e., an unconformity or its correlative conformity which bounds genetically related successions of strata) forms during the maximum rate of relative sea-level fall.

In Chapter 1 the fundamentals of wireline log interpretation were discussed, paying particular attention to the geological information contained in each wireline log. In this chapter the long-term trend with durations of 3-50 million years (i.e., second-order cycles) seen on the full suite of wireline logs over the Upper Jurassic interval will be discussed. In particular, the long-term trends seen on the gamma-ray logs are correlated with the relative sea-level curve constructed in this study which is based on the sequence stratigraphical field interpretation of the Upper Jurassic of Britain. The issue of whether trends seen on the gamma-ray logs can be related to rises and falls in relative sea-level will also be addressed.

4.2 Wireline log trends

The geological information obtained from wireline logs can be used to estimate lithology. Trends seen on the wireline logs may therefore equate with depositional trends, and patterns of sedimentary infill. Traditionally, only the spontaneous potential and gamma-ray wireline logs have been used in sand bodies to classify the wireline log trends (Serra & Sulpice 1975; Selley 1976; Galloway & Hobday 1983; Rider 1991). More

recently, log trends seen over large thicknesses have been used to interpret wireline logs in terms of sequence stratigraphy (Van Wagoner *et al.* 1990; Emery & Myers 1996; Rider 1996). A number of distinctive trends are commonly recognised on wireline logs, and are traditionally defined using the gamma-ray log (Fig. 4.1):

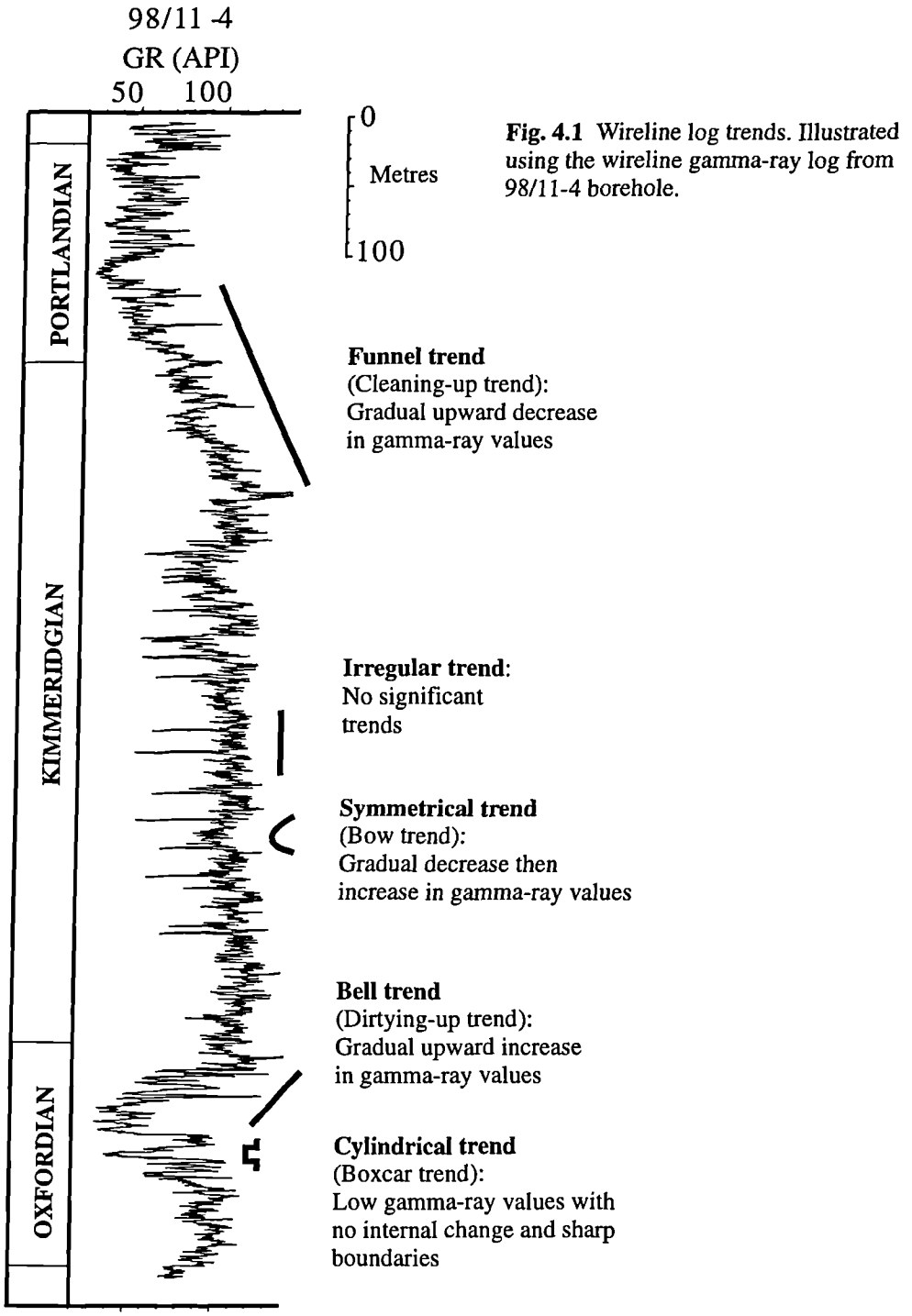

Fig. 4.1 Wireline log trends. Illustrated using the wireline gamma-ray log from 98/11-4 borehole.

- a) Funnel trend: shows a progressive upward decrease in the gamma-ray log reading representing a gradual upward change to a coarser-grained lithology, for example from mudstone to sandstone or from mudstone to coarse-grained carbonate.

- b) Bell trend: shows a progressive upward increase in the gamma-ray log reading, related to a gradual upward change to finer-grained lithology, for example from sandstone or carbonate to mudstone.

- c) Cylindrical trend (Boxcar log trend): low gamma-ray interval with a relatively constant gamma-ray reading, set within a higher gamma-ray background unit. The boundaries with the overlying and underlying intervals are abrupt.

- d) Symmetrical trend (Bow trend): consists of a funnel trend, overlain by a bell trend of similar thickness with no sharp break between the two.

- e) Irregular trend: no obvious systematic trend seen, and lacks the clean character of the cylindrical trend.

The general assumption made when interpreting trends on gamma-ray logs is that low gamma-ray values indicate clean formations (i.e. clay free) and high gamma-ray values indicate clay. This assumption is made because it has been shown that there is a close relationship between gamma-ray values and clay volume (Heslop 1974) and gamma-ray values and grain size (Serra & Sulpice 1975; Selley 1976). Low gamma-ray log values are interpreted to indicate a coarse grain-size while high values indicate fine grain-size. Taking this assumption one step further, it may be inferred that in general, high gamma-ray values indicate low energy environments and low gamma-ray values indicate high energy environments.

The significance of gamma-ray log trends in shallow and deep marine settings has been comprehensively discussed by Emery & Myers (1996). In shallow-marine settings, they suggested, the funnel trend is usually related to an upward transition from clay-rich to clay-poor lithologies, caused by an upward increase in depositional energy and upward coarsening. In the case of a prograding shoreline this may be interpreted as upward shallowing. By contrast, the bell trend often reflects a retrograding shoreline, resulting in upward deepening and a decrease in depositional energy.

In deep-marine settings, they suggested that, strong trends will generally only be seen on gamma-ray logs if coarser grained lithologies are introduced into the deep marine environment. For example funnel and bell trends are generally seen as part of symmetrical trends, which are related to an increase or decrease in the sand percentage of thinly bedded turbidites.

Occasionally, funnel trends may also be a result of a gradual change from clastic to carbonate deposition, or a gradual decrease in anoxicity, neither of which need be related necessarily to upward-shallowing (Emery & Myers 1996). By contrast, bell trends may also be a result of gradual increase in anoxicity, or a gradual change, perhaps climatically controlled, from carbonate to clastic deposition.

A symmetrical trend is generally the result of a waxing and waning of clastic sedimentation rate in a basinal setting, for example during the progradation and

retrogradation of a mud-rich fan system. Emery & Myers (1996) suggested that symmetrical trends are seldom developed in shallow-marine settings, but where they do occur they are usually associated with rift topography or growth faulting

In most cases subtle trends can be seen in what appears to be an irregular trend, if the log is redisplayed on a different scale (see Chapter 3). Emery & Myers (1996) suggested that irregular log trends are unlikely in any shelf or paralic facies, where cyclic changes in water depth are likely to be recognized as cyclic log trends.

Cylindrical trends, the interbedding of the two contrasting log units, implies the existence of two contrasting depositional energies, and an abrupt switching from one to the other. Cylindrical log trends are typical of some types of fluvial channel sands, tidal sand bodies, turbidites, and aeolian sands. Shallow-marine sand bodies may have truncated bases due to faulting, or sharp bases due to falls in relative sea-level or other factors. These therefore may have a cylindrical appearance, although systematic shifts in the shale line may be observable. In addition, evaporites often have a boxcar response on the gamma-ray log (Emery & Myers 1996).

Rider (1990), in his critical analysis of gamma-ray log shapes, concluded that neither the relationship between gamma-ray value and clay volume, nor the relationship between clay volume and grain size are consistent, as they should be if the shape of gamma-ray logs are to be used as a universally applicable facies indicator. For example, he shows a medium- to coarse-grained arkosic sandstone without clay but with up to 25% feldspar of which 10% is potassic and therefore radioactive, surrounded by a silty clay composed mainly of kaolinite with a very low natural radioactivity. This results in no gamma-ray trends because the radioactivity values of the silty clay and the sandstone are very similar.

In this study, therefore, the whole suite of wireline logs was used when interpreting trends seen on the gamma-ray log, always keeping in mind Rider's (1990) classic quote, "all that is radioactive is not necessarily clay and clay is not always radioactive".

4.2.1 Sequence stratigraphical interpretation of the wireline log trends

Sequence stratigraphy aims to use the vertical and lateral variations in sedimentary successions to divide the strata into cycles; these cycles are thought to be controlled by relative sea-level changes. The most important wireline log trends, therefore, are those which show progradation, retrogradation and aggradation. In a typical sequence cycle (Fig. 4.2), the lowermost systems tract would be represented by a progradational trend which may or may not show aggradation towards the top, the transgressive systems tract by a retrogradational trend, and the highstand systems tract by an aggradational and/or progradational gamma-ray trend.

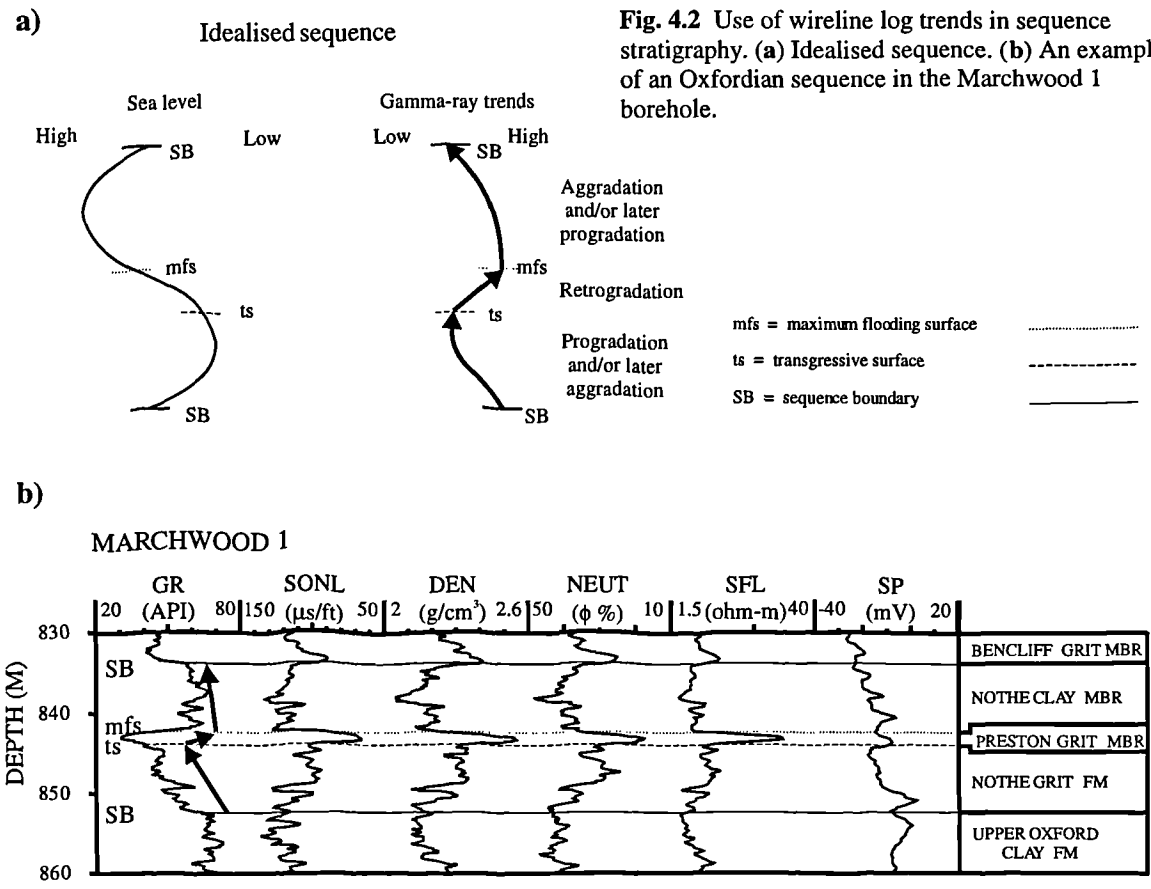

Fig. 4.2 Use of wireline log trends in sequence stratigraphy. (**a**) Idealised sequence. (**b**) An example of an Oxfordian sequence in the Marchwood 1 borehole.

Progradation can be recognized from a funnel trend (shallowing-upward unit). A prograding mudstone to siltstone unit (for example the upper part of the Kimmeridge Clay Formation; Fig. 4.3) can be recognized as a log unit with upward-decreasing gamma-ray and, and upward-increasing resistivity and velocity, representing an upward increase in the silt fraction.

Retrogradation of facies is recognized from a bell trend (deepening-upward unit). The only clear wireline log example of a long-term retrogradation trend in the Upper Jurassic succession of the Wessex Basin is that seen in the upper half of the Oxfordian (Fig. 4.3).

Irregular trends often represent aggradation of a fine-grained lithology, and may be typical of deep-water settings, a lacustrine succession, or muddy alluvial overbank facies (Emery & Myers 1996).

The interpretation of wireline trends in terms of rises and falls in relative sea-level (progradation, retrogradation and progradation) is vital in the detection of the key sequence stratigraphic boundaries (sequence boundary, transgressive surface and maximum flooding surface; Fig. 4.2).

Sequence boundaries resulting from a fall in relative sea-level should, in an ideal sequence, lie in between two funnel trends (Fig. 4.2). In cases where sequence boundaries

are unconformities and not correlative conformities, the sequence boundary should be easier to recognize from wireline data alone.

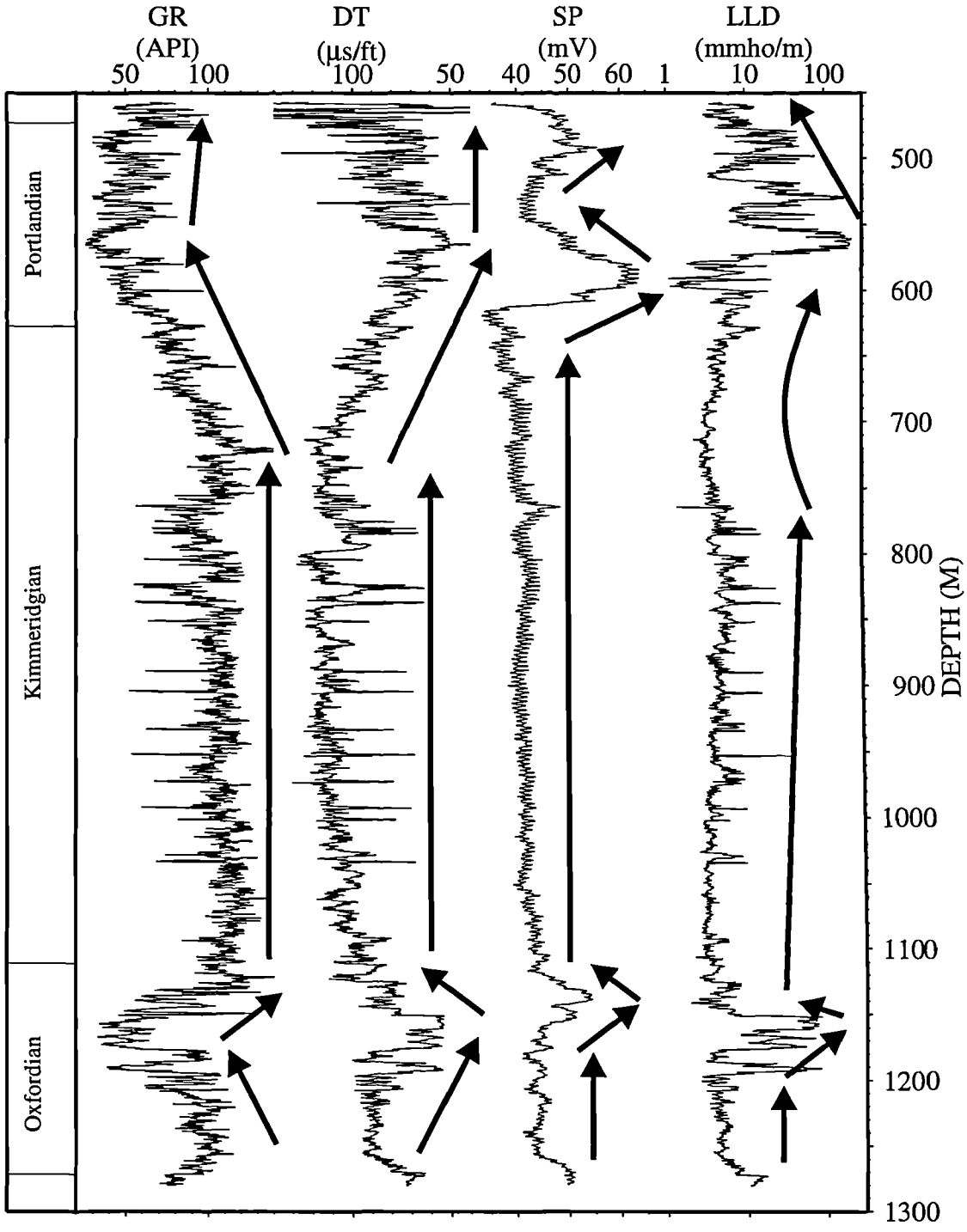

Fig. 4.3 Wireline log trends seen on the full suite of logs for borehole 98/11-4. See Figure 4.4 for location of 98/11-4.

The transgressive surface, the first significant marine flooding surface across the shelf within a sequence (Van Wagoner *et al.* 1988), is the surface between a funnel trend

(prograding unit) and a bell trend (retrograding unit). It marks the boundary between the lowermost systems tract and the transgressive systems tract (Fig. 4.2).

Maximum flooding surfaces can be recognized in proximal locations as the surface between a bell trend (retrograding unit) and an overlying irregular and/or funnel trend (aggradation and/or prograding unit). Where these are fining-upward and coarsening-upward units respectively, the maximum flooding surface will be a gamma-maximum. Maximum flooding surfaces pass laterally, at more distal locations, into condensed intervals. These may have a distinctive log response, such as a gamma peak, a resistivity trough, or a density maximum or minimum (Emery & Myers 1996). It should not be assumed that every gamma-ray peak is a maximum flooding surface. The key point is that the surface lies above a retrograding interval and below a prograding interval (Fig. 4.2).

4.3 Upper Jurassic long-term trends

4.3.1 Introduction

In this section four boreholes (Fig. 4.4), which are representative of all the boreholes in this study, have been selected to illustrate the Upper Jurassic long-term trends. Borehole 98/11-4 represents the full Upper Jurassic succession which is most like the Upper Jurassic exposures on the Dorset coast. Bletchingley and Cowden are representative of the boreholes in the Weald Sub-basin and Marchwood represents condensed Upper Jurassic successions which were developed on palaeohighs in the Wessex Basin.

4.3.2 Oxfordian

Looking at the gamma-ray log of borehole 98/11-4 (Fig. 4.3), where the full Oxfordian succession is present, it is evident that two trends are present in the Oxfordian: a funnel trend followed by a bell trend.

The funnel trend is developed when the Upper Oxford Clay, a mudstone, passes upwards into coarser-grained siliciclastics and then more calcareous beds which comprise the Corallian Group. The Upper Oxford Clay is characterized by a finely serrated log signature of high gamma-ray values and low sonic velocity, with discrete spikes where silty and calcareous beds are developed. The base of the Corallian Group has a similar log signature to that of the Upper Oxford Clay, but then shows a funnel trend (upward

coarsening) as the succession becomes sandier and passes to limestones and mudstones of the Osmington Oolite Formation.

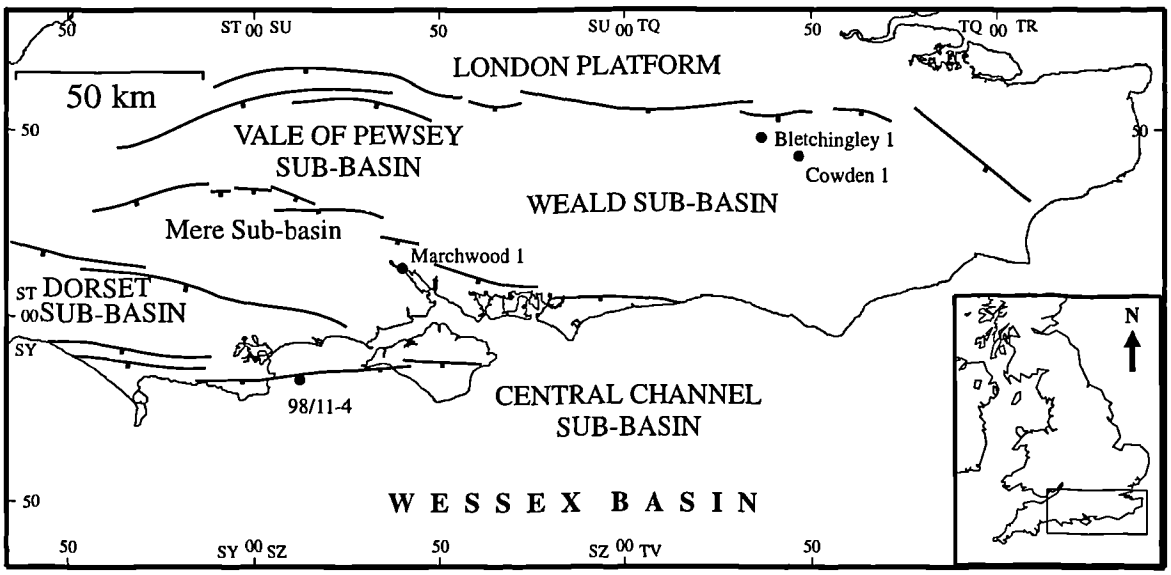

Fig. 4.4 Map showing the main structural features of the Wessex Basin (after Whittaker 1985) and the location of boreholes discussed in this chapter.

The bell shape is then developed as the overlying strata give rise to deeply serrated log profiles as the limestones of the Trigonia Clavellata Beds pass up to the Sandsfoot Clay and the other argillaceous beds of the upper Corallian Group.

In the Dorset Sub-basin (Fig. 4.4) the whole or part of the Corallian Beds have been eroded at the Base Cretaceous unconformity (Whittaker *et al.* 1985). Where they reappear to the north of the Isle of Wight (Mere Sub-basin), they are thin and only the lower Corallian Beds appear to be present beneath the Kimmeridge Clay Formation. This is shown in the Marchwood borehole where the funnel trend is clearly seen but the overlying bell trend is absent (Fig. 4.5). Such nonsequence or condensation of the upper part is widespread, and occurs even where the succession thickens northwards into the Vale of Pewsey Sub-basin (see Chapter 5; Whittaker *et al.* 1985).

Further east in the thick Weald Sub-basin succession, the Oxfordian succession can be divided into three units, the lower and upper units are composed of limestones, sandstones, siltstones and mudstones, whilst the middle unit is composed of a non-calcareous mudstone. This results in a more complex gamma-ray trend (Fig. 4.6) than the simple funnel trend followed by the bell trend which is seen in the rest of the Wessex Basin area. The main reason for the difference in trends is due to the development of a reef on the northern flank of the Weald Sub-basin (see Chapter 5, Section 5.3.5.6).

It was demonstrated in Chapter 2 that the Oxfordian sediments show marked lateral and vertical variation, thus making peak to peak wireline correlations impossible.

Nevertheless, where the full Oxfordian succession is present two distinctive logs trends can be seen on the gamma-ray log, a funnel trend followed by a bell trend. This is true for all of the Wessex Basin except for the Weald Sub-basin where a more complex pattern of trends is found.

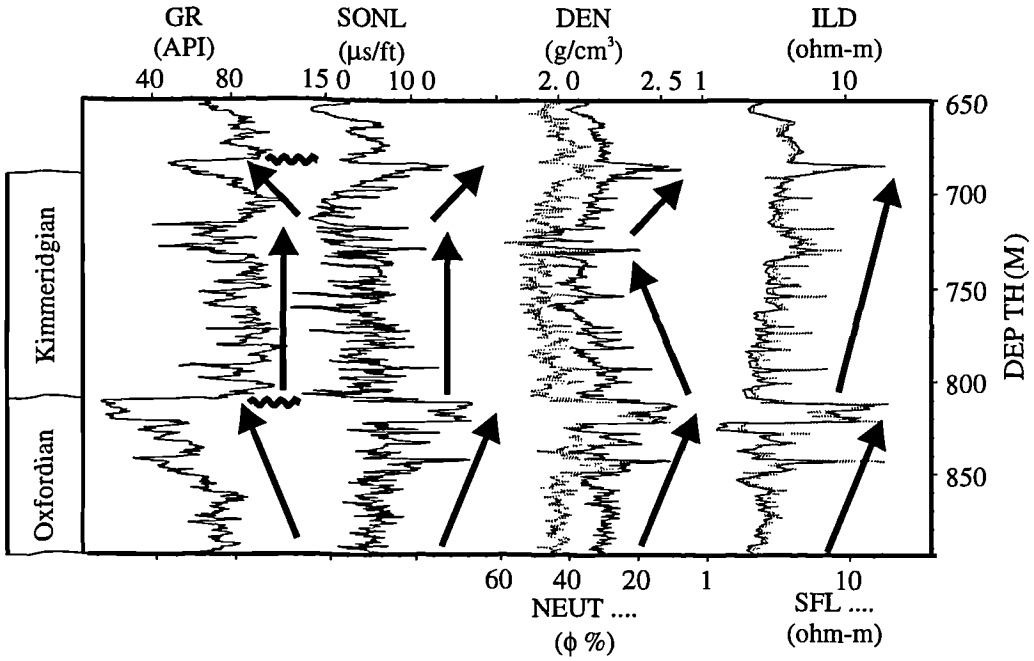

Fig. 4.5 Wireline trends on the full suite of logs from the Marchwood 1 borehole, which is representative of condensed Upper Jurassic successions. See Figure 4.4 for location of the Marchwood borehole.

4.3.3 Kimmeridgian

The Kimmeridge Clay Formation has a distinctive deeply serrated sonic and formation density log signature (Figs 4.3 & 4.6). Gamma-ray values are generally high, and show complementary but more subdued variation to those of the sonic log. The Kimmeridgian of Dorset is represented by interbedded organic-rich and organic-poor mudstones, with a few thin beds of fine-grained sandstones near the base and the top. Organic-rich mudstones are characterized by high gamma-ray, low sonic velocity and very low density values. Where sandstones/siltstones are present they give rise to a high velocity sonic spike and low gamma-ray values, although the latter values may be higher if phosphatized material is present (Whittaker *et al.* 1985). The more calcareous mudstones give rise to the lowest gamma-ray values and the highest sonic velocities. When these beds become limestone 'stone bands' (Cox & Gallois 1981), pronounced sonic and density spikes are registered. The coccolith-rich limestones on the other hand have prominent high velocity sonic spikes and low gamma-ray, but low density spikes.

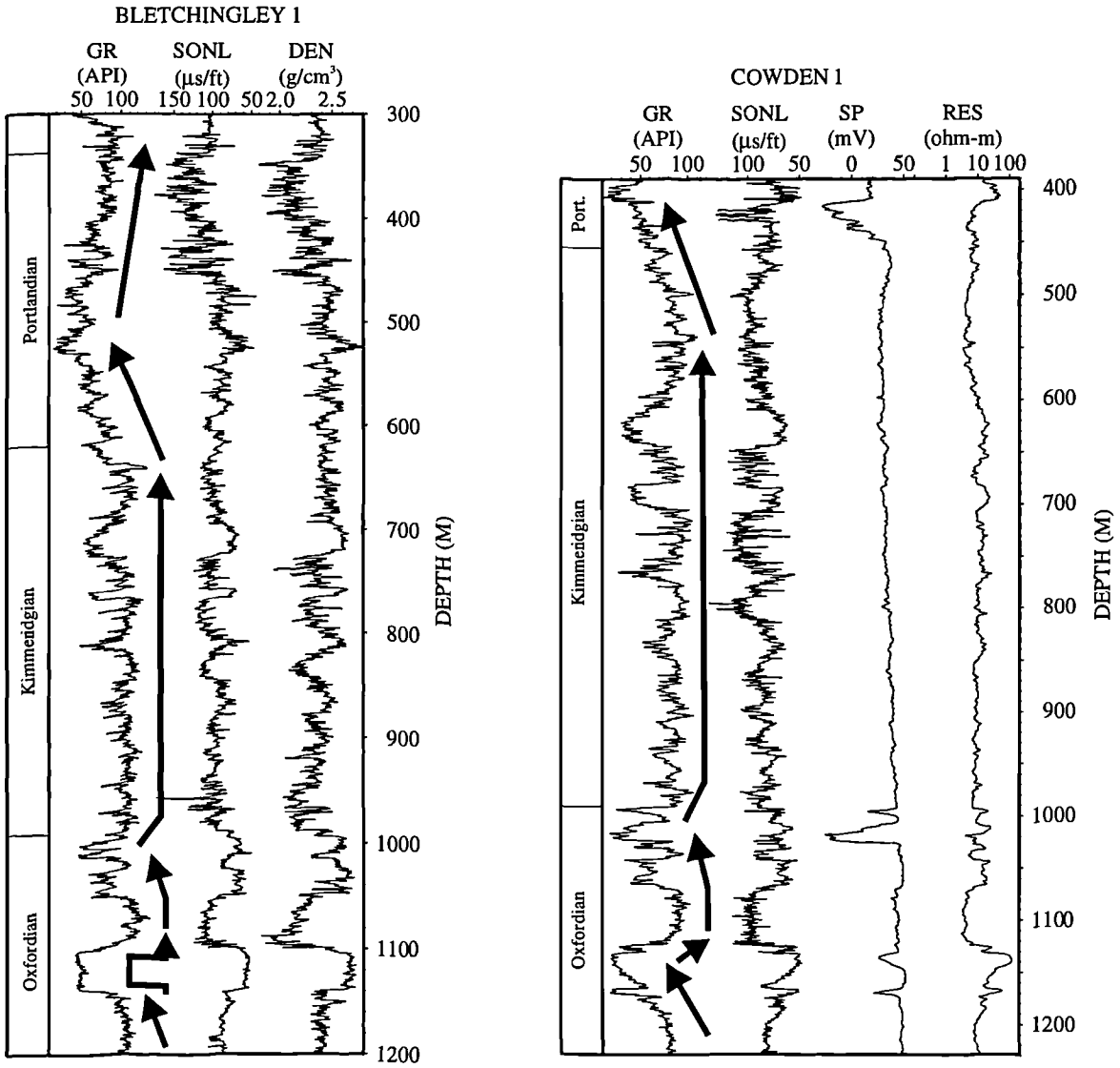

Fig. 4.6 Typical wireline log trends for the Upper Jurassic succession in the Weald Sub-basin. See Figure 4.4 for location of the boreholes.

The gamma-ray logs from boreholes 98/11-4, Bletchingley and Cowden (Figs 4.3 & 4.6) show that the lower three quarters of the Kimmeridgian is characterized by an irregular trend followed by a funnel trend which continues into the Portlandian. This is interpreted to represent a long-term sea-level rise followed by a fall. Superimposed on the longer term irregular and funnel trends are eight sequence stratigraphic cycles (Coe 1992; Chapter 6) in the Kimmeridgian. These shorter term sequence cycles are particularly evident in the upper part of the Kimmeridgian (Figs 4.3 & 4.5).

The same long-term irregular trend followed by a funnel trend can be seen in boreholes which penetrate condensed sections of Kimmeridgian strata (Fig. 4.5). For example, the Marchwood borehole, where the whole of the Kimmeridge Clay is just over 100 metres in thickness, shows the same overall trends as the wireline logs from the Weald and Central Channel Sub-basins, where the succession is up to five times thicker.

4.3.4 Portlandian

The Portlandian is represented by marine silty and clay-rich dolomites deposited in moderate water depth (Portland Sand Formation) overlain by shallow and non-marine carbonate ramp system comprised of the Portland Stone Formation and Lulworth Beds, which are part of Purbeck Formation (Coe 1996). The geophysical log signature of the Portland Sand Formation is characterized by a funnel trend and increasing sonic velocity as silty mudstones pass upwards into muddy dolomite and coarser dolomite (Figs 4.3 & 4.6). The signature may be spiky because of the occurrence of sporadic levels that are well cemented by dolomite or calcite or are even thin limestones. Thick units of low gamma-ray values associated with low sonic velocity may occur, reflecting the fact that substantial parts of Portland Sand are poorly cemented. Commonly, however, the gamma-ray values themselves are not particularly low since the dolomite is frequently argillaceous or glauconitic (Hamblin *et al.* 1992).

The geophysical log signature of the Purbeck Beds is characteristically highly serrated, reflecting the limestone/shale alternation (Figs 4.3 & 4.6). The stratigraphic succession also gives rise to an overall shape which is diagnostic throughout southern England (Whittaker *et al.* 1985). The increasingly argillaceous nature of the succession near the top results in a bell trend, with the lowest gamma-ray values and highest sonic velocity being found near the base of the Purbeck Beds and the highest gamma-ray value and lowest sonic velocity near the middle.

4.4 Upper Jurassic sea-level changes

A relative sea-level curve showing the long-term second-order regressive-transgressive cycles within the Upper Jurassic was constructed by A. L. Coe to show conceptually her sequence stratigraphic interpretation of the Upper Jurassic outcrops of Great Britain (Coe 1992; Fig. 4.7). She constructed the curve by assigning certain lithologies specific relative sea-level values. For example, the relative sea-level assigned for the Osmington Oolite Formation (Oxfordian) is the same level as the Portland Freestone Member (Portlandian), which is also oolitic. The time scale of this relative sea-level curve is based on ammonite zones which are assumed to have an equal duration. This process was taken one step further in this study by superimposing the third-order sequence cycles on the long-term regressive-transgressive cycles, resulting in a more detailed relative sea-level curve (Fig. 4.7).

The relative sea-level curve (Fig. 4.7) shows that in the Oxfordian there is a long-term regressive phase followed by a transgressive phase. At the base of the Kimmeridgian there is a minor regressive phase which is followed by a transgressive phase. The whole succession culminates in a long lasting regressive phase until the end of Portlandian.

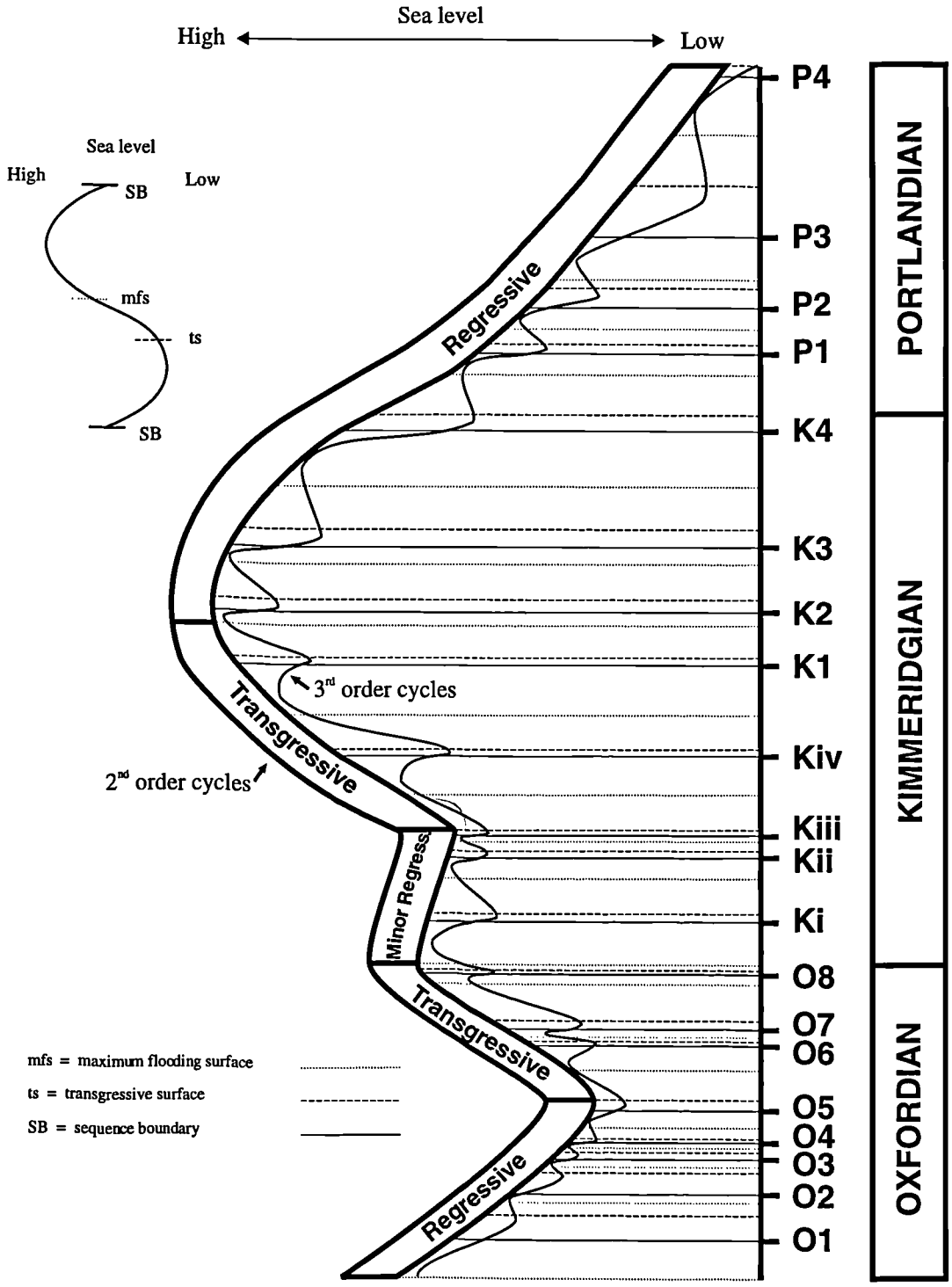

Fig. 4.7 Sea-level curve based on the sequence stratigraphic field interpretation of the Upper Jurassic exposures of the UK by A. L. Coe. See text for an explanation of the construction of the curves.

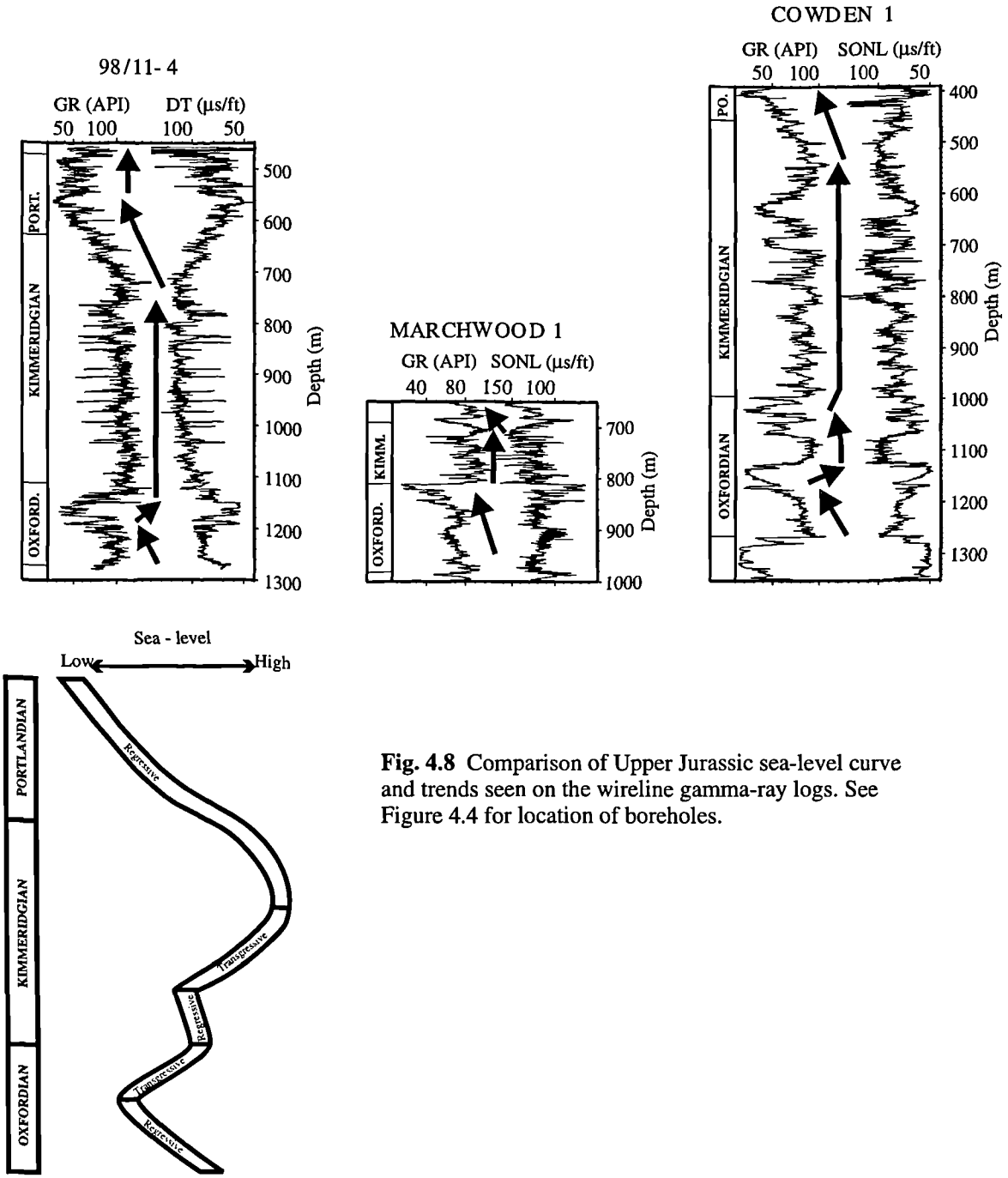

Fig. 4.8 Comparison of Upper Jurassic sea-level curve and trends seen on the wireline gamma-ray logs. See Figure 4.4 for location of boreholes.

Comparison of the relative sea-level curve for the Upper Jurassic with the wireline logs shows that the trends in the gamma-ray log do not exactly reflect the relative sea-level curve (Fig. 4.8). Borehole 98/11-4 is the closest borehole to the Upper Jurassic exposures on the Dorset coast in this study which penetrates the whole Upper Jurassic succession. The regressive-transgressive cycle seen on the relative sea-level curve in the Oxfordian is also depicted on the gamma-ray log of borehole 98/11-4, in the form of a funnel trend followed by a bell trend, which is interpreted as a prograding and retrograding cycle. The gamma-ray log for the Kimmeridgian shows an irregular trend through about three

quarters of the Kimmeridgian, followed by a funnel trend. The relative sea-level curve on the other hand shows a minor regressive phase at the base of the Kimmeridgian followed by a transgressive phase which lasts about two thirds of the way through the Kimmeridgian. This transgressive phase is then followed by a regressive phase. So, unlike the Oxfordian, it seems that changes in the relative sea-level curve are not reflected in the gamma-ray curve for the lower part of the Kimmeridgian.

The regressive phase which started in the Kimmeridgian continued to the top of the Portlandian. This is reflected in the gamma-ray log from borehole 98/11-4 which shows a funnel trend extending from the Kimmeridgian to the Portlandian, above which is a gently increasing bell trend.

The main differences, therefore, between the relative sea-level curve and the wireline gamma-ray log from 98/11-4 are firstly, that the minor regressive phase followed by the transgressive phase in Kimmeridgian is not reflected in the gamma-ray log (irregular trend seen); and, secondly, that the regressive phase which continues to the end of the Portlandian is not fully depicted on the gamma-ray log (shows funnel trend followed by slight bell trend).

Before going on to explain some of the possible causes of the discrepancies between the relative sea-level curve and the gamma-ray log, it is important to note that the vertical scale on the relative sea-level curve is in time, based on ammonite zones, whilst the vertical scale of the gamma-ray log is depth. Figure 4.9 was, therefore, constructed to try and solve this vertical scale problem. In this figure the relative sea-level curve for the Kimmeridgian has been stretched and squeezed so that the key sequence stratigraphical boundaries (sequence boundary, transgressive surface and maximum flooding surface) have been aligned with the key surfaces which have been picked on borehole 98/11-4 over the Kimmeridgian interval (see Chapter 6). This procedure has put the gamma-ray and relative sea-level curve on the same time scale, because sequence stratigraphic surfaces are chronostratigraphic.

Figure 4.9 shows that in general the third-order sea-level cycles have more effect on the gamma-ray curve than the second-order cycles. From sequence boundaries Ki to Kiv (see Chapter 6 for explanation of the sequences in the Kimmeridgian) the second-order sea-level curve shows a very slight regressive phase followed by a transgressive phase (Fig. 4.9). Over this interval the relative sea-level changes very gradually, which is probably the reason why an irregular trend (aggradation) is seen on the gamma-ray log. From sequence boundaries Kiv to K3 the second-order sea-level curve shows a strong transgressive phase followed by the start of the regressive phase (Fig. 4.9) which ends in the Portlandian (Fig. 4.7). Over this interval the gamma-ray curve seems to be influenced more by the third-order sea-level curve.

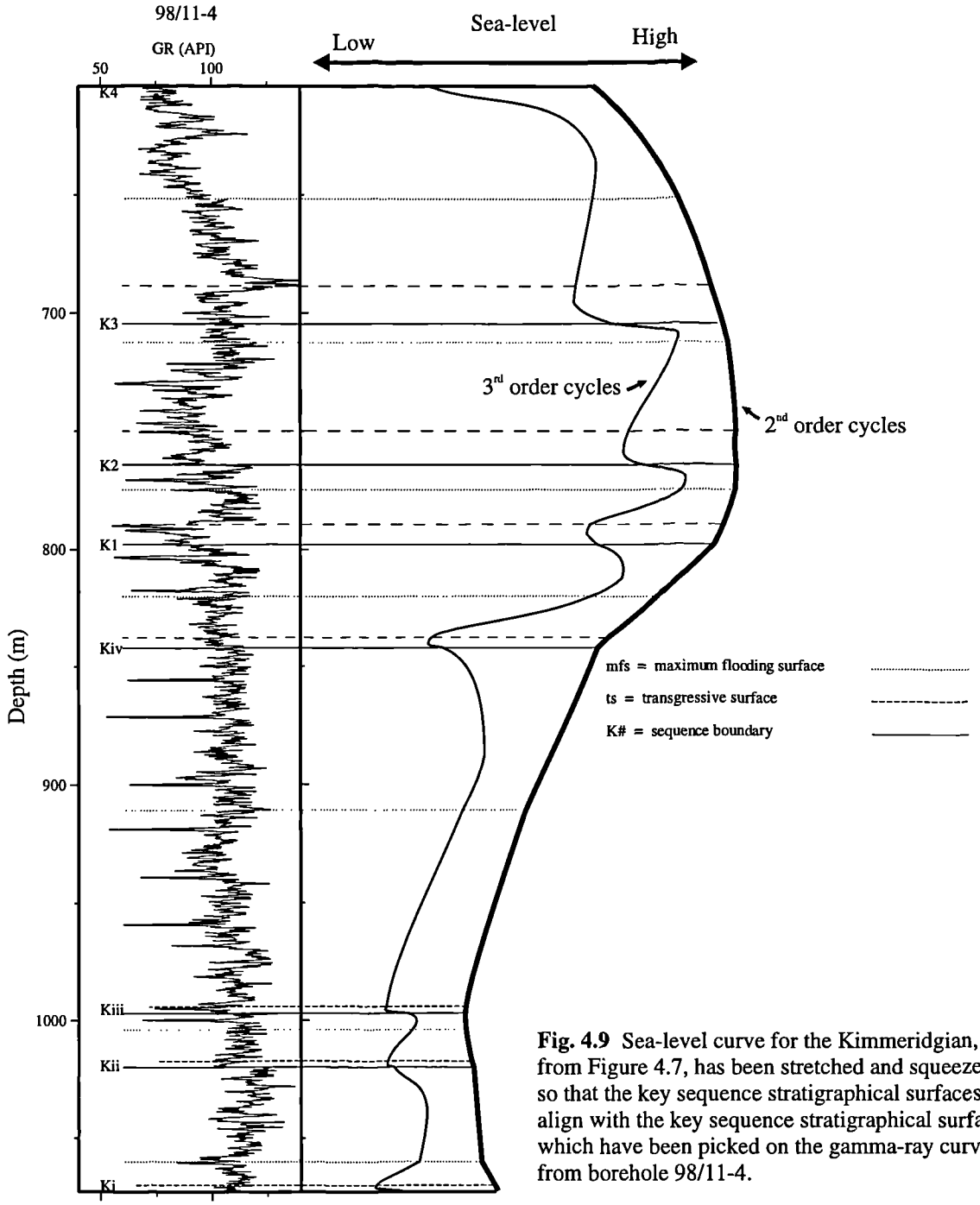

Fig. 4.9 Sea-level curve for the Kimmeridgian, from Figure 4.7, has been stretched and squeezed so that the key sequence stratigraphical surfaces align with the key sequence stratigraphical surfaces which have been picked on the gamma-ray curve from borehole 98/11-4.

4.5 Spectral gamma-ray curves as sea-level indicators

Total gamma-ray readings are made up of the gamma radiation emitted from potassium, uranium and thorium. One of the reasons for recording the spectral data in this study was to see if the spectral curves were better sea-level indicators than the total gamma-ray curve. Spectral gamma-ray theory was described in Chapter 2 and the

distribution of potassium, uranium and thorium in sedimentary rocks is described in Chapter 6.

The spectral gamma-ray data recorded over part of the Kimmeridge Clay Formation from the base of bed 32 in the *eudoxus* Zone to the top of bed 54 in the *pallasioides* Zone is shown in Figure 4.10 plotted alongside the second and third-order sea-level curves.

Over this part of the Kimmeridge Clay Formation the second-order sea-level curve does not show much change, hence the lack of significant long-term trends seen in the total gamma-ray curve (Fig. 4.10). The potassium curve looks very similar to the total gamma-ray curve whilst the uranium and thorium curves show more shorter term trends, which appear to be caused by the third-order changes in sea-level.

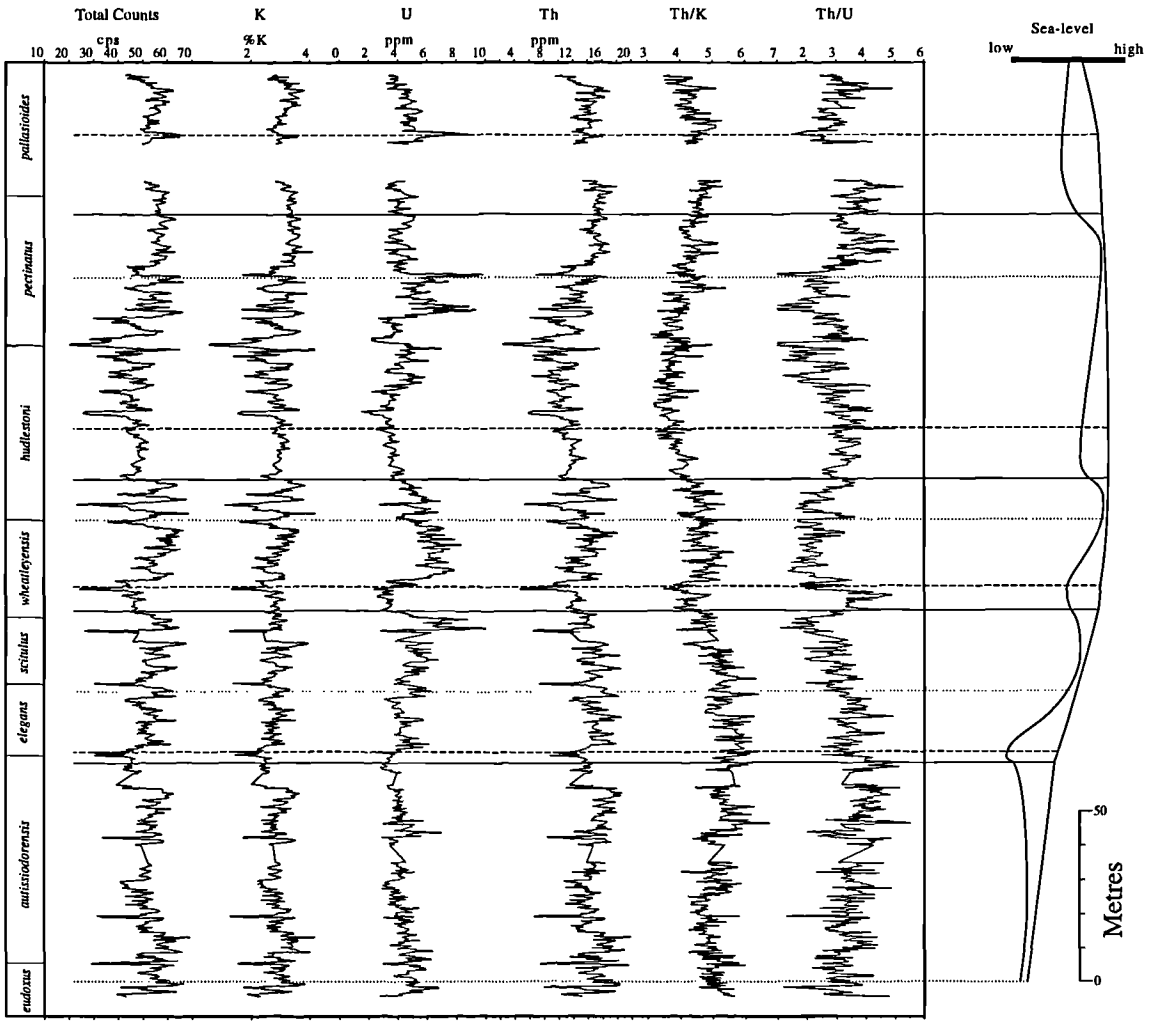

mfs = maximum flooding surface

ts = transgressive surface

SB = sequence boundary

Fig. 4.10 Spectral gamma-ray data, recorded over part of the Kimmeridge Clay Formation, plotted against sea-level curve.

The use of Th/K and Th/U ratios is discussed in Chapter 6. In term of relative sea-level, the Th/K ratio curve seems to be the best curve which reflects relative sea-level changes seen on both the second and third-order sea-level curves (Fig. 4.10). However, it clearly reflects the changes in the third-order sea-level changes better than the gradual changes seen in the second-order sea-level curve.

4.6 Discussion

Haq *et al.* (1987, 1988) produced a world-wide relative sea-level curve for the Mesozoic and Cenozoic based on a sequence stratigraphic interpretation of seismic, well-log and outcrop data. They stated that the bulk of the data for the Jurassic sequences came from sections in western Europe, in particular the English sections in Dorset and Yorkshire.

A comparison of the relative sea-level curves of the Upper Jurassic produced in this study with that of Haq *et al.* (1987, 1988) can be seen in Figure 4.11. This figure clearly shows that the third-order sea-level curve produced in this study which was based on the sequence stratigraphical interpretation of the Upper Jurassic of England by Coe (1992), is significantly more detailed than that produced by Haq *et al.* (1987, 1988).

Regarding the question of why the long-term second-order transgressive phase which occurs in the Upper Kimmeridgian is not reflected in the gamma-ray log trends, it is evident that the third-order sea-level changes seem to have more effect on the gamma-ray log trends than the second-order sea-level changes (Fig. 4.9). The spectral data in Figure 4.10 also shows that the third-order sea-level changes seem to have more effect on the spectral gamma-ray curves. Figure 4.10 also shows that the Th/K ratio curve is a better relative sea-level indicator than the total gamma-ray curve.

4.7 Conclusions

(1) - Trends seen on the total gamma-ray curve can be used to detect long-term transgressive/regressive sea-level changes in the Oxfordian and Portlandian.

(2) - The third-order sea-level changes have a bigger effect on both the total and spectral gamma-ray curves than the second-order sea-level changes in the Kimmeridgian.

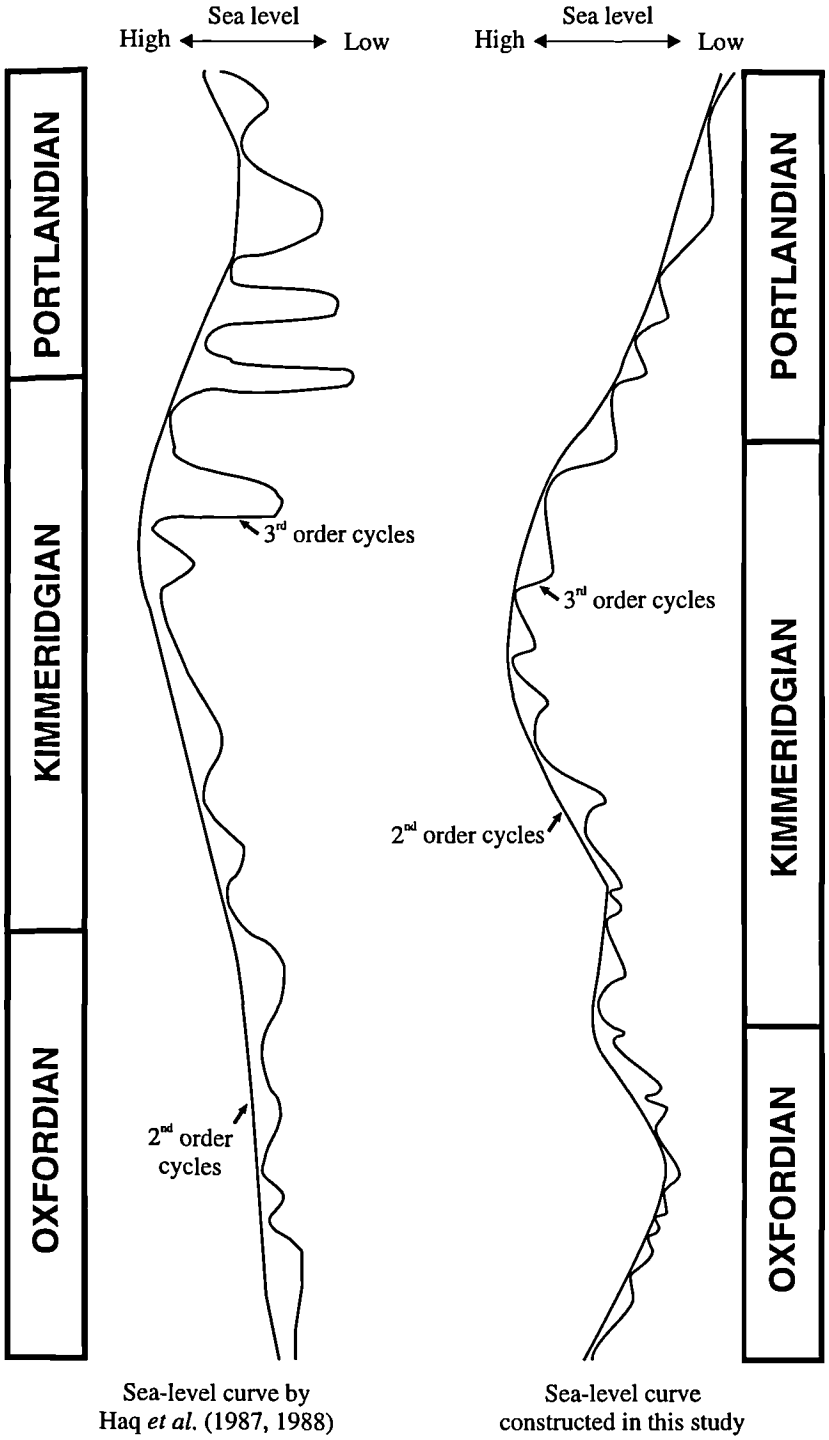

Fig. 4.11 Sea-level curve based on the sequence stratigraphic field interpretation of the Upper Jurassic exposures of the UK by A. L. Coe, plotted alongside the sea-level curve constructed by Haq *et al.* (1987, 1988).

(3) - Th/K ratio curve is a better sea-level indicator than the total and spectral gamma-ray curves.

(4) - The third-order sea-level curve produced in this study in significantly more detailed than that produced by Haq *et al.* (1987, 1988).

CHAPTER 5

Oxfordian

5.1 Introduction

The Oxfordian Stage in England is represented by the Upper Oxford Clay Formation and the Corallian Group. The Oxfordian outcrop stretches from Dorset to Yorkshire (Fig. 5.1). The exposures used in this study to produce the field gamma-ray and density logs (Chapter 2) are located on the Dorset coast (Furzy Cliff, Redcliff / Hamcliff, Bran Point and Black Head; Fig. 5.1).

The Oxfordian Stage encompasses the six North-West European ammonite zones, *Quenstedoceras mariae* through to *Ringsteadia pseudocordata*, and the constituent fifteen ammonite subzones, *Quenstedoceras scarburgense* through to *Ringsteadia evoluta* (Table 5.1). For more information on the ammonites and other fauna in the Oxfordian the reader is referred to Fürsich (1977), Wright (1981, 1986a, 1986b and references therein).

The Oxfordian succession of southern England has been extensively studied: lithostratigraphic and sedimentological studies have been carried out (Arkell 1933, 1947; Brookfield 1978a, b; Wright 1981, 1986a, b; Sun 1989; Sun & Wright 1989; Coe 1992, 1995; Wilson 1968; Talbot 1973; Allen & Underhill 1989; Bristow *et al.* 1995), as well as biostratigraphic (Arkell 1947; Fürsich 1977; Brookfield 1978a; Wright 1981, 1986a, b; Bristow *et al.* 1995), palaeogeographic (Brookfield 1973; Wilson 1968), diagenetic (Talbot 1971; Chowdhury 1982; De Wet 1987; Sun *et al.* 1992) and more recently sequence stratigraphic studies (Rioult *et al.* 1991; Wilson 1991; Coe 1992, 1995).

5.1.1 Upper Oxford Clay Formation

The Upper Oxford Clay Formation, on the Dorset coast, is split into three lithostratigraphic members: Furzedown Clay, Jordan Cliff Clays and the Bowleaze Clays. Furzy Cliff, on the Dorset coast, is the only good exposure of the Upper Oxford Clay in the Wessex Basin (Coe 1995; Fig. 5.1). The Furzedown Clay Member comprises fine-grained mudstones containing negligible amounts of fine-grained sand and is poorly exposed on the Dorset coast (Wright 1986a). The Jordan Cliff Clays are also fine-grained but can be easily distinguished from the Furzedown Clay due to the presence of numerous

Gryphaea dilatata (Wright 1986a). The Bowleaze Clays are predominantly very fine-grained, but contain common interbeds of sandy clay (Wright 1986a; Appendix B, Furzy Cliff log). The base of the Bowleaze Clays Member is easily recognized in the field because it is marked by a persistent band of white limestone nodules.

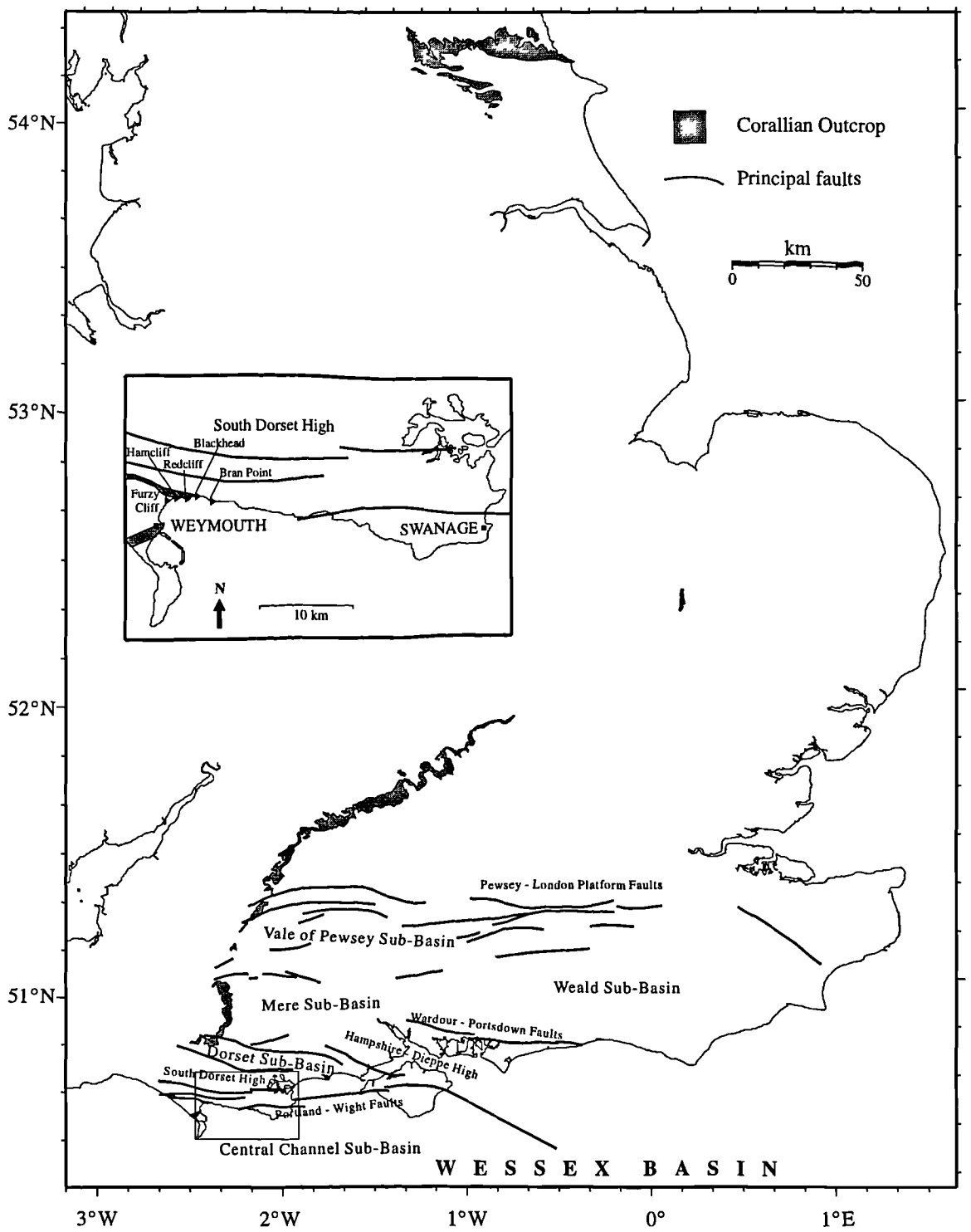

Fig. 5.1 Map of England showing the Corallian Group outcrop and the principal faults. The faults are after Whittaker (1985) and Hamblin *et al.* (1992). Insert shows location of the main Corallian Group exposures on the Dorset coast together with Furzy Cliff where part of the Upper Oxford Clay is exposed.

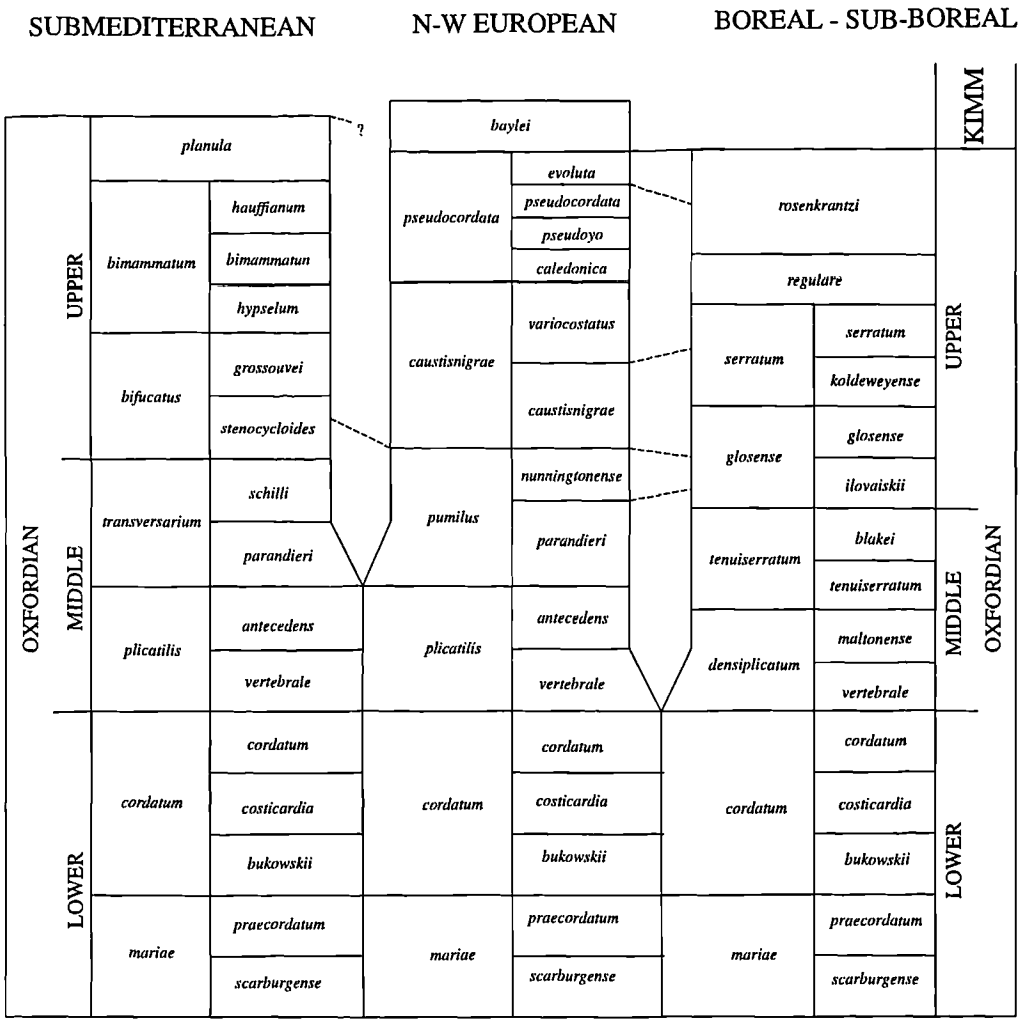

Table 5.1 Correlation of the Submediterranean, north-west European and Boreal zonal schemes for the Oxfordian (modified after Cope *et al.* (1980) and Cox (1990), originally from Sykes & Callomon (1979)).

5.1.2 Corallian Group

The Corallian Group is represented by a complex succession of shallow-marine siliciclastic and carbonate sedimentary rocks, which show marked lateral and vertical variation (Coe 1992, 1995). Because of the marked lateral sedimentological variation the lithostratigraphy of the three main outcrop areas, which lie on the eastern margin of the Wessex Basin, are briefly described. During the sequence stratigraphic interpretation of the wireline logs the outcrops closest to the boreholes have been used as a guide to predicting the sub-surface successions.

5.1.2.1 Dorset Coast

The Corallian Group is divided into six formations: the Nothe Grit, Redcliff, Osmington, Trigonia Clavellata, Sandsfoot and Ringstead Formations (Table 5.2; Wright 1986b). The Nothe Grit Formation, which has been divided into nine beds by Wright (1986b), comprises sandstones and argillaceous siltstones.

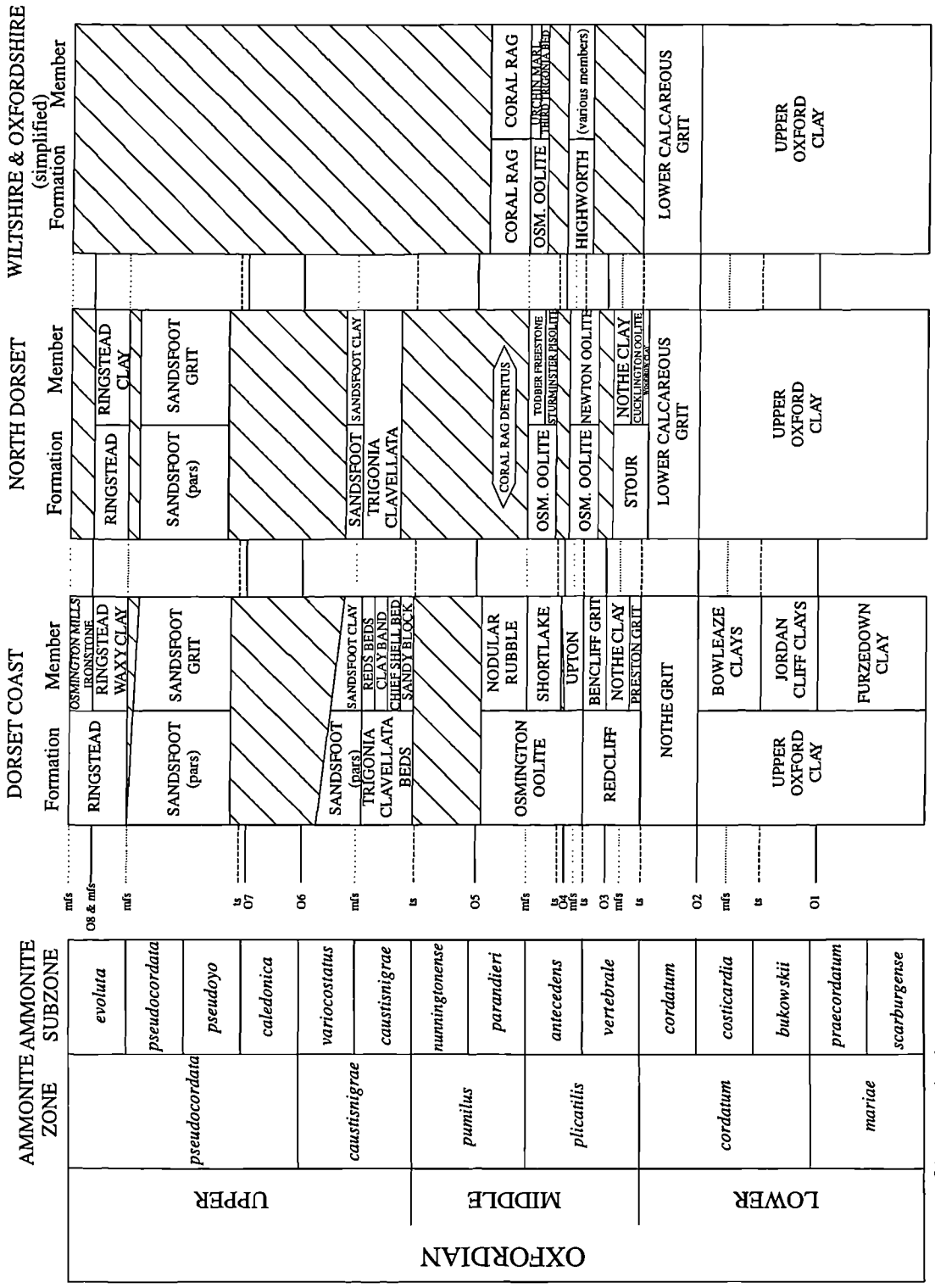

Table 5.2 Lithostratigraphic nomenclature for the Oxfordian of the Wessex Basin (modified after Coe 1992).

The Preston Grit, Nothe Clay and Bencliff Grit members make up the Redcliff Formation. The Preston Grit is a sandy limestone unit which grades into the Nothe Clay. The Nothe Clay is composed of a grey mudstone with limestone bands which have different compositions (Wright 1986b; Coe 1995). The Bencliff Grit comprises a series of thin bioturbated, argillaceous sands and silts separating three thicker cross-bedded sands (Wright 1986b). Allen & Underhill (1989) described the cross-bedded sands as being analogous to swaley cross-stratification, or amalgamated hummocky cross-stratification.

Wright (1986b) proposed the Upton, Shortlake and Nodular Rubble as formal members of the Osmington Oolite Formation. The Upton Member is composed of several thin argillaceous limestones separated by mudstones (Coe 1995). The Shortlake Member contains cross-bedded oolitic grainstones at it' base which grade into micritic bands interbedded with calcareous mudstones (Coe 1995). The third member of the Osmington Oolite Formation, the Nodular Rubble Member, is the most distinctive at outcrop. It comprises nodules of mictrite which are enclosed within marl (Coe 1995).

The Trigonia Clavellata Formation is made up of four members. The lowest being the Sandy Block Member, which consists of a sandy micritic limestone broken by several thin argillaceous beds (Coe 1995). The second is the Chief Shell Beds Member, which is an argillaceous oolite containing numerous fossils, in particular the bivalve *Morphella clavellata* (Wright 1986b; Coe 1995). A mudstone containing local ooids, known as the Clay Band Member is the third member in the formation. The last member is the Red Beds Member, which comprises alternations of oolite with sideritic micrite and shelly sideritic limestones (Wright 1986b; Coe 1995).

The Sandsfoot Formation contains the Sandsfoot Clay and Sandsfoot Grit members. The Sandsfoot Clay is a calcareous silty clay with local lenses of sandstone (Coe 1992). The Sandsfoot Grit, which has been divided into five units by Wright (1986b), is composed of calcareous sandstones, argillaceous sandstones and marls, and clays.

The final formation in the Corallian Group is the Ringstead Formation, which consist of the Ringstead Waxy Clay and Osmington Mills Ironstone members. The Ringstead Waxy Clay is a light-grey calcareous clay which contains distinctive red clay-filled *Chondrites* burrows and nodules. The Osmington Mills Ironstone Member is a thin limonite-oolite marl which locally is well enough cemented to form an impure limestone (Wright 1986b).

5.1.2.2 North Dorset

Until the work of Wright (1981) the Corallian of north Dorset was not systematically documented. Wright (1981) subdivided the Corallian Group of north Dorset

into six formations; Lower Calcareous Grit, Stour, Osmington Oolite, Trigonia Clavellata, Sandsfoot, and Ringstead (Table 5.2).

The Lower Calcareous Grit Formation, which is equivalent to the Nothe Grit Formation on the Dorset coast, is a bioturbated fossiliferous sandstone with cemented bands and doggers (Coe 1992).

The Stour Formation is split into three members, the first being the Woodrow Clay (Wright 1981), a calcareous mudstone which is not developed in south Dorset (Coe 1992). The second member is the Cucklington Oolite which is very similar in lithology to the Preston Grit in south Dorset. The Cucklington Oolite is made up of several shell beds, micrite, sand, clay and marl beds. The Nothe Clay Member, the third member of the Stour Formation, is a light-grey calcareous clay with scattered ooids (Wright 1981). It is the thickest clay unit in the north Dorset Corallian succession, and although it only outcrops in a small area in north Dorset due to a subsequent overstep, Wright (1981) believed that there is little doubt that it was laid down originally over the whole area, and that it was contiguous with the Nothe Clay of the Dorset Coast. This statement by Wright (1981) is supported by the presence of the Nothe Clay in most of the boreholes in the western side of the Wessex Basin (see sections 5.4.5 and 5.6).

The Osmington Oolite Formation is made up of the Newton Oolite Member, Sturminster Pisolite Member and the Todber Freestone Member. The Newton Oolite is made up of oolitic packstones and grainstones with local clay bands. The Sturminster Pisolite consists of interbedded pisolitic marl, pisolitic clay and pisolitic bioclastic wackstones-packstones. The Todber Freestone is a cross-bedded oolitic grainstones (Coe 1992).

The Coral Rag Formation, which is present in Wiltshire and Oxfordshire, is only present in a very small area in north Dorset. The Coral Rag in North Dorset is a rubbly limestone with numerous fossils.

The Trigonia Clavellata Beds Formation, which consist of bioclastic oolitic packstone, is not split into members as in south Dorset.

The Sandsfoot Formation is split into the Sandsfoot Clay and Grit members. Only 2.6 m of the Sandsfoot Clay Member is seen in North Dorset, and is described as a blue marl and mudstone with numerous small oysters (Coe 1992). The Sandsfoot Grit is a red argillaceous sand which contains some limonitic ooids and phosphatic nodules.

The Ringstead Formation in north Dorset is a clay with red claystone nodules and is thought to be equivalent to the Ringstead Waxy Clay on the Dorset coast (Coe 1992).

More recently the British Geological Survey has re-mapped the Corallian in north Dorset and published the 'Geology Around Shaftesbury Memoir' (Bristow *et al.* 1995). A comparison of the previous Corallian stratigraphy of north Dorset by Wright (1981) can be seen in Table 5.3. The main differences occur in Wright's Stour and Osmington

Formations. The British Geological Survey team amalgamated these two formations into one formation, the Stour Formation. They also renamed the Nothe Clay the Hinton St. Mary Clay, and the Lower Calcareous Grit Formation the Hazelbury Bryan Formation.

Formation	Member
RINGSTEAD CLAY	
SANDSFOOT FM	SANDSFOOT GRIT
	SANDSFOOT CLAY
TRIGONIA CLAVELLATA BEDS	
CORAL RAG	
OSMINGTON FM	TODBER FREESTONE
	STURMINSTER PISOLITE
	NEWTON OOLITE
STOUR FM	NOTHE CLAY
	CUCKLINGTON OOLITE
	WOODROW CLAY
LOWER CALCAREOUS GRIT	

Wright (1981) & Coe (1992; 1995)

Formation	Member
RINGSTEAD WAXYCLAY	
SANDSFOOT	SANDSFOOT GRIT
	SANDSFOOT CLAY
CLAVELLATA BEDS (including CORAL RAG)	ECCLIFFE
STOUR FM	TODBER FREESTONE
	NEWTON CLAY
	STURMINSTER PISOLITE
	HINTON St MARY CLAY
	CUCKLINGTON OOLITE
	WOODROW CLAY
HAZELBURY BRYAN	

Bristow *et al.* (1995)

Table 5.3 Corallian Group terminology in north Dorset

5.1.2.3 Wiltshire and Oxfordshire

In most areas of Wiltshire and Oxfordshire only parts of the lower Corallian Group have been preserved (*cordatum* to *parandieri* subzones), which consists of four formations: Lower Calcareous Grit, Highworth, Osmington Oolite and Coral Rag (Table 5.2).

The Lower Calcareous Grit Formation is similar to the Nothe Grit Formation in south Dorset and the Lower Calcareous Grit Formation of north Dorset. It is a fine-grained sandstone with a small amount of clay, cemented bands and doggers (Coe 1992).

The Highworth Formation is split into the Highworth Limestone, Highworth Clay and Highworth Grit members in Wiltshire. In Oxfordshire the Highworth Formation is split into the Lower Trigonia Bed, Upper Trigonia Bed and Pusey Flags members. In some parts of Oxfordshire the Highworth Formation is called the Cowley Shell Beds.

The Osmington Oolite Formation is present all over Wiltshire and Oxfordshire but the name of the various members varies across the region (Coe 1992). For example, in Wiltshire the Osmington Oolite is known as the Calne Freestone or the Faringdon Oolite depending on location of the exposure. Generally both the Calne Freestone and the Faringdon Oolite contain cross-bedded oolites at the base and mixed oolites and pisolites at the top. In Oxfordshire the Osmington Oolite Formation is split into the Third Trigonia Bed member and the Urchin Marl member.

The Coral Rag Formation in Wiltshire and Oxfordshire is a coral biolithite which has an average thickness of 6-10 m. The corals form large masses, whereas the inter-coralline portions are filled with bioclastic detritus set in a micritic matrix (Coe 1992).

5.2 Oxfordian palaeogeography of the Wessex Basin

This section briefly describes the various depositional models proposed for the Oxfordian succession of southern England. The more recent sequence stratigraphic models are discussed on Section 5.3.

Wilson (1968) carried out a detailed study of the Upper Oxfordian palaeogeography of southern England. He came to the conclusion that the palaeogeography of the period was dominated by the Portsdown Swell (called Hampshire - Dieppe High in this study), which separates two regions of subsidence, the Wessex (known as the Mere, Dorset and Central Channel sub-basins in this study) and Wealden Basins (known as the Vale of Pewsey and Weald sub-basins in this study). The main points of his model are as follows: the shorelines during the Upper Oxfordian probably trended east-west in the vicinity of London, and paralleled the present-day outcrop to the west (Fig. 5.2). In the west of the region the lower two quartzitic sandstone formations (Nothe Grit and Bencliff Grit) were derived from a north-westerly source. On these banks of quartz sands, tidal-flat regressive cycles of high-energy carbonate sediments formed. Quartz sand deposition appears to have caused shallowing to the extent that such sediments could form. Thus, carbonate deposition was the natural consequence of quartz sand bank formation in a region of former phyllosilicate clay deposition. He suggested that clay-sand-limestone cycles commenced with a rise in eustatic sea-level, but that quartz sand deposition and subsequent carbonate deposition was linked to events in the source

area, and not to sea-level changes. He also suggested that only two major eustatic changes, affecting the whole of southern England occurred during this time, the first during the *pumilus* Zone (when carbonate deposition was terminated) and the second at the beginning of Kimmeridgian times. Finally he stated that the contrast between the Corallian Beds, and the Oxford and Kimmeridge Clays probably does not reflect a more complex tectonic framework to the sedimentary basin at this time, but that shallower restricted marine conditions gave rise to sediments which revealed the form of the sedimentary basin more clearly during Upper Oxfordian times.

Brookfield (1973, 1978a) studied the lithostratigraphy and palaeogeography of the top three ammonite zones of the Oxfordian and the lower three ammonite zones of the Kimmeridgian. He suggested that the passage from Oxfordian to Kimmeridgian times is a gradual change from shallow-water carbonates, through delta-influenced conditions to open-shelf environments and that the common stratigraphic successions in all basins indicate a common overall control on sedimentation. The relative importance, therefore, of sea-level changes, climate and tectonic movements cannot be separated and may be interconnected (Brookfield 1973). Brookfield (1978a) also suggested that the Dorset outcrops appear to represent the western edge of a basin and that the sediments in N. W. France are similar to those of the outcrops in Dorset, and appear to represent similar basin-margin deposits.

Wright (1981, 1986a, 1986b) carried out a series of detailed sedimentological and stratigraphic studies of the Corallian of south Dorset (Wright 1986b), the Corallian of north Dorset (Wright 1981) and the Upper Oxford Clay of south Dorset (Wright 1986a). In all of these studies he re-examined the ammonite fauna and where necessary revised the ammonite zonal scheme. He suggested that the sediments in the Corallian Group in this area were laid down during a tectonically unstable period (Wright 1986b). In the middle Oxfordian, sediments accumulated in a series of extensional basins bounded by deep-seated crustal faults. Positive areas in between the basins rose, providing sediment. During the Upper Oxfordian, there was less tendency for localised basins to develop. More widespread regional subsidence occurred, punctuated by localised uplifts. On a broad scale, therefore, he suggested that as the regional stresses varied with time, subsidence in the basins would vary with the rate of movement of the bounding faults. Widespread clay deposition would occur in extensional phases, followed by a progression to shallow-marine sediment as the stress eased. This being a regional stress, each basin would have a similar history of subsidence and a generally similar stratigraphy, but the details of the stratigraphy would vary with the absolute subsidence and the availability of clastic and carbonate sediment.

De Wet (1987) proposed that syndepositional tectonics, which resulted in movement of the east-west trending fault-bounded blocks making up the Wessex Basin,

regulated local sea-level independently over each block. This resulted in the variable facies distributions. In the Oxford shallows area moderate- to high-energy currents created sand shoals which permitted patch reef development in a shallow subtidal shelf environment.

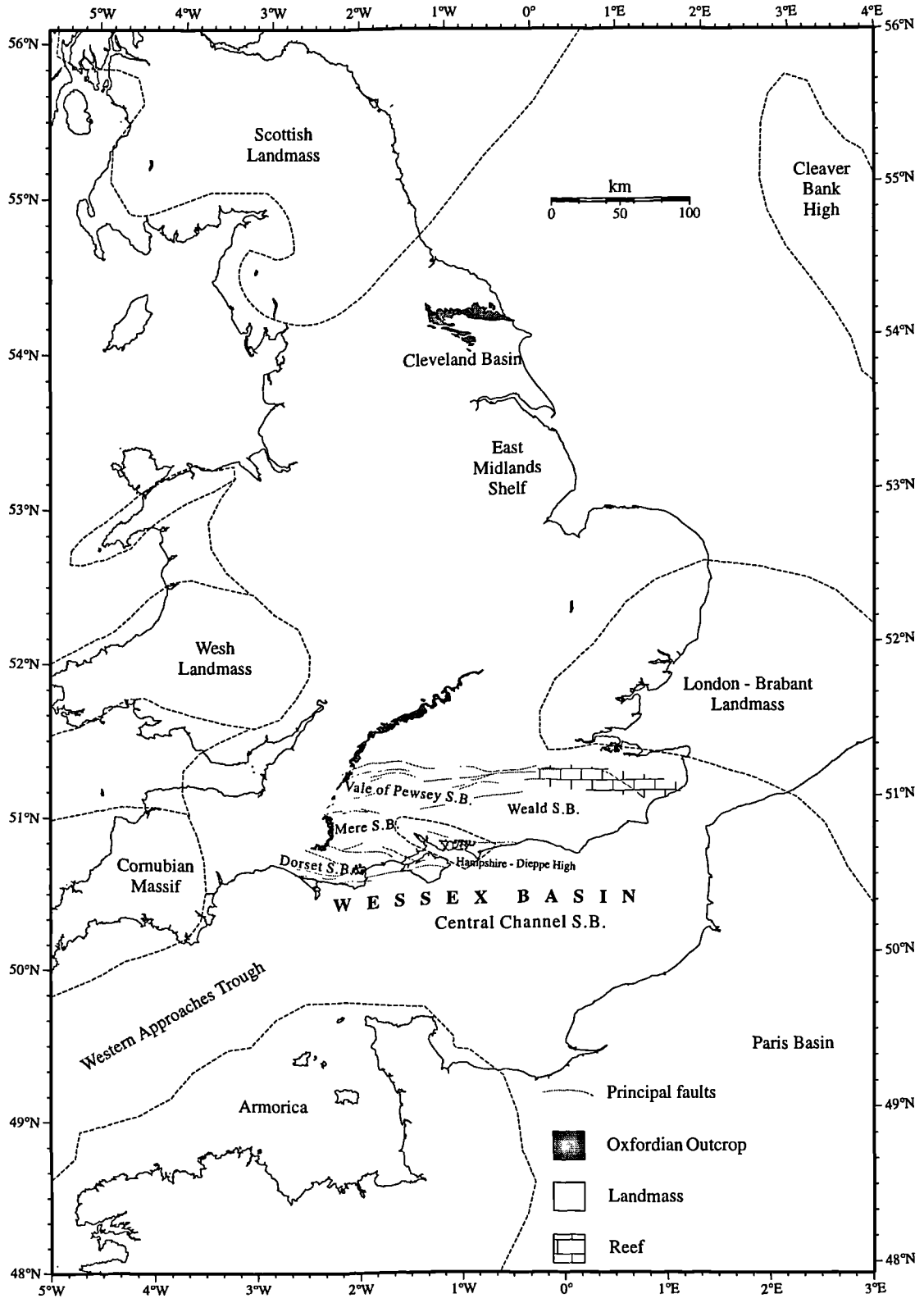

Fig. 5.2 Palaeogeographic map for the Oxfordian. Data from Wilson (1968), Brookfield (1973), Ziegler (1982), Bradshaw *et al.* (1992) and this study. The faults are after Whittaker (1985) and Hamblin *et al.* (1992).

5.3 Sequence stratigraphy of Oxfordian exposures

5.3.1 Introduction

To date the most detailed sequence stratigraphic study of the Oxfordian exposures in the UK has been carried out by Coe (1992, 1995). This section briefly describes the sequence stratigraphy of the Oxfordian exposures as interpreted by Coe (1992). The final part of this section discusses the other sequence stratigraphic studies completed on the Oxfordian of southern England and compares them to the interpretation made by Coe (1992, 1995).

5.3.2 Oxfordian sequence stratigraphy

The Oxfordian succession was deposited during a second-order regression-transgression cycle. The regressive phase started in the *mariae* Zone, at the base of the Oxfordian, and ended near the top of the *nunningtonense* Zone, at the top of the middle Oxfordian. Coe (1992, 1995 and pers. comm.) suggested that this regression-transgression cycle is punctuated by eight unconformities (Table 5.2), or their correlative conformities, which correspond to the base of eight small-scale cycles of relative sea-level change. She informally denoted these unconformities O1 to O8, and interpreted them to be sequence boundaries. The unconformities O7 and O8 were only seen in the Yorkshire exposures where the upper Oxfordian succession is more complete, in the Wessex Basin exposures these sequences are represented by hiatuses or highly condensed strata.

Sequence boundary O1 is within the Upper Oxford Clay Formation (late *praecordatum* Subzone), and is marked by an increase in quartz sand seen in the Jordan Cliff Clays. The transgressive surface is at the top of the Jordan Cliff Clays, and the maximum flooding is represented by the fossiliferous Red Nodule Bed which is in the mid-*costicardia* Subzone (Coe 1992).

Sequence boundary O2 is at the base of the Corallian Group in southern England (*costicardia/cordatum* Subzonal boundary). At outcrop it is the erosional surface between the Upper Oxford Clay Formation and the sands of the Nothe Grit or Lower Calcareous Grit Formation (Coe 1995). The transgressive surface is marked by distinctive faunal-rich sandy limestones (base *vertebrale* Subzone), and the maximum flooding surface is within the Nothe Clay (Table 5.2).

In Dorset the sequence boundary O3 is conformable and is overlain by the sandstones of the Bencliff Grit Member, whereas in marginal areas it is unconformable and commonly overlain by a pebble bed, indicating erosion (Coe 1995). The transgressive surface is located at the base of the *antecedens* Subzone and across the basin is marked by

deposition of a complex of condensed, richly fossiliferous limestones (Coe 1992). Maximum flooding occurred early in the *antecedens* Subzone and is associated by the deposition of an oncolite in Dorset.

In most of the exposures the sequence boundary O4 is unconformable, and an angular relationship between under- and overlying strata can be seen (Coe 1995). The boundary is dated as mid-*antecedens* Subzone and is, for the most part, overlain by carbonates. The transgressive surface is interpreted to be combined with the sequence boundary for the marginal areas. The maximum flooding occurs at the *antecedens/parandieri* zonal boundary. The carbonate deposition culminated in the buildup of coral patch reefs immediately after the time of maximum flooding. This increased biogenic production is related to a lack of siliciclastic input during the peak of the second-order regression (Coe 1995).

Sequence boundary O5 is associated with a biostratigraphic gap (*nunningtonense* Subzone) and is combined with the transgressive surface (Coe 1995). The maximum flooding surface is at the *cautisnigrae/variocostatus* sub-zonal boundary, and is marked by the deposition of clays. The general change of lithology and the associated stratal gap in this sequence, is related to the fairly rapid second-order change from regression to transgression (Coe 1995).

The O6 sequence is associated with a biostratigraphic gap across the whole of the Wessex Basin area (Table 5.2). The location of the O7 and O8 sequences seen in Table 5.2, as mentioned above were only documented from the Cleveland Basin (Coe 1995) and from exposures in Scotland (Coe, pers. comm.). Sequence boundary O7 is represented by the same biostratigraphic gap as O6 in southern England (Coe 1995) and O8 is within highly condensed strata.

5.3.3 Other sequence stratigraphic interpretations

Two sequence stratigraphic studies of the Oxfordian sediments have been carried out in addition to those of Coe (1992, 1995). Wilson (1991) and Sellwood & Wilson (1990) presented a preliminary sequence stratigraphic interpretation of the Corallian Group exposed on the Dorset coast. Most of the key sequence stratigraphic boundaries located by Wilson and Sellwood agree with those found by Coe except for the ones located in the Osmington Oolite Formation (Table 5.4).

Rioult *et al.* (1991) carried out a detailed sequence stratigraphic study of the Middle to early Upper Jurassic outcrops of Normandy, Maine and Dorset. The results of their sequence stratigraphic interpretation can be seen in Table 5.4. The table clearly shows that the sequence stratigraphic model proposed by Rioult *et al.* (1991) is very similar to

that of Coe (1992, 1995) except for those key sequence stratigraphic surfaces located within the Osmington Oolite Formation.

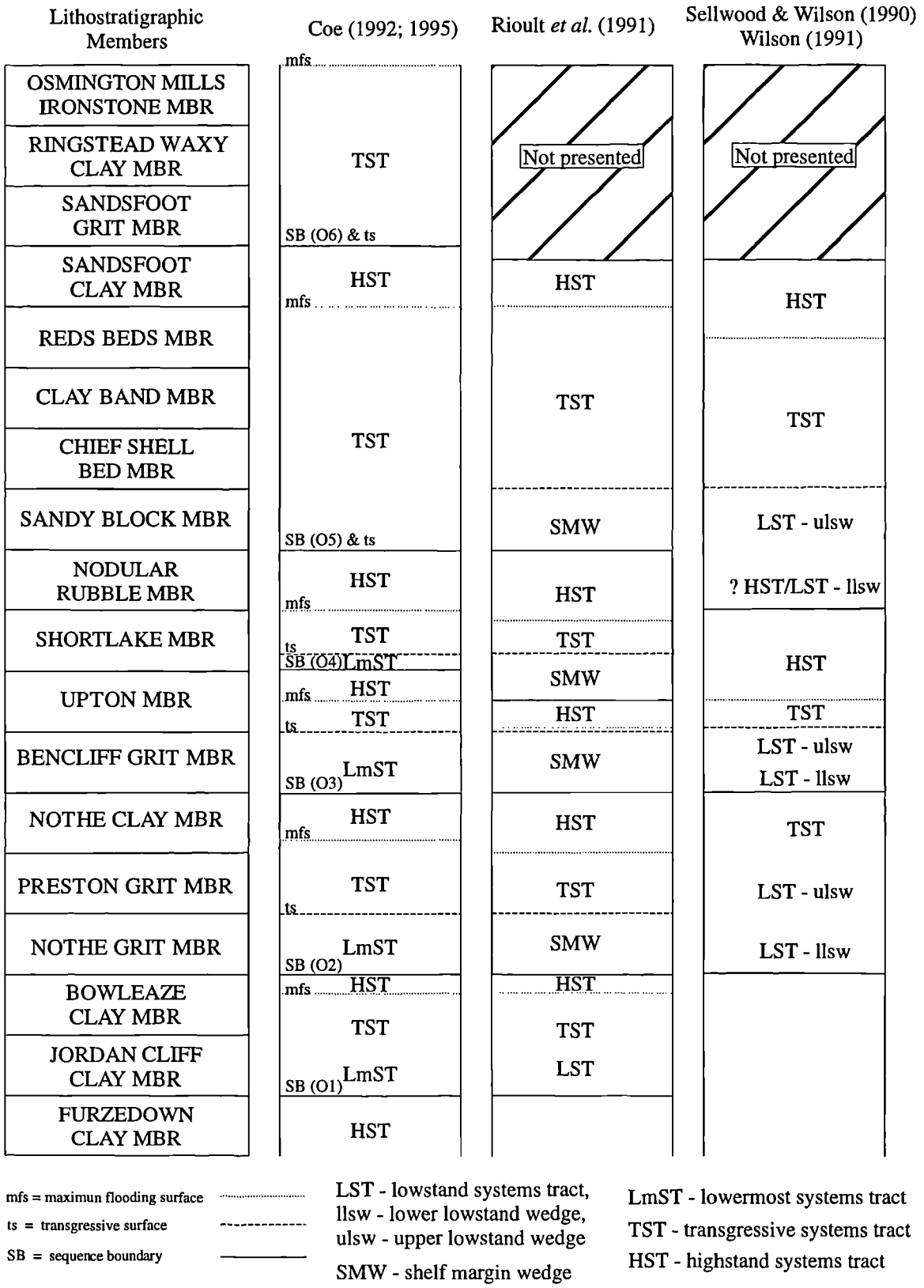

Table 5.4 Comparison of the different sequence stratigraphic interpretations of the Oxfordian succession exposed on the Dorset coast (modified after Coe 1992).

Coe's sequence stratigraphic study was used here because her study was the only one which incorporated all the Oxfordian exposures in the whole of the England and not just those exposed on the Dorset coast.

Older studies, which addressed cycles, transgressions and sea-level changes, have been carried out prior to the development of sequence stratigraphy by Vail *et al.* (1977). For example, Talbot (1973) described the Corallian Beds as consisting of four asymmetric, upward-shallowing cycles, where each cycle is separated from the next by a non-sequence, usually an erosion surface, which marks a marine transgression. He even went as far as saying that there is evidence of the same non-sequence occurring elsewhere in Britain and abroad, suggesting that the transgressions were the result of world-wide, eustatic sea-level changes.

5.4 Sequence stratigraphical interpretation of the wireline logs

5.4.1 Introduction

Thirty five boreholes in the Wessex Basin that contain both Oxfordian strata and wireline data were available for this study. The wireline logs from these thirty five boreholes have been subdivided both lithostratigraphically and biostratigraphically prior to being interpreted sequence stratigraphically.

Sequence stratigraphic interpretation of the wireline data was achieved by correlating the wireline data from the boreholes with the field gamma-ray and density logs constructed for the Oxfordian succession exposed on the Dorset coast, and by using the lithostratigraphical and biostratigraphical subdivisions of the logs to constrain the final sequence stratigraphic interpretation.

The format of this section is to briefly describe the field gamma-ray and density logs sequence stratigraphically (Section 5.4.2). The key wells used in the biostratigraphical and lithostratigraphic subdivision of the borehole data are then discussed in Section 5.4.3. The final part of the section (Section 5.4.4) describes the results of the sequence stratigraphic analysis of the Wessex Basin based on the wireline log data.

5.4.2 Field gamma-ray and density logs

The composite field gamma-ray log for the Oxfordian, as described in Chapter 2, was constructed by combining the data recorded over Furzy Cliff, Redcliff / Hamcliff, Bran

Point (up to the base of the Red Beds Member) and Black Head (from the base of the Red Beds Member) (Fig. 5.3; also see Appendix B for lithological logs of the above mentioned exposures). This composite field gamma-ray log was thus constructed using the Osmington Oolite Formation exposed at Bran Point.

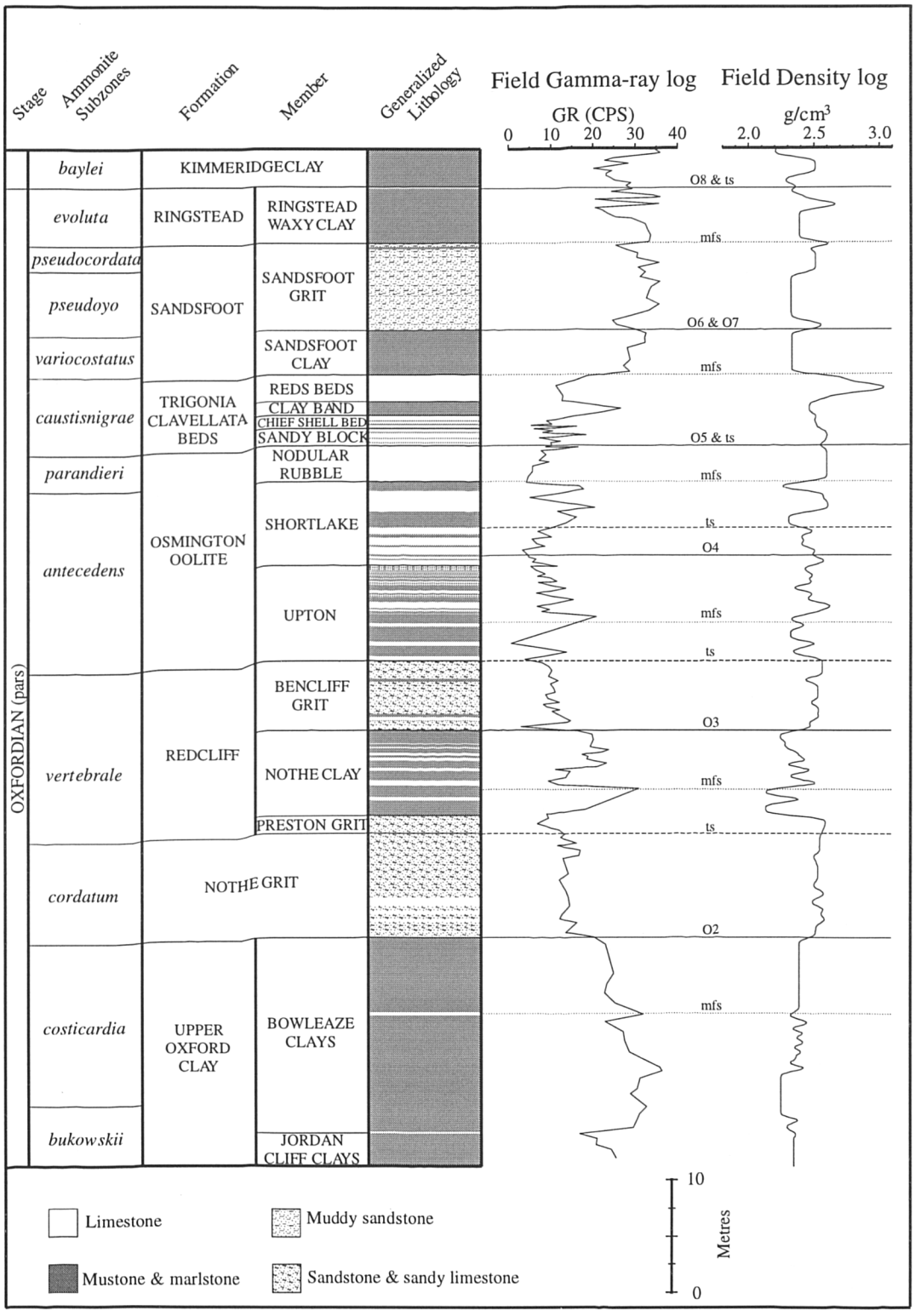

Fig. 5.3 Composite field gamma-ray and density field logs for the Oxfordian succession exposed on the Dorset coast, showing the key sequence stratigraphic surfaces.

Figure 5.4 shows the comparison of the field gamma-ray log constructed for the Osmington Oolite Formation exposed at Bran Point and that at Black Head (see also Appendix B). It is clear that lithological variations do occur, which account for the differences seen in the two field gamma-ray logs. However, despite the lithological variations the overall trends seen on the two field gamma-ray logs are similar.

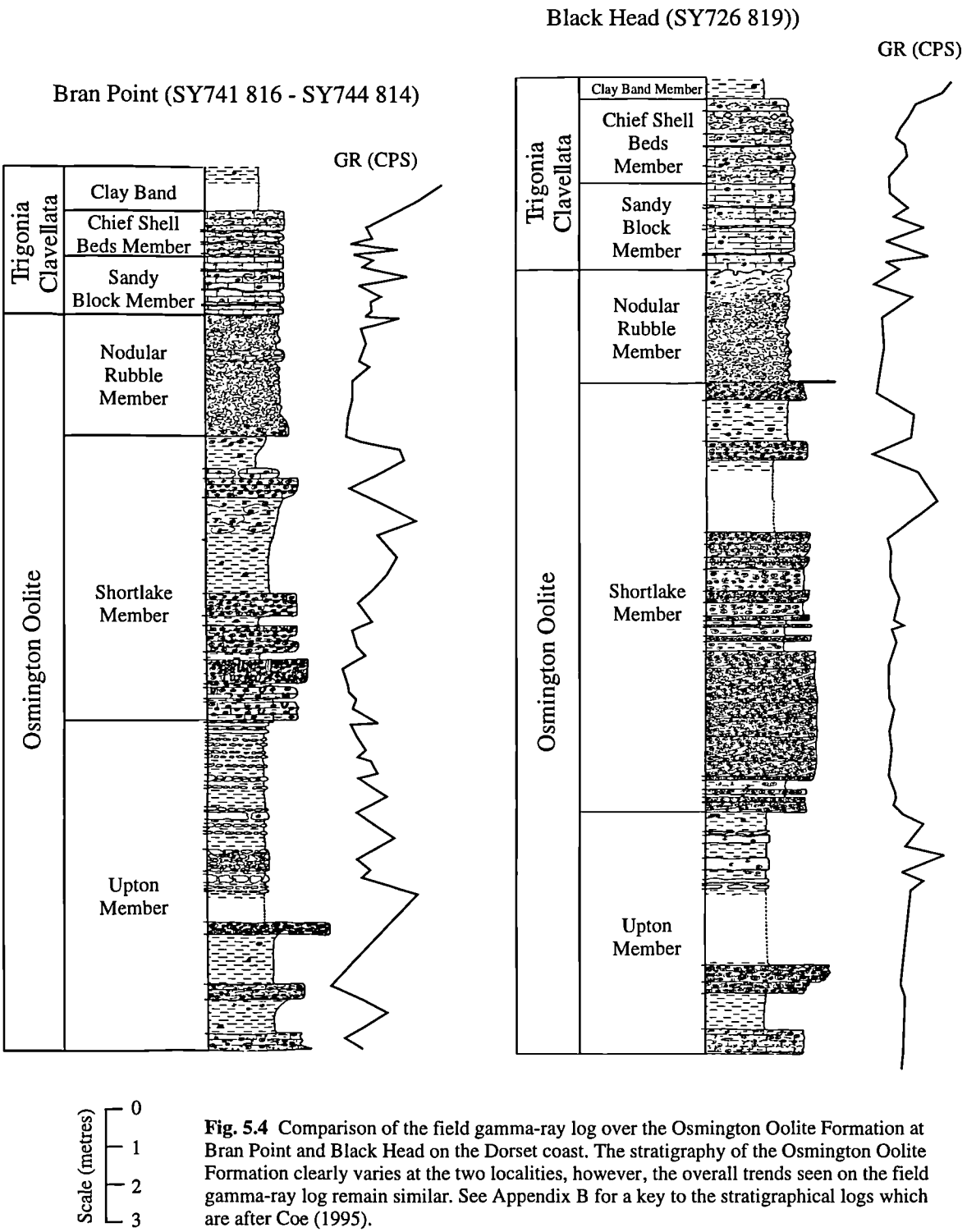

Fig. 5.4 Comparison of the field gamma-ray log over the Osmington Oolite Formation at Bran Point and Black Head on the Dorset coast. The stratigraphy of the Osmington Oolite Formation clearly varies at the two localities, however, the overall trends seen on the field gamma-ray log remain similar. See Appendix B for a key to the stratigraphical logs which are after Coe (1995).

Another factor which contributes to the difference seen in the two field gamma-ray logs is the fact that the exposure at Bran Point is better, and easier to record gamma-ray measurements on, than the exposure at Black Head. This is because the exposure at Bran Point is a vertical fairly smooth cliff which is easily accessible, while the lower part of the exposure at Black Head is on the foreshore and is only exposed at low tides. The beds form irregular ledges and grooves due to the variable lithology, and the grooves are usually still filled with sea-water at low tide: hence the lack of data over the Upton Member (see Black Head log in Appendix B, Fig. 5.4). For this reason the composite field gamma-ray log used in Chapter 2 and subsequently in this chapter is the one constructed with the Osmington Oolite Formation exposed at Bran Point, and because of this the field density log was also constructed using the Bran Point succession.

The positions of the key sequence stratigraphic surfaces found at outcrop have been placed on the field gamma-ray and density logs (Fig. 5.3). It is evident that the trends seen on the field gamma-ray log correspond very well with the trends expected in a typical theoretical sequence (see Chapter 4): for example, the lowermost systems tract should show progradation, the transgressive systems tract retrogradation and the highstand systems tract aggradation and/or progradation (Fig. 5.5).

It was demonstrated in Chapter 2 that the facies in the Oxfordian succession changes both laterally and vertically and, therefore, unlike the Kimmeridgian succession which can be correlated very accurately peak for peak, it is hard to correlate the Oxfordian between the boreholes just using the wireline signature alone. However, the trends seen on the field gamma-ray log (Fig. 5.5) have demonstrated that the Oxfordian succession can be interpreted in a sequence stratigraphic manner, which means that the boreholes can be quite successfully correlated using wireline trends related to the component parts of the depositional sequence.

5.4.3 Boreholes with biostratigraphical control

Only a few of the wells used in this study were cored over the Oxfordian interval, so most of the biostratigraphic data come from drill cuttings and side wall cores (see Chapter 3 for the disadvantages of drill cuttings).

For example, the biostratigraphic report for 98/11-3 by King & Allen (1987), was done using unwashed drill cuttings which were collected at 20ft (6m) intervals. The report stated that foraminiferid *Ammobaculites corprolithiformis*, indicating the Oxfordian age, was found between 905.2m 935.7m (King & Allen 1987). Microflora comprising mainly long-ranging taxa were also found over this interval, in particular *Hystrichogonyaulax cladophora* which is typical of Oxfordian sediments. Foraminifera *Lenticulina quenstedti* and *Epistomina mosquensis,* found in the depth range 981.4-987.5m indicate Early

Oxfordian / Late Callovian. Ostracods *Lophocythere scabra bucki* in the depth range 993.6-999.7m and *Nophrecythere cruciata* in the depth range 999.7-1005.8m indicate Early Oxfordian. There were also a lot of microflora found in the depth range 935.7-1006.7m, which were also indicative of Early Oxfordian age.

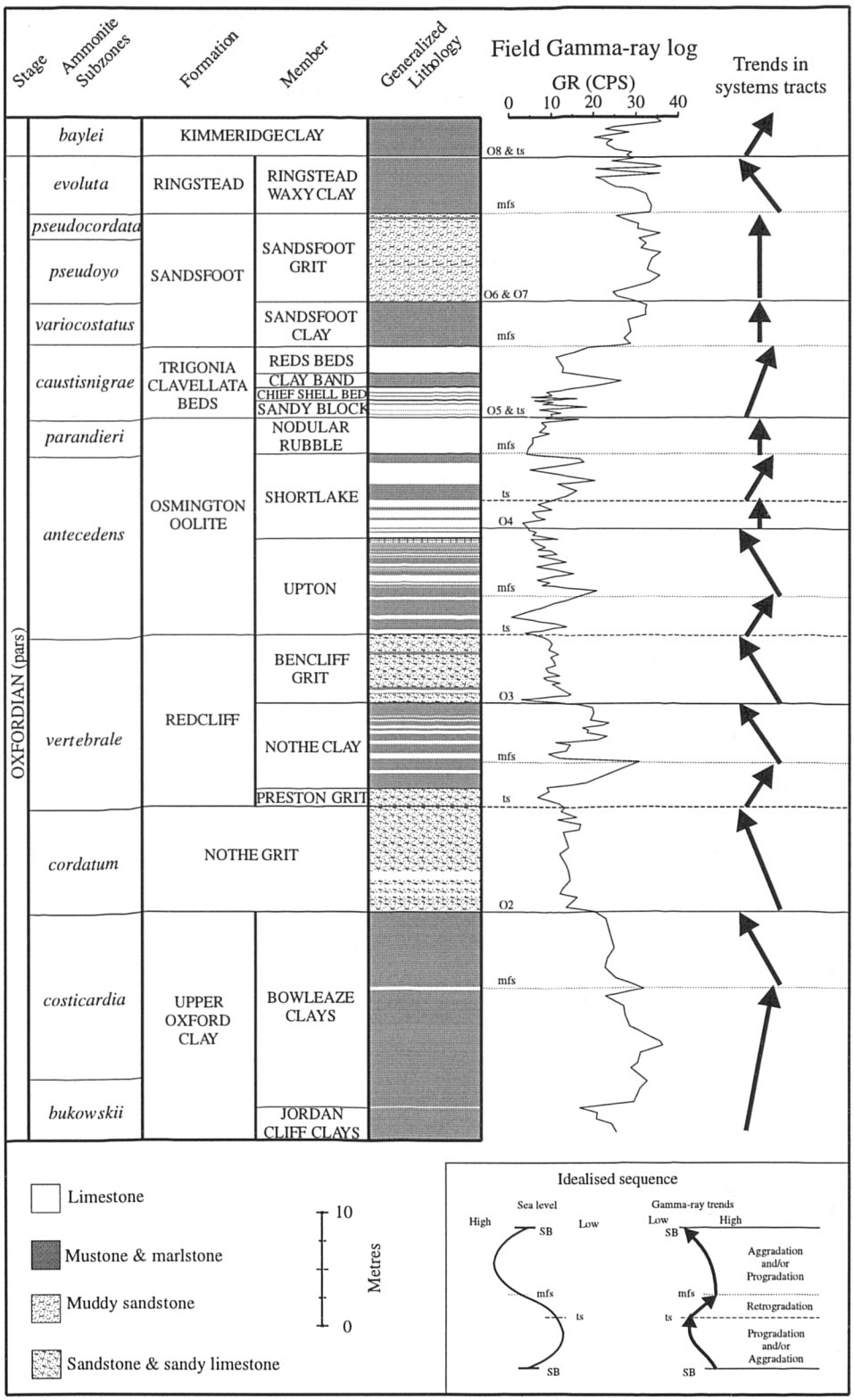

Fig. 5.5 Gamma-ray trends seen in each of the systems tracts on the composite field gamma-ray log for the Oxfordian succession exposed on the Dorset coast.

This type of biostratigraphic data clearly only tells us that Oxfordian-age sediments are present, but is not detailed enough to suggest ages down to the ammonite zone or subzone framework used in the exposures. On the other hand, where core is taken there is more chance of finding ammonites and/or other more informative fossils. For example, ammonites found in the Ashdown 1 core between depths of 929.6m and 960.7m are all indicative of the Upper Oxfordian and equivalent to part of the Ampthill Clay (Bristow & Bazley 1972). Further down, a specimen of *Amoeboceras* was found at 988.5 m indicating the *cautisnigae* Zone (Bristow & Bazley 1972), and at 1046.6 m ammonites which were described as possibly of the *cordatum* Zone (Bristow & Bazley 1972) were found (Fig. 5.6). In the Upper Oxford Clay at a depth of 1049m, an ammonite *Cardioceras (S.) alphacordatum* Spath was found, indicating *mariae* Zone (*praecordatum* Subzone) (Fig. 5.6).

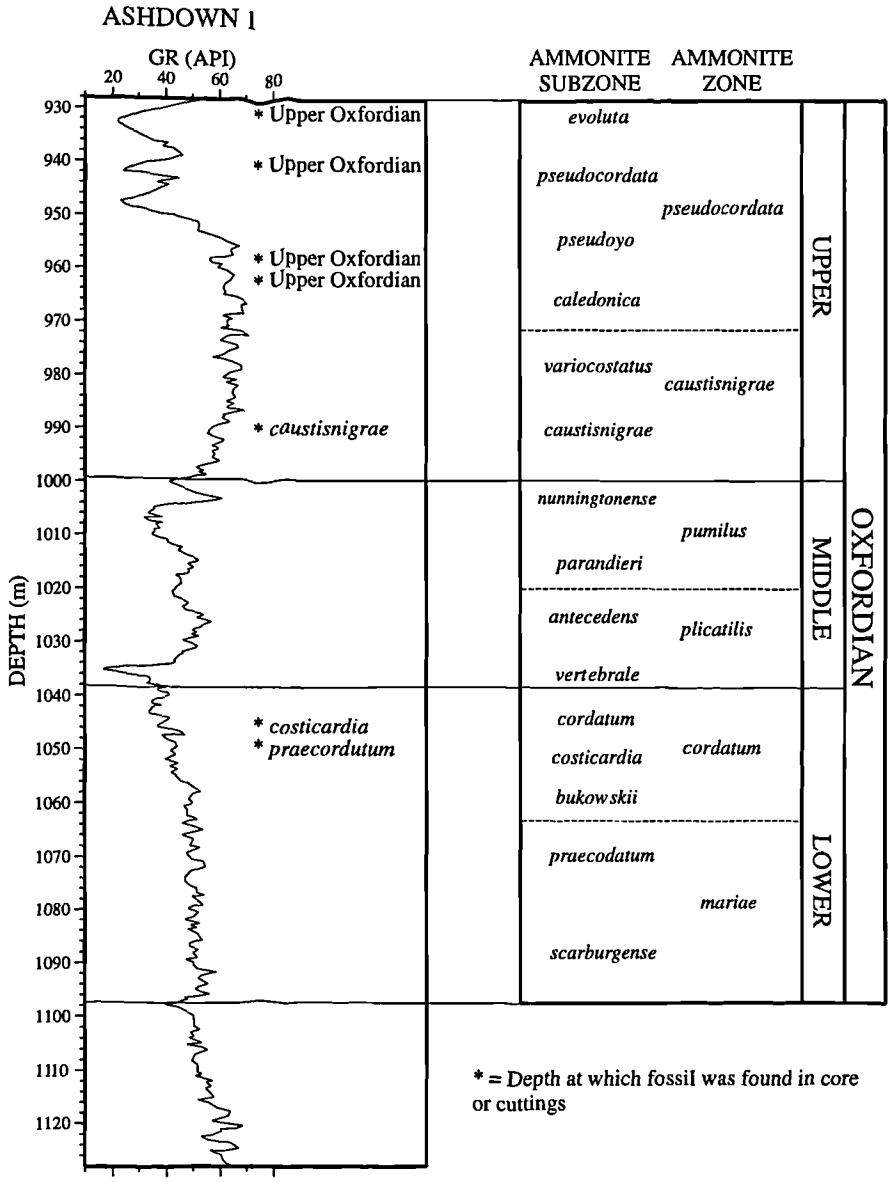

Fig. 5.6 Biostratigraphic information obtained from fossils found in core and cuttings from Ashdown 1 borehole. Fossil depths and ages from Bristow & Bazley (1972).

Ammonites were also found in the core from the Warlingham 1 borehole. For example, below the fault breccia at 911.8m are 1.3m of mudstone which contain ammonites. Callomon & Cope (1971) described these beds as clays of the same age and facies as the Ringstead Waxy Clays of the Dorset coast and assigned them to the *pseudocordata* Zone. These clays are said to rest with apparent conformity on the thick coralline limestone below (Fig. 5.7; Worssam & Ivimey-Cook 1971). No fossils have been found in the coralline limestone or the oolitic limestone units. However, in the ironshot silty beds rare oppeliid ammonites which may possibly indicate the *plicatilis* Zone were found (Callomon & Cope 1971).

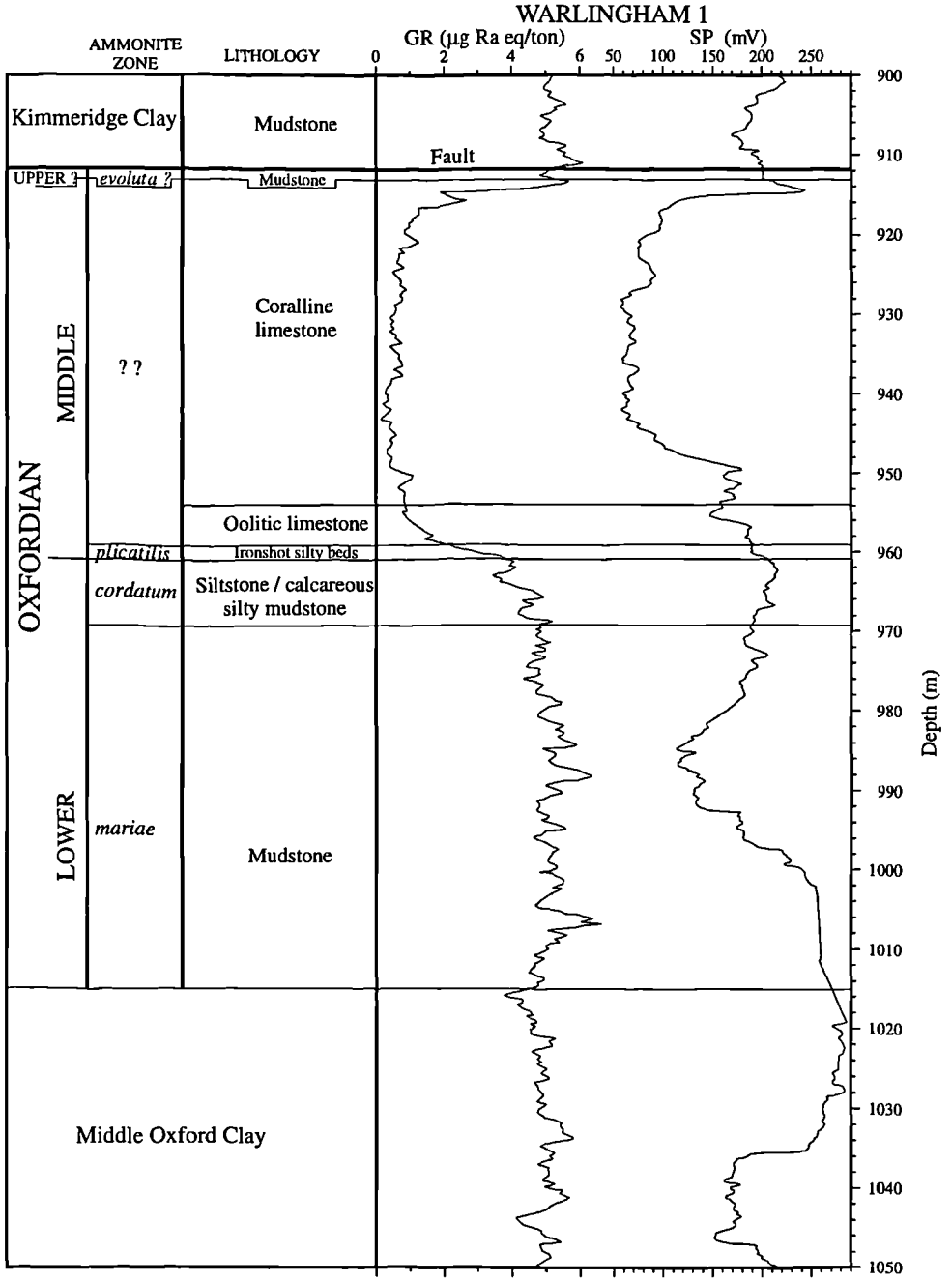

Fig. 5.7 Diagram showing the biostratigraphic information obtained from the Warlingham borehole core by Worssam & Ivimey-Cook (1971).

From the ammonite evidence, it has been suggested that the limestone in Warlingham 1 borehole ranges in age from the *plicatilis* Zone up to the *pseudocordata* Zone (Worssam & Ivimey-Cook 1971). Worssam & Ivimey-Cook (1971) also noted "a record by Downie (in Wilson 1968) that microplankton from near the top of the limestone at Warlingham suggest the *plicatilis* Zone does not entirely support such an inference". Cope *et al.* (1980) also noted that comparison of the Warlingham core with the Kent Coal field successions suggests a substantial stratigraphical break between the mudstones below the fault and the coralline limestone.

Boreholes for which no wireline data were available in this study but did contain core, have been used in this study to interprete nearby boreholes. For example, the biostratigraphy of the Brightling borehole was worked out by correlating the data with core taken over the Oxfordian interval from the Grove Hill borehole (Lake *et al.* 1987). The Arreton 1 and 2 boreholes, which are located on the Isle of Wight, were interpreted biostratigraphically by correlating them with the offshore wells in block 98/11. The Wareham 3 borehole was interpreted by correlating the data with Wareham C6 and Encombe boreholes, which were not available in this study but were shown in Bristow *et al.* (1995). Table 5.5 shows all the boreholes in the Wessex Basin for which biostratigraphic data exist and were used in this study as the key biostratigraphically controlled boreholes.

BOREHOLE	REFERENCE
98/11-1	Jacovides *et al.* (1983)
98/11-2	Jacovides & Woollam (1994)
98/11-3	King & Allen (1987)
98/11-4	King *et al.* (1987)
98/23-1	King & Jacovides (1983)
Ashdown 1	Bristow & Bazley (1972) Cope *et al.* (1980)
Ashdown 2	Bristow & Bazley (1972) Cope *et al.* (1980)
Bolney 1	Gallois & Worssam (1993)
Brightling 1	Lake *et al.* (1987)
Collendean Farm 1	Whittaker *et al.* (1985)
Detention 1	Perkins (1982)
Henfield 1	Young & Lake (1988)
Humbly Grove	BGS well file
Kimmeridge K5	BGS well file
Marchwood 1	Whittaker *et al.* (1985)
Warlingham 1	Worssam & Ivimey-Cook (1971) Cope *et al.* (1980)
Winterborne Kingston 1	Whittaker *et al.* (1985) Bristow *et al.* (1995)

Table 5.5 List of boreholes, in the Wessex Basin, with references containing biostratigraphical data for the Kimmeridgian.

5.4.4 Lithostratigraphy

As was shown in the previous section, biostratigraphic control for the Oxfordian strata encountered in boreholes is fairly limited. Ammonites are rarely found, and when they are, they are found in the clay facies. Other microflora and fauna tend to be long-ranging taxa. Therefore in this study identification of the various formations in the Oxfordian was carried out by a combination of lithological and petrophysical log characteristics. This was done by calculating the lithology from the so-called lithology logs (gamma-ray, density, neutron and sonic), and then comparing the wireline lithology with the known outcrop lithology. The wireline lithology was calculated using the Petra module of the TerraSation II software package, as described in Chapter 3, Section 3.5.

Figures 5.8 and 5.9 are examples of the results of the Petra module for two wells in the Wessex Basin. In the example shown for the 98/11-1 borehole (Fig. 5.8), the gamma-ray, sonic and density logs were used to calculate the lithology, and for the Ashour 1 borehole the gamma-ray, density and neutron logs were used (Fig. 5.9). For both examples only four components were entered into the program: sandstone, limestone, shale and porosity. These four components were chosen because for the majority of the Oxfordian succession these are the only components present in any significant quantity. In some beds, however, other lithologies such as phosphatic nodules, iron ooids and siderite cement are present, so the Petra solution is not ideal. For example, in the 98/11-1 borehole (Fig. 5.8) it is evident that the reconstructed Petra curves do not match the original gamma-ray and density wireline curves around 940m depth. It is believed that these beds represent a condensed section of the argillaceous upper part of the Corallian Beds above the Osmington Oolite Formation, where phosphatic nodules, iron ooids and siderite cement are all found (see lithology logs in Appendix B).

In this study, the lithology was calculated for all the boreholes which had at least two lithology logs. The calculated lithology for each well was then compared with the field gamma-ray and density logs, the nearest well with good biostratigraphic data, and the closest outcrop exposures, so that a final lithostratigraphic subdivision of the well could be undertaken. Figure 5.10 shows the final lithostratigraphic subdivision for 98/11-3 and 98/11-4 boreholes.

A few of the boreholes used in this study have been subdivided lithostratigraphically into formations by various authors (mainly in British Geological Survey publications). For example, the wireline data from the Winterbourne Kingston 1 borehole, located in north Dorset, were interpreted by Whittaker (1985) and re-interpreted by Bristow *et al.* (1995) using the known lithostratigraphy of the area (Fig. 5.11 & Table 5.3). These previous interpretations were only used as a guide in this study, because the whole wireline data set has been re-interpreted to ensure that the sequence stratigraphic interpretation (see next section) was consistent for all the boreholes in the Wessex Basin.

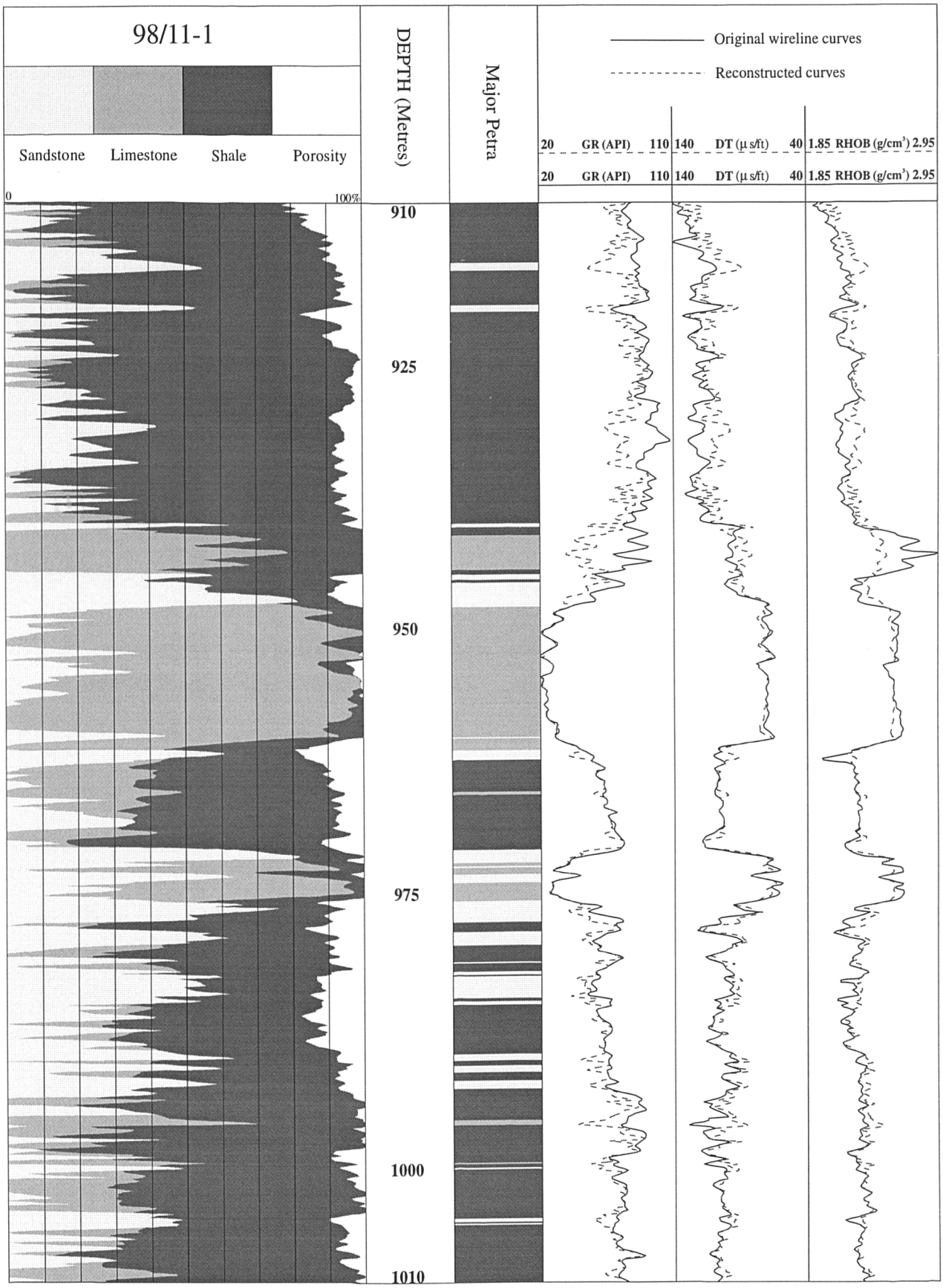

Fig. 5.8 Lithology calculated using the Petra module of the Terrastation II computer package, for the interval which encompasses the Oxfordian succession in the 98/11-1 borehole.

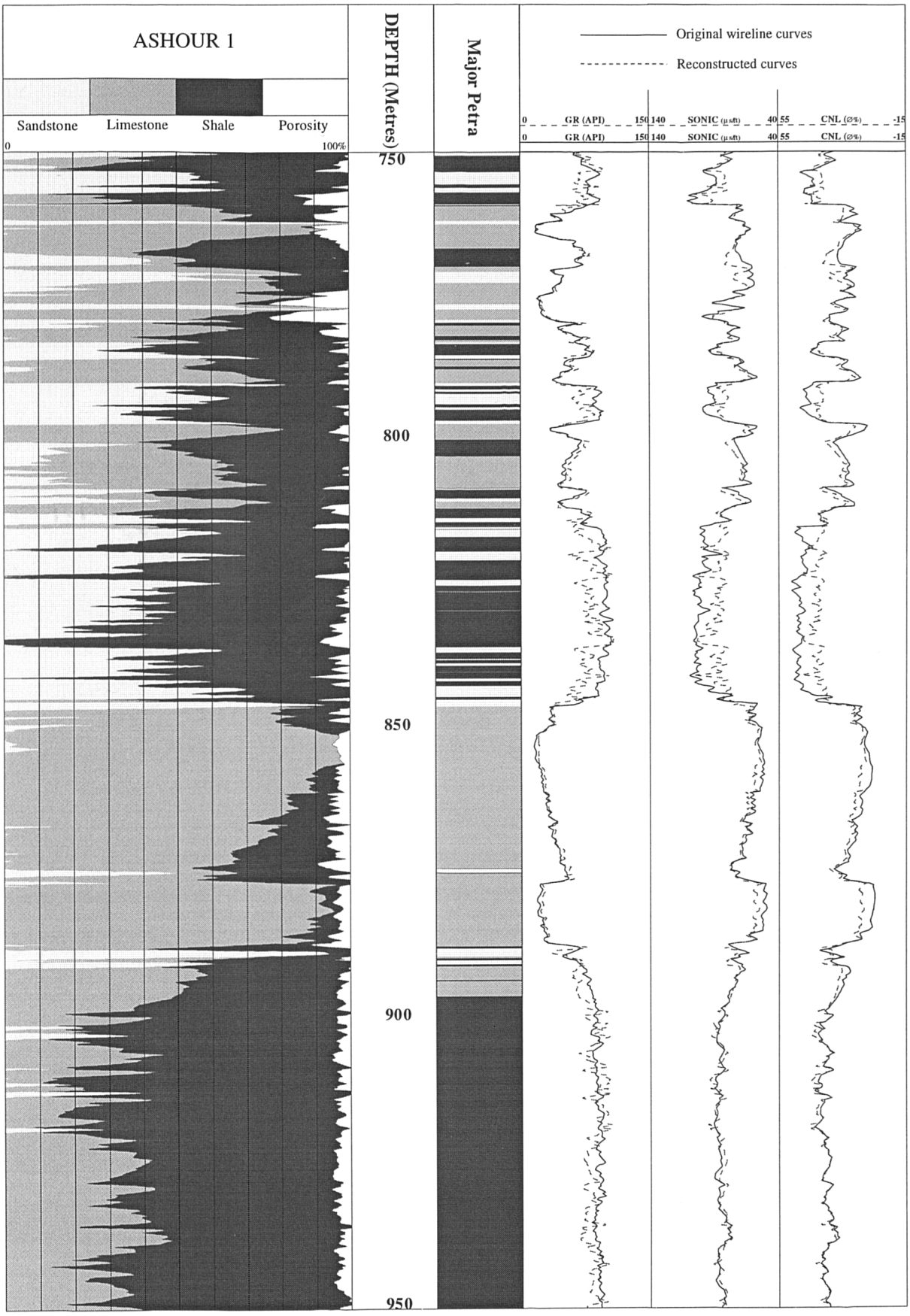

Fig. 5.9 Lithology calculated using the Petra module of the Terrastation II computer package, for the Oxfordian succession typical of the Weald Sub-basin.

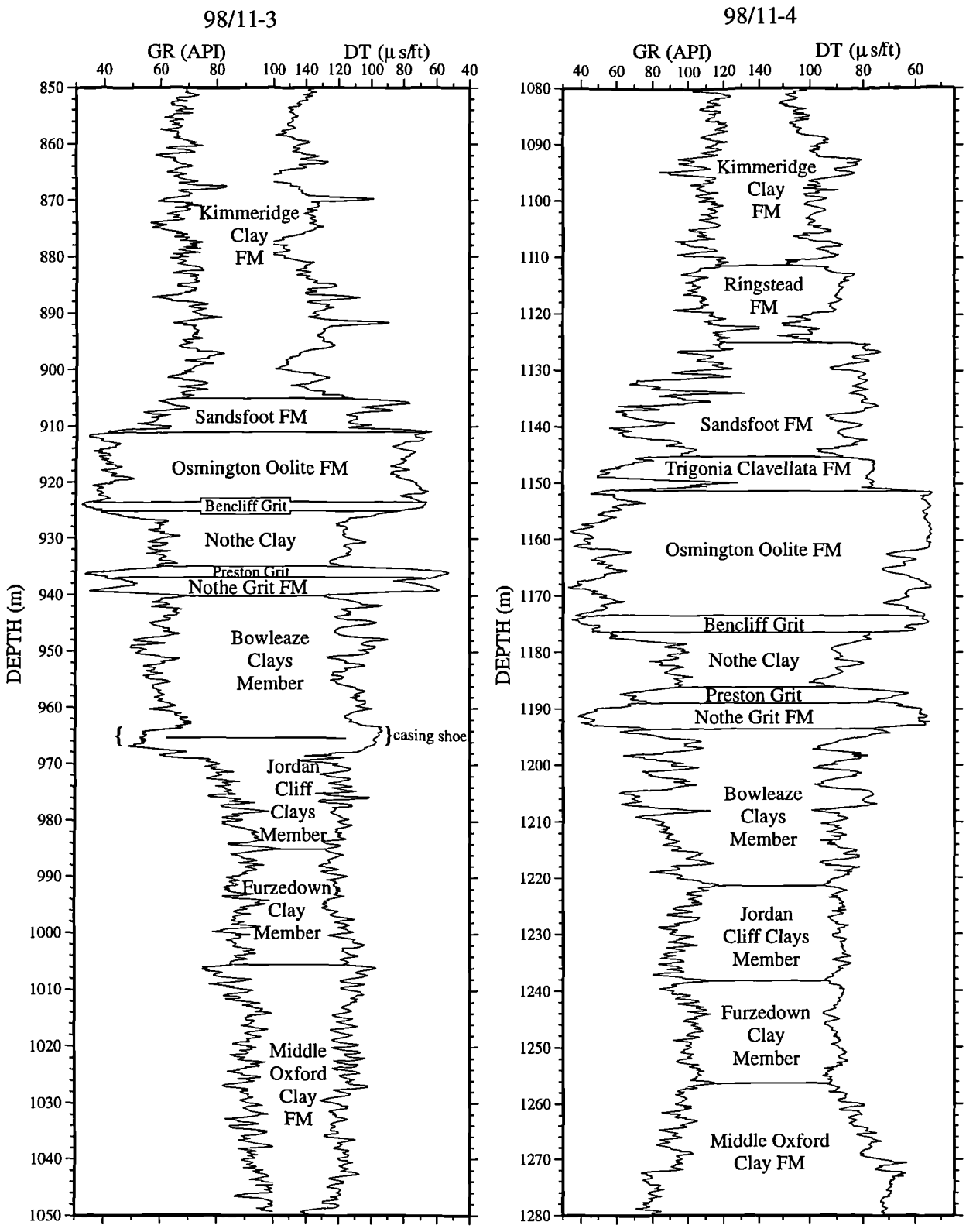

Fig. 5.10 Lithostratigraphic subdivision of the Oxfordian successions in the 98/11-3 and 98/11- 4 boreholes, based on the available biostratigraphic data, calculation of lithology using Petra and comparison with exposures on the Dorset coast using the field gamma-ray and density logs.

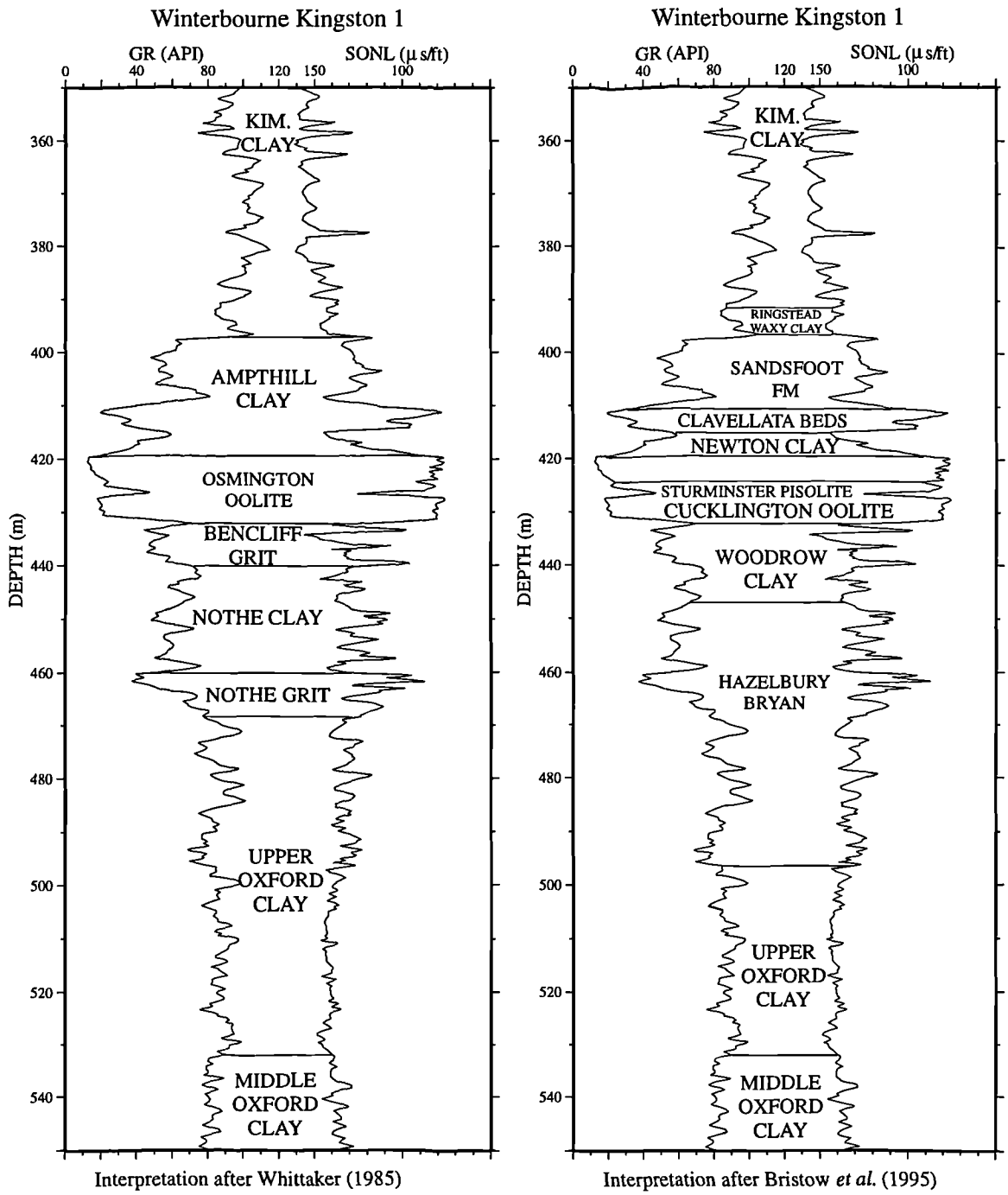

Fig. 5.11 Comparsion of two interpretations of the Oxfordian succession encountered in the Winterbourne Kingston 1 Borehole.

5.4.5 Wessex Basin

The lithology was calculated and the ammonite zones located on all the boreholes which contained biostratigraphic data. The next stage in the construction of the sequence stratigraphic wireline correlations (Figs 5.12 to 5.18) was to correlate these biostratigraphically controlled boreholes with the rest of the boreholes in the Wessex Basin and the field gamma-ray and density logs, using the techniques described in Chapter 3. Once all the ammonite zones had been picked on the entire borehole data set, the key

sequence stratigraphic surfaces were then picked using the ammonite zones as a constraint to the interpretations (see Chapter 3).

Whilst producing the wireline correlations, it was evident that the Oxfordian sediments did not correlate peak for peak as the Kimmeridge Clay Formation did (see Chapter 6) between boreholes within the sub-basins of the Wessex Basin. Therefore the interpretation of trends seen on the wireline logs proved to be very important for the wireline sequence stratigraphic interpretation.

The key sequence stratigraphic surfaces (sequence boundary, transgressive surface and maximum flooding surface) have been picked for the sequences O1 - O8 of Coe (1992, 1995) on most of the boreholes shown in the wireline correlations (Fig. 5.12 to 5.18).

The key sequence stratigraphic surfaces for the O1 sequence were only picked with confidence in the wells shown in the wireline correlation (Fig. 5.12) for two reasons. Firstly, the lower part of the O1 sequence is not exposed on the Dorset coast, so the full sequence was not incorporated in the field gamma-ray and density logs. Secondly, not many boreholes used in this study have been cored over the Upper Oxford Clay interval, and those that have been tend to have very generalised lithology descriptions of the core. The key sequence stratigraphic surfaces for the O1 sequence were picked in the wells correlated in Figure 5.12 with confidence, because the Oxfordian succession in these boreholes is similar to that seen in the exposures on the Dorset coast. Therefore, knowing the thickness of the three members of the Upper Oxford Clay from previous work done on exposures in the past, when the whole Upper Oxford Clay was exposed on the Dorset coast (Wright 1986; Cope *et al.* 1980), it was possible to locate the boundaries of the members on the wireline logs from the 98/11-3 and 98/11-4 boreholes (Fig. 5.10). Figure 5.10 shows that the boundaries of the members within the Upper Oxford Clay are not very distinctive and significant wireline marker horizons do not exist in the succession. Nevertheless, by changing the scale and using the simple mathematical techniques discussed in Chapter 3, which enhance the trends seen on the wireline logs, it was possible to locate the O1 sequence boundary, transgressive surface and maximum flooding surface on the rest of the wireline correlations (Figs 5.13 to 5.18). For example, in 98/11-4 borehole (Fig 5.12), where the O1 sequence boundary, transgressive surface and maximum flooding surface were located by correlating the borehole succession with the outcrops on the Dorset coast, it is evident that the trends seen on the gamma-ray log conform to what is expected in a typical sequence (i.e. progradation from the sequence boundary to the transgressive surface, retrogradation from the transgressive surface to the maximum flooding surface and finally progradation from the maximum flooding surface to the O2 sequence boundary). Therefore it was possible to extend the interpretation to the boreholes further away from the Dorset coast.

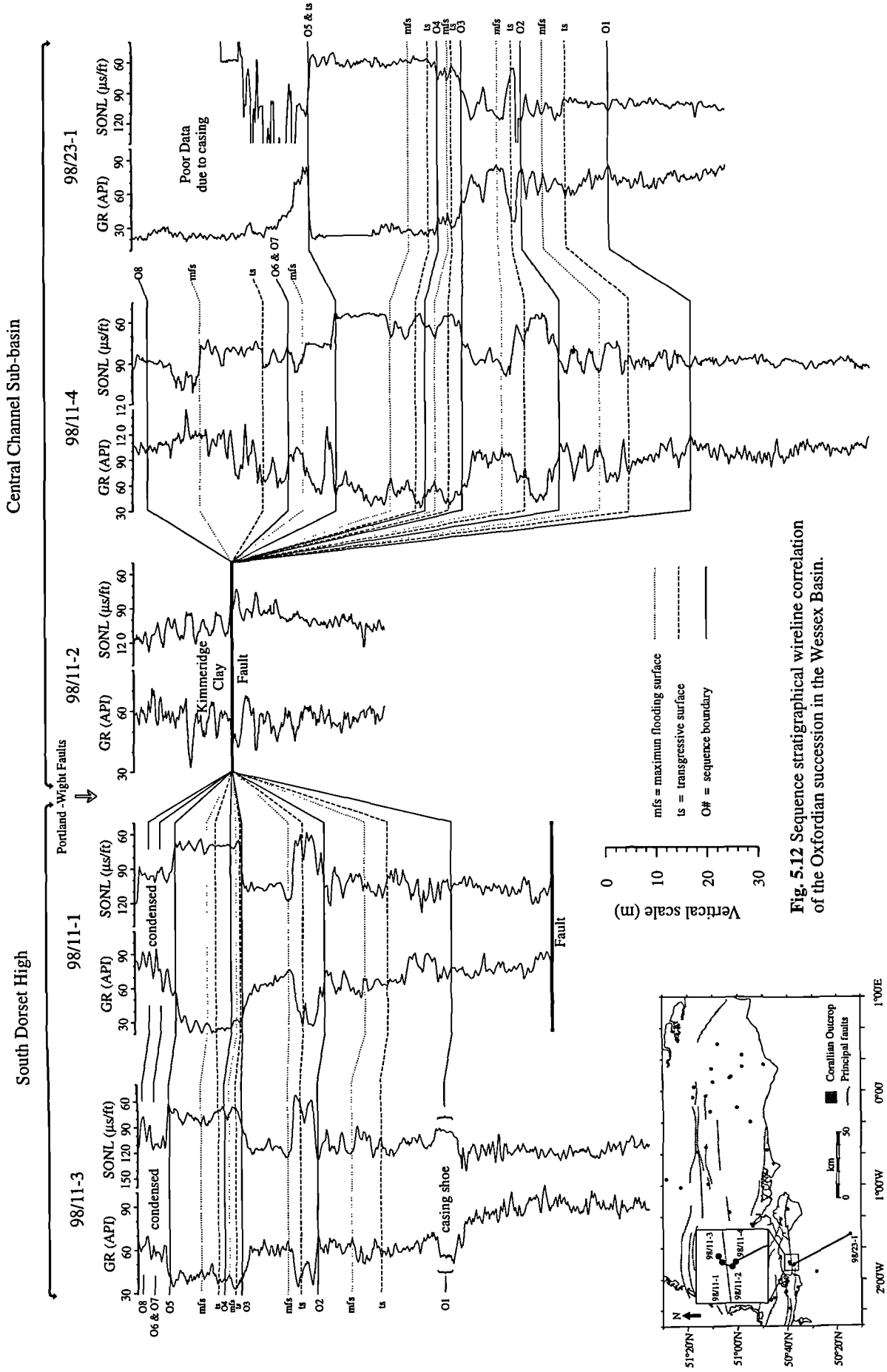

Fig. 5.12 Sequence stratigraphical wireline correlation of the Oxfordian succession in the Wessex Basin.

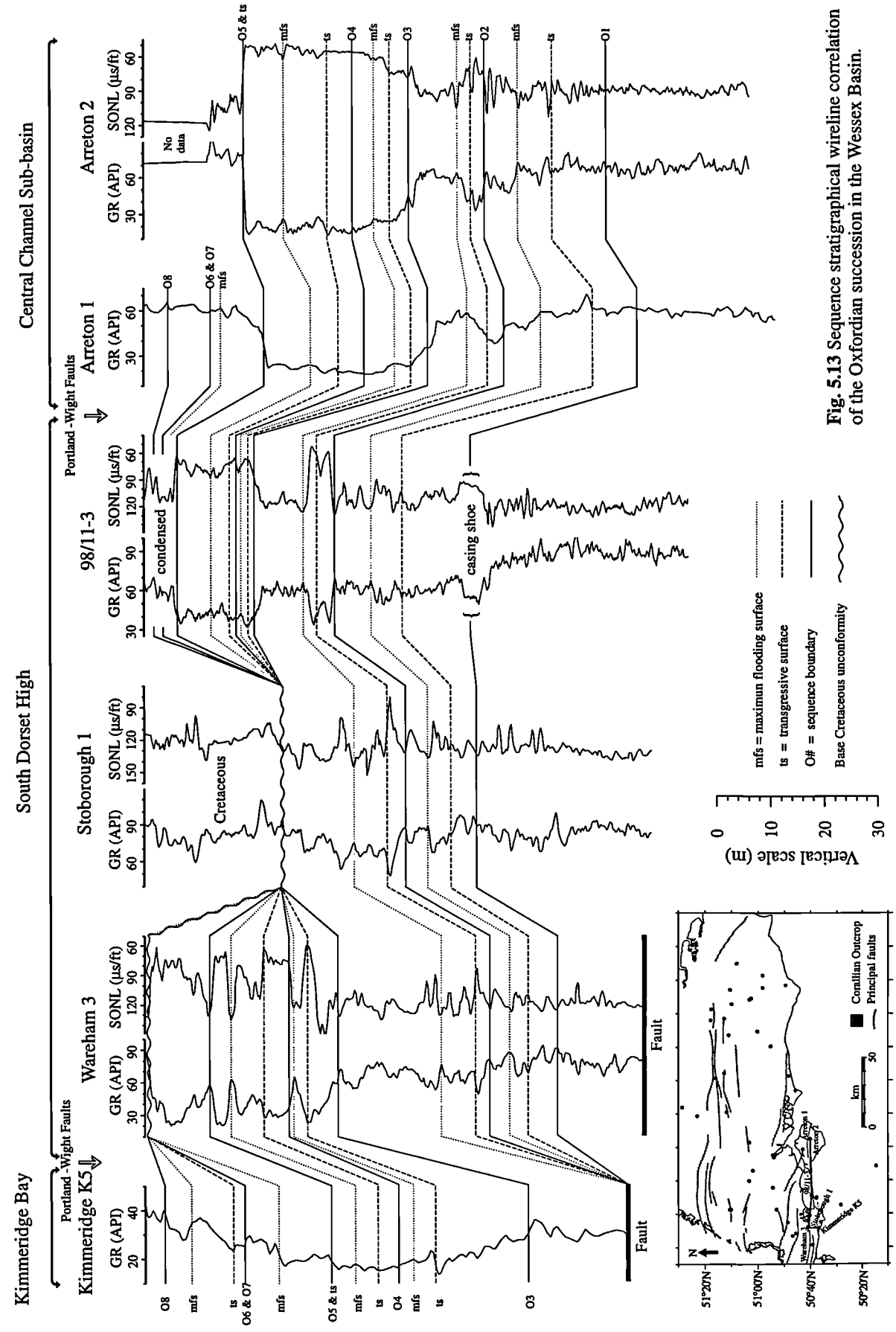

Fig. 5.13 Sequence stratigraphical wireline correlation of the Oxfordian succession in the Wessex Basin.

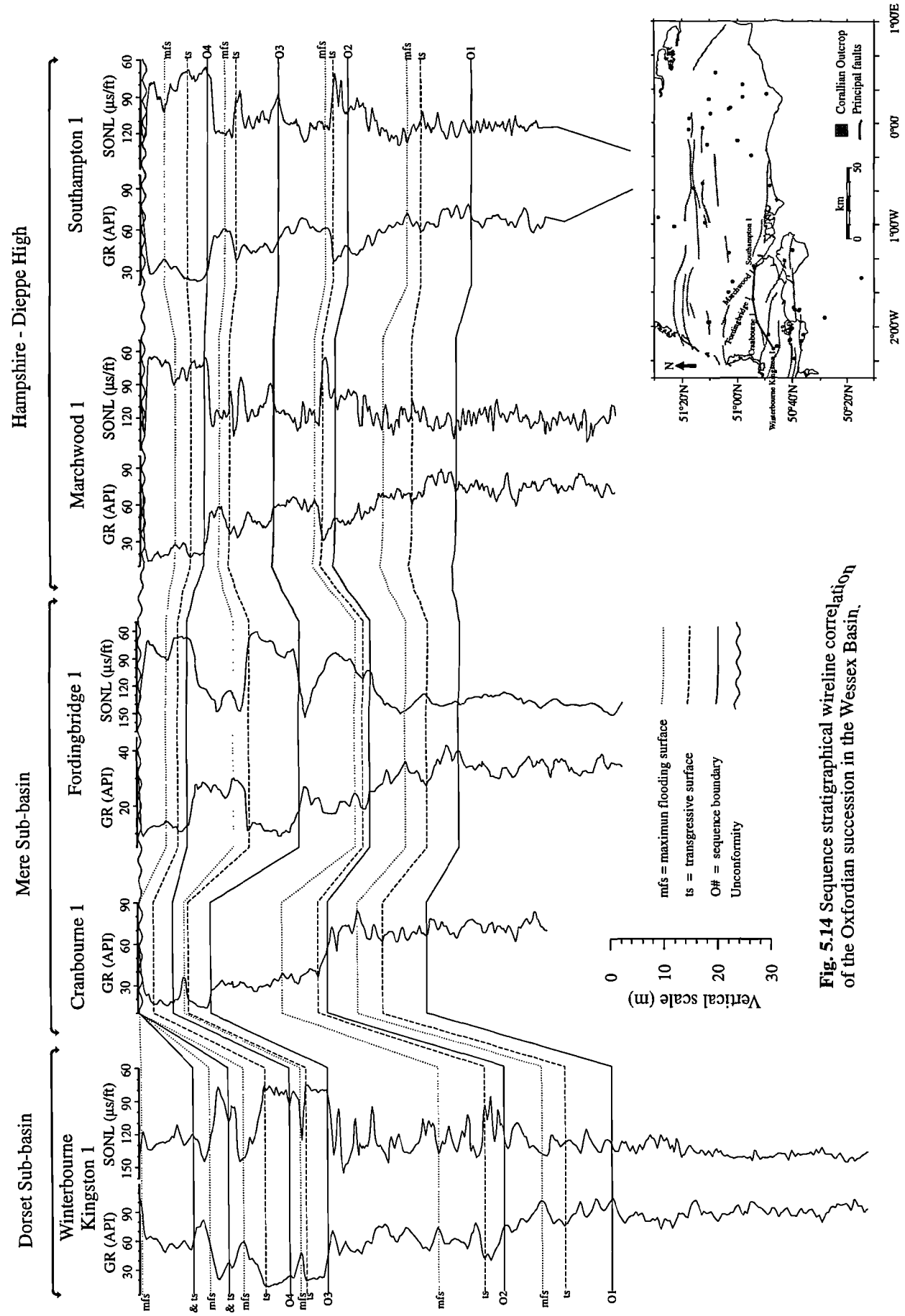

Fig. 5.14 Sequence stratigraphical wireline correlation of the Oxfordian succession in the Wessex Basin.

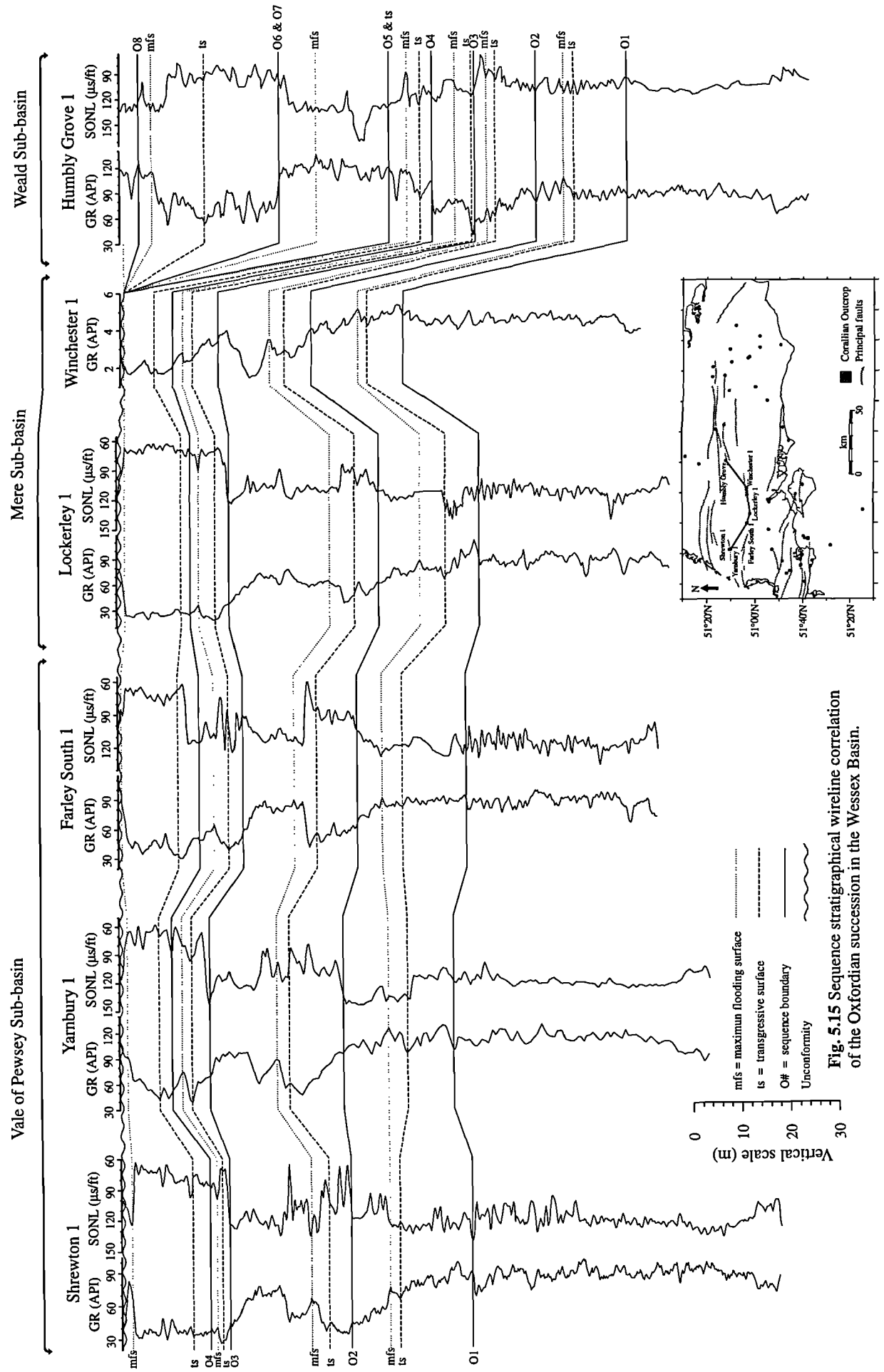

Fig. 5.15 Sequence stratigraphical wireline correlation of the Oxfordian succession in the Wessex Basin.

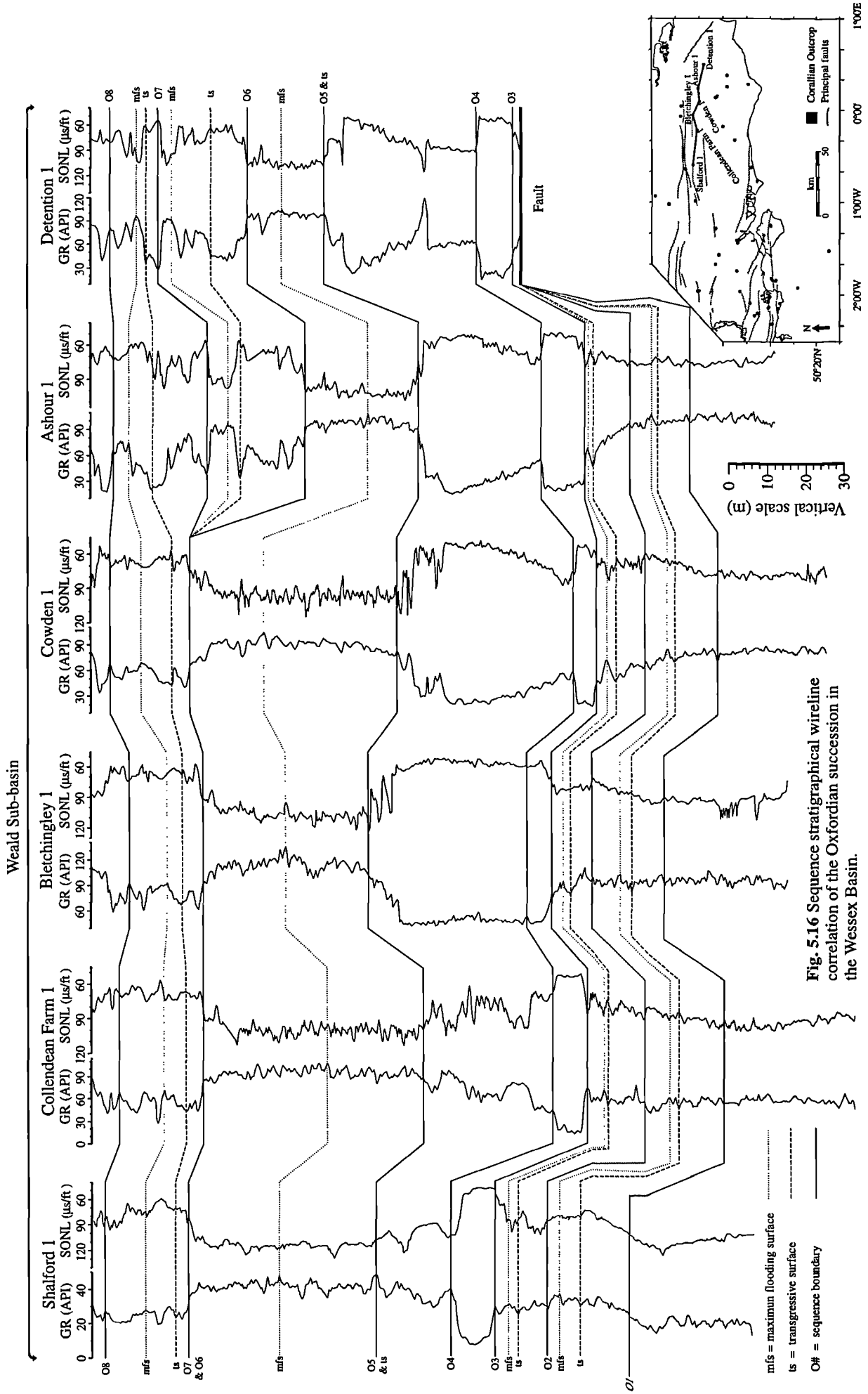

Fig. 5.16 Sequence stratigraphical wireline correlation of the Oxfordian succession in the Wessex Basin.

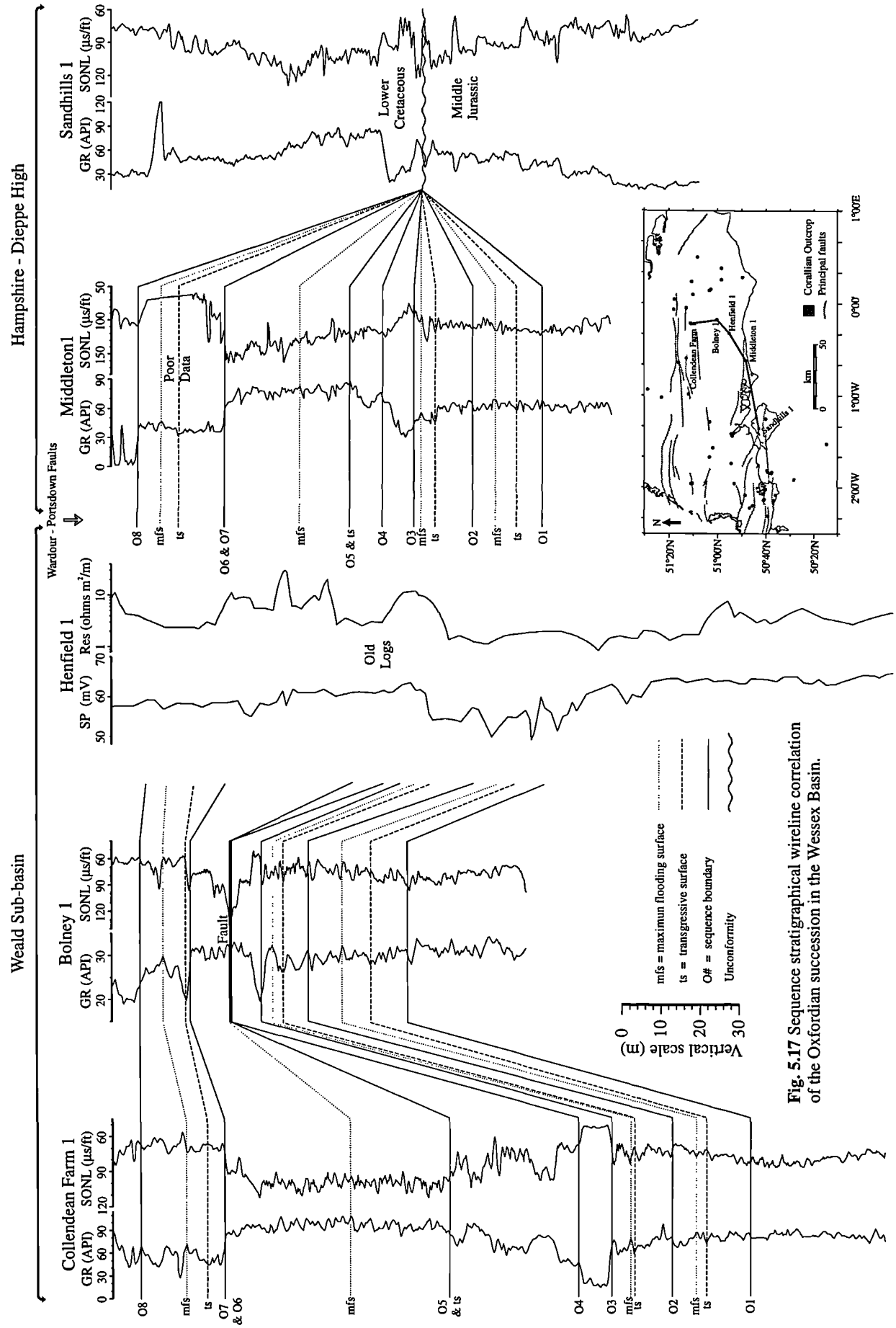

Fig. 5.17 Sequence stratigraphical wireline correlation of the Oxfordian succession in the Wessex Basin.

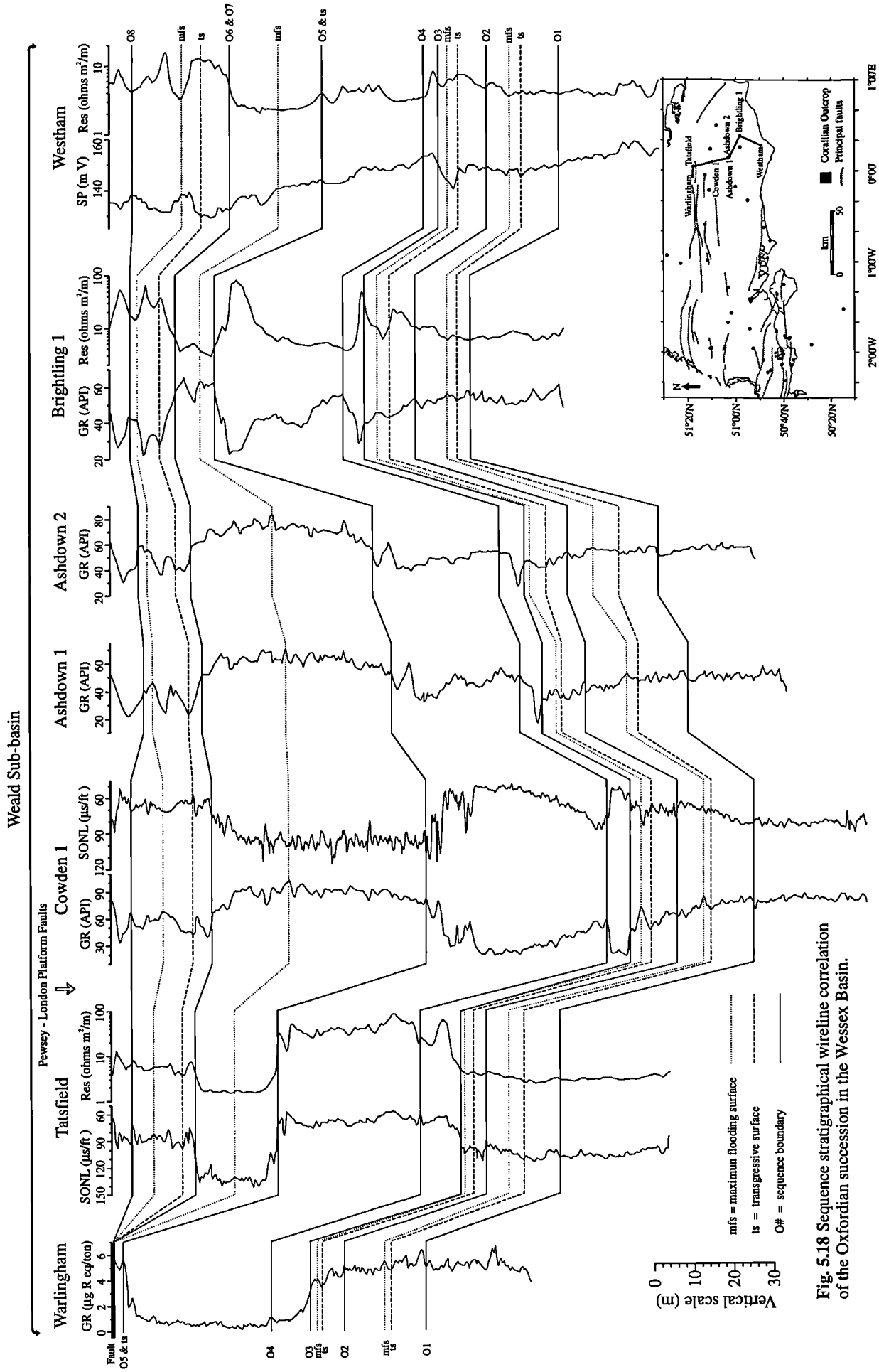

Fig. 5.18 Sequence stratigraphical wireline correlation of the Oxfordian succession in the Wessex Basin.

In the Weald Sub-basin, only the sequence boundary was picked for the O3 and O4 sequences (Figs 5.16 to 5.18) because a thick coralline reef is present over these sequences (see Section 5.4.5.6), making the detection of the transgressive surface and maximum flooding surface more difficult due to the lack of trends on the wireline logs. For example, the whole of the O3 sequence (Fig. 5.16) is characterized by a cylindrical trend (low gamma-ray interval with no internal change; see Chapter 4, Section 4.2).

The full Oxfordian succession (base of the Upper Oxford Clay to the top of the Corallian Beds) for each of the boreholes in the sequence stratigraphic wireline correlations are shown in Figures 5.12 to 5.18. Both the gamma-ray and sonic wireline log curves have been plotted for each borehole, except for the boreholes which did not have these wireline curves, in which case other useful wireline curves were plotted (see Chapter 3 for the discussion of which wireline logs are best for correlation purposes in this Upper Jurassic succession).

5.4.5.1 Central Channel Sub-basin

The Oxfordian succession encountered in the boreholes in the northern part of the Central Channel Sub-basin, Arreton 1 and 98/11-4 boreholes, for example, are very similar to the Oxfordian exposures on the Dorset coast. Because the successions are similar, both in lithology and thickness, and the Dorset coast exposures are not far from the boreholes which lie between Swanage and the Isle of Wight. It was assumed that the same unconformities that are present in the exposures are also present in the borehole sections.

The transgressive systems tract of the O2 sequence (Nothe Grit Formation) is significantly thinner in 98/23-1 than it is in 98/11-4 (Fig. 5.12). This would suggest that the succession encountered in the 98/23-1 borehole is more distal (farther away from the clastic source) than the succession in the 98/11-4.

The boreholes Arreton 1, Arreton 2 and 98/11-4, which are all located in the northern margin of the Central Channel Sub-basin (Figs 5.12 & 5.13), were drilled in 1952, 1974 and 1987, respectively. Looking at the wireline data from these wells, it is evident that the older the well, the poorer the wireline resolution (see Chapter 3 for more information about data quality).

5.4.5.2 Dorset Sub-basin & South Dorset High

The Oxfordian succession encountered in the Winterbourne Kingston borehole is similar to that seen at the north Dorset exposures. The limestone sediments which make up the O3 and O4 sequences are thinner in Winterbourne Kingston than those sediments in Wareham 3, which is located on the southern margin of the Dorset Sub-basin, and those

sediments in the Central Channel Sub-basin. This is assumed to be due to that fact that the unconformities which form O3 and O4 sequence boundaries have removed more sediment than the same unconformities in the southern part of the Dorset Sub-basin. This observation fits in with what is seen at outcrop (Table 5.2).

It is visibly evident, from looking at Figure 5.12, that the Oxfordian succession deposited on the south Dorset High is roughly half the thickness of the Oxfordian succession deposited south of the Portland - Wight faults, in the Central Channel Sub-basin. This is due to the fact that there was less subsidence during deposition on the south Dorset High than there was in the Central Channel Sub-basin, which resulted in less sediment accommodation space.

The more argillaceous sediments of the Upper Corallian (above the Osmington Oolite equivalent) seem very thin in the boreholes on the south Dorset High (Fig. 5.12). This could be either because the sediments are condensed or because part of the succession was eroded during the rise in relative sea-level at the onset of the Kimmeridgian times. Jacovides *et al.* (1983) suggested that it is possible that there is a hiatus at this level, in the 98/11-1 borehole, but stress that palaeontological control is very poor. Due to the long term transgression, very little strata have generally been preserved at outcrop (Coe 1992) over this interval which suggests that a hiatus is more likely. Whichever of these is correct, the succession cannot be accurately interpreted sequence stratigraphically for the sequences O5 to O8, due to the lack of strata.

Hamblin *et al.* (1992) suggested that the upper part of the Corallian Beds is faulted against Kimmeridge Clay, in the 98/11-1 borehole, and that the lower part may belong structurally to the southern flank of the Hampshire - Dieppe High. Looking at Figure 5.12, it is evident that this is clearly not the case. Firstly, the fault cuts the Oxfordian succession near the base of the Upper Oxford Clay and, secondly, the Corallian succession in 98/11-1 is very similar to the succession in 98/11-3, which is clearly located on the south Dorset High (Fig. 5.12).

5.4.5.3 Mere Sub-basin

The north Dorset exposures outcropping at the eastern end of the Mere Sub-basin (Table 5.2) contain an Oxfordian succession which spans the *mariae* to *pseudocordata* zones. At outcrop the sediments of *plicatilis* to *pseudocordata* zones are very thin and patchy in distribution (Coe 1992). The Oxfordian succession encountered in the boreholes in the Mere Sub-basin seem only to span the *mariae* to *plicatilis* zones. Both Wright (1981) and Whittaker *et al.* (1985) suggested that the upper Oxfordian has possibly been eroded by the occurrence of Kimmeridgian overstep. However, Whittaker *et al.* (1985) also suggested that the Kimmeridgian overstep may rest locally on superficially similar clays of Oxfordian age. If this were the case, they would be hard to distinguish on the

wireline logs. Detailed wireline correlation of the Kimmeridgian (Chapter 6), however, does suggest that the sediments of *plicatilis* to *pseudocordata* zones are not present in the boreholes of the Mere Sub-basin (Figs 5.14 & 5.15).

In the Fordingbridge 1 borehole there seems to be a thick clay which forms the highstand of the O3 sequence (Newton Clay; Table 5.3): this clay is significantly thinner in Cranbourne 1 (Fig. 5.14). This is probably due to the fact that Fordingbridge 1 borehole is in the centre of the Mere Sub-basin, whereas Cranbourne 1 lies on the southern margin of the sub-basin. The thin clay also seems to be present in the Lockerley 1 and Winchester 1 boreholes, which lie on the northern margin of the sub-basin (Fig. 5.15).

5.4.5.4 Hampshire - Dieppe High

Marchwood 1 and Southampton 1, which lie at the western end of the Hampshire - Dieppe High, have an Oxfordian succession which spans the *mariae* to *plicatilis* Zones, like the boreholes in the Mere Sub-basin. The upper part of the Oxfordian was probably not preserved due to the long term transgression, or was eroded due to the Kimmeridge Clay Formation overstep.

Because the succession encountered in Marchwood 1 and Southampton 1 was deposited on a palaeohigh, the succession is thinner than that seen in the nearby boreholes (Fig. 5.14). It is only slightly thinner than the Oxfordian succession in the Mere Sub-basin, which suggests that the Mere Sub-basin was not a significant depocentre like the Dorset, Central Channel and the Weald Sub-basins.

Towards the northern margin of the eastern end of the onshore part of the Hampshire - Dieppe High, the full Oxfordian succession is seen in the Middleton 1 borehole (Fig. 5.17). The Oxfordian succession in Middleton 1 is more like that seen in the Weald Sub-basin (see Section 5.4.5.6) than that seen in the rest of the Wessex Basin area.

On the southern margin of the Hampshire - Dieppe High, just north of the Portland - Wight faults on the Isle of Wight, the full Oxfordian succession in the Sandhills 1 borehole (Fig. 5.17) is absent due to the Cretaceous overstep. Wilson (1968) suggested that the distribution and succession of sediments were topographically controlled. The dominant feature was the Hampshire - Dieppe High (which Wilson called the Portsdown Swell), the rising (or non-subsidence) of which inhibited deposition or even led to erosion of earlier - formed beds, first in its south-east part, then later in the north-west.

5.4.5.5 Vale of Pewsey Sub-basin

The Oxfordian successions in the boreholes in the Vale of Pewsey Sub-basin (*mariae* to *parandieri* zones) are similar to the exposures in Wiltshire (Table 5.2, Fig. 5.15) which lie at the western end of the sub-basin (Fig. 5.1).

The thickness of the Corallian succession in the Vale of Pewsey Sub-basin is similar to that in the Mere Sub-basin. However, the Upper Oxford Clay is thicker in the Vale of Pewsey Sub-basin, in particular the succession in the Shrewton 1 and Yarnbury 1 boreholes, close to the centre of the sub-basin (Fig. 5.15).

5.4.5.6 Weald Sub-basin

The Oxfordian succession seen in the Weald Sub-basin is the thickest succession found in the whole of the Wessex Basin (164.5 m in Collendean farm 1 borehole, Fig. 5.16).

The Corallian succession can be split into three units based on the wireline data (Fig. 5.19). The lower and upper units consist of interbedded limestones, sandstones, siltstones and mudstones, and these are separated by an intervening mudstone which forms the third unit. The Corallian succession in the Weald Sub-basin is markedly different from the Corallian succession exposed on the Dorset coast and along the eastern margin of the Wessex Basin, making a comparison between the exposures and the borehole successions difficult (Sun 1989; Gallois 1992). This is only true if the lithologies are compared, however. This study has shown that they can be compared biostratigraphically and sequence stratigraphically. Biostratigraphically the lower unit spans the *cordatum* to *parandieri* subzones and the middle and upper units span the *nunningtonense* to *evoluta* subzones (Fig. 5.19).

The lower unit can be split into three intervals (Fig. 5.19). The first consists of siltstones and calcareous silty mudstones which are *cordatum* Subzone in age, therefore probably equivalent to the Nothe Grit on the Dorset coast and the Lower Calcareous Grit in the north Dorset, Wiltshire and Oxfordshire exposures. Above these beds is a silty bed of *plicatilis* Zone age, which has been described in the Warlingham 1 borehole as an ironshot silty bed (Fig. 5.7). The base of this lower interval has therefore been interpreted to be the O2 sequence boundary (Fig. 5.19).

The second interval consists of an oolitic limestone which forms a prominent gamma-ray low in all the boreholes in the Weald Sub-basin (Figs 5.16 to 5.18). This oolitic limestone is believed to be the same age as the Bencliff Grit seen in the Dorset coast exposures because, just below this interval, Sun & Wright (1989) described an oolitic wacke/packstone containing *Cardioceras* which is also found in the Preston Grit on the Dorset coast. Therefore the base of this second interval has been interpreted to be the O3 sequence boundary (Fig. 5.19).

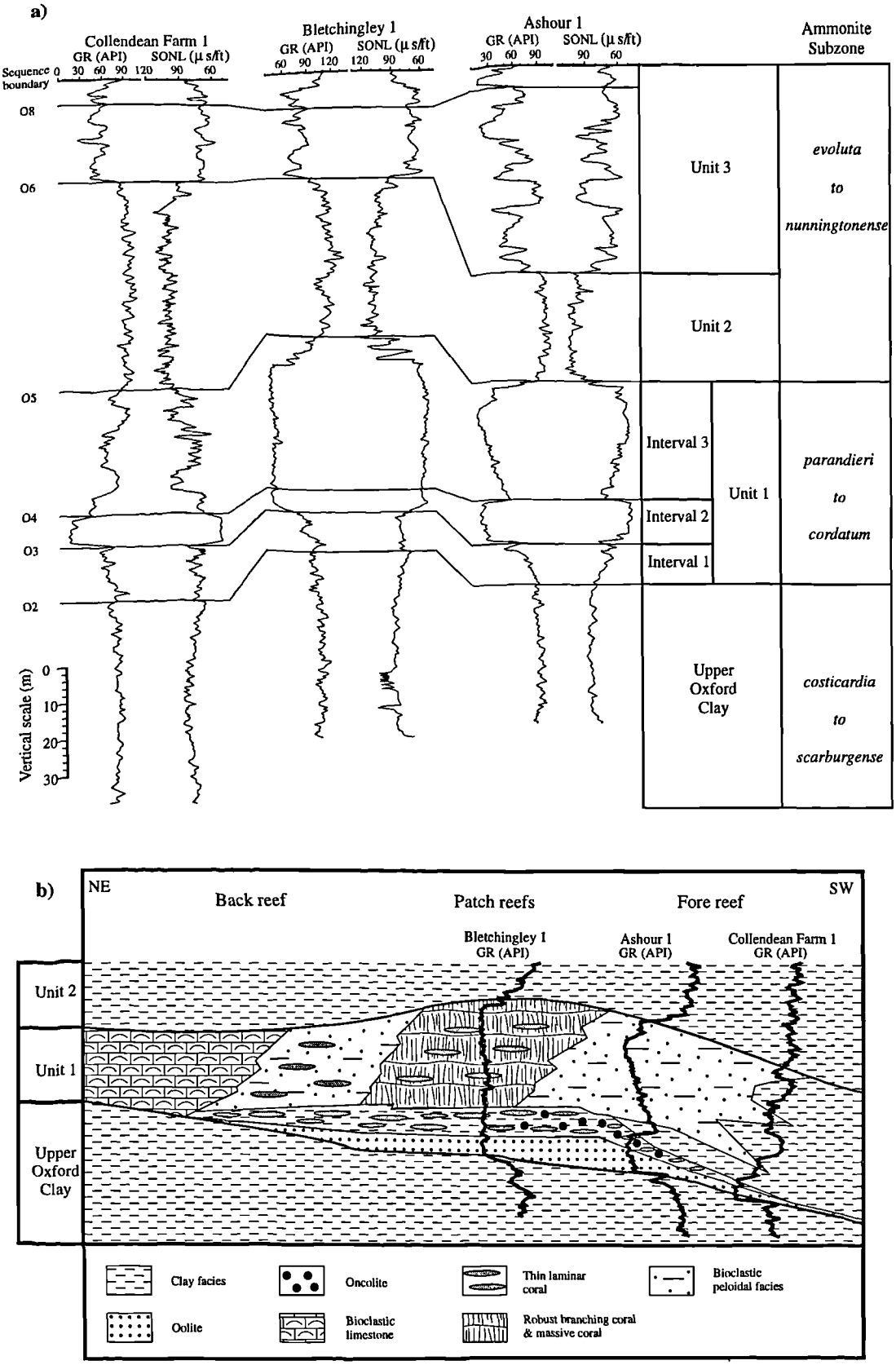

Fig. 5.19 Diagram showing the typical Oxfordian succession in the Weald Sub-basin. **(a)** Three boreholes in the Weald Sub-basin showing the typical wireline signature of the Oxfordian succession. **(b)** Simplified sketch of the reef, located on the northern margin of the sub-basin. The relative location of the three boreholes in a) have been plotted to show how the different intervals in unit 1 relate to each other. Reef architecture modifield after Sun *et al.* (1992).

The third interval consists of a thick coralline limestone which is only seen on the northern flank of the sub-basin. To the south, in the rest of the sub-basin, interbedded limestones, siltstones and calcareous mudstones are present. The thick limestones seen in this interval form the main part of the reef; therefore the change from the oolitic limestones to the reef facies has been interpreted to be the O4 sequence boundary (Fig. 5.19).

The thick coralline limestones seen in the boreholes on the northern flank of the Weald Sub-basin have been described by Gallois (1992) as fringing 'reefs' close to the shore. Sun & Wright (1989) described the coralline limestones as low relief, superimposed patch reefs which have an elongate geometry and parallel the palaeoshoreline (the London Platform). Sun *et al.* (1992) suggested that the reef is made up of three parts, the lower part consists predominantly of thin laminar corals with argillaceous skeletal matrices. The middle part consists of both laminar and digitate corals with extensive early marine peloidal cements and the upper part is primarily composed of robust branching and massive corals with a predominant bioclastic/introclastic pack/grainstone matrix.

Insalaco *et al.* (1997) carried out a comparative sedimentological and palaeoecological study of Oxfordian coral-dominated reefs in Europe, and developed a depositional model for these reefs. They incorporated Oxfordian exposures from Wiltshire and Oxfordshire but did not include the sub-surface reefs of the Weald Sub-basin. As part of their model, they suggested that Jurassic reef-bearing carbonates reached their maximum extent late in the period, primarily as a result of the relatively high sea-level stand at that time which created vast areas of relatively shallow epicontinental sea. This, together with the equable Jurassic climate, provided a suitable setting for extensive reef development.

In Section 5.4.3, it was mentioned that ammonites were found in the clay below the fault, in the Warlingham 1 borehole (Fig. 5.7), that were of the same age as the Ringstead Waxy Clays on the Dorset coast (*pseudocordata* Zone). Seeing as the clay rested with apparent conformity on the thick coralline limestone, it was suggested (Worssam & Ivimey-Cook 1971) that the limestone at Warlingham ranged in age from the *plicatilis* Zone up to the *pseudocordata* Zone. Cope *et al.* (1980) suggested that a substantial stratigraphical break occurred between the mudstones below the fault and the coralline limestone. However after interpreting the wireline data from the Weald Sub-basin sequence stratigraphically in this study (Figs. 5.16 to 5.18) it is believed that the age of the coralline limestone, in Warlingham 1, ranges from the *cordatum* to *parandieri* Subzones, which confirms the record of Downie (in Wilson 1968) that the top of the limestone was *plicatilis* Zone in age. It is suggested that, if the ammonites found in the mudstone below the fault were in fact from the *pseudocordata* Zone, then they and the mudstone in which they were found must be tectonically related to the fault.

The second unit of the Corallian succession in the Weald Sub-basin (Fig. 5.19) has been described in core from Ashdown 2 borehole as a dark grey non-calcareous shale (Bristow & Bazley 1972). This mudstone unit has a different wireline character from the mudstones in the overlying Kimmeridge Clay Formation and the underlying Oxford Clay Formation (Fig. 5.20).

The third unit consists of interbedded calcareous mudstones, limestones and siltstones (Figs 5.19 & 5.20). The wireline correlations (Figs 5.16 to 5.18) show that this unit remains fairly constant in thickness (~20 m) in most parts of the Weald Sub-basin, except in the north-east of the sub-basin where this unit is more that double the thickness (see Ashour 1 and Detention 1 borehole in Fig. 5.16). It is also evident that the mudstones of second unit are significantly thinner in this north-eastern part of the sub-basin where the third unit is thicker. This is probably related to the fact that the north-eastern part of the sub-basin is closer to the London - Brabant landmass, which might have resulted in less subsidence taking place in this area while the second unit was being deposited. Also, with increased transgression occurring late in the Oxfordian, more sediment would be deposited in the proximal areas.

5.5 Previous wireline correlations

Wireline correlations of the Oxfordian succession of the Wessex Basin are quite rare. This is probably due to the fact that the lithologies found within the Oxfordian succession vary greatly both laterally and vertically, making lithostratigraphic correlations hard. One previous detailed correlation was found in Bristow *et al.* (1995). They showed a detailed lithostratigraphic wireline correlation for seven boreholes (three of which were used in this study: Winterbourne Kingston, Encombe & Cranbourne) which stretches from Dorset to west Hampshire. Another, less detailed, correlation can be found in Hamblin *et al.* (1992). This wireline correlation shows six boreholes which stretch from the Isle of Wight to the south east corner of the Weald Sub-basin. However, the Oxfordian is only split into the Upper Oxford Clay, Lower and Upper Corallian beds.

The wireline correlations produced in this study (Figs 5.12 to 5.18) are, to the author's knowledge, the first attempt at a detailed chronostratigraphic wireline correlation of the Oxfordian succession across the whole of the Wessex basin.

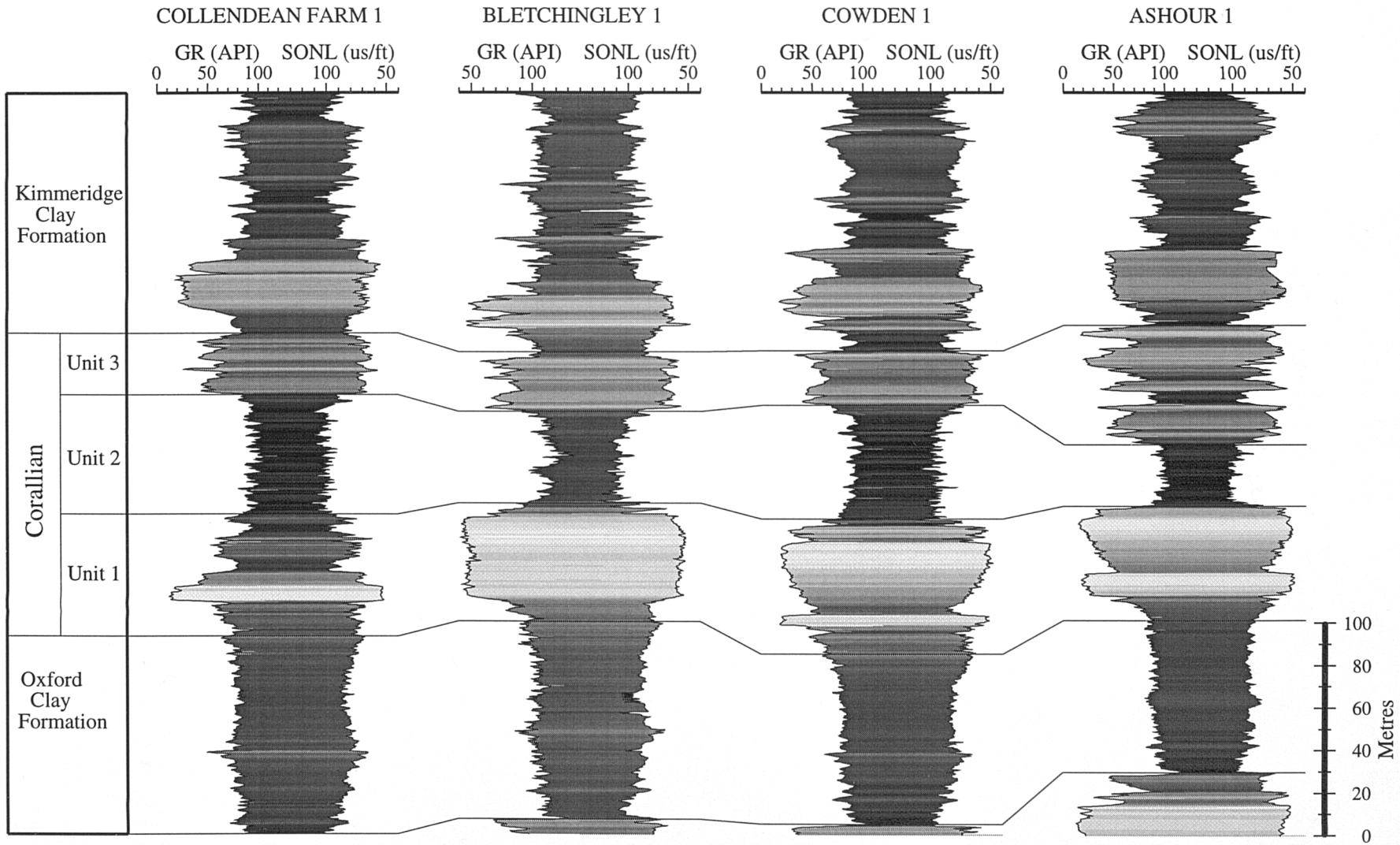

Fig. 5.20 Corallian succession in the Weald Sub-basin. The shading (black = high gamma-ray, white = low gamma-ray) shows that the mudstone of unit 2 in the Corallian has a different wireline character to the mudstones in the overlying Kimmeridge Clay Formation and the underlying Oxford Clay Formation. See figure 5.15 for location of the boreholes.

5.6 Discussion

In this section a general synthesis for the deposition of the Oxfordian succession in the Wessex Basin is discussed. The synthesis builds on and utilises certain aspects of the models described in sections 5.2 and 5.3.

The main palaeogeography of the Wessex Basin region can be seen in Figure 5.2. This figure is a simplified map showing the main palaeogeographic features of the Oxfordian. The data come from Wilson (1968), Brookfield (1973), Ziegler (1982) and Bradshaw *et al.* (1992). The work done by Wilson (1968) and Brookfield (1973) is specific to the Oxfordian of England, whilst the work of Ziegler (1982) and Bradshaw *et al.* (1992) span long time-scales and large geographic areas. The main difference between the maps produced by Wilson (1968) and Brookfield (1973) to those produced by Ziegler (1982) and Bradshaw *et al.* (1992) is the presence of the Hampshire - Dieppe High (known as Portsdown Swell in Wilson (1968)). This palaeohigh was probably omitted from the larger scale maps of Ziegler (1982) and Bradshaw *et al.* (1992) because the area appears to have only been a high at certain times throughout the Oxfordian.

The Oxford Clay facies was deposited during a regional transgression that began in Callovian times. By early Oxfordian times the relative sea-level began to fall; at outcrop this is marked by an increase in quartz sand in the Jordan Cliff Clays. The base of the Jordan Cliff Clays is interpreted as the O1 sequence boundary. The relative sea-level then rose slightly resulting in the loss of the quartz sand in the Bowleaze Clays. The transgressive surface is at the base of the Bowleaze Clays and the maximum flooding surface is marked by the presence of the Red Nodule Bed within the Bowleaze Clays Member. The relative sea-level changes which occur in the O1 sequence are hard to detect on the gamma-ray log because the Upper Oxford Clay succession generally has a monotonous high gamma-ray character. However the use of the techniques described in Chapter 3 to enhance wireline trends proved useful in the detection of the key sequence stratigraphic surfaces in the O1 sequence.

A fall in relative sea-level resulted in the deposition of the Nothe Grit Formation, in Dorset (Table 5.2), or Lower Calcareous Grit Formation, in Wiltshire and Oxfordshire (Table 5.2), which makes up the lowermost systems tract of the O2 sequence and is the lowest formation in the Corallian Group. This formation forms a prominent marker horizon across most of the basin (Figs 5.12 - 5.18). At outcrop a sharp erosional surface can be seen between this formation and the underlying Upper Oxford Clay. This sharp erosion surface is probably also present in the Central Channel, Dorset and Mere Sub-basins. The evidence for this is the sharp break seen in wireline logs (see O2 sequence boundary in Figs 5.12 - 5.14). Wright (1986b) recorded that the Nothe Grit Formation seen on the Dorset coast consists of fine-grained offshore silty sandstones which pass up

into well sorted subtidal sandstones which were deposited quite close to the beach environment. This would suggest that the source of the sand came from the west (i.e., the nearest landmass), probably the Cornubian Massif (Fig. 5.2). Evidence for this is that the lowermost systems tract for the O2 sequence seen in borehole 98/23-1 is significantly thinner than elsewhere in the Wessex Basin, except for the succession seen on the palaeohighs (Figs 5.12 - 5.18). 98/23-1 lies over 50 km to the south-east of the Dorset outcrops, and looking at the palaeogeographic map (Fig. 5.2) the southern edge of the Cornubian Massif followed the present-day Cornwall Coast line; in other words the Cornubian Massif curves away from the location of the 98/23-1.

In the Vale of Pewsey Sub-basin, and more so in the Weald Sub-basin, the boundary between the Upper Oxford Clay and the Corallian Group is more gradational, and a sharp break in the wireline logs is not seen (Figs 5.15 - 5.18). Also, unlike the rest of the basin where the lowermost systems tract of the O2 sequence is made up sandstones, in the Weald Sub-basin it consists of calcareous mudstones with calcareous siltstones (Fig. 5.7). This lack of coarser grained siliciclastic sediment confirms the fact that the siliciclastic source was probably from the western side of the Wessex Basin, and also suggests that the London - Brabant Massif was not a prominent high during this time in the Oxfordian.

Wright (1986b) suggested that there was a break in sedimentation and minor uplift prior to relative sea-level rising. The rise in relative sea-level resulted in the deposition of a transgressive beach deposit, the Preston Grit, in the Dorset coast area. The continuing rise in relative sea-level and the fact that subsidence was faster than the sedimentation rate resulted in the deposition of the Nothe Clay above the Preston Grit in the Dorset coast area. The Preston Grit and the lower part of the Nothe Clay makes up the transgressive systems tract of the O2 sequence, whilst the upper part of the Nothe Clay makes up the highstand systems tract of the O2 sequence. This pattern of sedimentation can be clearly seen on the wireline logs in the boreholes located in the northern part of the Central Channel Sub-basin and on the eastern side of the South Dorset High (Figs 5.12 & 5.13). Some boreholes and exposures on the Dorset coast contain prominent limestone bands that developed in the highstand systems tract of the O2 sequence, for example, 98/23-1 (Fig. 5.12), Shrewton 1 and Yarnbury 1 (Fig. 5.15). These limestone bands are shelfal limestones which were formed due to slight variations in siliciclastic mud supply. The highstand systems tract of the O2 sequence seen in the Winterbourne Kingston 1 borehole, located in the Dorset Sub-basin (Fig. 5.14), is very thick compared to that seen at outcrop on the Dorset coast and in the boreholes located between Swanage and the Isle of Wight (Fig. 5.12). This may suggest that tectonic activity occurred locally in the Dorset Sub-basin at this time, resulting in more sediment accommodation space for the Nothe Clay to

be deposited in, or may be related to the fact that Winterbourne Kingston 1 boreholes lies close to the Dorset Sub-basin bounding fault.

Relative sea-level then fell fairly quickly resulting in the deposition of the Bencliff Grit, which rests with a fairly sharp boundary on the Nothe Clay in the Dorset coast exposures. Wright (1986b) suggested that the source of the Bencliff Grit Member was to the north-east of the Dorset coast area, because the Bencliff Grit becomes more marine westwards. The base of the Bencliff Grit is the O3 sequence boundary and the Bencliff Grit itself makes up the lowermost systems tract of the O3 sequence. Relative sea-level then rose again, resulting in the deposition of the Upton Member which, on the Dorset coast, consists of several thin argillaceous limestones separated by mudstones and sandy mudstones. The transgressive surface of the O3 sequence is at the top of the Bencliff Grit, which is marked as an erosion surface; the maximum flooding surface is within the Upton Member.

The O3 sequence boundary is a very prominent marker on the wireline logs in the whole of the Wessex Basin (Fig. 5.12 - 5.18). This is mainly because the Bencliff Grit and the overlying Osmington Oolite Formation, in general, have the lowest gamma-ray and highest sonic values within the Oxfordian succession.

Coe (1995) and Allen & Underhill (1989) suggested that the Bencliff Grit on the Dorset coast was probably deposited near to land under high-energy conditions, with occasional tidal influences, possibly near the mouth of an estuary. Wright (1986b) stated that the source of the Bencliff Grit was a localised uplift to the north-east. If this were the case, the Hampshire - Dieppe high was probably the source area. Further evidence for this is that towards the eastern end of the Mere Sub-basin, which lies just to the west of the Hampshire - Dieppe high, a thick sandstone forms the lower-most systems tract for the O3 sequence, suggesting that another estuary may have formed on the northwestern end of the Hampshire - Dieppe high, as well as on the southern flank of the high which sourced the Dorset area.

In the Weald Sub-basin, the rapid relative sea-level fall which resulted in the O3 sequence boundary is marked by an oolitic limestone unit which forms a prominent wireline marker (Figs 5.15 - 5.18). The oolitic limestone unit thins to the west in the Humbly Grove 1 borehole (Fig. 5.15) and to the south in the Brightling 1 (Fig. 5.18) and in Bolney 1 (Fig. 5.17) boreholes. This suggest that the London - Brabant Massif may have been land, or at least more proximal to the boreholes in the northeast of the Weald Sub-basin. Oncolites present above the oolitic limestone (Sun & Wright 1989; Fig. 5.19), probably represent the maximum flooding surface. Similarly there are also oncolites present at the maximum flooding surface of the O3 sequence in the Dorset and Yorkshire exposures (Coe 1992, 1995).

Relative sea-level then fell again, resulting in the deposition of the Shortlake Member. Wright (1986b) suggested that gentle currents alternated with strong currents depositing the cross-bedded oolites in the Shortlake Member. Relative sea-level then rose and the Nodular Rubble Member was deposited in deeper calmer waters. Near the base of the Shortlake Member is the O4 sequence boundary, and the base of the Nodular Rubble is interpreted as the maximum flooding surface. On the wireline logs the O4 sequence is located in the large gamma-ray low which is the Osmington Oolite Formation in all but the Weald Sub-basin. The highstand systems tract of the O4 sequence as well as the rest of the Oxfordian succession has been eroded in the Dorset, Mere and Vale of Pewsey Sub-basins, and from the Hampshire-Dieppe and parts of the South Dorset Highs (Figs 5.12 - 5.15).

In the Weald Sub-basin, the fall in relative sea-level resulted in the development of a reef in the northern part of the sub-basin (Figs 5.2 & 5.19). Elsewhere calcareous mudstones and limestones were deposited. The base of the reef is the O4 sequence boundary.

Renewed block uplift resulted in a marine bench being cut into the Osmington Oolite Formation which was colonised by numerous burrowing organisms (Wright 1986b). The basin areas then subsided as relative sea-level rose, possibly due to increased tectonic subsidence, and the condensed Trigonia Clavellata Beds were deposited on the rocky sea floor. The surface between the Osmington Oolite Formation and the Trigonia Clavellata Beds Formation is the O5 sequence boundary and the transgressive surface combined. Relative sea-level then rose further, and the whole area was covered with clay of the Sandsfoot Clay Formation.

Similar successions which make up the O5 sequence are only seen in the Central Channel Sub-basin. Elsewhere in the Wessex Basin the upper part Oxfordian succession has been eroded by an unconformity (for example, in the Dorset, Mere and Vale of Pewsey Sub-basins) or is highly condensed (for example, in boreholes 98/11-1 and 98/11-3 on the South Dorset High, Fig. 5.12).

In the Weald Sub-basin, the rise in relative sea-level resulted in the flooding of the reefs in the northern part of the sub-basin, and is marked by the deposition of dark grey non-calcareous mudstones. The top of the reef is the O5 sequence boundary and also probably the transgressive surface combined. The maximum flooding surface of the O5 sequence can be clearly located in the boreholes in the Weald Sub-basin, as the highest gamma-ray peak at the end of a retrogradational trend and the start of a progradational trend (Figs 5.16 & 5.18).

The succession which makes up the O5 to O8 sequences has only been deposited or preserved in limited parts of the Wessex Basin. The isopach maps seen in Figure 5.21 show that the lower part of the Oxfordian succession (base of the Upper Oxford Clay to the transgressive surface of the O5 sequence), which was deposited during a second-order

regressive phase has generally been deposited and/or preserved all over the basin. On the other hand, the isopach maps show that the upper part of the Oxfordian succession (transgressive surface of the O5 sequence to the top of the Oxfordian), which was deposited during a second-order transgressive phase, has only been deposited and/or preserved in the Weald Sub-basin, Central Channel Sub-basin and parts of the Dorset Sub-basin (Fig. 5.21b). The succession seen in borehole 98/11-4 (Fig. 5.12) is most like that exposed on the Dorset coast, whilst the succession seen on the South Dorset High (Fig. 5.12) and Dorset Sub-basin (Fig. 5.14) is highly condensed. The only other place in the Wessex Basin where the upper part of the Oxfordian succession occurs is in the Weald Sub-basin (units 2 & 3 in Fig. 5.19).

The thickest succession of O6 to O8 sequences was found in the northeast part of the Weald Sub-basin. It was mentioned in Section 5.4.5.6 that this part of the sub-basin is closer to the London - Brabant landmass, and with increased transgression occurring late in the Oxfordian, more sediment would be deposited in the proximal areas. For this reason it is believed that the O6 sequence which is not preserved elsewhere in the Wessex Basin (Table 5.2; Figs 5.12 to 5.18) is actually present in the northeast part of the Weald Sub-basin in Ashour 1 and Detention 1 boreholes (Fig. 5.16).

The isopach map in Figure 5.21a shows that the thickest development of the lower part of the Oxfordian succession (base of the Upper Oxford Clay to the transgressive surface of the O5 sequence), which was deposited during a second-order regressive phase, can be found in the Mere and Vale of Pewsey Sub-basins. However, when the Corallian part of the lower Oxfordian succession is contoured (i.e., O2 sequence boundary to the transgressive surface of the O5 sequence; Fig. 5.21c), it is evident that the thickest succession is found in the Weald Sub-basin. This would suggest that the western part of the Wessex Basin was the more important depocentre during the thermal subsidence tectonic stage in which the Upper Oxford Clay Formation was deposited (Fig. 1.4). Then, during the following extensional tectonic stage in which the Corallian succession was deposited, the eastern part of the Wessex Basin was the more important depocentre (Fig. 1.4).

In conclusion, this study has shown that even though the lithology of the Oxfordian succession varies both laterally and vertically, due to local tectonic activity and physical nature of the various sub-basins, the effects of third-order sea-level changes can be deduced by the sequence stratigraphical interpretation of the wireline data.

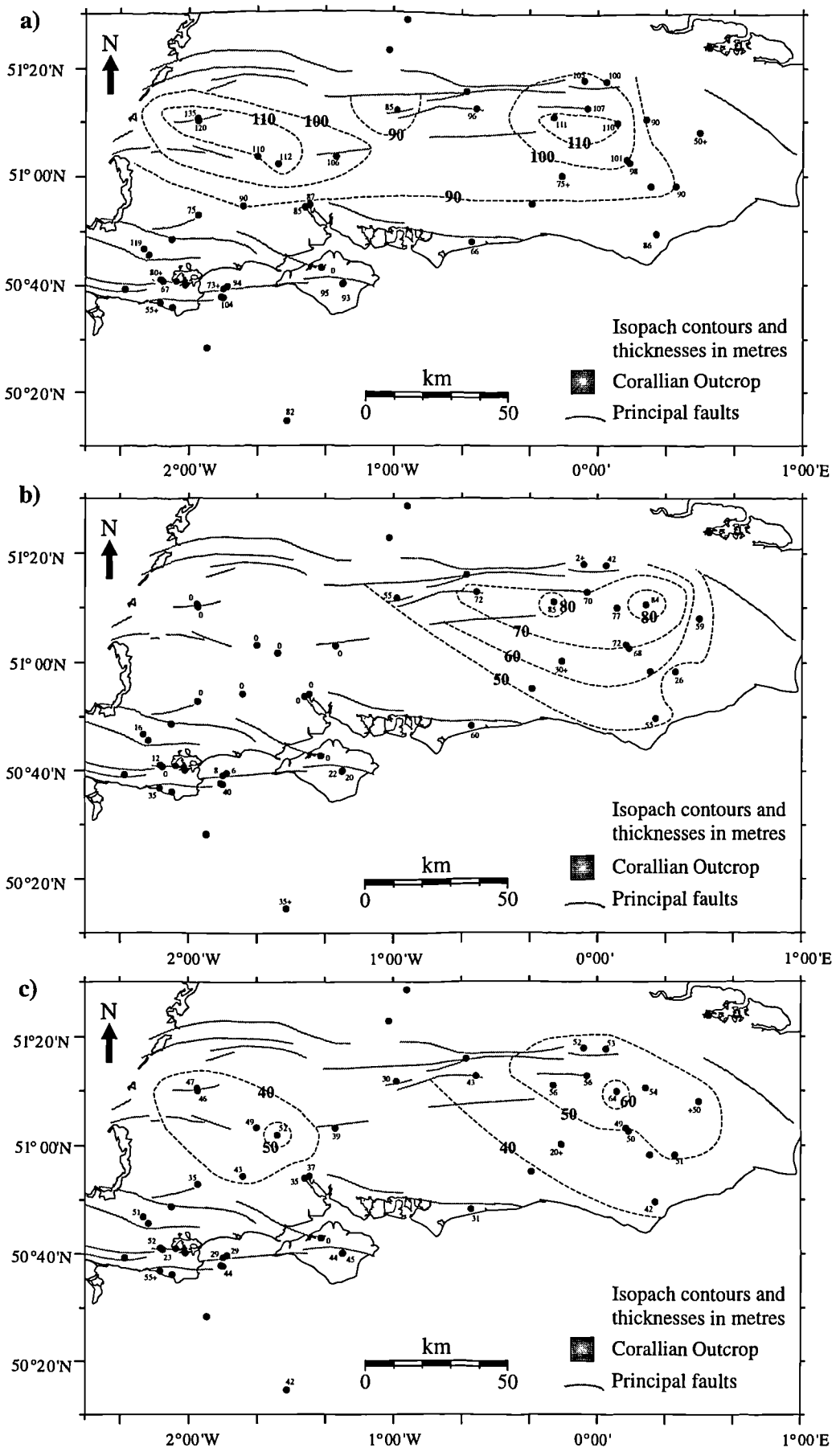

Fig. 5.21 **(a)** Isopach map of the second order regressive succession (base of the Upper Oxford Clay to the trangressive surface of the O5 sequence). **(b)** Isopach map of second order transgressive succession (transgressive surface of the O5 sequence to the top of the Oxfordian). **(c)** Isopach map of part of the second order regressive succession encompassing only the Corallian sediments (O2 sequence boundary to the trangressive surface of the O5 sequence).

5.7 Conclusions

(1) - The Oxfordian succession cannot be correlated peak for peak using the wireline logs, as the Kimmeridgian succession can be (Chapter 6). Nevertheless the Oxfordian can be correlated sequence stratigraphically using trends seen on the wireline logs. Lithology cannot be used to correlate the Oxfordian succession because it changes both laterally and vertically; however, the trends relating to sequence stratigraphy are seen basin-wide.

(2) - The sequences O2 to O5 of Coe (1992, 1995) can be picked on the wireline data from within the various sub-basins of the Wessex Basin with confidence. Due to the lack of core data and detailed biostratigraphy, the sequences O1, and O6-O8 were picked with less confidence and are thus provisional at this stage.

(3) - The wireline correlations seen in this chapter are the first attempt at a detailed sequence stratigraphic correlation of the Oxfordian succession across the whole of the Wessex Basin.

(4) - The effects of the third-order sea-level changes can be seen in the wireline data, even though the Oxfordian succession was deposited during a tectonically active time.

(5) - Considering the entire Wessex Basin area the O6 sequence is only preserved in the northeast part of the Weald Sub-basin.

CHAPTER 6

Kimmeridgian

6.1 Introduction

The Kimmeridgian Stage (*sensu anglico*) of the UK is represented entirely by the Kimmeridge Clay Formation which has outcrops in a band extending from Dorset to North Yorkshire (Fig. 6.1). There are also two exposures in Scotland, on the Isle of Skye and near Helmsdale (Gallois 1978). The type section is exposed on the Dorset coast in cliff sections at Kimmeridge (Hobarrow Bay to Chapman's Pool), Osmington Mills and Ringstead Bay (Fig. 6.1).

The Kimmeridgian Stage encompasses thirteen ammonite zones, *baylei* through to *fittoni* zones. The zonal scheme used in this study is based on Callomon (1968, 1971) for the Lower Kimmeridge Clay and Cope (1967, 1978) for the Upper Kimmeridge Clay. For more information on the ammonites and other fauna of the Kimmeridge Clay Formation the reader is referred to Gallois & Cox (1974, 1976), Cox & Gallois (1981) and Wignall (1990).

Blake in 1875 divided the Kimmeridge Clay Formation into the Lower Kimmeridge Clay and the Upper Kimmeridge Clay (Cox & Gallois 1981) on the basis that they were easily distinguishable by their ammonite faunas. The Lower Kimmeridge Clay spans from the base of the *baylei* Zone through to the top of the *autissioderensis* Zone, and the Upper Kimmeridge Clay from the base of the *elegans* Zone to the top of the *fittoni* Zone. The division has proved useful for descriptive purposes in the past (Arkell 1947; Cox & Gallois 1981; Coe 1992), and has also proved useful in this study because the lower and upper parts of the Kimmeridge Clay Formation have distinctive wireline signatures.

The exposures on the Dorset coast at Osmington Mills and Ringstead Bay, which expose most of the Kimmeridge Clay Formation, are unfortunately disturbed by tectonism and landslides. On the other hand the exposure between Hobarrow Bay and Chapman's Pool at Kimmeridge is largely undisturbed by tectonism and nearly the full succession, from the middle of the *eudoxus* Zone to the top of the *fittoni* Zone, is easily accessible (Fig. 6.2).

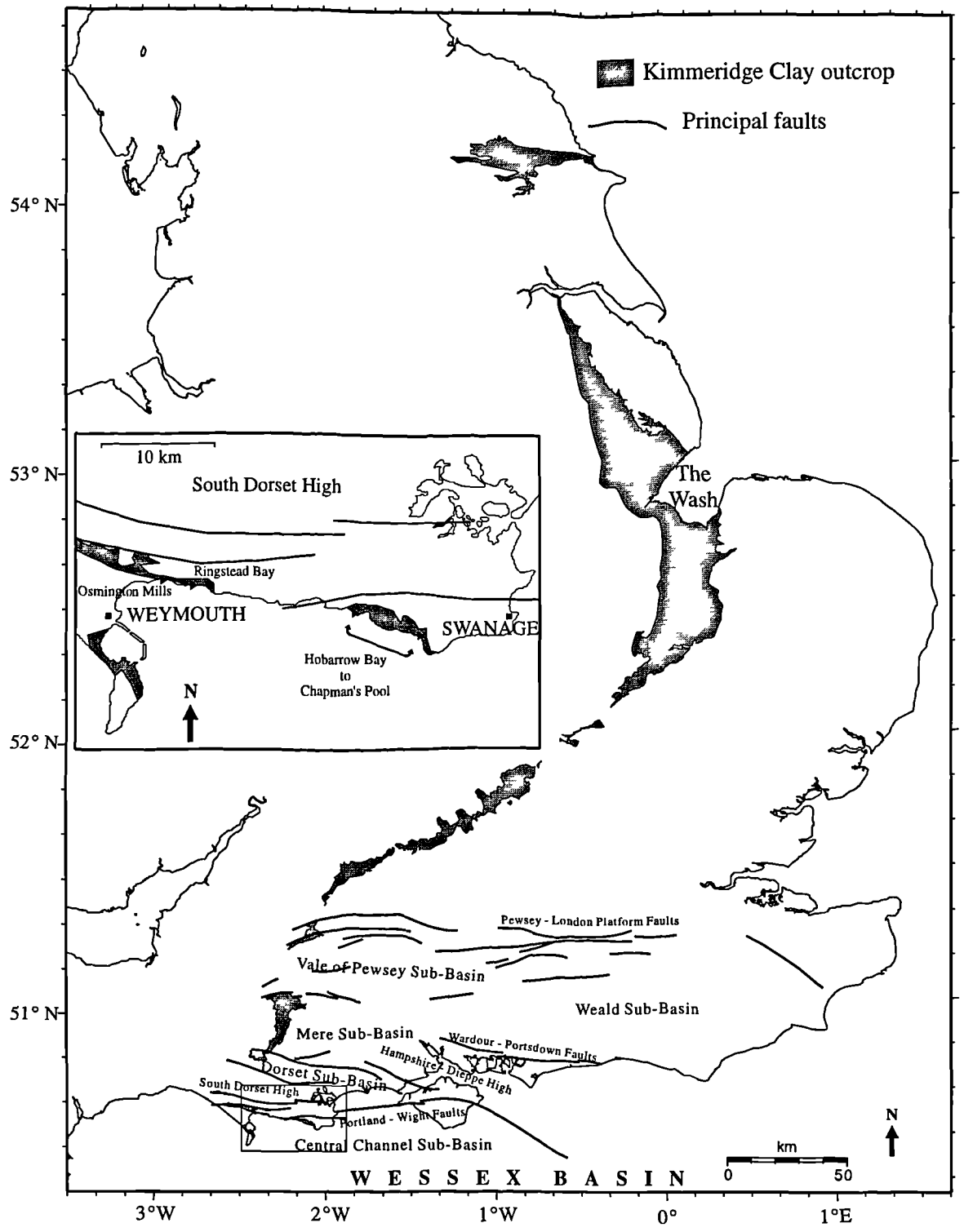

Fig. 6.1 Map of England showing the Kimmeridgian outcrop and the main structural features of the Wessex Basin, including the principal faults and the location of the various sub-basins. The insert shows the Kimmeridgian outcrops in Dorset. The faults are after Whittaker (1985) and Hamblin *et al.* (1992).

The bulk of the Kimmeridge Clay Formation is made up of interbedded mudstones, calcareous mudstones, bituminous mudstones and oil shales, with a few silty/sandy mudstone and limestone bands. The mudstones are most common in the Lower

Kimmeridge Clay whilst the calcareous mudstones are mainly found in the Upper Kimmeridge Clay. The silty mudstones are mainly found in the *baylei, cymodoce, mutabilis,* and *fittoni* zones.

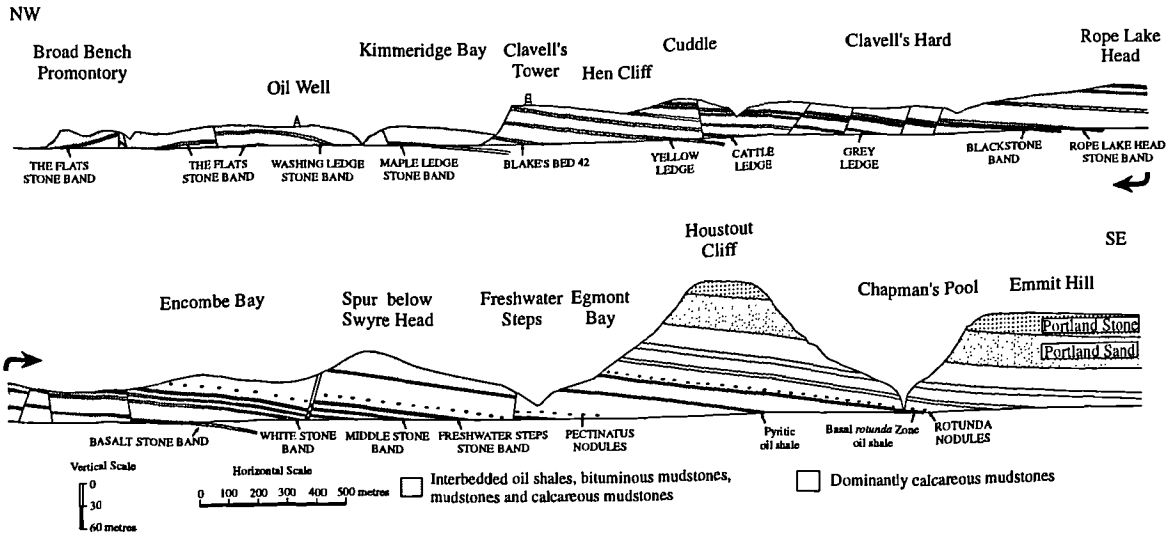

Fig. 6.2 Outcrop section exposed between Kimmeridge Bay and Chapman's Pool, showing the prominent 'Stone Band' marker horizons. After Coe (1992).

Arkell (1933, 1947) named the limestone bands (e.g. Washing Ledge Stone Band, Maple Ledge Stone Band etc.; Fig. 6.2) along the type section between Hobarrow Bay and Chapman's Pool, these limestone bands form prominent markers in the cliff section and are useful for identifying where you are in the succession. These 'Stone Bands' are also good marker horizons on the wireline logs because they have markedly different petrophysical properties than the mudstones which surround them. Several beds with distinctive fossil content are also good marker horizons. For example the *Astarte supracorallina* bed near the top of the *mutabilis* Zone and the *Nannocardioceras* bed near the top of the *eudoxus* Zone (Cox & Gallois 1981). Some of the 'Stone Bands' and the fossil marker horizons have been correlated from the exposures on the Dorset coast to the Warlingham 1 borehole, in the Weald Sub-basin and through to The Wash, East Anglia (Gallois & Cox 1974, 1976; Cox & Gallois 1981).

The Kimmeridge Clay Formation, from the *baylei* to the *pectinatus* zones, was divided into 48 beds (Gallois & Cox 1976; Gallois 1979; Cox & Gallois 1981). Wignall (1990) then added beds 49 - 55 which took the bed numbers up into the *rotunda* Zone. Coe (1992) further subdivided the original 48 beds (Gallois & Cox 1976; Gallois 1979; Cox & Gallois 1981) and added new beds up to the top of the *fittoni* Zone. The original bed numbers from 1 - 48 are thus now called bed group numbers because in most cases they have been subdivided into individual beds. In this study, therefore, bed group numbers 1 - 45 are after Cox & Gallois (1981), 46 - 50 after Coe (1992), 51 - 55 after Wignall

(1990) and 56 - 62 after Coe (1992), detailed lithostratigraphic logs showing the bed group numbers can be seen in Appendix B.

6.2 Sequence stratigraphy of Kimmeridgian exposures

6.2.1 Introduction

The most detailed sequence stratigraphic study of the Kimmeridgian exposures in the UK to date was carried out by Coe (1992). This section briefly describes the sequence stratigraphy of the Kimmeridgian exposures as interpreted by Coe (1992). The final part of this section discuses the other sequence stratigraphic studies done on the Kimmeridgian of the UK and compares them to the interpretation made by Coe (1992).

6.2.2 Lower Kimmeridge Clay

Three sequence boundaries were found in the Lower Kimmeridge Clay by Coe (1992) and a further one subsequently (Coe pers. comm.). All four of the sequence boundaries in the Lower Kimmeridge Clay are associated with thin sands/silts (Figs 6.3 & 6.4), and have been interpreted as coarse bases to fining upward transgressive packages. The evidence for this is that the sands have sharp erosive bases, in places contain phosphate nodules, and are all overlain by mudstone packages.

The first sequence boundary, Ki (base of bed 5), is at the base of the Wyke Siltstone which is also the base of the *cymodoce* Zone (Fig. 6.3). The base of the Wyke siltstone is erosive and has been interpreted as a sequence boundary and a transgressive surface combined. The maximum flooding surface has been interpreted to be the Supracorallina Bed which is at the *mutabilis / cymodoce* zonal boundary (top of bed 14).

The second sequence boundary, Kii (base of bed 17), is at the base of a siltstone in the middle of the *mutabilis* Zone. This surface has also been interpreted as the transgressive surface. Again the maximum flooding surface is associated with a Supracorallina Bed (top of bed 22) which, in this sequence, is located in the upper part of the *mutabilis* Zone. Coe (1992) attributes the fact that the sediments above the maximum flooding surface are thin to erosion beneath sequence boundary Kiii.

The third sequence boundary, Kiii (base of bed 24), is at the base of the siltstone which lies at the base of the *eudoxus* Zone. Again this surface is also interpreted to be the transgressive surface. The Nannocardioceras Bed (near top of bed 32) associated with the *eudoxus* oil shales have been interpreted as the maximum flooding surface (Coe 1992).

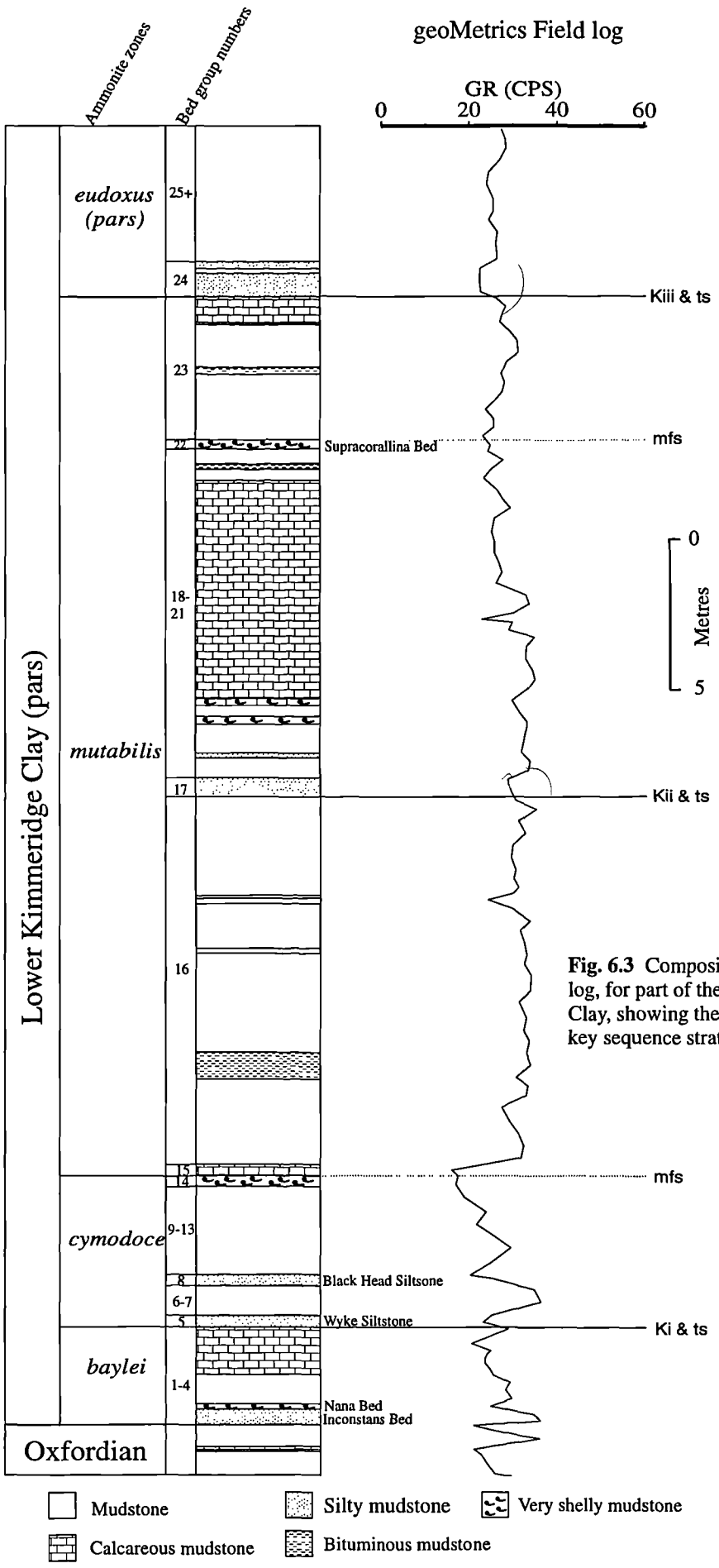

Fig. 6.3 Composite field gamma-ray log, for part of the Lower Kimmeridge Clay, showing the location of the key sequence stratigraphic surfaces.

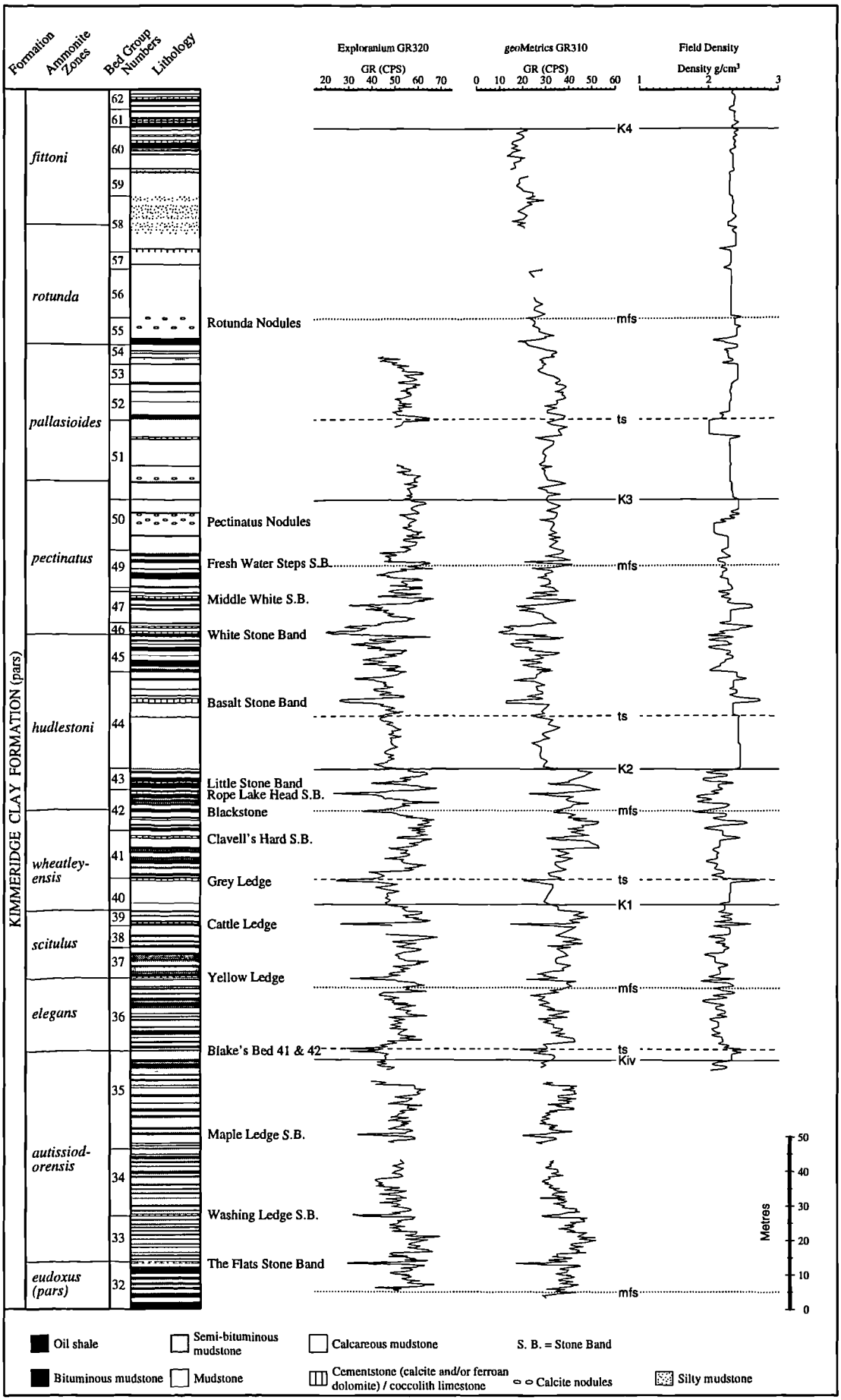

Fig. 6.4 Field gamma-ray and density logs, constructed over the Kimmeridgian exposures on the Dorset coast, showing the location of the key sequence stratigraphic surfaces.

The sediments below the maximum flooding surface are thicker than those above the maximum flooding surface for the Kii sequence. This conforms with the overall trend and the lack of obvious erosion below the Kiv sequence boundary.

The transgressive surface for the Ki, Kii and Kiii sequences could also be interpreted as being at the top of the siltstones, rather than being coincident with the sequence boundary at the base in all three of the sequences (Coe 1992).

The final sequence boundary in the Lower Kimmeridge Clay is Kiv (near top of bed 35). This sequence boundary, like the previous ones, is associated with silt but this time there is no sharp base. Therefore is likely to be a distal end of a lowermost systems tract. Unlike the previous sequences the transgressive surface is not interpreted as being coincident with the sequence boundary. In this sequence the transgressive surface is interpreted to be just above the *autissiodorensis / elegans* zonal boundary (top of Blake's bed 41; Fig. 6.4). The maximum flooding surface is not that clear in this sequence but is probably near the top of the *elegans* Zone (near top of bed 36) above some bituminous mudstone beds and below the Yellow Ledge stone band (Fig. 6.4; Coe 1992).

6.2.3 Upper Kimmeridge Clay

Four sequence boundaries have also been interpreted in the Upper Kimmeridge Clay. The depositional conditions, which had remained fairy constant during the *eudoxus* to *scitulus* zones, changed in the *wheatleyensis* Zone, from humid to semi-arid (Wignall & Ruffell 1990), resulting in the deposition of the first of two thick homogeneous calcareous mudstone units. The sequence boundary, K1 (in bed 40; Fig. 6.4), is interpreted to be at the base of the first thick homogeneous calcareous mudstone unit within the *wheatleyensis* Zone (Coe 1992). The transgressive surface is located at the base of bed 41 in the *wheatleyensis* Zone, from which point the sediments revert back to interbedded oil shales, bituminous mudstones and clays. The top of the organic-rich Blackstone band is interpreted to be the maximum flooding surface (in bed 42; Fig. 6.4; Coe 1992).

The second sequence boundary in the Upper Kimmeridge Clay, K2 (base of bed 44) is in the *hudlestoni* Zone at the base of the second thick homogeneous calcareous mudstone unit. Again the transgressive surface is located at the top of the thick homogeneous calcareous mudstone unit (in bed 44; Fig. 6.4). Above the transgressive surface interbedded oil shales, bituminous mudstones and clays are seen. The maximum flooding surface is associated with the oil shales around the Fresh Water Steps Stone Band in bed 49 (Fig. 6.4; Coe 1992).

The third sequence boundary, K3 (base of bed 51), is at the base of a sand near the top of the *pectinatus* Zone (Coe 1992). The transgressive surface is interpreted to be at the base of bed 52 in the *pallasioides* Zone above which deeper water sediments are seen. The

Rotunda Nodules (near top of bed 55; Fig. 6.4) are interpreted to be the maximum flooding surface.

The final sequence boundary in the Kimmeridge Clay Formation, K4 (near base of bed 61; Fig. 6.4), is marked by a rapid increase of quartz sand in a previously clay-dominated environment.

6.2.4 Other sequence stratigraphic interpretations

The only other sequence stratigraphic interpretation of the Kimmeridgian exposures of the England was done by Wignall (1991). Wignall (1991) recognized ten sequence boundaries in the Kimmeridgian Stage (Fig. 6.5). The position of Wignall's first sequence boundary K1, at the Oxfordian / Kimmeridgian stage boundary was interpreted by Coe (1992) as a maximum flooding surface. Wignall also places a sequence boundary (K3) at the base of the Black Head siltstone in the cymodoce Zone; this is probably not a valid sequence boundary because there is only a minor erosion surface at the base of the siltstone (Coe 1992).

Melnyk *et al.* (1994) recognized four possible hiatuses (sequence boundaries) and five possible maximum flooding surfaces, in their analysis of subsequence-scale depositional packages using digitally filtered gamma-ray logs. The location of their sequence boundaries compare very well with the interpretation made by Coe (1992) (Fig. 6.5). The maximum flooding surfaces at the *eudoxus/autissiodorensis* and *elegans/scitulus* zonal boundaries also compare very well.

Haq *et al.* (1987, 1988) constructed a world sea-level curve for the Mesozoic and Cenonzoic. They state that the bulk of the Upper Jurassic data came from sequences exposed between the Isle of Portland and Swanage in England and that outcrop studies in the Montsalvens area of Switzerland furnished further confirmation of the Late Jurassic sequences. A main criticism of the sea-level curves produced by Haq *et al.* (1987, 1988) is that they do not provide any detailed information about the fieldwork done or the evidence for the placement of the key sequence stratigraphic surfaces (this study and Neal *et al.* 1995). Nevertheless the sequence boundaries 136 to 144 of Haq *et al.* (1987, 1988) correlate very well with the interpretation of Coe (1992), even though the other key sequence stratigraphic surfaces (transgressive surface and maximum flooding surface) do not always match up (Fig. 6.5).

Partington *et al.* (1993) presented a genetic sequence stratigraphic interpretation for the Late Jurassic of the North Sea. They suggested that the systems tracts of the Upper Jurassic were below seismic resolution, so a complete sequence stratigraphic interpretation (the detection of the sequence boundaries, transgressive surfaces and maximum flooding surfaces) was impractical. They therefore carried out a preliminary subdivision of the

Upper Jurassic using maximum flooding surfaces. Figure 6.5 clearly shows that the sequence stratigraphic interpretation of the Upper Jurassic of the North Sea by Partington *et al.* (1993) does not remotely compare with any of the sequence stratigraphic interpretations of the Upper Jurassic of the Wessex Basin.

Several studies on the sequence stratigraphy of source rocks, using the Kimmeridge Clay Formation as an example have been carried out (Herbin *et al.* 1993, 1995; Tyson 1996).

6.3 Sequence stratigraphy as seen on the field gamma-ray and density logs

The reason for constructing the field gamma-ray and density logs (see Chapter 2) was to extend the sequence stratigraphic interpretation based on the exposures on the Dorset coast to the subsurface wireline data set. Therefore the first part of this section (Section 6.3.1) describes the field gamma-ray and density logs in terms of the sequence stratigraphic cycles. The second part of this chapter (Section 6.3.2) describes the spectral gamma-ray data recorded over part of the Kimmeridge Clay Formation, and describes its significance to the sequence stratigraphic interpretation.

6.3.1 Field gamma-ray and density logs

The position of the key sequence stratigraphic surfaces found at outcrop by Coe (1992), and described in the Sections 6.2.2 and 6.2.3, have been placed on the gamma-ray and density field logs (Figs 6.3 & 6.4). It was shown in Chapter 2 (Figs 2.17, 2.19 & 2.27) that both the gamma-ray and density field logs correlated well with boreholes within the Wessex Basin. These field logs have therefore been used to help pick the key sequence stratigraphic surfaces on all the boreholes which contain gamma-ray and density wireline data, thus enabling the extension of the sequence stratigraphic interpretation from the surface to the sub-surface.

The sequence boundaries for the Ki, Kii and Kiii sequences are all at the base of siltstones which occur, respectively, at the base of the *baylei* Zone, middle of the *mutabilis* Zone and base of the *eudoxus* Zone. These siltstones are all associated with gamma-ray lows (Fig. 6.3), but they are not very prominent in this interval because the siltstones have only marginally less radioactivity than the surrounding mudstones.

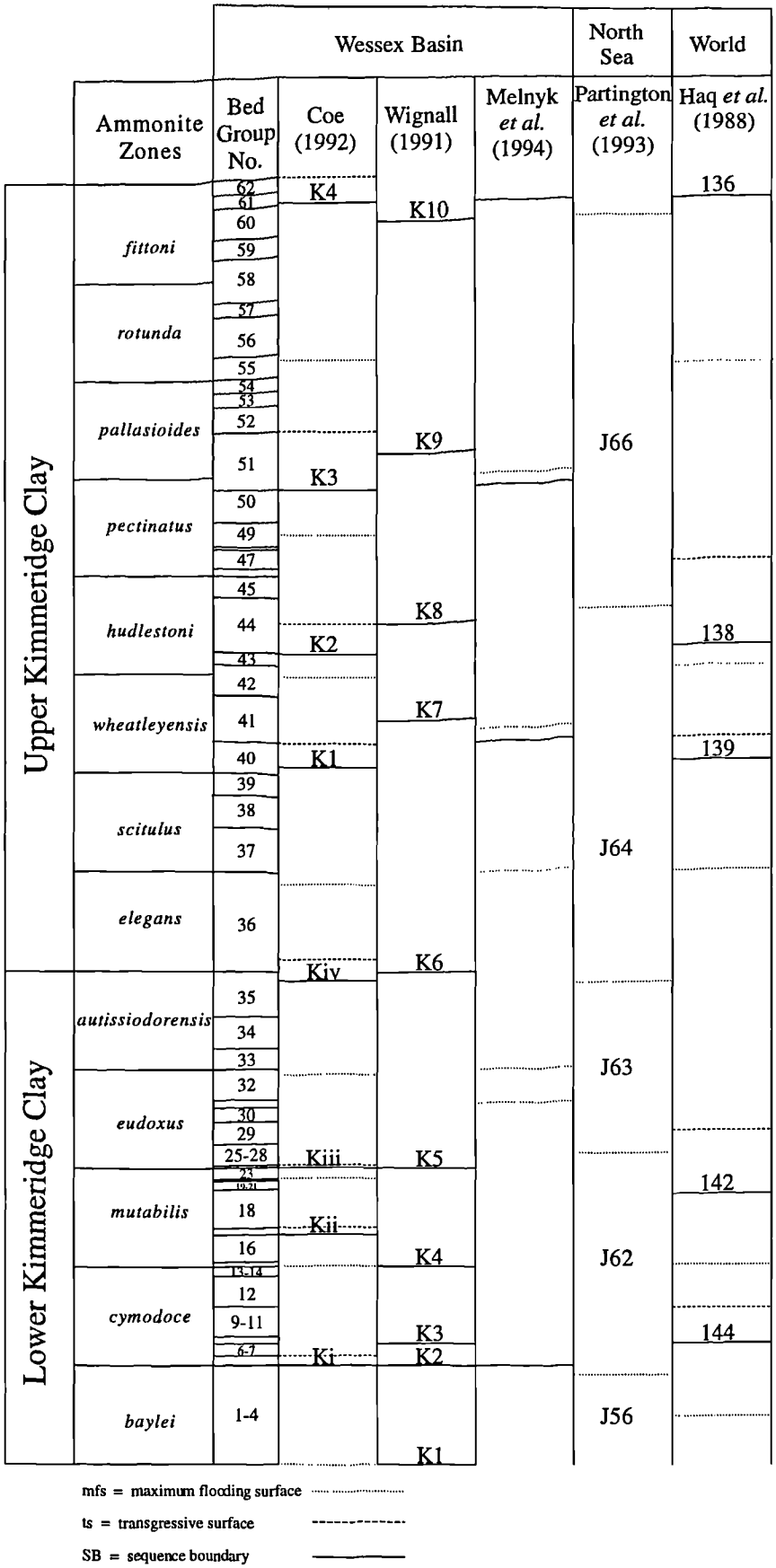

Fig. 6.5 Diagram showing the differences between the various sequence stratigraphic interpretations of Kimmeridgian strata. The interpretation of Coe (1992) was used in this study.

The field log over the part of the Lower Kimmeridge Clay shown in Figure 6.3 lacks significant trends and character. This is probably due to several reasons. Firstly, the lithologies present over this interval are fairly similar. Secondly, the exposure at Blackhead on the Dorset coast where this field gamma-ray log was measured (see Chapter 2) has been disturbed by tectonism and land slides. Thirdly, these exposures are north of the Portland - Wight Faults, and therefore were deposited on a palaeohigh which means that this interval is condensed compared to other successions of Lower Kimmeridge Clay deposited in the deeper sub-basins. The lower part of the Kimmeridge Clay field gamma-ray log does not show the trends expected in a typical sequence (i.e., typical sequence should show progradation from the sequence boundary to the transgressive surface, then retrogradation to the maximum flooding surface, and finally aggradation and/or progradation to the next sequence boundary; see Chapter 4).

The field gamma-ray log constructed from Hobarrow Bay to Chapman's Pool, at Kimmeridge (Fig. 6.4), on the other hand does show the trends expected in a typical sequence. Looking at the Kiv, K1, K2 and K3 sequences in Figure 6.4 you can see that they all show progradation from the sequence boundary to the transgressive surface, then retrogradation to the maximum flooding surface, and finally aggradation and/or progradation to the next sequence boundary.

The two thick homogeneous calcareous mudstone units seen at the base of the *wheatleyensis* Zone (bed group 40) and in the *hudlestoni* Zone (lower part of bed group 44) are the lowermost systems tracts of the K1 and K2 sequences respectively. The gamma-ray signature of these two lowermost systems tracts and the surrounding beds are very distinctive and can be easily correlated using the gamma-ray wireline logs from boreholes across the Wessex Basin (see Section 6.4.3 and Figs 6.25 - 6.30). The K2 sequence boundary also forms a very distinctive density signature which can also be easily correlated with density wireline logs around the basin (Fig. 2.27).

6.3.2 Spectral gamma-ray logs

6.3.2.1 Introduction

Spectral gamma-ray data were recorded along the Dorset coast from the base of bed 32 in the *eudoxus* Zone to the top of bed 54 in the *pallasioides* Zone (Fig. 6.6), covering the sediments from the maximum flooding surface of the Kiii sequence through to the transgressive surface of the K3 sequence. Details of the field logging procedure and the location of the Kimmeridge Clay exposures can be found in Chapter 2. Appendix B contains detailed field logs with the location and values of every field spectral gamma-ray measurement.

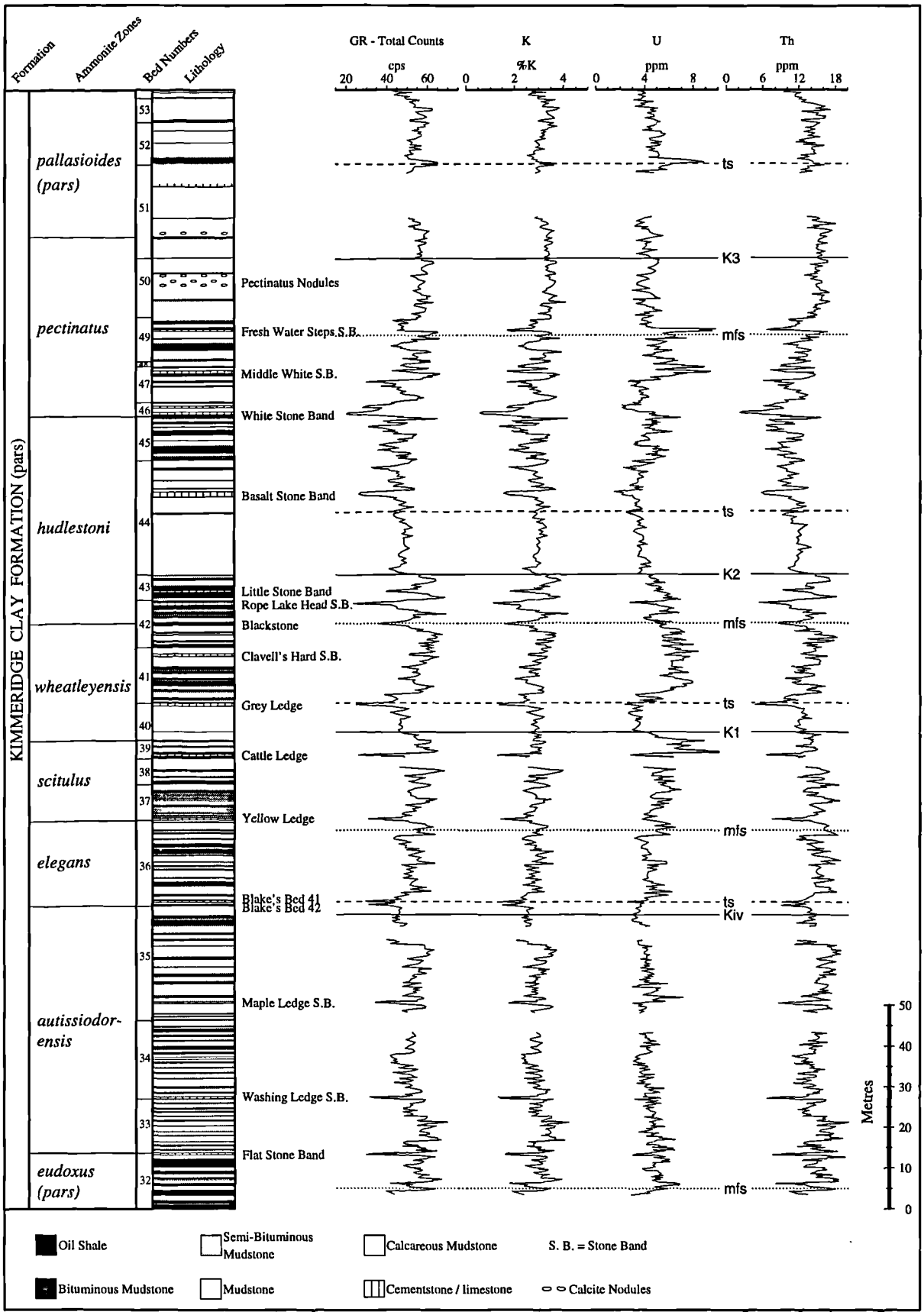

Fig. 6.6 Spectral gamma-ray data recorded over part of the Kimmeridge Clay Formation between Hobarrow Bay and Chapman's Pool, showing the key sequence stratigraphical surfaces.

The properties and distribution of potassium, uranium and thorium in sedimentary rocks are briefly described in Section 6.3.2.2. For more detailed information about the sedimentary geochemistry of potassium, uranium and thorium the reader is referred to Bell (1954), Adams & Weaver (1958), Myers (1987) and Rider (1996). The distribution of potassium, uranium and thorium in the ten lithologies within the Kimmeridge Clay Formation which are most easily recognisable in the field is discussed in Sections 6.3.2.3 to 6.3.2.5. The information gained from the Th/K and Th/U ratios will also be looked at (Sections 6.3.2.6 & 6.3.2.7). The discussion at the end of this section looks at the spectral gamma-ray data in terms of the sequence stratigraphic cycles.

6.3.2.2 Interpretation principles

6.3.2.2.1 Potassium

The source minerals of potassium are the alkali potassic feldspars and micas plus a large number of minerals of minor importance (Serra 1984). During alteration, feldspars are generally completely dissolved, resulting in the release of potassium in ionic form which is then transported in solution. Micas, on the other hand, may lose only part of their potassium during alteration, the remainder staying in the crystal lattice (Serra 1984).

In solution the potassium ion has a very weak ionic potential and can stay in solution under a wide range of pH (Hassan *et al.* 1976). Potassium ions may be absorbed onto the surfaces of clay particles, or absorbed by plants, to reappear in relatively insoluble complex organic compounds. Potassium also occurs in some of the less commonly occurring evaporites in very large quantities, between 10% and 50% K by weight (Rider 1996).

In sea-water, potassium is only present at 380 ppm (Serra 1984). It is thought to be low due to: a) dilution by river-water; b) biological activity; certain algae, for instance, accumulate potassium; and c) interactions between sea-water and detrital minerals, colloidal particles and clay minerals. Potassium minerals may also crystallize out of solution to form evaporites.

6.3.2.2.2 Uranium

The source rocks for uranium are the acidic igneous rocks in which uranium exists as a number of accessory minerals. Uranium is very soluble, thus is dissolved out during the alteration or leaching of source minerals. Because of its solubility it is transported mainly in solution, but rarely in suspension (Serra *et al.* 1980). These dissolved uranium salts are unstable and pass easily out of solution and are fixed into sediments in three geologically important ways (Serra *et al.* 1980): a) chemical precipitation in acid or

reducing environments; b) adsorption by organic matter, plants, plankton, shells, or by animal skeletons in certain environments; c) absorption of uranium by phosphates.

Uranium found in certain heavy minerals and complex organic compounds can be transported over large distances (Serra 1984). On the other hand uranium that is found in complex carbonates or sulphates are only transported short distances before being dissolved.

In general, uranium behaves as an independent constituent. It is not chemically combined in the principal molecules of rocks like potassium, but is loosely associated with secondary components. For this reason it has a very heterogeneous, original sedimentary distribution. Because of its continued solubility even in the subsurface, which is a function of its loose attachments, it is susceptible to leaching and redeposition and its distribution is therefore even more irregular (Serra 1984).

6.3.2.2.3 Thorium

Like uranium, thorium has its origins mainly in the acid and intermediate igneous rocks. However, it is extremely stable and, unlike uranium, will not generally pass into solution (Rider 1996). Almost all thorium is transported in suspension, and it is a common constituent of the detrital fraction of sediments. The small amount of thorium that passes into solution is readily absorbed onto clay minerals, or forms secondary products of hydrolysis with the resistant thorium bearing minerals (Serra 1984). Unlike uranium, thorium does not migrate during diagenesis.

Thorium minerals may be found as silt-sized particles in placer concentrations but more generally distributed throughout most mudstones where the thorium seems to become fixed by adsorption (Serra *et al.* 1980). Thorium shows an affinity for terrestrial minerals, because of its detrital nature and consequent transport by currents. Amongst the clay minerals for example it is more abundant in kaolinites (of terrestrial origin) than in glauconites (of marine origin) (Hassan *et al.* 1976).

6.3.2.2.4 Shales

In Chapter 4 the general assumption that there is a close relationship between total gamma-ray values and clay volume was made, as shown by Heslop (1974). The advantage of spectral gamma-ray curves over the total gamma-ray curve is that it allows the analysis of the relationship of the individual radioactive elements to the clay matrix to be examined.

Potassium occurs as part of the clay mineral structure and has a fairly constant distribution through most shales. However, the potassium content of different clay minerals varies considerably. Illites contain by far the greatest amount while kaolinite has very little or none (Table 6.1). Most clays are mixtures of several clay minerals which

result in a relatively constant potassium content of about 2.7% (Rider 1991). Potassium is thought to contribute about 35-45% to shale radioactivity (Dypvik & Eriksen 1983).

Mineral	K% by weight	Average K%	Composition
Illite	3.51 - 8.31	5.20	K, Al, Silicate
Glauconite	3.20 - 5.80	4.50	K, Mg, Fe, Al, Silicate
Kaolinite	0.00 - 1.49	0.63	Al, Silicate
Smectite	0.00 - 0.60	0.22	Ca, Na, Mg, Fe, Al, Silicate
Chlorite	0	0	Mg, Fe, Al, Silicate

Table 6.1 Potassium in clay minerals (modified from Rider (1991), original data from Serra *et al.* (1980), Dresser Atlas (1983)).

Uranium is often associated with secondary components because of its solubility and thus is generally distributed irregularly. Uranium is thought to only contribute 10-20% (Dypvik & Eriksen 1983) of the overall radioactivity of shales, but in certain cases this can increase dramatically (Rider 1991). For example uranium contributes up to 41% of the total radioactivity in black oil shales (Rider 1996), because uranium will tend to precipitate or concentrate in confined, reducing environments, which are themselves favourable to the accumulation and preservation of organic matter (Serra 1984). An environment of stagnant water and a relatively slow rate of deposition (Adams & Weaver 1958) is required to produce black shales. Uranium is therefore a poor shale indicator but a good oil shale indicator.

Thorium is generally considered a marine element and is associated only with detrital sediments. It has a constant value in almost all naturally-occurring shales, the average being about 12 ppm for a typical shale (Rider 1991). This constant value is said to contribute between 40-50% (Dypvik & Eriksen 1983) of the overall shale radioactivity. In mixtures of sandstone and shale, thorium will occur only in the shale fraction, except in rare occurrences where the sandstones are tufaceous in nature or contain heavy minerals (Western Atlas 1992).

6.3.2.3 Potassium content of the Kimmeridge Clay Formation

The potassium curve in Figure 6.6 shows that the overall potassium content, from bed 32 in the *eudoxus* Zone to bed 54 in the *pallasioides* Zone, remains generally similar at 3%, but over short intervals varies between 2.5% and 3.5%. An exception to this can be seen in two intervals, the first being at the base of the *hudlestoni* Zone, the second straddles the *hudlestoni / pectinatus* zonal boundary. In these two intervals the potassium content varies over a greater range. The lowest potassium content (0.58%) was recorded at the base of the *pectinatus* Zone in the 'White Stone Band' (coccolith limestone), in fact

all of the most prominent potassium lows were recorded in the 'Stone Bands' which are either carbonate cementstones or coccolith limestones (Cox & Gallois 1981).

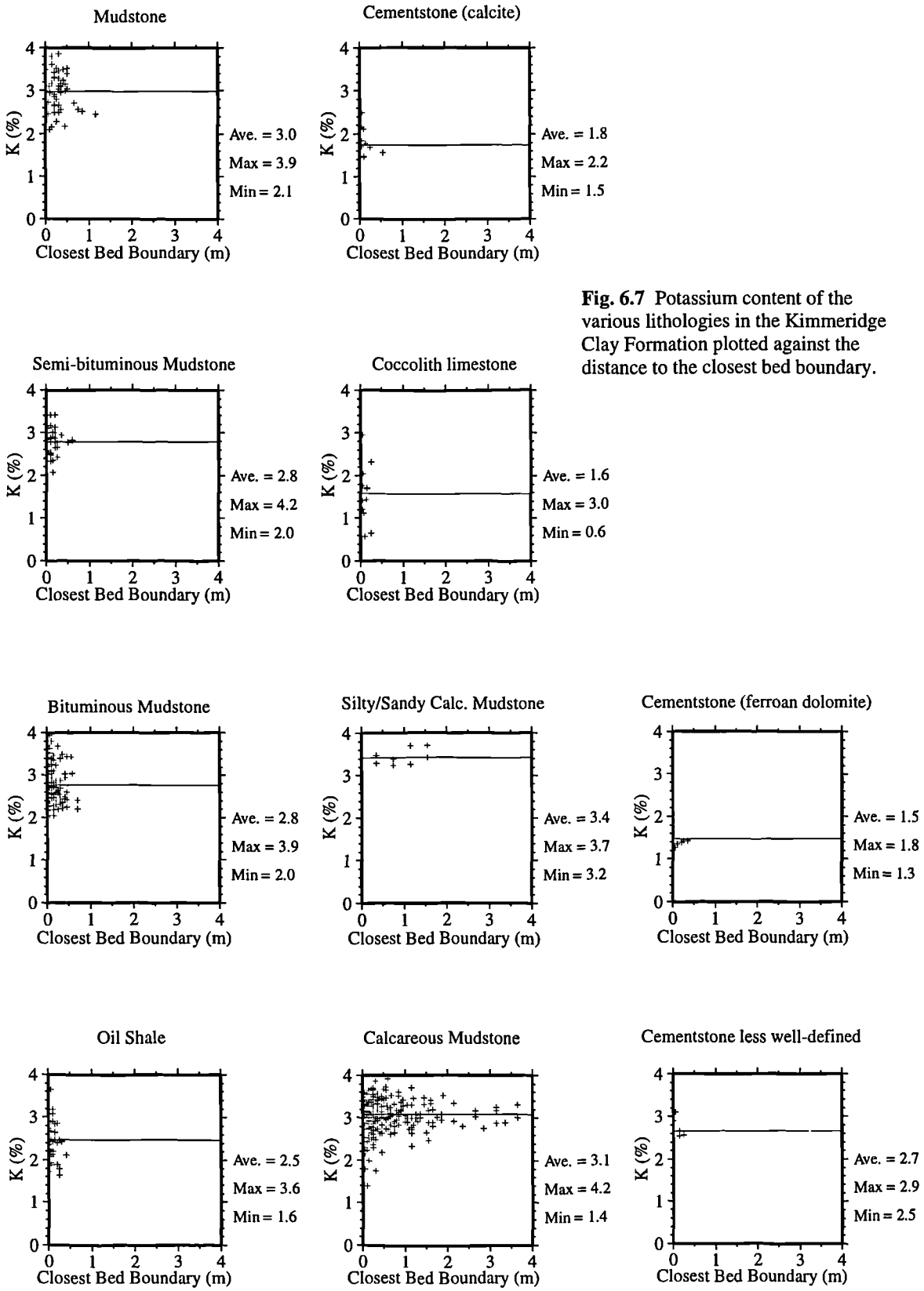

Fig. 6.7 Potassium content of the various lithologies in the Kimmeridge Clay Formation plotted against the distance to the closest bed boundary.

The three highest potassium values were recorded near the base of the *autissiodorensis* Zone in a mudstone (4.15%), near the base of the *hudlestoni* Zone in a semi-bituminous mudstone (4.17%) and at the top of the *hudlestoni* Zone in a calcareous mudstone (4.18%). It has been observed that the potassium content seems to be higher than average below the coccolith limestones and the thicker oil shales. A possible explanation for this is that potassium rich formation waters, which were trapped by the impermeable coccolith limestones and oil shales, reacted with the minerals present in the clays resulting in an increase in illite which are rich in potassium (pers. comm. J. Pearce).

The potassium content for each of the ten lithologies which are easily recognized in the field between the *eudoxus* and *pallasioides* zones have been plotted against the distance to the closest bed boundary to the position from which the potassium content was recorded (Fig. 6.7). Figure 6.7 clearly shows that the potassium measurements taken close to bed boundaries have large scatter, while those taken in thicker beds further away from the bed boundaries show less scatter (see calcareous mudstone plot in Fig. 6.7). This is due to the fact that the spectral gamma-ray tool has a radius of influence of approximately 80 cm (see Chapter 2, Section 2.2.4) and that the measurements were taken on the cliff face perpendicular to the bedding so the thinner beds would be influenced to some extent by the beds above and below. Figure 6.8 shows the potassium content of the calcareous mudstones plotted against the distance along the cliff, bed thickness and distance to the closest bed boundary. This diagram shows that the average potassium (average of all measurements) content of calcareous mudstones is not ideal, and to get a better average any measurement taken within the radius of influence of the tool (~80 cm) should be removed. This was not done for all the lithologies in this data set because only the calcareous mudstone lithology forms thick beds in this Kimmeridgian succession (Fig. 6.7). The averages seen in Figures 6.7, 6.9 and 6.10 are therefore only used for general descriptive purposes.

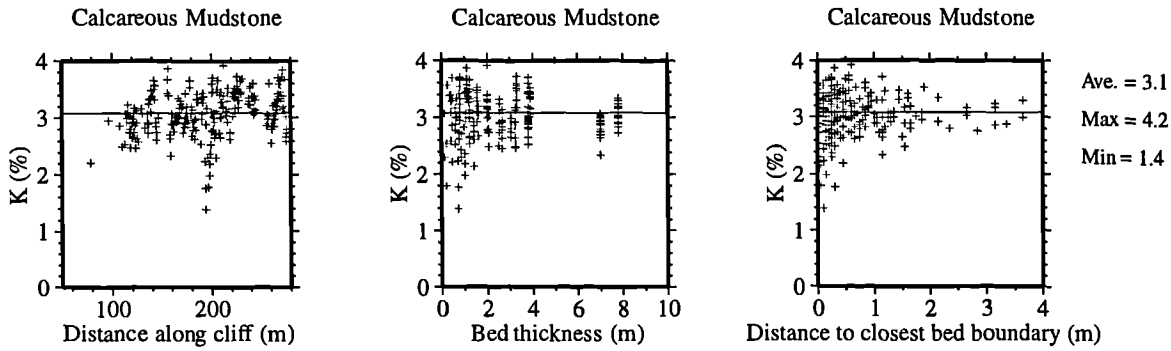

Fig. 6.8 Potassium content of the calcareous mudstone plotted against the distance along the cliff, bed thickness and distance to closest bed boundary.

The graphs in Figure 6.7 clearly show that the 'Stone Bands' contain the lowest average potassium values whilst the calcareous mudstones contain the highest average values.

6.3.2.4 Uranium content of the Kimmeridge Clay Formation

Unlike the potassium curve, which remains fairly constant, the uranium curve shows marked variation (Fig. 6.6). The lowest uranium content was recorded in the 'Basalt Stone Band' (1.6 ppm). Other low uranium values (average 4.4 ppm) are associated with the calcareous mudstones, especially those within bed 40 of the *wheatleyensis* Zone and those in bed 44 of the *hudlestoni* Zone.

The highest uranium value (11.4 ppm) was recorded in the oil shale above 'Cattle ledge' in bed 39 of the *scitulus* Zone (Fig. 6.6). Other oil shales also seem to have fairly high levels of uranium, for example the oil shale in bed 52 of the *pallasioides* Zone has a uranium content of 8.86 ppm. In general the uranium content is higher around oil shales and bituminous mudstones (average of 6 ppm as opposed to 3 ppm where oil shales and bituminous beds are not present).

An interesting observation is that two of the coccolith limestones, 'Freshwater Steps Stone Band' (9.82 ppm) and the 'Middle White Stone Band' (9.32 ppm), have high uranium contents whereas the other coccolith limestone bands (Rope Lake Head Stone Band, Little Stone Band and White Stone Band) have significantly lower uranium contents (see coccolith limestone graph in Fig. 6.9, and lithology logs in Appendix B). The coccolith bands are finely laminated with organic rich mudstones 'mm' scale, this suggests that probably the Freshwater Steps and the Middle White Stone Bands have a higher organic content, because uranium is generally associated with organic matter (see Section 6.3.2.2.2). Also in general the coccolith limestones have higher uranium content than the diagenetic stone bands due to the fact the diagenetic stone bands do not contain organic matter. For example the 'Basalt Stone Band' and 'Cattle Ledge' have low uranium contents (1.6 - 3.5 ppm). This is unlike potassium which has a low content in all the stone bands, because potassium is not associated with organic matter.

The oil shales and bituminous mudstones have the highest average uranium content of the various mudstone lithologies (Fig. 6.9). Looking at the average uranium content in the mudstone lithologies, a trend from higher uranium contents to lower uranium contents can be seen as the mudstones grade from oil shales to calcareous mudstones.

6.3.2.5 Thorium content of the Kimmeridge Clay Formation

The thorium curve is very similar in appearance to the potassium curve in that potassium highs and lows tend to correlate with thorium highs and lows (Fig. 6.6). But

unlike the potassium curve the thorium curve does show slight trends. For example the thorium curve remains fairly constant from the *eudoxus* Zone to the middle of the *scitulus* Zone, but thereafter the overall trend reduces from an average thorium value of 16 ppm to an average value of 8 ppm at the top of the *hudlestoni* Zone. The curve then increases to 16 ppm by the middle of the *pectinatus* Zone where it stays at that level to the top of the log.

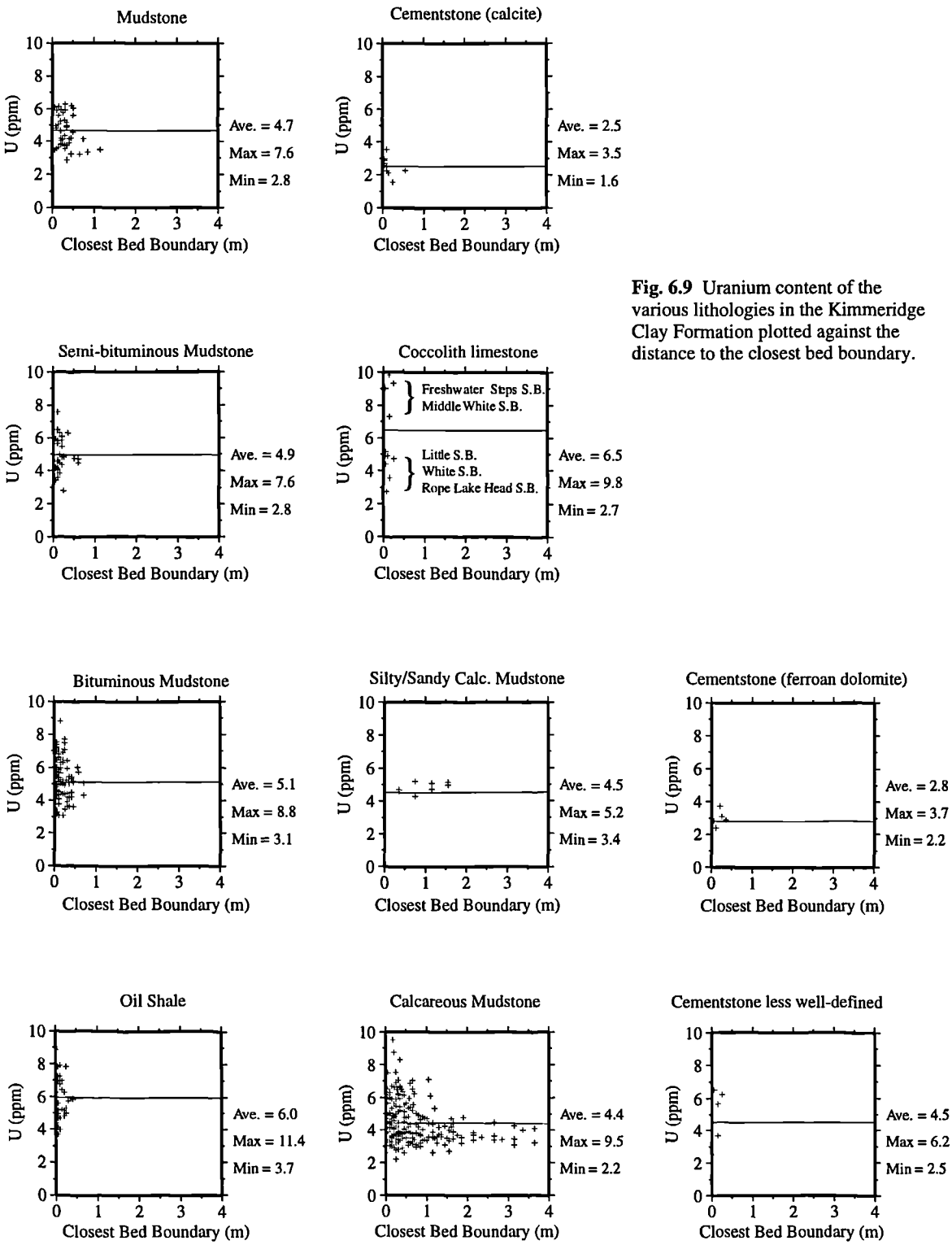

Fig. 6.9 Uranium content of the various lithologies in the Kimmeridge Clay Formation plotted against the distance to the closest bed boundary.

The lowest thorium value (2.34 ppm) was measured in the 'White Stone Band' (coccolith limestone). The other thorium lows like the potassium lows are associated with the 'Stone Bands' (Fig. 6.10). This is because thorium generally resides with clays (see Section 6.3.2.2.3), and the 'Stone Bands' are generally devoid of clays.

The highest thorium content (18.6 ppm) was measured in a mudstone in bed 33 of the *autissiodorensis* Zone. Of the mudstone lithologies the lowest average thorium content was found to be in the oil shales (11 ppm), and the highest average thorium content (15.5 ppm) in the silty/sandy calcareous mudstones (Fig. 6.10).

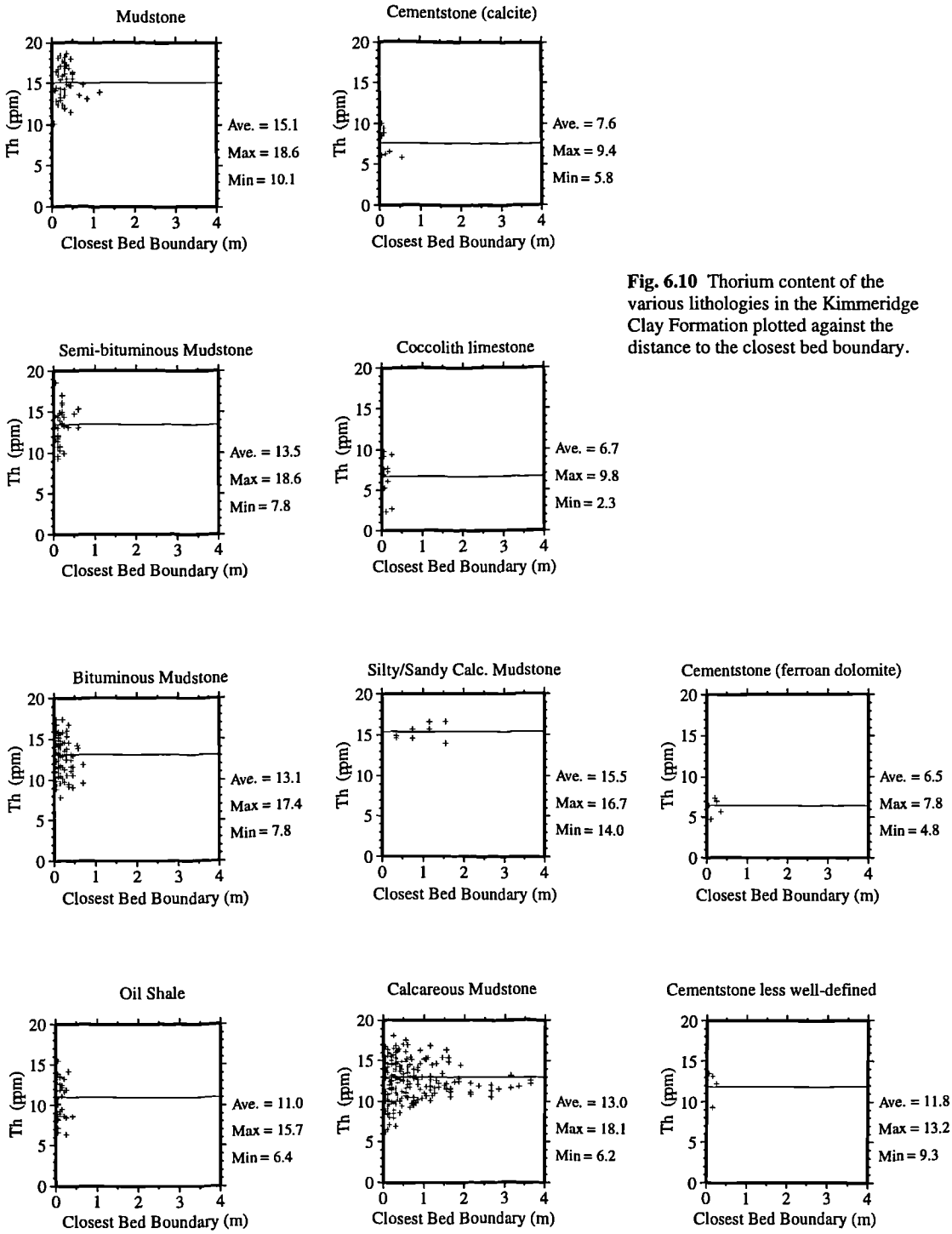

Fig. 6.10 Thorium content of the various lithologies in the Kimmeridge Clay Formation plotted against the distance to the closest bed boundary.

6.3.2.6 Th/K

Adams & Gasparini (1970) were the first to realise that potassium and thorium are closely correlated in mudrocks, and the data recorded in this study also agree with this observation (Fig. 6.11). They suggest that this is due to that fact that thorium resides with potassium in the clay fraction of the rock. Quinif *et al.* (1982) noticed that regression lines drawn on thorium and potassium cross plots rarely pass through the origin and commonly have a positive intercept on the thorium axis. The spectral data recorded in this study also agree with this observation (Fig. 6.11). This shows that there is an excess of thorium which is not associated with potassium. Quinif *et al.* (1982) defined an equation to express this relationship:

$$\text{Th ppm} = (C \times K\%) + d$$

They interpreted a positive value of d to represents Th in heavy minerals. Myers (1987) took this argument further by suggesting that a negative value of d, (i.e., a positive intercept on the K-axis), would indicate the presence of potassium which is not associated with thorium - most probably K-feldspar.

The Th/K cross plots may also be used for the identification of clay mineralogy (Hassan *et al.* 1976). They have been used to discriminate micas from clay minerals, owing to the higher content of potassium in mica. Illite has higher potassium than mixed-layer clays or smectite, while kaolinite has little or none (Doveton 1994). The data recorded in this study can be seen plotted on the Th/K cross plot (Fig. 6.12) constructed by Quirein *et al.* (1982) from standard mineral data (Edmundson & Raymer 1979). For comparative purposes the data in this study were also plotted on the Th/K cross plot developed by Western Atlas (1992) (Fig. 6.13). Comparing these two cross plots (Figs 6.12 & 6.13) it is evident that both tell us that the majority of the Kimmeridge Clay is made up of mixed layer clays. What is disturbing is the fact that the two data sets do not plot in the same regions on both graphs; for example most of the data plotted on the Quirein *et al.* (1982) cross plot lies just above the mixed layer clay / illite boundary, with some of the points actually falling into the illite zone (Fig. 6.12). On the other hand the same data plotted on the Western Atlas (1992) cross plot lie just above the mixed layer clay / kaolinite boundary, with some points falling into the kaolinite zone (Fig. 6.13). The Western Atlas (1992) graph does not come with any explanation on how the graph was produced, unlike the graph in Quirein *et al.* (1982). For this reason the graph produced by Quirein *et al.* (1982) has been taken as being more accurate in this study.

Doveton (1994) warns that the clay mineral zones on Th/K cross plots should be used with caution, because clay minerals show wide variability in composition and most shales contain mixtures of different clay mineral species. Hurst (1990) went further by

saying "there is no theoretical, and negligible analytical, basis for using Th/K cross-plots for mineral identification".

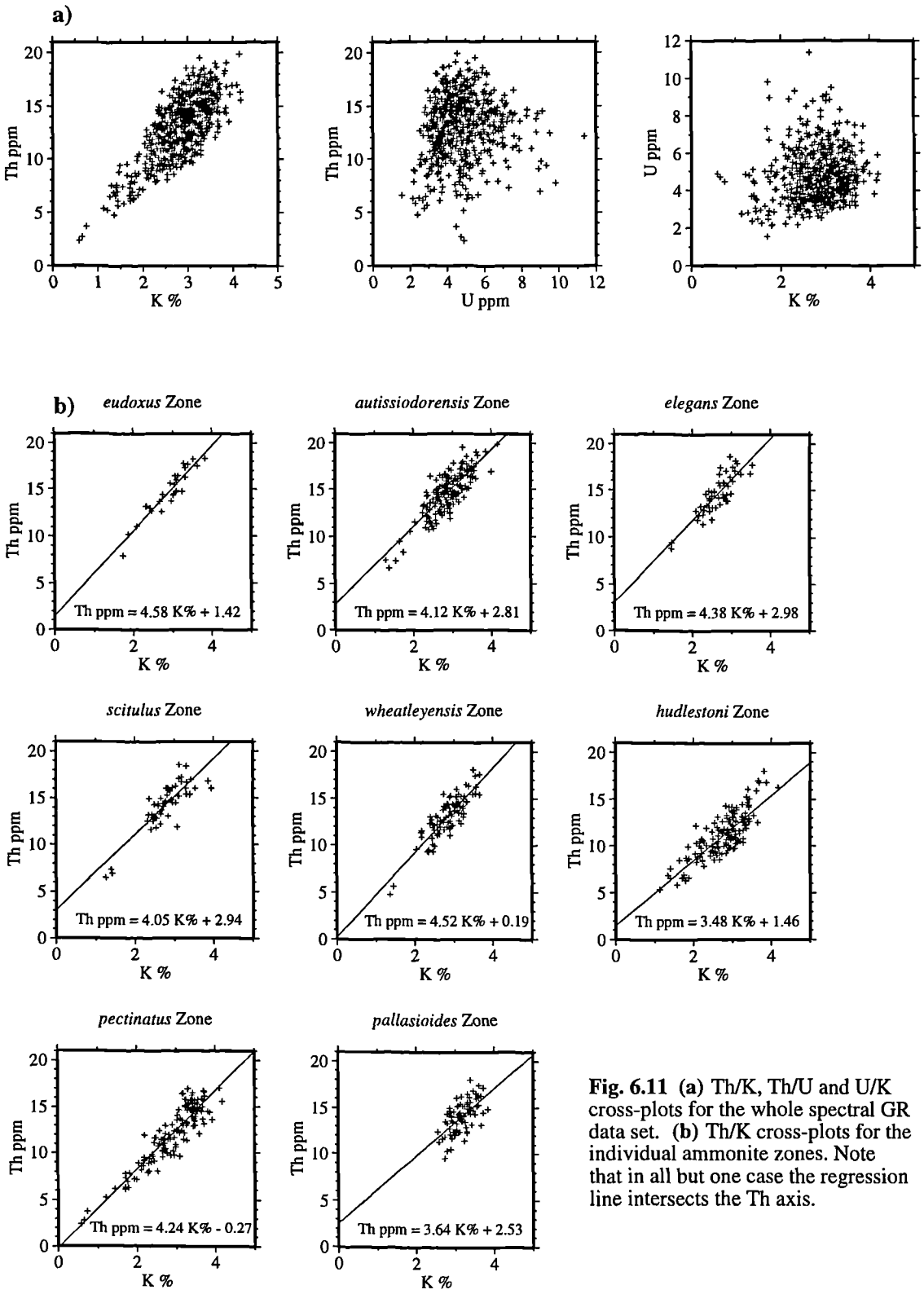

Fig. 6.11 **(a)** Th/K, Th/U and U/K cross-plots for the whole spectral GR data set. **(b)** Th/K cross-plots for the individual ammonite zones. Note that in all but one case the regression line intersects the Th axis.

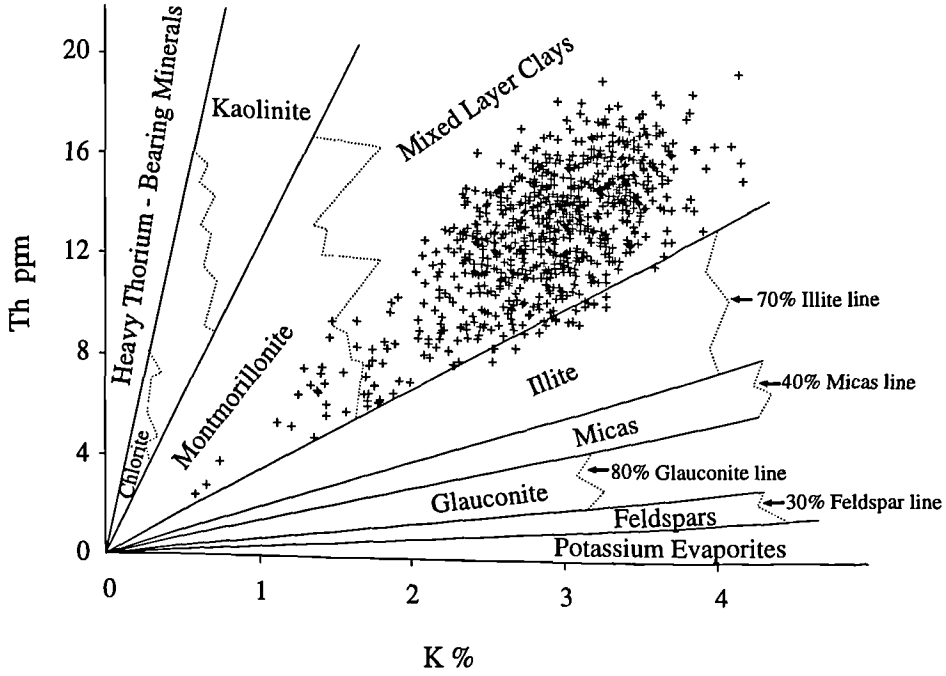

Fig. 6.12 Spectral gamma-ray data recorded over part of the Kimmeridge Clay Formation, plotted on the Th/K plot for the identification of clay minerals developed by Quirein *et al.* (1982).

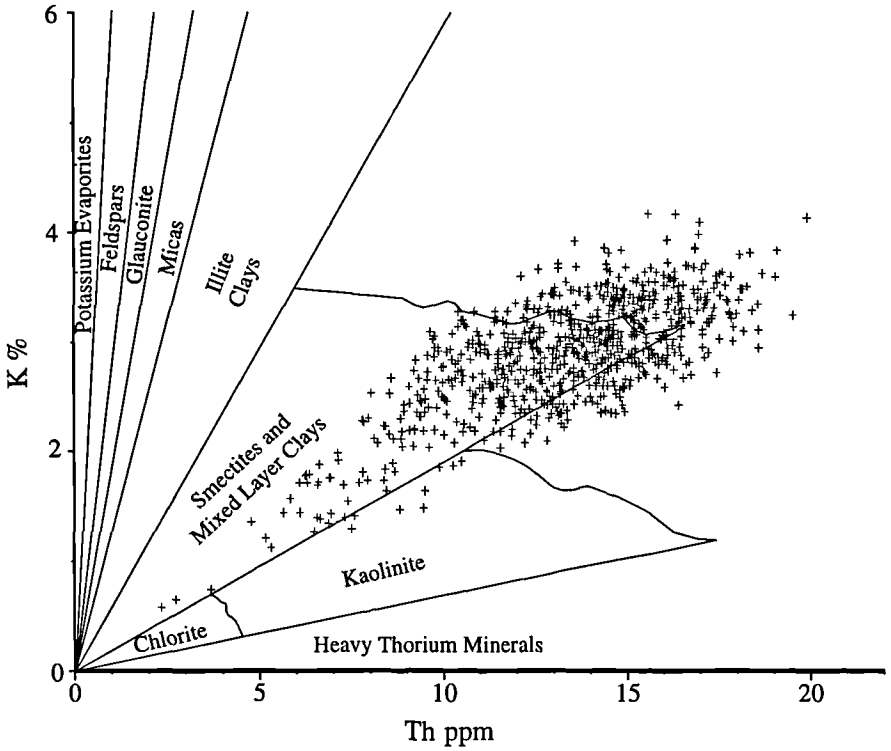

Fig. 6.13 Spectral gamma-ray data recorded over part of the Kimmeridge Clay Formation, plotted on the Th/K plot for the identification of clay minerals from Western Atlas (1992).

Lithologies	Clay minerals	Quartz	Calcium carbonate	Kerogen
Dark grey mudstone (Semi-bituminous mudstone)	45-65 %	10-30 %	5-20 % (depending on shell content)	<2%
Medium grey mudstone (Mudstone)	35-55 %	10-15 %	20-35 %	<1%
Pale grey mudstone (Calcareous mudstone)	25-45 %	8-15 %	25-55 %	<1%
Cementstone	10-20 %	2-6 %	60-90 %	<1%
Bituminous mudstone	30-50 %	10-20 %	10-25 %	2-10 %
Oil shale	20-40 %	10-15 %	10-25%	10-45%

Table 6.2 Bulk chemistry of the Kimmeridge Clay lithologies (after Cox & Gallois 1981). The lithology names in brackets are the names used in this study.

Clay minerals make up 30 - 65% of the mudstones in the Kimmeridge Clay Formation (Table 6.2). The dominant clay minerals are illite and kaolinite with minor amounts of smectite and chlorite (Cox & Gallois 1981). It is suggested that kaolinite is generally concentrated in near shore and deltaic facies, while illite dominates in offshore facies (Bjørlykke *et al.* 1975). Kaolinite/illite ratios have been used to show changes in climate (Bjørlykke *et al.* 1975; Wignall & Ruffell 1990; Hesselbo 1996) because kaolinite generally characterizes warm humid climates.

Myers (1987) suggests that kaolinite (and to a lesser extent smectite) will tend to increase the Th/K ratio, whereas illite will tend to decrease it. Thus indicating that the Th/K ratio can potentially yield important information concerning climate in the source area. The Th/K ratio of illitic clays is around 3-4 whereas for kaolinite and smectite it is around 40 (Myers 1987). The Th/K ratio from the spectral data in this study range from 3-7, which would indicate that the areas on the curve with the lower Th/K ratios represent more illitic clays (Fig. 6.14).

Hesselbo (1996) showed that Th/K ratios may correlate with kaolinite/illite ratios but only where glauconite is not developed. Seeing as there is no glauconite in the Kimmeridge Clay of Dorset the kaolinite/illite data from Wignall & Ruffell (1990) was plotted against the spectral gamma-ray data recorded in this study (Fig. 6.15) to test this suggestion. The general trends seen on the Th/K and the kaolinite/illite ratio curves do in fact seem to correlate (Fig. 6.15). The uranium curve seems to correlate better with the kaolinite/illite ratio curve, then the Th/K curve.

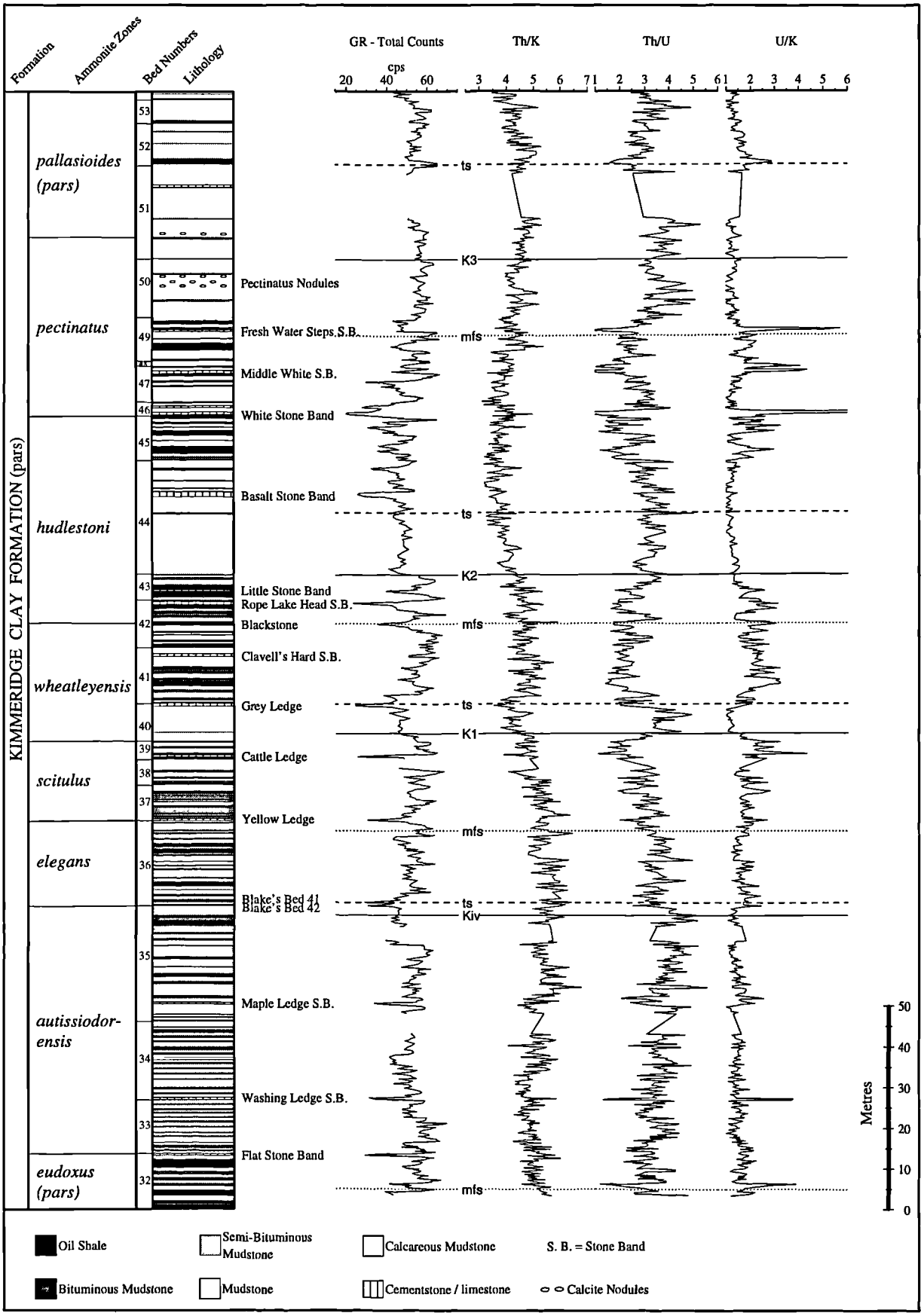

Fig. 6.14 Th/K, Th/U and U/K ratios for the part of the Kimmeridge Clay Formation exposed between Hobarrow Bay and Chapman's Pool, showing the key sequence stratigraphical surfaces.

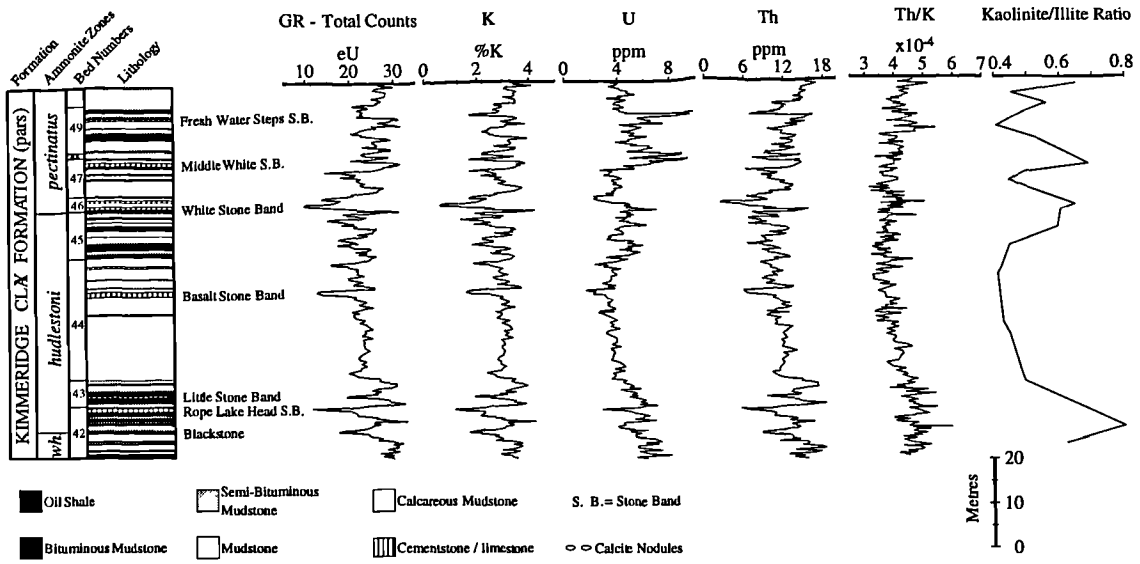

Fig. 6.15 Spectral gamma-ray data, recorded in this study, plotted with the kaolinite/illite ratio from Wignall & Ruffell (1990).

6.3.2.7 Th/U

After the work of Adams & Weaver (1958), the thorium/uranium ratio has been used in the identification of depositional environments. They suggested that when the ratio was computed to be less than 2 (uranium-rich), the depositional environment had probably promoted uranium fixation under reducing conditions, and was most commonly marine. By contrast, ratio values of greater than 7 (uranium-poor), implied uranium mobilization through weathering and/or leaching, and therefore indicated an oxidizing, possibly terrestrial environment.

Doveton (1994) combined the Th/K and Th/U ratios into one plot so that both composition and possible redox potential conditions could be assessed simultaneously. Figure 6.16 shows the spectral data recorded in this study plotted on Doveton's spectral gamma-ray KUT ratio plot. This plot shows that some of the spectral data recorded in this study has Th/U ratio values of less than 2 indicating reducing conditions, these data points correlate with the high uranium concentrations of the oil shales and bituminous mudstones (Fig. 6.9). Figure 6.16 also shows that the spectral data lies on the mixed-layer clays / illite boundary (i.e., the same place as seen on clay mineralogy plot of Quirein *et al.* (1982); Fig. 6.12).

6.3.2.8 Previous work

As was mentioned in Chapter 2 Myers (1987) recorded spectral gamma-ray measurements along the Dorset coast, from the base of the *elegans* Zone to about the middle of the *pectinatus* Zone. A comparison of Myers's spectral data and the spectral data recorded in this study can be seen in Figure 6.17. This diagram clearly shows that the data

recorded in both studies compare very well, the main difference being that the curves constructed in this study are more detailed and cover more of the Upper Kimmeridge Clay. Myers (1987) recorded the spectral gamma-ray data on horizontal bedding planes, mainly on wave cut platforms, whilst the measurements recorded in this study were taken on the cliff face (see Chapter 2), it is for this reason that Myers curves are not as detailed and as continuous as the curves from this study (Fig. 6.17).

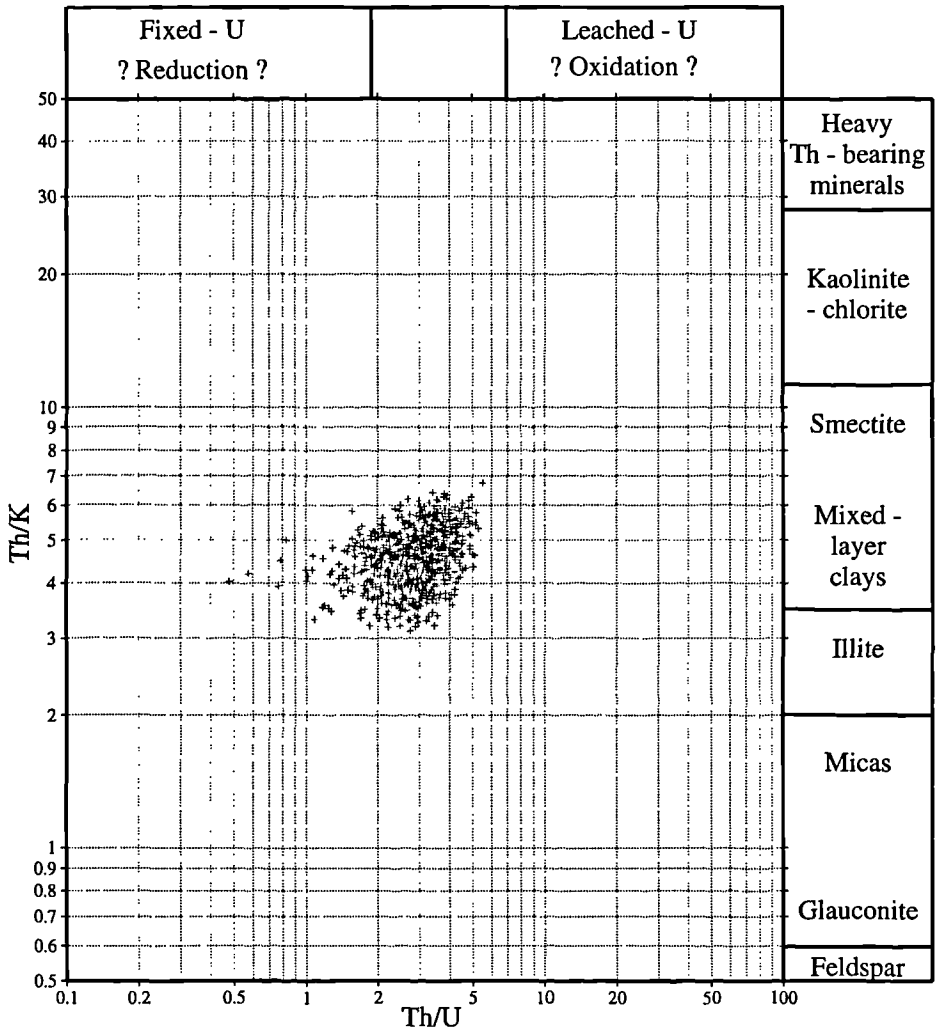

Fig. 6.16 Kimmeridge Clay spectral gamma-ray data ploted on spectral gamma-ray KUT ratio plot. The KUT ratio plot is after Doveton (1994).

Myers (1987) states that the average potassium content remains similar but varies over a greater range in the upper ammonite zones (Fig. 6.17). The data recorded in this study show the same observation over the interval from which Myers recorded spectral data, but Figure 6.17 clearly shows that above the middle of the *pectinatus* Zone the average potassium content reverts to remaining similar without varying over a greater range. He also states that the average thorium content steadily decreases upwards (Fig. 6.17). The extra data recorded in this study as compared to Myers's data clearly show that

the thorium content increases upwards again, from the *hudlestoni / pectinatus* zonal boundary, and reaches similar high thorium values as those seen lower in the succession.

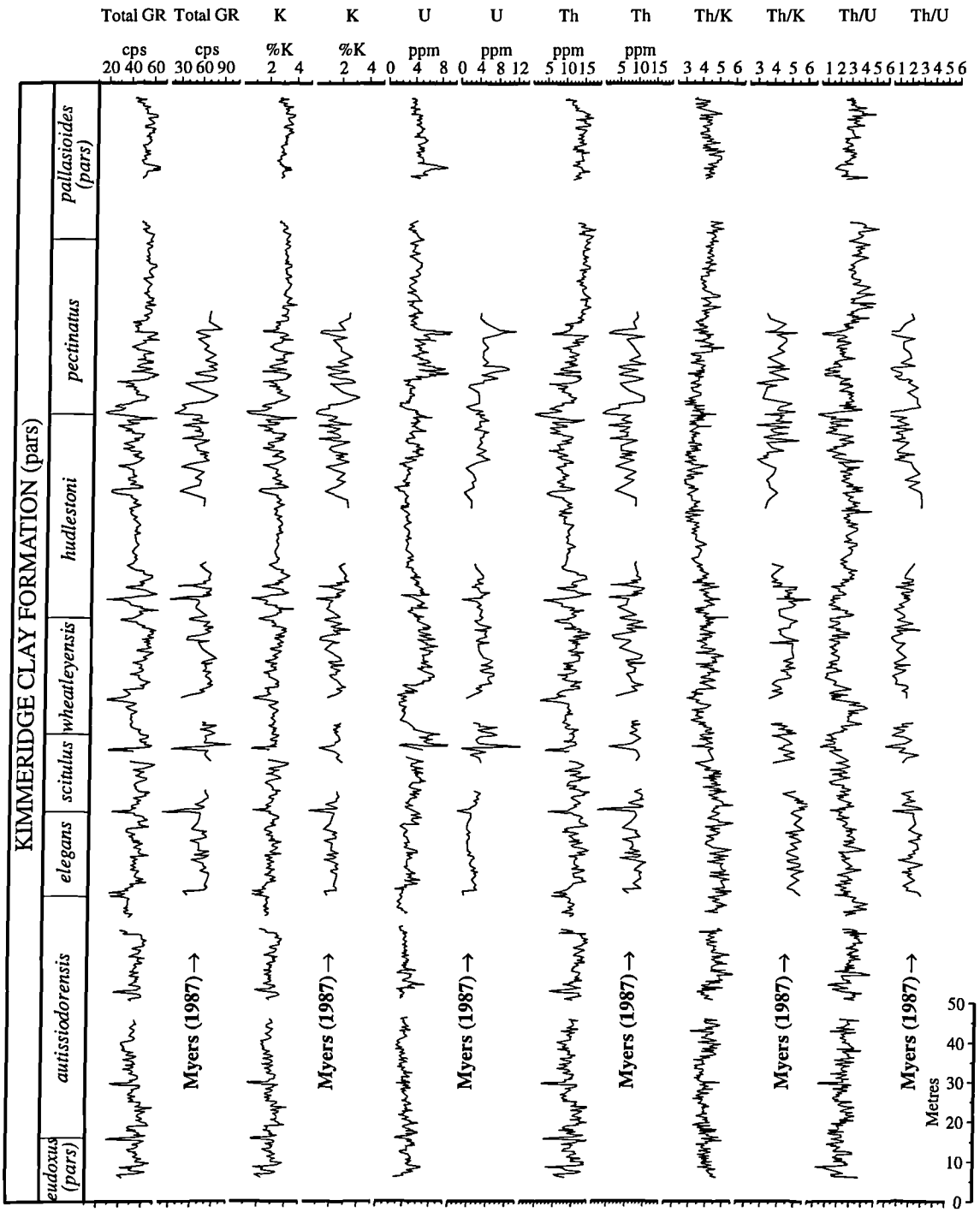

Fig. 6.17 Spectral gamma-ray data recorded in this study plotted alongside the spectral data recorded by Myers (1987).

6.3.2.9 Discussion

Looking at the spectral gamma-ray curves (potassium, uranium and thorium; Fig. 6.6) it is evident that the overall trends seen on the total gamma-ray curve are more

enhanced on the uranium curve. Also the lowermost systems tracts stand out more on the uranium curve than any of the curves.

The Th/K ratio curve (Fig. 6.14) is the best curve to show the trends expected in a typical sequence (i.e., progradation from sequence boundary to transgressive surface, retrogradation from the transgressive systems tract to the maximum flooding surface and finally progradation and or aggradation from the maximum flooding surface to the next sequence boundary).

Doveton (1994) used the Th/U curve as an indicator of transgression / regression cycles, and suggested that abrupt changes in the Th/U curve were due to periods of non-deposition. Abrupt changes can be seen in the Th/U curve from this study (Fig. 6.14); however, there are no periods of non-deposition in the Kimmeridgian succession over which the spectral gamma-ray data was recorded. Some of the abrupt changes do occur at the sequence boundaries: Kiv, K1 and K2, for example. This would suggest that the abrupt changes seen in the Th/U curve from this study are due to the change in lithology from that in the highstand systems tract to that in the lowermost systems tract, which occurred when the sea-level fell.

6.4 Sequence stratigraphical interpretation of the wireline logs

6.4.1 Introduction

Out of the 166 boreholes used in this study, 84 penetrate Kimmeridgian strata, and of these 58 have wireline data (Fig. 6.18). Each of these 58 wells has been interpreted sequence stratigraphically.

The first stage in the construction of the sequence stratigraphic wireline correlations (Figs 6.25 - 6.30) was to correlate the biostratigraphically controlled boreholes and the field gamma-ray and density logs with the rest of the boreholes in the Wessex Basin in order to pick the ammonite zonal boundaries. The techniques used to correlate the wireline data and the need for biostratigraphically controlled boreholes were described in Chapter 3. Once all the ammonite zones had been picked on the entire borehole data set the key sequence stratigraphic surfaces were then picked using the ammonite zones to constrain the interpretations. The location of the key sequence stratigraphic surfaces interpreted on the boreholes were then compared with the location of the key surfaces on the field gamma-ray and density logs as a final check on the interpretation.

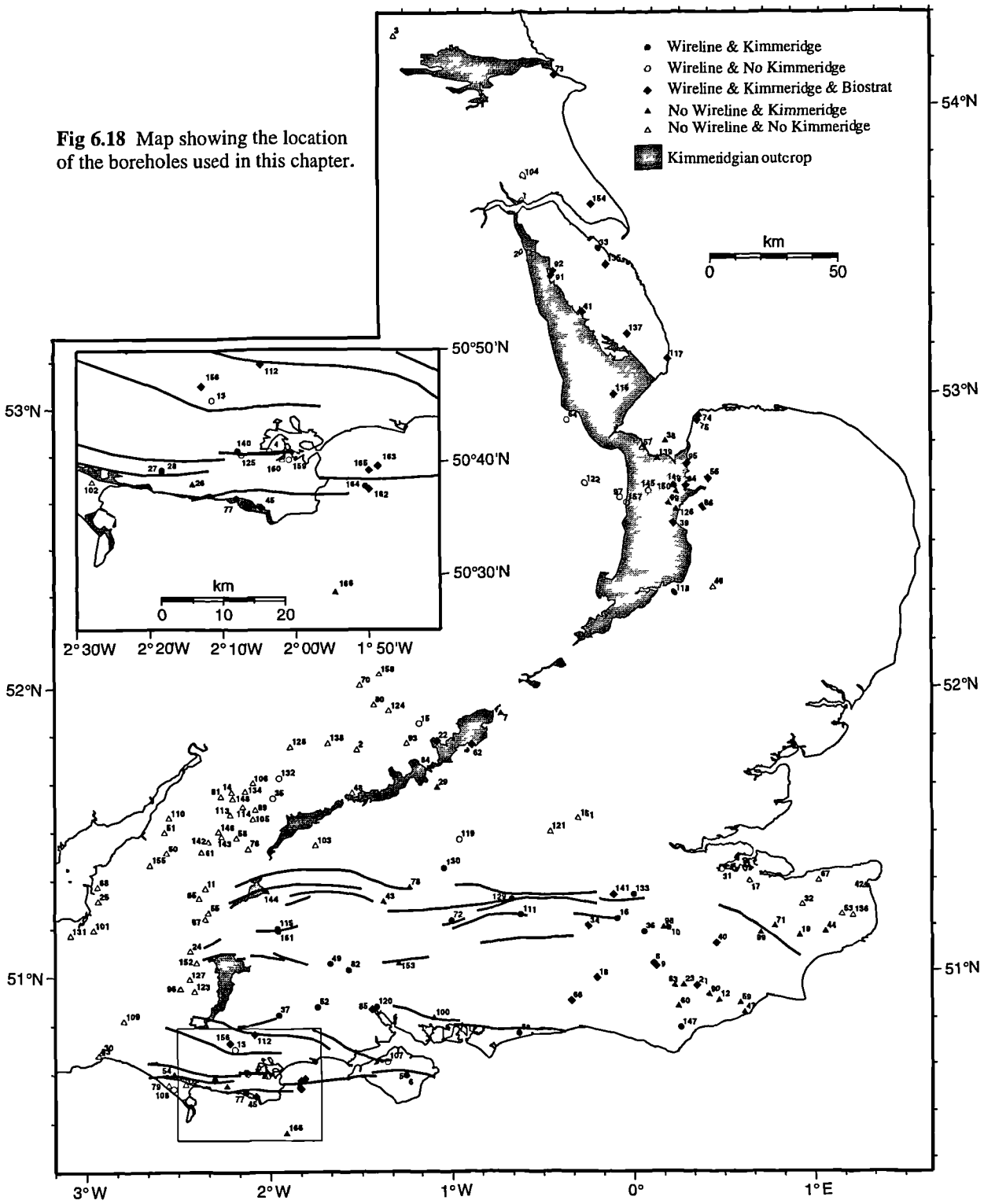

Fig 6.18 Map showing the location of the boreholes used in this chapter.

1 Alandale
2 Apley Barn
3 Arden Moor
4 Arne G1
5 Arreton 1
6 Arreton 2
7 Ascott Farm
8 Ashdown 1
9 Ashdown 2
10 Ashour 1
11 Baggridge 1
12 Battle
13 Bere Regis 1
14 Beverston
15 Bicester 1
16 Blechingley 1
17 Bobbing
18 Bolney 1
19 Branbourne
20 Brigg 1
21 Brightling 1
22 Brill
23 Broadoak
24 Burton
25 Burton Row
26 Chaldon Herring G2
27 Chaldon Herring 1
28 Chaldon Herring G3
29 Chalgrove
30 Charmouth
31 Chatham
32 Chilham
33 Cleethorpes
34 Collendean farm
35 Cooles Farm
36 Cowden 1
37 Cranbourne 1
38 Daseley's Sand
39 Denver Sluice 1
40 Detention 1
41 Donington on Bain
42 Ebbsfleet
43 Egbury
44 Elham
45 Encombe
46 Eriswell
47 Fairlight
48 Faringdon 1
49 Farley South 1
50 Filton 1
51 Filton 2
52 Fordingbridge 1
53 Freville
54 Friar Waddon
55 Frome
56 Gayton
57 Gedney Drove End
58 Grittleton
59 Guestling
60 H. Grove Hill 1
61 Hamswell
62 Hartwell
63 Heathfield 7
64 Helpringham 1
65 Hemington
66 Henfield 1
67 Herne
68 Hill Lane
69 Hook Drian
70 Hook Norton
71 Hothfield
72 Humbly Grove
73 Hunmanby 1
74 Hunstanton 1
75 Hunstanton IGS
76 Ivyfields 3
77 Kimmeridge K5
78 Kingsclere
79 Langton Herring 1
80 Ledwell
81 Leighterton
82 Lockerley 1
83 Lyme Regis
84 M40 site 9
85 Marchwood 1
86 Marham
87 Marston
88 Middleton 1
89 Milbourne 1
90 Mountfield 1
91 Nettleton
92 Nettleton Bottom
93 Noke Hill
94 North Runcton 1
95 North Wootton 1
96 Oborne
97 Parson Drove 1
98 Penhurst 1
99 Pluckley
100 Portsdown 2
101 Puriton
102 Radipole
103 Richmond
104 Risby 1
105 Rodbourne 1
106 Rodmarton A
107 Sandhills 1
108 Seabarn Farm
109 Seaborough
110 Severn Bridge Tunnel
111 Shalford 1
112 Shapwick 1
113 Sherston
114 Shipton Moyne 5A
115 Shrewton 1
116 Sibsey 1
117 Skegness
118 Soham 1
119 Sonning eye 1
120 Southhampton 1
121 Southhall
122 Spalding 1
123 Stalbridge
124 Steeple Aston
125 Stoborough 1
126 Stowbridge
127 Stowell
128 Stowell Park
129 Strat A1
130 Strat B1
131 Swang Farm 1
132 Swindon BH 2
133 Tatsfield 1
134 Tetbury
135 Tetney Lock
136 Tilmanstone
137 Ulceby Cross
138 Upton
139 Walkers Marsh
140 Wareham 3
141 Warlingham 1
142 West Farm
143 West Kington
144 West Lavington
145 West Walton Highway
146 Westfield Farm
147 Westham 1
148 Westonbirt
149 Wiggenhall 1
150 Wiggenhall St. Peter
151 Willesden
152 Wincanton
153 Winchester 1
154 Winestead 1
155 Winford
156 Winterbourne Kingston
157 Wisbech
158 Withycombe Farm
159 Wytch Farm 2
160 Wytch Farm D5
161 Yarnbury 1
162 98/11-4
163 98/11-3
164 98/11-2
165 98/11-1
166 98/16-1

The first part of this section (Section 6.4.2) describes the information gained from the boreholes which contained biostratigraphical data. The results of the wireline sequence stratigraphical interpretation for the Wessex Basin is described in Section 6.4.3, and for the Wash and Yorkshire in Section 6.4.4.

6.4.2 Boreholes with biostratigraphical control

6.4.2.1 Wessex Basin

The Warlingham 1 borehole, which was drilled between 1956-8 by the Institute of Geological Sciences (now British Geological Survey), contains the thickest cored section of Kimmeridgian strata in the whole of the Wessex Basin. A detailed core description can be found in Worssam & Ivimey-Cook (1971) and the stratigraphy and ammonite succession in Calloman & Cope (1971). Figure 6.19 shows the ammonite zones and the core lithology from the above mentioned references plotted against the gamma-ray and self potential wireline logs. The full succession from the *mutabilis* to the *pallasioides* zones is present in the Warlingham borehole, the top of the Kimmeridgian has been eroded and the bottom section of the Kimmeridgian was faulted out.

The core description in Worssam & Ivimey-Cook (1971) was examined in detail and compared to the Dorset exposures. This resulted in several of the key sequence stratigraphical surfaces being located. For example, in the core description in Worssam & Ivimey-Cook (1971), a silty fossiliferous mudstone (889 m) is described at the base of the *eudoxus* Zone. This has been correlated with the silty mudstone of bed 24 (Fig. 6.3) which has been interpreted as the Kiii sequence boundary.

A calcareous, hard brittle mudstone bed with conchoidal fractures is described at 775 to 780 m, at the base of the *wheatleyensis* Zone (Fig. 6.19). This bed is correlated with the first of the two thick homogeneous calcareous mudstone units seen on the Dorset coast (Fig. 6.4), at the base of which is the K1 sequence boundary. The base of the second of the two homogeneous calcareous mudstone units is at 755 m and is described as an unfossiliferous calcareous mudstone. The base of the second homogeneous calcareous mudstone is interpreted to be the K2 sequence boundary (Figs 6.4 & 6.19).

The Warlingham borehole provided the best biostratigraphical data of any borehole in Weald Sub-basin because it was the only borehole which was continuously cored through the Kimmeridgian succession. This was important to this study because the ammonite zones constrain the wireline sequence stratigraphic interpretation. The core descriptions were also very useful for the location of the sequence boundaries Kiii, K1 and K2.

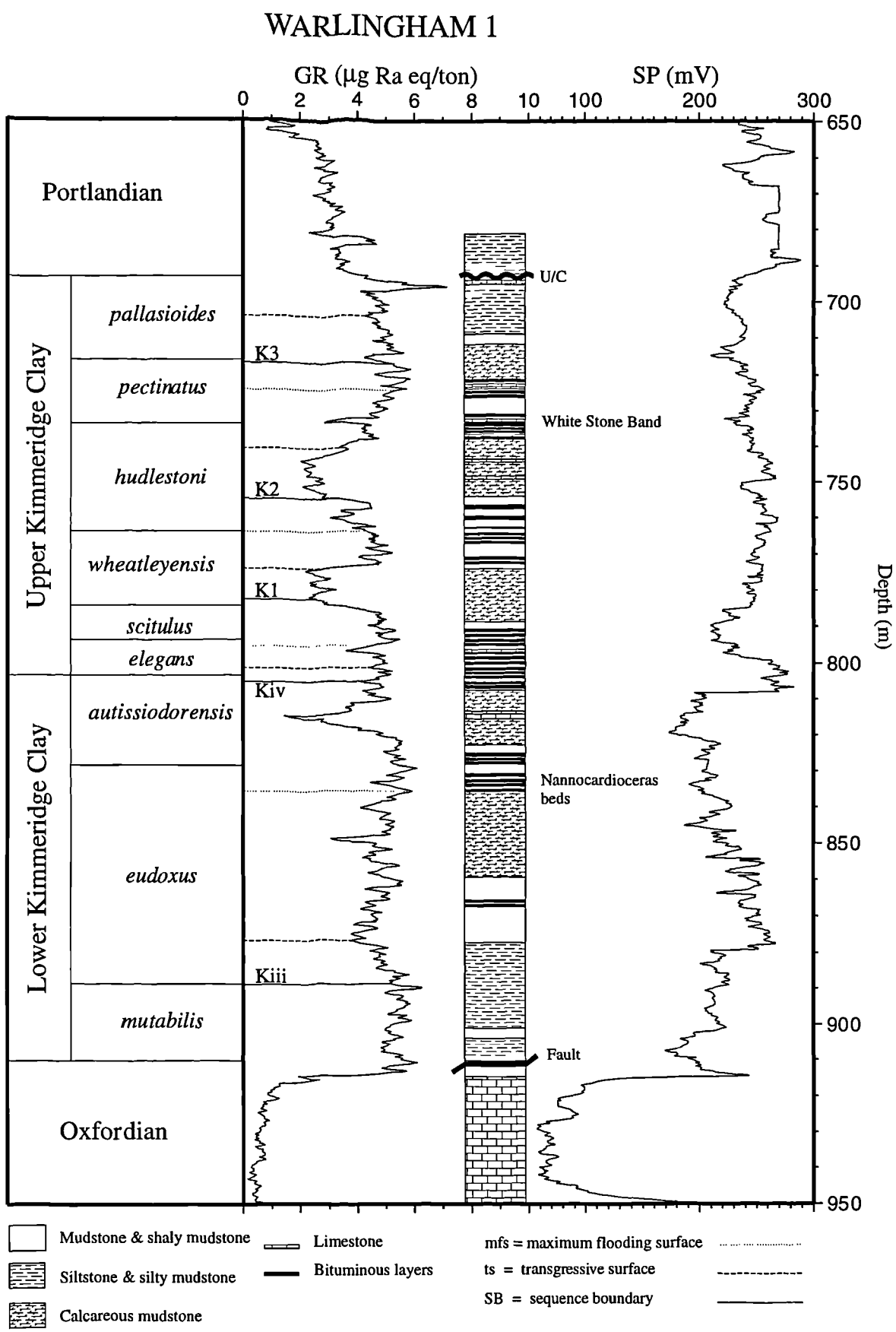

Fig. 6.19 Diagram showing the Warlingham borehole with the key sequence stratigraphic surfaces picked. The lithology and ammonite zones after Worssam & Ivimey-Cook (1971).

In 1976 the British Geological Survey drilled the Hartwell Borehole, near Aylesbury in Buckinghamshire (Cox *et al.* 1994). This borehole penetrated the whole of the Kimmeridge Clay Formation from the *baylei* to the *pallasioides* zones, and core was collected over the entire interval. Using the detailed description of the core by Cox *et al.* (1994), this borehole has been compared to nearby exposures and the Dorset coast and the key sequence stratigraphic surfaces located (Fig. 6.20).

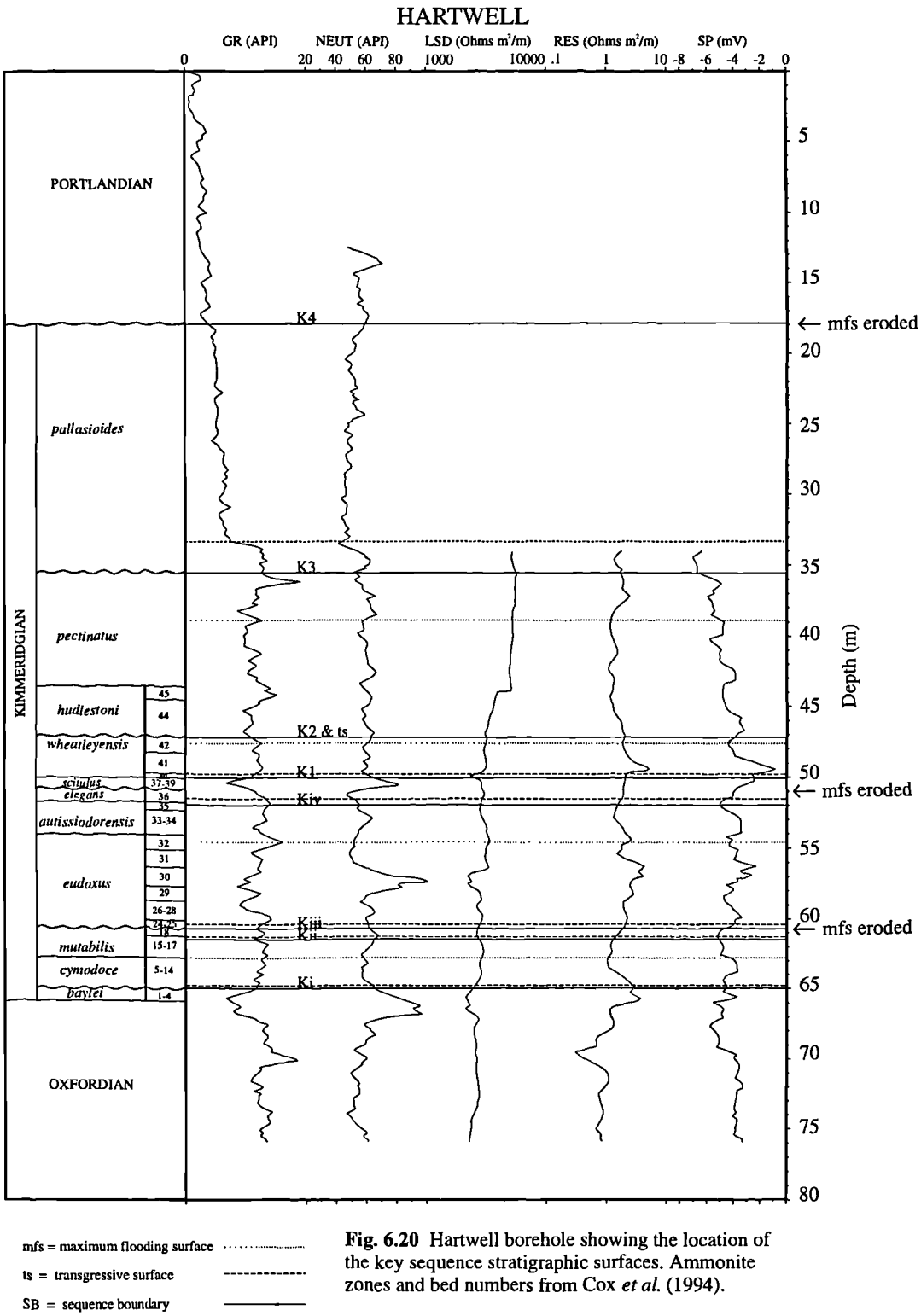

Fig. 6.20 Hartwell borehole showing the location of the key sequence stratigraphic surfaces. Ammonite zones and bed numbers from Cox *et al.* (1994).

The British Geological Survey also drilled and continuously cored the Brill borehole. Cox & Sumbler (1989) initially described the core and located the ammonite zonal boundaries and bed group numbers, but have subsequently revised their interpretation of the Oxfordian - Kimmeridgian boundary beds (Cox & Sumbler 1994). Like the Hartwell borehole, the Brill borehole was also compared to the Dorset coast and nearby exposures, and the key sequence stratigraphic surfaces located (Fig. 6.21).

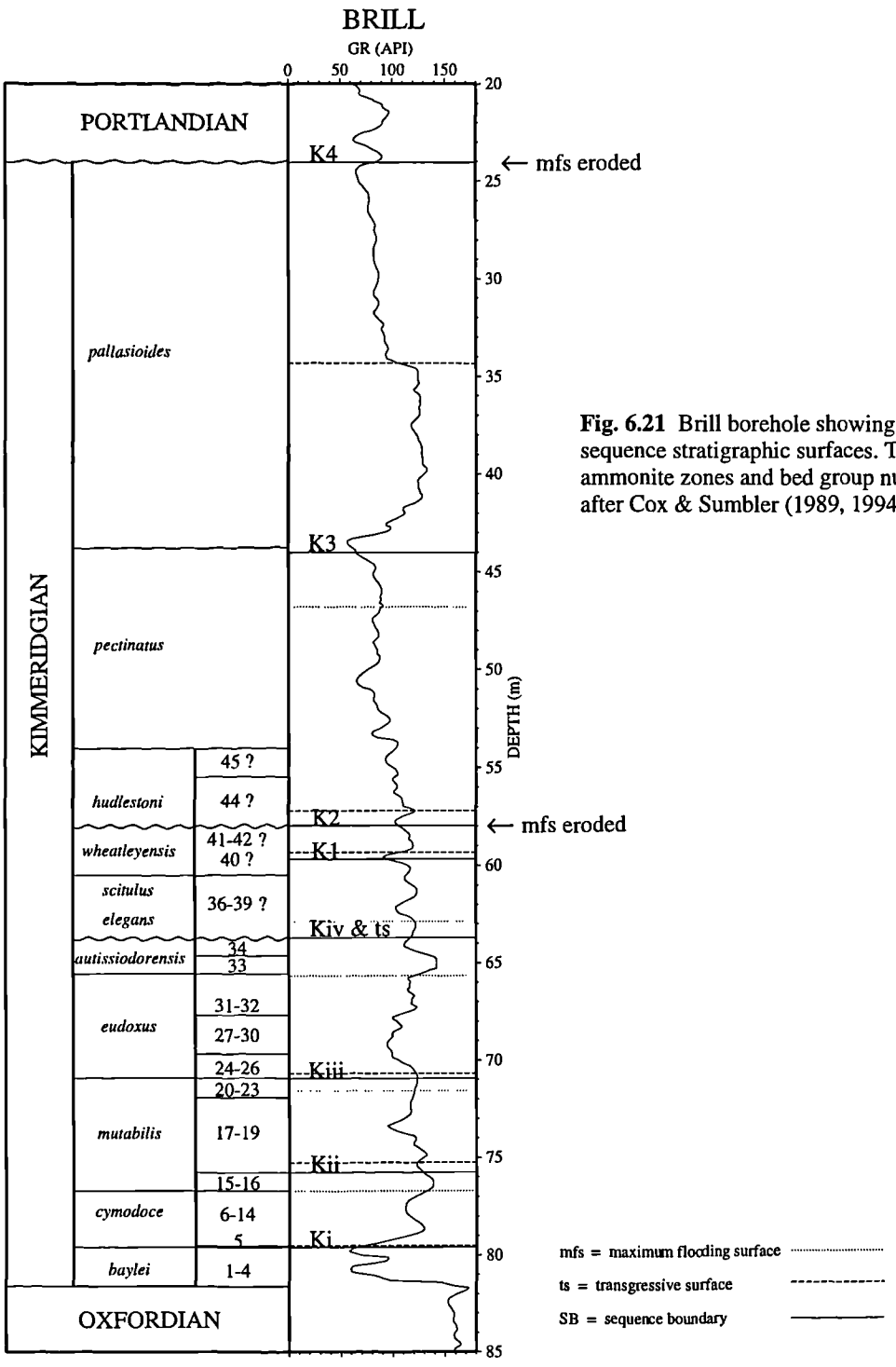

Fig. 6.21 Brill borehole showing the key sequence stratigraphic surfaces. The ammonite zones and bed group numbers after Cox & Sumbler (1989, 1994).

The best source of biostratigraphic data (i.e., ammonite zones) for this study has come from the work of the British Geological Survey, principally in their own fully cored boreholes. The other source of biostratigraphic data, albeit sparse, is from hydrocarbon exploration company well reports and reports done on behalf of the exploration companies by biostratigraphic contractors. Hydrocarbon exploration companies are generally only interested in coring the potential reservoir interval, so generally no core is cut in the Kimmeridgian succession in the Wessex Basin. The source of biostratigraphic information therefore comes from drill cuttings and side wall cores.

The Brightling 1 borehole drilled by British Petroleum in 1955 is a good example of a borehole with sparse biostratigraphic data. Only about 15 m of core was taken near the base of the Lower Kimmeridge Clay. The rest of the succession was only sampled with drill cuttings which contained scattered fragmentary ammonites giving some stratigraphic control (Lake *et al.* 1987). Examination of these samples by B. M. Cox resulted in the detection of the 'White Stone Band' which is at the base of the *pectinatus* Zone and the pentacrinus band located within the *mutabilis* Zone (Lake *et al.* 1987). Using this information and correlation with the Warlingham and other boreholes the rest of the ammonite zones were located in this borehole (Fig. 6.22).

Depths of biostratigraphic zones or marker horizons obtained from drill cuttings were not regarded as absolute in this study. For example King *et al.* (1987) described a drill cutting from 740 m in the 98/11-4 borehole as being a distinctive bed of white limestone with organic argillaceous laminae, which they stated probably represented the White Stone Band (the base of which is the *hudlestoni / pectinatus* zonal boundary). Correlation of the 98/11-4 gamma-ray log with the field gamma-ray log constructed in this study (see Chapter 2; Fig. 2.19) shows the White Stone Band to be at a depth about 25 m greater than the drill cutting suggests. It was also stated by King *et al.* (1987) that drill cuttings were only taken at 20 ft (6 m) intervals and due to the lag time (i.e., the time taken for cuttings to reach the surface (Rider 1996)) the sample depth is not very accurate. Even if the depth of the sample examined by King *et al.* (1987) was accurate then it does not necessarily have to be the White Stone Band; it could well be the Middle White Stone Band or the Fresh Water Steps Stone Band which are located higher up in the *pectinatus* Zone.

Even though biostratigraphic data from drill cuttings were not strictly adhered to in this study, there were some occasions when the data was of use. For example examination of the drill cuttings and side wall cores from borehole 98/11-3 showed that the highest part of the late Kimmeridgian strata was absent but the remaining section, although highly condensed, was essentially complete (King & Allen 1987). Looking at the position of 98/11-3 these observations seem quite reasonable. 98/11-3 lies just north of the Portland - Wight Faults (Fig. 6.18) on what was a palaeohigh (Penn *et al.* 1987) so the observations

that the Kimmeridgian strata is condensed makes sense and because the area was a palaeohigh the base Cretaceous unconformity which eroded most of the Upper Jurassic just to the west of 98/11-3 in the Wytch Farm area (Colter & Harvard 1981) is also most likely to have removed part of the Upper Jurassic in 98/11-3. This is also backed up by the fact that Cretaceous Lower Greensand Formation lies unconformably over the Kimmeridgian strata.

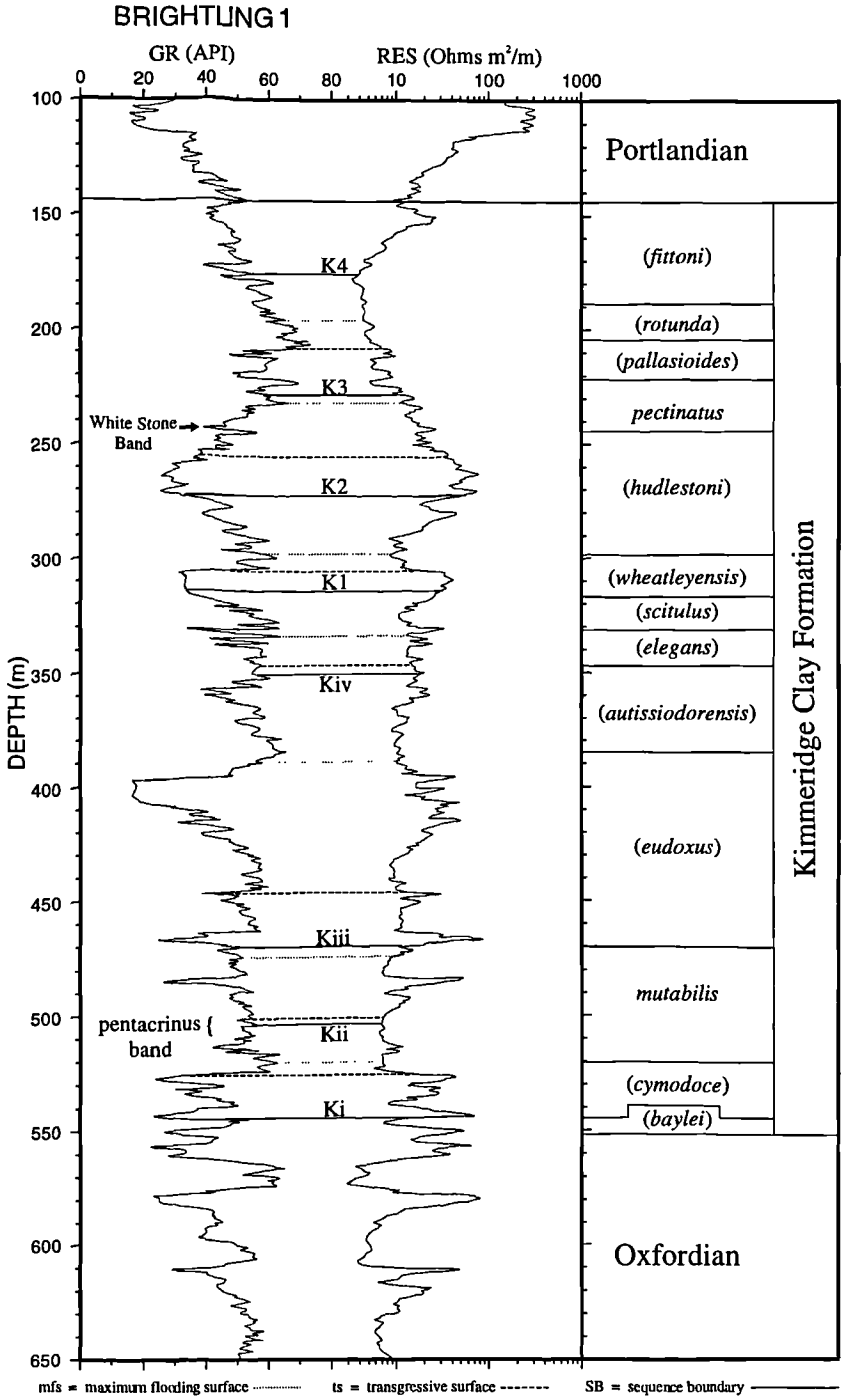

Fig. 6.22 Brightling 1 borehole showing the key sequence stratigraphic surfaces. Direct evidence for the *mutabilis* and *pectinatus* zones were found in drill cuttings and core (Lake *et al.* 1987). The other ammonite zones (in brackets) and the ammonite zonal boundaries were located in this study by correlating this borehole with the Warlingham 1 and other boreholes.

The table below shows all the boreholes in the Wessex Basin for which biostratigraphic data exists and were used in this study to aid in the location of the ammonite zones.

BOREHOLE	REFERENCE
98/11-1	Jacovides *et al.* (1983)
98/11-3	King & Allen (1987)
98/11-4	King *et al.* (1987)
Ashdown 1	Bristow & Bazley (1972)
Ashdown 2	Bristow & Bazley (1972)
Bolney 1	Gallois & Worssam (1993)
Brightling 1	Lake *et al.* (1987)
Brill 1	Cox & Sumbler (1989; 1994)
Collendean Farm 1	Gallois & Worssam (1993)
Detention 1	Perkins (1982)
Hartwell 1	Cox *et al.* (1994)
Henfield 1	Young & Lake (1988)
Marchwood 1	Whittaker *et al.* (1985)
Shapwick 1	Bristow *et al.* (1991)
Warlingham 1	Worssam & Ivimey-Cook (1971)
Winterborne Kingston 1	Whittaker *et al.* (1985)

Table 6.3 List of boreholes, in the Wessex Basin, with references containing biostratigraphical data for the Kimmeridgian.

6.4.2.2 The Wash and Yorkshire

Unlike the Wessex Basin, where most of the boreholes have been drilled by various companies for hydrocarbon exploration, most of the boreholes in the Wash and Yorkshire have been drilled and continuously cored by the British Geological Survey for stratigraphical, site-investigation, heat-flow and mineral exploration purposes (Penn *et al.* 1986). Because of this 13 out of the 18 boreholes used in this study, which penetrate the Kimmeridgian and contain wireline data, have good biostratigraphic data.

Skegness, Hunstanton IGS, Gayton and Marham boreholes were drilled in 1970 by the Institute of Geological Sciences (now BGS). Gallois (1973) showed that these boreholes could be correlated in detail using the wireline gamma-ray logs. Gallois & Cox (1974) described the stratigraphy of the Upper Kimmeridge Clay of these boreholes and later (Gallois & Cox 1976) described the stratigraphy of the Lower Kimmeridge Clay of Eastern England using the Denver Sluice, North Wootton and other wells not used in this study.

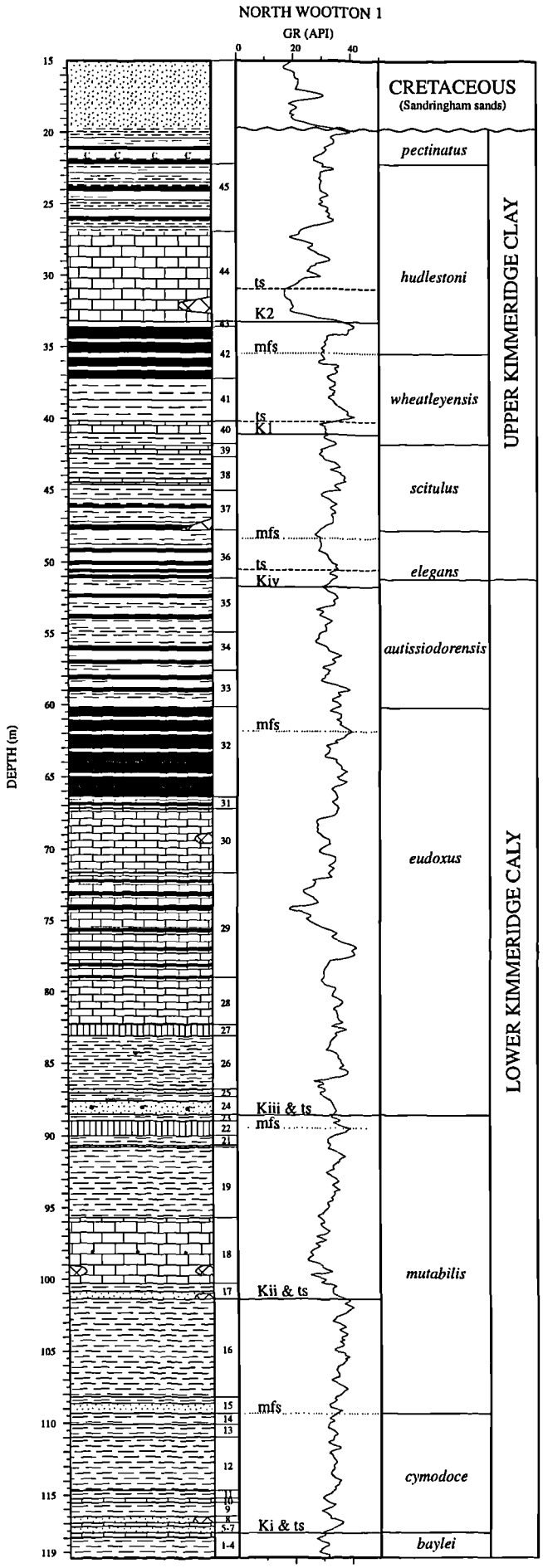

Fig. 6.23 North Wootton borehole showing the location of the key sequence stratigraphic surfaces. The lithology, bed group numbers and ammonite zones are after Gallois (1979).

Oil shale

Mudstone

Calcareous mudstone

Very shelly mudstone

Silty mudstone

The large number of cored boreholes with good quality data in the Wash area has lead to various detailed studies done on the Kimmeridgian in this area. Gallois (1979) carried out a study for the Wash water storage scheme: in this report detailed lithological logs for nine boreholes can be found, two of which can be seen in Figures 6.23 & 6.24. Penn *et al.* (1986) correlated the Upper Jurassic in 36 boreholes on the Eastern England Shelf. The correlations were done on a bed by bed basis (49 distinctive beds - now termed bed groups Coe 1992 and this study; Gallois & Cox 1976; Gallois 1979; Cox & Gallois 1981), using wireline gamma-ray logs which they calibrated against all the cored borehole sequences in the area.

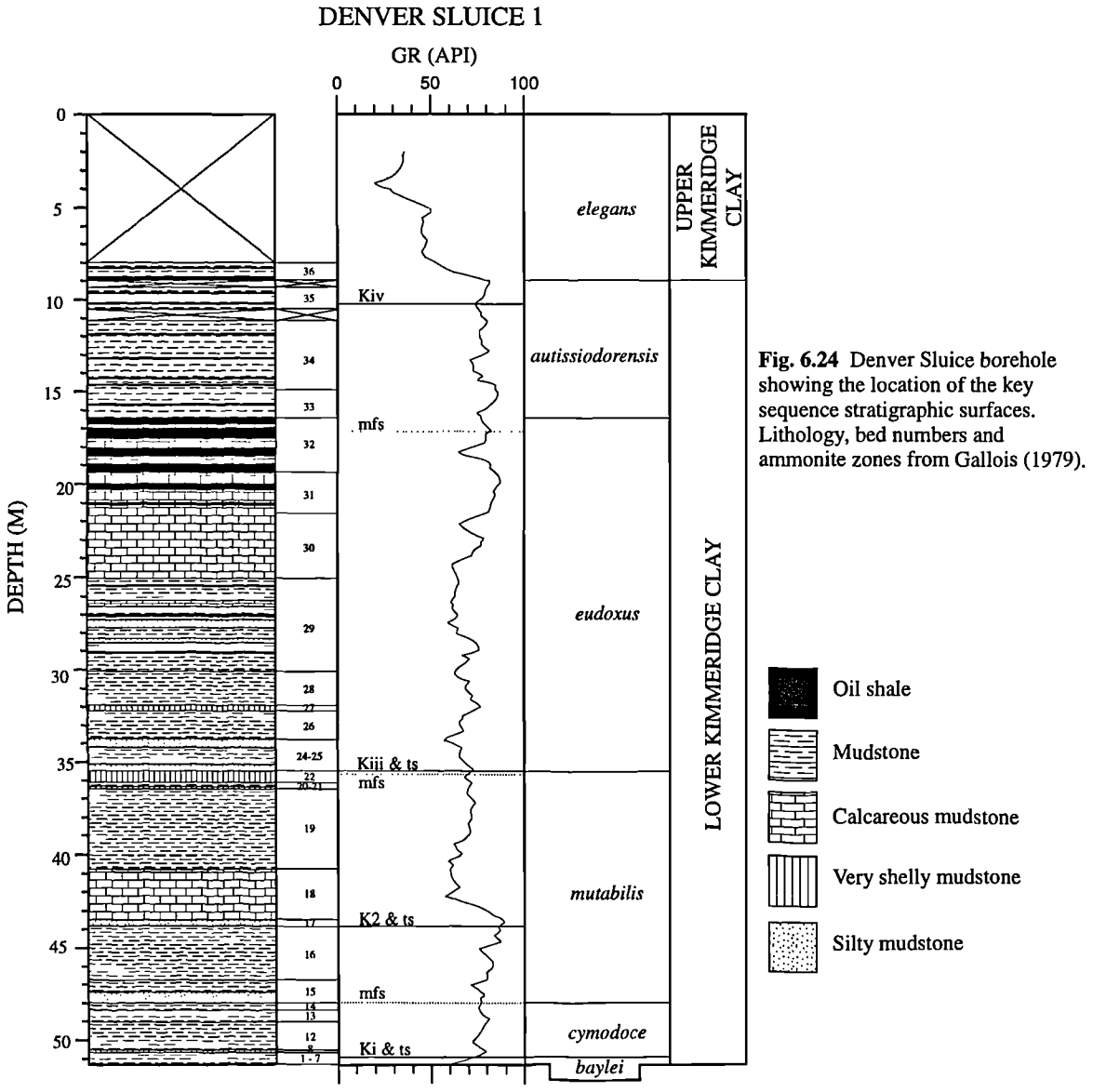

Fig. 6.24 Denver Sluice borehole showing the location of the key sequence stratigraphic surfaces. Lithology, bed numbers and ammonite zones from Gallois (1979).

The location of the ammonite zones for the boreholes in the Wash and Yorkshire were taken directly from Penn *et al.* (1986), Gallois (1979) and Whittaker *et al.* (1985),

except for the Soham, Gayton and Cleethorpes boreholes which were not incorporated in the previous studies.

6.4.3 Wessex Basin

Whilst producing the wireline correlations (Figs 6.25 - 6.30) it was evident that the Kimmeridge Clay Formation correlated very well between boreholes within the sub-basins of the Wessex Basin. In general the Upper Kimmeridge Clay was easier to correlate than the Lower Kimmeridge Clay, because the wireline signature of the Upper Kimmeridge Clay has more character and is more distinctive than the Lower Kimmeridge Clay. The lowermost systems tracts of the K1 and K2 sequences form very distinctive marker horizons; in fact these two systems tracts are also known as the middle Kimmeridgian limestones and form good seismic marker horizons (Hancock & Mithen 1987).

Correlating the Kimmeridge Clay Formation seen in the sub-basins with the successions on the palaeohighs (Hampshire - Dieppe High and South Dorset High) proved more difficult. However, with the aid of computer programs which allowed one wireline log to be stretched in relation to another wireline log (see Chapter 3, Section 3.4.3), the correlation between these areas was found to be possible.

Isopach maps for the first sequence in the Lower Kimmeridge Clay (Ki) and the first sequence in the Upper Kimmeridge Clay (K1) can be seen in Figure 6.31. The isopach maps and the results of the sequence stratigraphic wireline interpretation as seen in the various sub-basins and palaeohigh areas are discussed in the rest of this section.

6.4.3.1 Weald Sub-basin

The Weald Sub-basin contains the thickest succession of Kimmeridge Clay (584.9 m in the Cowden 1 borehole; Fig. 6.25). Most of the boreholes in the Weald Sub-basin penetrate the full Kimmeridgian succession from the *baylei* Zone through to the *fittoni* Zone. The boreholes which do not contain the full Kimmeridgian succession are mostly those which lie on the northern flank of the sub-basin near the Pewsey - London Platform faults, such as Collendean Farm 1 which has had the *fittoni*, *rotunda* and part of the *pallasioides* zones eroded away and Warlingham 1 which has also had the upper part of the succession eroded and has had the lower part faulted out (Figs 6.25 & 6.26). The Humbly Grove 1 borehole, which lies in the eastern end of the sub-basin, penetrated the thinnest full Kimmeridgian succession (178.5 m).

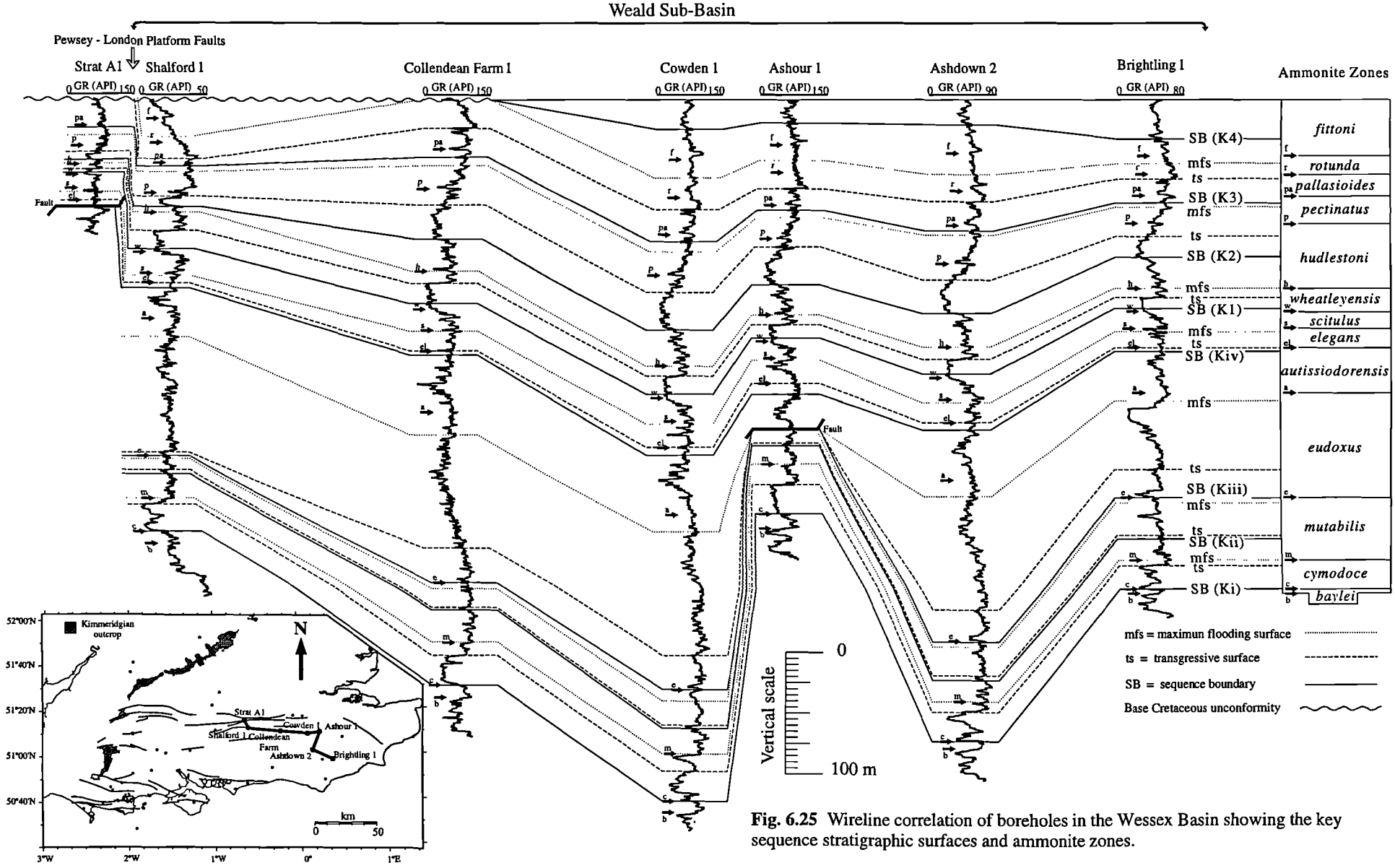

Fig. 6.25 Wireline correlation of boreholes in the Wessex Basin showing the key sequence stratigraphic surfaces and ammonite zones.

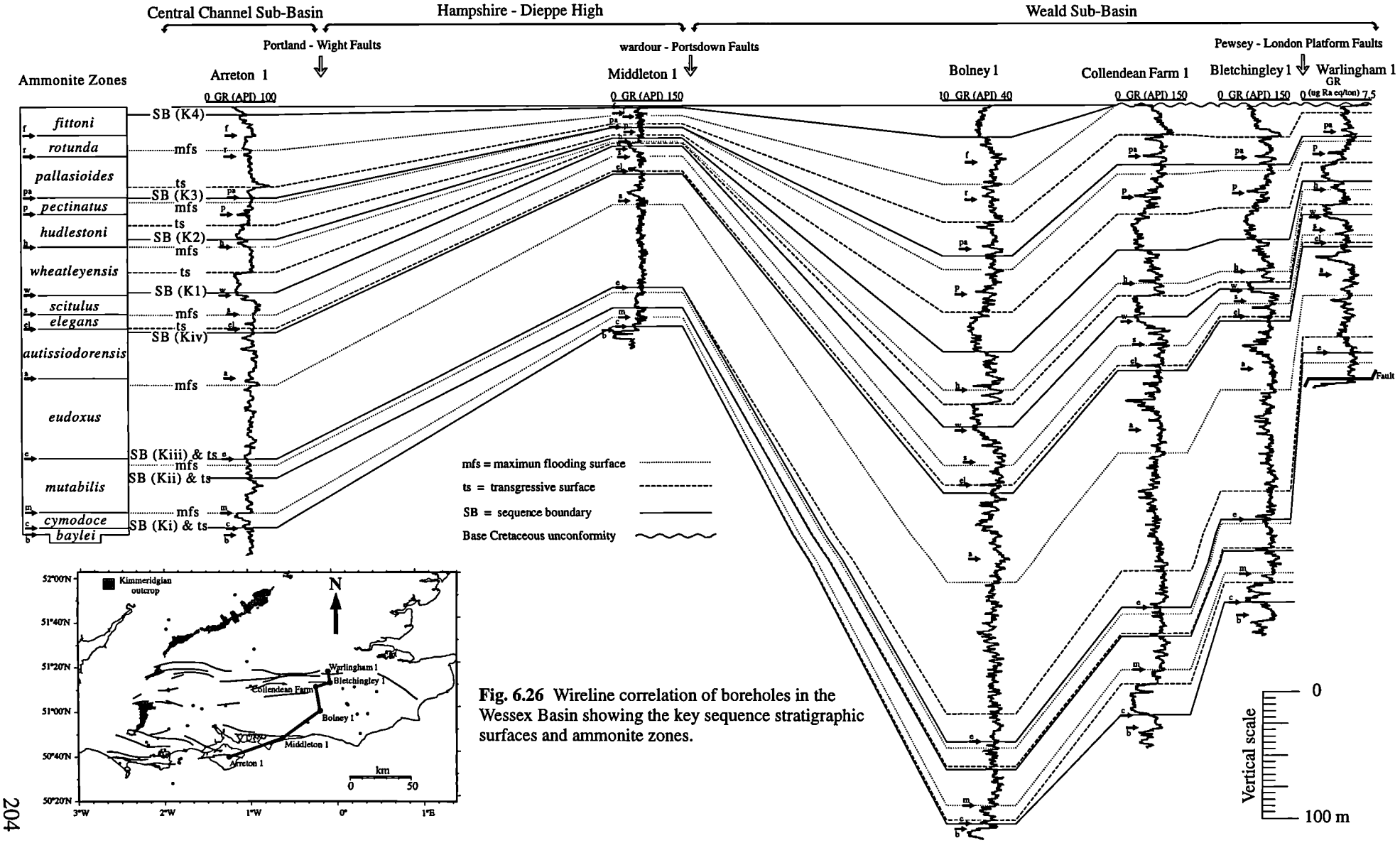

Fig. 6.26 Wireline correlation of boreholes in the Wessex Basin showing the key sequence stratigraphic surfaces and ammonite zones.

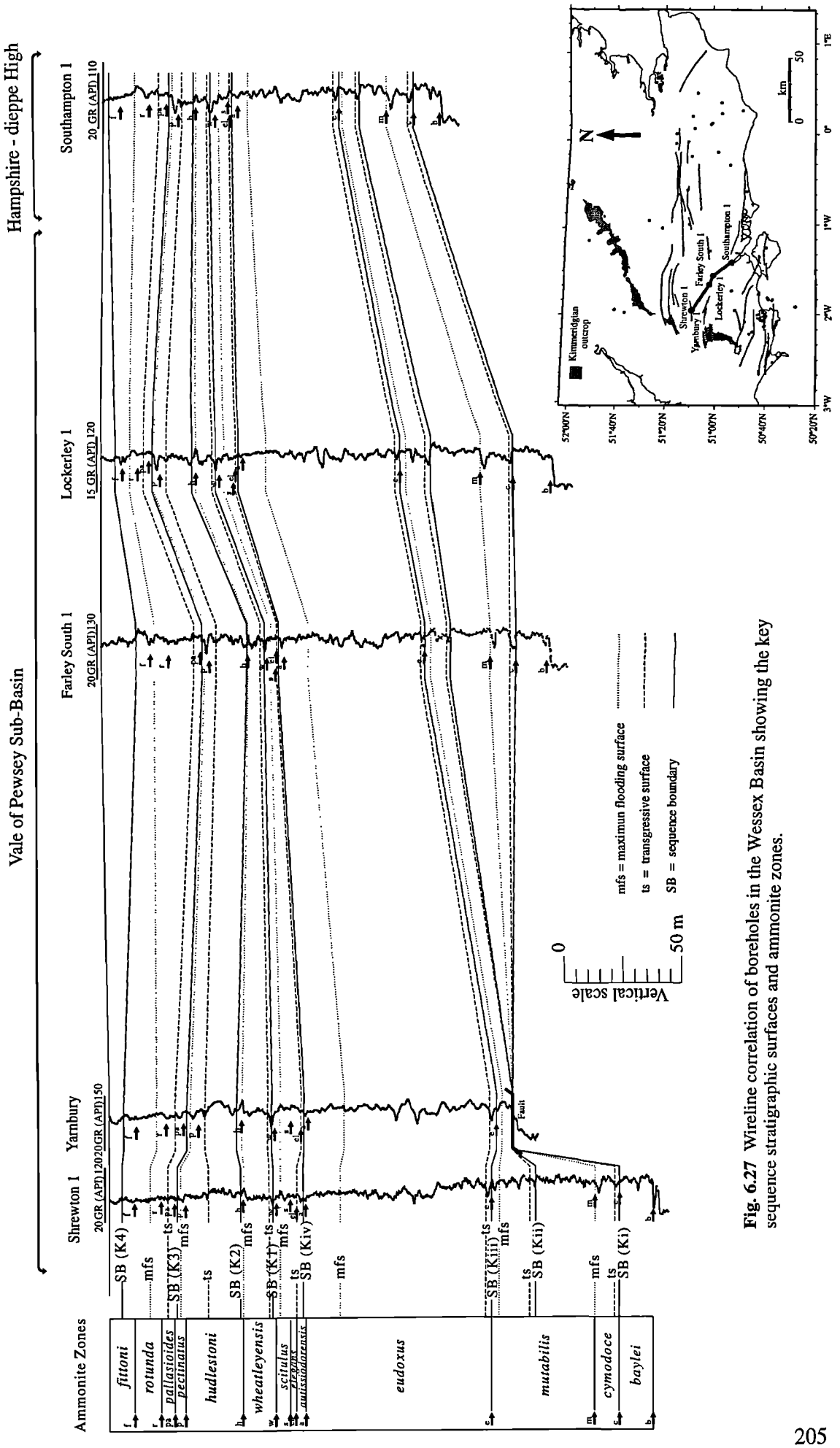

Fig. 6.27 Wireline correlation of boreholes in the Wessex Basin showing the key sequence stratigraphic surfaces and ammonite zones.

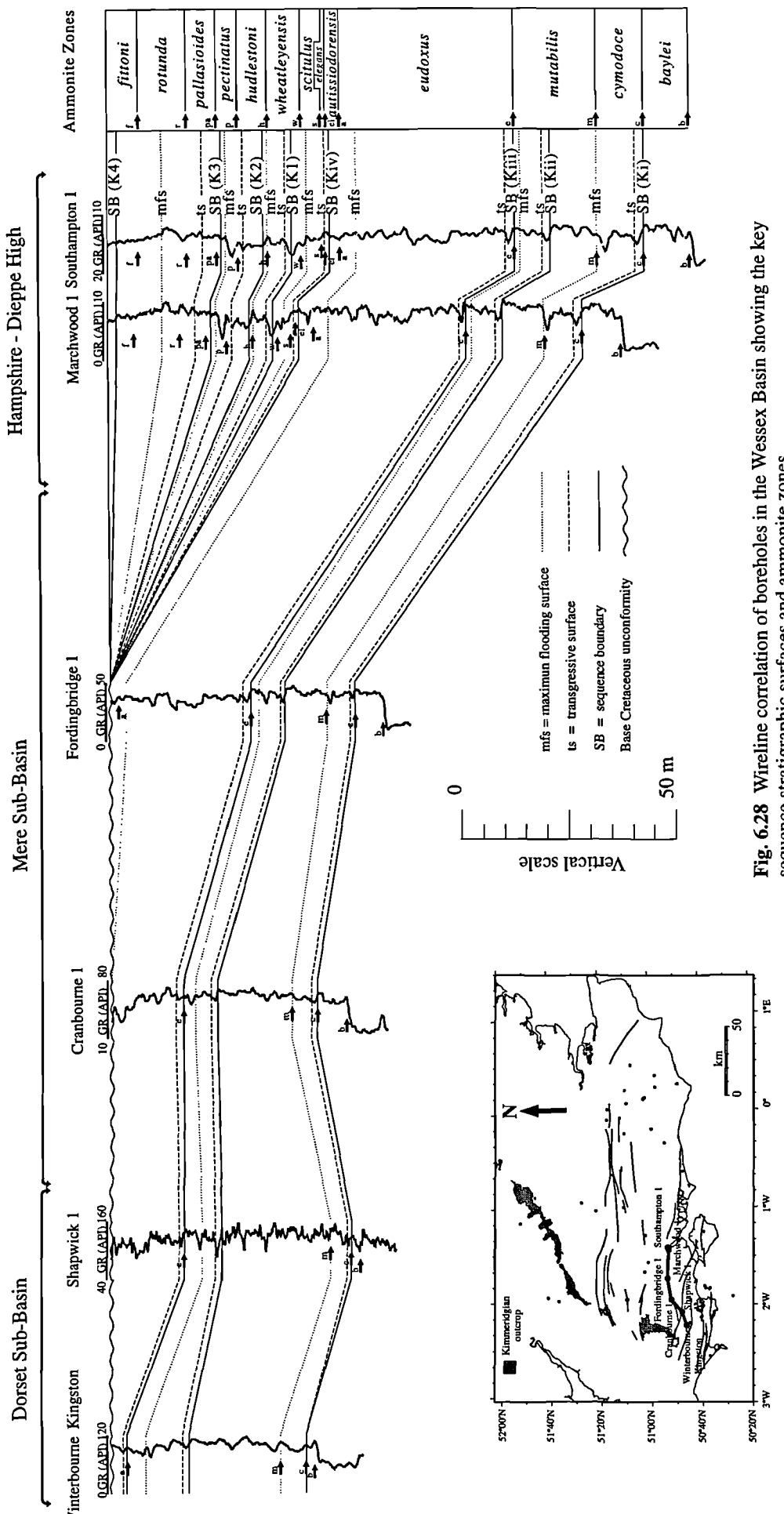

Fig. 6.28 Wireline correlation of boreholes in the Wessex Basin showing the key sequence stratigraphic surfaces and ammonite zones.

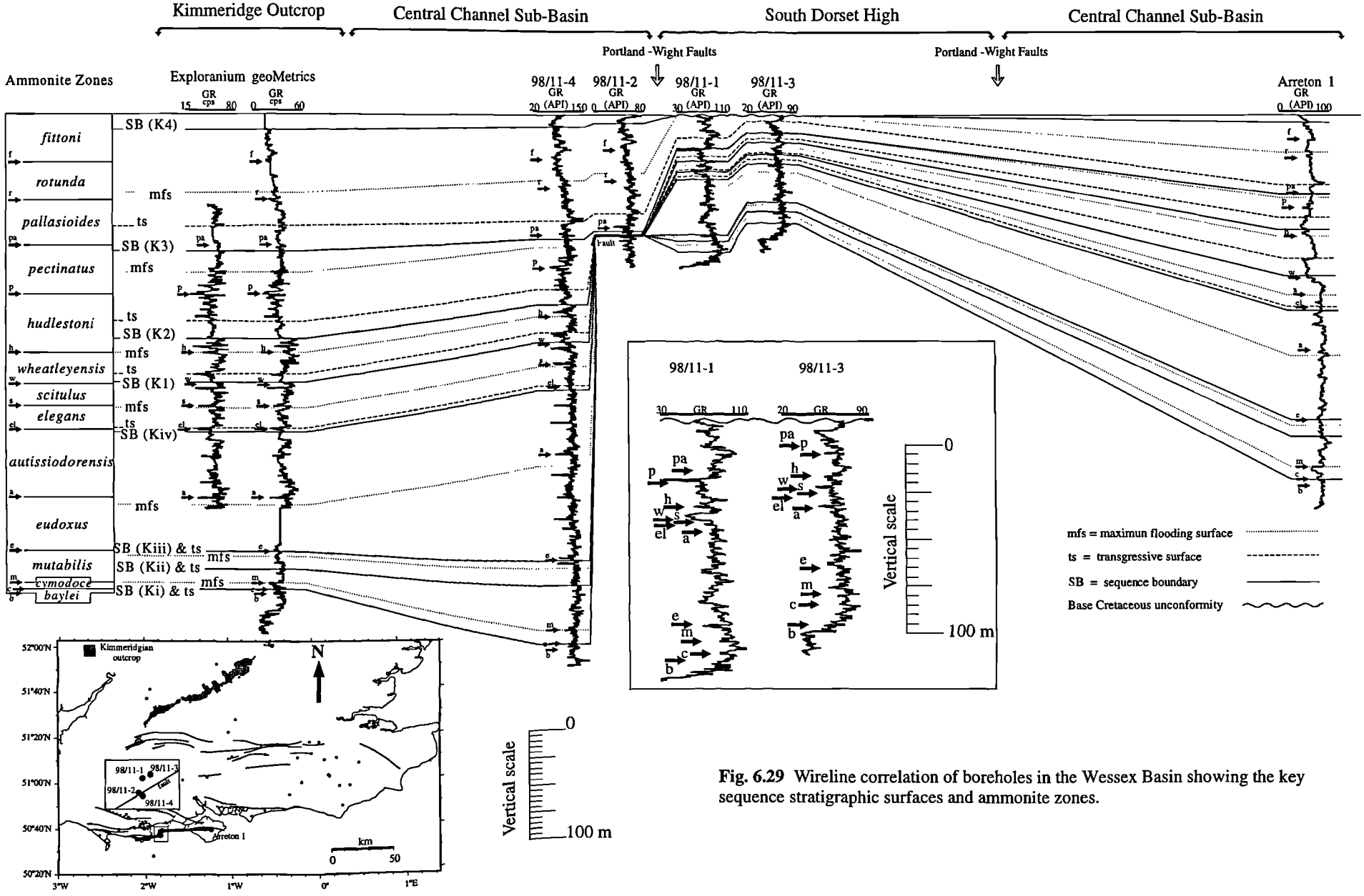

Fig. 6.29 Wireline correlation of boreholes in the Wessex Basin showing the key sequence stratigraphic surfaces and ammonite zones.

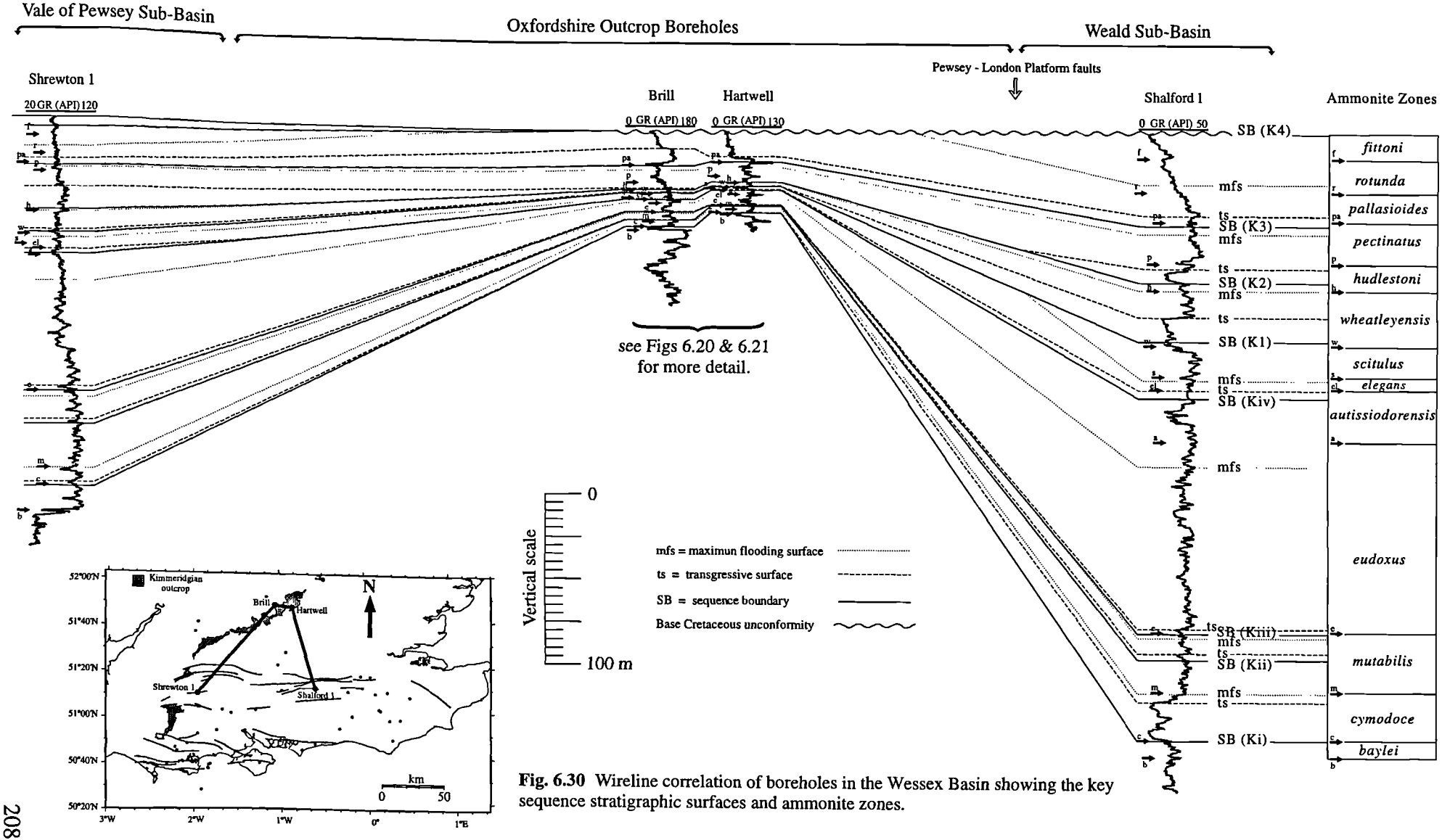

Fig. 6.30 Wireline correlation of boreholes in the Wessex Basin showing the key sequence stratigraphic surfaces and ammonite zones.

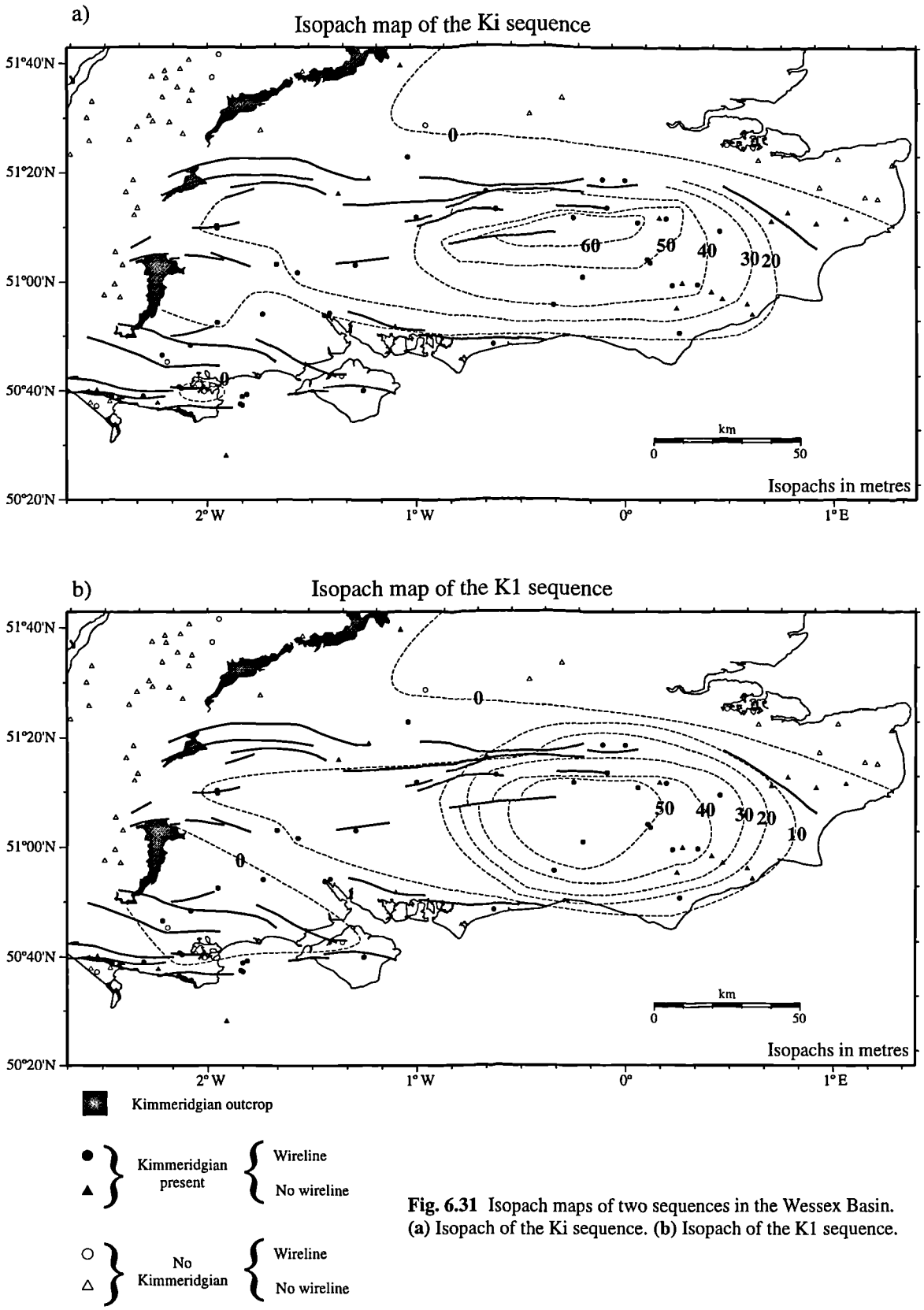

Fig. 6.31 Isopach maps of two sequences in the Wessex Basin. **(a)** Isopach of the Ki sequence. **(b)** Isopach of the K1 sequence.

Comparing the Kimmeridgian succession encountered in the Cowden 1 borehole with that exposed on the Dorset coast (Fig 6.32); see Chapter 3 Section 3.4.5 for information about graphical correlation), it is evident that the section from the base of the

baylei to the top of the *eudoxus* is significantly thicker in the Weald Sub-basin, confirming the fact that the part of the Lower Kimmeridge Clay exposed on the Dorset coast at Osmington Mills and Ringstead Bay was deposited on a palaeohigh and therefore is thinner than successions deposited in the sub-basin depocentres.

The main sequence stratigraphic difference is that the lowermost systems tract for the Ki sequence is significantly thicker (24.8 m in Cowden 1) than that on the Dorset coast, where it has a thickness of 0 m or 0.5 m depending on whether the transgressive surface is combined with the Ki sequence boundary or on top of the Wyke Siltstone (Fig. 6.3). The thick sand which forms the lowermost systems tract of the Ki sequence is thickest around the northern part of the sub-basin, for example it is 24.2 m thick in Ashdown 2, 24.6 m in Collendean Farm 1, 24.9 m in Cowden 1 and 22.4 m in Shalford 1 (Fig. 6.25). The sand thins off to the south (2.8 m in Bolney; Fig. 6.26), to the west (1.5 m in Humbley Grove) and to the east (19 m in Brightling; Fig. 6.25). The sands which form the lowermost systems tract for the Ki sequence are discussed further in Section 6.7.

The lowermost systems tracts for the K1 and K2 sequences are represented on the Dorset coast by thick homogeneous calcareous mudstone units, which on the field gamma-ray log show up as gamma-ray lows (Fig. 6.4). In the Weald Sub-basin these lowermost systems tracts are even more prominent on the wireline gamma-ray logs (Figs 6.25 & 6.26) which would indicate that these beds must be more calcareous (less radioactive) than those seen on the Dorset coast. In the Warlingham borehole these two beds are described as calcareous, hard brittle mudstone beds with conchoidal fractures (Worssam & Ivimey-Cook 1971).

6.4.3.2 Central Channel Sub-basin

The Central Channel Sub-basin contains the second thickest Kimmeridgian succession after the Weald Sub-basin. In borehole 98/11-4 which lies just south of the Portland - Wight Faults the Kimmeridgian is 485.3 m thick. Correlating the wireline gamma-ray log from borehole 98/11-4 with the field gamma-ray log of the exposures on the Dorset coast, it is evident that the two sections correlate very well (Figs 6.29 & 6.33). The main difference again is the thickness of the Lower Kimmeridge Clay, again due to the fact that the Lower Kimmeridge Clay exposed on the Dorset coast is condensed.

The thick sand which formed the lowermost systems tract in the Ki sequence of the Weald Sub-basin is not present in the Central Channel Sub-basin.

The lowermost systems tracts for the K1 and K2 sequences in boreholes 98/11-4 and Arreton 1 are not as prominent as they are in the Weald Sub-basin (Figs. 6.25 & 6.29), in fact they form gamma-ray lows with similar character and amplitude to the field gamma-ray logs (Fig. 6.29). This shows that the Kimmeridgian succession in the northern part of

the Central Channel Sub-basin, which lies just below the Portland - Wight Faults, is very similar to the upper part of the Kimmeridgian exposed on the Dorset coast.

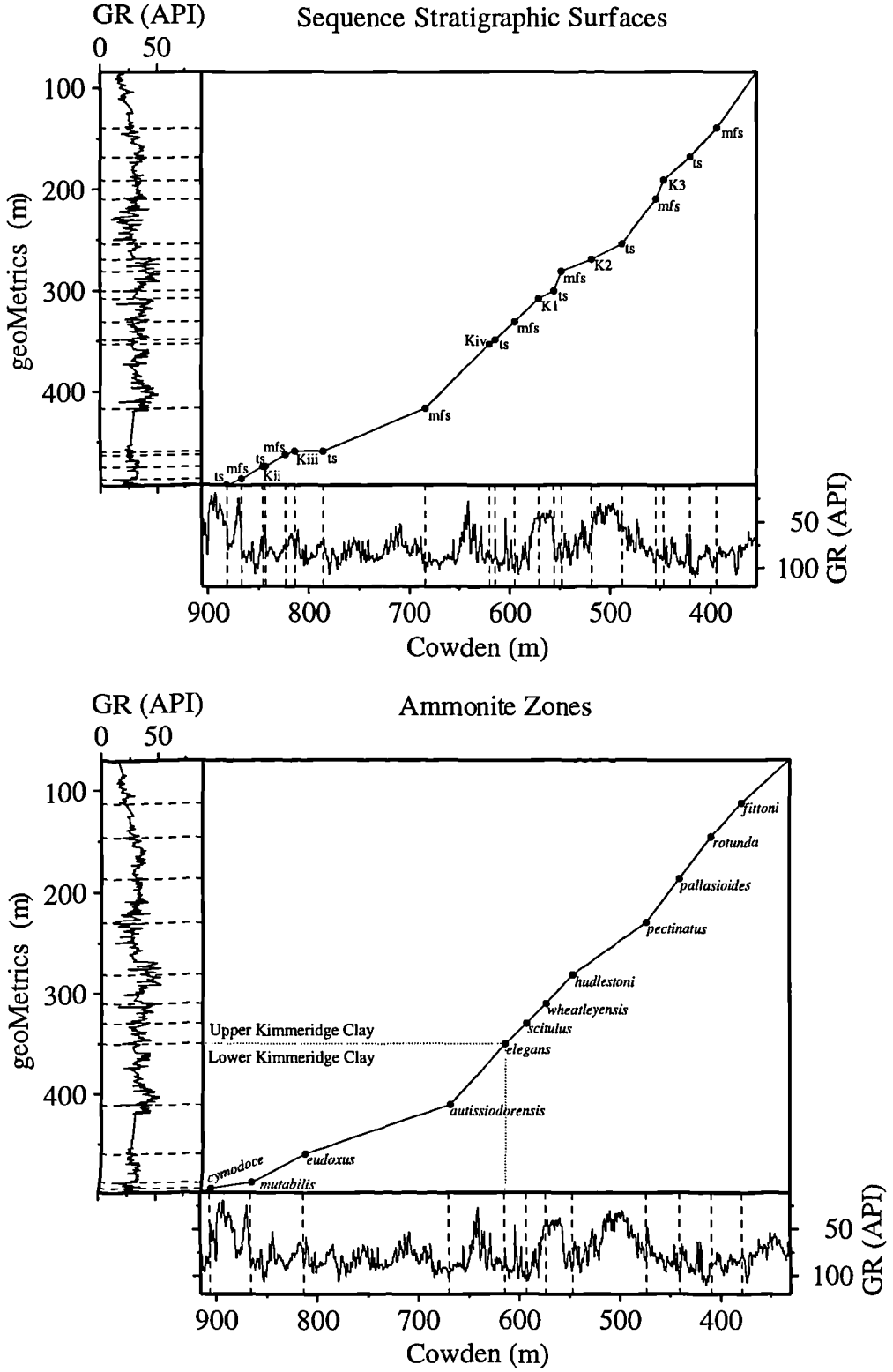

Fig. 6.32 Comparison of the Kimmeridgian succession in the Weald Sub-basin (Cowden 1) and the Kimmeridgian exposures on the Dorset coast (geoMetrics gamma-ray field log). The lowermost systems tracts are generally lower gradient than the transgressive and high stand systems tracts, this suggests that Cowden is more basinal but during transgressive phases sediments are blanketing onto both areas.

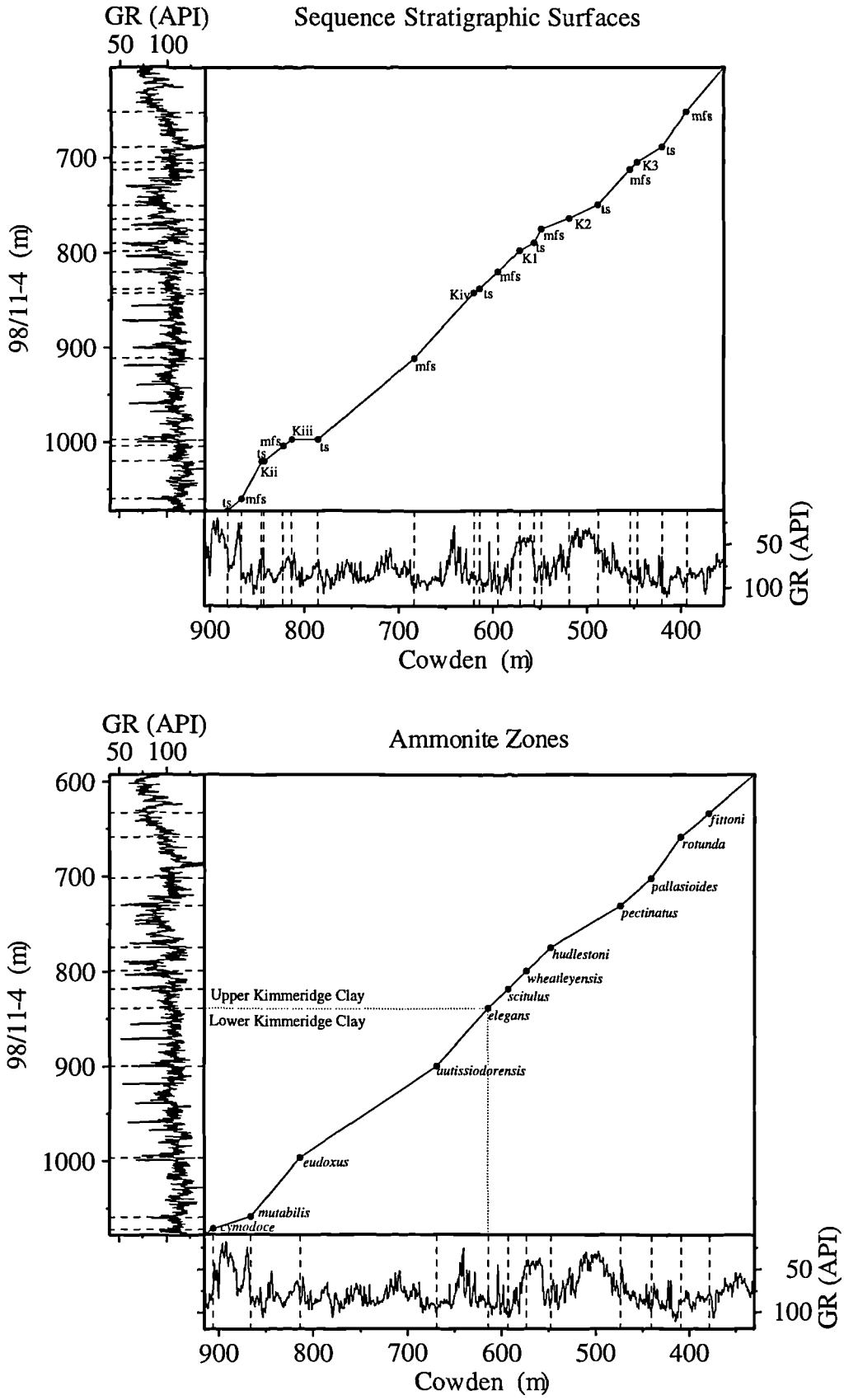

Fig. 6.33 Comparison of the Kimmeridgian succession in the Weald Sub-basin (Cowden 1) and the Kimmeridgian succession in the Central Channel Sub-basin (98/11-4).

6.4.3.3 Dorset Sub-basin & South Dorset High

Only part of the Lower Kimmeridge Clay is present in the Dorset Sub-basin, the rest of the succession has been eroded at the base Cretaceous unconformity. The thickest Kimmeridgian succession is found in the Shapwick 1 borehole (57.8 m; Fig. 6.28) where *baylei* through to part of the *eudoxus* zones are present, representing sequences Ki, Kii and part of Kiii.

The boreholes located on the western part of the South Dorset High, for example Arne G1, Stoborough 1 and Wytch Farm 2, contain no Kimmeridgian strata due to the base Cretaceous erosion. To the east in the offshore part of the South Dorset High just north of the Portland - Wight Faults between Swanage and the Isle of Wight nearly the full Kimmeridgian succession (*baylei* through to *pallasioides* zones) is penetrated by 98/11-1 and 98/11-3 (Fig. 6.29). Further to the east on the Isle of Wight in the Sandhills 1 borehole all the Kimmeridgian strata are again eroded at the base Cretaceous unconformity.

Comparing the thickness of the Lower Kimmeridge and the gamma-ray log character of the field gamma-ray log and borehole 98/11-1, it is evident that the two sections are very similar (Fig. 6.29). This confirms the observation that the Lower Kimmeridge Clay exposures on the Dorset coast are condensed.

The lowermost systems tract of the Ki sequence (which is probably silty/sand) seems to thicken to the east north-east from the Dorset Sub-basin to the Mere Sub-basin and onto the Hampshire - Dieppe High (Fig. 6.28). This suggests that the source of the sands/silts is towards the Weald Sub-basin, and is most probably the London Platform.

6.4.3.4 Mere Sub-basin

Like the Dorset Sub-basin the boreholes in the Mere Sub-basin have had the upper part of the Kimmeridge Clay Formation eroded away at the base Cretaceous unconformity. The thickest succession is found in the Fordingbridge 1 borehole (63.4 m; Fig. 6.28) where the sediments are of *baylei* through to lower *autissiodorensis* in age.

The extent of the base Cretaceous unconformity can be partly seen in Figure 6.31b, where the isopach map of the K1 sequence shows that the K1 sequence is not present in the Dorset and Mere Sub-basins.

The thickness of the Kimmeridgian strata which is penetrated by the Cranbourne 1 and Fordingbridge 1 boreholes is not significantly thicker than the same part of the Kimmeridgian succession encountered in the Hampshire -Dieppe High boreholes (Fig. 6.28). This suggests that the Mere Sub-basin was not a significant depocentre like the Weald and Central Channel Sub-basins.

6.4.3.5 Vale of Pewsey Sub-basin

The full Kimmeridgian succession is seen in the boreholes of the Vale of Pewsey Sub-basin. The Farley South 1 and Lockerley boreholes in the western part of the sub-basin (Fig. 6.27) have Kimmeridge Clay Formation thicknesses of 185 m and 186.3 m respectively. Shrewton 1 borehole in the eastern part of the sub-basin has a thickness of 227 m.

The lowermost systems tracts for the K1 and K2 sequences are not as prominent in the Vale of Pewsey Sub-basin as they are in the Weald Sub-basin (Figs 6.26 & 6.27). This is probably due to the fact that the Kimmeridgian is not very thick in the Vale of Pewsey, indicating that subsidence was not as active in the Vale of Pewsey Sub-basin as it was in the Weald Sub-basin where there would have been more accommodation space.

6.4.3.6 Hampshire - Dieppe High

The boreholes on the Hampshire - Dieppe High penetrate the thinnest full Kimmeridgian succession, from the *baylei* to *fittoni* zones, in the Wessex Basin. A thickness of 119.4 m is penetrated in the Marchwood 1 borehole and 135.6 m in the Southampton 1 borehole. A thicker succession is penetrated in the Middleton 1 borehole (175.8 m) which is located just south of the Wardour - Portsdown Faults which form the southern limit of the Weald Sub-basin.

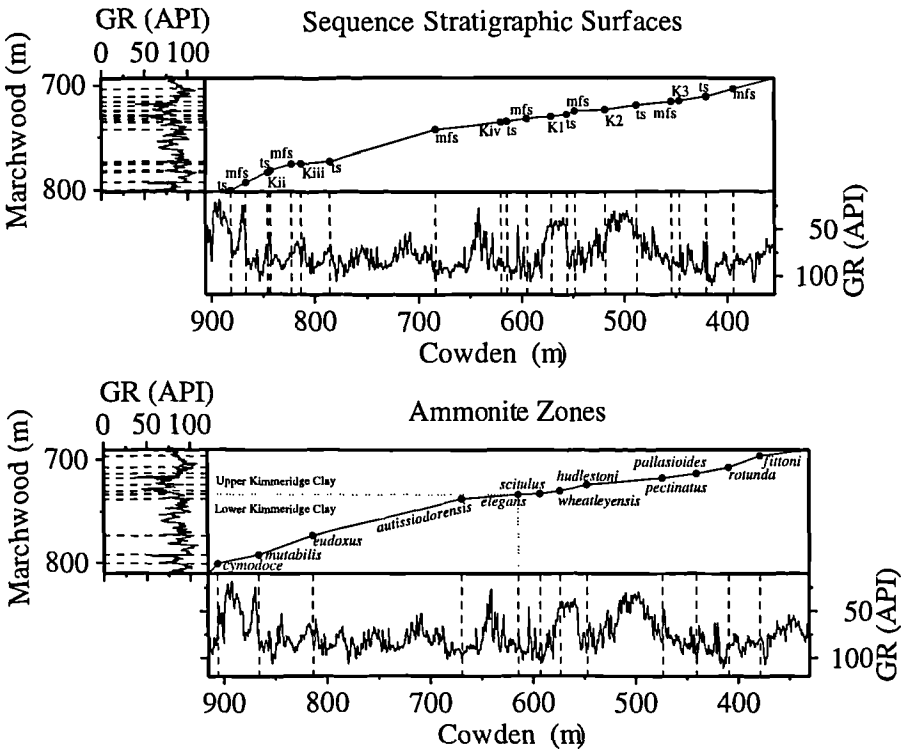

Fig. 6.34 Comparison of the Kimmeridgian succession in the Weald Sub-basin (Cowden 1) and the Kimmeridgian succession on the Hampshire - Dieppe High (Marchwood 1).

The Kimmeridgian succession is nearly five times thinner in the Marchwood borehole than the thickest Kimmeridgian succession in the Cowden 1 borehole in the Weald Sub-basin (Fig. 6.34). Comparing the Kimmeridgian succession encountered in the Marchwood 1 borehole with that in the Cowden 1 borehole of the Weald Sub-basin, it is evident that proportionally the thickness of each sequence is similar (the line of correlation in Figure 6.34 is close to being straight).

6.4.4 The Wash and Yorkshire

The sequence stratigraphic wireline correlations for the boreholes in the north of England can be seen in Figures 6.35 and 6.36. All of the boreholes in The Wash and Yorkshire have had the top part of the Kimmeridgian (part of the *pectinatus* through to the *fittoni*) eroded by the base Cretaceous unconformity. The thickest Kimmeridgian succession is found in the Ulcebly Cross 1 borehole (177.2 m).

The Kimmeridgian succession in The Wash and Yorkshire is significantly thinner than that found in the Weald Sub-basin (Fig. 6.37). On the other hand the Kimmeridgian succession between the two areas in Oxfordshire is thinner than both The Wash and the Weald succession (Figs. 6.30 & 6.35). Also the Kimmeridgian succession encountered in the Hartwell (Fig. 6.20) and Brill (Fig. 6.21) boreholes in Oxfordshire contain unconformities large enough to erode beds which are present in both the Wash and the Weald succession. The reason for unconformities within the Kimmeridgian succession in the Oxfordshire boreholes (Fig. 6.30) is that during Kimmeridgian times the Oxfordshire successions were deposited in a shallow sea way, which flowed from the Wash down to the Wessex Basin (Fig. 6.38; Miller 1990) and would probably, at certain times, have had strong currents flowing through it.

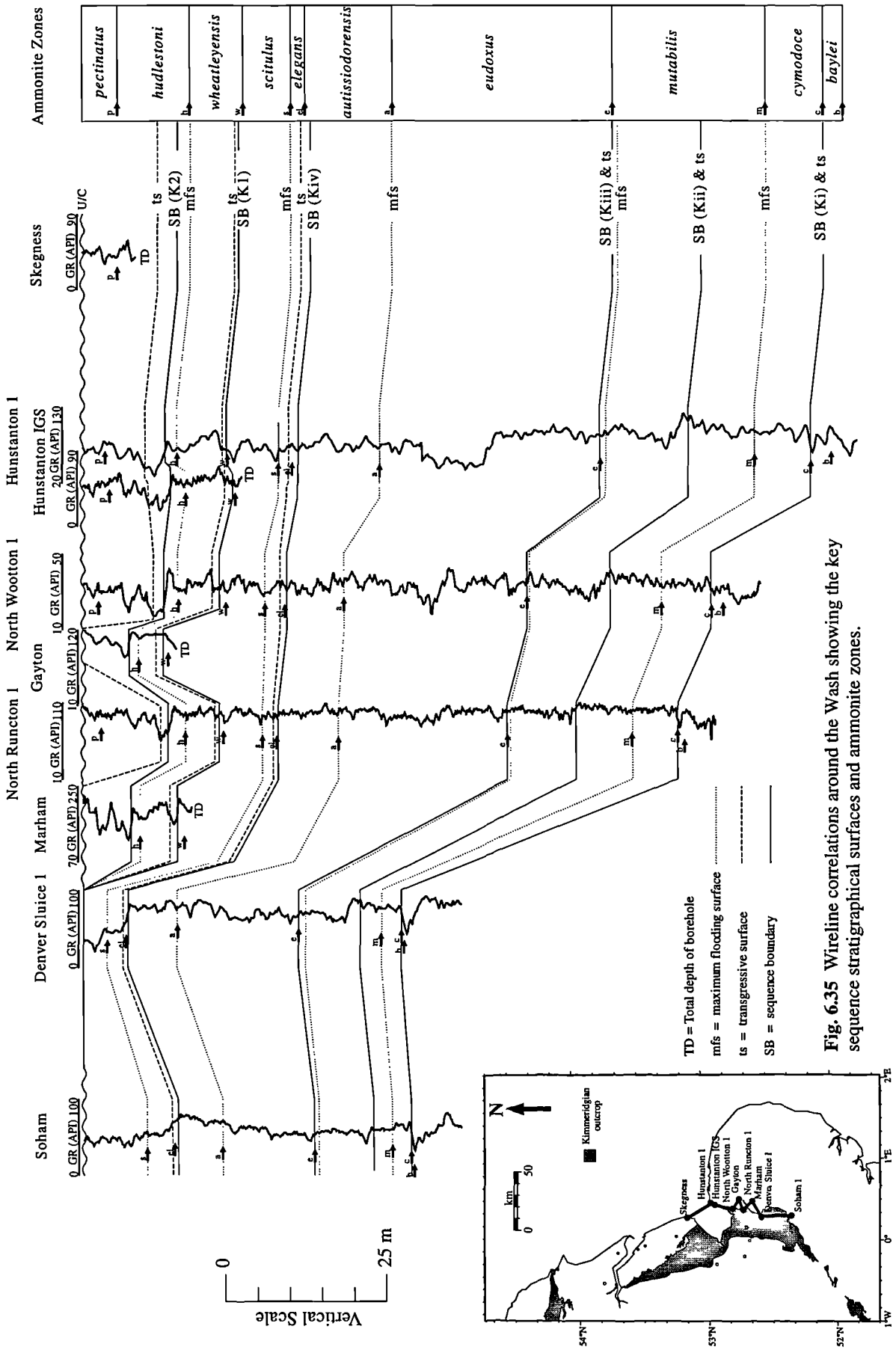

Fig. 6.35 Wireline correlations around the Wash showing the key sequence stratigraphical surfaces and ammonite zones.

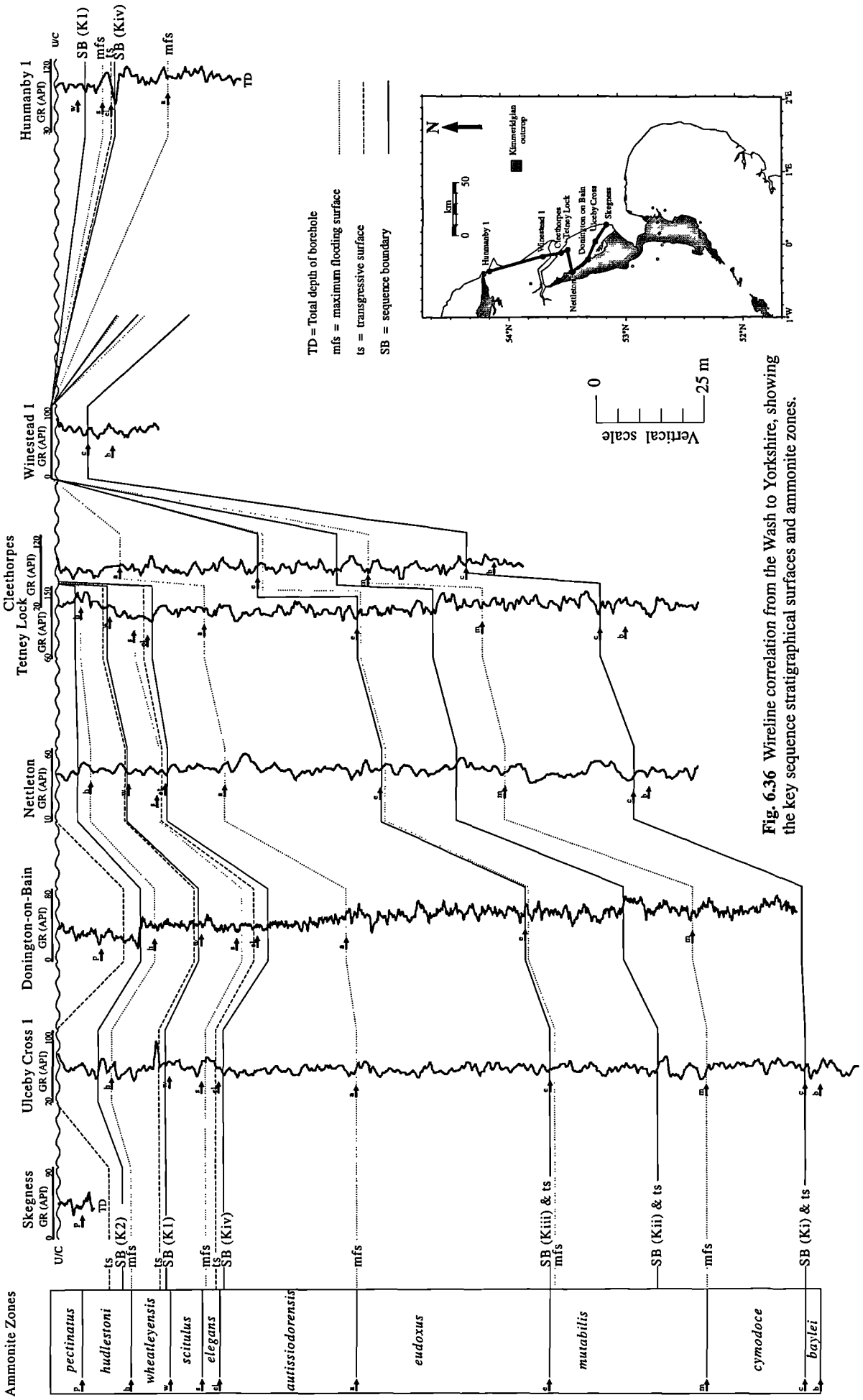

Fig. 6.36 Wireline correlation from the Wash to Yorkshire, showing the key sequence stratigraphical surfaces and ammonite zones.

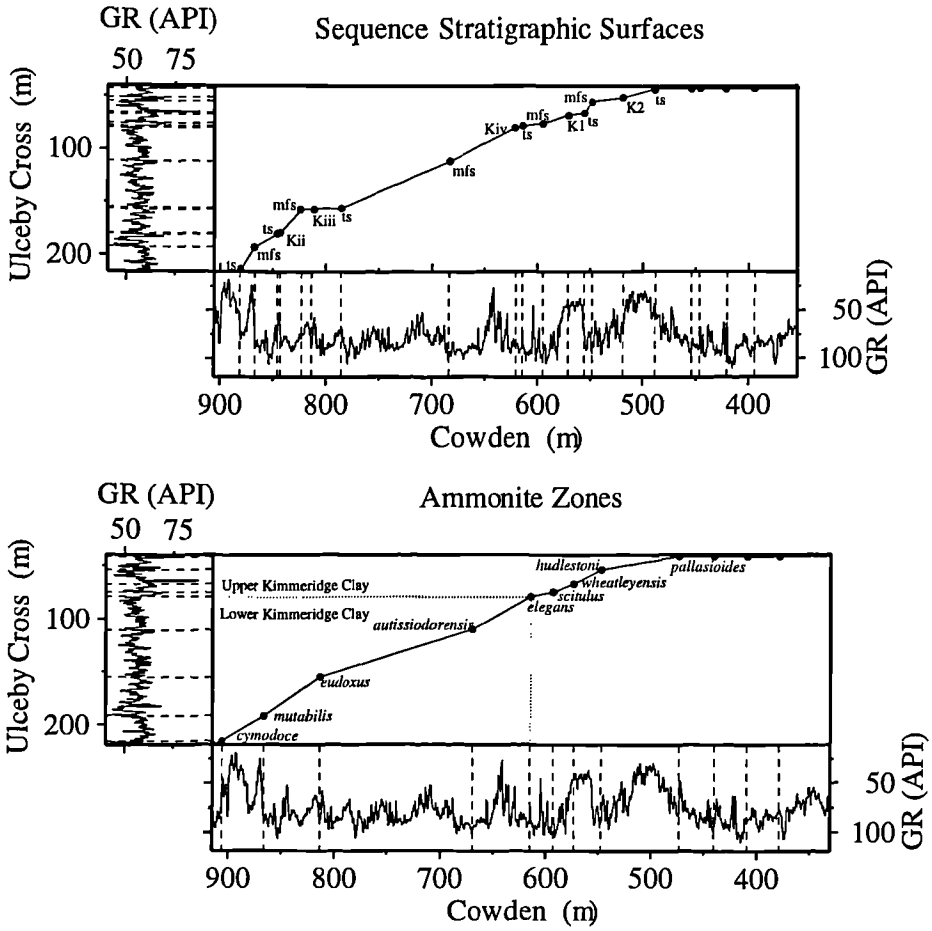

Fig. 6.37 Comparison of the Kimmeridgian succession in the Weald Sub-basin (Cowden 1) and the Kimmeridgian succession in The Wash (Ulceby Cross).

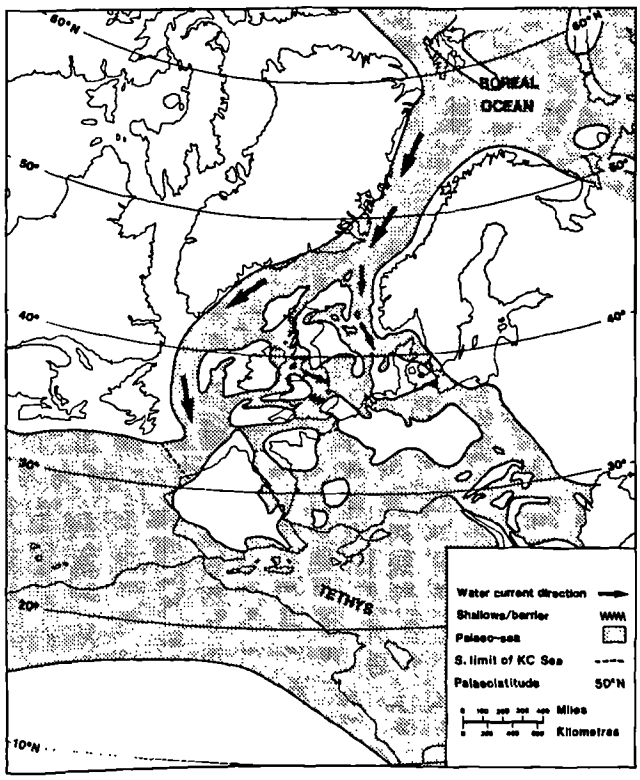

Fig. 6.38 Late Kimmeridgian paleogeography. Note the southward flow of the water currents from the Boreal Ocean. After Miller (1990).

6.5 Previous wireline correlations

Melnyk *et al.* (1994, 1995) showed wireline correlations for boreholes in the Wessex Basin, mainly from the Weald Sub-basin, as part of their study on the measurement of dispersion of ostracod and foraminifer extinction events. They filtered the digital wireline gamma-ray and sonic logs using a low frequency bandpass filter, which removed all variance at wavelengths of less than 4 m. As was shown in Chapter 3 Section 3.3.4, the filtering of the data in this manner does make wireline correlations easier, but does have the disadvantage of losing the small scale data which makes the picks less accurate. They correlated 13 gamma-ray highs in the Kimmeridgian, which they suggest may be cycle boundaries. They also suggest some locations for possible hiatuses and maximum flooding surfaces (Fig. 6.5). The gamma-ray highs which were correlated by Melnyk *et al.* (1994, 1995) are arbitrary; thus they were not picked on the basis of any sedimentological or biostratigraphical logic, unlike this study where both the ammonite zonal boundaries and the key sequence stratigraphical surfaces have been picked.

In Melnyk *et al.* (1995) an attempt was made to tie the correlations to the Kimmeridge Clay type section on the Dorset coast. They did this by scoring the lithologies, from measured sections on the Dorset coast, on an ordinal scale of decreasing radioactivity: black shales were assigned a value of 2, shales 1, mudstones 0, calcareous mudstones -1 and clean sands and limestones -2. Their attempt is clearly not as accurate and as detailed as the gamma-ray field logs constructed in this study (Fig. 6.39).

As was mentioned in Section 6.4.2.2, Penn *et al.* (1986) correlated the Upper Jurassic on a bed by bed basis for 36 boreholes located in the Eastern England Shelf (The Wash and Yorkshire). Of these boreholes 21 had been continuously cored so the wireline correlations were very well calibrated against the core. The location of the ammonite zones from Penn *et al.* (1986) were therefore confidently used in this study to constrain the sequence stratigraphic interpretation.

Besides the wireline correlation studies discussed above, the only other published wireline correlations are those found in British Geological Survey sheet memoirs and regional reports (Hamblin *et al.* 1992; Lake *et al.* 1987; Lake & Shephard-Thorn 1987) and in the occasional hydrocarbon industry paper (Colter & Harvard 1981; Hancock & Mithen 1987; Penn *et al.* 1987). The correlations in the British Geological Survey sheet memoirs tend to be quite detailed but cover very small areas, whilst the British Geological Survey regional reports and hydrocarbon industry papers tend to cover larger areas but tend to be very general (i.e., normally the Kimmeridgian is only split into the Upper Kimmeridge Clay and the Lower Kimmeridge Clay).

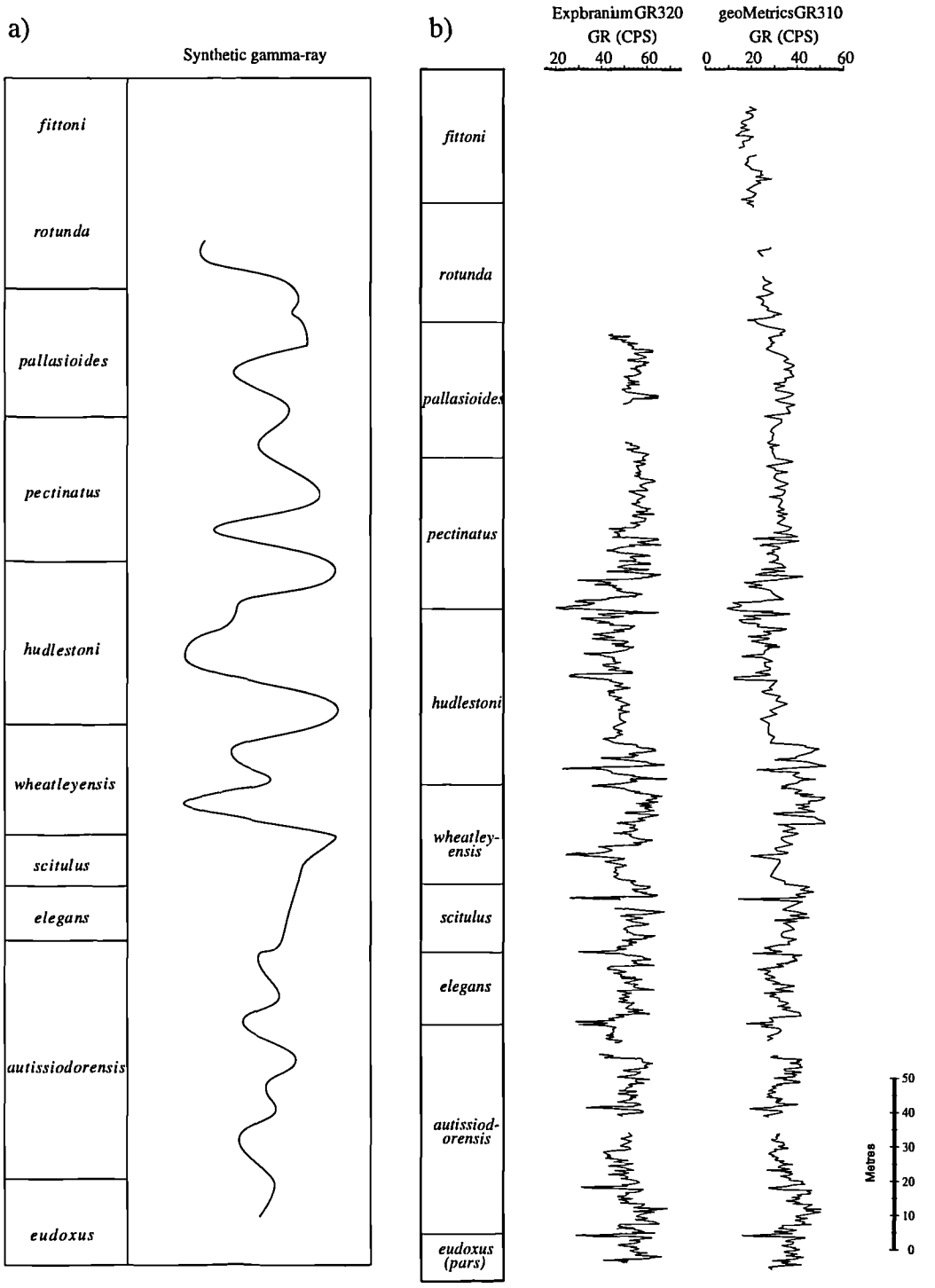

Fig. 6.39 Comparison of synthetic gamma-ray log of Melnyk *et al.* (1995) and field gamma-ray logs constructed in this study. **(a)** synthetic gamma-ray log of Melnyk *et al.* (1995), see text for an explanation of how the synthetic log was constructed. **(b)** Field gamma-ray logs constructed in this study.

6.6 Depositional models for the Kimmeridge Clay Formation

One of the first depositional models for the Kimmeridge Clay Formation was put forward by Gallois (1976). Gallois suggested that the Kimmeridge Clay Formation was deposited in an environment intermediate between an open ocean and a restricted marine basin, where the palaeogeographical influences and nutrient supply were particularly favourable to the formation of algal blooms. He noted that the organic content of the shales was largely derived from blooms, and that the blooms themselves, by deoxygenating and poisoning the water, provided the temporary anaerobic bottom conditions required to ensure the preservation of their organic content.

Comparisons of the Kimmeridge Clay Formation with Quaternary sediments in the Black Sea and Mediterranean lead Tyson *et al.* (1979) to believe that the algal blooms were not the cause, but rather a symptom of widespread anaerobic bottom conditions and that preservational factors rather than productivity were the major control on the accumulation of black shales. They argued that the deposition of the various lithologies in the Kimmeridge Clay Formation were attributed to the vertical movement of the O_2 : H_2S interface in a temporarily stratified water column. They suggested that the bituminous shales formed during periods of fluctuating aerobic/anaerobic conditions with a consequent preservation of greater amounts of organic matter, whilst the oil shales formed in predominantly anaerobic bottom conditions with only rare current activity and minimal clastic sedimentation. They interpreted the coccolith limestones to have been deposited at the maximum development of anaerobic bottom water.

The fact that oil shales are missing but the coccolith limestones are present in the upper part of the *hudlestoni* Zone and the lower part of the *pectinatus* Zone has been interpreted by Tyson *et al.* (1979) to be because these sediments were deposited in shallower water depths than lower in the Kimmeridge Clay where there are relatively thick oil shales. Once the bottom became anaerobic the O_2 : H_2S interface would take less time to rise to the thermocline and conditions suitable for oil shale formation would have been short lived. This fits in with the relative sea-level curve constructed in this study. Figure 4.7 shows that the relative sea-level during upper part of the *hudlestoni* Zone and the lower part of the *pectinatus* Zone is slightly lower than the relative sea-level around the *wheatleyensis* / *hudlestoni* zonal boundary where thick oil shales (i.e., the Blackstone Band) were deposited.

Irwin (1979) suggested that the coccolith limestones were deposited during increased water circulation immediately after the maximum anoxic conditions, because of bioturbation, ripples and encrusters seen within the coccolith limestones. Irwin's (1979) model seems to have been disproved, because only a small number of burrows have been

seen by other authors (Tyson 1979; Gallois & Medd 1979; Oschmann 1991; Wignall 1990), and no ripples have been documented by any other authors (Tyson 1979; Oschmann 1991; Coe 1992) except Wignall (1989), who suggested some small scale storm structures were seen in the coccolith limestones.

Oschmann (1988) proposed a model which he named the North Atlantic water passage model, which takes into account the overall palaeogeographic and palaeoclimatic situation. His model is based on a wind driven water current and counter current system in the North Atlantic Shelf Sea and the Arctic Ocean which caused a stable water stratification and anoxic bottom conditions. Oschmann (1988) also recognized four different orders of cycles which he incorporates into his model. The first-order cycle which formed the bases for all the other cycles was the late Jurassic transgression and regression which started in the Bathonian and ended in the latest Portlandian. He suggested that active rifting and spreading zones in the north and Central Atlantic were the cause of the first-order cycles. The second-order cycles were formed by minor transgressions and regressions. The current-counter-current system Oschmann's model depends on certain water depths, so at times of high relative sea-level stands a circulation system develops, whereas during low relative sea-level stands the currents could no longer pass each other and the watermass became mixed. The third-order cycles are caused by climatic variations and finally the fourth-order cycles are seasonal variations.

The models discussed above are all based on the type section on the Dorset coast. Miller (1990) stated that the type section is not representative of the whole formation and describes it as "being a corner of a carpet with a complex pattern". Miller's model tries to explain observations seen from the whole of the formation, which extends from offshore Norway to offshore Canada and the English Channel. The model involves the gradual formation of warm, saline, oxygen-deficient, bottom water beneath a sluggish surface current in a simple two-layer stratified shelf sea. It implies normal rates of marine organic productivity, low rates of sedimentation, and very efficient organic preservation. He argued that seawater flowed southwards from the Boreal Ocean to the Tethyan Ocean (Fig. 6.38) but, in the shallow waters around the present Britain mainland, evaporation created waters of increased salinity which sank and flowed as bottom currents into deeper water. Areas of deeper waters were most often in the more rapidly subsiding grabens and separated palaeohigh areas. In this way the more saline waters migrated along the sea bottom depressions, their paths being determined by local tectonic features but mostly from north to south.

Myers & Wignall (1987) looked at the palaeoecology and gamma-ray spectrometry of part of the Kimmeridge Clay Formation and proposed a model for Kimmeridge Clay Formation based on the data from *elegans* and *pectinatus* zones (Fig. 6.40). They suggested that climatic factors are the major driving mechanism for the cyclic alternations,

and that whilst palaeo-water-depth was also an important factor in accounting for the differences between the two zones it has no direct effect on the cyclicity. This model is discussed further in the next section.

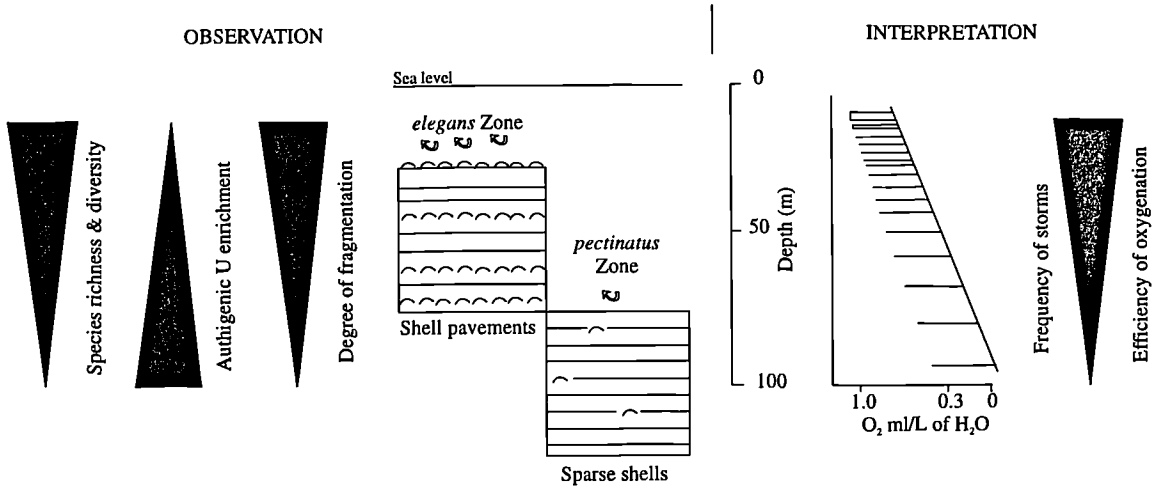

Fig. 6.40 Diagram showing the main points from the depositional model of Myers & Wignall (1987), for the Upper Kimmeridge Clay Formation.

Macquaker & Gawthorpe (1993) carried out a detailed lithofacies analysis of the Kimmeridge Clay Formation. They identified five lithofacies which they suggested were deposited in a marine shelf environment below fair-weather wave base, but in relatively shallow water close to storm wave base. One of their main conclusions was that organic matter is best preserved in areas of the basin where sediment accumulation rates were most rapid, organic-matter productivity is highest, bottom waters are anoxic, and the sediment is unwinnowed.

Coe (1992) suggested that the expanding puddle model proposed by Wignall (1991) for the lower Toarcian of England is to some extent applicable to the Kimmeridge Clay Formation; therefore she incorporated it into her general model described below.

Coe (1992) presented a general model for the deposition of the Kimmeridge Clay. She recognized three scales of cyclicity, which were incorporated in the model. The first scale, millimetre microlamination of kerogen and clay in the bituminous lithologies, were interpreted as being caused by movement of the O_2 : H_2S interface due to seasonal temperature stratification of the water column. The second scale of cycles, decimetre to metre scale, were also attributed to movement of the O_2 : H_2S interface due to temperature stratification of the water column. But in this case Coe (1992) suggested that the cycles were controlled by longer term changes in climate. The third scale of cycles, tens of metres thick (the short-term third-order sequence cycles), were interpreted to be caused by relative changes in sea-level which again may be controlled by climate.

A summary of Coe's general model is as follows: during the predominantly transgressive phase of the early Kimmeridgian, thin fining upwards packages of sediments were deposited. The transgressive trend was punctuated by a number of small scale relative sea-level changes. The first bituminous and oil shale beds were deposited during the *eudoxus* Zone, at which point the water-depth was deep enough for thermal stratification of the water-column. The thermoclines were affected by seasonal changes and longer term variations in climate which controlled the different orders of cyclicity.

The deepest water attained in the Kimmeridgian was during the *elegans* to *hudlestoni* zones, at which time the temperature stratification was still producing cyclic organic-rich sediments. The long term climatic change from humid to semi-arid influenced the general sediment type and fauna. During the *pectinatus* Zone cycles with increasing bituminous content were developed as well as coccolith limestones. The coccoliths were deposited when the O_2 : H_2S interface was at its highest.

The sudden climatic change from humid to semi-arid (Wignall & Ruffell 1990) is believed to be the cause of the culmination of the deposition of Kimmeridge Clay type sediments in both Miller (1990) and Coe (1992) models.

6.7 Discussion

At outcrop, on the Dorset coast, two thin siltstones (Wyke and Black Head Siltstones) can be seen in the *cymodoce* Zone (Fig. 6.3). The base of the Wyke Siltstone has been interpreted as the Ki sequence boundary. The Wyke Siltstone is quite thin and is not a clean sand, probably because the Dorset outcrop is not located close to the sediment source. Therefore it would be expected that the equivalent of the Wyke becomes thicker and cleaner closer to the sediment source. This is exactly what is seen in the northern part of the Weald Sub-basin (Fig. 6.25). The two stacked offshore sand bodies (Sun 1992) are probably the proximal equivalent of the Wyke and Black Head Siltstones. Looking at Figure 6.38 the only obvious source of these thick sandstones, which have been interpreted as the lowermost systems tract of the Ki sequence, is the London Platform.

The two thick homogeneous calcareous mudstone units seen at outcrop in the *wheatleyensis* and *hudlestoni* zones, which have been interpreted as the lowermost systems tracts for the K1 and K2 sequences, are devoid of bedding and sedimentary structures and have very few fossils (Cox & Gallois 1981; Wignall 1990; Coe 1992). Coe (1992) suggests that these mudstones were deposited rapidly from suspension and that mud-rich turbidity currents were responsible for the transportation of the clays. Assuming that the ammonite zones are of equal time duration then the lowermost systems tracts of the K1 and K2

sequences are shorter in time than the transgressive systems tracts and the highstand systems tracts. This means that the relative sea-level must have fallen relatively quickly. Also the overall relative sea-level was at its highest around the *wheatleyensis* and *hudlestoni* zones, in which case the London Platform may well have been drowned during the highstands and then during the relatively rapid fall in relative sea-level during the lowstands the clay and carbonates and on the London Platform would have been washed down into the Weald (according to Miller (1990) the current was from north to south; Fig. 6.38). This would explain the thicker and more calcareous nature of the lowermost systems tracts for the K1 and K2 sequences in the Weald Sub-basin, as opposed to that seen at outcrop and in the northern part of the Central Channel Sub-basin which are more distal than the Weald Sub-basin.

Myers & Wignall (1987) looked at the palaeoecology and gamma-ray spectrometry of the lower *pectinatus* Zone and the *elegans* Zone, and produced a depositional model for the Upper Kimmeridge Clay (Fig. 6.40). As part of this model they argued that the Th/K ratio decreases slightly with increasing water depth and distance from shoreline. For example the Th/K ratio over the *elegans* Zone which was deposited in shallower water than the *pectinatus* Zone, is higher than the Th/K ratio over the *pectinatus* Zone. Looking at Myers's Th/K ratio curve in Figure 6.17, you can see that the Th/K ratio is in fact slightly lower, on average, in the *pectinatus* Zone as opposed to the *elegans* Zone. However, Figure 6.17 also shows that Myers's data stop around the middle of the *pectinatus* Zone, whilst the data recorded in this study continue up past the *pectinatus* Zone and show that in fact the Th/K ratio increases to the same level as the *elegans* Zone above the point where Myers's data stop. Also Figure 6.41 clearly shows that the lowest Th/K ratio occurs over the lowermost systems tract of the K1 and K2 sequence and increases in transgressive systems tract of each of the sequences. Therefore the extra data recorded in this study show that in fact the Th/K ratio increases with water depth and does not decrease as Myers (1987) suggests. The model produced by Myers & Wignall (1987) does seem to work for the *elegans* and *pectinatus* zones, but it is important to note that this model cannot be used for the entire Upper Kimmeridge Clay because there is not a linear relationship between the palaeo-water-depth during *elegans* Zone through to the *pectinatus* Zone.

Wignall & Ruffell (1990) investigated the sudden climatic change, from humid to semi-arid, which they say that Myers & Partington pin pointed to be in bed 44 of the *hudlestoni* Zone based on palynological data. Wignall & Ruffell (1990) collected mudstones samples around *hudlestoni* Zone, and using XRD techniques measured the kaolinite and illite content of the mudstones (Fig. 6.15) to see if the climatic change is reflected in the kaolinite/illite ratio. The decline of kaolinite towards the centre of the *hudlestoni* Zone is strong evidence in favour of an aridity abundance at this time. Above

this level the kaolinite abundance does not remain uniformly low as Wignall & Ruffell (1990) expected (Fig. 6.15), but varies over short intervals. Wignall & Ruffell (1990) go on to say that bed 44 of the *hudlestoni* Zone is a regional lowstand, and that possible eustatic sea-level changes occur on a much coarser scale than the clay mineral fluctuations and they appear unrelated. They also mention that if the clay mineral signature was influenced by the position of the shoreline then the regressive conditions of bed 44 should have supplied more, rather then less, kaolinite to the Kimmeridge Bay area.

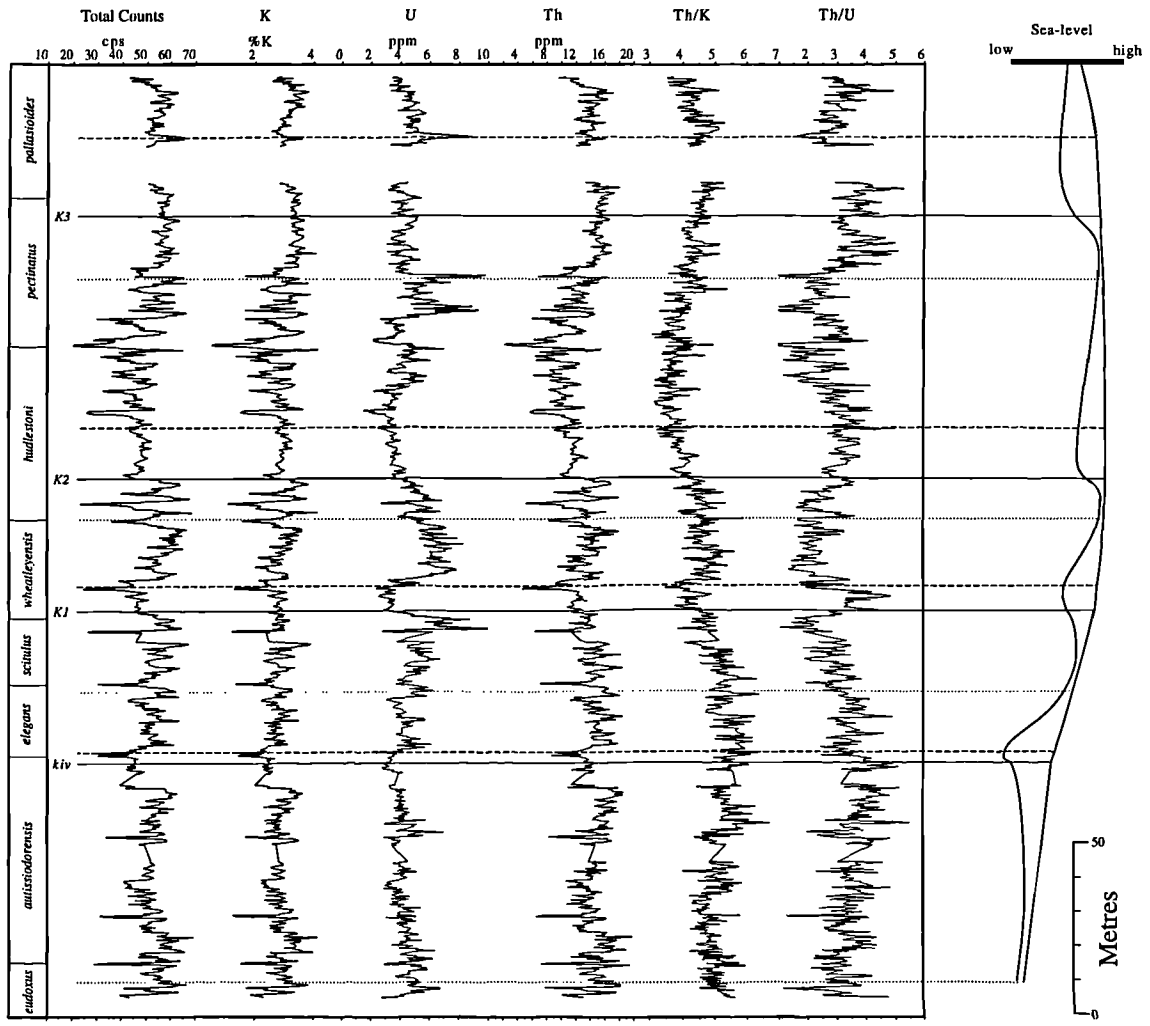

Fig. 6.41 Spectral gamma-ray data, recorded over part of the Kimmeridge Clay Formation, plotted against sea-level curve.

Kaolinite (and to a lesser extent smectite) increases the Th/K ratio, whereas illite tends to decrease it (Myers 1987). This is reflected in Figure 6.15. Looking at the Th/K ratio in Figure 6.14, you can see that the Th/K ratio decreases in two places in this Upper Jurassic interval, the first being in bed 40 of the *wheatleyensis* Zone and the second in bed 44 of the *hudlestoni* Zone. These two intervals are lowermost systems tracts for the K1

and K2 sequences. Myers (1987) states that a major change in the Th/K ratio occurs in the lower part of the *hudlestoni* Zone where the ratio switches from greater than 5 to less than 5 over an interval of a few metres (see Myers's Th/K curve in Fig. 6.17); this equates to bed 44. He does not notice the change in bed 40 because he did not take any measurements over this bed.

From the evidence provided from the spectral gamma-ray data recorded in this study, it is suggested therefore that the climatic change did not occur in bed 44 of the *hudlestoni* Zone but in fact started earlier, probably at the base of bed 40 of the *wheatleyensis* Zone. Also it is believed that the spectral gamma-ray data and the relative sea-level curve has shown that the relative sea-level strongly influences the patterns seen on the spectral curves (Fig. 6.41).

6.8 Conclusions

(1) - The Upper Kimmeridge Clay is easier to correlate using wireline logs than the Lower Kimmeridge Clay because it has more wireline character and trends due to greater individual bed thickness and lithological variation this therefore allows greater resolution.

(2) - The unconformities present in the Kimmeridgian successions of the Hartwell and Brill boreholes, which are located in Oxfordshire, are probably due to the fact that these successions were deposited in a shallow seaway between the Wessex Basin and the Wash.

(3) - The part of the Kimmeridge Clay Formation exposed between Hobarrow Bay and Chapman's Pool is most like the Kimmeridgian succession found in the northern part of the Central Channel Sub-basin (for example the 98/11-4 borehole).

(4) - The lower part of the Kimmeridge Clay Formation exposed on the Dorset coast is condensed because it was deposited on the palaeohigh on the footwall of the Portland - Wight fault complex.

(5) - The stacked offshore sand bodies, which have been interpreted as the lowermost systems tract of the Ki sequence, seen in the Weald Sub-basin are probably the proximal equivalent of the Wyke and Black Head Siltstones seen in the exposures on the Dorset coast. The source of these sandstones is probably the London Platform.

(6) - The climatic change from humid to semi-arid probably started at the base of bed 40 of the *wheatleyensis* Zone, rather than the base of bed 44 suggested by Wignall & Ruffell (1990).

(7) - The third-order changes in relative sea-level strongly influences the patterns seen on the gamma-ray and spectral gamma-ray curves particularly over the upper part of the Kimmeridge Clay.

CHAPTER 7

Conclusions

7.1 Introduction

Wireline logs have been used successfully in this study to extend the sequence stratigraphical interpretation of the Upper Jurassic outcrops of the Wessex Basin to the subsurface wireline data set. The wireline logs were interpreted sequence stratigraphically by first locating the ammonite zones on all the boreholes then interpreting the trends seen on the wireline logs. Biostratigraphic data is important in the sequence stratigraphic interpretation of wireline logs because it constrains the interpretation of the wireline trends.

Field gamma-ray and density logs, which were constructed from Upper Jurassic outcrops on the Dorset coast, were used very successfully to tie the outcrop interpretation to the subsurface wireline data set.

The main new data and interpretations in this study are :-

1. The construction of the composite field gamma-ray log for 503 m of Upper Jurassic in Dorset and its comparison and correlation with wireline gamma-ray logs.

2. The construction of a field density log for the whole of the Oxfordian and part of the Kimmeridgian in Dorset and its comparison and correlation with wireline density logs.

3. A review and development of a systematic method for enhancing and comparing wireline logs. Cross plots and change of scale are the most useful techniques.

4. Detailed comparison of gamma-ray logs from all over the Wessex Basin with a sea-level curve constructed in this study based on the sequence stratigraphical interpretation of Upper Jurassic outcrops of Great Britain. This enabled thickness changes in relation to sequence stratigraphy across the whole basin to be ascertained.

5. Detailed sequence stratigraphic wireline interpretations and correlations for the Oxfordian and Kimmeridgian successions of the Wessex Basin.

In Section 7.2 the overall conclusions for each chapter are summarised and in Section 7.3 possible future work is reviewed.

7.2 Conclusions

7.2.1 Surface - Subsurface Correlation

Field gamma-ray and density logs were used very successfully in this study to tie the sequence stratigraphical interpretation of the Upper Jurassic outcrops to the subsurface wireline data set.

The geoMetrics GR310 and Exploranium GR320 hand-held portable gamma-ray spectrometers were used to produce field gamma-ray logs which are comparable with borehole gamma-ray wireline logs. The most comparable signal between hand-held spectrometers and wireline log tools is produced by using the hand-held spectrometer perpendicular to the bedding and by using a sample spacing of 30 cm or less.

A composite field gamma-ray log was constructed which covered 503 m of the Oxfordian, Kimmeridgian and part of the Portlandian succession. This composite field gamma-ray log can be used to correlate, down to at least bed group scale (typically 10 m), with wireline gamma-ray data from nearby boreholes. Larger features can also be correlated with boreholes as far as 170 km away in the Weald Sub-basin.

Pervious workers have constructed field gamma-ray logs over short intervals of this Upper Jurassic interval. However a composite field gamma-ray log covering 503 m of this Upper Jurassic succession, with an average distance between measurements of 40 cm, has never been produced prior to this study.

A field density log was constructed for the whole of the Oxfordian and part of the Kimmeridgian successions. The field density log correlated very well with the wireline density log over the Kimmeridgian succession. To the authors knowledge this is the first time a field density log has been produced specifically to correlate with wireline density logs.

Due to the simplicity of the technique and small size of samples needed to measure density, it could be carried out following any sedimentological field study of outcrops where samples are generally collected for thin section and / or geochemical analysis. The technique could also be used to construct density logs, using core and / or drill cuttings, from older boreholes which contain no wireline data.

7.2.2 Wireline Correlation Methods and Techniques

A systematic technique for the sequence stratigraphic interpretation of wireline logs was developed in this study, starting with the quality control of the data and ending with a graphical correlation technique for checking the wireline correlations.

The simplest wireline log manipulation techniques, such as changing the scale and power and root transforms, proved to be of most use when trying to enhance the wireline trends.

Manual visual correlation of the wireline logs proved to be the best method of producing the wireline correlations. Shading the wireline logs and the ability to stretch one log in relation to another log proved to be the best aid during the manual wireline correlation.

The graphical correlation plots have been useful for spotting subtle differences in sedimentation rate, between boreholes across the study area, which would not necessarily be seen by looking at the wireline correlations.

7.2.3 Upper Jurassic Wireline Log Trends

Trends seen on the wireline logs are very important for sequence stratigraphic interpretations of wireline logs. Gamma-ray log trends for the Oxfordian and Portlandian successions have been shown to represent long-term (second-order) transgressive/regressive sea-level changes. The gamma-ray trends in the Kimmeridgian, on the other hand, are more influenced by the third-order sea-level changes.

It has been shown that the sea-level curve, constructed in this study, which was based on the sequence stratigraphic interpretation of the Upper Jurassic outcrops of Great Britain (Coe 1992, 1995, 1996) compared very well with the trends seen on the wireline gamma-ray logs. Figure 7.1 shows the gamma-ray log for the Oxfordian and Kimmeridgian successions from 98/11-4 plotted with the stretched and squeezed sea-level curve constructed in this study (Fig. 4.7), based on the sequence stratigraphic interpretation of the Upper Jurassic outcrops. Out of all the boreholes available in this study the Upper Jurassic succession in 98/11-4, which lies on the northern margin of the Central Channel Sub-basin, is most like that exposed on the Dorset coast from which the sequence stratigraphic interpretation was mainly based. This figure shows that the third-order sea-level curve compares very well with the trends seen on the gamma-ray log. For this Upper Jurassic succession, therefore, it is suggested that in general the trends seen on the gamma-ray log can be related to sea-level changes.

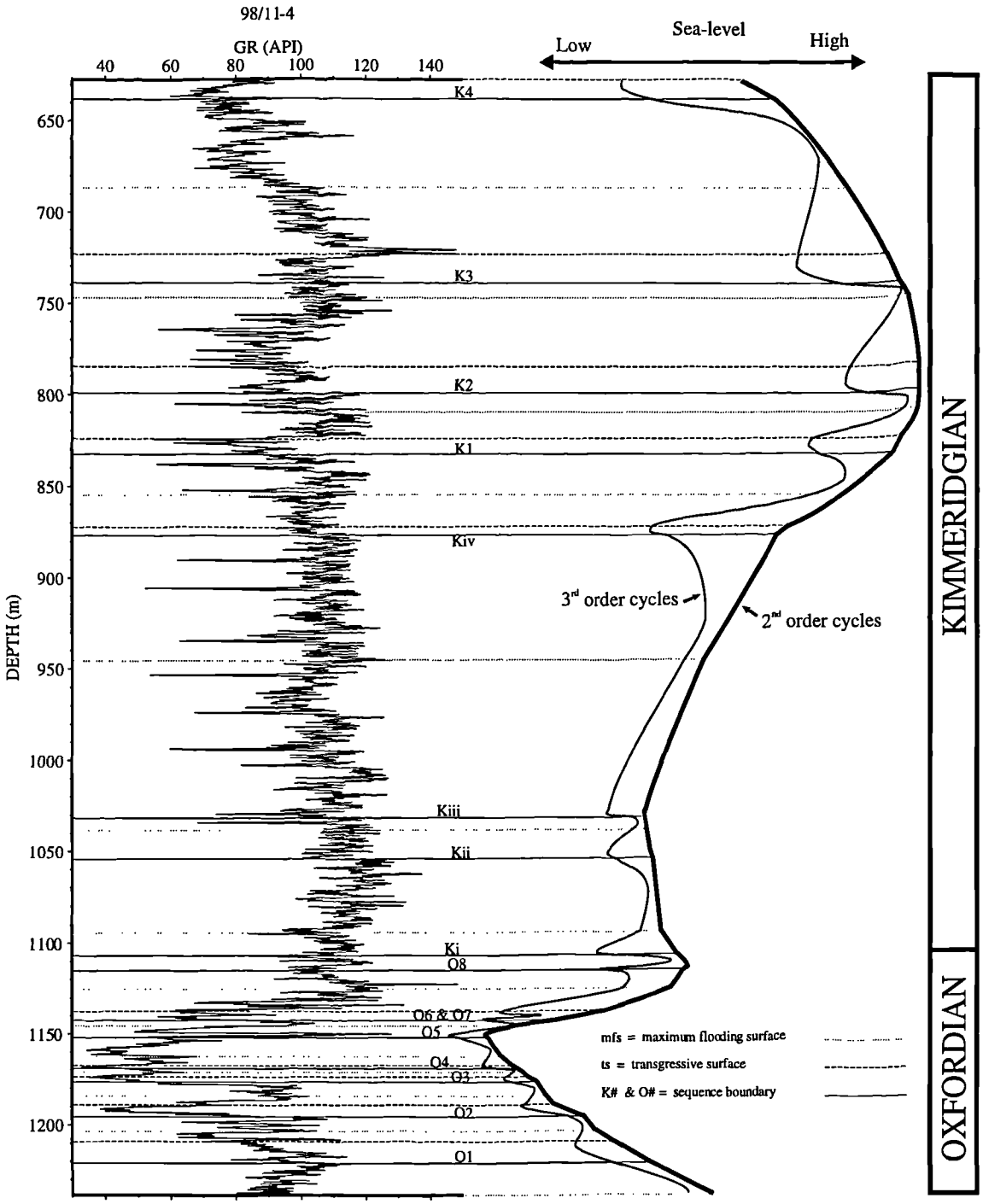

Fig. 7.1 Sea-level curve for the Oxfordian and Kimmeridgian, from Figure 4.7, has been stretched and squeezed so that the key sequence stratigraphical surfaces align with the key sequence stratigraphical surfaces which have been picked on the gamma-ray curve from borehole 98/11-4. The Upper Jurassic succession in 98/11-4 is very similar to that seen at outcrop from which the sequence stratigraphic interpretation was used to construct the sea-level curve.

The comparison of the spectral gamma-ray data recorded in this study with the third-order sea-level curve (Fig. 4.10) showed that the Th/K ratio curve is a better sea-level indicator than the total gamma-ray curve or the individual spectral gamma-ray curves.

When interpreting trends on the gamma-ray log, patterns of progradation, retrogradation and aggradation were used to locate the key sequence stratigraphic

surfaces. The lowermost systems tract would be represented by a progradational trend which may or may not show aggradation towards the top, the transgressive systems tract by a retrogradational trend, and the highstand systems tract by an aggradational and/or progradational gamma-ray trend.

The third-order sea-level curve produced in this study in significantly more detailed than that produced by Haq *et al.* (1987, 1988) and would be useful for comparison purposes for Jurassic workers in other geographic areas.

7.2.4 Oxfordian

The wireline logs over the Oxfordian succession can not be correlated peak for peak across the Wessex Basin because facies changes occur both laterally and vertically, but nevertheless can be correlated sequence stratigraphically using trends seen on the wireline logs.

The key sequence stratigraphic surfaces (sequence boundary, transgressive surface and maximum flooding surface) have been picked for sequences O2 to O5 on all the boreholes within the Wessex Basin. However due to the lack of core data, detailed biostratigraphy and the development of a reef in the Weald Sub-basin, the key sequence stratigraphic surfaces for O1 and O6-O8 could only be picked in some of the boreholes.

To the authors knowledge the wireline correlations seen in Chapter 5 is the first attempt at a detailed sequence stratigraphic correlation of the Oxfordian succession across the whole of the Wessex Basin.

The wireline correlations of the Oxfordian succession (Figs 5.12 to 5.18) have shown that the upper part of Oxfordian succession, down as far as highstand of the O4 sequence, in eastern part of the Wessex Basin was not deposited, has been eroded or is highly condensed (Fig. 7.2: Mere, Vale of Pewsey Sub-basins and the Hampshire - Dieppe High). The wireline correlations also showed that the development of the carbonate reef was restricted to the north-eastern part of the Weald Sub-basin (Fig. 7.2) probably paralleling the London - Brabant landmass which was prominent at the time.

The O6 sequence which is not present in any outcrops in the Wessex Basin has been interpreted to be present in the north-eastern part of the Weald Sub-basin (Fig. 7.2). The O6 sequence is probably preserved here because with increased transgression occurring late in the Oxfordian more sediment would be deposited in the proximal areas.

Figure 7.3 shows the graphical correlation of 98/11-4, which lies to the south of the Portland - Wight Faults in the Central Channel Sub-basin, with 98/11-3, which lies to the north of the Portland - Wight Faults on the south Dorset High. This figure shows the usefulness of the graphical correlation technique in detecting changes of sedimentation rates between boreholes. This example clearly shows that the succession above the O5

sequence boundary is condensed in 98/11-3 due to the lack of sediment accommodation space on the palaeohigh.

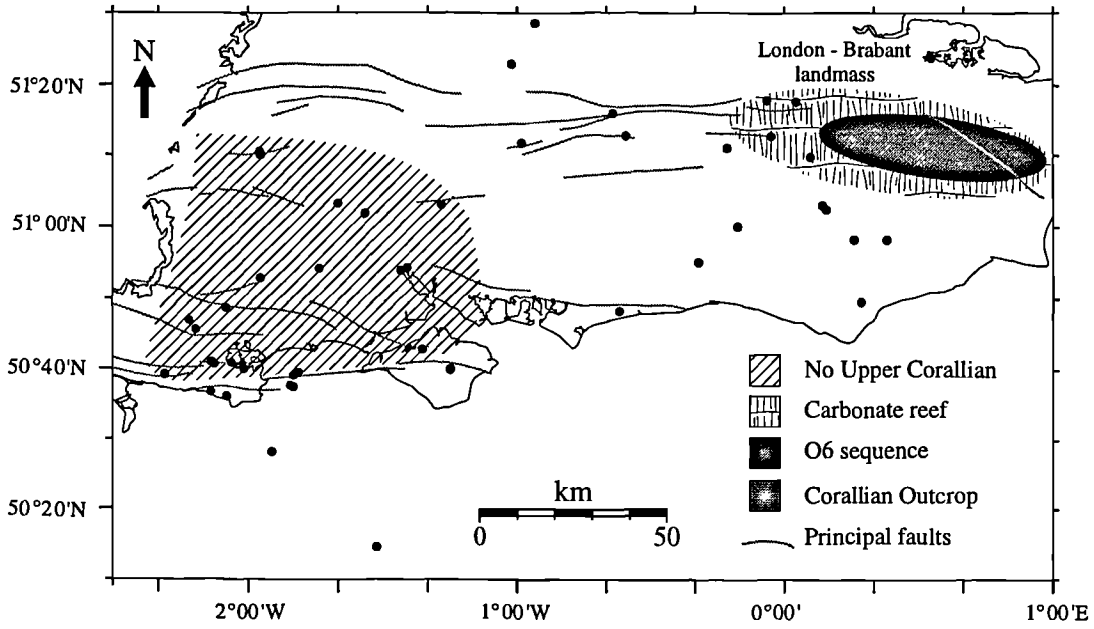

Fig. 7.2 Map of the Wessex Basin showing the location of the carbonate reef and the O6 sequence in the Weald Sub-basin. The map also shows the area where the part of the Upper Corallian is not present.

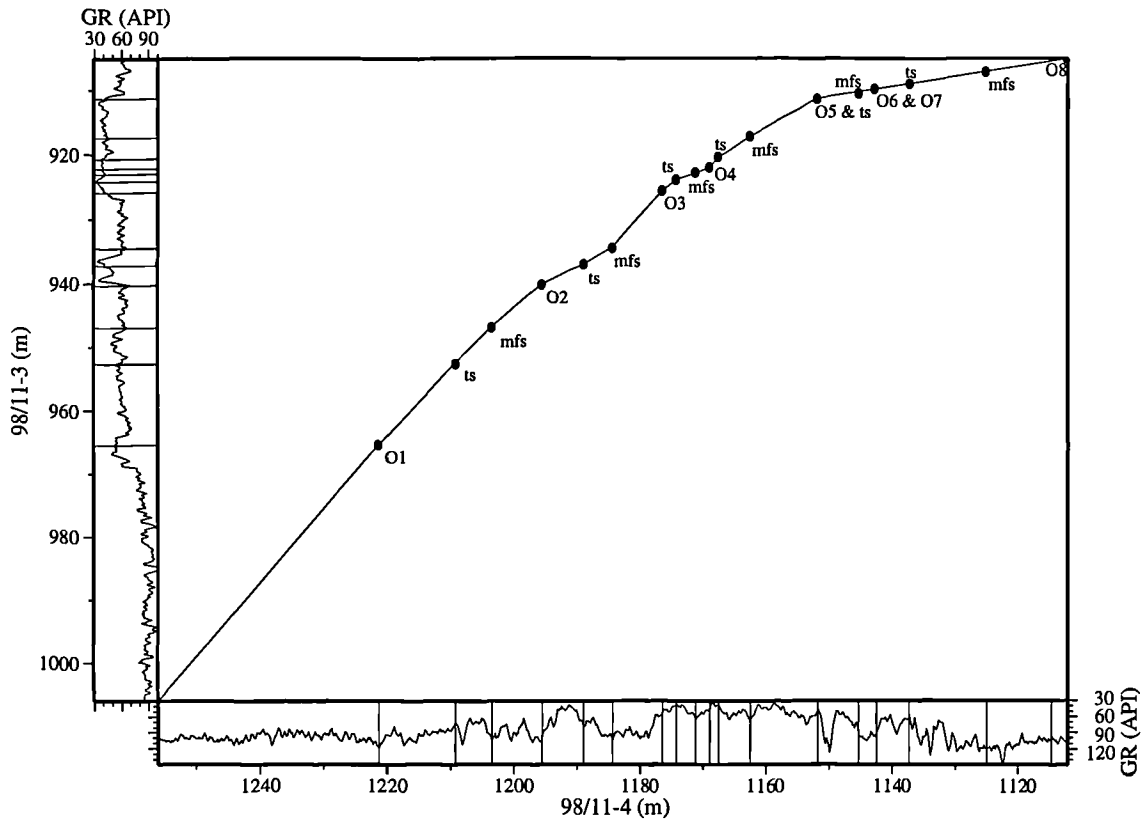

Fig. 7.3 Graphical correlation plot of the Oxfordian succession in 98/11-4, located in the Central Channel Sub-basin, and 98/11-3, located on the South Dorset High. The plot clearly shows that the upper part of the Oxfordian in 98/11-3 is condensed in relation to the succession in 98/11-4.

7.2.5 Kimmeridgian

The Kimmeridgian succession has been very successfully correlated in a sequence stratigraphic manner across the Wessex Basin and up into Yorkshire. Unlike the Oxfordian the Kimmeridgian succession could be correlated virtually peak for peak. The Upper Kimmeridge Clay was easier to correlate than the Lower Kimmeridge Clay because it has more wireline character and trends which are believed to be related to short-term third-order sea-level changes.

The part of the Kimmeridge Clay Formation exposed between Hobarrow Bay and Chapman's Pool is most like the Kimmeridgian succession found in the northern part of the Central Channel Sub-basin (for example the 98/11-4 borehole). The lower part of the Kimmeridge Clay Formation exposed on the Dorset coast is condensed because it was deposited on a palaeohigh.

The base Cretaceous unconformity has resulted in the removal of the upper part of the Kimmeridge Clay Formation, down to the transgressive systems tract of the Kiii sequence, in the Mere and Dorset Sub-basins (Fig. 7.4). On the onshore part of the south Dorset High the base Cretaceous unconformity has removed the whole of the Kimmeridge Clay Formation.

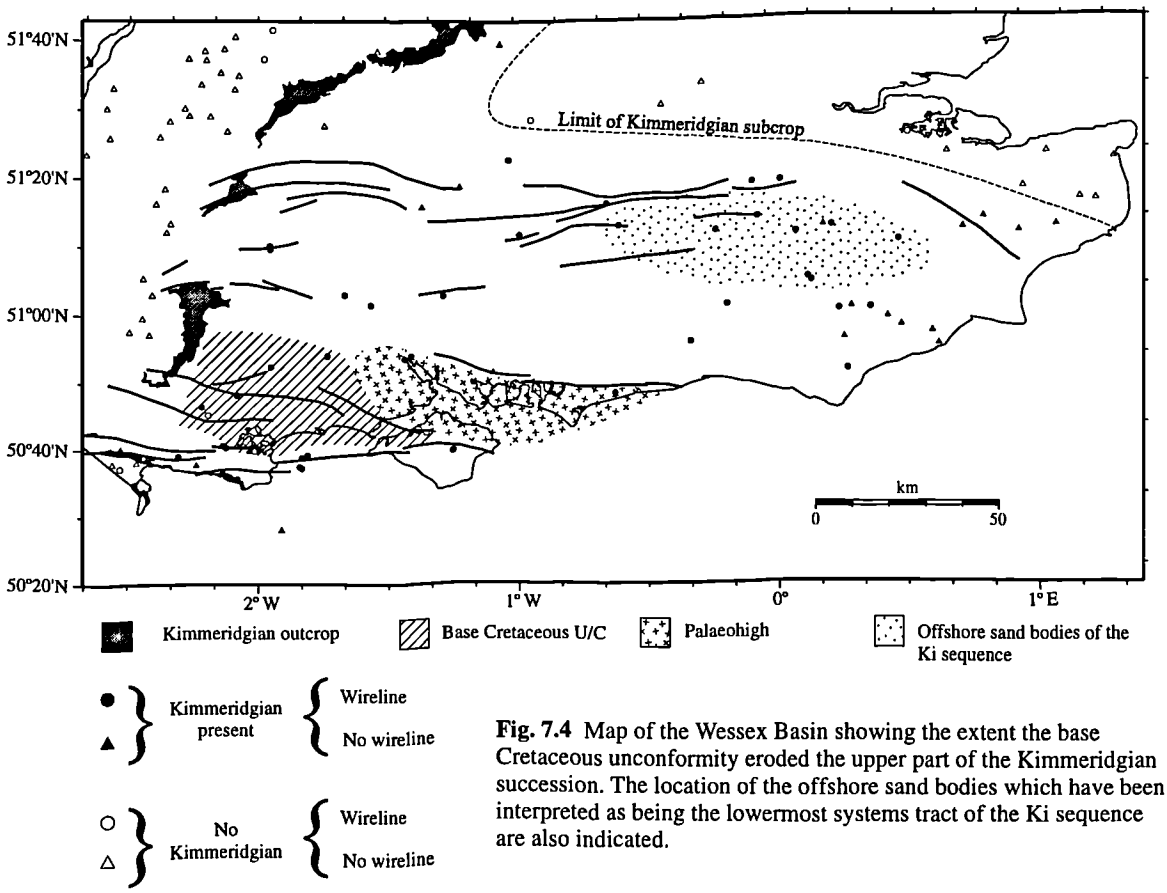

Fig. 7.4 Map of the Wessex Basin showing the extent the base Cretaceous unconformity eroded the upper part of the Kimmeridgian succession. The location of the offshore sand bodies which have been interpreted as being the lowermost systems tract of the Ki sequence are also indicated.

The wireline correlations of the Kimmeridgian succession (Figs 6.25 to 6.30, 6.35 and 6.36) have shown that the Weald Sub-basin was the most prominent depocentre in the Wessex Basin resulting in the thickest Kimmeridgian succession of 585 m. The Central Channel Sub-basin was the second most prominent depocentre with a thickest Kimmeridgian succession of 485 m. The thinnest full Kimmeridgian succession was seen on the Hampshire Dieppe High (Fig. 7.4), 119 m in the Marchwood borehole.

The stacked offshore sand bodies, which have been interpreted as the lowermost systems tract of the Ki sequence, seen in the Weald Sub-basin (Fig. 7.4) are probably the proximal equivalent of the Wyke and Black Head Siltstones seen in the exposures on the Dorset coast. The source of these sandstones is most probably the London - Brabant landmass. The lowermost systems tract for the Kii and Kii sequences are also thin siltstones on the Dorset coast, however there is no equivalent thick sandstone bodies in the Weald Sub-basin.

Interpretation of the spectral gamma-ray data recorded in this study suggests that third-order changes in sea-level strongly influences the patterns seen on the gamma-ray and spectral gamma-ray curves over the Upper Kimmeridge Clay , in particular. The spectral data recorded in this study also suggests that the climatic change from humid to semi-arid probably started at the base of bed 40 of the *wheatleyensis* Zone rather than the base of bed 44 as suggested by Wignall & Ruffell (1990).

The graphical correlations in Figure 7.5 show that the lowermost systems tracts generally have lower gradient than the transgressive systems tracts and the highstand systems tracts. This suggests that during lowstand the Weald Sub-basin, where Cowden is located, had either more sediment accommodation space or more likely a higher sediment supply from the London - Brabant massif during the lowstand than in the Central Channel Sub-basin (98/11-4), Hampshire - Dieppe high (Marchwood) and the Cleveland Basin (Ulceby Cross), but as transgression proceeded all areas received the same amount of sediment. The lowstand system tracts thus seem to show the most variability in sediment thickness across the basin, this is what the sequence stratigraphic model would predict.

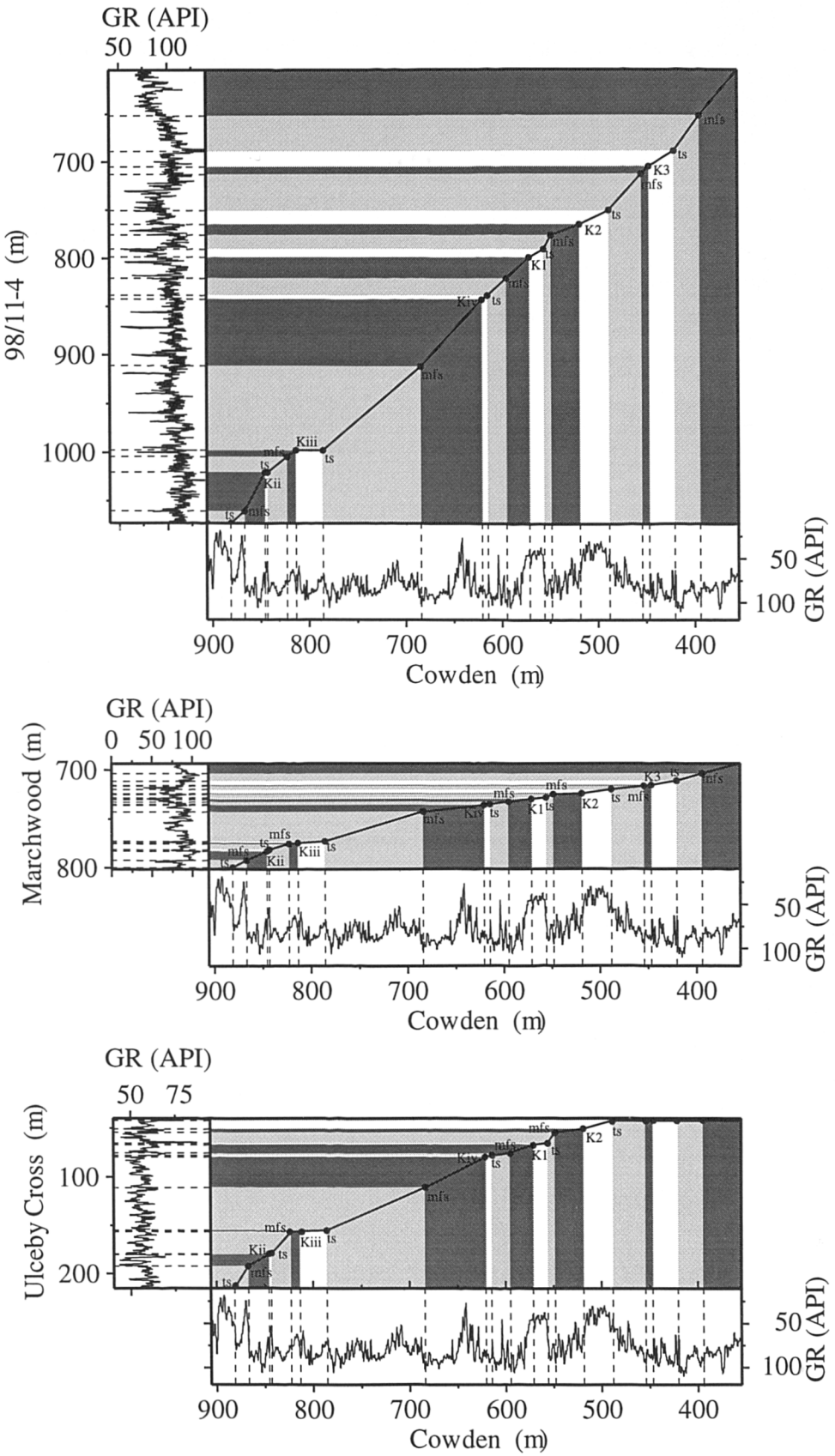

Fig. 7.5 Graphical correlation plots showing that the lowermost systems tract is generally lower gradient than the transgressive and highstand systems tracts.

7.3 Further work

The data used to construct the composite total gamma-ray, spectral gamma-ray and density field logs produced in this study are given in Appendix B. This data could be combined with other field gamma-ray and density logs measured along the Dorset coast in the future to produce composite field logs for the whole of the Mesozoic exposed along southern coast of England.

This study has extended the sequence stratigraphic interpretation of the Upper Jurassic outcrops of the Wessex Basin to the subsurface using wireline line logs. The next stage would be to compare the interpretation from this study to a seismic sequence stratigraphic interpretation of a seismic data set from the Wessex Basin. The integration of wireline correlations with seismic data could be achieved by constructing synthetic seismic sections for each of the boreholes. An example of a synthetic seismic, constructed using the Terrastation II software package, is shown in Figure 7.6 for 98/11-4. The location of the key sequence stratigraphic surfaces could be placed on the synthetic seismic and easily extended to the seismic data set. Even though the synthetic seismic shown in Figure 7.6 is a quick first attempt it does show that the sequences picked in this study are below seismic resolution, nevertheless it would be interesting to see how a seismic sequence stratigraphic interpretation compares with the wireline sequence stratigraphic interpretation.

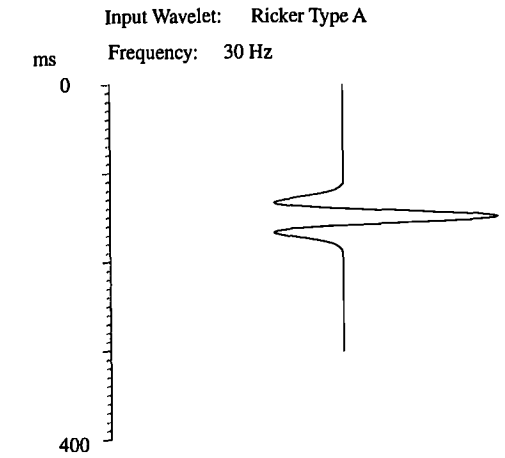

Fig. 7.6 Synthetic seismic for 98/11-4, constructed using the sonic and density logs.

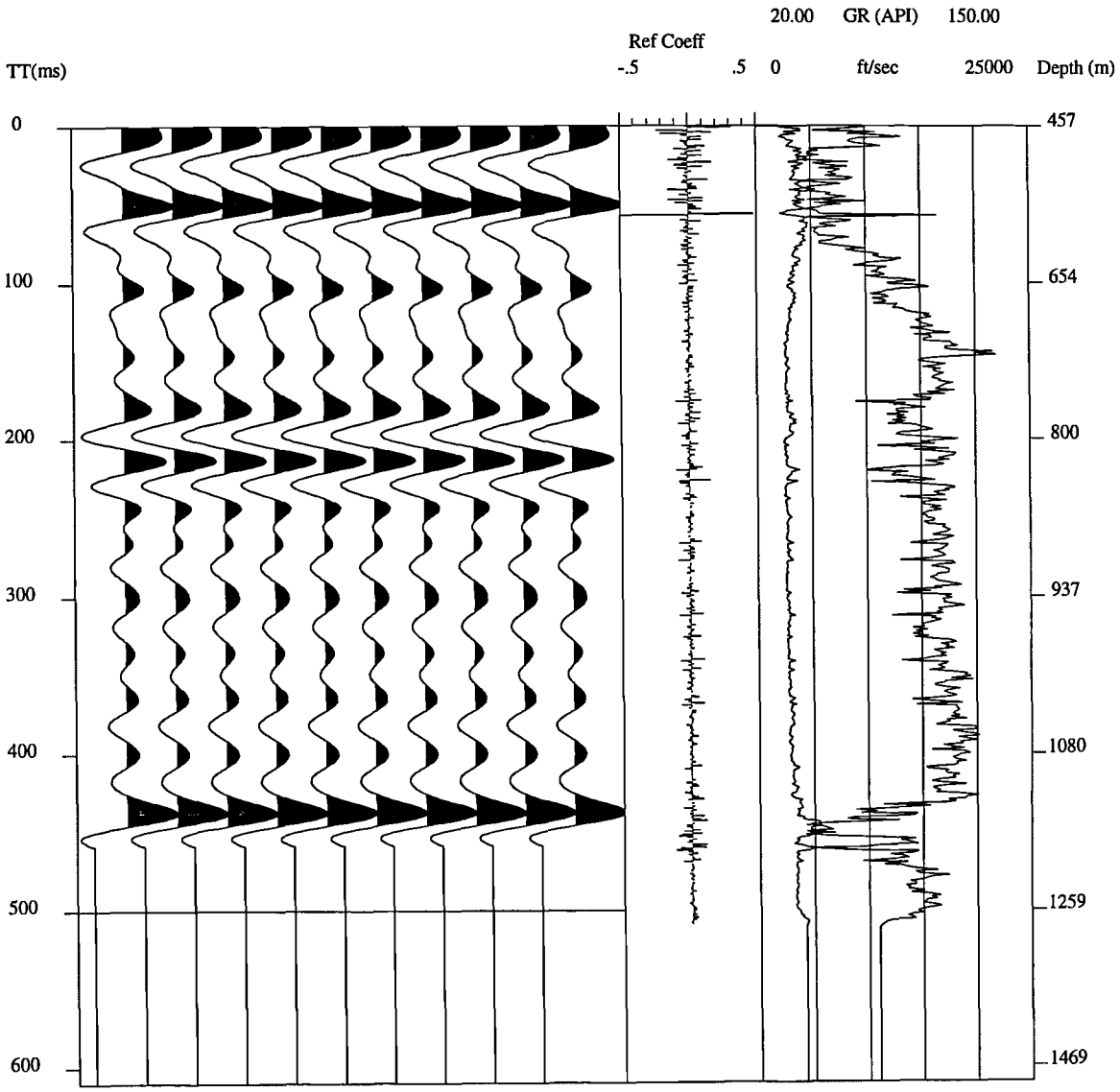

References

ADAMS, J. A. S. & WEAVER, C. E. 1958. Thorium-to-uranium ratios as indicators of sedimentary processes: example of concept of geo-chemical facies. *American Association of Petroleum Geologists Bulletin*, **42**, 387-430.

ADAMS, J. A. S. & GASPERINI, P. 1970. *Gamma-ray spectrometry of rocks*, Methods in Geochemistry and Geophysics 10, Elsevier.

ALLEN, P. A. & UNDERHILL, J. R. 1989. Swaley cross-stratification produced by unidirectional flows, Bencliff Grit (Upper Jurassic), Dorset, UK. *Journal of the Geological Society, London*, **146**, 241-252.

ARKELL, W. J. 1933. *The Jurassic System in Great Britain*. Clarendon Press, Oxford.

ARKELL, W. J. 1947. The geology of the country around Weymouth, Swanage, Corfe and Lulworth. *Memoir of the Geological Survey of Great Britain*, **Sheet 341, 342 & 343** (England & Wales).

ARMENTROUT, J. M., MALECEK, S. J., FEARN, L. B., SHEPPARD, C. E., NAYLOR, P. H., MILES, A.W., DESMARIAIS, R. J. & DUNAY, R. E. 1993. Log-motif analysis of Paleogene depositional system tracts, central and northern North Sea -- defined by sequence stratigraphic analysis. *In:* PARKER, J. R. (ed.). *4th conference on the petroleum geology of northwest Europe*, proceedings, **1**. The Geological Society London, 45-57.

ATLAS WIRELINE SERVICES 1985. *Log interpretation charts*. Western Atlas International.

ATLAS WIRELINE SERVICES 1992. *Introduction to Wireline Log Analysis*. Western Atlas International Inc., Houston, Texas.

ATLAS WIRELINE SERVICES 1994. *Well data system: advanced log evaluation - documentation*. Western Atlas International.

BATEMAN, R. M. 1985. *Open-hole log analysis and formation evaluation*. Reidel.

BAUM, G. R. & VAIL, P. R. 1988. Sequence stratigraphic concepts applied to Paleogene outcrops, Gulf and Atlantic Basins. *In*: WILGUS, C. K., HASTINGS, B. S., KENDALL, C. G. St C., POSAMENTIER, H. W., ROSS, C. A. & VAN WAGONER, J. C. (eds). *Sea-Level Changes - An intergrated approach*, Society of Economic Paleontologists and Mineralogists, Special Publication, **42**, 309-327.

BELL, K. G. 1954. Uranium and thorium in sedimentary rocks. *In*: FAUL, H. (ed.). *Nuclear Geology*. Chapman & Hall, London, 98-132.

BESSA, J. & HESSELBO, S. P. (In Press). Gamma-ray character and correlation of the Lower Lias, SW Britain. *Proceedings of the Geologists' Association, London.*

BIGELOW, E. L. 1987. *Fundamentals of Diplog analysis.* Atlas Wireline Services, Western Atlas International, Inc., Houston.

BJØRLYKKE, K., DYPVIK, H. & FINSTAD, K. G. 1975. The Kimmeridgian shale, its composition and radioactivity. *In*: FINSTAD, K. G. & SELLEY, R. C. (eds). *NFP Jurassic Northern North Sea Symposium*, Stavanger, **paper 12**, 1-20.

BOWEN, D. W., WEIMER, P. & SCOTT, A. J. 1993. Application of siliciclastic sequence stratigraphy to exploration: examples from frontier and mature basins, SPE-26438, *In:* SPE annual technical conference and exhibition proceedings, v. omega, Formation evaluation and reservoir geology: Society of Petroleum Engineers, 221-233.

BRADSHAW, M. J., COPE, J. C. W., CRIPPS, D. W., DONOVAN, D. T., HOWARTH, M. K., RAWSON, P. F., WEST, I. M. & WIMBLEDON, W. A. 1992. Jurassic. *In*: COPE, J. C. W., INGHAM, J. K. & RAWSON, P. F. (eds). *Atlas of palaeogeography and lithofacies.* Geological Society London Memoir, **13**, 107-129.

BRISTOW, C. R. & BAZLEY, R. A. 1972. Geology of the country around Royal Tunbridge Wells. *Memoir of the British Geological Survey of Great Britain*, **Sheet 303** (England & Wales).

BRISTOW, C. R., FRESHNEY, E. C. & PENN, I. E. 1991. Geology of the country around Bournemouth. *Memoir of the British Geological Survey*, **Sheet 329** (England & Wales).

BRISTOW, C. R., BARTON, C. M., FRESHNEY, E. C., WOOD, C. J., EVANS, D. J., COX, B. M., IVIMEY-COOK, H. C. & TAYLOR, R. T. 1995. Geology of the country around Shaftesbury. *Memoir of the British Geological Survey*, **Sheet 313** (England & Wales).

BROOKFIELD, M. E. 1973. Palaeogeography of the Upper Oxfordian and Lower Kimmeridgian (Jurassic) in Britain. *Palaeogeography, Palaeoclimatology, Palaeoecology*, **14**, 137-167.

BROOKFIELD, M. E. 1978a. The lithostratigraphy of the upper Oxfordian and lower Kimmeridgian Beds of south Dorset, England. *Proceedings of the Geologists' Association*, **89**, 1-32.

BROOKFIELD, M. E. 1978b. The use of coarse fraction analysis in paleo-environmental interpretation: upper Oxfordian and lower Kimmeridgian (Jurassic) sediments in Dorset, England. *Sedimentary Geology*, **20**, 249-280.

BROWN, L. F. & FISHER, W. L. 1977. Seismic-stratigraphic interpretation of depositional systems: examples from Brazil rift and pull-apart basins. *In*: PAYTON, C. E. (ed.). *Seismic stratigraphy - applications to hydrocarbon exploration.* American Association of Petroleum Geologists Memoir, **26**, 213-248.

BURKE, J. A., CURTIS, M. R. & COX, J. T. 1966. Computer processing of log data enables better production in Chaveroo field. *Society of Petroleum Engineers,* **paper 1576**, presented at the 41st Annual Meeting, Dallas, Oct. 2-5, 1966.

BURST, J. F. 1969. Diagenesis of Gulf Coast clayey sediments and its possible relation to petroleum migration. *American Association of Petroleum Geologists Bulletin*, **53**, 73-93.

BUTLER, M. & PULLAN, C. P. 1990. Tertiary structures and hydrocarbon entrapment in the Weald Basin of southern England. *In*: HARDMAN, R. F. P. & BROOKS, J. (eds). *Tectonic Events Responsible for Britain's Oil and Gas Reserves*, Geological Society Special Publication, **55**, 371-391.

CALLOMAN, J. H. 1968 (with TORRENS, H. C.). The Corallian Beds, the Ampthill Clay and the Kimmeridge Clay. Chapter 15. *In*: SYLVESTER-BRADLEY, P. C. & FORD, T. D. (eds). *The geology of the East Midlands*. Leicester University Press.

CALLOMON, J. H. 1971. Lower Kimmeridge Clay. *In:* CALLOMON, J. H. & COPE, J. C. W. (eds). The stratigraphy and ammonite succession of the Oxford and Kimmeridge Clays in the Warlingham Borehole. *Bulletin of the Geological Survey of Great Britain*, **36**, 152-168.

CALLOMON, J. H. & COPE, J. C. W. 1971. The stratigraphy and ammonite succession of the Oxford and Kimmeridge Clays in the Warlingham Borehole. *Bulletin of the Geological Survey of Great Britain*, **36**.

CHADWICK, R. A. 1986. Extension tectonics in the Wessex Basin, southern England. *Journal of the Geological Society, London*, **143**, 465-488.

CHAMBERLAIN, A. K. 1984. Surface gamma-ray logs: a correlation tool for frontier areas. *American Association of Petroleum Geologists Bulletin*, **68**, 1040-1043.

CHOWDHURY, A. N. 1982. Variations in diagenetic environments of the coral rag and underlying oolite of the Osmington Oolite Formation (Upper Oxfordian) of the Oxford-Berkshire area, U.K., and their implications. *Sedimentary Geology*, **32**, 247-263.

CLOETINGH, S. 1988. Intraplate stresses: A tectonic cause for third-order cycles in apparent sea level. *In*: WILGUS, C. K., HASTINGS, B. S., KENDALL, C. G. St C., POSAMENTIER, H. W., ROSS, C. A. & VAN WAGONER, J. C. (eds). *Sea-Level Changes - An intergrated approach*, Society of Economic Paleontologists and Mineralogists, Special Publication, **42**, 19-29.

COE, A. L. 1992. *Unconformities within the Upper Jurassic of the Wessex Basin, Southern England*, DPhil Thesis, University of Oxford.

COE, A. L. 1994. The Upper Jurassic of Britain from a sequence stratigraphical perspective. *In:* PARKINSON, N. & HESSELBO, S. (eds). *Progress in sequence stratigraphy: abstracts*. Geological Society London.

COE, A. L. 1995. A comparison of the Oxfordian successions of Dorset, Oxfordshire, and Yorkshire. *In*: Taylor, P. D. (ed.). *Field Geology of the British Jurassic*. Geological Society, London, 151-172.

COE, A. L. 1996. Unconformities within the Portlandian Stage of the Wessex Basin and their sequence-stratigraphical significance. *In*: HESSELBO, S. P. & PARKINSON, D. N. (eds). *Sequence Stratigraphy in British Geology*, Geological Society Special Publication, **103**, 109-143.

COE, A. L., HESSELBO, S. P. & JENKYNS, H. C. 1989. Jurassic sequence stratigraphy in relation to the tectonic development of the Wessex Basin. *Terra abstracts*, **1**, 76.

COLTER, V. S. & HARVARD, D. J. 1981. The Wytch Farm Oil Field, Dorset. *In:* ILLING, L. V. & HOBSON, G. D. (eds). *Petroleum Geology of the Continental Shelf of North-West Europe*, Heydon. 494-503.

COPE, J. C. W. 1967. The palaeontology and stratigraphy of the lower part of the Upper Kimmeridge Clay of Dorset. *Bulletin of the British Museum of Natural History (Geology)*, **15**, 3-79.

COPE, J. C. W. 1978. The ammonite faunas and stratigraphy of the upper part of the Upper Kimmeridge Clay of Dorset. *Palaeontology*, **21**, 469-533.

COPE, J. C. W. 1994. The nature and resolution of Jurassic Ammonite biozones. *In:* CARIOU, E. & HANTZPERGUE, P. (eds). *3rd International Symposium on Jurassic stratigraphy*, Poitiers 1991. Geobios, **17**, 127-132.

COPE, J. C. W., DUFF, K. L., PARSONS, C. F., TORRENS, H. S., WIMBLEDON, W. A. & WRIGHT, J. K. 1980. A Correlation of Jurassic Rocks in the British Isles - Part Two: Middle and Upper Jurassic. *The Geological Society, Special Report* **15.**

COPE, J. C. W., INGHAM, J. K. & RAWSON, P. F. (eds).1992. *Atlas of Palaeogeography and Lithofacies*. Geological Society, London, Memoir **13**.

COPESTAKE, P. 1993. Application of micropalaeontology to hydrocarbon exploration in the North Sea Basin. *In*: JENKINS, D. G. (ed.). *Applied microplaeontology*, Kluwer Academic Publishers.

COWAN, D. R. & MYERS, K. T. 1988. Surface gamma ray logs: A correlation tool for frontier areas: Discussion. *American Association of Petroleum Geologists Bulletin*, **72**, 634-636.

COX, B. M. 1990. A review of Jurassic chronostratigraphy and age indicators for the UK. *In*: HARDMAN, R. F. P. & BROOKS, J. (eds). *Tectonic events responsible for Britain's oil and gas reserves*, Geological Society Special Publication, **55**, 169-190.

COX, B. M. & GALLOIS, R. W. 1981. The stratigraphy of the Kimmeridge Clay of the Dorset type area and its correlation with some other Kimmeridgian sequences. *Report of the Institute of Geological Sciences*, **80/4**.

COX, B. M. & SUMBLER, M. G. 1989. The Upper Jurassic sequence at Red's Hill, Brill, Buckinghamshire, and the age of the Brill Serpulite Bed. *Proceedings of the Geologists' Association*, **100**, 353-362.

COX, B. M. & SUMBLER, M. G. 1994. The Oxfordian-Kimmeridgian boundary beds in Southern England (Dorset to Fenland). *In:* CARIOU, E. & HANTZPERGUE, P. (eds). *3rd International Symposium on Jurassic stratigraphy, Poitiers 1991.* Geobios, **17**, 133-140.

COX, B. M., GALLOIS, R. W. & SUMBLER, M. G. 1994. The stratigraphy of the BGS Hartwell Borehole, near Aylesbury, Buckinghamshire. *Proceedings of the Geologists' Association*, **105**, 209-224.

DAVIES, S. J. & ELLIOTT, T. 1996. Spectral gamma ray characterization of high resolution sequence stratigraphy -- examples from Upper Carboniferous fluvio-deltaic systems, County Clare, Ireland. *In:* HOWELL, J. A. & AITKEN, J. F. (eds). *High resolution sequence stratigraphy; innovations and applications.* Geological Society London Special Publication, **104**, 25-35.

DE WET, C. B. 1987. Deposition and diagenesis in an extensional basin: the Corallian Formation (Jurassic) near Oxford, England. *In*: MARSHALL, J. D. (ed.). *Diagenesis of Sedimentary Sequences*, Geological Society Special Publication, **36**, 339-353.

DOVETON, J. H. 1994a. Geologic log interpretation. *Society for Sedimentary Geology.* Society of Economic Paleontologists and Mineralogists, Short Course **29**.

DOVETON, J. H. 1994b. Geological log analysis using computer methods. *American Association of Petroleum Geologists,* Computer applications in Geology, **2**.

DOVETON, J. H. & CABLE, H. W. 1979. Fast matrix methods for the lithological interpretation of geophysical logs. *In*: GILL, D. & MERRIAM, D. F. (eds). *Geomathematical and petrophysical studies in sedimentology*, Pergamon Press.

DRANFIELD, P., BREGG, S. H. & CARTER, R. R. 1987. Wytch farm oilfield: reservoir characterization of the Triassic Sherwood Sandstone for input to reservoir simulation studies. *In*: BROOKS, J. & GLENNIE, K. (eds). *Petroleum Geology of North West Europe*, Graham & Trotman, 149-160.

DRESSER ATLAS 1982. *Well logging and interpretation techniques - the course for home study, third edition.* Dresser Atlas, Dresser Industries.

DRESSER ATLAS 1983. *Log interpretation charts.* Dresser Atlas, Dresser Industries.

DUVAL, B., CRAMEZ, C. & VAIL, P. 1992. Types and hierarchy of stratigraphic cycles. *Abstract volume for conference on sequence stratigraphy of European basins.* CNRS-IFP, Dijon, France (18-20th May 1992), 44-45.

DYPVIK, H. & ERIKSEN, D. O. 1983. Natural radioactivity of clastic sediments and the contributions of U, Th and K. *Journal of Petroleum Geology*, **5**, 409-416.

EDMUNDSON, H. & RAYMER, L. L. 1979. Radioactive logging parameters for common minerals. *The Society of Professional Well Log Analysts*, 22th Annual Logging Symposium, June 3-6, paper O.

ELLIS, D. V. 1987. *Well logging for earth scientists.* Elsevier.

EMERY, D. & MYERS, K. J. 1996. *Sequence stratigraphy*. Blackwell Science Ltd.

ETTENSOHN, F. R., FULTON, L. P. & KEPFERLE, R. C. 1979. Use of scintillometer and gamma-ray logs for correlation and stratigraphy in homogeneous black shales. *Geological Society of America Bulletin,* part II, **90**, 828-849.

EXPLORANIUM, 1996. *GR-320 portable gamma ray spectrometer - user manual.* Exploranium Ltd., Canada.

FANG, J. H., CHEN, H. C., SHULTZ, A. W. & MAHMOUD, W. 1992. Computer-aided well log correlation. *American Association of Petroleum Geologists Bulletin*, **76**, 307-317.

FOSTER, N. H. & BEAUMONT, W. A. (eds).1990a. Formation Evaluation I. *American Association of Petroleum Geologists,* Treatise of Petroleum Geology Reprint Series, **17**.

FOSTER, N. H. & BEAUMONT, W. A. (eds).1990b. Formation Evaluation II. *American Association of Petroleum Geologists,* Treatise of Petroleum Geology Reprint Series, **17**.

FRANK, R. W. 1986. *Prospecting with old E-Logs*. Schlumberger Educational Services, Houston, Texas.

FÜRSICH, F. T. 1977. Corallian (Upper Jurassic) marine benthic associations from England and Normandy. *Palaeontology*, **20**, 337-385.

GALLOIS, R. W. 1973. Some detailed correlations in the Upper Kimmeridge Clay in Norfolk and Lincolnshire. *Bulletin of Geological Survey of Great Britain*, **44**, 63-75.

GALLOIS, R. W. 1976. Coccolith blooms in the Kimmeridge Clay and origin of North Sea Oil. *Nature*, **259**, 473-475.

GALLOIS, R. W. 1978. A pilot study of oil shale occurrences in the Kimmeridge Clay. *Report of the Institute of Geological Sciences*, **78/13**.

GALLOIS, R. W. 1979. Geological investigations for the Wash Water Storage Scheme. *Report of the Institute of Geological Sciences*, **78/19**.

GALLOIS, R. W. 1992. *British Regional Geology - The Wealden District.* British Geological Survey.

GALLOIS, R. W. & COX, B. M. 1974. Stratigraphy of the Upper Kimmeridge Clay of the Wash area. *Bulletin of Geological Survey of Great Britain*, **47**, 1-16.

GALLOIS, R. W. & COX, B. M. 1976. The stratigraphy of the Lower Kimmeridge Clay of Eastern England. *Proceedings of the Yorkshire Geological Society*, **41**, 13-26.

GALLOIS, R. W. & MEDD, A. W. 1979. Coccolith-rich marker bands in the English Kimmeridge Clay. *Geological Magazine*, **116**, 247-260.

GALLOIS, R. W. & WORSSAM, B. C. 1993. Geology of the country around Horsham. *Memoir of the British Geological Survey*, **Sheet 302** (England & Wales).

GALLOWAY, W. E. & HOBDAY, D. K. 1983. *Terrigenous clastic depositional systems: applications to petroleum, coal and uranium exploration.* Springer-Verlag, New York.

GALLOWAY, W. E. 1989. Genetic stratigraphic sequences in basin analysis I: Architecture and genesis of flooding-surface bounded depositional units. *American Association of Petroleum Geologists Bulletin*, **73**, 125-142.

GEOMETRICS. *Operating manual - Model GR-310 Gamma Ray Spectrometer.* GeoMetrics.

GRASTY, R. L., HOLMAN, P. B. & BLANCHARD, Y. B. 1991. Transportable calibration pads for ground and airborne gamma-ray spectrometers. *Geological Survey of Canada,* **paper 90-23**.

HAMBLIN, R. J. O., CROSBY, A., BALSON, P. S., JONES, S. M., CHADWICK, R. A., PENN, I. E., & ARTHUR, M. J. 1992. *United Kingdom offshore regional report: the geology of the English Channel.* London: HMSO for the British Geological Survey.

HANCOCK, F. R. P. & MITHEN, D. P. 1987. The geology of the Humbly Grove Oilfield, Hampshire, UK. *In*: BROOKS, J. & GLENNIE, K. (eds). *Petroleum Geology of North West Europe*, Graham & Trotman, 161-170.

HAQ, B. U., HARDENBOL, J. & VAIL, P. R. 1987. Chronology of fluctuating sea-levels since the Triassic. *Science*, **235**, 1156-1166.

HAQ, B. U., HARDENBOL, J. & VAIL, P. R. 1988. Mesozoic and Cenozoic chronostratigraphy and cycles of sea-level change. *In*: WILGUS, C. K., HASTINGS, B. S., KENDALL, G. St. C., POSAMENTIER, H. W., ROSS, C. A. & VAN WAGONER, J. C. (eds). *Sea-Level Changes - An integrated approach*, Society of Economic Paleontologists and Mineralogists, Special Publication, **42**, 71-108.

HARDENBOL, J. 1992. The Mesozoic-Cenozoic global sequence stratigraphic framework. *Abstract volume for conference on sequence stratigraphy of European basins.* CNRS-IFP, Dijon, France (18-20th May 1992), 62.

HASSAN, M., HOSSIN, A. & COMBAZ, A. 1976. Fundamentals of differential gamma ray log. *The Society of Professional Well Log Analysts*, 17th Annual Logging Symposium, June 9-12, paper H.

HERBIN, J. P., MULLER, C., GEYSSANT, J. R., MELIERES, F., PENN, I. E. & GROUP, Y. 1993. Variation of the distribution of organic matter within a transgressive system tract: Kimmeridge Clay (Jurassic), England. *In*: KATZ, B. J. & PRATT, L. M. (eds). *Source rocks in a sequence stratigraphic framework*, American Association of Petroleum Geologists, Studies in Geology, **37**, 67-100.

HERBIN, J. P., FERNANDEZ-MARTINEZ, J. L., GEYSSANT, J. R., ALBANI, A. E., DECONINCK, J. F., PROUST, J. N., COLBEAUX, J. P. & VIDIER, J. P. 1995. Sequence stratigraphy of source rocks applied to the study of the Kimmeridgian/Tithonian in the north-west European shelf (Dorset/UK, Yorkshire/UK and Boulonnais/France). *Marine and Petroleum Geology*, **12**, 177-194.

HESLOP, A. 1974. Gamma-ray log response of shaly sandstone. *The Log Analyst*, **15**, 16-21.

HESSELBO, S. P. 1996. Spectral gamma-ray logs in relation to clay mineralogy and sequence stratigraphy, Cenozoic of the Atlantic Margin, offshore New Jersey. *In*: MOUNTAIN, G. S., MILLER, K. G., BLUM, P., POAG, C. W. & TWICHELL, D. C. (eds). *Proceedings of the Ocean Drilling Program Scientific Results*, **150**.

HURST, A. 1990. Natural gamma-ray spectrometry in hydrocarbon-bearing sandstones from the Norwegian Continental Shelf. *In:* HURST, A., LOVELL, M. A. & MORTON, A. C. (eds). *Geological Applications of Wireline Logs*. Geological Society Special Publication, **48**, 211-222.

IAEA, 1976. Radiometric reporting methods and calibration in uranium exploration. *International Atomic Energy Agency*, Technical Report **174**, Vienna.

INSALACO, E., HALLAM, A. & ROSEN, B. 1997. Oxfordian (Upper Jurassic) coral reefs in western Europe: reef types and conceptual depositional model. *Sedimentology*, **44**, 707-734.

IRWIN, H. 1979. On an environmental model for the type Kimmeridge Clay. *Nature*, **279**, 819.

JACOUIDES, J., KING, C. & TYKOEZINSKI, H. 1983 (unpublished). *Well 98/11-1 English Channel, stratigraphical / paleontological report - for British Gas Exploration.* Paleoservices.

JACOVIDES, J. & WOOLLAM, R. 1994 (unpublished). *Biostratigraphic analysis of British Gas wells 98/11-2 and 98/22-1B, English Channel.* Millennia Stratigraphic Consultants.

JERVEY, M. T. 1988. Quantitative geological modelling of siliciclastic rock sequences and their seismic expression. *In*: WILGUS, C. K., HASTINGS, B. S., KENDALL, C. G. St C., POSAMENTIER, H. W., ROSS, C. A. & VAN WAGONER, J. C. (eds). *Sea-Level Changes - An intergrated approach*, Society of Economic Paleontologists and Mineralogists, Special Publication, **42**, 47-69.

KARNER, G. D., LAKE, S. D., & DEWEY, J. F. 1987. The thermal and mechanical development of the Wessex Basin, southern England. *In*: COWARD, M. P., DEWEY, J. F. & HANCOCK, P. L. (eds). *Continental Extensional Tectonics*, Special Publication of the Geological Society, **28**, 517-536.

KENT, P. F. 1949. A structural contour map of the surface of the buried pre-Permian rocks of England and Wales. *Proceedings of the Geologists' Association*, **60**, 2, 87-104.

KING, C., & ALLEN, C. D. 1987 (unpublished). *Well 98/11-3 stratigraphical / paleontological report - for British Gas Exploration.* Paleoservices.

KING, C. & JACOVIDES, J. 1983 (unpublished). *Well 98/23-1 stratigraphical / paleontological report - for British Gas Exploration.* Paleoservices.

KING, C., JACOVIDES, J. & SHAW, D. 1987 (unpublished). *Well 98/11-4 stratigraphical / paleontological report - for British Gas Exploration.* Paleoservices.

LAKE, R. D. & SHEPHARD-THORN, E. R. 1987. Geology of the country around Hastings and Dungeness. *Memoir of the British Geological Survey*, **Sheet 320 and 321** (England & Wales).

LAKE, R. D., YOUNG, B., WOOD, C. J. & MORTIMORE, R. N. 1987. Geology of the country around Lewes. *Memoir of the British Geological Survey*, **Sheet 319** (England & Wales).

LAKE, S. D. & KARNER, G. D. 1987. The structure and evolution of the Wessex Basin, southern England: an example of inversion tectonics. *Tectonophysisc*, **137**, 347-378.

LOUTIT, T. S., HARDENBOL, J., VAIL, P. R. & BAUM, G. R. 1988. Condensed sections; the key to age determination and correlation of continental margin sequences. *In*: WILGUS, C. K., HASTINGS, B. S., KENDALL, C. G. St C., POSAMENTIER, H. W., ROSS, C. A. & VAN WAGONER, J. C. (eds). *Sea-Level Changes - An intergrated approach,* Society of Economic Paleontologists and Mineralogists, Special Publication, **42**, 183-213.

LØVBORG, L. 1984. *The calibration of portable and airborne gamma-ray spectrometers - theory, problems and facilities*, Report Risø-M-2456, Risø National Laboratory, Denmark.

LØVBORG, L. & MOSE, E. 1987. Counting statistics in radioelement assaying with a portable spectrometer. *Geophysics*, **52**, 555-563.

LØVBORG, L., WOLLENBERG, H., SORENSEN, P. & HANSEN, J. 1971. Field determination of uranium and thorium by gamma-ray spectrometry, exemplified by measurements in the Ilimaussaq alkaline intrusion, South Greenland. *Economic Geology*, **66**, 368-384.

MACQUAKER, J. H. S. & GAWTHORPE, R. L. 1993. Mudstone lithofacies in the Kimmeridge Clay Formation, Wessex Basin, southern England: implications for the origin and controls of the distribution of mudstones. *Journal of Sedimentary Petrology*, **63**, 1129-1143.

MANN, C. J. 1979. Obstacles to quantitative lithostratigraphic correlation. *In*: GILL, D. & MERRIAM, D. F. (eds). *Geomathematical and petrophysical studies in sedimentology*, Pergamon Press.

MANN, K. O., LANE, H. R. & SCHOLLE, P. A. 1995. Graphic correlation, *Society of Economic Paleontologists and Mineralogists, Special Publication*, **53**.

MARTINSON, D. G., MENKE, W. & STOFFA, P. 1982. An inverse approach to signal correlation. *Journal of Geophysical Research*, **87**, 4807-4818.

MARTINSON, D. G., MENKE, W. & STOFFA, P. 1984. Reply to Comments on "An inverse approach to signal correlation" by SHURE, L & CHAVE, A. D. *Journal of Geophysical Research*, **89**, 2501-2504.

MATUSZAK, D. R. 1972. Stratigraphic Correlation of Subsurface Geologic Data by Computer. *Mathematical Geology*, **4**, 331-343.

MCKENZIE, D. 1978. Some remarks on the development of sedimentary basins. *Earth and Planetary Science Letters*, **40**, 25-32.

MELNYK, D. H., ATHERSUCH, J. & SMITH, D. G. 1992. Estimating the dispersion of biostratigraphic events in the subsurface by graphic correlation: an example from the Late Jurassic of the Wessex Basin, UK. *Marine and Petroleum Geology*, **9**, 602-607.

MELNYK, D. H., SMITH D. G. & AMIRI-GARROUSSI, K. 1994. Filtering and frequency mapping as tools in subsurface cyclostratigraphy, with examples from the Wessex Basin, UK. *In*: DE BOER, P. L. & SMITH, D. G. (eds). *Orbital forcing and cyclic sedimentary sequences*, International Association of Sedimentologists, Special Publication **19**, 35-46.

MELNYK, D. H., ATHERSUCH, J., AINSWORTH, N. & BRITTON, P. D. 1995. Measuring the dispersion of ostracod and foraminifer extinction events in the subsurface Kimmeridge Clay and Portland beds, Upper Jurassic, United Kingdom. *In*: MANN, K. O., LANE, H. R. & SCHOLLE, P. A. (eds). *Graphic correlation*, Society of Economic Paleontologists and Mineralogists, Special Publication, **53**, 185-203.

MIALL, A. D. 1997. *The Geology of Stratigraphic Sequences*. Springer-Verlag.

MILLER, R. G. 1990. A paleoceanographic approach to the Kimmeridge Clay Formation. *In*: HUC, A. Y. (ed.). *Deposition of organic facies*. American Association of Petroleum Geologists, Studies in Geology **30**, 13-26.

MITCHUM, R. M. 1977. Seismic stratigraphy and global changes of sea-level, Part 1: glossary of terms used in seismic stratigraphy. *In*: PAYTON, C. E. (ed.). *Seismic stratigraphy - applications to hydrocarbon exploration.* American Association of Petroleum Geologists Memoir, **26**, 205-212.

MORAN, J. H., COUFLEAU, M. A., MILLER, G. K. & TIMMONS, J. P. 1962. Automatic computation of dipmeter logs digitally recorded on magnetic tapes. *Journal of Petroleum Technology*, **14**, 771-782.

MYERS, K. J. 1987. *Onshore-outcrop gamma-ray spectrometry as a tool in sedimentological studies*. PhD thesis, University of London.

MYERS, K. J. & WIGNALL, P. B. 1987. Understanding Jurassic organic-rich mudrocks - new concepts using gamma-ray spectrometry and palaeoecology: examples from the Kimmeridge Clay of Dorset and the Jet Rock of Yorkshire. *In*: LEGGETT, J. K. & ZUFFA, G. G. (eds). *Marine Clastic Sedimentology - concepts and case studies*, Graham & Trotman, London, 172-189.

MYERS, K. J. & BRISTOW, C. S. 1989. Detailed sedimentology and gamma-ray log characteristics of a Namurian deltaic succession II: gamma-ray logging. *In*: WHATELEY, M. K. G. & PICKERING, K. T. (eds). *Deltas: Sites and traps for fossil fuels*, Geological Society Special Publication, **41**, 81-88.

NEAL, J. E., STEIN, J. A. & GAMBER, J. H. 1995. Integration of the graphic correlation methodology in a sequence stratigraphic study: examples from North Sea Paleogene sections. *In:* MANN, K. O. & LANE, H. R. (eds). *Graphic Correlation*, Society of Economic Paleontologists and Mineralogists, Special Publication **53**, 95-113.

NORTH, F. K. 1990. *Petroleum Geology*. Unwin Hyman, Boston.

OLEA, R. A. 1988. CORRELATOR -- An interactive computer system for lithostratigraphic correlation of wireline logs. *Kansas Geological Survey Petrophysical Series*, **4**.

OLEA, R. A. 1994. Expert systems for automated correlation and Interpretation of Wireline Logs. *Mathematical Geology*, **26,** 879-897.

OSCHMANN, W. 1988. Kimmeridge clay sedimentation - a new cyclic model. *Palaeogeography, Palaeoclimatology, Palaeoecology*, **65**, 217-251.

OSCHMANN, W. 1991. Anaerobic-Poikiloaerobic-Aerobic: a new facies zonation for modern and ancient neritic redox facies. *In:* EINSELE, G., RICKEN, W. & SEILACHER, A. *Cycles and events in stratigraphy*, Springer-Verlag, 565-571.

PARKINSON, D. N. 1996. Gamma-ray spectrometry as a tool for stratigraphical interpretation: examples from the western European Lower Jurassic. *In*: HESSELBO, S. P. & PARKINSON, D. N. (eds). *Sequence Stratigraphy in British Geology*, Geological Society Special Publication, **103**, 103-255.

PARTINGTON, M. A., MITCHENER, B. C., MILTON, N. J. & FRASER, A. J. 1993. Genetic sequence stratigraphy for the North Sea Late Jurassic and Early Cretaceous: distribution and prediction of Kimmeridgian - Late Ryazanian in the North Sea and adjacent areas. *In:* PARKER, J. R. (ed.). *Petroleum Geology of Northwest Europe: proceedings of the 4th conference*. The Geological Society, London, 347-370.

PAYTON, C. E. (ed.)1977. Seismic stratigraphy-applications to hydrocarbon exploration. *Ammerican Association of Petroleum Geologists Memoir* **26**.

PENN, I. E., COX, B. M. & GALLOIS, R. W. 1986. Towards precision in stratigraphy: geophysical log correlation of Upper Jurassic (including Callovian) strata of the Eastern England Shelf. *Journal of the Geological Society, London*, **143**, 381-410.

PENN, I. E., CHADWICK, R. A, HOLLOWAY, S., ROBERTS, G., PHARAOH, T. C., ALLSOP, J. M., HULBERT, A. G. & BURNS, I. M. 1987. Principal features of the hydrocarbon prospectivity of the Wessex - Channel Basin, UK. *In:* BROOKS, J. & GLENNIE, K. (eds). *Petroleum Geology of North West Europe*, Graham & Trotman, 109-118.

PERKINS, S. 1982 (unpublished). *Detention No. 1 - Final geological report.* Conoco (UK) LTD.

POSAMENTIER, H. W., JERVEY, M. T. & VAIL, P. R. 1988. Eustatic controls on clastic deposition I - conceptual framework. *In*: WILGUS, C. K., HASTINGS, B. S., KENDALL, C. G. St C., POSAMENTIER, H. W., ROSS, C. A. & VAN WAGONER, J. C. (eds). *Sea-Level Changes - An intergrated approach*, Society of Economic Paleontologists and Mineralogists, Special Publication, **42**, 109-124.

PRENSKY, S. E. 1996. Bibliography of Well-Log Applications, Open-File Report 95-0064, *U. S. Department of the Interior, U. S. Geological Survey.*

PROSSER, S. & HOWELL, J. 1994 (unpublished). *Seismic and Sequence Stratigraphy Course for PhD Students*. Oxford Brookes University.

QUINIF, Y., CHARLET, J. M. & DUPUIS, C. 1982. Geochimie des radioelements: une nouvelle methode d'interpretation. Annales de la Societe Geologique de Belgique, **105**, 223-233.

QUIREIN, J. A., GARDEN, J. S. & WATSON, J. T. 1982. Combined natural gamma ray spectral/litho-density measurements applied to complex lithologies. *Society of Petroleum Engineers*. SPE **11143**, 1-14.

RIDER, M. H. 1990. Gamma-ray log shape used as a facies indicator: critical analysis of an oversimplified methodology. *In*: HURST, A., LOVELL, M. A. & MORTON, A. C. (eds). *Geological Applications of Wireline Logs*. Geological Society Special Publication, **48**, 27-37.

RIDER, M. H. 1986. *The geological interpretation of well logs*. Whittles Publishing, Caithness.

RIDER, M. H. 1991. *The geological interpretation of well logs*. Revised edition, Whittles Publishing, Caithness.

RIDER, M. H. 1996. *The geological interpretation of well logs*. Second edition, Whittles Publishing, Caithness.

RIOULT, M., DUGUE, O., JAN DU CHENE, R., PONSOT, C., FILY, G., MORON, J. & VAIL, P. R. 1991. Outcrop Sequence stratigraphy of the Anglo-Paris Basin, Middle to Upper Jurassic (Normandy, Maine, Dorset). *Bulletin des Centres de Reecheres Exploration-Production Elf-Aquitaine*, **15**, 101-194.

ROBINSON, J. E. 1975. Transforms to Enhance Correlation of Mechanical Well Logs. *Mathematical Geology*, **7**, 323-334.

RUDMAN, A. J. & LANKSTON, R. W. 1973. Stratigraphic correlation of well logs by computer techniques. *American Association of Petroleum Geologists Bulletin*, **57**, 577-588.

RUSKA INSTRUMENT CORPORATION 1973. *Ruska universal porometer - operating instructions*. Ruska Instrument Corporation, Houston, Texas.

SCHLUMBERGER 1989. *Log interpretation principles / applications*. Schlumberger Educational Services, Houston, Texas.

SCHLUMBERGER 1994. *Log interpretation charts.* Schlumberger Wireline & Testing, Houston, Texas.

SELLEY, R. C. 1976. Subsurface environmental analysis of North Sea sediments. *American Association of Petroleum Geologists Bulletin*, **60**, 184-195.

SELLWOOD, B. W. & WILSON, R. C. L. 1990. Jurassic sedimentary environments of the Wessex Basin, with contributions from I.M. West and A. Clitheroe. *Field Guide (No 7) for the 13th International Sedimentological Congress*, Nottingham, British Sedimentological Research Group.

SERRA, O. 1984. *Fundamentals of well-log interpretation 1. The acquisition of logging data.* Developments in Petroleum Science 15A. Elsevier.

SERRA, O. & SULPICE, L. 1975. Sedimentological analysis of sand-shale series from well logs. *The Society of Professional Well Log Analysts*, 16th Annual Logging Symposium, paper W, 1-23.

SERRA, O., BALDWIN, J., & QUIREIN, J., 1980. Theory, interpretation, and practical applications of natural gamma-ray spectroscopy, *Society of Professional Well Log Analysts*, 21st annual logging symposium transactions, paper Q. Reprinted in 1990, *In*: FOSTER, N. H., & BEAUMONT, E. A. (eds). Formation evaluation I--log evaluation: *American Association of Petroleum Geologists,* Treatise of Petroleum Geology Reprint Series, **16**, p. 297-326.

SHAW, A. B. 1964. *Time in stratigraphy.* New York, McGraw-Hill.

SHAW, B. R. & CUBITT, J. M. 1979. Stratigraphic correlation of well logs: an automated approach. *In*: GILL, D. & MERRIAM, D. F. (eds). *Geomathematical and petrophysical studies in sedimentology*, Pergamon Press.

SLATT, R. M., JORDAN, D. W., D'AGOSTINO, A. E. & GILLESPIE, R. H. 1992. Outcrop gamma-ray logging to improve understanding of subsurface well log correlation. *In:* HURST, A., GRIFFITHS, C. M. & WORTHINGTON, P. F. (eds). *Geological Applications of Wireline Logs II*, Geological Society Special Publication, **65**, 3-19.

SMITH, N. 1985. Contours on the top of the Pre-Permian surface of the United Kingdom (south). *British Geological Survey 150th Anniversary Publication.*

SUN, S. Q. 1989. A new interpretation of the Corallian (Upper Jurassic) cycles of the Dorset coast, Southern England. *Geological Journal*, **24**, 139-158.

SUN, S. Q. 1992. A storm-dominated offshore sandstone interval from the Corallian Group (upper Jurassic), Weald Basin, southern England. *Marine and Petroleum Geology*, **9**, 274-286.

SUN, S. Q. & WRIGHT, V. 1989. Peloidal fabrics in Upper Jurassic reefal limestones, Weald Basin, southern England. *Sedimentary Geology*, **65**, 165-181.

SUN, S. Q., Fallick, A. E. & Williams, B. P. J. 1992. Influence of original fabric on subsequent porosity evolution: an example from the Corallian (Upper Jurassic) reefal limestones, the Weald Basin, southern England. *Sedimentary Geology*, **79**, 139-160.

SYKES, R. M. & CALLOMON, J. H. 1979. The Amoeboceras zonation of the Boreal Upper Oxfordian. *Palaeontology*, **22**, 839-903.

TALBOT, M. R. 1971. Calcite cements in the Corallian Beds (Upper Oxfordian) of southern England. *Journal of sedimentary Petrology*, **41**, 261-273.

TALBOT, M. R. 1973. Major sedimentary cycles in the Corallian beds (Oxfordian) of southern England. *Palaeogeography, Palaeoclimatology, Palaeoecology*, **14**, 293-317.

TALWAR, A. D., HENDERSON, A. S. & HART, M. B. 1992. Simple gamma-ray response of the Upper Jurassic from the Dorset coast - a preliminary investigation using the scintillometer profile technique. *Proceedings of the Ussher Society*, **8**, 70-72.

TERRASCIENCES 1996. *TerraStation II Overview*. Terrasciences Inc.

TERRIS, A. P. & BULLERWELL, W. 1965. Investigations into the underground structure of Southern England. British *Association for the Advancement of Science*, 232-252.

TITTMAN, J. 1956. *Fundamentals of logging*, University of Kansas.

TYSON, R. V. 1979 (reply). On an environmental model for the type Kimmeridge Clay. *Nature*, **279**, 819-820.

TYSON, R. V., WILSON, R. C. L. & DOWNIE, C. 1979. A stratified water column environmental model for the type Kimmeridge Clay. *Nature*, **277**, 377-380.

TYSON, R. V. 1996. Sequence-stratigraphic interpretation of organic facies variations in marine siliciclastic systems: general principles and application to the onshore Kimmeridge Clay Formation, UK. *In:* HESSELBO, S. P. & PARKINSON, D. N. (eds). *Sequence Stratigraphy in British Geology*, Geological Society Special Publication, **103**, 75-76.

VAIL, P. R. 1987. Seismic stratigraphy interpretation procedure. *In*: BALLY, A. W. (ed.).*Atlas of seismic stratigraphy volume 1*. American Association of Petroleum Geologists, Studies in Geology **27**, 1-10.

VAIL, P. R. 1992. Opening address - summary Mesozoic and Cenozoic sequence stratigraphy of European basins. *Abstract volume for conference on sequence stratigraphy of European basins*. CNRS-IFP, Dijon, France (18-20th May 1992), 3-6.

VAIL, P. R. & WORNARDT, W. W. 1990. Well log - seismic sequence stratigraphy: an intergrated tool for the 90'S. *GCSSEPM Foundation Eleventh Annual Research Conference*. 379-388.

VAIL, P. R., MITCHUM, R. M. Jr. & THOMPSON, S. III. 1977. Seismic stratigraphy and global changes of sea level, part 3: relative changes in sea-level from coastal onlap. *In*:

PAYTON, C. E. (ed.). *Seismic stratigraphy - applications to hydrocarbon exploration.* Memoir of the American Association of Petroleum Geologists, **26**, 63-97.

VAN BUCHEM, F. S. P., MELNYK, D. H. & MCCAVE, I. N. 1992. Chemical cyclicity and correlation of Lower Lias mudstones using gamma ray logs, Yorkshire, UK. *Journal of the Geological Society, London*, **149**, 991-1002.

VAN WAGONER, J. C., POSAMENTIER, H. W., MITCHUM, R. M., VAIL, P. R., SARG. J. F., LOUTIT, T. S. & HARDENBOL, J. 1988. An overview of the fundamentals of sequence stratigraphy and key definitions. *In*: WILGUS, C. K., HASTINGS, B. S., KENDALL, C. G. St C., POSAMENTIER, H. W., ROSS, C. A. & VAN WAGONER, J. C. (eds). *Sea-Level Changes - An integrated approach*, Society of Economic Paleontologists and Mineralogists, Special Publication, **42**, 39-45.

VAN WAGONER, J. C., MITCHUM, R. M., CAMPION, K. M. & RAHMANIAN, V. D. 1990. Siliciclastic sequence stratigraphy in well logs, cores and outcrop: concepts for high resolution correlation of time and facies. *American Association of Petroleum Geologists,* Methods in Exploration Series, **7**.

WESSEL, P. & SMITH, W. H. F. 1991. Free software helps map and display data. *EOS Transactions American Geophysical Union*, **72**, 441.

WESSEL, P. & SMITH, W. H. F. 1995a. New Version of the Generic Mapping Tools Released. *EOS Transactions American Geophysical Union*, **76**, 329.

WESSEL, P. & SMITH, W. H. F. 1995b. *The Generic Mapping Tools (GMT) version 3.0 Technical Reference & Cookbook. SOEST/NOAA.*

WESTERN ATLAS 1992. *Introduction to Wireline Log Analysis.* Western Atlas International Inc., Houston, Texas.

WHITTAKER, A. (ed.) 1985. *Atlas of Onshore Sedimentary Basins in England and Wales: Post-Carboniferous Tectonics and Stratigraphy.* Blackie, Glasgow.

WHITTAKER, A., HOLLIDAY, D. W. & PENN, I. E. 1985. Geophysical logs in British stratigraphy. *The Geological Society: Special Report* **18.**

WIGNALL, P. B. 1989. Sedimentary dynamics of the Kimmeridge Clay: tempests and earthquakes. *Journal of the Geological Society, London*, **146**, 273-284.

WIGNALL, P. B. 1990. Bethic palaeoecology of the late Jurassic Kimmeridge Clay of England. *Special papers in palaentology*, **43**.

WIGNALL, P. B. 1991. Test of the concepts of sequence stratigraphy in the Kimmeridgian (Late Jurassic) of England and northern France. *Marine and Petroleum Geology*, **8**, 430-441.

WIGNALL, P. B. & RUFFELL, A. H. 1990. The influence of a sudden climatic change on marine deposition in the Kimmeridgian of northwest Europe. *Journal of the Geological Society, London*, **147**, 365-371.

WILSON, R. C. L. 1968. Upper Oxfordian palaeogeography of southern England. *Palaeogeography, Palaeoclimatology, Palaeoecology*, **4**, 5-28.

WILSON, R. C. L. 1991. Sequence Stratigraphy: an introduction. *Geoscientist*, **1**, 13-23.

WORSSAM, B. C. & IVIMEY-COOK, H. C. 1971. The stratigraphy of the Geological Survey Borehole at Warlingham, Surrey. *Bulletin of the Geological Survey of Great Britain*, **36**, 1-146.

WRIGHT, J. K. 1981. The Corallian rocks of north Dorset. *Proceedings of the Geologists' Association*, **92**, 17-32.

WRIGHT, J. K. 1986a. The Upper Oxford Clay at Furzy Cliff, Dorset: stratigraphy, palaeoenvironment and ammonite fauna. *Proceedings of the Geologists' Association*, **97**, 221-228.

WRIGHT, J. K. 1986b. A new look at the stratigraphy, sedimentology and ammonite fauna of the Corallian Group (Oxfordian) of south Dorset. *Proceedings of the Geologists' Association*, **97**, 1-21.

WU, X. & NYLAND, E. 1987. Automated stratigraphic interpretation of well-log data. *Geophysics*, **52**, 1665-1676.

YOUNG, B. & LAKE, R. D. 1988. Geology of the country around Brighton and Worthing. *Memoir of the British Geological Survey*, **Sheet 318 and 333** (England & Wales).

ZIEGLER, P. A. 1982. *Geological atlas of Western and Central Europe*. Shell Internationale Petroleum Maatschappij.

APPENDIX A

List of boreholes used in this study

This appendix contains a list of all the boreholes used in this study. A list of the wireline logging tool mnemonics used in this thesis can also be found in this appendix.

Table A.1 List of all the boreholes used in this study which contained wireline data.

WELL NAME	LAT. WGS 84	LONG. WGS 84	NATIONAL GRID	CAL	SP	GR	SON	NEUT	DEN	RES	KB (M)	DATE	OPERATOR
Alandale	53.71939	-0.485	TA 00070 25840			*					7.6	1972	BGS
Arne G1	50.68292	-2.06156	SY 95750 87040	*		*		*	*		7.93	1975	British Gas
Arreton 1	50.66794	-1.25042	SZ 53070 85640			*					38.1	1952	D' ARCY
Arreton 2	50.66939	-1.24856	SZ 53200 85800			*	*	*	*		38.1	1974	British Gas
Ashdown 1	51.05283	0.139528	TQ 50050 30350			*					189.9	1954	D' ARCY
Ashdown 2	51.04258	0.153583	TQ 51070 29240			*					178.43	1955	D' ARCY
Ashour 1	51.17594	0.236056	TQ 56400 44239			*	*	*			85.7	1981	CONOCO
Bere Regis 1	50.75994	-2.19392	SY 86420 95620			*	*				69.28	1959	BP
Bicester 1	51.88272	-1.14833	SP 58720 20810			*					87.69	1976	SHELL
Bletchingley 1	51.21242	-0.05106	TQ 36225 47727			*	*		*		68.6	1965	ESSO
Bolney 1	51.0035	-0.17689	TQ 28011 24269			*	*				70.8	1963	ESSO
Brigg 1	53.54397	-0.44147	TA 03370 06391			*	*				13.7	1981	BP
Brightling 1	50.97144	0.380778	TQ 67250 21820			*				*	152.7	1955	BP
Brill	51.82181	-1.04817	SP 65700 14120			*					0	1986	BGS
Chaldon Herring 1	50.65431	-2.3075	SY 78360 83900			*					87.17	1955	D' ARCY
Chaldon Herring G3	50.65547	-2.3075	SY 78360 84030			*					79.25	1955	D' ARCY
Chatham	51.39592	0.545083	TQ 77150 69400	*	*						20		
Cleethorpes	53.54428	-0.03594	TA 30237 07090			*	*				12.2	1984	D of E / BGS
Collendean Farm 1	51.18414	-0.21572	TQ 24800 44290		*	*	*	*		*	84.5	1964	ESSO
Cooles Farm 1	51.62797	-1.97769	SU 01641 92135			*	*				96.5	1976	SHELL
Cowden 1	51.16539	0.096528	TQ 46680 42778		*	*	*			*	125.5	1971	BALL & COLLINS
Cranbourne 1	50.88108	-1.95294	SU 03408 09073			*	*				68.3	1972	BP
Denver Sluice 1	52.58403	0.347083	TF 59110 01060			*					0	1972	Water Board
Detention 1	51.13433	0.496806	TQ 74781 40200			*	*	*	*		58.8	1981	CONOCO
Donington-on-Bain	53.31931	-0.14006	TF 23990 81880			*					73.2	1975	BGS
Encombe	50.60028	-2.07964	SY 94460 77850	*		*			*	*	0	1965	
Farley South 1	51.05556	-1.66481	SU 23589 28529	*		*	*				69.49	1980	SHELL
Fordingbridge 1	50.90531	-1.73458	SU 18760 11800			*	*				69.8	1958	BP
Gayton	52.74764	0.558722	TF 72800 19740			*					0	1970	BGS
Hartwell	51.80306	-0.85192	SP 79260 12230	*	*	*		*	*	*	0	1976	BGS
Heathfield 7	50.97092	0.257389	TQ 58590 21490			*					160.78	1955	D'ARCY
Helpringham 1	52.93406	-0.25278	TF 17530 38840			*		*			7.6	1969	BP
Henfield 1	50.91847	-0.32281	TQ 17990 14570		*					*	11	1936	D' ARCY
Humbly Grove 1	51.19831	-0.98308	SU 71150 44840	*	*	*	*	*		*	142.65		CARLESS
Hunmanby 1	54.16628	-0.27047	TA 13010 75880			*	*				4.15	1973	BURMAH
Hunstanton 1	52.95494	0.517806	TF 69230 42700			*	*				10.7	1969	Place Oil & Gas Ltd.
Hunstanton IGS	52.93792	0.506972	TF 68570 40780		*	*					21.3	1970	BGS
Kimmeridge K5	50.61372	-2.13678	SY 90420 79350			*					32.6	1980	BP
Lockerley 1	51.03167	-1.56389	SU 30680 25910	*		*	*	*	*		43.89	1981	SHELL
Marchwood 1	50.89867	-1.43386	SU 39910 11180		*	*	*	*	*	*	0	1980	IGS
Marham	52.64319	0.51875	TF 70510 08030			*					0	1970	BGS
Middleton 1	50.80392	-0.61842	SU 97450 01400			*	*				6.71	1971	PENZOIL
Nettleton	53.45267	-0.31714	TF 11847 96420			*					166.5	1972	Candecca Resources
Nettleton Bottom	53.46853	-0.30681	TF 12490 98200			*	*		*		101.1	1979	D of E / BGS
North Runcton 1	52.71892	0.427306	TF 64040 16240			*		*	*		15.9	1974	BGS
North Wootton 1	52.79361	0.436639	TF 64390 24570			*					0	1972	Water Board
Parson Drove 1	52.67478	0.038639	TF 37930 10520			*					1.85	1979	BGS
Risby 1	53.80847	-0.46678	TA 01057 35778			*					51.4	1972	Candecca Resources
Sandhills 1	50.71542	-1.35392	SZ 45710 90850	*		*	*	*	*	*	26.97	1982	BRITISH GAS
Seabarn Farm	50.62328	-2.52967	SY 62630 80540	*		*	*			*	0	1978	BGS
Shalford 1	51.21192	-0.59536	SU 98210 46800			*	*				48.6	1958	BP
Shapwick1	50.81153	-2.08253	ST 94284 01342			*	*				89.9	1968	BP
Shrewton 1	51.17708	-1.9565	SU 03137 41989	*	*	*	*	*	*	*	142.69	1979	D of E / IGS
Sibsey 1	53.03375	0.026722	TF 35996 50408			*					6.7	1970	Ball & Collins
Skegness	53.14978	0.347889	TF 57110 63980			*					3.35	1970	BGS
Soham 1	52.34522	0.336889	TL 59280 74480			*					5.18	1955	BGS
Sonning eye 1	51.47625	-0.93297	SU 74200 75800		*	*	*			*	40.24	1974	BRALORNE
Southampton 1	50.90608	-1.41031	SU 41559 12018	*	*	*	*		*	*	7.59	1981	IGS
Spalding 1	52.71636	-0.16058	TF 24344 14781			*					3.8	1971	TEXACO Ltd.
Stoborough 1	50.67883	-2.12508	SY 91260 86590			*	*	*	*	*	11.1	1977	BRITISH GAS

WELL NAME	LAT. WGS 84	LONG. WGS 84	NATIONAL GRID	CAL	SP	GR	SON	NEUT	DEN	RES	KB (M)	DATE	OPERATOR
Strat B1	51.38169	-1.02142	SU 68200 65200			*	*				54.1	1966	ESSO
Swindon BH 2	51.69789	-1.94281	SU 04050 99910			*					103		
Tatsfield 1	51.29469	0.041722	TQ 42450 57050		*		*		*	*	200.3	1966	ESSO
Tetney Lock	53.48794	0.006889	TA 33250 00900			*	*	*			5.6	1963	BP
Ulceby Cross 1	53.24283	0.117556	TF 41400 73850			*					100.6	1970	Empress Oil
Wareham 3	50.68439	-2.13469	SY 90590 87210	*		*	*	*	*		22.86	1977	BRITISH GAS
Warlingham 1	51.29783	-0.06844	TQ 34760 57190		*	*					54.4	1958	IGS
West Walton Highway	52.69558	0.205333	TF 49130 13160			*					0	1972	Water Board
Westham 1	50.82553	0.284139	TQ 60970 05350		*					*	8.84	1973	CAMBRIAN
Wiggenhall 1	52.71247	0.358417	TF 59410 15370			*	*				3.84	1971	TEXACO Ltd.
Winchester 1	51.05347	-1.28317	SU 50340 28490			*					62.48	1960	BP
Winestead 1	53.69989	-0.07153	TA 27410 24334			*					8.9	1972	Candecca Resources
Winterbourne Kingston 1	50.78094	-2.21839	SY 84700 97960	*		*	*		*		65.1	1977	IGS
Wisbech	52.65531	0.078083	TF 40660 08425			*					2.72	1971	TEXACO Ltd.
Wytch Farm 2	50.66944	-2.01625	SY 98950 85540			*	*				11.86	1975	BRITISH GAS
Yarnbury 1	51.16867	-1.95336	SU 03357 41053			*	*				158.2	1980	CARLESS
98/11-1	50.65369	-1.83202	SZ 11874 83857	*	*	*	*	*	*	*	29.26	1983	BRITISH GAS
98/11-2	50.63048	-1.84128	SZ 11225 81274	*		*	*				32.61		BRITISH GAS
98/11-3	50.66028	-1.81198	SZ 13288 84493	*		*	*				32.61	1986	BRITISH GAS
98/11-4	50.62659	-1.83209	SZ 11875 80844	*	*	*	*			*	34.44	1987	BRITISH GAS
98/16-1	50.47283	-1.91179											BRITISH GAS

Table A.2 List of the boreholes which penetrate Upper Jurassic strata but contain no wireline data.

WELL NAME	NATIONAL GRID	LAT. WGS 84	LONG. WGS 84
Arden Moor	SE 50370 91570	54.31725	-1.22718
Ascott Farm	SP 90780 24080	51.90783	-0.68177
Battle	TQ 75730 17060	50.92616	0.499141
Brabourne	TR 07750 42360	51.14273	0.968657
Broadoak	TQ 61950 22140	50.97584	0.305495
Chaldon Down G2	SY 83200 81600	50.63378	-2.23894
Chalgrove	SU 65650 96200	51.66071	-1.05228
Chilham	TR 08800 54550	51.25182	0.990731
Daseley's Sand	TF 55910 31890	52.86189	0.3145
Egbury	SU 44480 52360	51.26861	-1.36382
Elham	TR 18000 43900	51.15275	1.115898
Eriswell	TL 74230 78870	52.38011	0.558416
Fairlight	TQ 85920 11730	50.87509	0.641265
Faringdon 1	SU 32440 93990	51.64373	-1.53259
Fredville	TR 24450 51150	51.21535	1.212502
Friar Waddon	SY 62800 85900	50.6715	-2.52782
Gedney Drove End	TF 46650 29390	52.84203	0.175936
Guestling	TQ 84140 1533	50.908	0.617806
H. Grove Hill 1	TQ 60080 13590	50.89954	0.275127
Hook Drain	TF 57210 08270	52.64935	0.322476
Hothfield	TQ 98000 46000	51.17888	0.831458
Kingsclere	SU 54750 57850	51.31708	-1.21579
M40 site investigation 9	SP 63410 04290	51.7337	-1.08319
Mountfield 1	TQ 71950 19310	50.94752	0.446468
Penhurst 1	TQ 54160 44280	51.17692	0.204056
Pluckley	TQ 92430 43300	51.15653	0.750422
Portsdown 2	SU 63950 07500	50.86342	-1.09269
Stowbridge	TF 60220 06400	52.63167	0.366022
Walkers Marsh	TF 52680 25300	52.80362	0.263481
West Lavington	ST 98980 56330	51.30603	-2.01604
Wiggenhall St. Peter	TF 60300 13190	52.69264	0.370502

Table A.3 List of boreholes in the Wessex Basin which do not penetrate any Upper Jurassic strata.

WELL NAME	NATIONAL GRID	LATITUDE WGS 84	LONGITUDE WGS 84
Apley Barn	SP 34380 10660	51.7935	-1.50292
Baggridge 1	ST 74910 57010	51.31159	-2.36138
Beverston	ST 85620 94200	51.64636	-2.20925
Bobbing	TQ 88000 64000	51.34393	0.698014
Burton	ST 68960 32840	51.09397	-2.44465
Burton Row	ST 33560 52080	51.26394	-2.95367
Charmouth	SY 34825 94355	50.74506	-2.92515
Ebbsfleet	TR 33800 62000	51.309	1.35323
Filton 1	ST 60100 70500	51.43204	-2.57537
Filton 2	ST 59300 78500	51.50391	-2.5878
Frome	ST 76320 47690	51.22785	-2.34053
Grittleton	ST 87190 76750	51.4895	-2.18591
Hamswell	ST 73480 70880	51.43624	-2.38294
Hemington	ST 72500 53000	51.27542	-2.39565
Herne	TR 15200 64000	1.087995	51.334289
Hill Lane	ST 33460 57560	-2.956121	51.313193
Hook Norton	SP 35650 35880	52.02016	-1.4819
Ivyfields 3	ST 91760 72790	51.45398	-2.12
Langton Herring 1	SY 60630 81710	50.63368	-2.55808
Ledwell	SP 40932 28209	51.95083	-1.40584
Leighterton	ST 81340 92260	51.62879	-2.271
Lyme Regis	SY 33650 93000	50.73275	-2.94156
Marston	ST 75210 45280	51.20613	-2.35626
Milbourne 1	ST 94870 87630	51.58745	-2.07546
Noke Hill	SP 53800 13000	51.81301	-1.22099
Oborne	ST 65200 18300	50.963	-2.49694
Puriton	ST 31900 40900	51.16322	-2.97533
Radipole	SY 67000 82040	50.63705	-2.46804
Richmond	SU 18000 74000	51.46464	-1.74229
Rodbourne 1	ST 93680 84060	51.55534	-2.09257
Rodmarton A	ST 93880 98010	51.68077	-2.08993
Seaborough	ST 43480 06200	50.85248	-2.80432
Severn Bridge Tunnel	ST 61000 84000	51.55348	-2.56392
Sherston	ST 84740 85420	51.5674	-2.22158
Shipton Moyne 5A	ST 89910 88650	51.59656	-2.14708
Southhall	TQ 09800 79200	51.50103	-0.4195
Stalbridge	ST 70600 17400	50.95521	-2.41997
Steeple Aston	SP 46870 25860	51.92925	-1.31977
Stowell	ST 68700 21900	50.99558	-2.44741
Stowell Park	SP 08400 11800	51.80474	-1.87959
Swang Farm 1	ST 22950 38910	51.14419	-3.10288
Tetbury	ST 90870 94820	51.65205	-2.13338
Tilmanstone	TR 28750 50550	51.20826	1.273584
Upton	SP 23150 13130	51.81628	-1.66558
West Farm	ST 76250 75180	51.47503	-2.34338
West Kington	ST 81480 77000	51.49159	-2.26817
Westfield Farm	ST 80240 78850	51.50818	-2.28613

WELL NAME	NATIONAL GRID	LATITUDE WGS 84	LONGITUDE WGS 84
Westonbirt	ST 86000 91780	51.62461	-2.20366
Willesden	TQ 20860 84770	51.54883	-0.25832
Wincanton	ST 71300 28300	51.05326	-2.41087
Winford	ST 53700 66100	51.39199	-2.66686
Withycombe Farm	SP 43190 40170	52.0582	-1.37148
Wytch Farm D5	SY 97800 85500	50.6691	-2.03252

Wireline tool mnemonics

Resistivity :	RES	Old Resistivity Logs	ohm.m
	ES	Old Resistivity Logs	ohm.m
	LLD	Laterlog Deep	mmho/m
	ILD	Deep Induction Log	mmho/m
	ILM	Medium Induction Log	mmho/m
	MSFL	Micro Sperically Focused Log	mmho/m
	SFL	Sperically Focused Log	mmho/m
Electrical:	SP	Self Potential	mV
Sonic:	SONL	Borehole Compensated Sonic	us/ft
	DT	Borehole Compensated Sonic	us/ft
	SONIC	Borehole Compensated Sonic	us/ft
Nuclear:	GR	Gamma Ray	API or CPS
	K	Potassium	ppm
	U	Uranium	ppm
	Th	Thorium	ppm
	DEN	Compensated Bulk Density	g/cm^3
	RHOB	Formation Density Compensated	g/cm^3
	NEUT	Compensated Neutron Log	ϕN
	NPHI	Compensated Neutron Log	ϕN
	CNL	Compensated Neutron Log	ϕN
Mechanical:	CALI	Caliper	Inches

Miscellaneous mnemonics:

API	American Petroleum Institute
CPS	Counts Per Second

APPENDIX B

Stratigraphic logs showing location of the field gamma-ray and density measurements

B.1 Introduction

Sections B2, B3 and B4 of this appendix contain stratigraphic logs of the Oxfordian, Kimmeridgian and Portlandian exposures used in this study to construct the field gamma-ray and density logs (Fig. B.1). The location of every total gamma-ray measurement taken with the geoMetrics GR310 and the spectral gamma-ray measurements taken with the Exploranium GR320 is shown. The location of the hand specimens used to construct the field density log is also shown.

All the total gamma-ray and spectral gamma-ray data shown in this appendix has been corrected for background radiation.

The final three sections in this appendix contains the field gamma-ray and density data in such a format which allows other workers to plot up the field logs. Section B.5 contains the gamma-ray and distance value used to construct the composite total gamma-ray field log for the Upper Jurassic succession on the Dorset coast. Section B.6 contains the spectral data and distance value used to plot up the spectral curves over part of the Kimmeridge Clay Formation. This section also contains the raw spectral gamma-ray data and an explanation of how potassium, thorium and uranium concentrations are calculated from the raw data. Section B.7 contains the data used to construct the field density log.

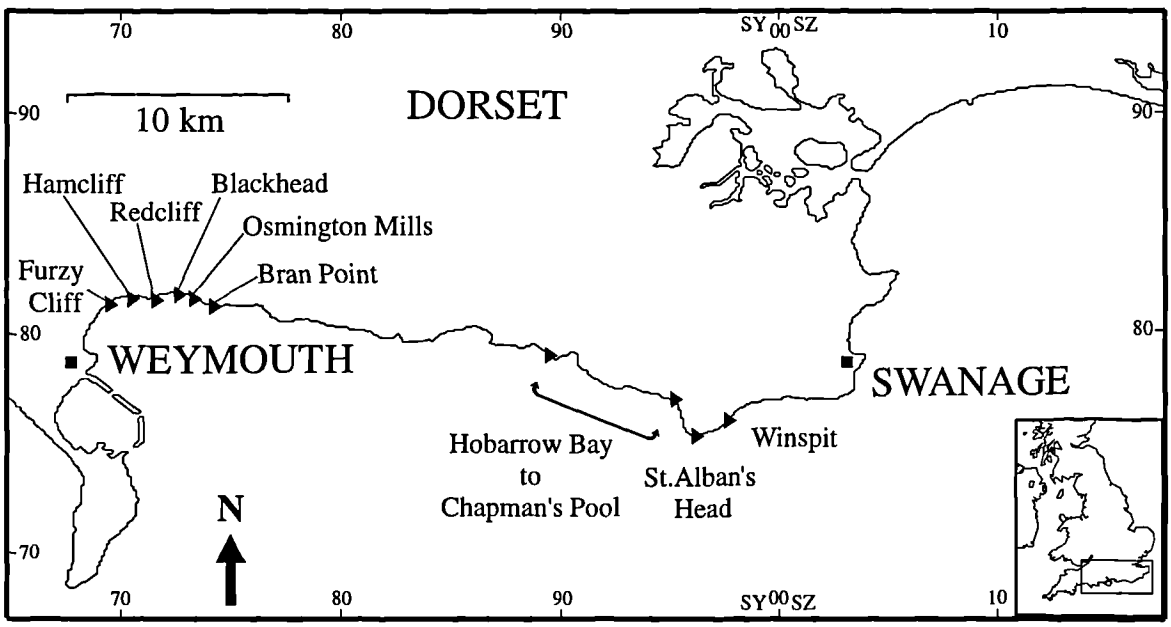

Fig. B.1 Map showing the location of the Upper Jurassic exposures on the Dorset coast.

B.2 Oxfordian

The stratigraphical / sedimentological logs seen in this section are after Coe (1992, 1995). The arrows show the location of the total gamma-ray measurements taken with the geoMetrics GR310, and the location from which hand specimens were taken to produce the field density log.

Key

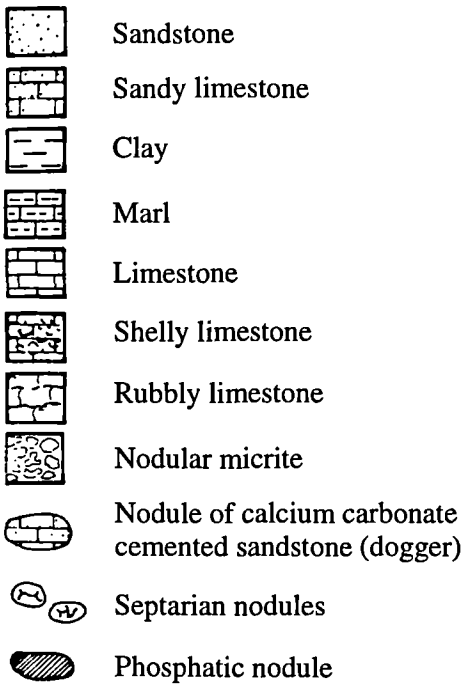

Furzy Cliff (SY 698817), Overcombe, south Dorset

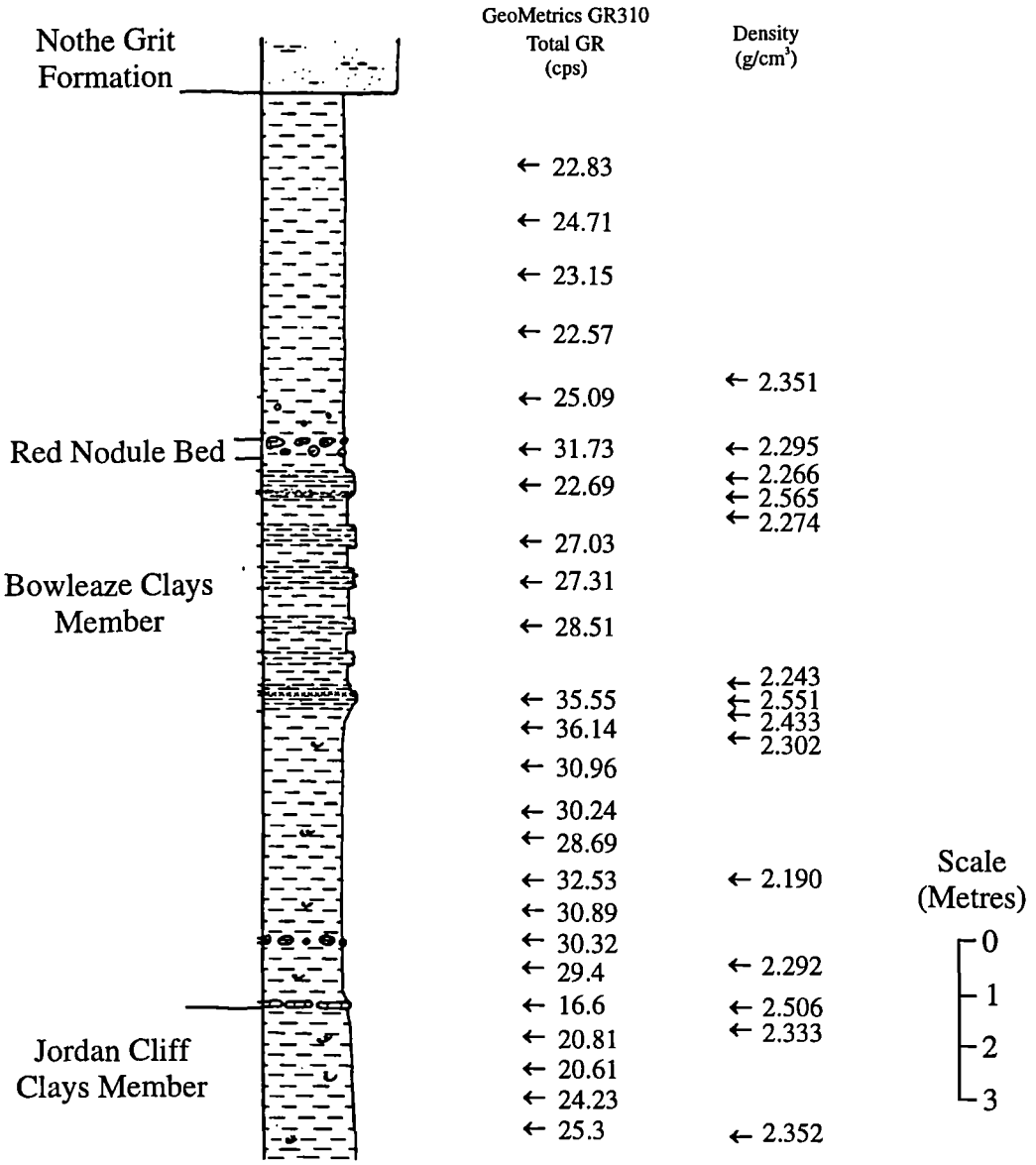

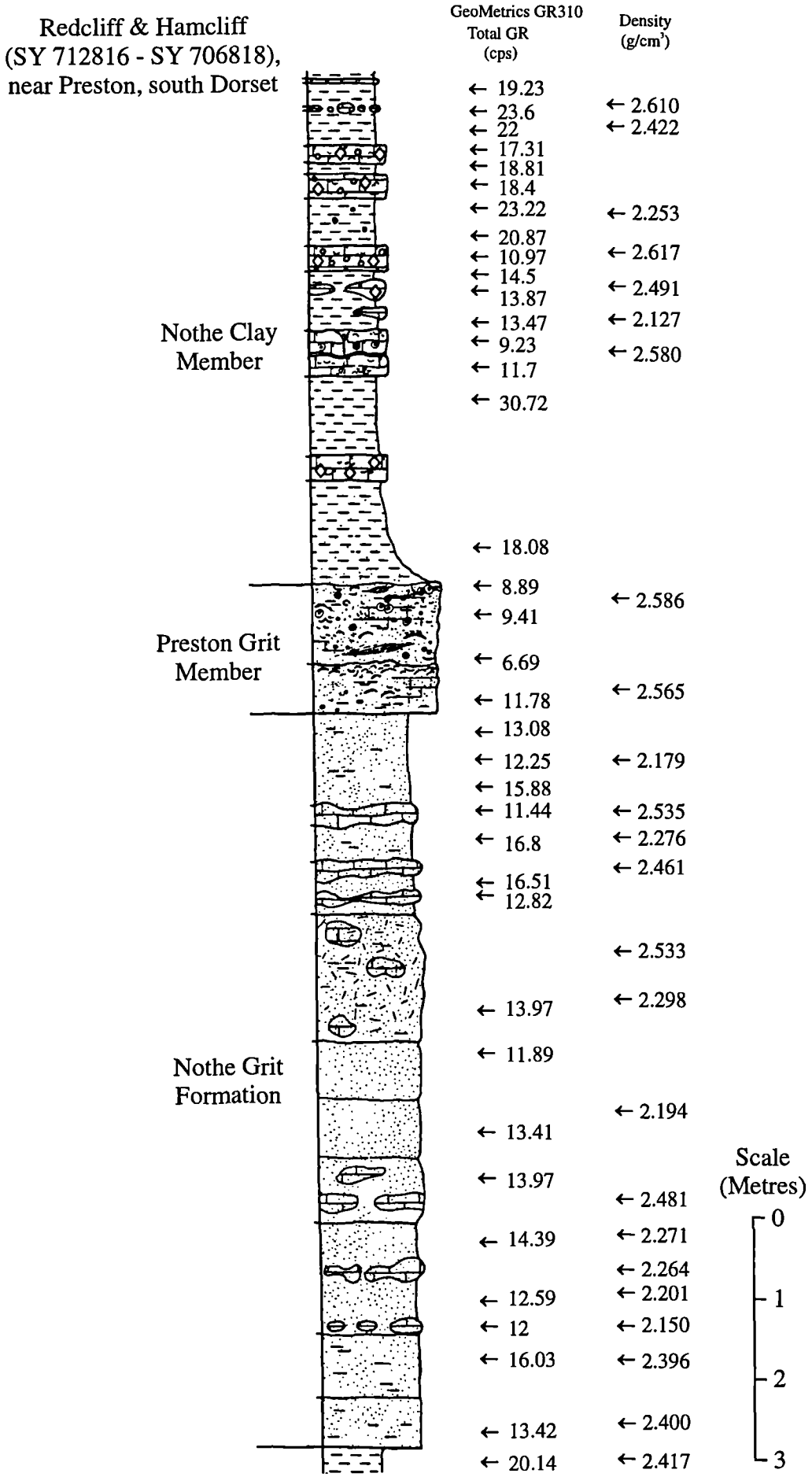
Redcliff & Hamcliff
(SY 712816 - SY 706818),
near Preston, south Dorset
GeoMetrics GR310
Total GR
(cps)
Density
(g/cm³)
Nothe Clay
Member
Preston Grit
Member
Nothe Grit
Formation
← 19.23
← 23.6
← 22
← 17.31
← 18.81
← 18.4
← 23.22
← 20.87
← 10.97
← 14.5
← 13.87
← 13.47
← 9.23
← 11.7
← 30.72
← 18.08
← 8.89
← 9.41
← 6.69
← 11.78
← 13.08
← 12.25
← 15.88
← 11.44
← 16.8
← 16.51
← 12.82
← 13.97
← 11.89
← 13.41
← 13.97
← 14.39
← 12.59
← 12
← 16.03
← 13.42
← 20.14
← 2.610
← 2.422
← 2.253
← 2.617
← 2.491
← 2.127
← 2.580
← 2.586
← 2.565
← 2.179
← 2.535
← 2.276
← 2.461
← 2.533
← 2.298
← 2.194
← 2.481
← 2.271
← 2.264
← 2.201
← 2.150
← 2.396
← 2.400
← 2.417
Scale
(Metres)
0
1
2
3

Bran Point (SY741 816 - SY744 814)

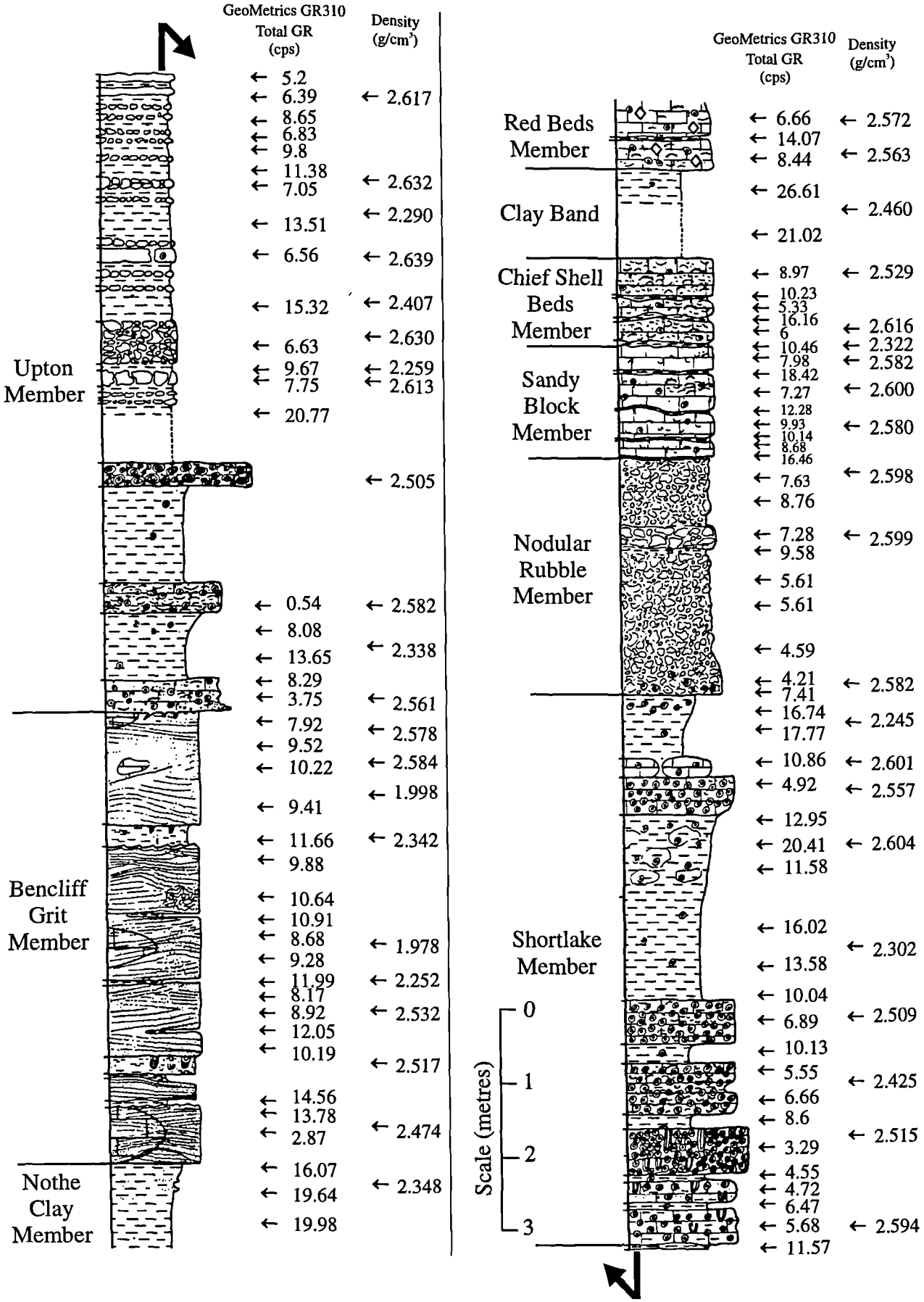

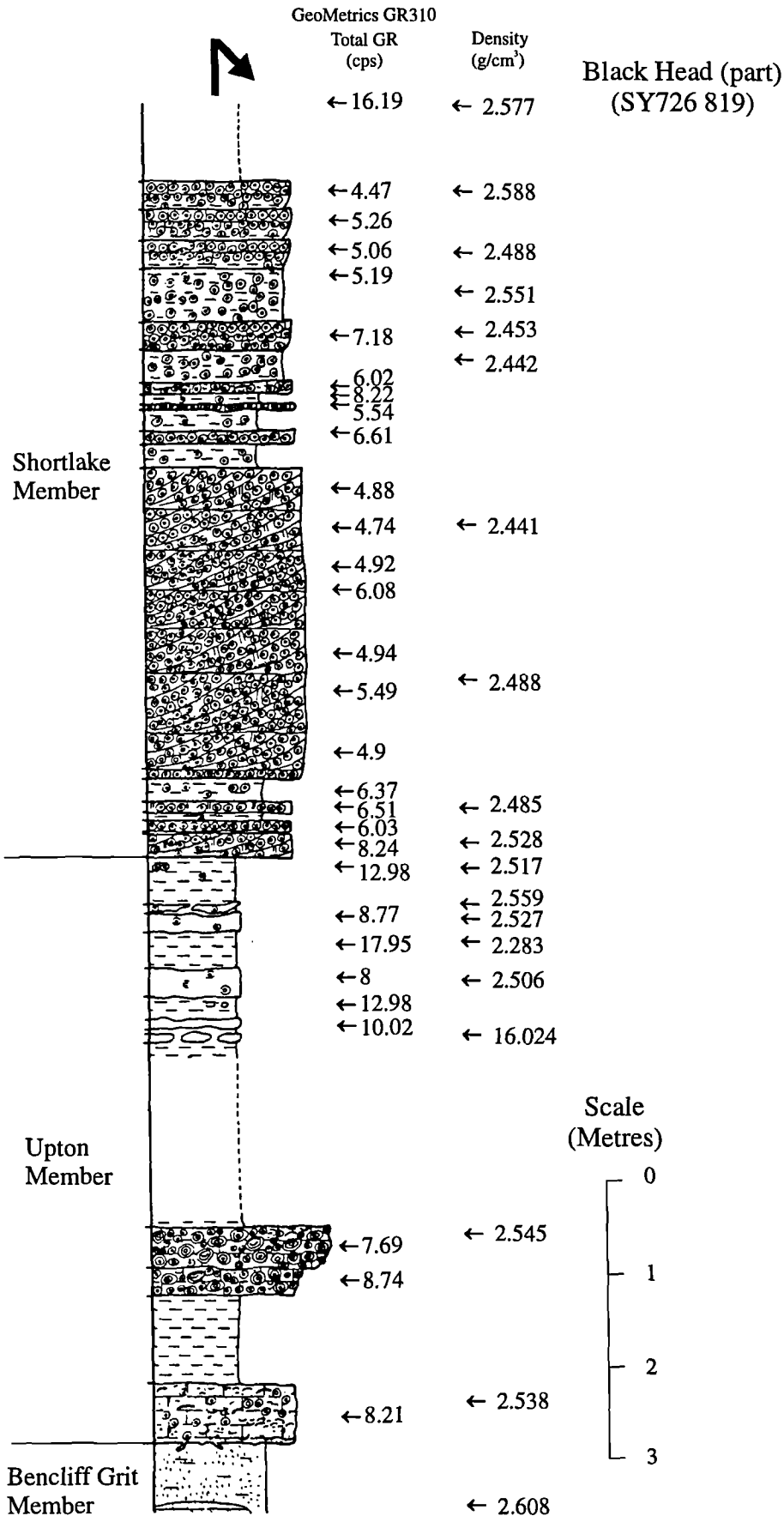
GeoMetrics GR310
Total GR (cps)
Density (g/cm³)
Black Head (part)
(SY726 819)
←16.19
← 2.577
←4.47
← 2.588
←5.26
←5.06
← 2.488
←5.19
← 2.551
←7.18
← 2.453
← 2.442
←6.02
←8.22
←5.54
←6.61
Shortlake Member
←4.88
←4.74
← 2.441
←4.92
←6.08
←4.94
←5.49
← 2.488
←4.9
←6.37
←6.51
← 2.485
←6.03
←8.24
← 2.528
←12.98
← 2.517
← 2.559
←8.77
← 2.527
←17.95
← 2.283
←8
← 2.506
←12.98
←10.02
← 16.024
Scale (Metres)
Upton Member
0
1
2
3
←7.69
← 2.545
←8.74
←8.21
← 2.538
Bencliff Grit Member
← 2.608

Black Head (continued)

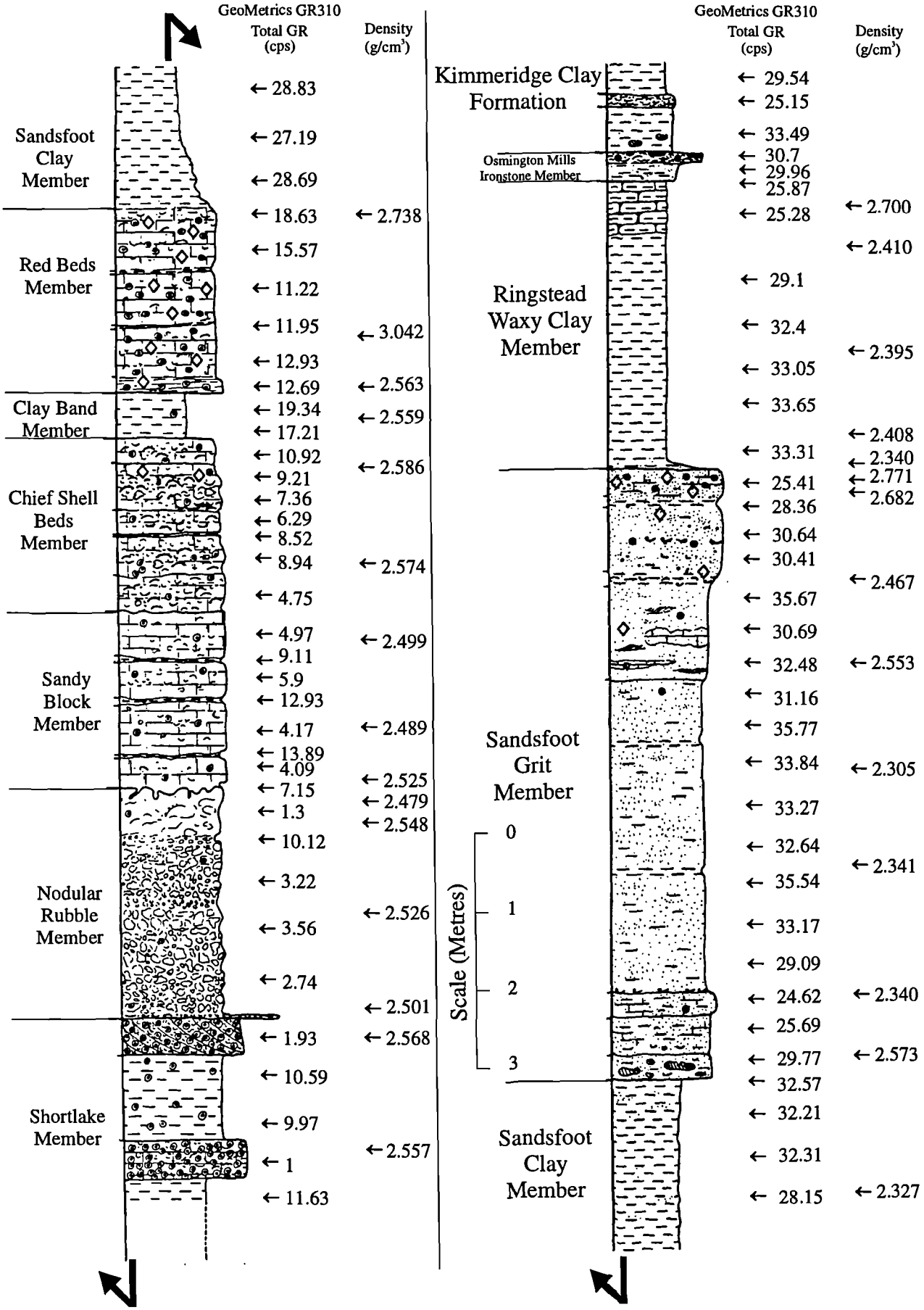

B.3 Kimmeridgian

This section contains the stratigraphical / sedimentological logs of the Kimmeridge Clay Formation. The Black Head log and the first three pages of the Hobarrow Bay to Chapman's Pool log (bed group 32 to 35) are after Cox & Gallios (1981), the rest of the logs are after Coe (1992).

The arrows show the location of the total gamma-ray measurements taken with the geoMetrics GR310, the spectral gamma-ray measurements taken with the Exploranium GR320 and the location from which hand specimens were taken to produce the field density log.

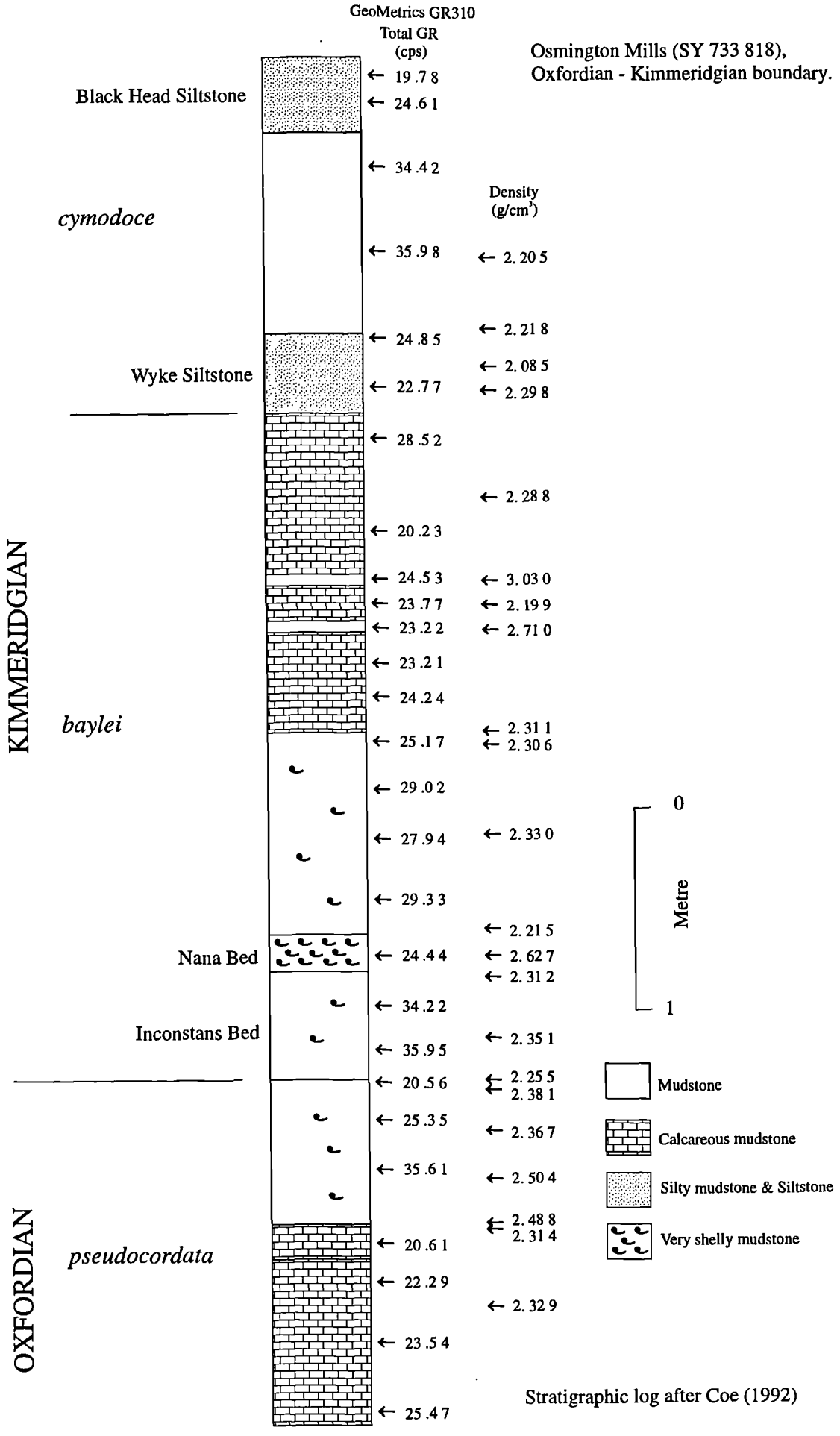
GeoMetrics GR310
Total GR
(cps)
Osmington Mills (SY 733 818),
Oxfordian - Kimmeridgian boundary.
Black Head Siltstone
← 19.7 8
← 24.6 1
← 34.4 2
Density
(g/cm³)
cymodoce
← 35.9 8
← 2.20 5
← 24.8 5
← 2.21 8
← 2.08 5
Wyke Siltstone
← 22.7 7
← 2.29 8
← 28.5 2
← 2.28 8
KIMMERIDGIAN
← 20.2 3
← 24.5 3
← 3.03 0
← 23.7 7
← 2.19 9
← 23.2 2
← 2.71 0
← 23.2 1
← 24.2 4
baylei
← 25.1 7
← 2.31 1
← 2.30 6
← 29.0 2
← 27.9 4
← 2.33 0
← 29.3 3
← 2.21 5
Nana Bed
← 24.4 4
← 2.62 7
← 2.31 2
← 34.2 2
Inconstans Bed
← 35.9 5
← 2.35 1
← 20.5 6
← 2.25 5
← 2.38 1
← 25.3 5
← 2.36 7
← 35.6 1
← 2.50 4
← 2.48 8
← 2.31 4
OXFORDIAN
pseudocordata
← 20.6 1
← 22.2 9
← 2.32 9
← 23.5 4
← 25.4 7
0
Metre
1
Mudstone
Calcareous mudstone
Silty mudstone & Siltstone
Very shelly mudstone
Stratigraphic log after Coe (1992)

Black Head (SY 7239 8195 for *baylei* & *cymodoce* zones;
SY 7259 8192 to 7258 8200 for remainder)

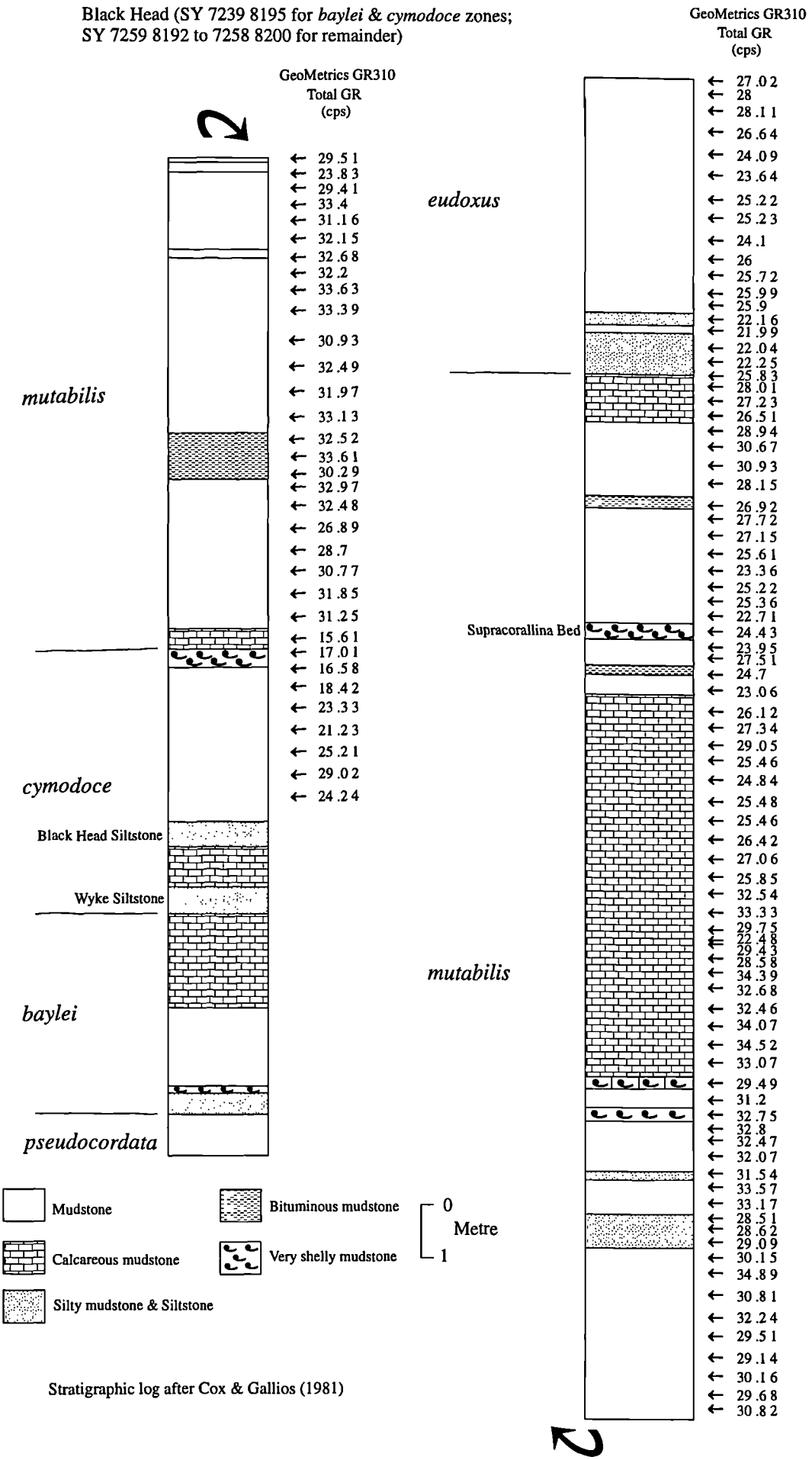

Stratigraphic log after Cox & Gallios (1981)

Kimmeridge Clay type section exposed between Hobarrow Bay and Chapman's Pool (SY896 790 - SY955 771).

Lithology Key

Oil shale

Bituminous mudstone

Semi-bituminous mudstone

Mudstone

Calcareous mudstone

Silty or sandy Calcareous mudstone

Dark-grey silty Calcareous mudstone

Dolomite, calcite, clay and silt

Coccolith limestone

Cementstone (calcite)

Cementstone (calcite) less well-defined

Cementstone (ferroan dolomite and calcite)

Calcite cemented silty or sandy mudstone

Septarian calcium carbonate nodule

{15.3} Distance from base of log (m) shown on particular page.

3 Bed Group Number of Coe (1992)

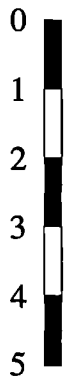

Scale (metres)

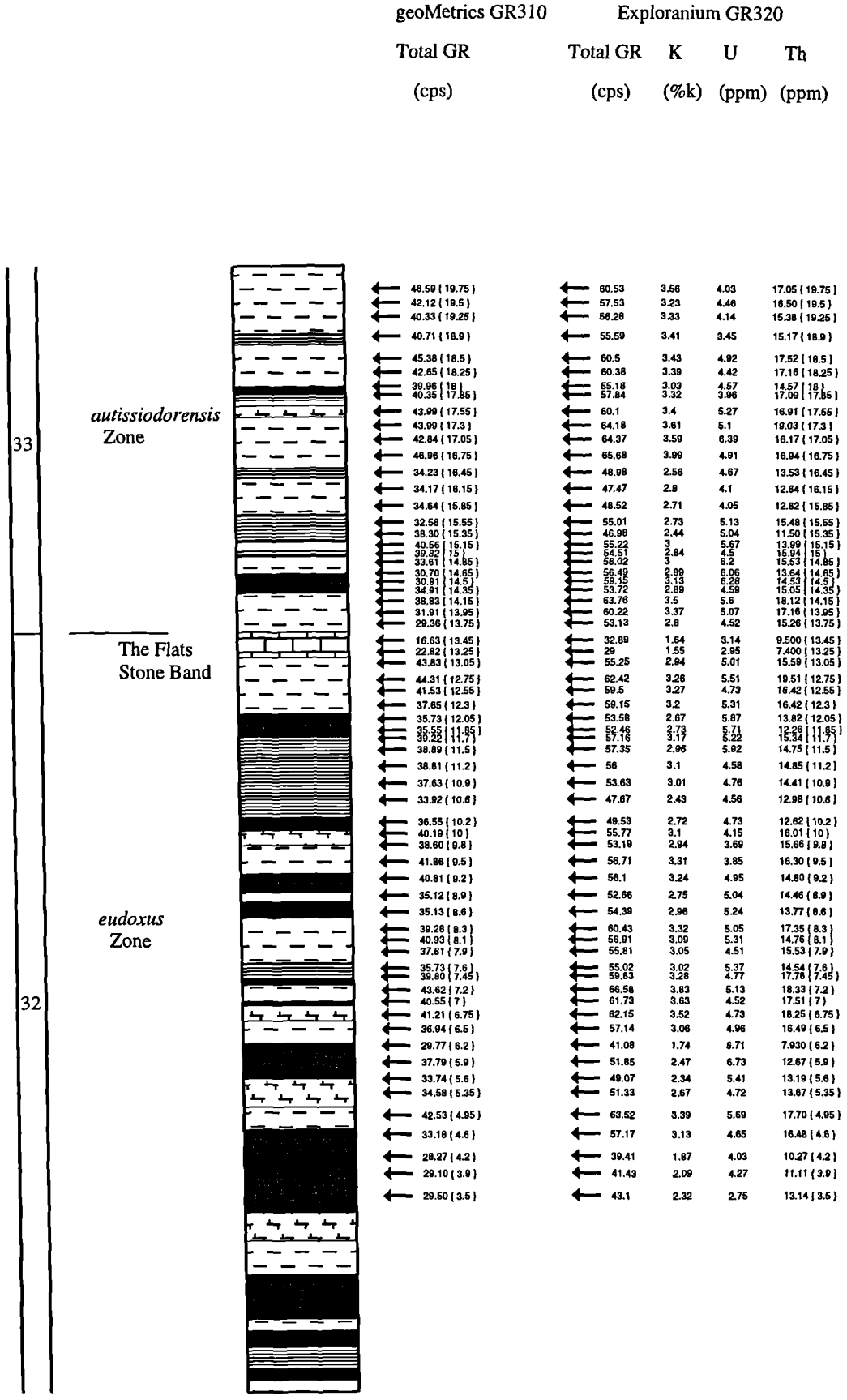
geoMetrics GR310
Exploranium GR320
Total GR
(cps)
Total GR
(cps)
K
(%k)
U
(ppm)
Th
(ppm)
33
32
autissiodorensis Zone
The Flats Stone Band
eudoxus Zone
46.59 (19.75)
42.12 (19.5)
40.33 (19.25)
40.71 (18.9)
45.38 (18.5)
42.65 (18.25)
39.96 (18)
40.35 (17.85)
43.99 (17.55)
43.99 (17.3)
42.84 (17.05)
46.96 (16.75)
34.23 (16.45)
34.17 (16.15)
34.64 (15.85)
32.56 (15.55)
38.30 (15.35)
40.56 (15.15)
39.82 (15)
33.61 (14.85)
30.70 (14.65)
30.91 (14.5)
34.91 (14.35)
38.83 (14.15)
31.91 (13.95)
29.36 (13.75)
16.63 (13.45)
22.82 (13.25)
43.83 (13.05)
44.31 (12.75)
41.53 (12.55)
37.65 (12.3)
35.73 (12.05)
35.55 (11.85)
39.22 (11.7)
38.89 (11.5)
38.81 (11.2)
37.63 (10.9)
33.92 (10.6)
36.55 (10.2)
40.19 (10)
38.60 (9.8)
41.86 (9.5)
40.81 (9.2)
35.12 (8.9)
35.13 (8.6)
39.28 (8.3)
40.93 (8.1)
37.81 (7.9)
35.73 (7.6)
39.80 (7.45)
43.62 (7.2)
40.55 (7)
41.21 (6.75)
36.94 (6.5)
29.77 (6.2)
37.79 (5.9)
33.74 (5.6)
34.58 (5.35)
42.53 (4.95)
33.18 (4.6)
28.27 (4.2)
29.10 (3.9)
29.50 (3.5)
60.53 3.56 4.03 17.05 (19.75)
57.53 3.23 4.46 16.50 (19.5)
56.28 3.33 4.14 15.38 (19.25)
55.59 3.41 3.45 15.17 (18.9)
60.5 3.43 4.92 17.52 (18.5)
60.38 3.39 4.42 17.16 (18.25)
55.18 3.03 4.57 14.57 (18)
57.84 3.32 3.96 17.09 (17.85)
60.1 3.4 5.27 16.91 (17.55)
64.18 3.61 5.1 19.03 (17.3)
64.37 3.59 6.39 16.17 (17.05)
65.68 3.99 4.91 16.94 (16.75)
48.98 2.56 4.67 13.53 (16.45)
47.47 2.8 4.1 12.64 (16.15)
48.52 2.71 4.05 12.62 (15.85)
55.01 2.73 5.13 15.48 (15.55)
46.98 2.44 5.04 11.50 (15.35)
55.22 3 5.67 13.99 (15.15)
54.51 2.84 4.5 15.94 (15)
56.02 3 6.2 15.53 (14.85)
56.49 2.89 6.06 13.64 (14.65)
59.15 3.13 6.28 14.53 (14.5)
53.72 2.89 4.59 15.05 (14.35)
63.76 3.5 5.6 18.12 (14.15)
60.22 3.37 5.07 17.16 (13.95)
53.13 2.8 4.52 15.26 (13.75)
32.89 1.64 3.14 9.500 (13.45)
29 1.55 2.95 7.400 (13.25)
55.25 2.94 5.01 15.59 (13.05)
62.42 3.26 5.51 19.51 (12.75)
59.5 3.27 4.73 16.42 (12.55)
59.15 3.2 5.31 16.42 (12.3)
53.58 2.67 5.87 13.82 (12.05)
52.46 2.73 5.71 12.26 (11.85)
57.16 3.17 5.22 15.34 (11.7)
57.35 2.96 5.92 14.75 (11.5)
56 3.1 4.58 14.85 (11.2)
53.63 3.01 4.76 14.41 (10.9)
47.67 2.43 4.56 12.98 (10.6)
49.53 2.72 4.73 12.62 (10.2)
55.77 3.1 4.15 16.01 (10)
53.19 2.94 3.69 15.66 (9.8)
56.71 3.31 3.85 16.30 (9.5)
56.1 3.24 4.95 14.80 (9.2)
52.66 2.75 5.04 14.46 (8.9)
54.39 2.96 5.24 13.77 (8.6)
60.43 3.32 5.05 17.35 (8.3)
56.91 3.09 5.31 14.76 (8.1)
55.81 3.05 4.51 15.53 (7.9)
55.02 3.02 5.37 14.54 (7.6)
59.83 3.28 4.77 17.76 (7.45)
66.58 3.83 5.13 18.33 (7.2)
61.73 3.63 4.52 17.51 (7)
62.15 3.52 4.73 18.25 (6.75)
57.14 3.06 4.96 16.49 (6.5)
41.08 1.74 6.71 7.930 (6.2)
51.85 2.47 6.73 12.67 (5.9)
49.07 2.34 5.41 13.19 (5.6)
51.33 2.67 4.72 13.67 (5.35)
63.52 3.39 5.69 17.70 (4.95)
57.17 3.13 4.65 16.48 (4.6)
39.41 1.87 4.03 10.27 (4.2)
41.43 2.09 4.27 11.11 (3.9)
43.1 2.32 2.75 13.14 (3.5)

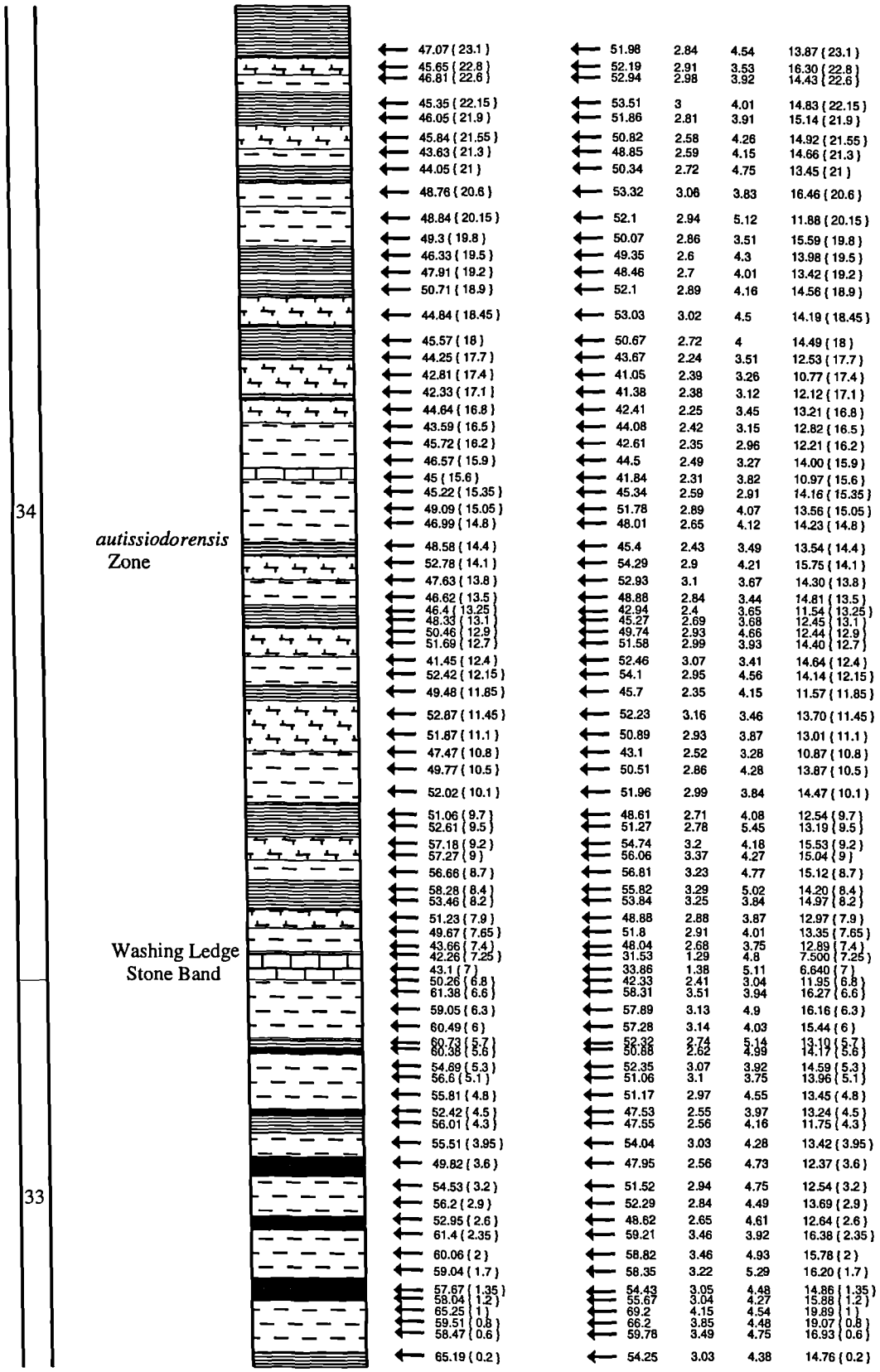
geoMetrics GR310
Exploranium GR320
Total GR (cps)
Total GR (cps)
K (%k)
U (ppm)
Th (ppm)
34
33
autissiodorensis Zone
Washing Ledge Stone Band
47.07 (23.1)
45.65 (22.8)
46.81 (22.6)
45.35 (22.15)
46.05 (21.9)
45.84 (21.55)
43.63 (21.3)
44.05 (21)
48.76 (20.6)
48.84 (20.15)
49.3 (19.8)
46.33 (19.5)
47.91 (19.2)
50.71 (18.9)
44.84 (18.45)
45.57 (18)
44.25 (17.7)
42.81 (17.4)
42.33 (17.1)
44.64 (16.8)
43.59 (16.5)
45.72 (16.2)
46.57 (15.9)
45 (15.6)
45.22 (15.35)
49.09 (15.05)
46.99 (14.8)
48.58 (14.4)
52.78 (14.1)
47.63 (13.8)
46.62 (13.5)
46.4 (13.25)
48.33 (13.1)
50.46 (12.9)
51.69 (12.7)
41.45 (12.4)
52.42 (12.15)
49.48 (11.85)
52.87 (11.45)
51.87 (11.1)
47.47 (10.8)
49.77 (10.5)
52.02 (10.1)
51.06 (9.7)
52.61 (9.5)
57.18 (9.2)
57.27 (9)
56.66 (8.7)
58.28 (8.4)
53.46 (8.2)
51.23 (7.9)
49.67 (7.65)
43.66 (7.4)
42.26 (7.25)
43.1 (7)
50.26 (6.8)
61.38 (6.6)
59.05 (6.3)
60.49 (6)
60.73 (5.7)
60.38 (5.6)
54.69 (5.3)
56.6 (5.1)
55.81 (4.8)
52.42 (4.5)
56.01 (4.3)
55.51 (3.95)
49.82 (3.6)
54.53 (3.2)
56.2 (2.9)
52.95 (2.6)
61.4 (2.35)
60.06 (2)
59.04 (1.7)
57.67 (1.35)
58.04 (1.2)
65.25 (1)
59.51 (0.8)
58.47 (0.6)
65.19 (0.2)
51.98 2.84 4.54 13.87 (23.1)
52.19 2.91 3.53 16.30 (22.8)
52.94 2.98 3.92 14.43 (22.6)
53.51 3 4.01 14.83 (22.15)
51.86 2.81 3.91 15.14 (21.9)
50.82 2.58 4.26 14.92 (21.55)
48.85 2.59 4.15 14.66 (21.3)
50.34 2.72 4.75 13.45 (21)
53.32 3.06 3.83 16.46 (20.6)
52.1 2.94 5.12 11.88 (20.15)
50.07 2.86 3.51 15.59 (19.8)
49.35 2.6 4.3 13.98 (19.5)
48.46 2.7 4.01 13.42 (19.2)
52.1 2.89 4.16 14.56 (18.9)
53.03 3.02 4.5 14.19 (18.45)
50.67 2.72 4 14.49 (18)
43.67 2.24 3.51 12.53 (17.7)
41.05 2.39 3.26 10.77 (17.4)
41.38 2.38 3.12 12.12 (17.1)
42.41 2.25 3.45 13.21 (16.8)
44.08 2.42 3.15 12.82 (16.5)
42.61 2.35 2.96 12.21 (16.2)
44.5 2.49 3.27 14.00 (15.9)
41.84 2.31 3.82 10.97 (15.6)
45.34 2.59 2.91 14.16 (15.35)
51.78 2.89 4.07 13.56 (15.05)
48.01 2.65 4.12 14.23 (14.8)
45.4 2.43 3.49 13.54 (14.4)
54.29 2.9 4.21 15.75 (14.1)
52.93 3.1 3.67 14.30 (13.8)
48.88 2.84 3.44 14.81 (13.5)
42.94 2.4 3.65 11.54 (13.25)
45.27 2.69 3.68 12.45 (13.1)
49.74 2.93 4.66 12.44 (12.9)
51.58 2.99 3.93 14.40 (12.7)
52.46 3.07 3.41 14.64 (12.4)
54.1 2.95 4.56 14.14 (12.15)
45.7 2.35 4.15 11.57 (11.85)
52.23 3.16 3.46 13.70 (11.45)
50.89 2.93 3.87 13.01 (11.1)
43.1 2.52 3.28 10.87 (10.8)
50.51 2.86 4.28 13.87 (10.5)
51.96 2.99 3.84 14.47 (10.1)
48.61 2.71 4.08 12.54 (9.7)
51.27 2.78 5.45 13.19 (9.5)
54.74 3.2 4.18 15.53 (9.2)
56.06 3.37 4.27 15.04 (9)
56.81 3.23 4.77 15.12 (8.7)
55.82 3.29 5.02 14.20 (8.4)
53.84 3.25 3.84 14.97 (8.2)
48.88 2.88 3.87 12.97 (7.9)
51.8 2.91 4.01 13.35 (7.65)
48.04 2.68 3.75 12.89 (7.4)
31.53 1.29 4.8 7.500 (7.25)
33.86 1.38 5.11 6.640 (7)
42.33 2.41 3.04 11.95 (6.8)
58.31 3.51 3.94 16.27 (6.6)
57.89 3.13 4.9 16.16 (6.3)
57.28 3.14 4.03 15.44 (6)
52.32 2.74 5.14 13.19 (5.7)
50.88 2.62 4.99 14.17 (5.6)
52.35 3.07 3.92 14.59 (5.3)
51.06 3.1 3.75 13.96 (5.1)
51.17 2.97 4.55 13.45 (4.8)
47.53 2.55 3.97 13.24 (4.5)
47.55 2.56 4.16 11.75 (4.3)
54.04 3.03 4.28 13.42 (3.95)
47.95 2.56 4.73 12.37 (3.6)
51.52 2.94 4.75 12.54 (3.2)
52.29 2.84 4.49 13.69 (2.9)
48.62 2.65 4.61 12.64 (2.6)
59.21 3.46 3.92 16.38 (2.35)
58.82 3.46 4.93 15.78 (2)
58.35 3.22 5.29 16.20 (1.7)
54.43 3.05 4.48 14.86 (1.35)
55.67 3.04 4.27 15.88 (1.2)
69.2 4.15 4.54 19.89 (1)
66.2 3.85 4.48 19.07 (0.8)
59.78 3.49 4.75 16.93 (0.6)
54.25 3.03 4.38 14.76 (0.2)

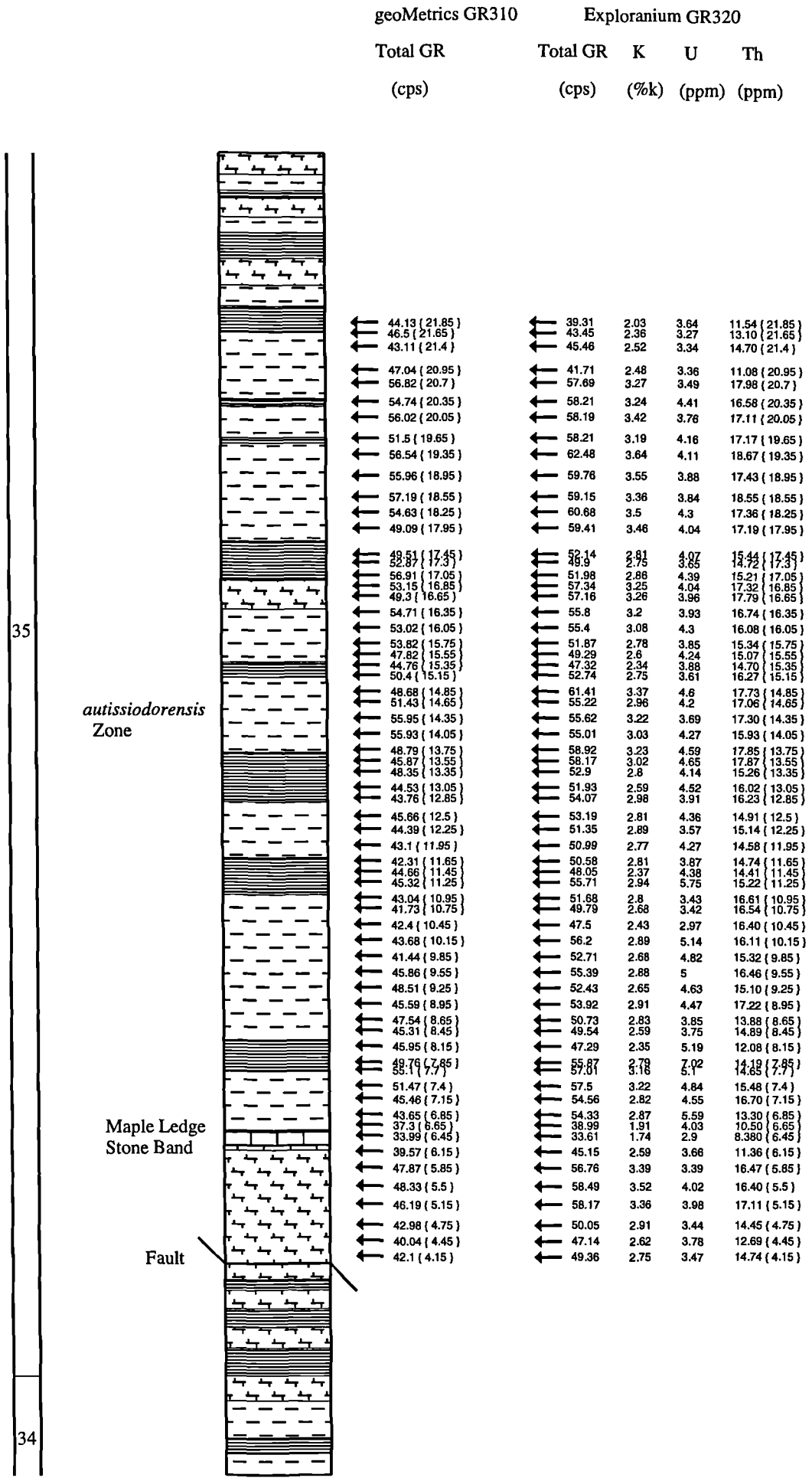
geoMetrics GR310
Total GR
(cps)
Exploranium GR320
Total GR K U Th
(cps) (%k) (ppm) (ppm)
35
34
autissiodorensis Zone
Maple Ledge Stone Band
Fault
44.13 (21.85)
46.5 (21.65)
43.11 (21.4)
47.04 (20.95)
56.82 (20.7)
54.74 (20.35)
56.02 (20.05)
51.5 (19.65)
56.54 (19.35)
55.96 (18.95)
57.19 (18.55)
54.63 (18.25)
49.09 (17.95)
49.51 (17.45)
52.87 (17.3)
56.91 (17.05)
53.15 (16.85)
49.3 (16.65)
54.71 (16.35)
53.02 (16.05)
53.82 (15.75)
47.82 (15.55)
44.76 (15.35)
50.4 (15.15)
48.68 (14.85)
51.43 (14.65)
55.95 (14.35)
55.93 (14.05)
48.79 (13.75)
45.87 (13.55)
48.35 (13.35)
44.53 (13.05)
43.76 (12.85)
45.66 (12.5)
44.39 (12.25)
43.1 (11.95)
42.31 (11.65)
44.66 (11.45)
45.32 (11.25)
43.04 (10.95)
41.73 (10.75)
42.4 (10.45)
43.68 (10.15)
41.44 (9.85)
45.86 (9.55)
48.51 (9.25)
45.59 (8.95)
47.54 (8.65)
45.31 (8.45)
45.95 (8.15)
49.76 (7.85)
55.1 (7.7)
51.47 (7.4)
45.46 (7.15)
43.65 (6.85)
37.3 (6.65)
33.99 (6.45)
39.57 (6.15)
47.87 (5.85)
48.33 (5.5)
46.19 (5.15)
42.98 (4.75)
40.04 (4.45)
42.1 (4.15)
39.31 2.03 3.64 11.54 (21.85)
43.45 2.36 3.27 13.10 (21.65)
45.46 2.52 3.34 14.70 (21.4)
41.71 2.48 3.36 11.08 (20.95)
57.69 3.27 3.49 17.98 (20.7)
58.21 3.24 4.41 16.58 (20.35)
58.19 3.42 3.76 17.11 (20.05)
58.21 3.19 4.16 17.17 (19.65)
62.48 3.64 4.11 18.67 (19.35)
59.76 3.55 3.88 17.43 (18.95)
59.15 3.36 3.84 18.55 (18.55)
60.68 3.5 4.3 17.36 (18.25)
59.41 3.46 4.04 17.19 (17.95)
52.14 2.81 4.07 15.44 (17.45)
49.9 2.75 3.65 14.72 (17.3)
51.98 2.86 4.39 15.21 (17.05)
57.34 3.25 4.04 17.32 (16.85)
57.16 3.26 3.96 17.79 (16.65)
55.8 3.2 3.93 16.74 (16.35)
55.4 3.08 4.3 16.08 (16.05)
51.87 2.78 3.85 15.34 (15.75)
49.29 2.6 4.24 15.07 (15.55)
47.32 2.34 3.88 14.70 (15.35)
52.74 2.75 3.61 16.27 (15.15)
61.41 3.37 4.6 17.73 (14.85)
55.22 2.96 4.2 17.06 (14.65)
55.62 3.22 3.69 17.30 (14.35)
55.01 3.03 4.27 15.93 (14.05)
58.92 3.23 4.59 17.85 (13.75)
58.17 3.02 4.65 17.87 (13.55)
52.9 2.8 4.14 15.26 (13.35)
51.93 2.59 4.52 16.02 (13.05)
54.07 2.98 3.91 16.23 (12.85)
53.19 2.81 4.36 14.91 (12.5)
51.35 2.89 3.57 15.14 (12.25)
50.99 2.77 4.27 14.58 (11.95)
50.58 2.81 3.87 14.74 (11.65)
48.05 2.37 4.38 14.41 (11.45)
55.71 2.94 5.75 15.22 (11.25)
51.68 2.8 3.43 16.61 (10.95)
49.79 2.68 3.42 16.54 (10.75)
47.5 2.43 2.97 16.40 (10.45)
56.2 2.89 5.14 16.11 (10.15)
52.71 2.68 4.82 15.32 (9.85)
55.39 2.88 5 16.46 (9.55)
52.43 2.65 4.63 15.10 (9.25)
53.92 2.91 4.47 17.22 (8.95)
50.73 2.83 3.85 13.88 (8.65)
49.54 2.59 3.75 14.89 (8.45)
47.29 2.35 5.19 12.08 (8.15)
55.87 2.79 7.02 14.19 (7.85)
57.01 3.16 5.1 14.65 (7.7)
57.5 3.22 4.84 15.48 (7.4)
54.56 2.82 4.55 16.70 (7.15)
54.33 2.87 5.59 13.30 (6.85)
38.99 1.91 4.03 10.50 (6.65)
33.61 1.74 2.9 8.380 (6.45)
45.15 2.59 3.66 11.36 (6.15)
56.76 3.39 3.39 16.47 (5.85)
58.49 3.52 4.02 16.40 (5.5)
58.17 3.36 3.98 17.11 (5.15)
50.05 2.91 3.44 14.45 (4.75)
47.14 2.62 3.78 12.69 (4.45)
49.36 2.75 3.47 14.74 (4.15)

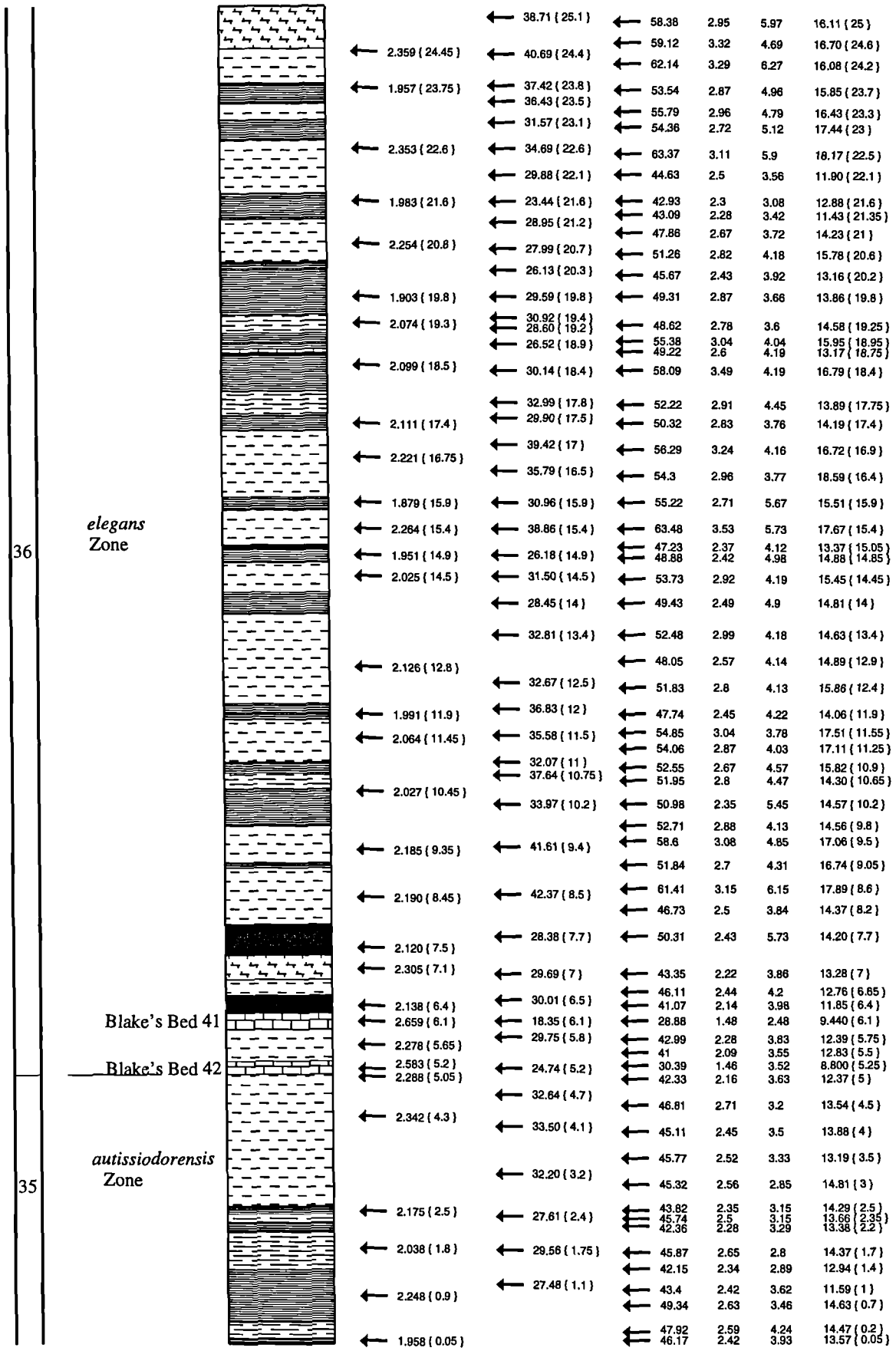
geoMetrics GR310
Exploranium GR320
Density (g/cm3)
Total GR (cps)
Total GR (cps)
K (%k)
U (ppm)
Th (ppm)
36
elegans Zone
Blake's Bed 41
Blake's Bed 42
35
autissiodorensis Zone
38.71 (25.1)
58.38 2.95 5.97 16.11 (25)
2.359 (24.45)
40.69 (24.4)
59.12 3.32 4.69 16.70 (24.6)
62.14 3.29 6.27 16.08 (24.2)
1.957 (23.75)
37.42 (23.8)
36.43 (23.5)
53.54 2.87 4.96 15.85 (23.7)
31.57 (23.1)
55.79 2.96 4.79 16.43 (23.3)
54.36 2.72 5.12 17.44 (23)
2.353 (22.6)
34.69 (22.6)
63.37 3.11 5.9 18.17 (22.5)
29.88 (22.1)
44.63 2.5 3.56 11.90 (22.1)
1.983 (21.6)
23.44 (21.6)
42.93 2.3 3.08 12.88 (21.6)
28.95 (21.2)
43.09 2.28 3.42 11.43 (21.35)
47.86 2.67 3.72 14.23 (21)
2.254 (20.8)
27.99 (20.7)
51.26 2.82 4.18 15.78 (20.6)
26.13 (20.3)
45.67 2.43 3.92 13.16 (20.2)
1.903 (19.8)
29.59 (19.8)
49.31 2.87 3.66 13.86 (19.8)
2.074 (19.3)
30.92 (19.4)
28.60 (19.2)
48.62 2.78 3.6 14.58 (19.25)
26.52 (18.9)
55.38 3.04 4.04 15.95 (18.95)
49.22 2.6 4.19 13.17 (18.75)
2.099 (18.5)
30.14 (18.4)
58.09 3.49 4.19 16.79 (18.4)
32.99 (17.8)
52.22 2.91 4.45 13.89 (17.75)
2.111 (17.4)
29.90 (17.5)
50.32 2.83 3.76 14.19 (17.4)
39.42 (17)
2.221 (16.75)
56.29 3.24 4.16 16.72 (16.9)
35.79 (16.5)
54.3 2.96 3.77 18.59 (16.4)
1.879 (15.9)
30.96 (15.9)
55.22 2.71 5.67 15.51 (15.9)
2.264 (15.4)
38.86 (15.4)
63.48 3.53 5.73 17.67 (15.4)
47.23 2.37 4.12 13.37 (15.05)
1.951 (14.9)
26.18 (14.9)
48.88 2.42 4.98 14.88 (14.85)
2.025 (14.5)
31.50 (14.5)
53.73 2.92 4.19 15.45 (14.45)
28.45 (14)
49.43 2.49 4.9 14.81 (14)
32.81 (13.4)
52.48 2.99 4.18 14.63 (13.4)
2.126 (12.8)
48.05 2.57 4.14 14.89 (12.9)
32.67 (12.5)
51.83 2.8 4.13 15.86 (12.4)
1.991 (11.9)
36.83 (12)
47.74 2.45 4.22 14.06 (11.9)
2.064 (11.45)
35.58 (11.5)
54.85 3.04 3.78 17.51 (11.55)
54.06 2.87 4.03 17.11 (11.25)
32.07 (11)
52.55 2.67 4.57 15.82 (10.9)
37.64 (10.75)
51.95 2.8 4.47 14.30 (10.65)
2.027 (10.45)
33.97 (10.2)
50.98 2.35 5.45 14.57 (10.2)
52.71 2.88 4.13 14.56 (9.8)
2.185 (9.35)
41.61 (9.4)
58.6 3.08 4.85 17.06 (9.5)
51.84 2.7 4.31 16.74 (9.05)
2.190 (8.45)
42.37 (8.5)
61.41 3.15 6.15 17.89 (8.6)
46.73 2.5 3.84 14.37 (8.2)
28.38 (7.7)
50.31 2.43 5.73 14.20 (7.7)
2.120 (7.5)
2.305 (7.1)
29.69 (7)
43.35 2.22 3.86 13.28 (7)
46.11 2.44 4.2 12.76 (6.65)
2.138 (6.4)
30.01 (6.5)
41.07 2.14 3.98 11.85 (6.4)
2.659 (6.1)
18.35 (6.1)
28.86 1.48 2.48 9.440 (6.1)
2.278 (5.65)
29.75 (5.8)
42.99 2.28 3.83 12.39 (5.75)
41 2.09 3.55 12.83 (5.5)
2.583 (5.2)
2.288 (5.05)
24.74 (5.2)
30.39 1.46 3.52 8.800 (5.25)
42.33 2.16 3.63 12.37 (5)
32.64 (4.7)
2.342 (4.3)
46.81 2.71 3.2 13.54 (4.5)
33.50 (4.1)
45.11 2.45 3.5 13.88 (4)
45.77 2.52 3.33 13.19 (3.5)
32.20 (3.2)
45.32 2.56 2.85 14.81 (3)
2.175 (2.5)
27.61 (2.4)
43.82 2.35 3.15 14.29 (2.5)
45.74 2.5 3.15 13.66 (2.35)
42.36 2.28 3.29 13.38 (2.2)
2.038 (1.8)
29.56 (1.75)
45.87 2.65 2.8 14.37 (1.7)
42.15 2.34 2.89 12.94 (1.4)
27.48 (1.1)
43.4 2.42 3.62 11.59 (1)
2.248 (0.9)
49.34 2.63 3.46 14.63 (0.7)
47.92 2.59 4.24 14.47 (0.2)
1.958 (0.05)
46.17 2.42 3.93 13.57 (0.05)

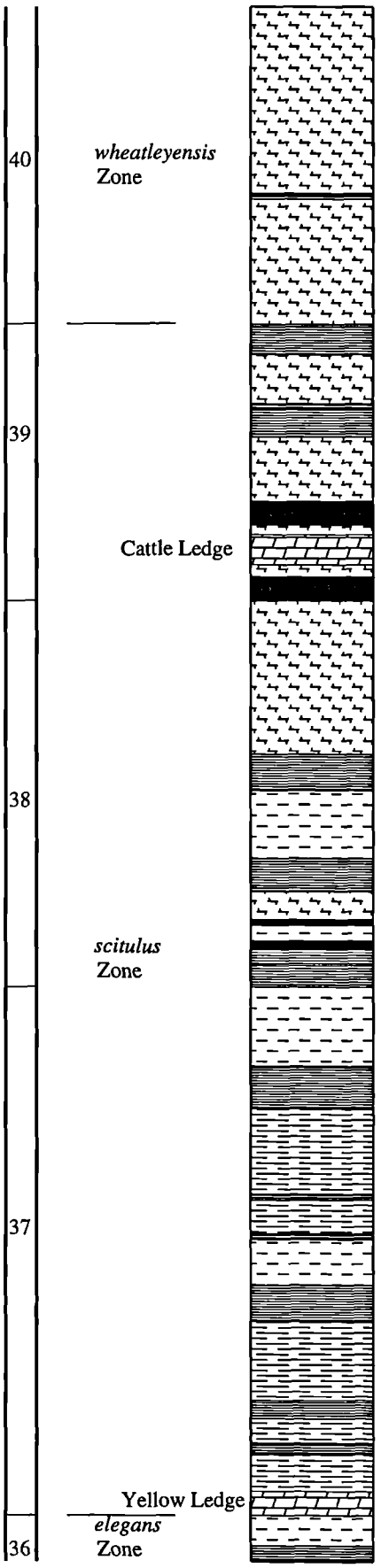

	geoMetrics GR310	Exploranium GR320			
	Density	Total GR	Total GR	K	U	Th
	(g/cm^3)	(cps)	(cps)	(%k)	(ppm)	(ppm)
		30.63 (25.4)	46.24	2.94	3.62	12.06 (25.4)
			46.12	2.75	3.2	11.62 (25)
			46.72	2.9	3.57	11.83 (24.5)
			45.52	2.65	3.49	11.96 (24)
		28.69 (23.3)	47.6	2.9	3.34	11.01 (23.5)
			47.15	2.98	3.2	12.11 (23.1)
	2.285 (22.65)		45.5	2.8	2.91	12.99 (22.7)
	1.737 (22.4)	31.35 (22.5)	46.14	2.82	3.44	11.96 (22.4)
			46.72	2.49	4.18	11.64 (22.1)
		34.90 (21.8)	48.25	2.74	4.36	12.47 (21.8)
	2.216 (21.35)		55.12	3.05	4.69	15.21 (21.4)
		34.80 (21)	52.97	2.8	5.01	13.97 (21.1)
			53.64	3.02	4.78	14.11 (20.8)
			54.24	2.75	5.94	12.78 (20.5)
	2.106 (20.05)	45.73 (20.2)	54.95	2.75	6.62	14.15 (20.25)
			61.52	2.73	8.8	13.80 (20)
			61.32	3.23	7.54	14.18 (19.8)
	2.330 (19.35)	41.66 (19.4)	61.47	3.23	6.96	14.00 (19.6)
			59.3	3.09	6.96	13.75 (19.3)
		47.57 (18.8)	53.67	2.72	5.72	13.77 (19)
			55.29	2.62	7.7	11.26 (18.75)
			54.5	2.65	6.94	12.67 (18.5)
			60.14	3.06	6.7	14.51 (18.3)
	2.314 (17.95)	39.77 (18)	57.92	2.99	6.38	14.30 (18.1)
		41.31 (17.6)	59.17	2.93	6.72	14.87 (17.8)
		43.96 (17.3)	64.65	3.04	9.12	14.49 (17.5)
		37.70 (17)	62.97	2.65	11.36	12.19 (17.2)
		14.51 (16.7)	50.77	3.07	5.04	11.91 (16.9)
	2.669 (16.6)		28.19	1.43	3.08	6.930 (16.65)
	2.310 (16.3)	33.99 (16.3)	26.35	1.26	2.82	6.470 (16.45)
		42.59 (16)	48	2.54	4.44	12.82 (16.25)
			48.44	2.41	6.28	11.65 (16)
	2.288 (13.75)					
		33.95 (13.6)	45.94	2.5	3.8	12.89 (13.6)
			54.67	3.1	4.91	15.18 (13.25)
		40.59 (13)	62.82	3.39	6.41	15.38 (13)
	1.962 (12.7)		67.64	3.94	5.48	16.09 (12.75)
	2.221 (12.35)	44.60 (12.4)	64.54	3.86	5.27	16.84 (12.4)
			60.24	3.53	4.56	16.07 (12.1)
		37.39 (11.9)	57.82	3.32	4.64	15.45 (11.8)
	2.068 (11.35)		48.74	2.55	4.49	12.81 (11.45)
		45.54 (11.3)	51.35	2.54	6.26	11.78 (11.2)
			58.47	3.3	5.06	15.41 (11)
		35.53 (10.8)	56.1	2.86	5.35	15.98 (10.75)
		30.36 (10.55)	54.25	2.89	4.69	15.69 (10.5)
		40.47 (10.3)	53.92	2.74	6.07	14.09 (10.3)
	2.135 (10.1)		50.8	2.35	6.3	13.22 (10.1)
		34.35 (9.8)	52.4	2.77	5.04	14.57 (9.9)
	2.289 (9.55)		56.69	3.12	5.67	15.22 (9.6)
			61.02	3.3	5.24	18.41 (9.3)
		37.10 (8.9)	60.59	3.4	5.56	15.48 (9)
			57.6	3.04	6.01	16.27 (8.7)
			53.49	2.66	5.94	13.26 (8.4)
			52.09	2.46	6.78	12.93 (8.1)
	1.916 (7.85)	39.06 (7.9)	50.22	2.32	5.94	12.54 (7.8)
			49.97	2.47	5.99	12.53 (7.55)
		34.37 (7.2)	51.44	2.66	4.8	14.95 (7.3)
			51.49	2.78	4.75	14.72 (7)
		33.57 (6.5)	51.25	2.84	4.49	13.06 (6.7)
			53.79	2.87	4.35	15.85 (6.3)
	2.072 (6)		54.27	2.83	4.61	16.06 (6)
		34.01 (5.7)	63.87	3.42	6.11	16.99 (5.8)
			62.2	3.12	5.92	18.58 (5.5)
			59.25	3.12	5.43	17.06 (5.35)
			58.97	3.18	5.03	16.74 (5.2)
	2.266 (5)	40.32 (5)	60.44	3.18	4.93	17.24 (5)
			56.92	2.95	5.88	14.48 (4.7)
		36.56 (4.3)	49.29	2.64	4.44	13.54 (4.35)
			52.74	2.59	5.43	14.16 (4)
	1.980 (3.75)		55.94	2.9	5.46	14.76 (3.8)
		37.23 (3.6)				
		32.70 (3.3)	52.3	2.82	4.72	15.33 (3.4)
	2.310 (3.1)					
			54.02	2.8	4.35	16.09 (2.9)
	2.174 (2.4)	26.24 (2.5)	47.89	2.49	4.28	14.29 (2.5)
		29.41 (2.2)	47.2	2.36	3.83	14.94 (2.15)
		28.45 (1.9)	51.44	2.71	4.3	14.40 (1.85)
		34.10 (1.5)	47.22	2.43	4.86	13.26 (1.55)
	1.954 (1.25)	30.62 (1.2)	46.67	2.49	4.04	12.98 (1.3)
	2.564 (1)	21.26 (1)	30.42	1.4	3.73	7.320 (1)
	1.816 (0.7)					
		42.68 (0.5)	49.96	2.69	4.65	13.68 (0.5)
	1.990 (0.15)	38.66 (0.05)	50.73	2.59	5.4	14.35 (0.1)

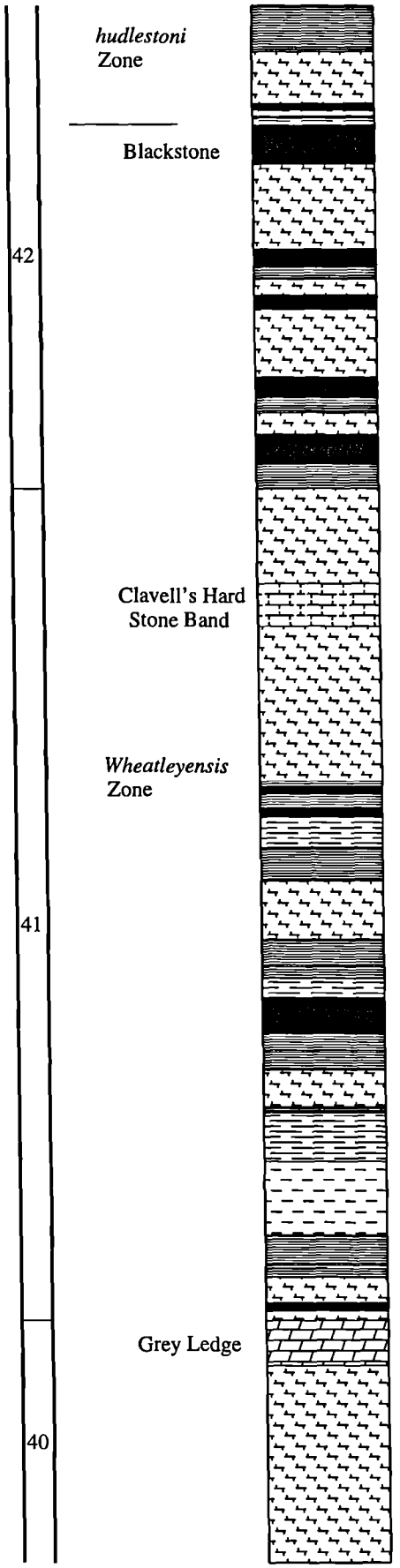

	geoMetrics GR310		Exploranium GR320			
	Density	Total GR	Total GR	K	U	Th
	(g/cm³)	(cps)	(cps)	(%k)	(ppm)	(ppm)
hudlestoni Zone	2.277 (25.3)	41.82 (25.4)	52.99	3.11	4.36	13.93 (25.5)
	2.303 (24.9)		53	3.24	4.37	12.92 (25.1)
			55.91	3.33	4.5	13.60 (24.85)
		40.38 (24.5)	52.54	2.99	3.91	14.25 (24.6)
	2.231 (24.25)		51.41	3	4.07	13.68 (24.3)
	2.039 (23.95)		49.2	2.65	5.15	11.76 (23.95)
	1.918 (23.95)		47.57	2.67	4.69	12.04 (23.85)
	2.018 (23.85)	33.61 (23.85)	45.41	2.07	5.16	12.21 (23.75)
	2.090 (23.7)	36.18 (23.75)	46.13	2.22	6.16	10.72 (23.7)
	1.328 (23.6)		38.46	1.89	4.82	8.620 (23.5)
	2.268 (23.5)	33.46 (23.3)	36.02	1.64	5.01	8.450 (23.3)
	1.517 (23.4)					
	1.996 (23.35)	38.14 (23)	43.66	2.15	5.68	10.02 (23)
	1.416 (23.05)		50.37	2.75	5.21	12.65 (22.7)
	2.260 (22.9)	42.47 (22.4)	50.8	2.62	5.21	13.19 (22.4)
			52.19	2.85	5.57	13.07 (22.1)
	2.221 (21.85)	39.53 (21.8)	57.12	2.92	6.72	14.22 (21.8)
	1.950 (21.55)	39.58 (21.6)	54.77	2.64	7	11.13 (21.5)
		47.43 (21.3)	61.44	3.27	7.19	15.27 (21.2)
	2.229 (21)	41.71 (21.1)	63.72	3.56	5.99	15.58 (21)
	2.089 (20.7)	42.69 (20.8)	66.73	3.65	6.97	15.48 (20.7)
		52.55 (20.4)	61.87	3.32	6.32	14.600 (20.55)
			63.16	3.57	5.46	16.26 (20.3)
		51.89 (19.9)	64.55	3.65	5.37	17.58 (20.1)
	2.543 (19.75)	50.27 (19.6)	63.82	3.5	5.49	18.08 (19.8)
	2.036 (19.4)	45.13 (19.4)	59.76	3.19	6.99	13.44 (19.45)
		46.03 (19.1)	59.49	2.89	7.26	13.91 (19.25)
	2.218 (19)	45.80 (18.8)	65.01	3.54	5.52	17.44 (19)
	1.882 (18.75)	39.81 (18.4)	62.21	3.38	6.02	16.39 (18.7)
			55.5	2.85	6.45	12.46 (18.45)
	2.212 (18)	45.79 (17.9)	60.73	2.9	7.94	13.58 (18.2)
		40.76 (17.5)	62.27	3.26	7.1	14.93 (18)
			56.94	3.26	5.35	13.35 (17.8)
		44.49 (17)	62.39	3.48	6.15	15.45 (17.4)
			59.06	3.08	6.86	14.24 (17.1)
	2.186 (16.45)	48.01 (16.5)	60.04	3.11	6.49	14.50 (16.8)
			63.47	3.34	8.32	14.64 (16.5)
Clavell's Hard Stone Band		30.15 (16)	58.66	3.11	6.53	13.49 (16.1)
	2.474 (15.8)	30.60 (15.7)	51.29	2.56	6.21	12.26 (15.9)
	2.428 (15.6)		50.73	2.54	5.65	13.18 (15.6)
			65.24	3.32	7.58	16.48 (15.2)
		48.16 (14.9)	61.63	3.24	7.03	13.04 (14.8)
		49.51 (14.3)	60.54	2.89	7.13	15.12 (14.4)
			56.04	2.73	6.1	15.45 (14)
	2.146 (13.75)	52.17 (13.6)	59.46	3.07	6.21	15.14 (13.6)
			56.65	2.92	6.2	15.24 (13.2)
		52.56 (13)	50.66	2.38	6.13	12.34 (12.8)
		32.02 (12.75)	47.04	2.18	6.24	10.86 (12.7)
Wheatleyensis Zone		35.38 (12.6)	49.45	2.18	6.95	11.54 (12.5)
	2.088 (12.5)	34.78 (12.4)	51.19	2.43	6.6	12.74 (12.3)
		37.58 (12)	55.16	3.01	5.86	13.63 (12.1)
		39.57 (11.6)	54.47	2.89	6.49	11.73 (11.9)
	2.136 (11.35)		54.68	2.59	6.89	13.01 (11.6)
			52.53	2.58	7.5	11.07 (11.3)
	2.107 (10.75)	34.07 (10.8)	55.88	2.94	5.92	13.34 (11.1)
			56.15	2.83	6.15	14.42 (10.8)
		40.97 (10.1)	54.76	2.97	5.27	14.37 (10.5)
			51.58	2.4	6.3	13.06 (10.1)
			45.38	2.04	6.45	9.610 (9.8)
	1.983 (9.4)	38.01 (9.5)	53.4	2.5	7.57	12.17 (9.45)
		33.50 (9)	52.53	2.46	7.85	11.93 (9.1)
			52.97	2.45	7.85	10.80 (8.8)
		33.50 (8.45)	53.68	2.58	7.07	11.29 (8.5)
			57.1	2.85	7.37	14.34 (8.2)
		35.03 (7.8)	62.57	3.07	7.1	15.98 (7.85)
	2.106 (7.65)		59.33	3.16	6.16	14.06 (7.6)
	2.076 (7.25)		60.01	3.11	6.4	14.63 (7.45)
			57.97	3.14	6.04	13.47 (7.25)
		38.41 (7)	54.23	2.95	6.31	13.10 (7)
			57.6	3.18	5.64	15.19 (6.7)
			56.06	3.12	5.15	15.46 (6.3)
		30.58 (5.9)	38.9	2.17	3.22	11.36 (5.9)
			42.5	2.46	3.48	10.10 (5.5)
	2.026 (5.2)	31.50 (5.1)	43.98	2.36	5.01	9.500 (5.1)
			44.98	2.47	5.37	9.380 (4.8)
		36.28 (4.6)	43.56	2.59	3.55	11.62 (4.5)
	1.692 (4.25)	35.51 (4.25)	42.29	2.36	4.88	9.280 (4.2)
		30.70 (4.1)	39.69	2.32	3.48	9.360 (4.05)
Grey Ledge		20.07 (3.7)	25.14	1.44	2.89	5.650 (3.7)
	2.748 (3.5)		24.64	1.36	2.4	4.770 (3.4)
			41.51	2.5	3.76	9.960 (3.1)
	2.188 (2.95)		44.36	2.64	3.5	11.25 (2.85)
		32.57 (2.7)	50.47	3.13	2.97	12.63 (2.45)
			47.52	2.91	3.71	12.58 (2)
		32.62 (1.8)	41.51	2.47	2.69	12.20 (1.6)
			43.68	2.64	2.59	12.63 (1.2)
			47.07	2.87	2.94	13.16 (0.8)
	2.416 (0.45)		51.12	3.18	3.69	12.29 (0.4)
			48.37	3.03	3.26	13.71 (0)

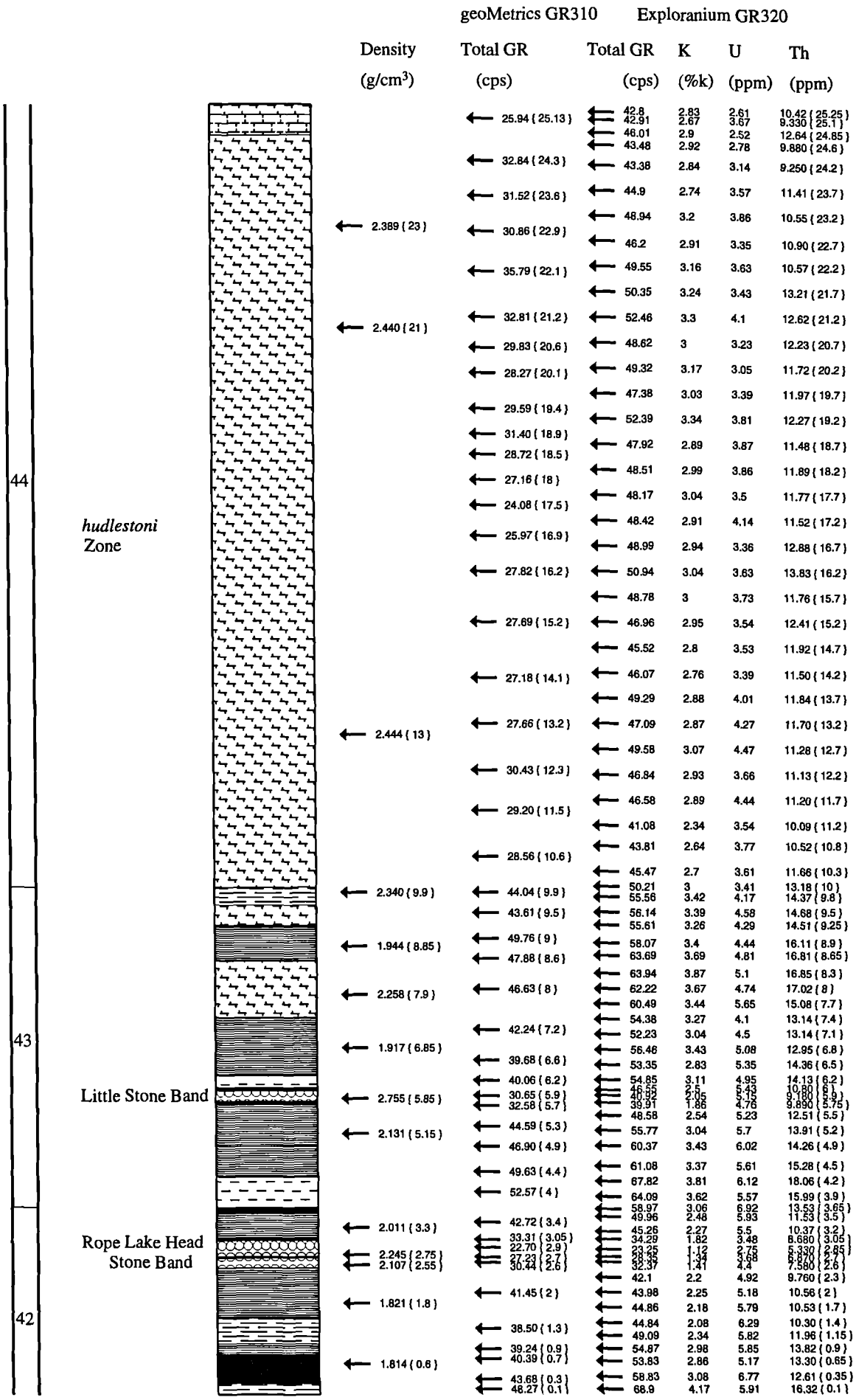
geoMetrics GR310
Exploranium GR320
Density (g/cm³)
Total GR (cps)
Total GR (cps)
K (%k)
U (ppm)
Th (ppm)
44
43
42
hudlestoni Zone
Little Stone Band
Rope Lake Head Stone Band
2.389 (23)
2.440 (21)
2.444 (13)
2.340 (9.9)
1.944 (8.85)
2.258 (7.9)
1.917 (6.85)
2.755 (5.85)
2.131 (5.15)
2.011 (3.3)
2.245 (2.75)
2.107 (2.55)
1.821 (1.8)
1.814 (0.6)
25.94 (25.13)
32.84 (24.3)
31.52 (23.6)
30.86 (22.9)
35.79 (22.1)
32.81 (21.2)
29.83 (20.6)
28.27 (20.1)
29.59 (19.4)
31.40 (18.9)
28.72 (18.5)
27.16 (18)
24.08 (17.5)
25.97 (16.9)
27.82 (16.2)
27.69 (15.2)
27.18 (14.1)
27.66 (13.2)
30.43 (12.3)
29.20 (11.5)
28.56 (10.6)
44.04 (9.9)
43.61 (9.5)
49.76 (9)
47.88 (8.6)
46.63 (8)
42.24 (7.2)
39.68 (6.6)
40.06 (6.2)
30.65 (5.9)
32.58 (5.7)
44.59 (5.3)
46.90 (4.9)
49.63 (4.4)
52.57 (4)
42.72 (3.4)
33.31 (3.05)
22.70 (2.9)
27.23 (2.7)
30.44 (2.6)
41.45 (2)
38.50 (1.3)
39.24 (0.9)
40.39 (0.7)
43.68 (0.3)
48.27 (0.1)
42.8 2.83 2.61 10.42 (25.25)
42.91 2.67 3.67 9.330 (25.1)
46.01 2.9 2.52 12.64 (24.85)
43.48 2.92 2.78 9.880 (24.6)
43.38 2.84 3.14 9.250 (24.2)
44.9 2.74 3.57 11.41 (23.7)
46.94 3.2 3.86 10.55 (23.2)
46.2 2.91 3.35 10.90 (22.7)
49.55 3.16 3.63 10.57 (22.2)
50.35 3.24 3.43 13.21 (21.7)
52.46 3.3 4.1 12.62 (21.2)
48.62 3 3.23 12.23 (20.7)
49.32 3.17 3.05 11.72 (20.2)
47.38 3.03 3.39 11.97 (19.7)
52.39 3.34 3.81 12.27 (19.2)
47.92 2.89 3.87 11.48 (18.7)
48.51 2.99 3.86 11.89 (18.2)
48.17 3.04 3.5 11.77 (17.7)
48.42 2.91 4.14 11.52 (17.2)
48.99 2.94 3.36 12.88 (16.7)
50.94 3.04 3.83 13.83 (16.2)
48.78 3 3.73 11.76 (15.7)
46.96 2.95 3.54 12.41 (15.2)
45.52 2.8 3.53 11.92 (14.7)
46.07 2.76 3.39 11.50 (14.2)
49.29 2.88 4.01 11.84 (13.7)
47.09 2.87 4.27 11.70 (13.2)
49.58 3.07 4.47 11.28 (12.7)
46.84 2.93 3.66 11.13 (12.2)
46.58 2.89 4.44 11.20 (11.7)
41.08 2.34 3.54 10.09 (11.2)
43.81 2.64 3.77 10.52 (10.8)
45.47 2.7 3.61 11.66 (10.3)
50.21 3 3.41 13.18 (10)
55.56 3.42 4.17 14.37 (9.8)
56.14 3.39 4.58 14.68 (9.5)
55.61 3.26 4.29 14.51 (9.25)
58.07 3.4 4.44 16.11 (8.9)
63.69 3.69 4.81 16.81 (8.65)
63.94 3.87 5.1 16.85 (8.3)
62.22 3.67 4.74 17.02 (8)
60.49 3.44 5.65 15.08 (7.7)
54.38 3.27 4.1 13.14 (7.4)
52.23 3.04 4.5 13.14 (7.1)
56.46 3.43 5.08 12.95 (6.8)
53.35 2.83 5.35 14.36 (6.5)
54.85 3.11 4.95 14.13 (6.2)
46.55 2.5 5.43 10.80 (6)
40.92 2.05 5.15 9.180 (5.9)
39.91 1.86 4.76 9.890 (5.75)
48.58 2.54 5.23 12.51 (5.5)
55.77 3.04 5.7 13.91 (5.2)
60.37 3.43 6.02 14.26 (4.9)
61.08 3.37 5.61 15.28 (4.5)
67.82 3.81 6.12 18.06 (4.2)
64.09 3.62 5.57 15.99 (3.9)
58.97 3.06 6.92 13.53 (3.65)
49.96 2.48 5.93 11.53 (3.5)
45.26 2.27 5.5 10.37 (3.2)
34.29 1.82 3.48 8.680 (3.05)
23.25 1.12 2.75 5.330 (2.85)
28.95 1.44 3.68 6.870 (2.7)
32.37 1.47 4.4 7.580 (2.6)
42.1 2.2 4.92 9.760 (2.3)
43.98 2.25 5.18 10.56 (2)
44.86 2.18 5.79 10.53 (1.7)
44.84 2.08 6.29 10.30 (1.4)
49.09 2.34 5.82 11.96 (1.15)
54.87 2.98 5.85 13.82 (0.9)
53.83 2.86 5.17 13.30 (0.65)
58.83 3.08 6.77 12.61 (0.35)
68.9 4.17 5.91 16.32 (0.1)

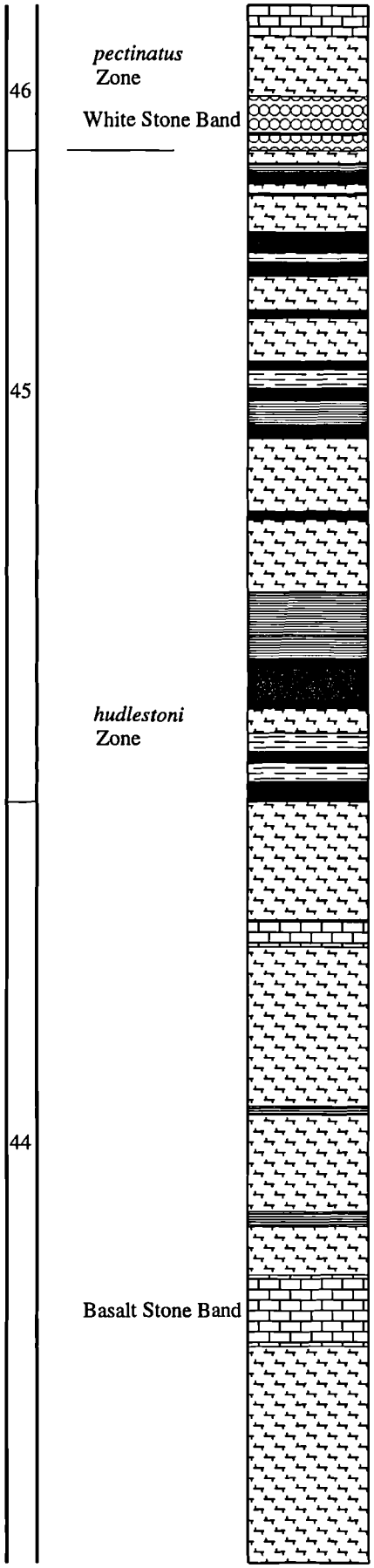

Density (g/cm³)	geoMetrics GR310 Total GR (cps)	Exploranium GR320 Total GR (cps)	K (%k)	U (ppm)	Th (ppm)
2.689 (25.7)	12.12 (25.7)	30.38	1.81	2.19	7.810 (25.8)
		28.44	1.71	2.47	6.300 (25.5)
	15.85 (25.1)	37.35	2.37	2.19	8.940 (25.2)
2.435 (24.9)	15.41 (24.7)	36.14	2.19	2.59	9.460 (24.9)
		33.46	1.99	3.27	7.130 (24.6)
		27.81	1.44	3.57	6.100 (24.3)
	9.610 (24.1)	20.88	0.65	4.73	2.730 (24.2)
2.127 (24)		20.26	0.58	4.89	2.340 (23.95)
	11.47 (23.8)	22.88	0.74	4.47	3.690 (23.75)
	15.34 (23.6)	28.65	1.21	4.85	5.180 (23.6)
	29.56 (23.4)	36.67	1.76	5.02	6.240 (23.4)
	29.57 (23.2)	38.88	2.04	4.6	5.890 (23.25)
1.520 (23)	24.39 (23.1)	48.59	2.68	5.99	10.81 (23.1)
	28.10 (22.9)	45.46	2.3	5.9	8.840 (22.9)
	33.26 (22.8)	55.42	2.82	6.96	12.02 (22.75)
2.368 (22.45)	37.10 (22.6)	65.07	4.18	4.89	15.58 (22.6)
	32.65 (22.3)	51.78	3.16	4.16	13.58 (22.3)
	16.65 (22)	38.7	1.92	4.97	7.150 (22)
	19.20 (21.85)	41.28	2.28	4.63	7.810 (21.8)
1.898 (21.55)	22.02 (21.6)	40.59	2.12	5.2	8.120 (21.6)
		49.9	2.99	4.67	10.95 (21.4)
	24.32 (21.2)	48.31	2.87	4.97	9.760 (21.2)
2.051 (20.8)	14.74 (20.85)	46.56	2.88	3.79	11.23 (21)
		33.43	1.72	4.7	6.610 (20.8)
2.343 (20.4)	15.72 (20.4)	31.34	1.46	4.51	6.560 (20.7)
		33.35	1.76	4.44	6.940 (20.5)
	16.75 (20)	38.37	2.24	4.06	8.430 (20.2)
2.008 (19.75)	22.43 (19.8)	40.46	2.24	4.84	8.380 (20)
	23.74 (19.5)	43.8	2.52	4.65	9.300 (19.75)
	22.71 (19.2)	38.04	1.88	5.63	6.630 (19.5)
2.106 (18.85)	23.00 (18.9)	44.87	2.27	6.12	7.840 (19.3)
		45.56	2.55	5.54	9.880 (19.1)
		43.58	2.48	4.13	10.04 (18.85)
		54.71	3.37	4.11	12.28 (18.6)
2.307 (18.2)	35.47 (18.3)	53.85	3.44	3.77	12.69 (18.4)
	33.69 (17.9)	52.85	3.27	4.09	12.58 (18.1)
		52.92	3.36	4.3	11.96 (17.8)
2.113 (17.5)	25.44 (17.5)	45.46	2.65	4.39	9.790 (17.45)
		48.74	3.06	4.42	10.97 (17.3)
2.342 (17)		50.19	3.32	3.62	12.25 (17.1)
	28.90 (16.9)	46.55	2.97	3.24	11.13 (16.8)
	26.54 (16.4)	40.32	2.54	3.45	8.540 (16.5)
2.274 (16.15)	18.82 (16.1)	36.49	2.18	3.14	8.870 (16.2)
2.186 (15.9)		39.53	2.21	3.63	9.220 (15.9)
	28.13 (15.6)	44.25	2.6	5.16	9.070 (15.6)
	27.49 (15.3)	45.91	2.6	4.96	10.25 (15.35)
		38.4	2.08	4.69	8.220 (15.1)
2.160 (14.9)		36.15	1.79	5.32	6.370 (14.9)
	20.20 (14.7)	41.89	2.11	5.84	8.650 (14.7)
	23.15 (14.3)	43.05	2.43	4.72	8.930 (14.4)
2.163 (14.15)		51.17	3.08	5.05	10.25 (14.2)
	27.98 (14)	51.93	3.28	4.99	10.84 (14)
		50.28	3.18	4.1	11.39 (13.8)
	31.40 (13.6)	50.66	3.02	5	10.81 (13.7)
	25.93 (13.35)	44.67	2.68	4.66	8.600 (13.45)
	32.59 (13.1)	50.03	2.88	5.65	9.580 (13.2)
1.955 (12.75)	27.17 (12.8)	46.17	2.48	5.23	9.510 (12.9)
	27.78 (12.5)	50.82	3.14	4.88	10.63 (12.7)
		54.45	3.28	4.85	11.76 (12.55)
	25.97 (12)	52.41	3.41	3.51	12.64 (12.25)
2.397 (11.7)		51.55	3.32	3.07	12.84 (12)
	25.84 (11.5)	51	3.28	4.73	10.42 (11.7)
		47.85	2.98	4.17	11.00 (11.3)
	25.49 (11)	44.67	2.78	3.72	10.00 (11)
	20.48 (10.7)	32.6	1.84	2.86	8.420 (10.7)
	16.02 (10.3)	33.59	2.11	2.24	8.850 (10.4)
	24.83 (10.1)	40.87	2.45	3.26	9.420 (10.2)
2.348 (9.75)		41.45	2.63	2.88	9.980 (9.9)
	26.49 (9.6)	45.95	2.95	4.17	9.850 (9.5)
	29.31 (9)	44.87	2.84	3.49	10.74 (9.1)
		46.15	2.78	3.53	11.79 (8.8)
	25.64 (8.5)	45.13	2.91	3.81	10.11 (8.4)
		48.69	3.14	3.88	10.41 (8.1)
	26.14 (7.9)	46.11	2.91	3.48	10.89 (7.8)
1.982 (7.5)	26.05 (7.5)	40.73	2.57	3.39	9.480 (7.5)
	28.45 (7)	41.22	2.68	3.47	8.570 (7.1)
		46.44	3.06	3.4	9.770 (6.8)
2.394 (6.45)	28.47 (6.5)	47.98	3.2	3.28	10.50 (6.5)
	24.09 (6)	43.87	3.03	2.81	9.730 (6.2)
2.222 (5.7)	21.95 (5.6)	43.26	2.74	3.13	9.200 (5.9)
	27.75 (5.35)	48.31	3.1	3.78	10.93 (5.75)
2.374 (5.15)	28.32 (5)	53.62	3.54	3.19	13.34 (5.4)
		53.59	3.66	3.72	12.58 (5.1)
		40.04	2.5	2.55	9.980 (4.8)
	12.90 (4.3)	26.88	1.69	1.55	6.570 (4.6)
2.730 (4.1)		25.94	1.57	2.25	5.830 (4.2)
	12.58 (3.7)	28.84	1.79	2.13	6.280 (3.8)
2.389 (3.5)	31.29 (3.4)	39.28	2.53	3	8.550 (3.5)
		44.72	2.95	3.04	10.67 (3.1)
	30.36 (2.65)	43.54	2.84	3.19	10.23 (2.8)
		45.86	2.99	3.59	10.99 (2.4)
	28.98 (1.9)	49.44	3.19	3.45	11.63 (2)
2.288 (1.6)		48.13	3.09	3.16	12.75 (1.7)
	27.95 (1.3)	45.91	2.89	3.32	11.50 (1.4)
		48.19	3.08	3.19	11.66 (1.1)
	29.26 (0.7)	52.77	3.42	3.38	13.00 (0.8)
		48.54	3.03	3.76	12.15 (0.5)
	24.69 (0.2)	47	2.98	3.75	10.81 (0.2)

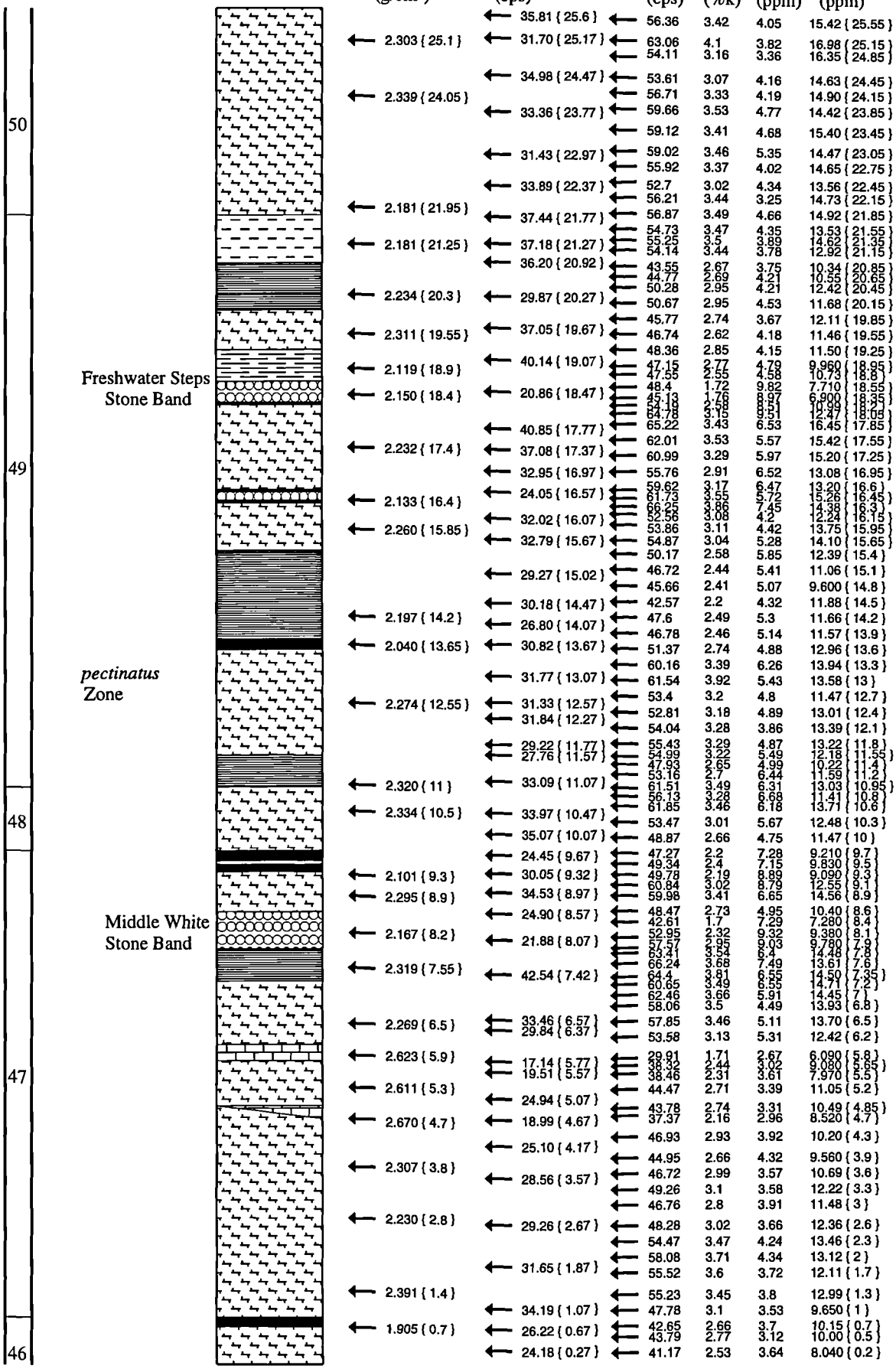
geoMetrics GR310
Exploranium GR320
Density (g/cm³)
Total GR (cps)
Total GR (cps)
K (%k)
U (ppm)
Th (ppm)
50
49
48
47
46
Freshwater Steps Stone Band
pectinatus Zone
Middle White Stone Band
2.303 { 25.1 }
2.339 { 24.05 }
2.181 { 21.95 }
2.181 { 21.25 }
2.234 { 20.3 }
2.311 { 19.55 }
2.119 { 18.9 }
2.150 { 18.4 }
2.232 { 17.4 }
2.133 { 16.4 }
2.260 { 15.85 }
2.197 { 14.2 }
2.040 { 13.65 }
2.274 { 12.55 }
2.320 { 11 }
2.334 { 10.5 }
2.101 { 9.3 }
2.295 { 8.9 }
2.167 { 8.2 }
2.319 { 7.55 }
2.269 { 6.5 }
2.623 { 5.9 }
2.611 { 5.3 }
2.670 { 4.7 }
2.307 { 3.8 }
2.230 { 2.8 }
2.391 { 1.4 }
1.905 { 0.7 }
35.81 { 25.6 }
31.70 { 25.17 }
34.98 { 24.47 }
33.36 { 23.77 }
31.43 { 22.97 }
33.89 { 22.37 }
37.44 { 21.77 }
37.18 { 21.27 }
36.20 { 20.92 }
29.87 { 20.27 }
37.05 { 19.67 }
40.14 { 19.07 }
20.86 { 18.47 }
40.85 { 17.77 }
37.08 { 17.37 }
32.95 { 16.97 }
24.05 { 16.57 }
32.02 { 16.07 }
32.79 { 15.67 }
29.27 { 15.02 }
30.18 { 14.47 }
26.80 { 14.07 }
30.82 { 13.67 }
31.77 { 13.07 }
31.33 { 12.57 }
31.84 { 12.27 }
29.22 { 11.77 }
27.76 { 11.57 }
33.09 { 11.07 }
33.97 { 10.47 }
35.07 { 10.07 }
24.45 { 9.67 }
30.05 { 9.32 }
34.53 { 8.97 }
24.90 { 8.57 }
21.88 { 8.07 }
42.54 { 7.42 }
33.46 { 6.57 }
29.84 { 6.37 }
17.14 { 5.77 }
19.51 { 5.57 }
24.94 { 5.07 }
18.99 { 4.67 }
25.10 { 4.17 }
28.56 { 3.57 }
29.26 { 2.67 }
31.65 { 1.87 }
34.19 { 1.07 }
26.22 { 0.67 }
24.18 { 0.27 }
56.36 3.42 4.05 15.42 { 25.55 }
63.06 4.1 3.82 16.98 { 25.15 }
54.11 3.16 3.36 16.35 { 24.85 }
53.61 3.07 4.16 14.63 { 24.45 }
56.71 3.33 4.19 14.90 { 24.15 }
59.66 3.53 4.77 14.42 { 23.85 }
59.12 3.41 4.68 15.40 { 23.45 }
59.02 3.46 5.35 14.47 { 23.05 }
55.92 3.37 4.02 14.65 { 22.75 }
52.7 3.02 4.34 13.56 { 22.45 }
56.21 3.44 3.25 14.73 { 22.15 }
56.87 3.49 4.66 14.92 { 21.85 }
54.73 3.47 4.35 13.53 { 21.55 }
55.25 3.5 3.89 14.62 { 21.35 }
54.14 3.44 3.78 12.92 { 21.15 }
43.55 2.67 3.75 10.34 { 20.85 }
44.77 2.69 4.21 10.55 { 20.65 }
50.28 2.95 4.21 12.42 { 20.45 }
50.67 2.95 4.53 11.68 { 20.15 }
45.77 2.74 3.67 12.11 { 19.85 }
46.74 2.62 4.18 11.46 { 19.55 }
48.36 2.85 4.15 11.50 { 19.25 }
47.15 2.77 4.79 9.960 { 18.95 }
47.55 2.55 4.58 10.73 { 18.6 }
48.4 1.72 9.82 7.710 { 18.55 }
45.13 1.76 8.97 6.900 { 18.35 }
54.51 2.58 8.91 10.69 { 18.25 }
64.78 3.15 9.51 12.47 { 18.05 }
65.22 3.43 6.53 16.45 { 17.85 }
62.01 3.53 5.57 15.42 { 17.55 }
60.99 3.29 5.97 15.20 { 17.25 }
55.76 2.91 6.52 13.08 { 16.95 }
59.62 3.17 6.47 13.20 { 16.6 }
61.73 3.55 5.72 15.26 { 16.45 }
66.25 3.86 7.45 14.38 { 16.3 }
52.56 3.08 4.2 12.24 { 16.15 }
53.86 3.11 4.42 13.75 { 15.95 }
54.87 3.04 5.28 14.10 { 15.65 }
50.17 2.58 5.85 12.39 { 15.4 }
46.72 2.44 5.41 11.06 { 15.1 }
45.66 2.41 5.07 9.600 { 14.8 }
42.57 2.2 4.32 11.88 { 14.5 }
47.6 2.49 5.3 11.66 { 14.2 }
46.78 2.46 5.14 11.57 { 13.9 }
51.37 2.74 4.88 12.96 { 13.6 }
60.16 3.39 6.26 13.94 { 13.3 }
61.54 3.92 5.43 13.58 { 13 }
53.4 3.2 4.8 11.47 { 12.7 }
52.81 3.18 4.89 13.01 { 12.4 }
54.04 3.28 3.86 13.39 { 12.1 }
55.43 3.29 4.87 13.22 { 11.8 }
54.99 3.22 5.49 12.18 { 11.55 }
47.93 2.65 4.99 10.22 { 11.4 }
53.16 2.7 6.44 11.59 { 11.2 }
61.51 3.49 6.31 13.03 { 10.95 }
56.13 3.28 6.68 11.41 { 10.8 }
61.85 3.46 6.18 13.71 { 10.6 }
53.47 3.01 5.67 12.48 { 10.3 }
48.87 2.66 4.75 11.47 { 10 }
47.27 2.2 7.28 9.210 { 9.7 }
49.34 2.4 7.15 9.830 { 9.5 }
49.78 2.19 8.89 9.090 { 9.3 }
60.84 3.02 8.79 12.55 { 9.1 }
59.98 3.41 6.65 14.56 { 8.9 }
48.47 2.73 4.95 10.40 { 8.6 }
42.61 1.7 7.29 7.280 { 8.4 }
52.95 2.32 9.32 9.380 { 8.1 }
57.57 2.95 9.03 9.780 { 7.8 }
53.41 3.54 9.4 14.48 { 7.8 }
66.24 3.68 7.49 13.61 { 7.6 }
64.4 3.81 6.55 14.50 { 7.35 }
60.65 3.49 6.55 14.71 { 7.2 }
62.46 3.66 5.91 14.45 { 7 }
58.06 3.5 4.49 13.93 { 6.8 }
57.85 3.46 5.11 13.70 { 6.5 }
53.58 3.13 5.31 12.42 { 6.2 }
29.91 1.71 2.67 6.090 { 5.8 }
38.32 2.44 3.02 9.080 { 5.65 }
38.46 2.31 3.61 7.970 { 5.5 }
44.47 2.71 3.39 11.05 { 5.2 }
43.78 2.74 3.31 10.49 { 4.85 }
37.37 2.16 2.96 8.520 { 4.7 }
46.93 2.93 3.92 10.20 { 4.3 }
44.95 2.66 4.32 9.560 { 3.9 }
46.72 2.99 3.57 10.69 { 3.6 }
49.26 3.1 3.58 12.22 { 3.3 }
46.76 2.8 3.91 11.48 { 3 }
48.28 3.02 3.66 12.36 { 2.6 }
54.47 3.47 4.24 13.46 { 2.3 }
58.08 3.71 4.34 13.12 { 2 }
55.52 3.6 3.72 12.11 { 1.7 }
55.23 3.45 3.8 12.99 { 1.3 }
47.78 3.1 3.53 9.650 { 1 }
42.65 2.66 3.7 10.15 { 0.7 }
43.79 2.77 3.12 10.00 { 0.5 }
41.17 2.53 3.64 8.040 { 0.2 }

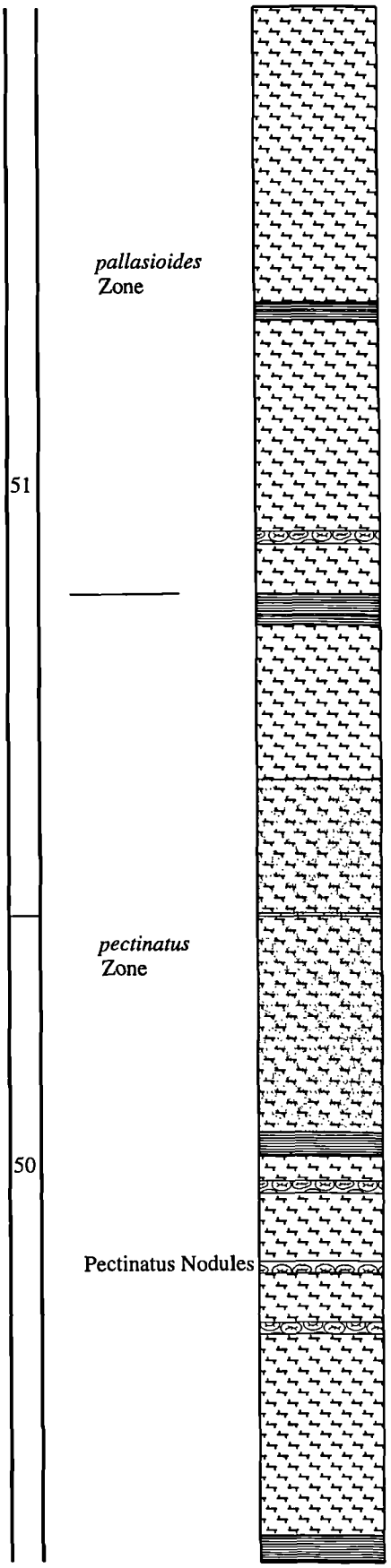

Density (g/cm³)	geoMetrics GR310 Total GR (cps)	Exploranium GR320 Total GR (cps)	K (%k)	U (ppm)	Th (ppm)
	29.05 { 50.67 }				
	28.42 { 49.77 }				
2.280 { 23.4 }	29.97 { 48.97 }				
	29.07 { 48.07 }				
	29.36 { 47.27 }				
	27.19 { 46.47 }				
	27.84 { 46.12 }	51.12	2.94	4.54	13.40 { 20.4 }
2.332 { 20.2 }	32.25 { 45.77 }	50.76	2.85	3.95	15.02 { 20.15 }
		53.5	3.14	3.73	15.39 { 19.85 }
2.308 { 19.55 }	28.13 { 45.27 }	52.62	3.1	3.36	14.26 { 19.45 }
	29.65 { 44.67 }	56.55	3.32	3.92	15.59 { 19.05 }
		56.38	3.39	3.41	18.02 { 18.65 }
	29.05 { 43.97 }	51.16	3.11	3.18	14.43 { 18.25 }
		53.86	3.05	4.21	15.13 { 17.95 }
	29.67 { 43.27 }	53.3	3.16	3.75	13.58 { 17.65 }
		57.07	3.36	4.29	16.10 { 17.35 }
		60.72	3.61	4.36	17.41 { 17.05 }
2.284 { 16.65 }	30.32 { 42.47 }	59.49	3.46	4.44	16.81 { 16.6 }
	30.45 { 41.97 }	58.16	3.39	4.75	15.61 { 16.15 }
	35.28 { 41.47 }	58.48	3.3	5.42	15.43 { 15.75 }
2.292 { 15.45 }		58.07	3.31	4.84	16.47 { 15.5 }
	38.22 { 40.97 }	59.55	3.53	4.4	15.99 { 15.25 }
		54.11	3.24	3.36	15.20 { 14.75 }
	32.38 { 40.27 }	59.35	3.56	4.5	15.16 { 14.25 }
	26.64 { 39.67 }	58.53	3.53	4.01	16.52 { 13.85 }
2.323 { 13.55 }		55.27	3.3	4.15	14.88 { 13.45 }
	30.27 { 38.97 }	55.95	3.23	4.05	15.09 { 13.15 }
	30.57 { 38.37 }	56.43	3.36	3.8	14.78 { 12.65 }
2.338 { 12.2 }	35.86 { 37.87 }	56.4	3.24	4.91	15.15 { 12.25 }
		57.37	3.41	4.08	16.20 { 11.85 }
	30.90 { 37.37 }	54.98	3.41	3.36	14.93 { 11.45 }
	30.57 { 36.87 }	57.17	3.43	3.98	15.60 { 11.15 }
		56.84	3.36	4.33	15.70 { 10.85 }
2.446 { 10.5 }	29.87 { 36.37 }	54.39	3.24	4.38	15.01 { 10.55 }
		56.96	3.48	4.54	14.90 { 10.25 }
	30.70 { 35.77 }	57.11	3.23	5.2	15.79 { 9.85 }
2.416 { 9.4 }	32.70 { 35.27 }	62.77	3.7	5.08	16.67 { 9.45 }
		63.37	3.71	5.13	16.60 { 9.05 }
	36.04 { 34.57 }	59.6	3.42	4.97	13.98 { 8.65 }
	34.25 { 33.87 }	57.97	3.26	4.73	15.79 { 8.25 }
2.394 { 8 }		56.81	3.39	4.29	14.62 { 7.85 }
	30.42 { 33.27 }	57.18	3.29	4.7	14.65 { 7.45 }
		58.99	3.42	4.92	15.33 { 7.05 }
2.306 { 6.8 }	34.86 { 32.57 }	59.82	3.64	4.77	14.53 { 6.75 }
2.317 { 6.35 }		60.24	3.68	4.55	14.96 { 6.45 }
	34.59 { 31.97 }	52.02	3.27	3.42	13.02 { 6.05 }
		54.5	3.46	4	14.87 { 5.55 }
2.292 { 5.45 }	33.51 { 31.07 }				
	27.90 { 30.67 }	55.59	3.42	4.37	13.91 { 5.05 }
2.579 { 4.8 }					
	32.74 { 30.17 }	59.04	3.69	3.74	15.65 { 4.55 }
2.152 { 4.3 }		57.94	3.65	3.39	15.80 { 4.15 }
2.427 { 3.8 }	33.62 { 29.47 }	56.2	3.59	3.4	14.78 { 3.75 }
		55.56	3.47	3.9	14.89 { 3.25 }
	32.60 { 28.57 }				
2.159 { 2.7 }		56.91	3.3	4.37	15.35 { 2.75 }
		53.28	3.31	3.09	15.44 { 2.35 }
	31.78 { 27.77 }	55.19	3.18	3.99	16.40 { 2.05 }
1.989 { 1.6 }		56.91	3.3	4.43	16.91 { 1.65 }
	34.51 { 26.97 }	57.14	3.51	4.63	14.17 { 1.35 }
		61.37	3.73	4.79	16.10 { 1.05 }
	31.06 { 26.37 }	59.52	3.56	4.84	15.76 { 0.75 }
2.126 { 0.2 }	33.03 { 25.97 }	60.31	3.47	5.22	15.72 { 0.35 }
		55.11	3.4	3.09	15.75 { 0.15 }

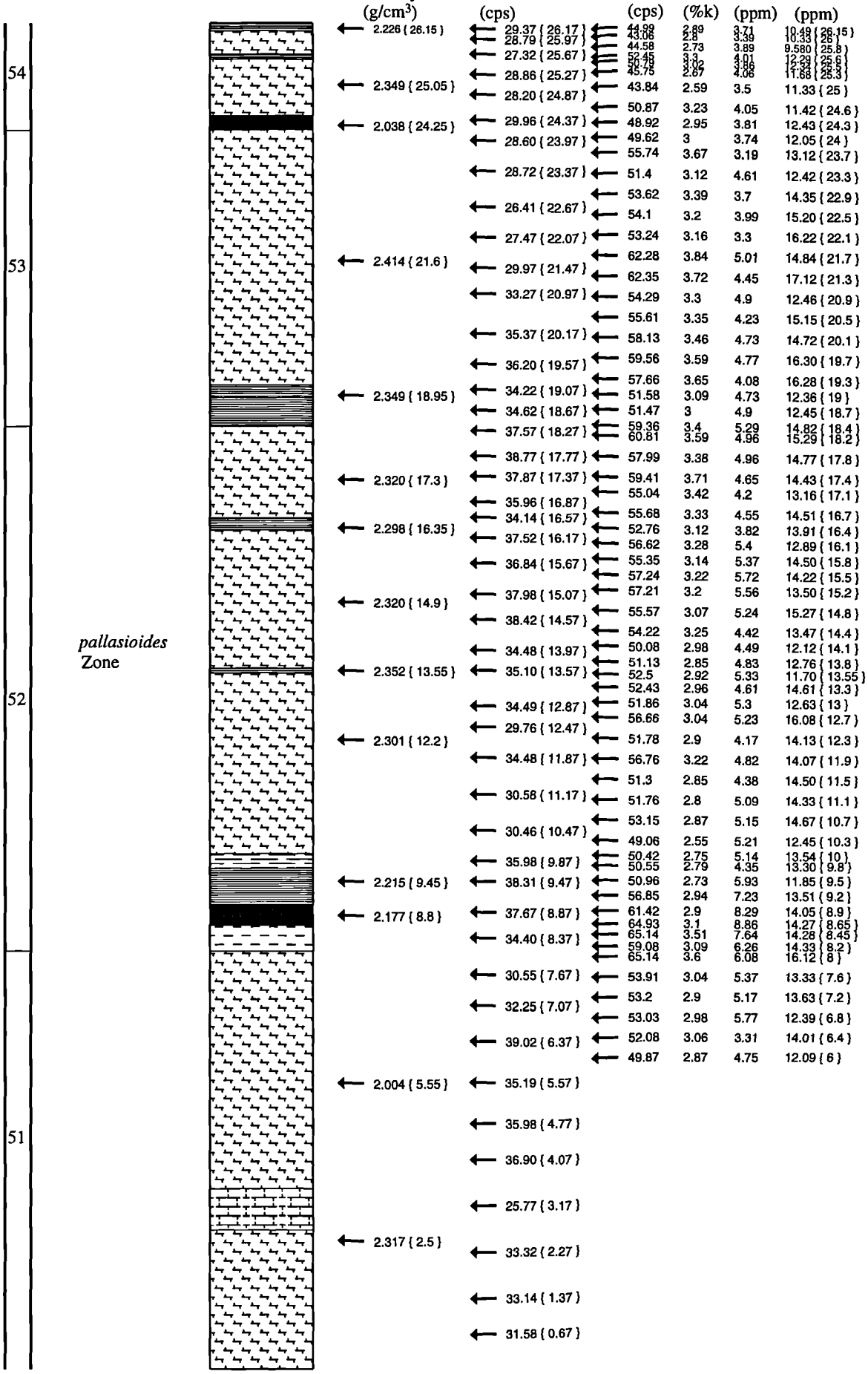
geoMetrics GR310
Exploranium GR320
Density (g/cm³)
Total GR (cps)
Total GR (cps)
K (%k)
U (ppm)
Th (ppm)
54
53
52
51
pallasioides Zone
2.226 { 26.15 }
2.349 { 25.05 }
2.038 { 24.25 }
2.414 { 21.6 }
2.349 { 18.95 }
2.320 { 17.3 }
2.298 { 16.35 }
2.320 { 14.9 }
2.352 { 13.55 }
2.301 { 12.2 }
2.215 { 9.45 }
2.177 { 8.8 }
2.004 { 5.55 }
2.317 { 2.5 }
29.37 { 26.17 }
28.79 { 25.97 }
27.32 { 25.67 }
28.86 { 25.27 }
28.20 { 24.87 }
29.96 { 24.37 }
28.60 { 23.97 }
28.72 { 23.37 }
26.41 { 22.67 }
27.47 { 22.07 }
29.97 { 21.47 }
33.27 { 20.97 }
35.37 { 20.17 }
36.20 { 19.57 }
34.22 { 19.07 }
34.62 { 18.67 }
37.57 { 18.27 }
38.77 { 17.77 }
37.87 { 17.37 }
35.96 { 16.87 }
34.14 { 16.57 }
37.52 { 16.17 }
36.84 { 15.67 }
37.98 { 15.07 }
38.42 { 14.57 }
34.48 { 13.97 }
35.10 { 13.57 }
34.49 { 12.87 }
29.76 { 12.47 }
34.48 { 11.87 }
30.58 { 11.17 }
30.46 { 10.47 }
35.98 { 9.87 }
38.31 { 9.47 }
37.67 { 8.87 }
34.40 { 8.37 }
30.55 { 7.67 }
32.25 { 7.07 }
39.02 { 6.37 }
35.19 { 5.57 }
35.98 { 4.77 }
36.90 { 4.07 }
25.77 { 3.17 }
33.32 { 2.27 }
33.14 { 1.37 }
31.58 { 0.67 }
44.89 2.89 3.71 10.49 { 26.15 }
43.06 2.8 3.39 10.33 { 25.8 }
44.58 2.73 3.89 9.580 { 25.8 }
52.45 3.3 4.01 12.29 { 25.6 }
50.79 3.02 3.86 12.34 { 25.5 }
45.75 2.67 4.06 11.68 { 25.3 }
43.84 2.59 3.5 11.33 { 25 }
50.87 3.23 4.05 11.42 { 24.6 }
48.92 2.95 3.81 12.43 { 24.3 }
49.62 3 3.74 12.05 { 24 }
55.74 3.67 3.19 13.12 { 23.7 }
51.4 3.12 4.61 12.42 { 23.3 }
53.62 3.39 3.7 14.35 { 22.9 }
54.1 3.2 3.99 15.20 { 22.5 }
53.24 3.16 3.3 16.22 { 22.1 }
62.28 3.84 5.01 14.84 { 21.7 }
62.35 3.72 4.45 17.12 { 21.3 }
54.29 3.3 4.9 12.46 { 20.9 }
55.61 3.35 4.23 15.15 { 20.5 }
58.13 3.46 4.73 14.72 { 20.1 }
59.56 3.59 4.77 16.30 { 19.7 }
57.66 3.65 4.08 16.28 { 19.3 }
51.58 3.09 4.73 12.36 { 19 }
51.47 3 4.9 12.45 { 18.7 }
59.36 3.4 5.29 14.82 { 18.4 }
60.81 3.59 4.96 15.29 { 18.2 }
57.99 3.38 4.96 14.77 { 17.8 }
59.41 3.71 4.65 14.43 { 17.4 }
55.04 3.42 4.2 13.16 { 17.1 }
55.68 3.33 4.55 14.51 { 16.7 }
52.76 3.12 3.82 13.91 { 16.4 }
56.62 3.28 5.4 12.89 { 16.1 }
55.35 3.14 5.37 14.50 { 15.8 }
57.24 3.22 5.72 14.22 { 15.5 }
57.21 3.2 5.56 13.50 { 15.2 }
55.57 3.07 5.24 15.27 { 14.8 }
54.22 3.25 4.42 13.47 { 14.4 }
50.08 2.98 4.49 12.12 { 14.1 }
51.13 2.85 4.83 12.76 { 13.8 }
52.5 2.92 5.33 11.70 { 13.55 }
52.43 2.96 4.61 14.61 { 13.3 }
51.86 3.04 5.3 12.63 { 13 }
56.66 3.04 5.23 16.08 { 12.7 }
51.78 2.9 4.17 14.13 { 12.3 }
56.76 3.22 4.82 14.07 { 11.9 }
51.3 2.85 4.38 14.50 { 11.5 }
51.76 2.8 5.09 14.33 { 11.1 }
53.15 2.87 5.15 14.67 { 10.7 }
49.06 2.55 5.21 12.45 { 10.3 }
50.42 2.75 5.14 13.54 { 10 }
50.55 2.79 4.35 13.30 { 9.8 }
50.96 2.73 5.93 11.85 { 9.5 }
56.85 2.94 7.23 13.51 { 9.2 }
61.42 2.9 8.29 14.05 { 8.9 }
64.93 3.1 8.86 14.27 { 8.65 }
65.14 3.51 7.64 14.28 { 8.45 }
59.08 3.09 6.26 14.33 { 8.2 }
65.14 3.6 6.08 16.12 { 8 }
53.91 3.04 5.37 13.33 { 7.6 }
53.2 2.9 5.17 13.63 { 7.2 }
53.03 2.98 5.77 12.39 { 6.8 }
52.08 3.06 3.31 14.01 { 6.4 }
49.87 2.87 4.75 12.09 { 6 }

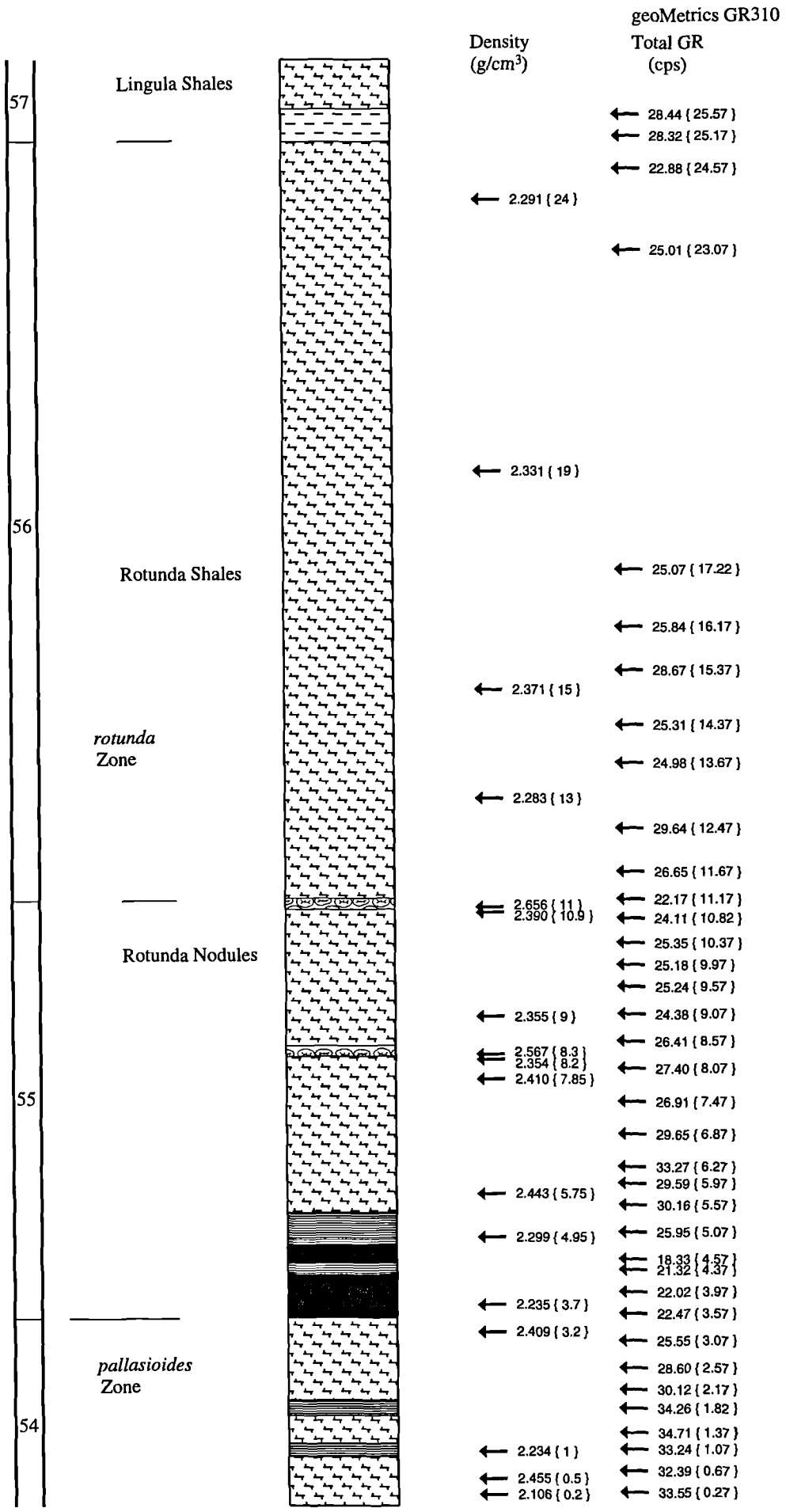
geoMetrics GR310
Density (g/cm³)
Total GR (cps)
57
Lingula Shales
56
Rotunda Shales
rotunda Zone
Rotunda Nodules
55
pallasioides Zone
54
28.44 { 25.57 }
28.32 { 25.17 }
22.88 { 24.57 }
2.291 { 24 }
25.01 { 23.07 }
2.331 { 19 }
25.07 { 17.22 }
25.84 { 16.17 }
28.67 { 15.37 }
2.371 { 15 }
25.31 { 14.37 }
24.98 { 13.67 }
2.283 { 13 }
29.64 { 12.47 }
26.65 { 11.67 }
2.656 { 11 }
22.17 { 11.17 }
2.390 { 10.9 }
24.11 { 10.82 }
25.35 { 10.37 }
25.18 { 9.97 }
25.24 { 9.57 }
2.355 { 9 }
24.38 { 9.07 }
26.41 { 8.57 }
2.567 { 8.3 }
2.354 { 8.2 }
27.40 { 8.07 }
2.410 { 7.85 }
26.91 { 7.47 }
29.65 { 6.87 }
33.27 { 6.27 }
29.59 { 5.97 }
2.443 { 5.75 }
30.16 { 5.57 }
2.299 { 4.95 }
25.95 { 5.07 }
18.33 { 4.57 }
21.32 { 4.37 }
22.02 { 3.97 }
2.235 { 3.7 }
22.47 { 3.57 }
2.409 { 3.2 }
25.55 { 3.07 }
28.60 { 2.57 }
30.12 { 2.17 }
34.26 { 1.82 }
34.71 { 1.37 }
2.234 { 1 }
33.24 { 1.07 }
32.39 { 0.67 }
2.455 { 0.5 }
2.106 { 0.2 }
33.55 { 0.27 }

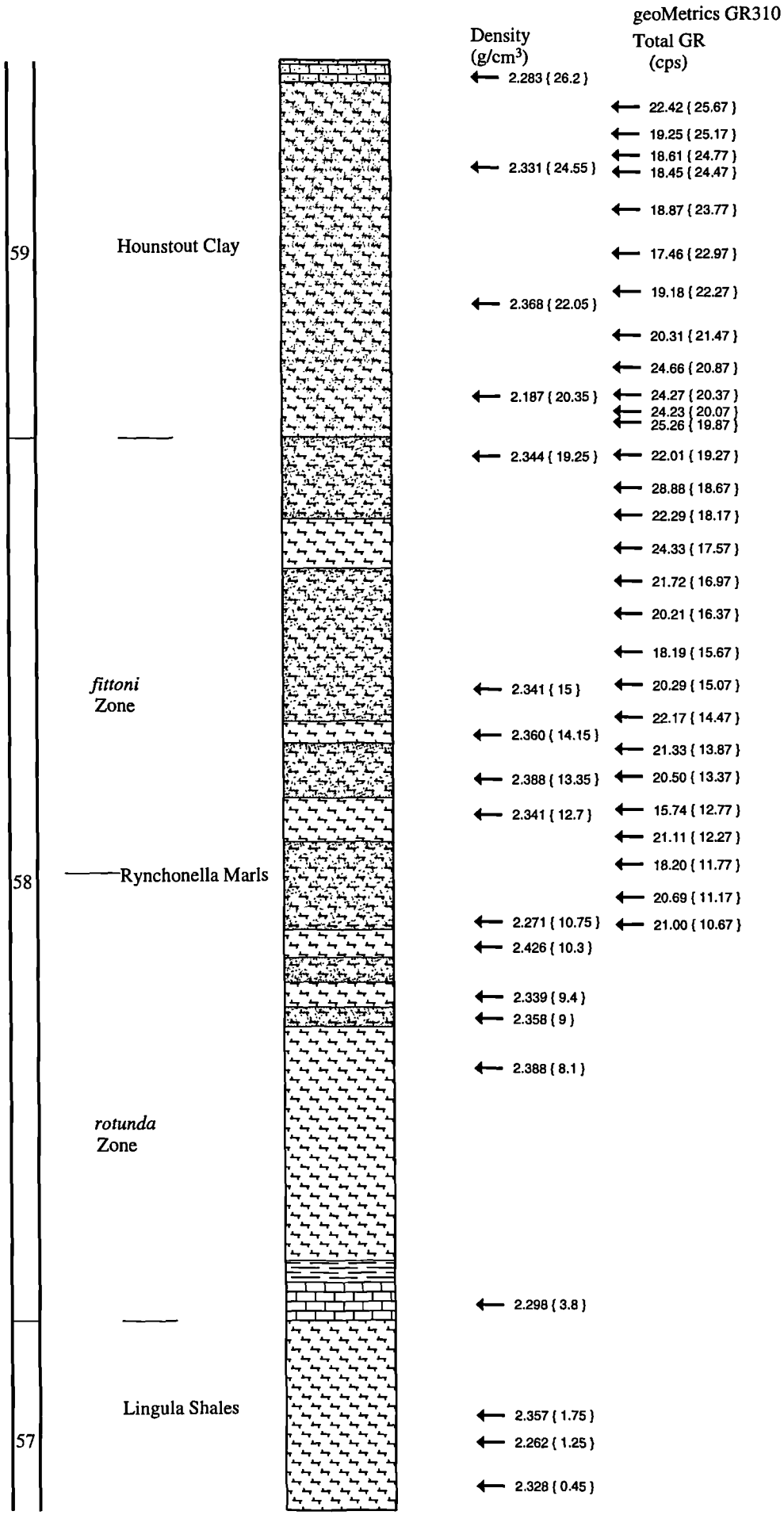
geoMetrics GR310
Density (g/cm³)
Total GR (cps)
59
Hounstout Clay
fittoni Zone
58
Rynchonella Marls
rotunda Zone
Lingula Shales
57
2.283 (26.2)
22.42 (25.67)
19.25 (25.17)
18.61 (24.77)
2.331 (24.55)
18.45 (24.47)
18.87 (23.77)
17.46 (22.97)
19.18 (22.27)
2.368 (22.05)
20.31 (21.47)
24.66 (20.87)
2.187 (20.35)
24.27 (20.37)
24.23 (20.07)
25.26 (19.87)
2.344 (19.25)
22.01 (19.27)
28.88 (18.67)
22.29 (18.17)
24.33 (17.57)
21.72 (16.97)
20.21 (16.37)
18.19 (15.67)
2.341 (15)
20.29 (15.07)
22.17 (14.47)
2.360 (14.15)
21.33 (13.87)
2.388 (13.35)
20.50 (13.37)
2.341 (12.7)
15.74 (12.77)
21.11 (12.27)
18.20 (11.77)
20.69 (11.17)
2.271 (10.75)
21.00 (10.67)
2.426 (10.3)
2.339 (9.4)
2.358 (9)
2.388 (8.1)
2.298 (3.8)
2.357 (1.75)
2.262 (1.25)
2.328 (0.45)

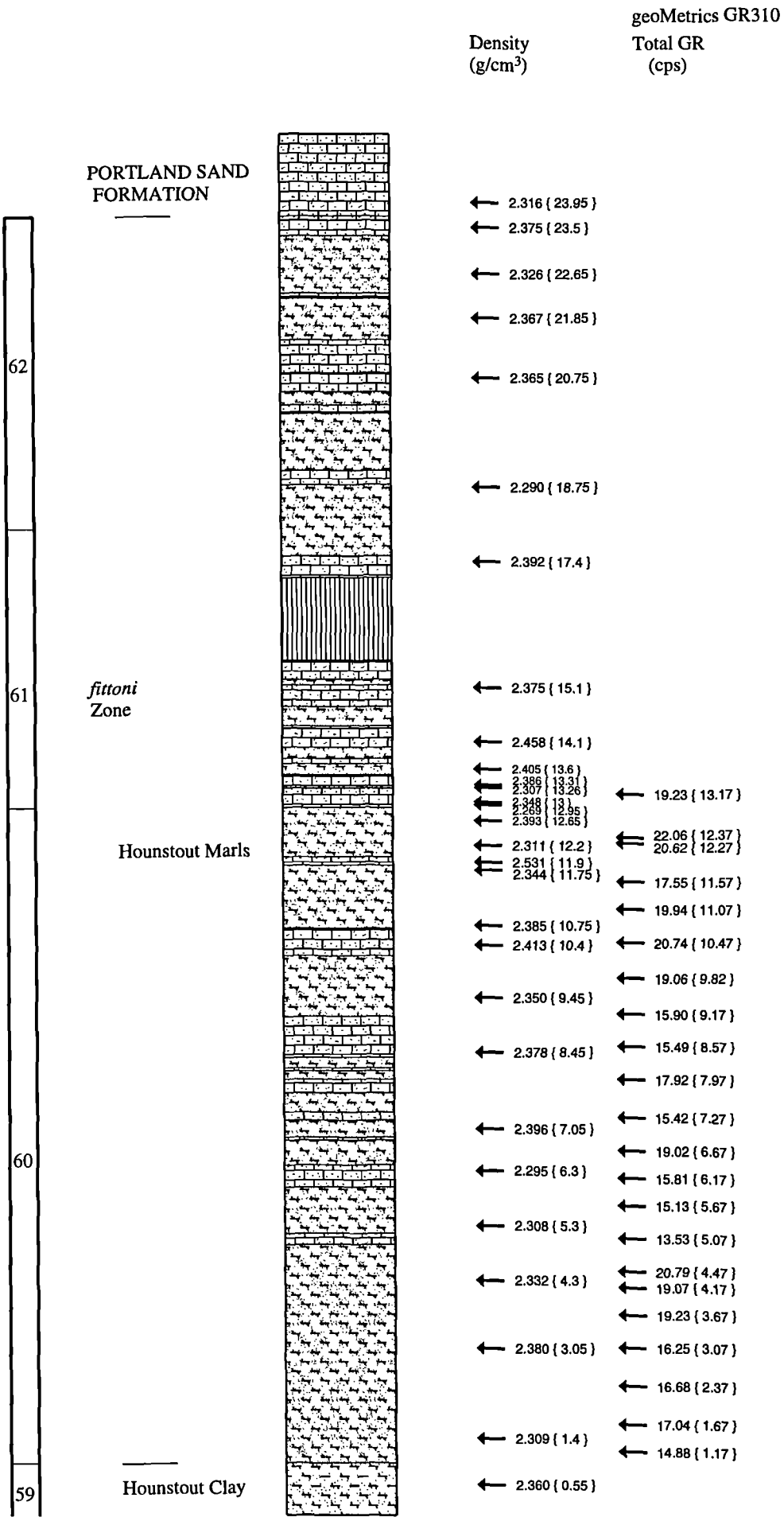
geoMetrics GR310
Density (g/cm³)
Total GR (cps)
PORTLAND SAND FORMATION
62
61
fittoni Zone
Hounstout Marls
60
59
Hounstout Clay
2.316 { 23.95 }
2.375 { 23.5 }
2.326 { 22.65 }
2.367 { 21.85 }
2.365 { 20.75 }
2.290 { 18.75 }
2.392 { 17.4 }
2.375 { 15.1 }
2.458 { 14.1 }
2.405 { 13.6 }
2.386 { 13.31 }
2.307 { 13.26 }
2.348 { 13 }
2.269 { 12.95 }
2.393 { 12.65 }
2.311 { 12.2 }
2.531 { 11.9 }
2.344 { 11.75 }
2.385 { 10.75 }
2.413 { 10.4 }
2.350 { 9.45 }
2.378 { 8.45 }
2.396 { 7.05 }
2.295 { 6.3 }
2.308 { 5.3 }
2.332 { 4.3 }
2.380 { 3.05 }
2.309 { 1.4 }
2.360 { 0.55 }
19.23 { 13.17 }
22.06 { 12.37 }
20.62 { 12.27 }
17.55 { 11.57 }
19.94 { 11.07 }
20.74 { 10.47 }
19.06 { 9.82 }
15.90 { 9.17 }
15.49 { 8.57 }
17.92 { 7.97 }
15.42 { 7.27 }
19.02 { 6.67 }
15.81 { 6.17 }
15.13 { 5.67 }
13.53 { 5.07 }
20.79 { 4.47 }
19.07 { 4.17 }
19.23 { 3.67 }
16.25 { 3.07 }
16.68 { 2.37 }
17.04 { 1.67 }
14.88 { 1.17 }

B.4 Portlandian

This section contains the stratigraphical / sedimentological logs of the Portlandian succession exposed at Winspit (SY 977761) and St. Alban's Head (SY 960754), Isle of Purbeck. The arrows show the location of the total gamma-ray measurements taken with the geoMetrics GR310. For more detailed stratigraphical and sedimentological logs of this Portlandian interval the reader is referred to Coe (1996).

Winspit (SY 977761) & St. Alban's Head
(SY 960754), Isle of Purbeck.

KEY

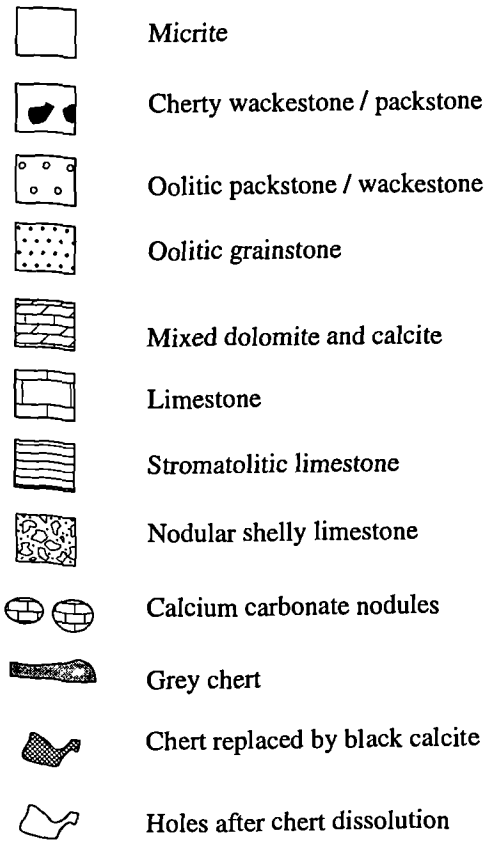

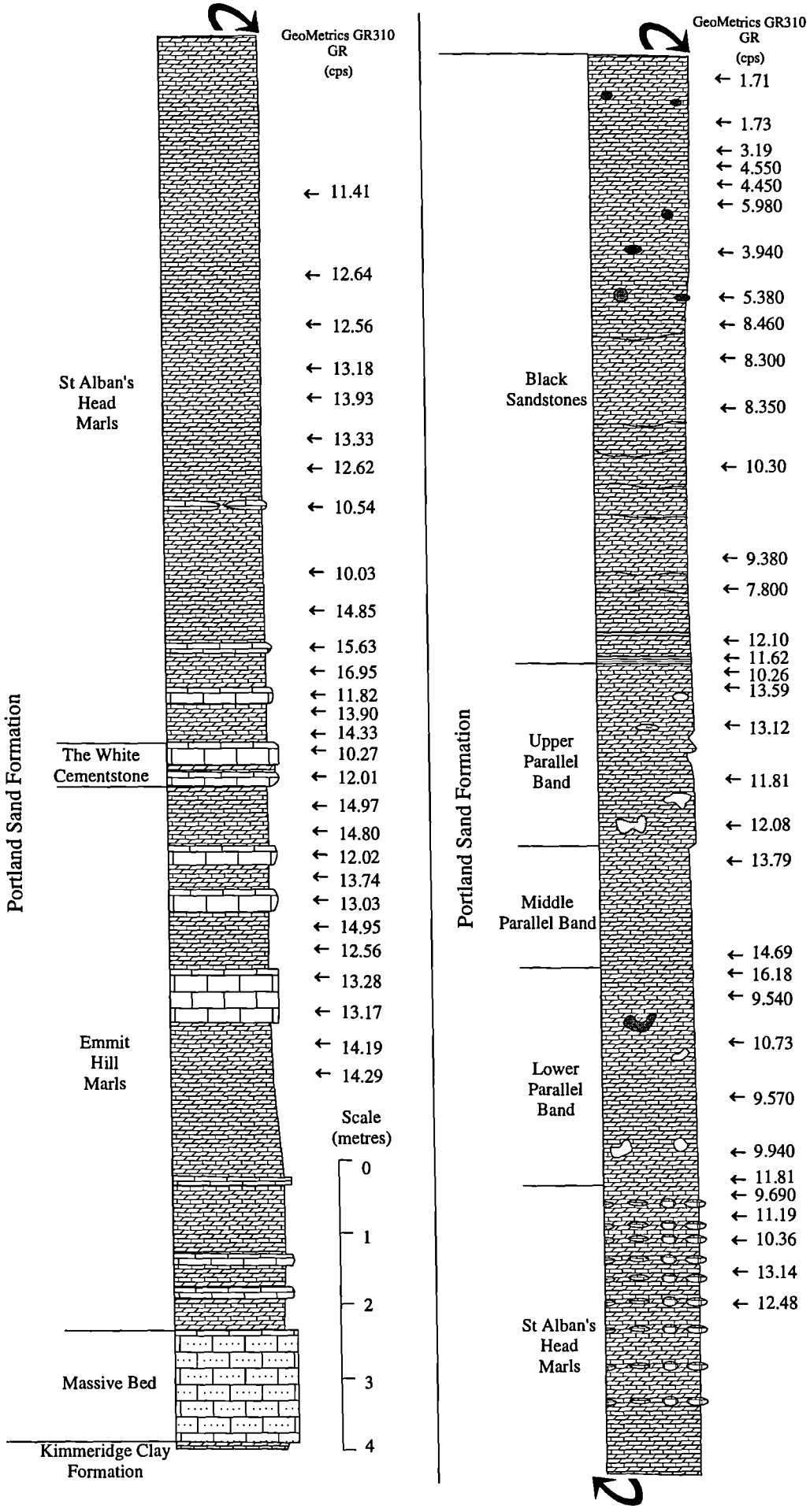
GeoMetrics GR310
GR
(cps)
← 11.41
← 12.64
← 12.56
← 13.18
← 13.93
← 13.33
← 12.62
← 10.54
← 10.03
← 14.85
← 15.63
← 16.95
← 11.82
← 13.90
← 14.33
← 10.27
← 12.01
← 14.97
← 14.80
← 12.02
← 13.74
← 13.03
← 14.95
← 12.56
← 13.28
← 13.17
← 14.19
← 14.29
Portland Sand Formation
St Alban's Head Marls
The White Cementstone
Emmit Hill Marls
Massive Bed
Kimmeridge Clay Formation
Scale (metres)
0
1
2
3
4
GeoMetrics GR310
GR
(cps)
← 1.71
← 1.73
← 3.19
← 4.550
← 4.450
← 5.980
← 3.940
← 5.380
← 8.460
← 8.300
← 8.350
← 10.30
← 9.380
← 7.800
← 12.10
← 11.62
← 10.26
← 13.59
← 13.12
← 11.81
← 12.08
← 13.79
← 14.69
← 16.18
← 9.540
← 10.73
← 9.570
← 9.940
← 11.81
← 9.690
← 11.19
← 10.36
← 13.14
← 12.48
Portland Sand Formation
Black Sandstones
Upper Parallel Band
Middle Parallel Band
Lower Parallel Band
St Alban's Head Marls

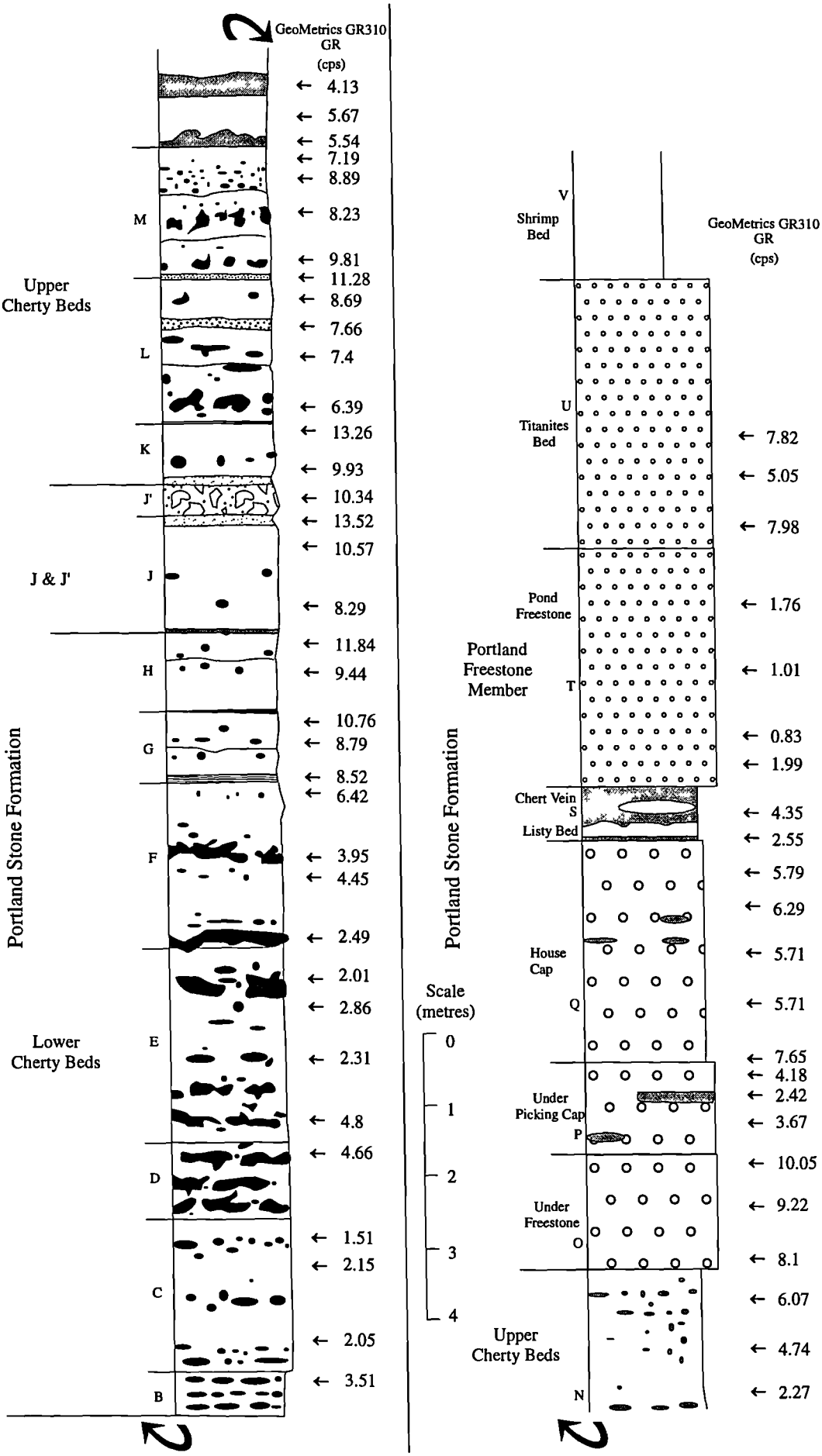
GeoMetrics GR310
GR
(cps)
← 4.13
← 5.67
← 5.54
← 7.19
← 8.89
M
← 8.23
← 9.81
← 11.28
Upper
Cherty Beds
← 8.69
← 7.66
L
← 7.4
← 6.39
← 13.26
K
← 9.93
J'
← 10.34
← 13.52
← 10.57
J & J'
J
← 8.29
← 11.84
H
← 9.44
← 10.76
G
← 8.79
← 8.52
← 6.42
Portland Stone Formation
F
← 3.95
← 4.45
← 2.49
← 2.01
← 2.86
Lower
Cherty Beds
E
← 2.31
← 4.8
← 4.66
D
← 1.51
← 2.15
C
← 2.05
← 3.51
B
Scale
(metres)
0
1
2
3
4
V
Shrimp
Bed
GeoMetrics GR310
GR
(cps)
U
Titanites
Bed
← 7.82
← 5.05
← 7.98
Pond
Freestone
← 1.76
Portland
Freestone
Member
T
← 1.01
← 0.83
← 1.99
Chert Vein
S
Listy Bed
← 4.35
← 2.55
← 5.79
← 6.29
House
Cap
← 5.71
Q
← 5.71
← 7.65
← 4.18
Under
Picking Cap
← 2.42
← 3.67
P
← 10.05
Under
Freestone
O
← 9.22
← 8.1
← 6.07
Upper
Cherty Beds
← 4.74
N
← 2.27
Portland Stone Formation

B.5 geoMetrics GR310 field log

The following table contains the total gamma-ray measurements made with the geoMetrics GR310 over most of the Upper Jurassic succession on the Dorset coast. The composite field gamma-ray log in Figure 2.2 was plotted using this data set.

General Statistics:
True vertical thickness = 503.52 m
Average distance between readings = 0.44 m
Number of readings = 1124
Total recording time = 31.22 hours (100 seconds each recording)

The total gamma-ray data in counts per second seen in Table B.5.1 has been corrected for background radiation. The background radiation recorded of Swanage in this study was 14.29 counts per second, therefore all the raw data was subtracted by 14.29 cps.

Table B.5.1

metres	GR (cps)
Furzy Cliff	
0.7	25.3
1.5	24.23
1.9	20.61
2.45	20.81
2.9	16.6
3.4	29.4
4.1	30.32
4.6	30.89
5.2	32.53
6.35	28.69
6.8	30.24
7.7	30.96
8.35	36.14
8.7	35.55
10	28.51
11	27.31
11.8	27.03
12.7	22.69
13.3	31.73
14.3	25.09
15.2	22.57
16	23.15
16.9	24.71
19.44	22.83
Redcliff &Hamcliff	
20.07	20.14
20.49	13.42
21.33	16.03
21.68	12
22.1	12.59
22.8	14.39
23.57	13.97
24.13	13.41
25.11	11.89
25.67	13.97
27	12.82
27.21	16.51
27.7	16.8
28.12	11.44
28.33	15.88
28.82	12.25
29.17	13.08
29.52	11.78
30.08	6.69
30.57	9.41
30.92	8.89

metres	GR (cps)
31.34	18.08
33.16	30.72
33.51	11.7
33.86	9.23
34.14	13.47
34.42	13.87
34.7	14.5
34.875	10.97
35.12	20.87
35.4	23.22
35.75	18.4
35.96	18.81
36.17	17.31
36.38	22
36.59	23.6
36.87	19.23
Branpoint	
37.48	19.98
37.97	19.64
38.25	16.07
38.6	2.87
39.02	13.78
39.16	14.56
39.93	10.19
40.07	12.05
40.35	8.92
40.56	8.17
40.7	11.99
41.05	9.28
41.4	8.68
41.61	10.91
41.96	10.64
42.345	9.88
42.625	11.66
43.01	9.41
43.5	10.22
43.85	9.52
44.2	7.92
44.48	3.75
44.76	8.29
45.145	13.65
45.46	8.08
45.88	0.54
48.26	20.77
48.68	7.75
48.89	9.67

metres	GR (cps)
49.17	6.63
49.73	15.32
50.36	6.56
50.78	13.51
51.27	7.05
51.41	11.38
51.725	9.8
51.83	6.83
52.04	8.65
52.39	6.39
52.705	5.2
52.74	11.57
53.09	5.68
53.335	6.47
53.51	4.72
53.72	4.55
54.14	3.29
54.49	8.6
54.7	6.66
55.12	5.55
55.365	10.13
55.82	6.89
56.17	10.04
56.59	13.58
57.08	16.02
57.64	11.58
57.99	20.41
58.41	12.95
58.865	4.92
59.18	10.86
59.6	17.77
59.88	16.74
60.09	7.41
60.23	4.21
60.72	4.59
61.21	5.61
61.665	5.61
62.05	9.58
62.19	7.28
62.68	8.76
63.03	7.63
63.31	16.46
63.38	8.68
63.52	10.14
63.73	9.93
63.87	12.28

metres	GR (cps)
64.15	7.27
64.43	18.42
64.64	7.98
64.815	10.46
64.99	6
65.13	16.16
65.27	5.33
65.41	10.23
65.69	8.97
66.39	21.02
66.81	26.61
Blackhead	
67.49	12.69
67.91	12.93
68.4	11.95
68.82	11.22
69.24	15.57
69.66	18.63
70.08	28.69
70.57	27.19
71.13	28.83
72.18	28.15
72.67	32.31
73.125	32.21
73.51	32.57
73.895	29.77
74.245	25.69
74.63	24.62
75.05	29.09
75.54	33.17
76.1	35.54
76.625	32.64
77.22	33.27
77.64	33.84
78.13	35.77
78.55	31.16
78.97	32.48
79.39	30.69
79.81	35.67
80.23	30.41
80.65	30.64
80.93	28.36
81.35	25.41
81.7	33.31
82.26	33.65
82.75	33.05

metres	GR (cps)
83.275	32.4
83.8	29.1
Osmington Mills	
83.87	25.47
84.22	23.54
84.52	22.29
84.72	20.61
85.08	35.61
85.34	25.35
85.51	20.56
85.68	35.95
85.9	34.22
86.15	24.44
86.42	29.33
86.72	27.94
86.97	29.02
87.2	25.17
87.42	24.24
87.6	23.21
87.77	23.22
87.91	23.77
88.02	24.53
88.25	20.23
88.74	28.52
88.97	22.77
89.2	24.85
89.65	35.98
90.05	34.42
90.42	24.61
90.54	19.78
Blackhead	
90.94	24.24
91.44	29.02
91.84	25.21
92.24	21.23
92.64	23.33
93.14	18.42
93.54	16.58
93.84	17.01
94.04	15.61
94.44	31.25
94.84	31.85
95.24	30.77
95.64	28.7
96.14	26.89
96.54	32.48

metres	GR (cps)
96.84	32.97
97.14	30.29
97.54	33.61
97.94	32.52
98.34	33.13
98.69	31.97
99.14	32.49
99.64	30.93
100.04	33.39
100.54	33.63
100.94	32.2
101.24	32.68
101.64	32.15
102.04	31.16
102.34	33.4
102.74	29.41
103.04	23.83
103.24	29.51
103.44	30.82
103.74	29.68
104.04	30.16
104.44	29.14
104.84	29.51
105.24	32.24
105.64	30.81
106.04	34.89
106.34	30.15
106.64	29.09
106.84	28.62
107.04	28.51
107.34	33.17
107.64	33.57
107.94	31.54
108.24	32.07
108.54	32.47
108.74	32.8
108.94	32.75
109.24	31.2
109.64	29.49
110.04	33.07
110.34	34.52
110.64	34.07
111.04	32.46
111.44	32.68
111.74	34.39
111.99	28.58
112.24	29.43
112.34	22.48
112.54	29.75
112.84	33.33
113.14	32.54
113.54	25.85
113.89	27.06
114.24	26.42

metres	GR (cps)
114.54	25.46
114.94	25.48
115.24	24.84
115.69	25.46
116.04	29.05
116.34	27.34
116.64	26.12
117.04	23.06
117.34	24.7
117.64	27.51
117.94	23.95
118.14	24.43
118.44	22.71
118.74	25.36
119.04	25.22
119.34	23.36
119.64	25.61
119.94	27.15
120.24	27.72
120.54	26.92
120.94	28.15
121.24	30.93
121.64	30.67
121.94	28.94
122.24	26.51
122.54	27.23
122.74	28.01
123.04	25.83
123.24	22.25
123.54	22.04
123.84	21.99
124.04	22.16
124.34	25.9
124.54	25.99
124.84	25.72
125.24	26
125.64	24.1
125.94	25.23
126.34	25.22
126.84	23.64
127.24	24.09
127.64	26.64
128.04	28.11
128.34	28
128.64	27.02
Hobarrow Bay to Chapman's Pool	
160.82	29.5
161.22	29.1
161.52	28.27
161.92	33.18
162.27	42.53
162.67	34.58
162.92	33.74

metres	GR (cps)
163.22	37.79
163.52	29.77
163.82	36.94
164.07	41.21
164.32	40.55
164.52	43.62
164.77	39.8
164.92	35.73
165.22	37.81
165.42	40.93
165.62	39.28
165.92	35.13
166.22	35.12
166.52	40.81
166.82	41.86
167.12	38.6
167.32	40.19
167.52	36.55
167.92	33.92
168.22	37.63
168.52	38.81
168.82	38.89
169.02	39.22
169.17	35.55
169.37	35.73
169.62	37.65
169.87	41.53
170.07	44.31
170.37	43.83
170.57	22.82
170.77	16.63
171.07	29.36
171.27	31.91
171.47	38.83
171.67	34.91
171.82	30.91
171.97	30.7
172.17	33.61
172.32	39.82
172.47	40.56
172.67	38.3
172.87	32.56
173.17	34.64
173.47	34.17
173.77	34.23
174.07	46.96
174.37	42.84
174.62	43.99
174.87	43.99
175.17	40.35
175.32	39.96
175.57	42.65
175.82	45.38
176.22	40.71

metres	GR (cps)
176.57	40.33
176.82	42.12
177.07	46.59
177.47	49.43
177.67	50.9
178.07	44.18
178.27	45.22
178.47	50.96
178.67	43.75
178.82	43.38
179.17	44.75
179.47	45.77
179.82	47.11
180.07	38.66
180.37	41.91
180.67	40.24
181.07	35.53
181.42	41.22
181.77	41.72
181.97	38.13
182.27	41.52
182.57	42.31
182.77	40.4
183.07	46.09
183.17	46.44
183.47	46.2
183.77	44.76
184.07	47.09
184.27	35.97
184.47	28.81
184.72	27.97
184.87	29.37
185.12	35.38
185.37	36.94
185.67	39.17
185.87	43.99
186.17	42.37
186.47	42.98
186.67	42.89
186.97	38.32
187.17	36.77
187.57	37.73
187.97	35.48
188.27	33.18
188.57	37.58
188.92	38.58
189.32	35.19
189.62	38.13
189.87	27.16
190.17	37.4
190.37	36.17
190.57	34.04
190.72	32.11
190.97	32.33

metres	GR (cps)
191.27	33.34
191.57	38.49
191.87	34.29
192.27	32.7
192.52	34.8
192.82	30.93
193.07	30.71
193.37	32.28
193.67	31.43
193.97	29.3
194.27	30.35
194.57	28.04
194.87	28.52
195.17	29.96
195.47	31.28
195.92	30.55
196.37	36.42
196.67	33.62
196.97	32.04
197.27	35.01
197.62	34.55
198.07	34.47
198.47	29.76
198.77	29.34
199.02	31.55
199.37	31.76
199.62	31.06
200.07	32.52
200.27	31.36
200.57	32.78
205.47	27.81
205.77	25.75
206.07	28.69
206.47	31.9
206.82	34.04
207.17	33.58
207.47	25.28
207.77	19.7
207.97	23.01
208.17	29.36
208.47	31.17
208.72	37.18
209.02	40.81
209.17	35.47
209.47	31.66
209.77	31.02
209.97	33.25
210.27	31.3
210.57	34.22
210.87	31.57
211.17	27.15
211.47	29.39
211.77	28.11
212.07	27.44

metres	GR (cps)
212.27	28.75
212.57	31.03
212.77	30.37
212.97	28.02
213.27	28.81
213.57	30.1
213.82	31.37
214.17	29.47
214.37	30.24
214.67	34.06
214.87	31.58
215.07	34.5
215.37	41.64
215.67	41.66
215.97	37.14
216.17	34.39
216.47	36.11
216.67	30.47
216.87	33.53
217.07	39.53
217.37	38.73
217.67	40.42
217.97	35.01
218.17	38.86
218.37	42.62
218.62	38.58
218.77	35.22
219.27	34.8
219.57	40.34
219.87	42.9
220.27	41.67
220.67	42.25
220.97	37.21
221.37	41.73
221.67	40.45
222.02	42.53
222.27	32.75
222.72	28.82
222.97	32.21
223.17	29.84
227.47	27.48
228.12	29.56
228.77	27.61
229.57	32.2
230.47	33.5
231.07	32.64
231.57	24.74
232.17	29.75
232.47	18.35
232.87	30.01
233.37	29.69
234.07	28.38
234.87	42.37
235.77	41.61

metres	GR (cps)
236.57	33.97
237.12	37.64
237.37	32.07
237.87	35.58
238.37	36.83
238.87	32.67
239.77	32.81
240.37	28.45
240.87	31.5
241.27	26.18
241.77	38.86
242.27	30.96
242.87	35.79
243.37	39.42
243.87	29.9
244.17	32.99
244.77	30.14
245.27	26.52
245.57	28.6
245.77	30.92
246.17	29.59
246.67	26.13
247.07	27.99
247.57	28.95
247.97	23.44
248.47	29.88
248.97	34.69
249.47	31.57
249.87	36.43
250.17	37.42
250.77	40.69
251.47	38.71
251.72	38.66
252.17	42.68
252.67	21.26
252.87	30.62
253.17	34.1
253.57	28.45
253.87	29.41
254.17	26.24
254.97	32.7
255.27	37.23
255.97	36.56
256.67	40.32
257.37	34.01
258.17	33.57
258.87	34.37
259.57	39.06
260.57	37.1
261.47	34.35
261.97	40.47
262.22	30.36
262.47	35.53
262.97	45.54

metres	GR (cps)
263.57	37.39
264.07	44.6
264.67	40.59
265.27	33.95
267.67	42.59
267.97	33.99
268.37	14.51
268.67	37.7
268.97	43.96
269.27	41.31
269.67	39.77
270.47	47.57
271.07	41.66
271.87	45.73
272.67	34.8
273.47	34.9
274.17	31.35
274.97	28.69
277.07	30.63
278.97	32.62
279.87	32.57
280.87	20.07
281.27	30.7
281.42	35.51
281.77	36.28
282.27	31.5
283.07	30.58
284.17	38.41
284.97	35.03
285.62	33.5
286.17	33.5
286.67	38.01
287.27	40.97
287.97	34.07
288.77	39.57
289.17	37.58
289.57	34.78
289.77	35.38
289.92	32.02
290.17	52.56
290.77	52.17
291.47	49.51
292.07	48.16
292.87	30.6
293.17	30.15
293.67	48.01
294.17	44.49
294.67	40.76
295.07	45.79
295.57	39.81
295.97	45.8
296.27	46.03
296.57	45.13
296.77	50.27

metres	GR (cps)
297.07	51.89
297.57	52.55
297.97	42.69
298.27	41.71
298.47	47.43
298.77	39.58
298.97	39.53
299.57	42.47
300.17	38.14
300.47	33.46
300.92	36.18
301.02	33.61
301.67	40.38
302.57	41.82
302.87	48.27
303.07	43.68
303.47	40.39
303.67	39.24
304.07	38.5
304.77	41.45
305.37	30.44
305.47	27.23
305.67	22.7
305.82	33.31
306.17	42.72
306.77	52.57
307.17	49.63
307.67	46.9
308.07	44.59
308.47	32.58
308.67	30.65
308.97	40.06
309.37	39.68
309.97	42.24
310.77	46.63
311.37	47.88
311.77	49.76
312.27	43.61
312.67	44.04
313.37	28.56
314.27	29.2
315.07	30.43
315.97	27.66
316.87	27.18
317.97	27.69
318.97	27.82
319.67	25.97
320.27	24.08
320.77	27.16
321.27	28.72
321.67	31.4
322.17	29.59
322.87	28.27
323.37	29.83

metres	GR (cps)
323.97	32.81
324.87	35.79
325.67	30.86
326.37	31.52
327.07	32.84
327.9	25.94
328.37	24.69
328.87	29.26
329.47	27.95
330.07	28.98
330.82	30.36
331.57	31.29
331.87	12.58
332.47	12.9
333.17	28.32
333.52	27.75
333.77	21.95
334.17	24.09
334.67	28.47
335.17	28.45
335.67	26.05
336.07	26.14
336.67	25.64
337.17	29.31
337.77	26.49
338.27	24.83
338.47	16.02
338.87	20.48
339.17	25.49
339.67	25.84
340.17	25.97
340.67	27.78
340.97	27.17
341.27	32.59
341.52	25.93
341.77	31.4
342.17	27.98
342.47	23.15
342.87	20.2
343.47	27.49
343.77	28.13
344.27	18.82
344.57	26.54
345.07	28.9
345.67	25.44
346.07	33.69
346.47	35.47
347.07	23
347.37	22.71
347.67	23.74
347.97	22.43
348.17	16.75
348.57	15.72
349.02	14.74

metres	GR (cps)
349.37	24.32
349.77	22.02
350.02	19.2
350.17	16.65
350.47	32.65
350.77	37.1
350.97	33.26
351.07	28.1
351.17	24.39
351.37	28.57
351.57	29.56
351.77	15.34
351.97	11.47
352.27	9.61
352.87	15.41
353.27	15.85
353.87	12.12
354.27	24.18
354.67	26.22
355.07	34.19
355.87	31.65
356.67	29.26
357.57	28.56
358.17	25.1
358.67	18.99
359.07	24.94
359.57	19.51
359.77	17.14
360.37	29.84
360.57	33.46
361.42	42.54
362.07	21.88
362.57	24.9
362.97	34.53
363.32	30.05
363.67	24.45
364.07	35.07
364.47	33.97
365.07	33.09
365.57	27.76
365.77	29.22
366.27	31.84
366.57	31.33
367.07	31.77
367.67	30.82
368.07	26.8
368.47	30.18
369.02	29.27
369.67	32.79
370.07	32.02
370.57	24.05
370.97	32.95
371.37	37.08
371.77	40.85

metres	GR (cps)
372.47	20.86
373.07	40.14
373.67	37.05
374.27	29.87
374.92	36.2
375.27	37.18
375.77	37.44
376.37	33.89
376.97	31.43
377.77	33.36
378.47	34.98
379.17	31.7
379.6	35.81
379.97	33.03
380.37	31.06
380.97	34.51
381.77	31.78
382.57	32.6
383.47	33.62
384.17	32.74
384.67	27.9
385.07	33.51
385.97	34.59
386.57	34.86
387.27	30.42
387.87	34.25
388.57	36.04
389.27	32.7
389.77	30.7
390.37	29.87
390.87	30.57
391.37	30.9
391.87	35.86
392.37	30.57
392.97	30.27
393.67	26.64
394.27	32.38
394.97	38.22
395.47	35.28
395.97	30.45
396.47	30.32
397.27	29.67
397.97	29.05
398.67	29.65
399.27	28.13
399.77	32.25
400.12	27.84
400.47	27.19
401.27	29.36
402.07	29.07
402.97	29.97
403.77	28.42
404.67	29.05
405.62	31.58

metres	GR (cps)
406.32	33.14
407.22	33.32
408.12	25.77
409.02	36.9
409.72	35.98
410.52	35.19
411.32	39.02
412.02	32.25
412.62	30.55
413.32	34.4
413.82	37.67
414.42	38.31
414.82	35.98
415.42	30.46
416.12	30.58
416.82	34.48
417.42	29.76
417.82	34.49
418.52	35.1
418.92	34.48
419.52	38.42
420.02	37.98
420.62	36.84
421.12	37.52
421.52	34.14
421.82	35.96
422.32	37.87
422.72	38.77
423.22	37.57
423.62	34.62
424.02	34.22
424.52	36.2
425.12	35.37
425.92	33.27
426.42	29.97
427.02	27.47
427.62	26.41
428.32	28.72
428.92	28.6
429.32	29.96
429.82	28.2
430.22	28.86
430.62	27.32
430.92	28.79
431.12	29.37
431.47	33.55
431.87	32.39
432.27	33.24
432.57	34.71
433.02	34.26
433.37	30.12
433.77	28.6
434.27	25.55
434.77	22.47

metres	GR (cps)
435.17	22.02
435.57	21.32
435.77	18.33
436.27	25.95
436.77	30.16
437.17	29.59
437.47	33.27
438.07	29.65
438.67	26.91
439.27	27.4
439.77	26.41
440.27	24.38
440.77	25.24
441.17	25.18
441.57	25.35
442.02	24.11
442.37	22.17
442.87	26.65
443.67	29.64
444.87	24.98
445.57	25.31
446.57	28.67
447.37	25.84
448.42	25.07
454.27	25.01
455.77	22.88
456.37	28.32
456.77	28.44
468.42	21
468.92	20.69
469.52	18.2
470.02	21.11
470.52	15.74
471.12	20.5
471.62	21.33
472.22	22.17
472.82	20.29
473.42	18.19
474.12	20.21
474.72	21.72
475.32	24.33
475.92	22.29
476.42	28.88
477.02	22.01
477.62	25.26
477.82	24.23
478.12	24.27
478.62	24.66
479.22	20.31
480.02	19.18
480.72	17.46
481.52	18.87
482.22	18.45
482.52	18.61

metres	GR (cps)
482.92	19.25
483.42	22.42
485.42	14.88
485.92	17.04
486.62	16.68
487.32	16.25
487.92	19.23
488.42	19.07
488.72	20.79
489.32	13.53
489.92	15.13
490.42	15.81
490.92	19.02
491.52	15.42
492.22	17.92
492.82	15.49
493.42	15.9
494.07	19.06
494.72	20.74
495.32	19.94
495.82	17.55
496.52	20.62
496.62	22.06
497.42	19.23
St Albans Head & Winspit	
513.87	14.29
514.37	14.19
514.97	13.17
515.37	13.28
515.77	12.56
516.17	14.95
516.52	13.03
516.87	13.74
517.17	12.02
517.57	14.8
517.87	14.97
518.17	12.01
518.57	10.27
518.87	14.33
519.07	13.9
519.37	11.82
519.67	16.95
519.97	15.63
520.47	14.85
521.07	10.03
521.92	10.54
522.37	12.62
522.87	13.33
523.37	13.93
523.87	13.18
524.37	12.56
524.87	12.64
525.87	11.41

metres	GR (cps)
530.37	12.48
530.87	13.14
531.37	10.36
531.97	11.19
532.27	9.69
532.47	11.81
532.87	9.94
533.47	9.57
534.37	10.73
534.87	9.54
535.17	16.18
535.52	14.69
536.87	13.79
537.27	12.08
538.14	11.81
538.67	13.12
539.07	13.59
539.37	10.26
539.62	11.62
539.77	12.1
540.77	7.8
541.17	9.38
542.17	10.3
543.07	8.35
543.47	8.3
544.17	8.46
544.52	5.38
545.12	3.94
545.82	5.98
546.12	4.45
546.32	4.55
546.62	3.19
547.02	1.73
547.62	1.71
548.42	3.51
549.02	2.05
549.82	2.15
550.32	1.51
551.52	4.66
552.02	4.8
552.82	2.31
553.62	2.86
553.82	2.01
554.52	2.49
555.32	4.45
555.82	3.95
556.52	6.42
557.995	8.52
558.42	8.79
558.72	10.76
559.42	9.44
559.82	11.84
560.02	8.29
561.27	10.57

metres	GR (cps)
561.495	13.52
561.82	10.34
562.32	9.93
562.77	13.26
563.07	6.39
563.62	7.4
564.17	7.66
564.57	8.69
564.87	11.28
565.12	9.81
565.37	8.23
565.72	8.89
566.47	7.19
566.77	5.54
567.07	5.67
567.57	4.13
568.145	2.27
569.07	4.74
569.57	6.07
570.12	8.1
570.82	9.22
571.57	10.05
572.07	3.67
572.52	2.42
572.82	4.18
573.02	7.65
573.57	5.71
574.07	5.71
574.62	6.29
575.17	5.79
575.57	2.55
575.92	4.35
576.52	1.99
576.97	0.83
578.02	1.01
579.17	1.76
579.92	7.98
580.52	5.05
581.07	7.82

B.6 Exploranium GR320 field log

The following table contains the spectral gamma-ray data recorded with the Exploranium GR320 over part of the Kimmeridge Clay Formation from the *eudoxus* to the *pallasioides* zones. The calculated concentrations of potassium, uranium and thorium data can be seen in Figure 2.9.

General Statistics:
Total thickness = 251 m
Average distance between readings = 0.30 m
Number of readings = 824
Total recording time = 45.77 hours (200 seconds each recording)

The stripping ratios and sensitivities for the Exploranium GR320 were determined from the calibration of the tool by EXPLORANIUM Ltd.

Stripping ratios:
alpha = 0.505127
beta = 0.62867
gamma = 0.924962
a = 0.046021

Sensitivities:
ksens = 3.443526
usens = 0.324028
tsens = 0.138008

Calibration total = 126 (used for eU conversion)

The background recorded in this study 2 km offshore Swanage:
Total counts (TCback) = 314.8286 counts per minute
Potassium (kback) = 28.45714 counts per minute
Uranium (uback) = 12 counts per minute
Thorium (tback) = 5.828571 counts per minute

The Exploranium GR320 displays and saves the total counts (ROI TC) and counts in the potassium (ROI K), uranium (ROI U) and thorium (ROI Th) windows after each measurement. As a precaution these values were noted in a field note book after each measurement. The Live Time is the actual time the detector crystal is counting gamma-rays during any one measurement. The Live Time is not displayed on the tool and is only available once the data is down loaded into a computer. In the Table B.6.1 it can be seen that the Live Time is not present for all the measurements, this loss of data was due to the tool's memory crashing in the field. The Live Time was needed to calculate the counts into concentrations of potassium, uranium and thorium, therefore because a constant recording time of 200 seconds was used the average of all the Live Times (194127.9) was used for these missing Live Time values.

Below is a brief explanation of how the counts measured by the tool were converted to counts per second (cps) and then concentrations, for more detail the reader is referred to IAEA (1976).

$$\text{Total counts (cps)} = \left(\frac{\text{ROI TC}}{\left(\frac{\text{Live Time}}{1000} \right) \times 60} - \text{TCback} \right) \div 60$$

$$\text{K (cps)} = \left(\frac{\text{ROI K}}{\left(\frac{\text{Live Time}}{1000} \right) \times 60} - \text{kback} \right) \div 60$$

$$\text{U (cps)} = \left(\frac{\text{ROI U}}{\left(\frac{\text{Live Time}}{1000} \right) \times 60} - \text{uback} \right) \div 60$$

$$\text{Th (cps)} = \left(\frac{\text{ROI Th}}{\left(\frac{\text{Live Time}}{1000} \right) \times 60} - \text{tback} \right) \div 60$$

To covert Total counts (cps) to Total counts (ppm eU):

$$\text{Total counts (ppm eU)} = \left(\frac{\text{ROI TC}}{\left(\frac{\text{Live Time}}{1000} \right) \times 60} - \text{TCback} \right) \div \text{Calibration Total}$$

To convert the ROI counts for K, U and Th to concentrations of K, U and Th:

Kcps = K counts per second, Ucps = U counts per second, Thcps = Th counts per second

uSTRIP = (Ucps - alpha * Thcps) / (1 - a * alpha)
tSTRIP = (Tcps - a * Ucps) / (1 - a * alpha)
kSTRIP = Kcps - (gamma * uSTRIP) - (beta * tSTRIP)

tconc - Int(tSTRIP / tsens * 100) / 100
uconc - Int(uSTRIP / usens * 100) / 100
kconc - Int(kSTRIP / ksens * 100) / 100

Where tconc, uconc and kconc are equal to Th ppm, U ppm and K % respectively.

Table B.6.1

Distance (M)	Live Time	ROI TC	ROI K	ROI U	ROI Th	Total count cps	K cps	U cps	Th cps	Total count ppm eU	K %k	U ppm	Th ppm
0	194196	9388	2029	390	379	43.1	9.97	1.81	1.85	20.52	2.32	2.75	13.14
0.4	194176	9063	1926	458	329	41.43	9.44	2.16	1.6	19.73	2.09	4.27	11.11
0.7	194288	8677	1755	432	306	39.41	8.56	2.02	1.48	18.77	1.87	4.03	10.27
1.1	194124	12117	2736	555	474	57.17	13.62	2.66	2.34	27.22	3.13	4.65	16.48
1.45	193884	13332	2987	636	509	63.52	14.93	3.08	2.53	30.25	3.39	5.69	17.7
1.85	194124	10983	2386	521	399	51.33	11.82	2.48	1.96	24.44	2.67	4.72	13.67
2.1	194160	10546	2200	558	388	49.07	10.86	2.67	1.9	23.37	2.34	5.41	13.19
2.4	194096	11083	2352	634	378	51.85	11.64	3.07	1.85	24.69	2.47	6.73	12.67
2.7	194280	9001	1781	569	251	41.08	8.69	2.73	1.19	19.56	1.74	6.71	7.93
3	194072	12108	2710	574	475	57.14	13.49	2.76	2.35	27.21	3.06	4.96	16.49
3.25	193940	13071	3031	583	521	62.15	15.15	2.81	2.59	29.6	3.52	4.73	18.25
3.5	194044	12996	3078	560	501	61.73	15.39	2.69	2.48	29.39	3.63	4.52	17.51
3.7	193800	13920	3258	609	524	66.58	16.34	2.94	2.61	31.7	3.83	5.13	18.33
3.95	194100	12632	2864	580	509	59.83	14.28	2.79	2.53	28.49	3.28	4.77	17.78
4.1	194124	11699	2674	574	424	55.02	13.3	2.76	2.09	26.2	3.02	5.37	14.54
4.4	194020	11847	2659	533	448	55.81	13.23	2.55	2.21	26.58	3.05	4.51	15.53
4.6	194172	12070	2722	573	430	56.91	13.54	2.75	2.12	27.1	3.09	5.31	14.76
4.8	194004	12741	2897	591	498	60.43	14.46	2.85	2.47	28.77	3.32	5.05	17.35
5.1	194120	11577	2614	555	403	54.39	12.99	2.66	1.98	25.9	2.96	5.24	13.77
5.4	194164	11244	2468	552	421	52.66	12.24	2.64	2.07	25.08	2.75	5.04	14.46
5.7	194148	11911	2800	551	430	56.1	13.95	2.64	2.12	26.72	3.24	4.95	14.8
6	194220	12034	2805	502	467	56.71	13.97	2.38	2.31	27.01	3.31	3.85	16.3
6.3	194080	11342	2541	483	449	53.19	12.62	2.29	2.22	25.33	2.94	3.69	15.66
6.5	194116	11845	2681	517	460	55.77	13.34	2.46	2.27	26.56	3.1	4.15	16.01
6.7	194188	10637	2406	508	371	49.53	11.92	2.42	1.81	23.59	2.72	4.73	12.62
7.1	194116	10272	2207	502	380	47.67	10.9	2.39	1.86	22.7	2.43	4.56	12.98
7.4	194232	11435	2627	534	419	53.63	13.05	2.55	2.06	25.54	3.01	4.76	14.41
7.7	194104	11889	2682	528	430	56	13.34	2.52	2.12	26.67	3.1	4.58	14.85
8	194008	12145	2669	611	431	57.35	13.28	2.95	2.12	27.31	2.96	5.92	14.75
8.2	194076	12112	2776	575	445	57.16	13.83	2.76	2.2	27.22	3.17	5.22	15.34
8.35	194120	11203	2460	564	364	52.46	12.2	2.71	1.78	24.98	2.73	5.71	12.26
8.55	193988	11412	2454	595	406	53.58	12.18	2.87	2	25.51	2.67	5.87	13.82
8.8	193984	12492	2816	595	474	59.15	14.04	2.87	2.35	28.17	3.2	5.31	16.42
9.05	193916	12555	2828	558	472	59.5	14.11	2.68	2.34	28.33	3.27	4.73	16.42
9.25	193904	13120	2920	649	557	62.42	14.58	3.15	2.78	29.72	3.26	5.51	19.51
9.55	193992	11736	2613	565	451	55.25	13	2.71	2.23	26.31	2.94	5.01	15.59
9.75	194348	6655	1432	325	226	29	6.89	1.47	1.07	13.81	1.55	2.95	7.4
9.95	194408	7414	1539	366	283	32.89	7.44	1.68	1.36	15.66	1.64	3.14	9.5
10.25	194128	11332	2490	530	441	53.13	12.35	2.53	2.17	25.3	2.8	4.52	15.26
10.45	194004	12700	2931	590	493	60.22	14.63	2.84	2.44	28.67	3.37	5.07	17.16
10.65	193884	13379	3063	636	520	63.76	15.32	3.08	2.58	30.36	3.5	5.6	18.12
10.85	193940	11437	2544	531	435	53.72	12.64	2.54	2.15	25.58	2.89	4.59	15.05
11	193960	12491	2798	630	426	59.15	13.95	3.05	2.1	28.17	3.13	6.28	14.53
11.15	194116	11985	2613	605	402	56.49	12.99	2.92	1.97	26.9	2.89	6.06	13.64
11.35	194072	12278	2725	639	453	58.02	13.57	3.09	2.24	27.63	3	6.2	15.53
11.5	194052	11596	2525	538	459	54.51	12.54	2.57	2.27	25.96	2.84	4.5	15.94
11.65	193976	11730	2668	585	410	55.22	13.28	2.82	2.02	26.3	3	5.67	13.99
11.85	194236	10145	2212	512	342	46.98	10.91	2.44	1.66	22.37	2.44	5.04	11.5
12.05	193924	11685	2478	571	448	55.01	12.3	2.74	2.21	26.19	2.73	5.13	15.48
12.35	194200	10441	2356	465	369	48.52	11.66	2.19	1.8	23.1	2.71	4.05	12.62
12.65	194328	10244	2422	469	370	47.47	11.99	2.21	1.81	22.6	2.8	4.1	12.64
12.95	194096	10525	2309	516	395	48.98	11.42	2.46	1.94	23.32	2.56	4.67	13.53
13.25	193732	13741	3324	576	486	65.68	16.68	2.77	2.41	31.28	3.99	4.91	16.94
13.55	193792	13491	3133	659	470	64.37	15.69	3.2	2.33	30.65	3.59	6.39	16.17
13.8	193908	13462	3126	617	543	64.18	15.65	2.98	2.7	30.56	3.61	5.1	19.03
14.05	194064	12681	2961	599	487	60.1	14.78	2.89	2.41	28.62	3.4	5.27	16.91
14.35	194012	12240	2833	519	488	57.84	14.13	2.48	2.42	27.54	3.32	3.96	17.09
14.5	193916	11717	2628	523	422	55.18	13.08	2.5	2.08	26.27	3.03	4.57	14.57
14.75	193924	12727	2905	549	491	60.38	14.51	2.63	2.43	28.75	3.39	4.42	17.16
15	193928	12750	2966	585	502	60.5	14.82	2.82	2.49	28.81	3.43	4.92	17.52
15.4	194000	11803	2829	461	435	55.59	14.11	2.18	2.15	26.47	3.41	3.45	15.17
15.75	194096	11942	2819	508	443	56.28	14.05	2.42	2.19	26.8	3.33	4.14	15.38
16	194168	12189	2791	543	474	57.53	13.9	2.6	2.34	27.39	3.23	4.46	16.5
16.25	193996	12760	2997	523	487	60.53	14.97	2.5	2.41	28.82	3.56	4.03	17.05
16.65	193676	13322	3120	625	511	63.54	15.64	3.03	2.54	30.26	3.61	5.5	17.81
16.85	194024	11544	2622	514	427	54.25	13.04	2.45	2.1	25.83	3.03	4.38	14.76
17.25	194040	12617	2991	567	486	59.78	14.94	2.72	2.41	28.46	3.49	4.75	16.93
17.45	193820	13847	3248	578	542	66.2	16.28	2.78	2.7	31.52	3.85	4.48	19.07
17.65	193736	14424	3460	593	564	69.2	17.39	2.86	2.81	32.95	4.15	4.54	19.89

Distance						Total count	K	U	Th	Total count	K	U	Th
(M)	Live Time	ROI TC	ROI K	ROI U	ROI Th	cps	cps	cps	cps	ppm eU	%k	ppm	ppm
17.85	194220	11831	2645	523	457	55.67	13.14	2.49	2.26	26.51	3.04	4.27	15.88
18	194104	11583	2645	522	430	54.43	13.15	2.49	2.12	25.92	3.05	4.48	14.86
18.35	194040	12341	2831	591	468	58.35	14.12	2.85	2.31	27.79	3.22	5.29	16.2
18.65	194112	12437	2958	563	456	58.82	14.76	2.7	2.25	28.01	3.46	4.93	15.78
19	194024	12507	2910	507	469	59.21	14.52	2.41	2.32	28.2	3.46	3.92	16.38
19.25	194068	10453	2350	500	371	48.62	11.63	2.38	1.81	23.15	2.65	4.61	12.64
19.55	194260	11178	2486	507	399	52.29	12.32	2.41	1.96	24.9	2.84	4.49	13.69
19.85	194224	11026	2547	508	369	51.52	12.64	2.42	1.8	24.53	2.94	4.75	12.54
20.25	194048	10323	2287	504	364	47.95	11.31	2.4	1.78	22.83	2.56	4.73	12.37
20.6	194152	11511	2597	490	391	54.04	12.9	2.32	1.92	25.73	3.03	4.28	13.42
20.95	194220	10254	2247	460	346	47.55	11.1	2.17	1.68	22.64	2.56	4.16	11.75
21.15	194084	10243	2254	468	385	47.53	11.14	2.21	1.89	22.63	2.55	3.97	13.24
21.45	194300	10962	2572	508	393	51.17	12.76	2.41	1.93	24.37	2.97	4.55	13.45
21.75	194164	10932	2624	464	404	51.06	13.04	2.19	1.98	24.31	3.1	3.75	13.96
21.95	194068	11178	2624	483	421	52.35	13.05	2.29	2.07	24.93	3.07	3.92	14.59
22.25	194096	10894	2379	545	413	50.88	11.78	2.61	2.03	24.23	2.62	4.99	14.17
22.35	194156	11177	2447	540	385	52.32	12.13	2.58	1.89	24.91	2.74	5.14	13.1
22.65	193968	12128	2688	501	444	57.28	13.38	2.38	2.19	27.28	3.14	4.03	15.44
22.95	194020	12250	2742	566	466	57.89	13.66	2.72	2.3	27.57	3.13	4.9	16.16
23.25	193976	12328	2944	507	466	58.31	14.7	2.41	2.31	27.77	3.51	3.94	16.27
23.45	194228	9240	2087	392	348	42.33	10.27	1.82	1.69	20.16	2.41	3.04	11.95
23.65	194300	7599	1426	451	212	33.86	6.86	2.12	0.99	16.12	1.38	5.11	6.64
23.9	194328	7146	1365	443	234	31.53	6.55	2.08	1.11	15.01	1.29	4.8	7.5
24.05	194028	10339	2322	449	375	48.04	11.49	2.11	1.84	22.88	2.68	3.75	12.89
24.3	193992	11067	2496	472	388	51.8	12.39	2.23	1.9	24.67	2.91	4.01	13.35
24.55	193264	10461	2453	456	376	48.88	12.22	2.16	1.85	23.28	2.88	3.87	12.97
24.85	194056	11467	2746	483	431	53.84	13.68	2.29	2.12	25.64	3.25	3.84	14.97
25.05	194124	11855	2827	547	414	55.82	14.09	2.62	2.04	26.58	3.29	5.02	14.2
25.35	194120	12046	2790	544	438	56.81	13.9	2.6	2.16	27.05	3.23	4.77	15.12
25.65	194000	11894	2848	511	434	56.06	14.21	2.43	2.14	26.7	3.37	4.27	15.04
25.85	194112	11644	2737	512	447	54.74	13.63	2.44	2.21	26.07	3.2	4.18	15.53
26.15	194032	10967	2495	560	388	51.27	12.38	2.69	1.9	24.42	2.78	5.45	13.19
26.35	194192	10458	2356	466	367	48.61	11.66	2.2	1.79	23.15	2.71	4.08	12.54
26.75	194160	11108	2564	477	418	51.96	12.73	2.26	2.06	24.74	2.99	3.84	14.47
27.15	194132	10825	2487	496	403	50.51	12.34	2.35	1.98	24.05	2.86	4.28	13.87
27.45	194296	9393	2155	393	320	43.1	10.62	1.82	1.55	20.52	2.52	3.28	10.87
27.75	194224	10904	2497	459	379	50.89	12.38	2.16	1.85	24.24	2.93	3.87	13.01
28.1	194036	11152	2640	442	396	52.23	13.13	2.08	1.94	24.87	3.16	3.46	13.7
28.5	194140	9890	2100	457	341	45.7	10.34	2.15	1.66	21.76	2.35	4.15	11.57
28.8	194064	11518	2572	517	411	54.1	12.78	2.46	2.02	25.76	2.95	4.56	14.14
29.05	194088	11200	2594	452	421	52.46	12.89	2.13	2.07	24.98	3.07	3.41	14.64
29.35	194016	11025	2566	481	416	51.58	12.75	2.28	2.05	24.56	2.99	3.93	14.4
29.55	194260	10681	2537	501	366	49.74	12.59	2.38	1.79	23.68	2.93	4.66	12.44
29.75	194072	9804	2314	439	363	45.27	11.45	2.06	1.77	21.56	2.69	3.68	12.45
29.9	194236	9360	2106	425	339	42.94	10.37	1.99	1.65	20.45	2.4	3.65	11.54
30.15	194220	10513	2445	456	426	48.88	12.11	2.15	2.1	23.28	2.84	3.44	14.81
30.45	194224	11300	2621	464	413	52.93	13.02	2.19	2.03	25.21	3.1	3.67	14.3
30.75	194068	11554	2543	517	453	54.29	12.63	2.46	2.24	25.85	2.9	4.21	15.75
31.05	194212	9837	2155	442	392	45.4	10.62	2.08	1.92	21.62	2.43	3.49	13.54
31.45	194080	10337	2347	491	412	48.01	11.62	2.33	2.03	22.86	2.65	4.12	14.23
31.7	194140	11072	2491	479	394	51.78	12.36	2.27	1.93	24.66	2.89	4.07	13.56
32	194236	9825	2234	414	407	45.34	11.03	1.93	2	21.59	2.59	2.91	14.16
32.25	194220	9146	2046	428	324	41.84	10.06	2	1.57	19.93	2.31	3.82	10.97
32.55	194288	9665	2186	435	404	44.5	10.78	2.04	1.98	21.19	2.49	3.27	14
32.85	194244	9296	2043	391	355	42.61	10.04	1.81	1.73	20.29	2.35	2.96	12.21
33.15	194340	9587	2116	411	372	44.08	10.41	1.91	1.82	20.99	2.42	3.15	12.82
33.45	194188	9255	2026	435	383	42.41	9.96	2.04	1.88	20.2	2.25	3.45	13.21
33.75	194252	9057	2071	400	353	41.38	10.19	1.86	1.72	19.7	2.38	3.12	12.12
34.05	194088	8986	2061	390	317	41.05	10.14	1.81	1.54	19.55	2.39	3.26	10.77
34.35	194264	9503	2011	430	365	43.67	9.88	2.01	1.78	20.8	2.24	3.51	12.53
34.65	194216	10860	2392	487	419	50.67	11.84	2.31	2.06	24.13	2.72	4	14.49
35.1	194028	11308	2617	514	412	53.03	13.01	2.45	2.03	25.25	3.02	4.5	14.19
35.55	194028	11126	2512	498	421	52.1	12.47	2.37	2.07	24.81	2.89	4.16	14.56
35.85	194092	10425	2357	473	390	48.46	11.67	2.24	1.91	23.08	2.7	4.01	13.42
36.15	194132	10600	2318	499	406	49.35	11.47	2.37	1.99	23.5	2.6	4.3	13.98
36.45	194228	10745	2474	471	447	50.07	12.26	2.22	2.2	23.84	2.86	3.51	15.59
36.8	194128	11132	2560	522	352	52.1	12.71	2.49	1.72	24.81	2.94	5.12	11.88
37.25	194148	11371	2644	503	471	53.32	13.14	2.39	2.33	25.39	3.06	3.83	16.46
37.65	194112	10791	2416	520	393	50.34	11.97	2.48	1.93	23.97	2.72	4.75	13.45
37.95	194168	10504	2315	499	424	48.85	11.45	2.37	2.09	23.26	2.59	4.15	14.66

Distance						Total count	K	U	Th	Total count	K	U	Th
(M)	Live Time	ROI TC	ROI K	ROI U	ROI Th	cps	cps	cps	cps	ppm eU	%k	ppm	ppm
38.2	194084	10881	2317	509	431	50.82	11.46	2.42	2.12	24.2	2.58	4.26	14.92
38.55	194116	11085	2458	490	436	51.86	12.19	2.32	2.15	24.69	2.81	3.91	15.14
38.8	194176	11409	2586	492	428	53.51	12.84	2.33	2.11	25.48	3	4.01	14.83
39.25	194132	11296	2561	481	417	52.94	12.72	2.28	2.05	25.21	2.98	3.92	14.43
39.45	194144	11152	2522	482	466	52.19	12.52	2.28	2.3	24.85	2.91	3.53	16.3
39.75	194248	11116	2491	513	404	51.98	12.35	2.44	1.98	24.75	2.84	4.54	13.87
44.65		10600	2382	457	424	49.36	11.8	2.15	2.09	23.5	2.75	3.47	14.74
44.95		10170	2280	449	370	47.14	11.27	2.11	1.81	22.45	2.62	3.78	12.69
45.25		10735	2486	451	416	50.05	12.33	2.12	2.05	23.83	2.91	3.44	14.45
45.65		12311	2863	521	489	58.17	14.27	2.48	2.42	27.7	3.36	3.98	17.11
46		12374	2956	514	470	58.49	14.75	2.45	2.32	27.85	3.52	4.02	16.4
46.35		12037	2833	475	470	56.76	14.12	2.25	2.32	27.03	3.39	3.39	16.47
46.65		9783	2231	423	334	45.15	11.02	1.98	1.62	21.5	2.59	3.66	11.36
46.95		7543	1569	335	252	33.61	7.61	1.53	1.2	16	1.74	2.9	8.38
47.15		8588	1783	435	312	38.99	8.71	2.04	1.51	18.57	1.91	4.03	10.5
47.35	193928	11554	2558	570	391	54.33	12.72	2.74	1.92	25.87	2.87	5.59	13.3
47.65	193912	11598	2522	551	479	54.56	12.53	2.64	2.37	25.98	2.82	4.55	16.7
47.9	193812	12162	2786	552	447	57.5	13.9	2.65	2.21	27.38	3.22	4.84	15.48
48.2	194012	12079	2747	558	426	57.01	13.68	2.68	2.1	27.15	3.16	5.1	14.65
48.35	193956	11855	2604	672	419	55.87	12.95	3.26	2.06	26.61	2.79	7.02	14.19
48.65	194356	10211	2174	530	358	47.29	10.71	2.53	1.74	22.52	2.35	5.19	12.08
48.95	194180	10638	2299	477	429	49.54	11.37	2.26	2.11	23.59	2.59	3.75	14.89
49.15	194096	10864	2443	469	402	50.73	12.11	2.22	1.97	24.15	2.83	3.85	13.88
49.45	194016	11479	2592	553	493	53.92	12.89	2.65	2.44	25.68	2.91	4.47	17.22
49.75	194152	11199	2392	535	437	52.43	11.85	2.56	2.15	24.97	2.65	4.63	15.1
50.05	193972	11761	2585	576	474	55.39	12.85	2.77	2.35	26.37	2.88	5	16.46
50.35	193992	11244	2426	549	443	52.71	12.03	2.63	2.19	25.1	2.68	4.82	15.32
50.65	193956	11918	2593	580	465	56.2	12.89	2.79	2.3	26.76	2.89	5.14	16.11
50.95	194136	10240	2170	448	467	47.5	10.7	2.11	2.31	22.62	2.43	2.97	16.4
51.25	194164	10687	2366	478	472	49.79	11.71	2.26	2.33	23.71	2.68	3.42	16.54
51.45	194120	11051	2448	480	474	51.68	12.14	2.27	2.34	24.61	2.8	3.43	16.61
51.75	193912	11821	2647	606	443	55.71	13.18	2.93	2.19	26.53	2.94	5.75	15.22
51.95	194224	10352	2177	510	418	48.05	10.73	2.43	2.06	22.88	2.37	4.38	14.41
52.15	194068	10834	2446	482	425	50.58	12.13	2.28	2.09	24.09	2.81	3.87	14.74
52.45	194120	10917	2438	505	422	50.99	12.08	2.4	2.08	24.28	2.77	4.27	14.58
52.75	194168	10990	2490	469	435	51.35	12.35	2.22	2.14	24.45	2.89	3.57	15.14
53	194112	11344	2480	515	431	53.19	12.3	2.45	2.12	25.33	2.81	4.36	14.91
53.35	194116	11514	2589	505	465	54.07	12.86	2.4	2.3	25.75	2.98	3.91	16.23
53.55	194048	11095	2360	540	461	51.93	11.69	2.58	2.28	24.73	2.59	4.52	16.02
53.85	193820	11270	2461	505	439	52.9	12.22	2.41	2.17	25.19	2.8	4.14	15.26
54.05	194004	12304	2685	573	511	58.17	13.37	2.75	2.54	27.7	3.02	4.65	17.87
54.25	193912	12442	2820	569	510	58.92	14.07	2.73	2.53	28.06	3.23	4.59	17.85
54.55	194092	11696	2640	523	458	55.01	13.13	2.49	2.26	26.2	3.03	4.27	15.93
54.85	194072	11812	2754	505	493	55.62	13.72	2.4	2.44	26.48	3.22	3.69	17.3
55.15	194076	11736	2606	534	488	55.22	12.95	2.55	2.42	26.3	2.96	4.2	17.06
55.35	194048	12935	2914	568	507	61.41	14.54	2.73	2.52	29.24	3.37	4.6	17.73
55.65	193984	11248	2418	486	465	52.74	11.99	2.31	2.3	25.11	2.75	3.61	16.27
55.85	194100	10203	2135	482	424	47.32	10.53	2.28	2.09	22.53	2.34	3.88	14.7
56.05	194168	10590	2333	510	435	49.29	11.54	2.43	2.14	23.47	2.6	4.24	15.07
56.25	194108	11087	2439	489	441	51.87	12.09	2.32	2.17	24.7	2.78	3.85	15.34
56.55	194020	11766	2677	527	462	55.4	13.32	2.52	2.28	26.38	3.08	4.3	16.08
56.85	194188	11855	2743	513	479	55.8	13.65	2.44	2.37	26.57	3.2	3.93	16.74
57.15	194140	12116	2805	529	507	57.16	13.97	2.52	2.51	27.22	3.26	3.96	17.79
57.35	194212	12156	2796	528	495	57.34	13.92	2.52	2.45	27.31	3.25	4.04	17.32
57.65	193996	11101	2521	521	439	51.98	12.52	2.49	2.17	24.75	2.86	4.39	15.21
57.9	194120	10705	2395	468	424	49.9	11.86	2.21	2.09	23.76	2.75	3.65	14.72
58.05	193952	11131	2469	504	444	52.14	12.26	2.4	2.19	24.83	2.81	4.07	15.44
58.55	194056	12548	2933	526	491	59.41	14.64	2.51	2.43	28.29	3.46	4.04	17.19
58.85	193948	12786	2977	544	496	60.68	14.88	2.6	2.46	28.89	3.5	4.3	17.36
59.15	194100	12500	2878	532	527	59.15	14.35	2.54	2.62	28.17	3.36	3.84	18.55
59.55	194064	12616	2984	519	497	59.76	14.9	2.47	2.46	28.46	3.55	3.88	17.43
59.95	194052	13142	3079	550	531	62.48	15.39	2.63	2.64	29.75	3.64	4.11	18.67
60.25	194060	12315	2760	533	491	58.21	13.75	2.55	2.43	27.72	3.19	4.16	17.17
60.65	194012	12308	2886	507	488	58.19	14.4	2.41	2.42	27.71	3.42	3.76	17.11
60.95	194144	12319	2796	541	476	58.21	13.93	2.59	2.35	27.72	3.24	4.41	16.58
61.3	194152	12219	2791	502	511	57.69	13.9	2.39	2.53	27.47	3.27	3.49	17.98
61.55	194448	9130	2136	401	326	41.71	10.51	1.86	1.58	19.86	2.48	3.36	11.08
62	194400	9857	2225	449	423	45.46	10.97	2.11	2.08	21.65	2.52	3.34	14.7
62.25	194420	9468	2088	423	380	43.45	10.27	1.98	1.86	20.69	2.36	3.27	13.1
62.45	194344	8659	1864	425	339	39.31	9.12	1.99	1.65	18.72	2.03	3.64	11.54

Distance						Total count	K	U	Th	Total count	K	U	Th
(M)	Live Time	ROI TC	ROI K	ROI U	ROI Th	cps	cps	cps	cps	ppm eU	%k	ppm	ppm
65.7		9981	2170	470	394	46.17	10.7	2.22	1.93	21.98	2.42	3.93	13.57
65.85		10321	2319	502	419	47.92	11.47	2.39	2.06	22.82	2.59	4.24	14.47
66.35		10596	2299	455	421	49.34	11.37	2.14	2.07	23.49	2.63	3.46	14.63
66.65		9444	2122	424	340	43.4	10.46	1.98	1.65	20.67	2.42	3.62	11.59
67.05		9201	2045	396	374	42.15	10.06	1.84	1.83	20.07	2.34	2.89	12.94
67.35		9923	2271	410	412	45.87	11.22	1.91	2.03	21.84	2.65	2.8	14.37
67.85		9241	2039	427	387	42.36	10.03	2	1.9	20.17	2.28	3.29	13.38
68		9898	2179	422	394	45.74	10.75	1.97	1.93	21.78	2.5	3.15	13.66
68.15		9526	2093	431	411	43.82	10.31	2.02	2.02	20.87	2.35	3.15	14.29
68.65		9817	2220	419	424	45.32	10.96	1.96	2.09	21.58	2.56	2.85	14.81
69.15		9903	2196	427	382	45.77	10.84	2	1.87	21.79	2.52	3.33	13.19
69.65		9776	2170	447	401	45.11	10.7	2.1	1.97	21.48	2.45	3.5	13.88
70.15		10106	2323	424	391	46.81	11.49	1.98	1.92	22.29	2.71	3.2	13.54
70.65		9237	1962	435	361	42.33	9.63	2.04	1.76	20.16	2.16	3.63	12.37
70.9		6918	1423	380	265	30.39	6.86	1.76	1.27	14.47	1.46	3.52	8.8
71.15		8978	1916	436	373	41	9.4	2.05	1.82	19.52	2.09	3.55	12.83
71.4		9365	2053	448	362	42.99	10.1	2.11	1.77	20.47	2.28	3.83	12.39
71.75		6625	1387	323	279	28.88	6.67	1.46	1.34	13.75	1.48	2.48	9.44
72.05		8992	1960	450	348	41.07	9.62	2.12	1.7	19.56	2.14	3.98	11.85
72.3		9970	2189	476	373	46.11	10.8	2.25	1.82	21.96	2.44	4.2	12.76
72.65		9434	2027	462	386	43.35	9.97	2.18	1.89	20.64	2.22	3.86	13.28
73.35		10785	2293	592	416	50.31	11.34	2.85	2.05	23.96	2.43	5.73	14.2
73.85		10091	2230	475	415	46.73	11.01	2.25	2.04	22.25	2.5	3.84	14.37
74.25		12940	2859	668	516	61.41	14.25	3.24	2.56	29.24	3.15	6.15	17.89
74.7		11083	2434	537	480	51.84	12.06	2.57	2.38	24.69	2.7	4.31	16.74
75.15		12395	2723	575	490	58.6	13.55	2.76	2.43	27.91	3.08	4.85	17.06
75.45		11252	2509	496	421	52.71	12.45	2.36	2.07	25.1	2.88	4.13	14.56
75.85		10916	2231	579	425	50.98	11.02	2.78	2.09	24.28	2.35	5.45	14.57
76.3		11104	2471	514	415	51.95	12.25	2.45	2.04	24.74	2.8	4.47	14.3
76.55		11220	2414	541	456	52.55	11.96	2.59	2.25	25.02	2.67	4.57	15.82
76.9		11514	2534	524	489	54.06	12.58	2.5	2.42	25.74	2.87	4.03	17.11
77.2		11667	2646	514	499	54.85	13.16	2.45	2.47	26.12	3.04	3.78	17.51
77.55		10286	2213	495	408	47.74	10.93	2.35	2	22.73	2.45	4.22	14.06
78.05		11081	2475	514	456	51.83	12.28	2.45	2.25	24.68	2.8	4.13	15.86
78.55		10347	2303	501	430	48.05	11.39	2.38	2.12	22.88	2.57	4.14	14.89
79.05		11206	2587	500	423	52.48	12.85	2.38	2.08	24.99	2.99	4.18	14.63
79.65		10614	2292	548	430	49.43	11.33	2.62	2.12	23.54	2.49	4.9	14.81
80.1		11449	2554	512	445	53.73	12.68	2.44	2.2	25.59	2.92	4.19	15.45
80.5		10507	2251	554	432	48.88	11.12	2.65	2.13	23.27	2.42	4.98	14.88
80.7		10187	2143	479	389	47.23	10.56	2.27	1.91	22.49	2.37	4.12	13.37
81.05		13342	3087	639	509	63.48	15.43	3.09	2.52	30.23	3.53	5.73	17.67
81.55		11739	2502	606	451	55.22	12.41	2.92	2.23	26.3	2.71	5.67	15.51
82.05		11560	2610	528	528	54.3	12.97	2.52	2.62	25.86	2.96	3.77	18.59
82.55		11946	2788	527	479	56.29	13.89	2.51	2.37	26.8	3.24	4.16	16.72
83.05		10788	2445	468	410	50.32	12.12	2.21	2.01	23.96	2.83	3.76	14.19
83.4		11156	2535	507	404	52.22	12.58	2.41	1.98	24.87	2.91	4.45	13.89
84.05		12295	2954	530	481	58.09	14.74	2.53	2.38	27.66	3.49	4.19	16.79
84.4		10574	2299	481	384	49.22	11.37	2.28	1.88	23.44	2.6	4.19	13.17
84.6		11769	2631	509	458	55.38	13.08	2.42	2.26	26.37	3.04	4.04	15.95
84.9		10457	2409	463	420	48.62	11.94	2.19	2.07	23.15	2.78	3.6	14.58
85.45		10592	2458	457	401	49.31	12.19	2.15	1.97	23.48	2.87	3.66	13.86
85.85		9884	2169	464	383	45.67	10.7	2.19	1.88	21.75	2.43	3.92	13.16
86.25		10970	2492	516	454	51.26	12.36	2.46	2.24	24.41	2.82	4.18	15.78
86.65		10309	2340	466	411	47.86	11.58	2.2	2.02	22.79	2.67	3.72	14.23
87		9384	2010	409	335	43.09	9.88	1.91	1.63	20.52	2.28	3.42	11.43
87.25		9353	2032	407	373	42.93	9.99	1.9	1.82	20.44	2.3	3.08	12.88
87.75		9682	2174	424	348	44.63	10.72	1.98	1.7	21.25	2.5	3.56	11.9
88.15		13320	2824	656	523	63.37	14.07	3.18	2.6	30.17	3.11	5.9	18.17
88.65		11571	2504	597	501	54.36	12.42	2.88	2.48	25.88	2.72	5.12	17.44
88.95		11849	2633	563	473	55.79	13.09	2.7	2.34	26.57	2.96	4.79	16.43
89.35		11413	2567	566	458	53.54	12.75	2.72	2.26	25.5	2.87	4.96	15.85
89.85		13081	2931	651	468	62.14	14.62	3.15	2.31	29.59	3.29	6.27	16.08
90.25		12495	2872	560	480	59.12	14.32	2.68	2.38	28.15	3.32	4.69	16.7
90.65		12351	2684	633	468	58.38	13.35	3.06	2.31	27.8	2.95	5.97	16.11
91.05		10866	2384	573	419	50.73	11.81	2.75	2.06	24.16	2.59	5.4	14.35
91.45		10717	2396	517	399	49.96	11.87	2.46	1.96	23.79	2.69	4.65	13.68
91.95		6924	1373	373	226	30.42	6.6	1.72	1.07	14.49	1.4	3.73	7.32
92.25		10078	2216	469	379	46.67	10.94	2.22	1.85	22.22	2.49	4.04	12.98
92.5		10185	2229	524	388	47.22	11.01	2.5	1.9	22.49	2.43	4.86	13.26
92.8		11004	2397	505	417	51.44	11.88	2.4	2.05	24.49	2.71	4.3	14.4

Distance						Total count	K	U	Th	Total count	K	U	Th
(M)	Live Time	ROI TC	ROI K	ROI U	ROI Th	cps	cps	cps	cps	ppm eU	%k	ppm	ppm
93.1		10182	2145	482	430	47.2	10.58	2.28	2.12	22.48	2.36	3.83	14.94
93.45		10315	2252	501	414	47.89	11.13	2.38	2.04	22.8	2.49	4.28	14.29
93.85		11505	2495	531	463	54.02	12.38	2.53	2.29	25.72	2.8	4.35	16.09
94.35		11172	2514	544	443	52.3	12.48	2.6	2.19	24.91	2.82	4.72	15.33
94.75		11877	2601	582	430	55.94	12.93	2.8	2.12	26.64	2.9	5.46	14.76
94.95		11256	2385	573	414	52.74	11.81	2.75	2.04	25.11	2.59	5.43	14.16
95.3		10586	2349	501	395	49.29	11.63	2.38	1.94	23.47	2.64	4.44	13.54
95.65		12068	2653	605	424	56.92	13.19	2.92	2.09	27.1	2.95	5.88	14.48
95.95		12751	2799	582	495	60.44	13.94	2.8	2.45	28.78	3.18	4.93	17.24
96.15		12466	2799	582	482	58.97	13.94	2.8	2.39	28.08	3.18	5.03	16.74
96.3		12521	2786	612	492	59.25	13.88	2.95	2.44	28.22	3.12	5.43	17.06
96.45		13094	2838	663	534	62.2	14.14	3.22	2.65	29.62	3.12	5.92	18.58
96.75		13417	3025	654	492	63.87	15.11	3.17	2.44	30.41	3.42	6.11	16.99
96.95		11554	2527	547	463	54.27	12.54	2.62	2.29	25.84	2.83	4.61	16.06
97.25		11460	2533	527	456	53.79	12.58	2.52	2.25	25.61	2.87	4.35	15.85
97.65		10968	2475	498	382	51.25	12.28	2.37	1.87	24.41	2.84	4.49	13.06
97.95		11014	2482	537	427	51.49	12.31	2.57	2.1	24.52	2.78	4.75	14.72
98.25		11004	2407	544	434	51.44	11.93	2.6	2.14	24.49	2.66	4.8	14.95
98.5		10719	2307	586	372	49.97	11.41	2.82	1.82	23.8	2.47	5.99	12.53
98.75		10768	2207	582	372	50.22	10.89	2.8	1.82	23.91	2.32	5.94	12.54
99.05		11130	2352	641	385	52.09	11.64	3.1	1.89	24.8	2.46	6.78	12.93
99.35		11402	2446	592	391	53.49	12.13	2.85	1.92	25.47	2.66	5.94	13.26
99.65		12201	2753	637	472	57.6	13.71	3.08	2.34	27.43	3.04	6.01	16.27
99.95		12780	2951	599	450	60.59	14.73	2.88	2.22	28.85	3.4	5.56	15.48
100.25		12864	2915	618	527	61.02	14.54	2.98	2.62	29.06	3.3	5.24	18.41
100.55		12023	2770	602	443	56.69	13.79	2.9	2.19	26.99	3.12	5.67	15.22
100.85		11191	2485	553	424	52.4	12.33	2.65	2.09	24.95	2.77	5.04	14.57
101.05		10881	2258	615	391	50.8	11.16	2.97	1.92	24.19	2.35	6.3	13.22
101.25		11486	2517	612	414	53.92	12.49	2.95	2.04	25.68	2.74	6.07	14.09
101.45		11551	2562	547	453	54.25	12.73	2.62	2.24	25.83	2.89	4.69	15.69
101.7		11910	2585	592	463	56.1	12.84	2.85	2.29	26.72	2.86	5.35	15.98
101.95		12369	2854	566	446	58.47	14.23	2.72	2.2	27.84	3.3	5.06	15.41
102.15		10988	2355	592	353	51.35	11.66	2.85	1.72	24.45	2.54	6.26	11.78
102.4		10480	2278	495	375	48.74	11.26	2.35	1.84	23.21	2.55	4.49	12.81
102.75		12243	2844	540	446	57.82	14.18	2.58	2.2	27.53	3.32	4.64	15.45
103.05		12712	2990	544	463	60.24	14.93	2.6	2.29	28.68	3.53	4.56	16.07
103.35		13547	3265	599	485	64.54	16.34	2.88	2.4	30.73	3.86	5.27	16.84
103.7		14149	3320	602	466	67.64	16.63	2.9	2.3	32.21	3.94	5.48	16.09
103.95		13214	2996	650	450	62.82	14.96	3.15	2.22	29.91	3.39	6.41	15.38
104.2		11631	2708	553	440	54.67	13.48	2.65	2.17	26.03	3.1	4.91	15.18
104.55		9936	2207	453	375	45.94	10.89	2.13	1.84	21.87	2.5	3.8	12.89
106.95		10421	2271	592	349	48.44	11.23	2.85	1.7	23.06	2.41	6.28	11.65
107.2		10337	2265	492	375	48	11.19	2.33	1.84	22.86	2.54	4.44	12.82
107.4		6134	1210	304	201	26.35	5.76	1.37	0.94	12.55	1.26	2.82	6.47
107.6		6490	1349	327	214	28.19	6.48	1.48	1	13.42	1.43	3.08	6.93
107.85		10874	2640	518	353	50.77	13.13	2.47	1.72	24.18	3.07	5.04	11.91
108.15		13243	2731	919	379	62.97	13.59	4.53	1.85	29.99	2.65	11.36	12.19
108.45		13570	2905	809	434	64.65	14.49	3.97	2.14	30.79	3.04	9.12	14.49
108.75		12505	2698	663	437	59.17	13.43	3.22	2.15	28.18	2.93	6.72	14.87
109.05		12262	2705	634	421	57.92	13.46	3.07	2.07	27.58	2.99	6.38	14.3
109.25		12693	2773	657	427	60.14	13.81	3.18	2.1	28.64	3.06	6.7	14.51
109.45		11599	2485	647	379	54.5	12.33	3.13	1.85	25.95	2.65	6.94	12.67
109.7		11751	2485	676	343	55.29	12.33	3.28	1.67	26.33	2.62	7.7	11.26
109.95		11437	2478	586	404	53.67	12.29	2.82	1.99	25.56	2.72	5.72	13.77
110.25		12531	2799	663	408	59.3	13.94	3.22	2	28.24	3.09	6.96	13.75
110.55		12952	2896	667	414	61.47	14.44	3.23	2.04	29.27	3.23	6.96	14
110.75		12922	2931	705	421	61.32	14.63	3.43	2.07	29.2	3.23	7.54	14.18
110.95		12961	2666	780	414	61.52	13.26	3.82	2.04	29.3	2.73	8.8	13.8
111.2		11686	2559	647	417	54.95	12.71	3.13	2.05	26.17	2.75	6.62	14.15
111.45		11547	2498	586	379	54.24	12.39	2.82	1.85	25.83	2.75	5.94	12.78
111.75		11431	2627	531	411	53.64	13.06	2.53	2.02	25.54	3.02	4.78	14.11
112.05		11301	2495	544	408	52.97	12.38	2.6	2	25.22	2.8	5.01	13.97
112.35		11719	2663	540	440	55.12	13.24	2.58	2.17	26.25	3.05	4.69	15.21
112.75		10386	2394	482	366	48.25	11.86	2.28	1.79	22.98	2.74	4.36	12.47
113.05		10088	2197	459	343	46.72	10.84	2.17	1.67	22.25	2.49	4.18	11.64
113.35		9975	2381	417	349	46.14	11.79	1.95	1.7	21.97	2.82	3.44	11.96
113.65		9852	2355	398	375	45.5	11.66	1.85	1.84	21.67	2.8	2.91	12.99
114.05		10172	2475	404	353	47.15	12.28	1.88	1.72	22.45	2.98	3.2	12.11
114.45		10260	2414	398	324	47.6	11.96	1.85	1.57	22.67	2.9	3.34	11.01
114.95		9855	2275	421	349	45.52	11.24	1.97	1.7	21.68	2.65	3.49	11.96

Distance						Total count	K	U	Th	Total count	K	U	Th
(M)	Live Time	ROI TC	ROI K	ROI U	ROI Th	cps	cps	cps	cps	ppm eU	%k	ppm	ppm
115.45		10088	2443	424	346	46.72	12.11	1.98	1.69	22.25	2.9	3.57	11.83
115.95		9972	2317	398	340	46.12	11.46	1.85	1.65	21.96	2.75	3.2	11.62
116.35		9994	2475	430	353	46.24	12.28	2.02	1.72	22.02	2.94	3.62	12.06
116.45	194248	10415	2545	430	396	48.37	12.63	2.01	1.94	23.03	3.03	3.26	13.71
116.85	194172	10944	2645	438	359	51.12	13.15	2.06	1.75	24.34	3.18	3.69	12.29
117.25	194052	10153	2408	402	380	47.07	11.93	1.87	1.86	22.42	2.87	2.94	13.16
117.65	194260	9504	2225	373	365	43.68	10.98	1.72	1.78	20.8	2.64	2.59	12.63
118.05	194340	9087	2114	374	354	41.51	10.4	1.72	1.72	19.77	2.47	2.69	12.2
118.45	194256	10250	2470	443	367	47.52	12.24	2.08	1.79	22.63	2.91	3.71	12.58
118.9	194164	10818	2572	397	366	50.47	12.77	1.84	1.79	24.03	3.13	2.97	12.63
119.3	194400	9644	2258	412	331	44.36	11.14	1.92	1.61	21.12	2.64	3.5	11.25
119.55	194340	9086	2155	411	297	41.51	10.61	1.91	1.43	19.76	2.5	3.76	9.96
119.85	194432	5811	1225	255	154	24.64	5.83	1.11	0.69	11.73	1.36	2.4	4.77
120.15	194448	5908	1326	298	179	25.14	6.35	1.33	0.82	11.97	1.44	2.89	5.65
120.5	194324	8732	2007	385	280	39.69	9.85	1.78	1.34	18.9	2.32	3.48	9.36
120.65	194232	9233	2115	472	282	42.29	10.41	2.23	1.35	20.14	2.36	4.88	9.28
120.95	194308	9483	2234	420	341	43.56	11.02	1.96	1.66	20.74	2.59	3.55	11.62
121.25	194140	9751	2216	504	286	44.98	10.94	2.4	1.38	21.42	2.47	5.37	9.38
121.55	194136	9556	2122	483	288	43.98	10.46	2.29	1.39	20.94	2.36	5.01	9.5
121.95	194300	9278	2115	395	300	42.5	10.41	1.83	1.45	20.24	2.46	3.48	10.1
122.35	194352	8580	1926	396	333	38.9	9.44	1.84	1.62	18.52	2.17	3.22	11.36
122.75	194036	11895	2738	572	448	56.06	13.64	2.75	2.21	26.69	3.12	5.15	15.46
123.15	193972	12190	2802	599	442	57.6	13.97	2.89	2.18	27.43	3.18	5.64	15.19
123.45	193968	11537	2653	613	388	54.23	13.2	2.96	1.9	25.82	2.95	6.31	13.1
123.7	193908	12259	2767	601	397	57.97	13.8	2.9	1.95	27.61	3.14	6.04	13.47
123.9	193880	12652	2791	639	429	60.01	13.92	3.1	2.12	28.58	3.11	6.4	14.63
124.05	193856	12519	2799	616	413	59.33	13.96	2.98	2.03	28.25	3.16	6.16	14.06
124.3	193832	13145	2828	701	467	62.57	14.12	3.42	2.31	29.79	3.07	7.1	15.98
124.65	193896	12088	2668	696	424	57.1	13.29	3.39	2.09	27.19	2.85	7.37	14.34
124.95	194164	11441	2420	637	342	53.68	11.99	3.08	1.66	25.56	2.58	7.07	11.29
125.25	194012	11295	2370	679	331	52.97	11.74	3.3	1.61	25.22	2.45	7.85	10.8
125.55	193944	11205	2396	694	361	52.53	11.88	3.38	1.76	25.01	2.46	7.85	11.93
125.9	194104	11383	2414	680	367	53.4	11.96	3.3	1.79	25.43	2.5	7.57	12.17
126.25	194076	9826	1997	575	295	45.38	9.82	2.76	1.42	21.61	2.04	6.45	9.61
126.55	194088	11030	2285	612	387	51.58	11.3	2.95	1.9	24.56	2.4	6.3	13.06
126.95	193996	11641	2628	565	419	54.76	13.07	2.71	2.06	26.08	2.97	5.27	14.37
127.25	194020	11912	2585	621	423	56.15	12.85	3	2.08	26.74	2.83	6.15	14.42
127.55	193848	11849	2626	591	393	55.88	13.07	2.85	1.93	26.61	2.94	5.92	13.34
127.75	193964	11206	2444	660	337	52.53	12.13	3.2	1.64	25.01	2.58	7.5	11.07
128.05	193876	11618	2446	648	387	54.68	12.14	3.14	1.9	26.04	2.59	6.89	13.01
128.35	194116	11593	2602	606	352	54.47	12.93	2.92	1.72	25.94	2.89	6.49	11.73
128.55	194004	11719	2674	592	401	55.16	13.31	2.85	1.97	26.27	3.01	5.86	13.63
128.75	193900	10943	2313	626	379	51.19	11.45	3.03	1.86	24.38	2.43	6.6	12.74
128.95	194016	10613	2149	632	348	49.45	10.6	3.06	1.7	23.55	2.18	6.95	11.54
129.15	194144	10152	2101	579	328	47.04	10.35	2.78	1.59	22.4	2.18	6.24	10.86
129.25	193968	10844	2247	591	367	50.66	11.11	2.85	1.79	24.12	2.38	6.13	12.34
129.65	193988	12008	2662	635	445	56.65	13.25	3.07	2.2	26.98	2.92	6.2	15.24
130.05	193908	12548	2758	634	442	59.46	13.75	3.07	2.18	28.32	3.07	6.21	15.14
130.45	193904	11884	2534	631	450	56.04	12.59	3.05	2.22	26.69	2.73	6.1	15.45
130.85	193824	12752	2690	691	444	60.54	13.4	3.37	2.19	28.83	2.89	7.13	15.12
131.25	193832	12962	2886	657	388	61.63	14.41	3.19	1.9	29.35	3.24	7.03	13.04
131.65	193900	13667	3032	738	482	65.24	15.16	3.61	2.39	31.07	3.32	7.58	16.48
132.05	193880	10853	2344	572	388	50.73	11.62	2.75	1.9	24.16	2.54	5.65	13.18
132.35	193920	10964	2372	595	365	51.29	11.76	2.87	1.79	24.42	2.56	6.21	12.26
132.55	194016	12399	2783	632	399	58.66	13.87	3.06	1.96	27.93	3.11	6.53	13.49
132.95	193956	13328	3059	760	435	63.47	15.3	3.72	2.15	30.22	3.34	8.32	14.64
133.25	193956	12662	2792	643	426	60.04	13.92	3.12	2.1	28.59	3.11	6.49	14.5
133.55	194016	12477	2794	663	420	59.06	13.93	3.22	2.07	28.12	3.08	6.86	14.24
133.85	193848	13111	3033	634	450	62.39	15.17	3.07	2.22	29.71	3.48	6.15	15.45
134.25	194036	12066	2807	556	392	56.94	13.99	2.67	1.92	27.11	3.26	5.35	13.35
134.45	193840	13087	2934	687	439	62.27	14.66	3.34	2.17	29.65	3.26	7.1	14.93
134.65	193748	12783	2720	721	405	60.73	13.56	3.52	1.99	28.92	2.9	7.94	13.58
134.9	193916	11780	2581	613	371	55.5	12.84	2.96	1.82	26.43	2.85	6.45	12.46
135.15	193916	13081	2975	639	475	62.21	14.87	3.1	2.35	29.62	3.38	6.02	16.39
135.45	193696	13608	3068	621	501	65.01	15.36	3.01	2.49	30.96	3.54	5.52	17.44
135.7	193860	12549	2683	683	412	59.49	13.37	3.32	2.03	28.33	2.89	7.26	13.91
135.9	193928	12607	2859	660	399	59.76	14.27	3.2	1.96	28.46	3.19	6.99	13.44
136.25	193992	13399	3055	629	519	63.82	15.27	3.04	2.58	30.39	3.5	5.49	18.08
136.55	193896	13533	3140	614	505	64.55	15.72	2.97	2.51	30.74	3.65	5.37	17.58
136.75	193968	13269	3068	602	470	63.16	15.34	2.9	2.33	30.08	3.57	5.46	16.26

Distance						Total count	K	U	Th	Total count	K	U	Th
(M)	Live Time	ROI TC	ROI K	ROI U	ROI Th	cps	cps	cps	cps	ppm eU	%k	ppm	ppm
137	193972	13019	2924	634	428	61.87	14.6	3.07	2.11	29.46	3.32	6.32	14.6
137.15	193748	13946	3198	686	453	66.73	16.03	3.34	2.24	31.78	3.65	6.97	15.48
137.45	193856	13369	3084	626	453	63.72	15.43	3.03	2.24	30.34	3.56	5.99	15.58
137.65	193764	12921	2950	697	448	61.44	14.75	3.4	2.21	29.26	3.27	7.19	15.27
137.95	193868	11635	2454	629	337	54.77	12.18	3.04	1.64	26.08	2.64	7	11.13
138.25	193940	12095	2679	654	419	57.12	13.34	3.17	2.06	27.2	2.92	6.72	14.22
138.55	193916	11138	2543	566	385	52.19	12.64	2.72	1.89	24.85	2.85	5.57	13.07
138.85	193944	10870	2371	545	387	50.8	11.75	2.61	1.9	24.19	2.62	5.21	13.19
139.15	194072	10793	2450	538	373	50.37	12.15	2.57	1.82	23.98	2.75	5.21	12.65
139.45	194136	9494	2032	532	304	43.66	9.99	2.54	1.47	20.79	2.15	5.68	10.02
139.75	194288	8018	1625	469	260	36.02	7.89	2.21	1.24	17.15	1.64	5.01	8.45
139.95	194140	8485	1787	459	264	38.46	8.73	2.16	1.26	18.31	1.89	4.82	8.62
140.15	194108	9973	2120	572	324	46.13	10.45	2.75	1.57	21.97	2.22	6.16	10.72
140.2	194040	9830	1987	529	361	45.41	9.77	2.53	1.76	21.63	2.07	5.16	12.21
140.3	194048	10250	2318	497	355	47.57	11.47	2.36	1.73	22.65	2.61	4.69	12.04
140.4	194088	10568	2365	522	349	49.2	11.71	2.49	1.7	23.43	2.65	5.15	11.76
140.75	193996	10992	2564	480	397	51.41	12.74	2.27	1.95	24.48	3	4.07	13.68
141.05	194076	11216	2562	478	412	52.54	12.73	2.26	2.03	25.02	2.99	3.91	14.25
141.3	193972	11863	2812	506	396	55.91	14.02	2.41	1.94	26.62	3.33	4.5	13.6
141.55	194176	11311	2736	489	378	53	13.62	2.32	1.85	25.24	3.24	4.37	12.92
141.95	194156	11307	2661	502	405	52.99	13.23	2.39	1.99	25.23	3.11	4.36	13.93
142.15	193952	14381	3497	631	473	68.9	17.56	3.05	2.34	32.81	4.17	5.91	16.32
142.4	193952	12428	2757	635	376	58.83	13.74	3.07	1.84	28.01	3.08	6.77	12.61
142.7	194004	11462	2530	544	390	53.83	12.57	2.6	1.91	25.64	2.86	5.17	13.3
142.95	194072	11667	2661	594	406	54.87	13.24	2.86	1.99	26.13	2.98	5.85	13.82
143.2	194040	10544	2196	567	356	49.09	10.84	2.72	1.74	23.38	2.34	5.82	11.96
143.45	194088	9721	2024	574	313	44.84	9.95	2.76	1.52	21.35	2.08	6.29	10.3
143.75	194192	9730	2066	546	318	44.86	10.16	2.61	1.54	21.36	2.18	5.79	10.53
144.05	194260	9563	2078	508	317	43.98	10.22	2.42	1.53	20.94	2.25	5.18	10.56
144.35	194300	9199	2022	481	295	42.1	9.93	2.28	1.42	20.05	2.2	4.92	9.76
144.65	194276	7309	1420	419	235	32.37	6.83	1.96	1.11	15.42	1.41	4.4	7.58
144.75	194452	6533	1325	364	214	28.35	6.34	1.67	1	13.5	1.34	3.68	6.87
144.9	194436	5541	1093	285	170	23.25	5.15	1.27	0.78	11.07	1.12	2.75	5.33
145.1	194376	7686	1661	376	262	34.29	8.07	1.73	1.25	16.33	1.82	3.48	8.68
145.25	194192	9808	2110	526	313	45.26	10.39	2.51	1.51	21.55	2.27	5.5	10.37
145.55	194080	10714	2294	568	345	49.96	11.35	2.73	1.68	23.79	2.48	5.93	11.53
145.7	193892	12451	2767	657	401	58.97	13.8	3.19	1.97	28.08	3.06	6.92	13.53
145.95	193888	13443	3106	605	463	64.09	15.55	2.92	2.29	30.52	3.62	5.57	15.99
146.25	193864	14165	3302	668	520	67.82	16.56	3.25	2.59	32.3	3.81	6.12	18.06
146.55	193900	12861	2929	598	444	61.08	14.63	2.88	2.19	29.09	3.37	5.61	15.28
146.95	193848	12720	2973	610	418	60.37	14.86	2.95	2.06	28.75	3.43	6.02	14.26
147.25	194052	11840	2696	586	408	55.77	13.42	2.82	2.01	26.56	3.04	5.7	13.91
147.55	193968	10440	2307	537	369	48.58	11.42	2.57	1.81	23.13	2.54	5.23	12.51
147.8	194292	8773	1787	473	298	39.91	8.72	2.23	1.44	19	1.86	4.76	9.89
147.95	194284	8970	1919	488	280	40.92	9.4	2.31	1.34	19.49	2.05	5.15	9.18
148.05	194132	10056	2262	527	324	46.55	11.18	2.51	1.57	22.17	2.5	5.43	10.8
148.25	194116	11665	2704	542	412	54.85	13.46	2.59	2.03	26.12	3.11	4.95	14.13
148.55	193992	11367	2541	570	419	53.35	12.62	2.74	2.06	25.4	2.83	5.35	14.36
148.85	193860	11963	2898	533	380	56.46	14.47	2.55	1.86	26.89	3.43	5.08	12.95
149.15	194088	11155	2612	500	384	52.23	12.98	2.38	1.88	24.87	3.04	4.5	13.14
149.45	194128	11576	2739	475	383	54.38	13.63	2.25	1.88	25.9	3.27	4.1	13.14
149.75	194008	12753	2976	598	439	60.49	14.87	2.88	2.17	28.8	3.44	5.65	15.08
150.05	193888	13082	3106	567	488	62.22	15.55	2.72	2.42	29.63	3.67	4.74	17.02
150.35	194016	13423	3259	588	485	63.94	16.32	2.83	2.4	30.45	3.87	5.1	16.85
150.7	194016	13374	3122	569	483	63.69	15.62	2.73	2.39	30.33	3.69	4.81	16.81
150.95	193896	12276	2894	536	463	58.07	14.45	2.56	2.29	27.65	3.4	4.44	16.11
151.3	194072	11810	2769	505	420	55.61	13.79	2.4	2.07	26.48	3.26	4.29	14.51
151.55	193844	11900	2872	525	425	56.14	14.34	2.51	2.1	26.73	3.39	4.58	14.68
151.85	194136	11804	2865	496	416	55.56	14.28	2.35	2.05	26.46	3.42	4.17	14.37
152.05	194196	10770	2525	432	382	50.21	12.53	2.02	1.87	23.91	3	3.41	13.18
152.35	194188	9849	2306	424	342	45.47	11.4	1.98	1.66	21.65	2.7	3.61	11.66
152.85	194356	9535	2262	419	312	43.81	11.16	1.96	1.51	20.86	2.64	3.77	10.52
153.25	194376	9004	2036	399	300	41.08	10	1.85	1.45	19.56	2.34	3.54	10.09
153.75	194228	10067	2477	470	332	46.58	12.28	2.22	1.61	22.18	2.89	4.44	11.2
154.25	194200	10116	2453	420	328	46.84	12.16	1.96	1.59	22.31	2.93	3.66	11.13
154.75	194116	10643	2597	473	334	49.58	12.9	2.24	1.62	23.61	3.07	4.47	11.28
155.25	194168	10163	2461	466	345	47.09	12.2	2.2	1.68	22.43	2.87	4.27	11.7
155.75	194212	10591	2454	452	348	49.29	12.16	2.13	1.69	23.47	2.88	4.01	11.84
156.25	194256	9969	2331	408	337	46.07	11.53	1.9	1.64	21.94	2.76	3.39	11.5
156.75	194340	9866	2375	423	349	45.52	11.75	1.98	1.7	21.68	2.8	3.53	11.92

Distance						Total count	K	U	Th	Total count	K	U	Th
(M)	Live Time	ROI TC	ROI K	ROI U	ROI Th	cps	cps	cps	cps	ppm eU	%k	ppm	ppm
157.25	194292	10144	2488	430	362	46.96	12.33	2.01	1.77	22.36	2.95	3.54	12.41
157.75	194260	10495	2521	433	345	48.78	12.5	2.03	1.68	23.23	3	3.73	11.76
158.25	194140	10909	2574	455	400	50.94	12.78	2.14	1.96	24.26	3.04	3.63	13.83
158.75	194228	10534	2473	425	374	48.99	12.26	1.99	1.83	23.33	2.94	3.36	12.88
159.25	194268	10425	2480	456	340	48.42	12.29	2.15	1.65	23.06	2.91	4.14	11.52
159.75	194368	10383	2534	419	345	48.17	12.56	1.96	1.68	22.94	3.04	3.5	11.77
160.25	194288	10444	2524	443	349	48.51	12.52	2.08	1.7	23.1	2.99	3.86	11.89
160.75	194236	10327	2450	438	338	47.92	12.14	2.05	1.64	22.82	2.89	3.87	11.48
161.25	194188	11193	2758	445	359	52.39	13.73	2.09	1.75	24.95	3.34	3.81	12.27
161.75	194396	10231	2523	415	350	47.38	12.5	1.93	1.7	22.56	3.03	3.39	11.97
162.25	194160	10594	2589	390	342	49.32	12.86	1.81	1.66	23.48	3.17	3.05	11.72
162.75	194088	10455	2492	408	356	48.62	12.37	1.9	1.74	23.15	3	3.23	12.23
163.25	194152	11204	2752	468	369	52.46	13.7	2.21	1.8	24.98	3.3	4.1	12.62
163.75	194268	10801	2683	434	383	50.35	13.34	2.03	1.87	23.98	3.24	3.43	13.21
164.25	194232	10643	2602	411	313	49.55	12.92	1.92	1.51	23.59	3.16	3.63	10.57
164.75	194304	9997	2422	398	321	46.2	11.99	1.85	1.55	22	2.91	3.35	10.9
165.25	194240	10525	2640	425	313	48.94	13.12	1.99	1.51	23.3	3.2	3.86	10.55
165.75	194160	9736	2327	418	335	44.9	11.51	1.95	1.63	21.38	2.74	3.57	11.41
166.25	194132	9441	2334	362	276	43.38	11.55	1.66	1.32	20.66	2.84	3.14	9.25
166.65	194304	9467	2376	348	292	43.48	11.75	1.59	1.41	20.7	2.92	2.78	9.88
166.9	194164	9953	2392	369	365	46.01	11.85	1.7	1.78	21.91	2.9	2.52	12.64
167.15	194420	9362	2253	397	280	42.91	11.11	1.84	1.34	20.43	2.67	3.67	9.33
167.3	194368	9338	2316	345	306	42.8	11.44	1.57	1.48	20.38	2.83	2.61	10.42
167.65	194424	10158	2489	422	320	47	12.33	1.97	1.55	22.38	2.98	3.75	10.81
167.95	194396	10456	2551	441	356	48.54	12.65	2.07	1.73	23.11	3.03	3.76	12.15
168.25	194132	11263	2800	428	377	52.77	13.95	2	1.84	25.13	3.42	3.38	13
168.55	194280	10382	2538	398	341	48.19	12.59	1.85	1.66	22.95	3.08	3.19	11.66
168.85	194220	9936	2413	404	337	45.91	11.95	1.88	1.64	21.86	2.89	3.32	11.5
169.15	194256	10369	2565	411	370	48.13	12.73	1.92	1.81	22.92	3.09	3.16	12.75
169.45	194364	10629	2626	414	341	49.44	13.04	1.93	1.66	23.54	3.19	3.45	11.63
169.85	194296	9930	2492	414	324	45.86	12.35	1.93	1.57	21.84	2.99	3.59	10.99
170.25	194496	9488	2359	379	303	43.54	11.65	1.75	1.46	20.73	2.84	3.19	10.23
170.55	194340	9711	2429	375	314	44.72	12.02	1.73	1.52	21.3	2.95	3.04	10.67
170.95	194380	8656	2108	344	257	39.28	10.37	1.57	1.23	18.71	2.53	3	8.55
171.25	194656	6635	1526	259	194	28.84	7.37	1.13	0.9	13.73	1.79	2.13	6.28
171.65	194516	6067	1379	260	182	25.94	6.62	1.14	0.84	12.35	1.57	2.25	5.83
172.05	194612	6252	1430	226	200	26.88	6.87	0.96	0.93	12.8	1.69	1.55	6.57
172.25	194308	8800	2086	335	294	40.04	10.26	1.52	1.42	19.07	2.5	2.55	9.98
172.55	194240	11429	2971	444	367	53.59	14.82	2.09	1.79	25.52	3.66	3.72	12.58
172.85	194240	11434	2876	421	386	53.62	14.33	1.97	1.89	25.53	3.54	3.19	13.34
173.2	194184	10400	2576	425	323	48.31	12.79	1.99	1.57	23	3.1	3.78	10.93
173.35	194400	9429	2266	361	275	43.26	11.18	1.66	1.32	20.6	2.74	3.13	9.2
173.65	194240	9541	2450	348	288	43.87	12.14	1.59	1.39	20.89	3.03	2.81	9.73
173.95	194200	10336	2601	388	310	47.98	12.92	1.8	1.5	22.85	3.2	3.28	10.5
174.25	194356	10045	2506	386	291	46.44	12.42	1.79	1.4	22.11	3.06	3.4	9.77
174.55	194472	9036	2236	374	259	41.22	11.02	1.72	1.23	19.63	2.68	3.47	8.57
174.95	194344	8936	2176	381	283	40.73	10.72	1.76	1.36	19.4	2.57	3.39	9.48
175.25	194252	9977	2426	406	321	46.11	12.01	1.89	1.56	21.96	2.91	3.48	10.89
175.55	194084	10469	2596	424	309	48.69	12.9	1.98	1.49	23.19	3.14	3.88	10.41
175.85	194180	9782	2437	416	301	45.13	12.08	1.94	1.45	21.49	2.91	3.81	10.11
176.25	194144	9978	2357	421	345	46.15	11.67	1.97	1.68	21.98	2.78	3.53	11.79
176.55	194212	9734	2376	404	317	44.87	11.76	1.88	1.54	21.37	2.84	3.49	10.74
176.95	194184	9942	2477	435	295	45.95	12.28	2.04	1.42	21.88	2.95	4.17	9.85
177.35	194372	9077	2191	356	295	41.45	10.8	1.63	1.42	19.74	2.63	2.88	9.98
177.65	194316	8962	2082	372	281	40.87	10.24	1.71	1.35	19.46	2.45	3.26	9.42
177.85	194372	7548	1788	300	263	33.59	8.72	1.34	1.26	15.99	2.11	2.24	8.85
178.15	194276	7352	1637	333	253	32.6	7.95	1.51	1.21	15.52	1.84	2.86	8.42
178.45	194308	9699	2344	409	298	44.67	11.59	1.9	1.44	21.27	2.78	3.72	10
178.75	194300	10316	2519	451	326	47.85	12.49	2.12	1.58	22.78	2.98	4.17	11
179.15	194252	10926	2738	478	312	51	13.62	2.26	1.51	24.29	3.28	4.73	10.42
179.45	194152	11027	2711	406	372	51.55	13.49	1.89	1.82	24.55	3.32	3.07	12.84
179.7	194232	11199	2796	431	368	52.41	13.92	2.02	1.8	24.96	3.41	3.51	12.64
180	194052	11585	2768	503	348	54.45	13.79	2.39	1.7	25.93	3.28	4.85	11.76
180.15	194208	10888	2656	490	318	50.82	13.2	2.32	1.54	24.2	3.14	4.88	10.63
180.35	194128	9981	2219	497	289	46.17	10.96	2.36	1.39	21.98	2.48	5.23	9.51
180.65	194124	10731	2510	524	292	50.03	12.46	2.5	1.41	23.82	2.88	5.65	9.58
180.9	194280	9698	2306	449	263	44.67	11.4	2.11	1.26	21.27	2.68	4.66	8.6
181.15	194068	10850	2587	500	323	50.66	12.86	2.38	1.57	24.12	3.02	5	10.81
181.25	194132	10780	2649	451	336	50.28	13.17	2.12	1.63	23.94	3.18	4.1	11.39
181.45	194244	11106	2763	500	324	51.93	13.75	2.37	1.57	24.73	3.28	4.99	10.84

Distance						Total count	K	U	Th	Total count	K	U	Th
(M)	Live Time	ROI TC	ROI K	ROI U	ROI Th	cps	cps	cps	cps	ppm eU	%k	ppm	ppm
181.65	193992	10944	2617	495	308	51.17	13.02	2.35	1.49	24.37	3.08	5.05	10.25
181.85	194252	9382	2146	457	272	43.05	10.57	2.15	1.3	20.5	2.43	4.72	8.93
182.15	194296	9158	1996	524	268	41.89	9.8	2.5	1.28	19.95	2.11	5.84	8.65
182.35	194188	8039	1707	460	205	36.15	8.32	2.17	0.96	17.21	1.79	5.32	6.37
182.55	194300	8481	1899	446	253	38.4	9.3	2.1	1.2	18.29	2.08	4.69	8.22
182.8	194196	9934	2294	490	308	45.91	11.34	2.32	1.49	21.86	2.6	4.96	10.25
183.05	194212	9612	2285	487	277	44.25	11.29	2.31	1.33	21.07	2.6	5.16	9.07
183.35	194440	8707	1943	393	277	39.53	9.52	1.82	1.33	18.83	2.21	3.63	9.22
183.65	194412	8114	1885	357	266	36.49	9.22	1.64	1.27	17.38	2.18	3.14	8.87
183.95	194360	8857	2140	372	258	40.32	10.54	1.71	1.23	19.2	2.54	3.45	8.54
184.25	194324	10066	2459	394	327	46.55	12.18	1.83	1.59	22.17	2.97	3.24	11.13
184.55	194236	10767	2732	433	358	50.19	13.59	2.03	1.75	23.9	3.32	3.62	12.25
184.75	194300	10489	2584	466	326	48.74	12.82	2.2	1.58	23.21	3.06	4.42	10.97
184.9	194172	9845	2291	448	294	45.46	11.32	2.11	1.42	21.65	2.65	4.39	9.79
185.25	194228	11297	2793	472	352	52.92	13.91	2.23	1.72	25.2	3.36	4.3	11.96
185.55	194224	11283	2730	467	368	52.85	13.58	2.2	1.8	25.16	3.27	4.09	12.58
185.85	194196	11476	2826	448	370	53.85	14.08	2.11	1.81	25.64	3.44	3.77	12.69
186.05	194164	11641	2796	464	360	54.71	13.93	2.19	1.76	26.05	3.37	4.11	12.28
186.3	194228	9483	2163	435	300	43.58	10.66	2.04	1.45	20.75	2.48	4.13	10.04
186.55	194260	9870	2294	522	300	45.56	11.33	2.49	1.45	21.7	2.55	5.54	9.88
186.75	194312	9739	2106	531	247	44.87	10.36	2.53	1.17	21.37	2.27	6.12	7.84
186.95	194172	8406	1793	483	213	38.04	8.76	2.29	1	18.12	1.88	5.63	6.63
187.2	194308	9531	2209	458	282	43.8	10.89	2.16	1.35	20.86	2.52	4.65	9.3
187.45	194416	8887	2020	458	258	40.46	9.92	2.16	1.23	19.27	2.24	4.84	8.38
187.65	194416	8479	1972	409	257	38.37	9.67	1.9	1.22	18.27	2.24	4.06	8.43
187.95	194380	7503	1650	413	218	33.35	8.01	1.92	1.02	15.88	1.76	4.44	6.94
188.15	194328	7110	1398	412	208	31.34	6.72	1.92	0.97	14.92	1.39	4.51	6.56
188.25	194392	7519	1636	425	210	33.43	7.94	1.99	0.98	15.92	1.72	4.7	6.61
188.45	194192	10060	2434	430	331	46.56	12.06	2.01	1.61	22.17	2.88	3.79	11.23
188.65	194128	10397	2469	484	295	48.31	12.24	2.29	1.42	23	2.87	4.97	9.76
188.85	194120	10706	2553	481	326	49.9	12.68	2.28	1.58	23.76	2.99	4.67	10.95
189.05	194340	8908	1955	477	252	40.59	9.59	2.25	1.2	19.33	2.12	5.2	8.12
189.25	194412	9046	2026	437	242	41.28	9.95	2.05	1.15	19.66	2.28	4.63	7.81
189.45	194204	8535	1790	449	225	38.7	8.74	2.11	1.06	18.43	1.92	4.97	7.15
189.75	194248	11077	2678	485	395	51.78	13.31	2.3	1.94	24.66	3.16	4.16	13.58
190.05	193852	13631	3432	557	450	65.07	17.23	2.67	2.22	30.99	4.18	4.89	15.58
190.2	193988	11768	2587	639	361	55.42	12.86	3.09	1.76	26.39	2.82	6.96	12.02
190.35	194232	9849	2128	530	273	45.46	10.48	2.53	1.31	21.65	2.3	5.9	8.84
190.45	194088	10449	2415	562	326	48.59	11.97	2.7	1.58	23.14	2.68	5.99	10.81
190.7	194504	8583	1884	450	271	38.88	9.21	2.11	1.3	18.51	2.04	4.6	8.89
190.85	194472	8151	1686	440	201	36.67	8.2	2.06	0.94	17.46	1.78	5.02	6.24
191.05	194260	6585	1276	415	172	28.65	6.09	1.94	0.79	13.64	1.21	4.85	5.18
191.2	194504	5471	914	371	131	22.88	4.22	1.71	0.58	10.9	0.74	4.47	3.69
191.4	194528	4962	807	379	96	20.26	3.67	1.75	0.4	9.65	0.58	4.89	2.34
191.65	194444	5081	852	374	106	20.88	3.91	1.72	0.45	9.94	0.65	4.73	2.73
191.75	194428	6427	1372	347	193	27.81	6.58	1.58	0.9	13.24	1.44	3.57	6.1
192.05	194480	7527	1740	342	220	33.46	8.47	1.56	1.03	15.93	1.99	3.27	7.13
192.35	194236	8038	1871	330	280	36.14	9.16	1.5	1.34	17.21	2.19	2.59	9.46
192.65	194256	8274	1959	298	265	37.35	9.61	1.33	1.27	17.78	2.37	2.19	8.94
192.95	194284	6545	1488	280	195	28.44	7.18	1.24	0.91	13.54	1.71	2.47	6.3
193.25	194504	6930	1566	283	235	30.38	7.58	1.25	1.11	14.47	1.81	2.19	7.81
193.55	194252	9016	2136	377	245	41.17	10.52	1.74	1.16	19.6	2.53	3.64	8.04
193.85	194244	9525	2302	371	296	43.79	11.38	1.71	1.43	20.85	2.77	3.12	10
194.05	194380	9310	2264	410	302	42.65	11.17	1.91	1.46	20.31	2.66	3.7	10.15
194.35	194208	10298	2540	392	288	47.78	12.6	1.82	1.39	22.75	3.1	3.53	9.65
194.65	194116	11740	2841	454	378	55.23	14.16	2.14	1.85	26.3	3.45	3.8	12.99
195.05	194028	11790	2919	437	354	55.52	14.57	2.05	1.73	26.44	3.6	3.72	12.11
195.35	194116	12292	3047	490	383	58.08	15.22	2.32	1.88	27.66	3.71	4.34	13.12
195.65	194184	11596	2888	488	392	54.47	14.4	2.31	1.92	25.94	3.47	4.24	13.46
195.95	194244	10397	2534	437	361	48.28	12.57	2.05	1.76	22.99	3.02	3.66	12.36
196.35	194252	10103	2391	441	338	46.76	11.83	2.07	1.64	22.27	2.8	3.91	11.48
196.65	194292	10591	2585	430	357	49.26	12.83	2.01	1.74	23.46	3.1	3.58	12.22
196.95	194328	10099	2487	409	316	46.72	12.32	1.9	1.53	22.25	2.99	3.57	10.69
197.25	194308	9754	2288	441	288	44.95	11.3	2.07	1.39	21.41	2.66	4.32	9.56
197.65	194292	10137	2458	424	304	46.93	12.18	1.98	1.47	22.35	2.93	3.92	10.2
198.05	194160	8275	1859	341	256	37.37	9.1	1.56	1.22	17.8	2.16	2.96	8.52
198.2	194340	9527	2302	390	310	43.78	11.37	1.81	1.5	20.85	2.74	3.31	10.49
198.55	194228	9657	2295	402	325	44.47	11.34	1.87	1.58	21.18	2.71	3.39	11.05
198.85	194148	8485	1983	374	243	38.46	9.74	1.73	1.15	18.31	2.31	3.61	7.97
199	194216	8462	2053	352	271	38.32	10.1	1.61	1.3	18.25	2.44	3.02	9.08

Distance						Total count	K	U	Th	Total count	K	U	Th
(M)	Live Time	ROI TC	ROI K	ROI U	ROI Th	cps	cps	cps	cps	ppm eU	%k	ppm	ppm
199.15	194216	6828	1501	290	190	29.91	7.25	1.29	0.88	14.24	1.71	2.67	6.09
199.55	194120	11420	2706	541	367	53.58	13.47	2.59	1.79	25.52	3.13	5.31	12.42
199.85	194168	12251	2935	546	401	57.85	14.64	2.61	1.97	27.55	3.46	5.11	13.7
200.15	194088	12288	2933	510	405	58.06	14.64	2.43	1.99	27.65	3.5	4.49	13.93
200.35	193984	13134	3129	606	423	62.46	15.66	2.92	2.08	29.74	3.66	5.91	14.45
200.55	194060	12788	3054	650	432	60.65	15.26	3.15	2.13	28.88	3.49	6.55	14.71
200.7	193912	13506	3264	647	426	64.4	16.36	3.14	2.1	30.67	3.81	6.55	14.5
200.95	194020	13870	3218	694	405	66.24	16.11	3.38	1.99	31.54	3.68	7.49	13.61
201.15	193916	13313	3076	637	425	63.41	15.39	3.08	2.09	30.19	3.54	6.4	14.48
201.25	193964	12185	2756	739	307	57.57	13.73	3.61	1.49	27.42	2.95	9.03	9.78
201.45	193948	11288	2343	752	297	52.95	11.61	3.68	1.43	25.22	2.32	9.32	9.38
201.75	194108	9290	1778	596	235	42.61	8.69	2.87	1.11	20.29	1.7	7.29	7.28
201.95	194084	10426	2386	491	312	48.47	11.82	2.33	1.51	23.08	2.73	4.95	10.4
202.25	194036	12657	3006	654	428	59.98	15.02	3.17	2.11	28.56	3.41	6.65	14.56
202.45	193832	12809	2830	761	380	60.84	14.13	3.73	1.86	28.97	3.02	8.79	12.55
202.65	194008	10675	2229	721	288	49.78	11.01	3.52	1.39	23.7	2.19	8.89	9.09
202.85	194060	10594	2283	622	303	49.34	11.29	3.01	1.46	23.5	2.4	7.15	9.83
203.05	194212	10200	2143	622	287	47.27	10.56	3	1.38	22.51	2.2	7.28	9.21
203.35	194156	10508	2345	493	340	48.87	11.6	2.34	1.65	23.27	2.66	4.75	11.47
203.65	194184	11402	2649	565	370	53.47	13.17	2.71	1.81	25.46	3.01	5.67	12.48
203.95	194008	13017	3000	613	404	61.85	14.99	2.96	1.99	29.45	3.46	6.18	13.71
204.15	194156	11917	2869	614	344	56.13	14.3	2.96	1.67	26.73	3.28	6.68	11.41
204.3	193996	12950	3013	612	386	61.51	15.06	2.95	1.89	29.29	3.49	6.31	13.03
204.55	194012	11332	2466	601	348	53.16	12.24	2.9	1.7	25.32	2.7	6.44	11.59
204.75	193960	10314	2329	491	307	47.93	11.53	2.33	1.49	22.82	2.65	4.99	10.22
204.9	193944	11682	2768	549	361	54.99	13.8	2.63	1.76	26.18	3.22	5.49	12.18
205.15	194036	11773	2802	524	387	55.43	13.97	2.5	1.9	26.39	3.29	4.87	13.22
205.45	194120	11508	2737	463	389	54.04	13.63	2.19	1.91	25.73	3.28	3.86	13.39
205.75	194236	11276	2727	523	382	52.81	13.57	2.49	1.87	25.15	3.18	4.89	13.01
206.05	194028	11379	2704	496	340	53.4	13.46	2.36	1.66	25.43	3.2	4.8	11.47
206.35	193840	12946	3257	564	398	61.54	16.33	2.71	1.96	29.3	3.92	5.43	13.58
206.65	193892	12681	2958	621	410	60.16	14.78	3	2.02	28.65	3.39	6.26	13.94
206.95	193992	10983	2426	521	380	51.37	12.03	2.49	1.86	24.46	2.74	4.88	12.96
207.25	194172	10103	2234	519	344	46.78	11.03	2.47	1.67	22.28	2.46	5.14	11.57
207.55	194268	10267	2267	531	347	47.6	11.2	2.53	1.69	22.67	2.49	5.3	11.66
207.85	194244	9288	2020	472	350	42.57	9.93	2.23	1.7	20.27	2.2	4.32	11.88
208.15	194128	9883	2166	488	291	45.66	10.68	2.31	1.4	21.74	2.41	5.07	9.6
208.45	194084	10086	2225	529	331	46.72	10.99	2.53	1.61	22.25	2.44	5.41	11.06
208.75	194184	10762	2373	575	368	50.17	11.75	2.76	1.8	23.89	2.58	5.85	12.39
209	194084	11668	2675	562	412	54.87	13.31	2.7	2.03	26.13	3.04	5.28	14.1
209.3	194080	11471	2666	503	400	53.86	13.26	2.39	1.96	25.65	3.11	4.42	13.75
209.5	194136	11223	2604	469	359	52.56	12.94	2.22	1.75	25.03	3.08	4.2	12.24
209.65	193796	13856	3344	701	425	66.25	16.78	3.42	2.1	31.55	3.86	7.45	14.38
209.8	193972	12991	3056	605	444	61.73	15.28	2.92	2.19	29.39	3.55	5.72	15.26
209.95	193912	12578	2813	624	391	59.62	14.03	3.02	1.92	28.39	3.17	6.47	13.2
210.3	193960	11832	2641	626	388	55.76	13.14	3.03	1.9	26.55	2.91	6.52	13.08
210.6	193904	12844	2896	620	443	60.99	14.46	3	2.19	29.04	3.29	5.97	15.2
210.9	194064	13052	3038	598	448	62.01	15.18	2.88	2.21	29.53	3.53	5.57	15.42
211.2	193884	13663	3044	672	478	65.22	15.23	3.27	2.37	31.06	3.43	6.53	16.45
211.4	193780	13569	2957	805	380	64.78	14.79	3.95	1.86	30.85	3.15	9.51	12.47
211.55	194052	11533	2501	723	338	54.19	12.41	3.53	1.64	25.8	2.58	8.51	10.99
211.7	194172	9781	1914	697	230	45.13	9.38	3.39	1.09	21.49	1.76	8.97	6.9
211.9	194052	10410	1946	761	254	48.4	9.55	3.72	1.21	23.05	1.72	9.82	7.71
212.15	194288	10257	2247	473	320	47.55	11.09	2.23	1.55	22.64	2.55	4.58	10.73
212.3	194280	10180	2399	476	300	47.15	11.87	2.25	1.45	22.45	2.77	4.79	9.96
212.6		10406	2435	456	339	48.36	12.07	2.15	1.65	23.03	2.85	4.15	11.5
212.9	194120	10091	2284	457	338	46.74	11.29	2.15	1.64	22.26	2.62	4.18	11.46
213.2		9904	2342	434	354	45.77	11.59	2.04	1.73	21.8	2.74	3.67	12.11
213.5	194136	10856	2527	482	345	50.67	12.54	2.28	1.68	24.13	2.95	4.53	11.68
213.8		10780	2520	472	364	50.28	12.51	2.23	1.78	23.94	2.95	4.21	12.42
214	194284	9717	2319	447	314	44.77	11.46	2.1	1.52	21.32	2.69	4.21	10.55
214.2		9472	2272	415	307	43.55	11.23	1.94	1.48	20.74	2.67	3.75	10.34
214.5		11528	2834	452	376	54.14	14.12	2.13	1.84	25.78	3.44	3.78	12.92
214.7		11745	2908	482	422	55.25	14.51	2.28	2.08	26.31	3.5	3.89	14.62
214.9		11644	2897	496	394	54.73	14.45	2.36	1.93	26.06	3.47	4.35	13.53
215.2	193992	12051	2951	534	432	56.87	14.74	2.55	2.13	27.08	3.49	4.66	14.92
215.5		11931	2835	443	423	56.21	14.13	2.08	2.08	26.77	3.44	3.25	14.73
215.8	194252	11257	2600	496	395	52.7	12.91	2.35	1.94	25.1	3.02	4.34	13.56
216.1	194092	11872	2829	490	423	55.92	14.1	2.32	2.08	26.63	3.37	4.02	14.65
216.4	194004	12468	2964	571	422	59.02	14.8	2.74	2.08	28.1	3.46	5.35	14.47

Distance						Total count	K	U	Th	Total count	K	U	Th
(M)	Live Time	ROI TC	ROI K	ROI U	ROI Th	cps	cps	cps	cps	ppm eU	%k	ppm	ppm
216.8	194028	12489	2904	542	445	59.12	14.49	2.59	2.2	28.15	3.41	4.68	15.4
217.2	194012	12592	2974	534	419	59.66	14.85	2.55	2.06	28.41	3.53	4.77	14.42
217.5	194044	12023	2816	504	430	56.71	14.04	2.4	2.12	27.01	3.33	4.19	14.9
217.8	194088	11424	2634	499	423	53.61	13.1	2.37	2.08	25.53	3.07	4.16	14.63
218.2	194188	11527	2681	472	467	54.11	13.33	2.23	2.31	25.77	3.16	3.36	16.35
218.5	193764	13235	3341	508	484	63.06	16.77	2.42	2.4	30.03	4.1	3.82	16.98
218.9	194212	11965	2881	503	444	56.36	14.36	2.39	2.19	26.84	3.42	4.05	15.42
219.2	194172	11720	2814	447	450	55.11	14.02	2.1	2.22	26.24	3.4	3.09	15.75
219.4	194056	12722	2986	580	455	60.31	14.91	2.79	2.25	28.72	3.47	5.22	15.72
219.8	194060	12569	3022	557	455	59.52	15.1	2.67	2.25	28.34	3.56	4.84	15.76
220.1	194012	12925	3136	558	464	61.37	15.69	2.68	2.29	29.22	3.73	4.79	16.1
220.4	194048	12106	2948	522	412	57.14	14.72	2.49	2.03	27.21	3.51	4.63	14.17
220.7	194212	12071	2843	547	485	56.91	14.16	2.62	2.4	27.1	3.3	4.43	16.91
221.1	194160	11735	2730	512	470	55.19	13.59	2.44	2.32	26.28	3.18	3.99	16.4
221.4	194332	11373	2750	443	442	53.28	13.68	2.08	2.18	25.37	3.31	3.09	15.44
221.8	194200	12070	2816	522	443	56.91	14.03	2.49	2.18	27.1	3.3	4.37	15.35
222.3	194044	11800	2889	486	429	55.56	14.41	2.3	2.11	26.46	3.47	3.9	14.89
222.8	194172	11931	2942	453	425	56.2	14.68	2.13	2.09	26.76	3.59	3.4	14.78
223.2	194080	12264	2998	466	452	57.94	14.97	2.2	2.23	27.59	3.65	3.39	15.8
223.6	194024	12474	3043	486	449	59.04	15.21	2.3	2.22	28.12	3.69	3.74	15.65
224.1	193980	11801	2871	502	404	55.59	14.33	2.39	1.99	26.47	3.42	4.37	13.91
224.6	194156	11601	2891	492	429	54.5	14.42	2.33	2.11	25.95	3.46	4	14.87
225.1	194276	11126	2700	431	378	52.02	13.42	2.02	1.85	24.77	3.27	3.42	13.02
225.5	194088	12711	3075	528	433	60.24	15.37	2.52	2.13	28.69	3.68	4.55	14.96
225.8	194052	12627	3050	536	422	59.82	15.24	2.56	2.08	28.49	3.64	4.77	14.53
226.1	194164	12472	2925	556	444	58.99	14.59	2.66	2.19	28.09	3.42	4.92	15.33
226.5	194120	12119	2813	533	425	57.18	14.02	2.55	2.09	27.23	3.29	4.7	14.65
226.9	194060	12042	2854	507	423	56.81	14.23	2.41	2.08	27.05	3.39	4.29	14.62
227.3	194280	12282	2820	551	456	57.97	14.04	2.64	2.25	27.61	3.26	4.73	15.79
227.7	194108	12588	2906	541	408	59.6	14.5	2.59	2	28.38	3.42	4.97	13.98
228.1	193912	13305	3153	586	478	63.37	15.79	2.82	2.37	30.17	3.71	5.13	16.6
228.5	194032	13198	3144	584	480	62.77	15.73	2.81	2.38	29.89	3.7	5.08	16.67
228.9	194032	12099	2823	580	457	57.11	14.07	2.79	2.26	27.19	3.23	5.2	15.79
229.3	193948	12064	2933	526	431	56.96	14.65	2.51	2.13	27.12	3.48	4.54	14.9
229.6	194196	11581	2771	518	434	54.39	13.79	2.47	2.14	25.9	3.24	4.38	15.01
229.9	194060	12048	2860	524	452	56.84	14.26	2.5	2.23	27.07	3.36	4.33	15.7
230.2	193928	12104	2882	500	448	57.17	14.39	2.38	2.21	27.22	3.43	3.98	15.6
230.5	194248	11699	2826	453	429	54.98	14.07	2.13	2.11	26.18	3.41	3.36	14.93
230.9	194176	12158	2883	515	465	57.37	14.37	2.45	2.3	27.32	3.41	4.08	16.2
231.3	194084	11965	2799	553	439	56.4	13.95	2.65	2.16	26.86	3.24	4.91	15.15
231.7	194112	11973	2813	478	426	56.43	14.02	2.26	2.1	26.87	3.36	3.8	14.78
232.2	194124	11880	2742	498	435	55.95	13.65	2.37	2.14	26.64	3.23	4.05	15.09
232.5	194232	11755	2794	502	430	55.27	13.91	2.38	2.12	26.32	3.3	4.15	14.88
232.9	194088	12379	2968	515	473	58.53	14.82	2.45	2.34	27.87	3.53	4.01	16.52
233.3	194060	12536	2989	527	438	59.35	14.93	2.52	2.16	28.26	3.56	4.5	15.16
233.8	194112	11521	2711	456	436	54.11	13.49	2.15	2.15	25.76	3.24	3.36	15.2
234.3	194104	12577	2981	532	460	59.55	14.88	2.54	2.27	28.36	3.53	4.4	15.99
234.55	194000	12283	2863	566	474	58.07	14.28	2.72	2.35	27.65	3.31	4.84	16.47
234.8	194076	12368	2876	589	448	58.48	14.34	2.83	2.21	27.85	3.3	5.42	15.43
235.2	194124	12308	2898	549	451	58.16	14.45	2.63	2.23	27.69	3.39	4.75	15.61
235.65	194084	12565	2951	546	482	59.49	14.73	2.61	2.39	28.33	3.46	4.44	16.81
236.1	194152	12807	3055	549	498	60.72	15.26	2.63	2.47	28.91	3.61	4.36	17.41
236.4	194176	12100	2863	527	463	57.07	14.27	2.51	2.29	27.17	3.36	4.29	16.1
236.7	194296	11375	2657	459	394	53.3	13.2	2.16	1.93	25.38	3.16	3.75	13.58
237	194276	11483	2639	509	437	53.86	13.11	2.42	2.15	25.65	3.05	4.21	15.13
237.3	194228	10956	2607	435	415	51.16	12.95	2.04	2.04	24.36	3.11	3.18	14.43
237.7	194212	11969	2863	498	512	56.38	14.27	2.36	2.54	26.85	3.39	3.41	18.02
238.1	194096	11995	2803	497	448	56.55	13.97	2.36	2.21	26.93	3.32	3.92	15.59
238.5	194244	11240	2603	444	411	52.62	12.93	2.09	2.02	25.06	3.1	3.36	14.26
238.9	194092	11402	2673	482	442	53.5	13.3	2.28	2.18	25.48	3.14	3.73	15.39
239.2	194248	10879	2487	491	433	50.76	12.33	2.33	2.13	24.17	2.85	3.95	15.02
239.45	194088	10940	2550	506	391	51.12	12.66	2.41	1.92	24.34	2.94	4.54	13.4
250.3	194260	10707	2494	502	357	49.87	12.36	2.38	1.74	23.75	2.87	4.75	12.09
250.7	194104	11128	2570	437	404	52.08	12.77	2.05	1.98	24.8	3.06	3.31	14.01
251.1	194248	11320	2636	570	368	53.03	13.1	2.73	1.8	25.25	2.98	5.77	12.39
251.5	194112	11346	2565	549	399	53.2	12.74	2.63	1.96	25.34	2.9	5.17	13.63
251.9	194216	11490	2665	558	392	53.91	13.25	2.67	1.92	25.67	3.04	5.37	13.33
252.3	193924	13649	3125	639	468	65.14	15.64	3.1	2.32	31.02	3.6	6.08	16.12
252.5	194108	12487	2765	627	421	59.08	13.77	3.03	2.07	28.13	3.09	6.26	14.33
252.75	193812	13642	3121	712	423	65.14	15.63	3.47	2.09	31.02	3.51	7.64	14.28

Distance						Total count	K	U	Th	Total count	K	U	Th
(M)	Live Time	ROI TC	ROI K	ROI U	ROI Th	cps	cps	cps	cps	ppm eU	%k	ppm	ppm
252.95	193748	13596	2916	788	426	64.93	14.58	3.87	2.1	30.92	3.1	8.86	14.27
253.2	193988	12933	2750	750	419	61.42	13.7	3.67	2.06	29.25	2.9	8.29	14.05
253.5	194120	12054	2712	677	402	56.85	13.5	3.29	1.97	27.07	2.94	7.23	13.51
253.8	194284	10920	2468	573	354	50.96	12.23	2.75	1.72	24.27	2.73	5.93	11.85
254.1	194196	10836	2440	493	388	50.55	12.09	2.34	1.9	24.07	2.79	4.35	13.3
254.3	194296	10815	2465	546	397	50.42	12.21	2.61	1.95	24.01	2.75	5.14	13.54
254.6	194376	10556	2316	536	368	49.06	11.44	2.56	1.8	23.36	2.55	5.21	12.45
255	194204	11340	2560	562	427	53.15	12.71	2.69	2.1	25.31	2.87	5.15	14.67
255.4	194264	11074	2505	554	418	51.76	12.42	2.65	2.05	24.65	2.8	5.09	14.33
255.8	194100	10975	2502	511	420	51.3	12.42	2.43	2.07	24.43	2.85	4.38	14.5
256.2	194152	12038	2765	533	410	56.76	13.77	2.55	2.01	27.03	3.22	4.82	14.07
256.6	194340	11083	2515	493	410	51.78	12.47	2.34	2.01	24.66	2.9	4.17	14.13
257	194136	12018	2704	586	465	56.66	13.45	2.82	2.3	26.98	3.04	5.23	16.08
257.3	194296	11096	2654	544	373	51.86	13.19	2.6	1.82	24.7	3.04	5.3	12.63
257.6	194228	11202	2591	527	424	52.43	12.87	2.51	2.09	24.97	2.96	4.61	14.61
257.85	194176	11214	2558	533	348	52.5	12.7	2.54	1.7	25	2.92	5.33	11.7
258.1	194220	10949	2497	516	375	51.13	12.38	2.46	1.83	24.35	2.85	4.83	12.76
258.4	194232	10746	2556	486	357	50.08	12.69	2.3	1.74	23.85	2.98	4.49	12.12
258.7	194224	11550	2756	500	393	54.22	13.72	2.37	1.93	25.82	3.25	4.42	13.47
259.1	194028	11801	2711	575	443	55.57	13.5	2.76	2.19	26.46	3.07	5.24	15.27
259.5	194188	12128	2784	572	397	57.21	13.86	2.75	1.95	27.24	3.2	5.56	13.5
259.8	194284	12141	2820	592	417	57.24	14.04	2.85	2.05	27.26	3.22	5.72	14.22
260.1	194140	11765	2752	573	423	55.35	13.7	2.75	2.08	26.36	3.14	5.37	14.5
260.4	194084	12008	2820	553	380	56.62	14.06	2.65	1.86	26.96	3.28	5.4	12.89
260.7	194208	11265	2636	468	403	52.76	13.1	2.21	1.98	25.12	3.12	3.82	13.91
261	194112	11826	2828	522	421	55.68	14.09	2.49	2.07	26.51	3.33	4.55	14.51
261.4	194268	11711	2853	482	384	55.04	14.21	2.28	1.88	26.21	3.42	4.2	13.16
261.7	194076	12548	3092	527	419	59.41	15.46	2.52	2.06	28.29	3.71	4.65	14.43
262.1	194128	12276	2895	551	429	57.99	14.44	2.64	2.11	27.61	3.38	4.96	14.77
262.5	194180	12827	3041	558	443	60.81	15.19	2.67	2.18	28.96	3.59	4.96	15.29
262.7	194004	12535	2922	572	431	59.36	14.59	2.75	2.12	28.27	3.4	5.29	14.82
263	194248	11017	2600	516	367	51.47	12.91	2.46	1.79	24.51	3	4.9	12.45
263.3	194184	11035	2647	504	364	51.58	13.16	2.4	1.78	24.56	3.09	4.73	12.36
263.6	194144	12214	3046	516	467	57.66	15.22	2.46	2.31	27.46	3.65	4.08	16.28
264	193868	12565	3046	559	469	59.56	15.24	2.68	2.32	28.36	3.59	4.77	16.3
264.4	194120	12303	2935	536	427	58.13	14.65	2.56	2.1	27.68	3.46	4.73	14.72
264.8	194084	11811	2838	510	437	55.61	14.15	2.43	2.15	26.48	3.35	4.23	15.15
265.2	194136	11559	2795	516	367	54.29	13.92	2.46	1.79	25.85	3.3	4.9	12.46
265.6	193956	13110	3129	550	490	62.35	15.66	2.64	2.43	29.69	3.72	4.45	17.12
266	194128	13109	3207	555	431	62.28	16.05	2.66	2.12	29.66	3.84	5.01	14.84
266.4	194112	11354	2675	466	463	53.24	13.31	2.2	2.29	25.35	3.16	3.3	16.22
266.8	194216	11526	2723	496	438	54.1	13.55	2.35	2.16	25.76	3.2	3.99	15.2
267.2	194100	11426	2817	466	414	53.62	14.04	2.2	2.04	25.53	3.39	3.7	14.35
267.6	194084	10994	2660	497	365	51.4	13.23	2.36	1.78	24.48	3.12	4.61	12.42
268	194284	11848	2955	418	380	55.74	14.74	1.95	1.86	26.54	3.67	3.19	13.12
268.3	194288	10660	2526	438	353	49.62	12.53	2.05	1.72	23.63	3	3.74	12.05
268.6	194140	10516	2497	447	363	48.92	12.39	2.1	1.77	23.3	2.95	3.81	12.43
268.9	194256	10902	2685	449	337	50.87	13.35	2.11	1.64	24.23	3.23	4.05	11.42
269.3	194288	9538	2221	413	333	43.84	10.96	1.93	1.62	20.88	2.59	3.5	11.33
269.6	194308	9910	2316	453	344	45.75	11.44	2.13	1.67	21.79	2.67	4.06	11.68
269.8	194196	10882	2547	449	361	50.79	12.64	2.11	1.76	24.19	3.02	3.86	12.34
269.9	194124	11200	2744	458	360	52.45	13.66	2.16	1.76	24.98	3.3	4.01	12.29
270.1	194220	9677	2311	414	287	44.58	11.42	1.93	1.38	21.23	2.73	3.89	9.58
270.3	194384	9390	2344	393	306	43.06	11.58	1.82	1.48	20.5	2.8	3.39	10.33
270.45	194248	9758	2422	415	311	44.99	11.99	1.94	1.5	21.42	2.89	3.71	10.49

B.7 Density data

This section contains the density data used to produce the field density logs. Table B.7.1 contains the density measurements made from the hand specimens collected from the Oxfordian succession. Table B.7.2 contains the output from the program 'DEN', the box curve and final filtered field density data for the Oxfordian succession (see Chapter 2). The data in Tables B.7.1 and B.7.2 were used to plot the curves (raw density, box curve and filtered density) seen in Figure 2.20.

Table B.7.3 contains the density measurements made from the hand specimens collected from the Kimmeridgian succession. Table B.7.4 contains the output from the program 'DEN', the box curve and final filtered field density data for the Kimmeridgian succession (see Chapter 2).The data in Tables B.7.3 and B.7.4 were used to plot the curves (raw density, box curve and filtered density) seen in Figure 2.21.

Table B.7.1

Distance (m)	Density (g/cm3)	Distance (m)	Density (g/cm3)	Distance (m)	Density (g/cm3)
0.15	2.352	43.75	2.584	83	2.408
2.6	2.333	44.15	2.578	84	2.395
2.95	2.506	44.55	2.562	84.5	2.41
3.3	2.292	45.45	2.338	84.9	2.7
4.4	2.19	45.85	2.582	85.3	2.488
7.5	2.302	47.45	2.505	85.52	2.504
8.5	2.433	48.75	2.613	85.75	2.367
8.7	2.551	48.95	2.259	85.98	2.381
9	2.243	49.25	2.63	86.02	2.255
12.2	2.274	49.75	2.407	86.21	2.351
12.5	2.565	50.35	2.639	86.51	2.312
12.7	2.266	50.85	2.29	86.61	2.627
13.35	2.295	51.35	2.632	86.75	2.215
14.5	2.351	52.53	2.617	87.2	2.33
19.8	2.417	53	2.594	87.64	2.306
20.3	2.4	54.1	2.515	87.71	2.311
21	2.396	54.9	2.425	88.22	2.71
21.5	2.15	55.8	2.509	88.33	2.199
21.8	2.201	56.7	2.302	88.46	3.03
22.15	2.264	57.8	2.604	88.86	2.288
22.6	2.271	58.8	2.557	89.39	2.298
23	2.481	59.2	2.601	89.5	2.085
24.1	2.194	59.6	2.245	89.68	2.218
25.3	2.298	60.7	2.582	90.04	2.205
26.2	2.533	62.35	2.599		
27.3	2.461	63.3	2.598		
27.6	2.276	63.8	2.58		
28	2.535	64.3	2.6		
28.6	2.179	64.8	2.582		
29.4	2.565	65.08	2.322		
30.4	2.586	65.2	2.616		
33.6	2.58	65.8	2.529		
34	2.127	66.8	2.46		
34.5	2.491	67.5	2.563		
34.9	2.617	68.4	3.042		
35.3	2.253	69.7	2.738		
36.4	2.422	71	2.327		
36.75	2.61	74	2.573		
37.95	2.348	74.8	2.34		
38.45	2.474	76	2.341		
39.55	2.517	77.3	2.305		
40.15	2.532	79.2	2.553		
40.73	2.252	80	2.467		
41.05	1.978	81.3	2.682		
42.75	2.342	81.5	2.771		
43.45	1.998	82	2.34		

Table B.7.2

Distance (m)	Box curve (g/cm3)	Filtered (g/cm3)
0	2.342	2.342
0.1	2.342	2.342
0.2	2.342	2.342
0.3	2.342	2.342
0.4	2.342	2.342
0.5	2.342	2.342
0.6	2.342	2.342
0.7	2.342	2.342
0.8	2.342	2.342
0.9	2.342	2.342
1	2.342	2.342
1.1	2.342	2.342
1.2	2.342	2.342
1.3	2.342	2.342
1.4	2.342	2.342
1.5	2.342	2.342
1.6	2.342	2.342
1.7	2.342	2.342
1.8	2.342	2.342
1.9	2.342	2.342
2	2.342	2.342
2.1	2.342	2.342
2.2	2.342	2.342
2.3	2.342	2.342
2.4	2.342	2.343
2.5	2.342	2.347
2.6	2.342	2.353
2.7	2.342	2.358
2.8	2.342	2.358
2.9	2.506	2.353
3	2.292	2.34
3.1	2.292	2.325
3.2	2.292	2.31
3.3	2.292	2.299
3.4	2.292	2.293
3.5	2.292	2.294
3.6	2.292	2.301
3.7	2.292	2.318
3.8	2.292	2.341
3.9	2.292	2.363
4	2.547	2.372
4.1	2.547	2.365
4.2	2.246	2.34
4.3	2.246	2.308
4.4	2.246	2.277
4.5	2.246	2.257
4.6	2.246	2.248
4.7	2.246	2.246
4.8	2.246	2.246
4.9	2.246	2.246
5	2.246	2.246
5.1	2.246	2.246
5.2	2.246	2.246
5.3	2.246	2.246
5.4	2.246	2.246
5.5	2.246	2.246
5.6	2.246	2.246
5.7	2.246	2.246
5.8	2.246	2.246
5.9	2.246	2.246
6	2.246	2.246
6.1	2.246	2.246
6.2	2.246	2.246
6.3	2.246	2.246
6.4	2.246	2.246
6.5	2.246	2.246
6.6	2.246	2.246
6.7	2.246	2.246
6.8	2.246	2.246
6.9	2.246	2.246
7	2.246	2.246
7.1	2.246	2.246
7.2	2.246	2.246
7.3	2.246	2.246
7.4	2.246	2.246
7.5	2.246	2.246
7.6	2.246	2.246
7.7	2.246	2.246
7.8	2.246	2.246
7.9	2.246	2.247
8	2.246	2.253
8.1	2.246	2.266
8.2	2.246	2.291
8.3	2.246	2.326
8.4	2.433	2.366
8.5	2.433	2.4
8.6	2.433	2.416
8.7	2.551	2.409
8.8	2.466	2.382
8.9	2.243	2.349
9	2.243	2.324
9.1	2.243	2.317
9.2	2.243	2.326
9.3	2.466	2.342
9.4	2.466	2.354
9.5	2.318	2.359
9.6	2.318	2.361
9.7	2.318	2.367
9.8	2.318	2.378
9.9	2.466	2.391
10	2.466	2.396
10.1	2.466	2.39
10.2	2.318	2.374
10.3	2.318	2.357
10.4	2.318	2.35
10.5	2.318	2.358
10.6	2.318	2.378
10.7	2.466	2.401
10.8	2.466	2.415
10.9	2.466	2.415
11	2.466	2.402
11.1	2.318	2.383
11.2	2.318	2.369
11.3	2.318	2.369
11.4	2.318	2.382
11.5	2.466	2.4
11.6	2.466	2.41
11.7	2.466	2.405
11.8	2.466	2.384
11.9	2.274	2.358
12	2.274	2.34
12.1	2.274	2.34
12.2	2.274	2.359
12.3	2.466	2.389
12.4	2.466	2.42
12.5	2.466	2.44
12.6	2.466	2.443
12.7	2.466	2.43
12.8	2.466	2.405
12.9	2.318	2.376
13	2.318	2.348
13.1	2.318	2.328
13.2	2.295	2.319
13.3	2.295	2.322
13.4	2.295	2.334
13.5	2.384	2.349
13.6	2.384	2.363
13.7	2.384	2.374
13.8	2.384	2.381
13.9	2.384	2.383
14	2.384	2.384
14.1	2.384	2.384
14.2	2.384	2.384
14.3	2.384	2.384
14.4	2.384	2.384
14.5	2.384	2.384
14.6	2.384	2.384
14.7	2.384	2.384
14.8	2.384	2.384
14.9	2.384	2.384
15	2.384	2.384
15.1	2.384	2.384
15.2	2.384	2.384
15.3	2.384	2.384
15.4	2.384	2.384
15.5	2.384	2.384
15.6	2.384	2.384
15.7	2.384	2.384
15.8	2.384	2.384
15.9	2.384	2.384
16	2.384	2.384
16.1	2.384	2.384
16.2	2.384	2.384
16.3	2.384	2.384
16.4	2.384	2.384
16.5	2.384	2.384
16.6	2.384	2.384
16.7	2.384	2.384
16.8	2.384	2.384
16.9	2.384	2.384
17	2.384	2.384
17.1	2.384	2.384
17.2	2.384	2.384
17.3	2.384	2.384
17.4	2.384	2.384
17.5	2.384	2.384
17.6	2.384	2.384
17.7	2.384	2.384
17.8	2.384	2.384
17.9	2.384	2.384
18	2.384	2.384
18.1	2.384	2.384
18.2	2.384	2.384
18.3	2.384	2.384
18.4	2.384	2.384
18.5	2.384	2.384
18.6	2.384	2.384
18.7	2.384	2.384
18.8	2.384	2.384
18.9	2.384	2.384
19	2.384	2.384
19.1	2.384	2.384
19.2	2.384	2.384
19.3	2.384	2.384
19.4	2.384	2.384
19.5	2.384	2.385
19.6	2.384	2.388
19.7	2.384	2.398
19.8	2.384	2.413
19.9	2.384	2.434
20	2.508	2.458
20.1	2.508	2.479
20.2	2.508	2.494
20.3	2.508	2.504
20.4	2.508	2.508
20.5	2.508	2.509
20.6	2.508	2.51
20.7	2.514	2.512
20.8	2.514	2.513
20.9	2.514	2.514

Distance (m)	Box curve (g/cm3)	Filtered (g/cm3)
21	2.514	2.517
21.1	2.514	2.524
21.2	2.514	2.535
21.3	2.514	2.549
21.4	2.611	2.562
21.5	2.611	2.572
21.6	2.572	2.577
21.7	2.572	2.576
21.8	2.572	2.571
21.9	2.572	2.563
22	2.572	2.557
22.1	2.528	2.553
22.2	2.528	2.554
22.3	2.528	2.559
22.4	2.595	2.565
22.5	2.595	2.567
22.6	2.595	2.561
22.7	2.595	2.546
22.8	2.481	2.527
22.9	2.481	2.508
23	2.481	2.493
23.1	2.481	2.486
23.2	2.481	2.485
23.3	2.481	2.492
23.4	2.481	2.504
23.5	2.481	2.521
23.6	2.579	2.539
23.7	2.579	2.556
23.8	2.579	2.568
23.9	2.579	2.572
24	2.579	2.569
24.1	2.579	2.558
24.2	2.579	2.544
24.3	2.492	2.527
24.4	2.492	2.512
24.5	2.492	2.502
24.6	2.492	2.496
24.7	2.492	2.496
24.8	2.492	2.5
24.9	2.492	2.506
25	2.527	2.513
25.1	2.527	2.519
25.2	2.527	2.523
25.3	2.527	2.526
25.4	2.527	2.527
25.5	2.527	2.527
25.6	2.527	2.527
25.7	2.527	2.527
25.8	2.527	2.527
25.9	2.527	2.527
26	2.527	2.527
26.1	2.527	2.527
26.2	2.527	2.527
26.3	2.527	2.526
26.4	2.527	2.524
26.5	2.527	2.521
26.6	2.527	2.517
26.7	2.492	2.514
26.8	2.492	2.509
26.9	2.552	2.504
27	2.492	2.499
27.1	2.492	2.497
27.2	2.461	2.499
27.3	2.461	2.506
27.4	2.549	2.516
27.5	2.549	2.528
27.6	2.549	2.536
27.7	2.549	2.54
27.8	2.535	2.541
27.9	2.535	2.54

Distance (m)	Box curve (g/cm3)	Filtered (g/cm3)
28	2.535	2.539
28.1	2.542	2.54
28.2	2.542	2.54
28.3	2.542	2.541
28.4	2.542	2.542
28.5	2.542	2.542
28.6	2.542	2.542
28.7	2.542	2.542
28.8	2.542	2.543
28.9	2.542	2.545
29	2.542	2.547
29.1	2.542	2.551
29.2	2.565	2.556
29.3	2.565	2.56
29.4	2.565	2.563
29.5	2.565	2.566
29.6	2.565	2.57
29.7	2.565	2.574
29.8	2.586	2.577
29.9	2.586	2.581
30	2.586	2.584
30.1	2.586	2.585
30.2	2.586	2.586
30.3	2.586	2.583
30.4	2.586	2.57
30.5	2.586	2.536
30.6	2.586	2.478
30.7	2.586	2.4
30.8	2.127	2.313
30.9	2.127	2.235
31	2.127	2.177
31.1	2.127	2.143
31.2	2.127	2.13
31.3	2.127	2.127
31.4	2.127	2.127
31.5	2.127	2.127
31.6	2.127	2.13
31.7	2.127	2.144
31.8	2.127	2.178
31.9	2.127	2.235
32	2.127	2.302
32.1	2.599	2.355
32.2	2.599	2.376
32.3	2.599	2.355
32.4	2.127	2.302
32.5	2.127	2.235
32.6	2.127	2.178
32.7	2.127	2.144
32.8	2.127	2.13
32.9	2.127	2.13
33	2.127	2.143
33.1	2.127	2.176
33.2	2.127	2.234
33.3	2.127	2.311
33.4	2.58	2.394
33.5	2.58	2.463
33.6	2.58	2.501
33.7	2.58	2.5
33.8	2.58	2.467
33.9	2.309	2.419
34	2.309	2.373
34.1	2.309	2.339
34.2	2.309	2.32
34.3	2.309	2.322
34.4	2.309	2.343
34.5	2.309	2.379
34.6	2.309	2.421
34.7	2.617	2.452
34.8	2.617	2.459
34.9	2.617	2.435

Distance (m)	Box curve (g/cm3)	Filtered (g/cm3)
35	2.253	2.39
35.1	2.253	2.339
35.2	2.253	2.305
35.3	2.253	2.304
35.4	2.253	2.334
35.5	2.253	2.377
35.6	2.599	2.409
35.7	2.599	2.423
35.8	2.599	2.419
35.9	2.127	2.406
36	2.127	2.392
36.1	2.599	2.382
36.2	2.599	2.375
36.3	2.274	2.367
36.4	2.274	2.353
36.5	2.274	2.333
36.6	2.274	2.311
36.7	2.61	2.294
36.8	2.127	2.283
36.9	2.127	2.276
37	2.127	2.274
37.1	2.599	2.276
37.2	2.237	2.276
37.3	2.237	2.271
37.4	2.237	2.26
37.5	2.237	2.248
37.6	2.237	2.24
37.7	2.237	2.238
37.8	2.237	2.239
37.9	2.237	2.246
38	2.237	2.263
38.1	2.237	2.293
38.2	2.237	2.334
38.3	2.474	2.378
38.4	2.474	2.418
38.5	2.474	2.448
38.6	2.474	2.465
38.7	2.474	2.468
38.8	2.474	2.466
38.9	2.474	2.464
39	2.474	2.468
39.1	2.318	2.479
39.2	2.563	2.495
39.3	2.563	2.511
39.4	2.563	2.524
39.5	2.517	2.529
39.6	2.517	2.53
39.7	2.517	2.528
39.8	2.532	2.528
39.9	2.532	2.529
40	2.532	2.53
40.1	2.532	2.531
40.2	2.532	2.53
40.3	2.532	2.524
40.4	2.532	2.511
40.5	2.532	2.496
40.6	2.532	2.483
40.7	2.252	2.478
40.8	2.528	2.482
40.9	2.528	2.493
41	2.528	2.508
41.1	2.528	2.52
41.2	2.528	2.526
41.3	2.528	2.528
41.4	2.528	2.528
41.5	2.528	2.528
41.6	2.528	2.528
41.7	2.528	2.528
41.8	2.528	2.528
41.9	2.528	2.528

Distance (m)	Box curve (g/cm3)	Filtered (g/cm3)
42	2.528	2.528
42.1	2.528	2.527
42.2	2.528	2.521
42.3	2.528	2.508
42.4	2.528	2.485
42.5	2.528	2.46
42.6	2.342	2.441
42.7	2.342	2.437
42.8	2.342	2.451
42.9	2.56	2.478
43	2.56	2.51
43.1	2.56	2.536
43.2	2.56	2.552
43.3	2.56	2.559
43.4	2.56	2.56
43.5	2.56	2.56
43.6	2.56	2.56
43.7	2.56	2.56
43.8	2.56	2.56
43.9	2.56	2.56
44	2.56	2.56
44.1	2.56	2.56
44.2	2.56	2.56
44.3	2.56	2.559
44.4	2.561	2.553
44.5	2.561	2.536
44.6	2.561	2.508
44.7	2.561	2.47
44.8	2.338	2.429
44.9	2.338	2.391
45	2.338	2.362
45.1	2.338	2.346
45.2	2.338	2.341
45.3	2.338	2.347
45.4	2.338	2.365
45.5	2.338	2.396
45.6	2.338	2.436
45.7	2.582	2.473
45.8	2.582	2.496
45.9	2.582	2.493
46	2.582	2.466
46.1	2.318	2.424
46.2	2.318	2.38
46.3	2.318	2.347
46.4	2.318	2.327
46.5	2.318	2.319
46.6	2.318	2.318
46.7	2.318	2.318
46.8	2.318	2.318
46.9	2.318	2.319
47	2.318	2.325
47.1	2.318	2.338
47.2	2.318	2.361
47.3	2.318	2.387
47.4	2.505	2.409
47.5	2.505	2.417
47.6	2.505	2.409
47.7	2.318	2.387
47.8	2.318	2.361
47.9	2.318	2.338
48	2.318	2.326
48.1	2.318	2.329
48.2	2.318	2.348
48.3	2.318	2.378
48.4	2.318	2.415
48.5	2.609	2.454
48.6	2.609	2.492
48.7	2.318	2.526
48.8	2.613	2.555
48.9	2.613	2.58

Distance (m)	Box curve (g/cm3)	Filtered (g/cm3)
49	2.63	2.601
49.1	2.63	2.616
49.2	2.63	2.618
49.3	2.63	2.605
49.4	2.63	2.577
49.5	2.63	2.541
49.6	2.407	2.503
49.7	2.407	2.473
49.8	2.407	2.456
49.9	2.407	2.452
50	2.609	2.458
50.1	2.318	2.47
50.2	2.609	2.48
50.3	2.318	2.481
50.4	2.639	2.467
50.5	2.609	2.439
50.6	2.29	2.402
50.7	2.29	2.368
50.8	2.29	2.35
50.9	2.29	2.356
51	2.29	2.385
51.1	2.609	2.424
51.2	2.318	2.456
51.3	2.632	2.473
51.4	2.632	2.474
51.5	2.318	2.467
51.6	2.318	2.462
51.7	2.609	2.465
51.8	2.318	2.474
51.9	2.609	2.482
52	2.609	2.482
52.1	2.318	2.472
52.2	2.609	2.455
52.3	2.318	2.441
52.4	2.318	2.431
52.5	2.617	2.429
52.6	2.318	2.437
52.7	2.492	2.455
52.8	2.318	2.482
52.9	2.594	2.512
53	2.594	2.542
53.1	2.594	2.564
53.2	2.594	2.572
53.3	2.594	2.565
53.4	2.544	2.547
53.5	2.544	2.524
53.6	2.544	2.504
53.7	2.318	2.491
53.8	2.515	2.488
53.9	2.515	2.493
54	2.515	2.5
54.1	2.515	2.502
54.2	2.515	2.493
54.3	2.515	2.472
54.4	2.515	2.447
54.5	2.318	2.423
54.6	2.318	2.408
54.7	2.425	2.403
54.8	2.425	2.407
54.9	2.425	2.414
55	2.425	2.417
55.1	2.425	2.414
55.2	2.425	2.407
55.3	2.425	2.402
55.4	2.318	2.406
55.5	2.318	2.421
55.6	2.509	2.443
55.7	2.509	2.467
55.8	2.509	2.481
55.9	2.509	2.48

Distance (m)	Box curve (g/cm3)	Filtered (g/cm3)
56	2.509	2.459
56.1	2.509	2.425
56.2	2.302	2.386
56.3	2.302	2.351
56.4	2.302	2.325
56.5	2.302	2.309
56.6	2.302	2.303
56.7	2.302	2.302
56.8	2.302	2.302
56.9	2.302	2.302
57	2.302	2.302
57.1	2.302	2.304
57.2	2.302	2.313
57.3	2.302	2.335
57.4	2.302	2.373
57.5	2.302	2.425
57.6	2.604	2.481
57.7	2.604	2.533
57.8	2.604	2.571
57.9	2.604	2.593
58	2.604	2.602
58.1	2.604	2.604
58.2	2.604	2.604
58.3	2.604	2.602
58.4	2.604	2.599
58.5	2.604	2.593
58.6	2.604	2.585
58.7	2.557	2.576
58.8	2.557	2.57
58.9	2.557	2.567
59	2.557	2.567
59.1	2.557	2.562
59.2	2.601	2.544
59.3	2.601	2.507
59.4	2.601	2.452
59.5	2.245	2.388
59.6	2.245	2.329
59.7	2.245	2.284
59.8	2.245	2.26
59.9	2.245	2.26
60	2.245	2.283
60.1	2.245	2.327
60.2	2.245	2.386
60.3	2.593	2.452
60.4	2.593	2.511
60.5	2.593	2.555
60.6	2.593	2.581
60.7	2.593	2.591
60.8	2.593	2.593
60.9	2.593	2.593
61	2.593	2.593
61.1	2.593	2.593
61.2	2.593	2.593
61.3	2.593	2.593
61.4	2.593	2.593
61.5	2.593	2.593
61.6	2.593	2.593
61.7	2.593	2.593
61.8	2.593	2.593
61.9	2.593	2.593
62	2.593	2.593
62.1	2.593	2.593
62.2	2.593	2.593
62.3	2.593	2.593
62.4	2.593	2.593
62.5	2.593	2.593
62.6	2.593	2.593
62.7	2.593	2.593
62.8	2.593	2.593
62.9	2.593	2.593

Distance (m)	Box curve (g/cm3)	Filtered (g/cm3)
63	2.593	2.591
63.1	2.593	2.585
63.2	2.593	2.574
63.3	2.593	2.561
63.4	2.593	2.551
63.5	2.318	2.547
63.6	2.617	2.552
63.7	2.617	2.562
63.8	2.58	2.573
63.9	2.58	2.582
64	2.58	2.587
64.1	2.58	2.589
64.2	2.6	2.592
64.3	2.6	2.595
64.4	2.6	2.596
64.5	2.6	2.595
64.6	2.6	2.591
64.7	2.582	2.582
64.8	2.582	2.568
64.9	2.582	2.553
65	2.582	2.537
65.1	2.322	2.525
65.2	2.616	2.519
65.3	2.616	2.515
65.4	2.318	2.513
65.5	2.617	2.509
65.6	2.617	2.506
65.7	2.318	2.503
65.8	2.529	2.505
65.9	2.529	2.508
66	2.529	2.509
66.1	2.529	2.507
66.2	2.529	2.5
66.3	2.46	2.488
66.4	2.46	2.476
66.5	2.46	2.468
66.6	2.46	2.462
66.7	2.46	2.46
66.8	2.46	2.46
66.9	2.46	2.46
67	2.46	2.461
67.1	2.46	2.464
67.2	2.46	2.473
67.3	2.46	2.49
67.4	2.46	2.515
67.5	2.563	2.543
67.6	2.617	2.571
67.7	2.617	2.596
67.8	2.617	2.623
67.9	2.617	2.661
68	2.617	2.717
68.1	2.617	2.79
68.2	3.042	2.869
68.3	3.042	2.942
68.4	3.042	2.996
68.5	3.042	3.025
68.6	3.042	3.029
68.7	3.042	3.009
68.8	3.042	2.97
68.9	3.042	2.919
69	2.738	2.861
69.1	2.738	2.81
69.2	2.738	2.771
69.3	2.738	2.746
69.4	2.738	2.725
69.5	2.738	2.693
69.6	2.738	2.641
69.7	2.738	2.571
69.8	2.327	2.494
69.9	2.327	2.424

Distance (m)	Box curve (g/cm3)	Filtered (g/cm3)
70	2.327	2.372
70.1	2.327	2.342
70.2	2.327	2.329
70.3	2.327	2.327
70.4	2.327	2.327
70.5	2.327	2.327
70.6	2.327	2.327
70.7	2.327	2.327
70.8	2.327	2.327
70.9	2.327	2.327
71	2.327	2.327
71.1	2.327	2.327
71.2	2.327	2.327
71.3	2.327	2.327
71.4	2.327	2.327
71.5	2.327	2.327
71.6	2.327	2.327
71.7	2.327	2.327
71.8	2.327	2.327
71.9	2.327	2.327
72	2.327	2.327
72.1	2.327	2.327
72.2	2.327	2.327
72.3	2.327	2.327
72.4	2.327	2.327
72.5	2.327	2.327
72.6	2.327	2.327
72.7	2.327	2.327
72.8	2.327	2.327
72.9	2.327	2.327
73	2.327	2.327
73.1	2.327	2.327
73.2	2.327	2.327
73.3	2.327	2.328
73.4	2.327	2.336
73.5	2.327	2.354
73.6	2.327	2.385
73.7	2.327	2.426
73.8	2.573	2.471
73.9	2.573	2.51
74	2.573	2.537
74.1	2.552	2.55
74.2	2.552	2.548
74.3	2.552	2.531
74.4	2.552	2.502
74.5	2.552	2.465
74.6	2.34	2.424
74.7	2.34	2.386
74.8	2.34	2.356
74.9	2.323	2.337
75	2.323	2.328
75.1	2.323	2.325
75.2	2.323	2.324
75.3	2.323	2.323
75.4	2.323	2.323
75.5	2.323	2.323
75.6	2.323	2.323
75.7	2.323	2.323
75.8	2.323	2.323
75.9	2.323	2.323
76	2.323	2.323
76.1	2.323	2.323
76.2	2.323	2.323
76.3	2.323	2.323
76.4	2.323	2.323
76.5	2.323	2.323
76.6	2.323	2.323
76.7	2.323	2.323
76.8	2.323	2.323
76.9	2.323	2.323

Distance (m)	Box curve (g/cm3)	Filtered (g/cm3)
77	2.323	2.323
77.1	2.323	2.323
77.2	2.323	2.323
77.3	2.323	2.323
77.4	2.323	2.323
77.5	2.323	2.323
77.6	2.323	2.323
77.7	2.323	2.323
77.8	2.323	2.323
77.9	2.323	2.323
78	2.323	2.323
78.1	2.323	2.323
78.2	2.323	2.323
78.3	2.323	2.323
78.4	2.323	2.324
78.5	2.323	2.33
78.6	2.323	2.343
78.7	2.323	2.367
78.8	2.323	2.399
78.9	2.51	2.434
79	2.51	2.466
79.1	2.51	2.49
79.2	2.51	2.503
79.3	2.51	2.509
79.4	2.51	2.51
79.5	2.51	2.51
79.6	2.51	2.51
79.7	2.51	2.51
79.8	2.51	2.51
79.9	2.51	2.51
80	2.51	2.51
80.1	2.51	2.51
80.2	2.51	2.51
80.3	2.51	2.51
80.4	2.51	2.51
80.5	2.51	2.51
80.6	2.51	2.509
80.7	2.51	2.503
80.8	2.51	2.491
80.9	2.51	2.479
81	2.51	2.477
81.1	2.318	2.492
81.2	2.318	2.527
81.3	2.727	2.569
81.4	2.727	2.6
81.5	2.727	2.603
81.6	2.727	2.574
81.7	2.388	2.523
81.8	2.388	2.468
81.9	2.388	2.425
82	2.388	2.4
82.1	2.388	2.39
82.2	2.388	2.388
82.3	2.388	2.388
82.4	2.388	2.388
82.5	2.388	2.388
82.6	2.388	2.388
82.7	2.388	2.388
82.8	2.388	2.388
82.9	2.388	2.388
83	2.388	2.388
83.1	2.388	2.388
83.2	2.388	2.388
83.3	2.388	2.388
83.4	2.388	2.388
83.5	2.388	2.388
83.6	2.388	2.388
83.7	2.388	2.388
83.8	2.388	2.388
83.9	2.388	2.388

Distance (m)	Box curve (g/cm3)	Filtered (g/cm3)
84	2.388	2.388
84.1	2.388	2.388
84.2	2.388	2.39
84.3	2.388	2.399
84.4	2.388	2.422
84.5	2.388	2.462
84.6	2.388	2.515
84.7	2.7	2.573
84.8	2.7	2.625
84.9	2.7	2.656
85	2.7	2.66
85.1	2.7	2.636
85.2	2.7	2.592
85.3	2.435	2.543
85.4	2.435	2.497
85.5	2.435	2.463
85.6	2.435	2.44
85.7	2.435	2.422
85.8	2.435	2.405
85.9	2.435	2.383
86	2.306	2.358
86.1	2.306	2.338
86.2	2.306	2.33
86.3	2.306	2.333
86.4	2.306	2.345
86.5	2.306	2.355
86.6	2.627	2.357
86.7	2.284	2.347
86.8	2.284	2.33
86.9	2.284	2.31
87	2.284	2.294
87.1	2.284	2.286
87.2	2.284	2.285
87.3	2.284	2.292
87.4	2.284	2.308
87.5	2.284	2.336
87.6	2.284	2.375
87.7	2.508	2.417
87.8	2.508	2.455
87.9	2.508	2.483
88	2.508	2.5
88.1	2.508	2.506
88.2	2.508	2.508
88.3	2.508	2.508
88.4	2.508	2.508
88.5	2.508	2.508
88.6	2.508	2.508
88.7	2.508	2.508
88.8	2.508	2.506
88.9	2.508	2.496
89	2.508	2.473
89.1	2.508	2.433
89.2	2.508	2.379
89.3	2.191	2.321
89.4	2.191	2.268
89.5	2.191	2.231
89.6	2.191	2.211
89.7	2.211	2.205
89.8	2.211	2.207
89.9	2.211	2.209
90	2.211	2.211

Table B.7.3

Distance (m)	Density (g/cm3)	Distance (m)	Density (g/cm3)	Distance (m)	Density (g/cm3)	Distance (m)	Density (g/cm3)
0.05	1.958	62.15	2.136	124.25	2.368	204.8	2.226
0.9	2.248	63.3	2.088	124.8	1.52	205.1	2.106
1.8	2.038	64.55	2.146	125.8	2.127	205.4	2.455
2.5	2.175	66.4	2.428	126.7	2.435	205.9	2.234
4.3	2.342	66.6	2.474	127.5	2.689	208.1	2.409
5.05	2.288	67.25	2.186	128.4	1.905	208.6	2.235
5.2	2.583	68.8	2.212	129.1	2.391	209.85	2.299
5.65	2.278	69.55	1.882	130.5	2.23	210.65	2.443
6.1	2.659	69.8	2.218	131.5	2.307	212.75	2.41
6.4	2.138	70.2	2.036	132.4	2.67	213.1	2.354
7.1	2.305	70.55	2.543	133	2.611	213.2	2.567
7.5	2.12	71.5	2.089	133.6	2.623	213.9	2.355
8.45	2.19	71.8	2.229	134.2	2.269	215.8	2.39
9.35	2.185	72.35	1.95	135.25	2.319	215.9	2.656
10.45	2.027	72.65	2.221	135.9	2.167	217.9	2.283
11.45	2.064	73.7	2.26	136.6	2.295	219.9	2.371
11.9	1.991	73.85	1.41	137	2.101	223.9	2.331
12.8	2.126	74.15	1.992	138.2	2.334	228.9	2.291
14.5	2.025	74.2	1.517	138.7	2.32	231.9	2.328
14.9	1.951	74.4	1.428	140.25	2.274	232.7	2.262
15.4	2.264	74.3	2.775	141.35	2.04	233.2	2.357
15.9	1.879	74.3	2.893	141.9	2.197	235.25	2.298
16.75	2.221	74.5	2.09	143.55	2.26	239.55	2.388
17.4	2.111	74.65	2.019	144.1	2.133	240.45	2.358
18.5	2.099	74.75	1.918	145.1	2.232	240.85	2.339
19.3	2.074	74.79	2.039	146.1	2.15	241.75	2.426
19.8	1.903	75.05	2.231	146.6	2.119	242.2	2.271
20.8	2.254	75.7	2.303	147.25	2.311	244.15	2.341
21.6	1.983	76.1	2.277	148	2.234	244.8	2.388
22.6	2.353	77	1.814	148.95	2.181	245.6	2.36
23.75	1.957	78.2	1.821	149.65	2.181	246.45	2.341
24.45	2.359	78.95	2.107	151.75	2.339	250.7	2.344
25.45	1.99	79.15	2.245	152.8	2.303	251.8	2.187
26	1.816	79.7	2.011	153.6	2.126	253.5	2.368
26.3	2.564	81.55	2.131	155	1.989	256	2.331
26.55	1.954	82.25	2.755	156.1	2.159	257.65	2.283
27.7	2.174	83.25	1.917	157.2	2.427	258.5	2.36
28.4	2.31	84.3	2.258	157.7	2.152	259.35	2.309
29.05	1.98	85.25	1.944	158.2	2.579	261	2.38
30.3	2.266	86.3	2.34	158.85	2.292	262.25	2.332
31.3	2.072	89.4	2.444	159.75	2.317	263.25	2.308
33.15	1.916	97.4	2.44	160.2	2.306	264.25	2.295
34.85	2.289	99.4	2.389	161.4	2.394	265	2.396
35.4	2.135	103.4	2.288	162.8	2.416	266.4	2.378
36.65	2.068	105.3	2.389	163.9	2.446	267.4	2.35
37.65	2.221	105.9	2.73	165.6	2.338	268.35	2.413
38	1.962	106.95	2.374	166.95	2.323	268.7	2.385
39.05	2.288	107.5	2.222	168.85	2.292	269.7	2.344
41.6	2.31	108.25	2.394	170.05	2.284	269.85	2.531
41.9	2.669	109.3	1.982	172.95	2.308	270.15	2.311
43.25	2.314	111.55	2.348	173.6	2.332	270.6	2.393
44.65	2.33	113.5	2.397	176.8	2.28	270.9	2.269
45.35	2.106	114.55	1.955	181.15	2.317	270.95	2.348
46.65	2.216	115.95	2.163	184.2	2.004	271.21	2.307
47.7	1.737	116.7	2.16	187.45	2.177	271.26	2.386
47.95	2.285	117.7	2.186	188.1	2.215	271.55	2.405
51.25	2.416	117.95	2.274	190.85	2.301	272.05	2.458
53.75	2.188	118.8	2.342	192.2	2.352	273.05	2.375
54.3	2.748	119.3	2.113	193.55	2.32	275.35	2.392
55.05	1.692	120	2.307	195	2.298	276.7	2.29
56	2.026	120.65	2.106	195.95	2.32	278.7	2.365
58.05	2.076	121.55	2.008	197.6	2.349	279.8	2.367
58.45	2.106	122.2	2.343	200.25	2.414	280.6	2.326
60.2	1.983	122.6	2.051	202.9	2.038	281.45	2.375
61.55	2.107	123.35	1.898	203.7	2.349	281.9	2.316

Table B.7.4

Distance (m)	Box curve (g/cm3)	Filtered (g/cm3)
0	1.958	2.015
0.1	2.083	2.05
0.2	2.083	2.092
0.3	2.083	2.136
0.4	2.248	2.176
0.5	2.248	2.208
0.6	2.248	2.23
0.7	2.248	2.242
0.8	2.248	2.247
0.9	2.248	2.247
1	2.248	2.241
1.1	2.248	2.225
1.2	2.248	2.198
1.3	2.248	2.163
1.4	2.038	2.123
1.5	2.038	2.088
1.6	2.038	2.061
1.7	2.038	2.049
1.8	2.038	2.048
1.9	2.038	2.057
2	2.038	2.069
2.1	2.124	2.083
2.2	2.124	2.102
2.3	2.083	2.127
2.4	2.083	2.16
2.5	2.175	2.198
2.6	2.315	2.238
2.7	2.315	2.272
2.8	2.315	2.296
2.9	2.315	2.309
3	2.315	2.314
3.1	2.315	2.315
3.2	2.315	2.315
3.3	2.315	2.315
3.4	2.315	2.315
3.5	2.315	2.315
3.6	2.315	2.315
3.7	2.315	2.315
3.8	2.315	2.315
3.9	2.315	2.315
4	2.315	2.315
4.1	2.315	2.315
4.2	2.315	2.315
4.3	2.315	2.315
4.4	2.315	2.315
4.5	2.315	2.315
4.6	2.315	2.317
4.7	2.315	2.325
4.8	2.315	2.344
4.9	2.315	2.376
5	2.315	2.413
5.1	2.583	2.441
5.2	2.583	2.448
5.3	2.583	2.43
5.4	2.278	2.392
5.5	2.278	2.351
5.6	2.278	2.325
5.7	2.278	2.33
5.8	2.278	2.367
5.9	2.278	2.414
6	2.659	2.447
6.1	2.659	2.447
6.2	2.659	2.408
6.3	2.138	2.343
6.4	2.138	2.275
6.5	2.138	2.226
6.6	2.205	2.207
6.7	2.205	2.216
6.8	2.205	2.238
6.9	2.305	2.261
7	2.305	2.274
7.1	2.305	2.274
7.2	2.305	2.258
7.3	2.305	2.229
7.4	2.12	2.195
7.5	2.12	2.164
7.6	2.12	2.143
7.7	2.12	2.134
7.8	2.12	2.138
7.9	2.12	2.148
8	2.19	2.162
8.1	2.19	2.173
8.2	2.19	2.182
8.3	2.19	2.188
8.4	2.19	2.19
8.5	2.19	2.19
8.6	2.19	2.188
8.7	2.19	2.185
8.8	2.19	2.181
8.9	2.19	2.178
9	2.124	2.176
9.1	2.185	2.176
9.2	2.185	2.178
9.3	2.185	2.18
9.4	2.185	2.178
9.5	2.185	2.167
9.6	2.185	2.148
9.7	2.185	2.121
9.8	2.027	2.091
9.9	2.027	2.064
10	2.027	2.045
10.1	2.027	2.039
10.2	2.027	2.047
10.3	2.027	2.069
10.4	2.027	2.096
10.5	2.205	2.124
10.6	2.205	2.142
10.7	2.205	2.146
10.8	2.124	2.136
10.9	2.124	2.118
11	2.064	2.097
11.1	2.064	2.081
11.2	2.064	2.071
11.3	2.064	2.066
11.4	2.064	2.062
11.5	2.064	2.056
11.6	2.064	2.048
11.7	2.064	2.039
11.8	1.991	2.035
11.9	1.991	2.04
12	1.991	2.054
12.1	2.126	2.074
12.2	2.126	2.095
12.3	2.126	2.111
12.4	2.126	2.121
12.5	2.126	2.125
12.6	2.126	2.126
12.7	2.126	2.126
12.8	2.126	2.126
12.9	2.126	2.126
13	2.126	2.126
13.1	2.126	2.126
13.2	2.126	2.126
13.3	2.126	2.126
13.4	2.126	2.126
13.5	2.126	2.126
13.6	2.126	2.126
13.7	2.126	2.125
13.8	2.124	2.121
13.9	2.124	2.114
14	2.124	2.101
14.1	2.124	2.084
14.2	2.025	2.065
14.3	2.025	2.048
14.4	2.025	2.033
14.5	2.025	2.02
14.6	2.025	2.01
14.7	2.025	2.006
14.8	1.951	2.015
14.9	1.951	2.042
15	1.951	2.086
15.1	2.264	2.139
15.2	2.264	2.191
15.3	2.264	2.228
15.4	2.264	2.239
15.5	2.264	2.222
15.6	2.264	2.185
15.7	2.264	2.145
15.8	1.879	2.116
15.9	1.879	2.109
16	2.221	2.124
16.1	2.221	2.154
16.2	2.221	2.186
16.3	2.221	2.209
16.4	2.221	2.219
16.5	2.221	2.221
16.6	2.221	2.221
16.7	2.221	2.221
16.8	2.221	2.22
16.9	2.221	2.217
17	2.221	2.209
17.1	2.221	2.195
17.2	2.221	2.175
17.3	2.111	2.153
17.4	2.111	2.13
17.5	2.111	2.112
17.6	2.083	2.099
17.7	2.083	2.092
17.8	2.083	2.09
17.9	2.083	2.09
18	2.099	2.092
18.1	2.099	2.095
18.2	2.099	2.1
18.3	2.099	2.114
18.4	2.099	2.137
18.5	2.099	2.166
18.6	2.099	2.191
18.7	2.607	2.203
18.8	2.124	2.195
18.9	2.124	2.171
19	2.124	2.137
19.1	2.074	2.102
19.2	2.074	2.07
19.3	2.074	2.039
19.4	2.074	2.006
19.5	1.903	1.973
19.6	1.903	1.943
19.7	1.903	1.922
19.8	1.903	1.909
19.9	1.903	1.904
20	1.903	1.905
20.1	1.903	1.916
20.2	1.903	1.941
20.3	1.903	1.986
20.4	1.903	2.046
20.5	2.254	2.111
20.6	2.254	2.171
20.7	2.254	2.216
20.8	2.254	2.24
20.9	2.254	2.242
21	2.254	2.224
21.1	2.254	2.19
21.2	2.254	2.144
21.3	1.983	2.095
21.4	1.983	2.06
21.5	1.983	2.053
21.6	1.983	2.08
21.7	1.983	2.135
21.8	2.353	2.203
21.9	2.353	2.266
22	2.353	2.313
22.1	2.353	2.34
22.2	2.353	2.351
22.3	2.353	2.352
22.4	2.353	2.345
22.5	2.353	2.328
22.6	2.353	2.299
22.7	2.353	2.26
22.8	2.124	2.22
22.9	2.124	2.187
23	2.124	2.167
23.1	2.124	2.156
23.2	2.205	2.146
23.3	2.205	2.127
23.4	2.205	2.098
23.5	1.957	2.069
23.6	1.957	2.059
23.7	1.957	2.079
23.8	1.957	2.129
23.9	2.359	2.197
24	2.359	2.264
24.1	2.359	2.313
24.2	2.359	2.338
24.3	2.359	2.343
24.4	2.359	2.335
24.5	2.299	2.323
24.6	2.299	2.313
24.7	2.299	2.306
24.8	2.299	2.299
24.9	2.299	2.288
25	2.299	2.265
25.1	2.299	2.225
25.2	2.299	2.167
25.3	1.99	2.097
25.4	1.99	2.022
25.5	1.99	1.953
25.6	1.816	1.902
25.7	1.816	1.886
25.8	1.816	1.917
25.9	1.816	1.999
26	1.816	2.117
26.1	2.564	2.238
26.2	2.564	2.321
26.3	2.564	2.338
26.4	2.564	2.289
26.5	1.954	2.197
26.6	1.954	2.099
26.7	1.954	2.027
26.8	1.954	1.994
26.9	1.954	1.996
27	1.954	2.019
27.1	2.124	2.045
27.2	2.124	2.068
27.3	2.083	2.084
27.4	2.083	2.096
27.5	2.083	2.107
27.6	2.083	2.12
27.7	2.174	2.134
27.8	2.174	2.146
27.9	2.174	2.152
28	2.145	2.154
28.1	2.145	2.151
28.2	2.145	2.148
28.3	2.145	2.146
28.4	2.145	2.145
28.5	2.145	2.145
28.6	2.145	2.145
28.7	2.145	2.145
28.8	2.145	2.145
28.9	2.145	2.144
29	2.145	2.143
29.1	2.145	2.14
29.2	2.145	2.136
29.3	2.124	2.132
29.4	2.124	2.13
29.5	2.124	2.131
29.6	2.124	2.14
29.7	2.124	2.158
29.8	2.124	2.182
29.9	2.266	2.208
30	2.266	2.232
30.1	2.266	2.25
30.2	2.266	2.256
30.3	2.266	2.248
30.4	2.266	2.228
30.5	2.266	2.199
30.6	2.124	2.165
30.7	2.083	2.133
30.8	2.083	2.108
30.9	2.083	2.092
31	2.083	2.084
31.1	2.083	2.081

Distance (m)	Box curve (g/cm3)	Filtered (g/cm3)
31.2	2.083	2.081
31.3	2.072	2.081
31.4	2.083	2.081
31.5	2.083	2.081
31.6	2.083	2.082
31.7	2.083	2.082
31.8	2.083	2.083
31.9	2.083	2.083
32	2.083	2.083
32.1	2.083	2.083
32.2	2.083	2.083
32.3	2.083	2.082
32.4	2.083	2.077
32.5	2.083	2.064
32.6	2.083	2.043
32.7	2.083	2.015
32.8	1.916	1.984
32.9	1.916	1.955
33	1.916	1.936
33.1	1.916	1.932
33.2	1.916	1.949
33.3	1.916	1.984
33.4	1.916	2.033
33.5	2.205	2.088
33.6	2.205	2.137
33.7	2.205	2.174
33.8	2.205	2.195
33.9	2.205	2.203
34	2.205	2.205
34.1	2.205	2.205
34.2	2.205	2.205
34.3	2.205	2.206
34.4	2.205	2.208
34.5	2.205	2.214
34.6	2.205	2.225
34.7	2.205	2.239
34.8	2.289	2.255
34.9	2.289	2.268
35	2.289	2.275
35.1	2.289	2.272
35.2	2.289	2.26
35.3	2.289	2.242
35.4	2.135	2.219
35.5	2.205	2.198
35.6	2.205	2.184
35.7	2.205	2.182
35.8	1.954	2.193
35.9	2.299	2.209
36	2.299	2.22
36.1	2.299	2.216
36.2	2.299	2.194
36.3	2.068	2.16
36.4	2.068	2.123
36.5	2.068	2.099
36.6	2.068	2.093
36.7	2.068	2.105
36.8	2.068	2.13
36.9	2.221	2.159
37	2.221	2.185
37.1	2.221	2.204
37.2	2.221	2.216
37.3	2.221	2.22
37.4	2.221	2.221
37.5	2.221	2.219
37.6	2.221	2.212
37.7	2.221	2.193
37.8	2.221	2.16
37.9	2.221	2.116
38	1.962	2.067
38.1	1.962	2.025
38.2	1.962	2.002
38.3	1.962	2.007
38.4	1.962	2.04
38.5	1.962	2.094
38.6	2.288	2.156
38.7	2.288	2.211
38.8	2.288	2.252
38.9	2.288	2.276

Distance (m)	Box curve (g/cm3)	Filtered (g/cm3)
39	2.288	2.286
39.1	2.288	2.288
39.2	2.288	2.288
39.3	2.288	2.288
39.4	2.288	2.288
39.5	2.288	2.288
39.6	2.288	2.288
39.7	2.288	2.288
39.8	2.288	2.288
39.9	2.288	2.288
40	2.288	2.288
40.1	2.288	2.288
40.2	2.288	2.288
40.3	2.288	2.288
40.4	2.288	2.288
40.5	2.288	2.288
40.6	2.288	2.286
40.7	2.288	2.276
40.8	2.288	2.252
40.9	2.288	2.209
41	2.288	2.154
41.1	1.954	2.102
41.2	1.954	2.074
41.3	1.954	2.087
41.4	1.954	2.15
41.5	2.31	2.252
41.6	2.31	2.372
41.7	2.669	2.482
41.8	2.669	2.556
41.9	2.669	2.575
42	2.669	2.531
42.1	2.669	2.435
42.2	2.299	2.311
42.3	1.954	2.194
42.4	1.954	2.115
42.5	1.954	2.09
42.6	1.954	2.115
42.7	2.314	2.17
42.8	2.314	2.229
42.9	2.314	2.275
43	2.314	2.301
43.1	2.314	2.312
43.2	2.314	2.314
43.3	2.314	2.313
43.4	2.314	2.307
43.5	2.314	2.293
43.6	2.314	2.269
43.7	2.314	2.237
43.8	2.124	2.202
43.9	2.124	2.176
44	2.124	2.167
44.1	2.124	2.179
44.2	2.124	2.209
44.3	2.33	2.246
44.4	2.33	2.281
44.5	2.33	2.307
44.6	2.33	2.321
44.7	2.33	2.321
44.8	2.33	2.306
44.9	2.33	2.277
45	2.33	2.239
45.1	2.106	2.198
45.2	2.106	2.163
45.3	2.106	2.142
45.4	2.106	2.14
45.5	2.106	2.152
45.6	2.216	2.171
45.7	2.216	2.19
45.8	2.216	2.204
45.9	2.216	2.212
46	2.216	2.215
46.1	2.216	2.216
46.2	2.216	2.216
46.3	2.216	2.216
46.4	2.216	2.216
46.5	2.216	2.216
46.6	2.216	2.216
46.7	2.216	2.216

Distance (m)	Box curve (g/cm3)	Filtered (g/cm3)
46.8	2.216	2.216
46.9	2.216	2.216
47	2.216	2.216
47.1	2.216	2.216
47.2	2.216	2.213
47.3	2.216	2.202
47.4	2.216	2.183
47.5	2.216	2.163
47.6	2.216	2.151
47.7	1.737	2.154
47.8	2.285	2.175
47.9	2.285	2.208
48	2.285	2.242
48.1	2.285	2.268
48.2	2.285	2.282
48.3	2.285	2.285
48.4	2.285	2.285
48.5	2.285	2.285
48.6	2.285	2.285
48.7	2.285	2.285
48.8	2.285	2.285
48.9	2.285	2.285
49	2.285	2.285
49.1	2.285	2.285
49.2	2.285	2.285
49.3	2.285	2.285
49.4	2.285	2.285
49.5	2.285	2.285
49.6	2.285	2.285
49.7	2.285	2.285
49.8	2.285	2.285
49.9	2.285	2.285
50	2.285	2.285
50.1	2.285	2.285
50.2	2.285	2.285
50.3	2.285	2.285
50.4	2.285	2.286
50.5	2.285	2.287
50.6	2.285	2.289
50.7	2.285	2.292
50.8	2.302	2.295
50.9	2.302	2.298
51	2.302	2.3
51.1	2.302	2.301
51.2	2.302	2.302
51.3	2.302	2.302
51.4	2.302	2.302
51.5	2.302	2.302
51.6	2.302	2.302
51.7	2.302	2.302
51.8	2.302	2.302
51.9	2.302	2.302
52	2.302	2.302
52.1	2.302	2.302
52.2	2.302	2.302
52.3	2.302	2.302
52.4	2.302	2.302
52.5	2.302	2.302
52.6	2.302	2.302
52.7	2.302	2.302
52.8	2.302	2.302
52.9	2.302	2.302
53	2.302	2.302
53.1	2.302	2.302
53.2	2.302	2.302
53.3	2.302	2.302
53.4	2.302	2.302
53.5	2.302	2.302
53.6	2.302	2.305
53.7	2.302	2.318
53.8	2.302	2.351
53.9	2.302	2.407
54	2.302	2.483
54.1	2.748	2.567
54.2	2.748	2.643
54.3	2.748	2.696
54.4	2.748	2.71
54.5	2.748	2.675

Distance (m)	Box curve (g/cm3)	Filtered (g/cm3)
54.6	2.748	2.589
54.7	2.748	2.469
54.8	2.124	2.342
54.9	2.124	2.239
55	1.692	2.181
55.1	2.299	2.167
55.2	2.299	2.177
55.3	2.299	2.184
55.4	2.299	2.169
55.5	2.026	2.133
55.6	2.026	2.09
55.7	2.026	2.057
55.8	2.026	2.042
55.9	2.026	2.047
56	2.026	2.068
56.1	2.026	2.099
56.2	2.205	2.132
56.3	2.205	2.163
56.4	2.205	2.186
56.5	2.205	2.199
56.6	2.205	2.204
56.7	2.205	2.205
56.8	2.205	2.205
56.9	2.205	2.204
57	2.205	2.201
57.1	2.205	2.191
57.2	2.205	2.175
57.3	2.205	2.153
57.4	2.076	2.128
57.5	2.076	2.106
57.6	2.076	2.09
57.7	2.076	2.081
57.8	2.076	2.078
57.9	2.076	2.081
58	2.076	2.085
58.1	2.076	2.091
58.2	2.124	2.097
58.3	2.106	2.102
58.4	2.106	2.105
58.5	2.106	2.107
58.6	2.106	2.108
58.7	2.106	2.11
58.8	2.106	2.113
58.9	2.124	2.117
59	2.124	2.119
59.1	2.124	2.116
59.2	2.124	2.105
59.3	2.124	2.084
59.4	2.124	2.055
59.5	1.954	2.023
59.6	1.954	1.994
59.7	1.954	1.974
59.8	1.954	1.963
59.9	1.954	1.963
60	1.954	1.971
60.1	1.983	1.987
60.2	1.983	2.009
60.3	1.983	2.037
60.4	2.124	2.066
60.5	2.124	2.091
60.6	2.124	2.108
60.7	2.124	2.118
60.8	2.124	2.121
60.9	2.124	2.12
61	2.124	2.117
61.1	2.107	2.114
61.2	2.107	2.111
61.3	2.107	2.109
61.4	2.107	2.108
61.5	2.107	2.107
61.6	2.107	2.108
61.7	2.107	2.11
61.8	2.107	2.114
61.9	2.107	2.119
62	2.136	2.124
62.1	2.136	2.129
62.2	2.136	2.131
62.3	2.136	2.129

Distance (m)	Box curve (g/cm3)	Filtered (g/cm3)
62.4	2.136	2.123
62.5	2.136	2.114
62.6	2.083	2.104
62.7	2.083	2.091
62.8	2.083	2.079
62.9	2.083	2.069
63	2.083	2.061
63.1	1.954	2.057
63.2	2.088	2.055
63.3	2.088	2.058
63.4	2.088	2.066
63.5	1.954	2.079
63.6	2.124	2.095
63.7	2.146	2.112
63.8	2.146	2.127
63.9	2.146	2.138
64	2.146	2.144
64.1	2.146	2.146
64.2	2.146	2.146
64.3	2.146	2.146
64.4	2.146	2.146
64.5	2.146	2.146
64.6	2.146	2.146
64.7	2.146	2.146
64.8	2.146	2.146
64.9	2.146	2.146
65	2.146	2.146
65.1	2.146	2.146
65.2	2.146	2.146
65.3	2.146	2.146
65.4	2.146	2.146
65.5	2.146	2.146
65.6	2.146	2.146
65.7	2.146	2.148
65.8	2.146	2.157
65.9	2.146	2.179
66	2.146	2.218
66.1	2.146	2.27
66.2	2.451	2.327
66.3	2.451	2.379
66.4	2.451	2.416
66.5	2.451	2.431
66.6	2.451	2.42
66.7	2.451	2.389
66.8	2.451	2.343
66.9	2.186	2.294
67	2.186	2.248
67.1	2.186	2.215
67.2	2.186	2.195
67.3	2.186	2.188
67.4	2.186	2.186
67.5	2.186	2.186
67.6	2.186	2.186
67.7	2.186	2.186
67.8	2.186	2.186
67.9	2.186	2.186
68	2.186	2.186
68.1	2.186	2.187
68.2	2.186	2.189
68.3	2.186	2.192
68.4	2.186	2.195
68.5	2.212	2.192
68.6	2.212	2.178
68.7	2.212	2.148
68.8	2.212	2.106
68.9	1.954	2.058
69	1.954	2.012
69.1	1.954	1.974
69.2	1.954	1.948
69.3	1.954	1.938
69.4	1.882	1.948
69.5	1.882	1.977
69.6	1.882	2.02
69.7	2.218	2.064
69.8	2.218	2.099
69.9	2.218	2.125
70	2.036	2.153
70.1	2.036	2.196
70.2	2.036	2.262
70.3	2.543	2.344
70.4	2.543	2.425
70.5	2.543	2.488
70.6	2.543	2.525
70.7	2.543	2.54
70.8	2.543	2.543
70.9	2.543	2.54
71	2.543	2.527
71.1	2.543	2.493
71.2	2.543	2.437
71.3	2.543	2.364
71.4	2.089	2.288
71.5	2.089	2.225
71.6	2.089	2.183
71.7	2.229	2.157
71.8	2.229	2.137
71.9	2.124	2.112
72	2.124	2.083
72.1	1.95	2.063
72.2	1.95	2.063
72.3	1.95	2.088
72.4	2.24	2.129
72.5	2.24	2.173
72.6	2.24	2.209
72.7	2.24	2.23
72.8	2.24	2.239
72.9	2.24	2.24
73	2.24	2.24
73.1	2.24	2.24
73.2	2.24	2.24
73.3	2.24	2.237
73.4	2.24	2.219
73.5	2.24	2.175
73.6	2.24	2.099
73.7	2.24	1.996
73.8	1.64	1.891
73.9	1.64	1.816
74	1.64	1.789
74.1	1.64	1.812
74.2	1.64	1.866
74.3	2.834	1.925
74.4	1.428	1.969
74.5	2.09	1.996
74.6	2.019	2.016
74.7	1.979	2.041
74.8	2.083	2.077
74.9	2.083	2.121
75	2.231	2.161
75.1	2.231	2.193
75.2	2.231	2.215
75.3	2.231	2.228
75.4	2.231	2.237
75.5	2.231	2.245
75.6	2.231	2.255
75.7	2.29	2.266
75.8	2.29	2.276
75.9	2.29	2.283
76	2.29	2.282
76.1	2.29	2.27
76.2	2.29	2.24
76.3	2.29	2.189
76.4	2.124	2.118
76.5	2.124	2.037
76.6	1.814	1.958
76.7	1.814	1.894
76.8	1.814	1.854
76.9	1.814	1.841
77	1.814	1.853
77.1	1.814	1.885
77.2	1.954	1.927
77.3	1.954	1.973
77.4	2.083	2.013
77.5	2.083	2.038
77.6	2.083	2.039
77.7	2.083	2.016
77.8	2.083	1.976
77.9	1.821	1.927
78	1.821	1.883
78.1	1.821	1.85
78.2	1.821	1.83
78.3	1.821	1.823
78.4	1.821	1.823
78.5	1.821	1.831
78.6	1.821	1.851
78.7	1.821	1.885
78.8	1.821	1.931
78.9	2.107	1.987
79	2.107	2.045
79.1	1.954	2.095
79.2	2.245	2.127
79.3	2.245	2.136
79.4	2.245	2.124
79.5	2.011	2.096
79.6	2.011	2.064
79.7	2.011	2.039
79.8	2.011	2.033
79.9	2.011	2.048
80	1.954	2.079
80.1	2.205	2.117
80.2	2.205	2.152
80.3	2.205	2.177
80.4	2.205	2.188
80.5	2.205	2.186
80.6	2.205	2.175
80.7	2.131	2.161
80.8	2.131	2.148
80.9	2.131	2.139
81	2.131	2.134
81.1	2.131	2.131
81.2	2.131	2.131
81.3	2.131	2.131
81.4	2.131	2.131
81.5	2.131	2.131
81.6	2.131	2.131
81.7	2.131	2.135
81.8	2.131	2.153
81.9	2.131	2.194
82	2.131	2.251
82.1	2.131	2.306
82.2	2.755	2.338
82.3	2.755	2.331
82.4	1.954	2.282
82.5	2.205	2.202
82.6	2.205	2.113
82.7	1.917	2.035
82.8	1.917	1.981
82.9	1.917	1.947
83	1.917	1.927
83.1	1.917	1.919
83.2	1.917	1.917
83.3	1.917	1.917
83.4	1.917	1.919
83.5	1.917	1.929
83.6	1.917	1.954
83.7	1.917	1.997
83.8	1.917	2.056
83.9	2.258	2.119
84	2.258	2.178
84.1	2.258	2.221
84.2	2.258	2.246
84.3	2.258	2.256
84.4	2.258	2.258
84.5	2.258	2.256
84.6	2.258	2.247
84.7	2.258	2.224
84.8	2.258	2.184
84.9	2.258	2.13
85	1.944	2.072
85.1	1.944	2.018
85.2	1.944	1.98
85.3	1.944	1.968
85.4	1.944	1.985
85.5	1.944	2.028
85.6	1.944	2.089
85.7	2.299	2.156
85.8	2.299	2.22
85.9	2.299	2.271
86	2.299	2.307
86.1	2.34	2.333
86.2	2.34	2.355
86.3	2.34	2.378
86.4	2.444	2.4
86.5	2.444	2.419
86.6	2.444	2.433
86.7	2.444	2.44
86.8	2.444	2.443
86.9	2.444	2.444
87	2.444	2.444
87.1	2.444	2.444
87.2	2.444	2.444
87.3	2.444	2.444
87.4	2.444	2.444
87.5	2.444	2.444
87.6	2.444	2.444
87.7	2.444	2.444
87.8	2.444	2.444
87.9	2.444	2.444
88	2.444	2.444
88.1	2.444	2.444
88.2	2.444	2.444
88.3	2.444	2.444
88.4	2.444	2.444
88.5	2.444	2.444
88.6	2.444	2.444
88.7	2.444	2.444
88.8	2.444	2.444
88.9	2.444	2.444
89	2.444	2.444
89.1	2.444	2.444
89.2	2.444	2.444
89.3	2.444	2.444
89.4	2.444	2.444
89.5	2.444	2.444
89.6	2.444	2.444
89.7	2.444	2.444
89.8	2.444	2.444
89.9	2.444	2.444
90	2.444	2.444
90.1	2.444	2.444
90.2	2.444	2.444
90.3	2.444	2.444
90.4	2.444	2.444
90.5	2.444	2.444
90.6	2.444	2.444
90.7	2.444	2.444
90.8	2.444	2.444
90.9	2.444	2.444
91	2.444	2.444
91.1	2.444	2.444
91.2	2.444	2.444
91.3	2.444	2.444
91.4	2.444	2.444
91.5	2.444	2.444
91.6	2.444	2.444
91.7	2.444	2.444
91.8	2.444	2.444
91.9	2.444	2.444
92	2.444	2.444
92.1	2.444	2.444
92.2	2.444	2.444
92.3	2.444	2.444
92.4	2.444	2.444
92.5	2.444	2.444
92.6	2.444	2.444
92.7	2.444	2.444
92.8	2.444	2.444
92.9	2.444	2.444
93	2.444	2.443
93.1	2.444	2.441
93.2	2.444	2.437
93.3	2.444	2.432
93.4	2.414	2.426
93.5	2.414	2.421

Distance (m)	Box curve (g/cm3)	Filtered (g/cm3)
93.6	2.414	2.418
93.7	2.414	2.416
93.8	2.414	2.415
93.9	2.414	2.415
94	2.414	2.415
94.1	2.414	2.415
94.2	2.414	2.415
94.3	2.414	2.415
94.4	2.414	2.415
94.5	2.414	2.415
94.6	2.414	2.415
94.7	2.414	2.415
94.8	2.414	2.415
94.9	2.414	2.415
95	2.414	2.415
95.1	2.414	2.415
95.2	2.414	2.415
95.3	2.414	2.415
95.4	2.414	2.415
95.5	2.414	2.415
95.6	2.414	2.415
95.7	2.414	2.415
95.8	2.414	2.415
95.9	2.414	2.415
96	2.414	2.415
96.1	2.414	2.415
96.2	2.414	2.415
96.3	2.414	2.415
96.4	2.414	2.415
96.5	2.414	2.415
96.6	2.414	2.415
96.7	2.414	2.415
96.8	2.414	2.415
96.9	2.414	2.415
97	2.414	2.415
97.1	2.414	2.415
97.2	2.414	2.415
97.3	2.414	2.415
97.4	2.414	2.415
97.5	2.414	2.415
97.6	2.414	2.415
97.7	2.414	2.415
97.8	2.414	2.415
97.9	2.414	2.415
98	2.414	2.415
98.1	2.414	2.415
98.2	2.414	2.415
98.3	2.414	2.415
98.4	2.414	2.415
98.5	2.414	2.415
98.6	2.414	2.415
98.7	2.414	2.415
98.8	2.414	2.415
98.9	2.414	2.415
99	2.414	2.415
99.1	2.414	2.415
99.2	2.414	2.415
99.3	2.414	2.415
99.4	2.414	2.415
99.5	2.414	2.415
99.6	2.414	2.415
99.7	2.414	2.415
99.8	2.414	2.415
99.9	2.414	2.415
100	2.414	2.415
100.1	2.414	2.415
100.2	2.414	2.415
100.3	2.414	2.415
100.4	2.414	2.415
100.5	2.414	2.415
100.6	2.414	2.415
100.7	2.414	2.415
100.8	2.414	2.416
100.9	2.414	2.418
101	2.414	2.423
101.1	2.414	2.429
101.2	2.451	2.432
101.3	2.451	2.43

Distance (m)	Box curve (g/cm3)	Filtered (g/cm3)
101.4	2.451	2.42
101.5	2.451	2.404
101.6	2.339	2.384
101.7	2.339	2.365
101.8	2.339	2.351
101.9	2.339	2.343
102	2.339	2.339
102.1	2.339	2.339
102.2	2.339	2.339
102.3	2.339	2.339
102.4	2.339	2.339
102.5	2.339	2.339
102.6	2.339	2.339
102.7	2.339	2.339
102.8	2.339	2.339
102.9	2.339	2.339
103	2.339	2.339
103.1	2.339	2.339
103.2	2.339	2.339
103.3	2.339	2.339
103.4	2.339	2.339
103.5	2.339	2.339
103.6	2.339	2.339
103.7	2.339	2.339
103.8	2.339	2.339
103.9	2.339	2.339
104	2.339	2.339
104.1	2.339	2.339
104.2	2.339	2.339
104.3	2.339	2.339
104.4	2.339	2.339
104.5	2.339	2.339
104.6	2.339	2.339
104.7	2.339	2.339
104.8	2.339	2.339
104.9	2.339	2.341
105	2.339	2.352
105.1	2.339	2.381
105.2	2.339	2.431
105.3	2.339	2.498
105.4	2.73	2.571
105.5	2.73	2.638
105.6	2.73	2.687
105.7	2.73	2.716
105.8	2.73	2.728
105.9	2.73	2.73
106	2.73	2.73
106.1	2.73	2.728
106.2	2.73	2.717
106.3	2.73	2.691
106.4	2.73	2.646
106.5	2.73	2.585
106.6	2.374	2.519
106.7	2.374	2.458
106.8	2.374	2.413
106.9	2.374	2.386
107	2.374	2.371
107.1	2.374	2.357
107.2	2.374	2.339
107.3	2.374	2.318
107.4	2.222	2.303
107.5	2.222	2.298
107.6	2.222	2.308
107.7	2.394	2.33
107.8	2.394	2.354
107.9	2.394	2.375
108	2.394	2.388
108.1	2.394	2.393
108.2	2.394	2.394
108.3	2.394	2.394
108.4	2.394	2.394
108.5	2.394	2.394
108.6	2.394	2.394
108.7	2.394	2.394
108.8	2.394	2.392
108.9	2.394	2.381
109	2.394	2.362
109.1	2.394	2.337

Distance (m)	Box curve (g/cm3)	Filtered (g/cm3)
109.2	2.394	2.313
109.3	1.982	2.298
109.4	2.348	2.296
109.5	2.348	2.307
109.6	2.348	2.323
109.7	2.348	2.337
109.8	2.348	2.346
109.9	2.348	2.348
110	2.348	2.348
110.1	2.348	2.348
110.2	2.348	2.348
110.3	2.348	2.348
110.4	2.348	2.348
110.5	2.348	2.348
110.6	2.348	2.348
110.7	2.348	2.348
110.8	2.348	2.348
110.9	2.348	2.348
111	2.348	2.348
111.1	2.348	2.348
111.2	2.348	2.348
111.3	2.348	2.348
111.4	2.348	2.348
111.5	2.348	2.348
111.6	2.348	2.35
111.7	2.348	2.357
111.8	2.348	2.376
111.9	2.348	2.409
112	2.348	2.452
112.1	2.607	2.495
112.2	2.607	2.523
112.3	2.607	2.529
112.4	2.607	2.513
112.5	2.397	2.481
112.6	2.397	2.447
112.7	2.397	2.42
112.8	2.397	2.405
112.9	2.397	2.398
113	2.397	2.397
113.1	2.397	2.397
113.2	2.397	2.397
113.3	2.397	2.397
113.4	2.397	2.397
113.5	2.397	2.397
113.6	2.397	2.397
113.7	2.397	2.397
113.8	2.397	2.397
113.9	2.397	2.397
114	2.397	2.394
114.1	2.397	2.381
114.2	2.397	2.349
114.3	2.397	2.293
114.4	2.397	2.218
114.5	1.955	2.139
114.6	1.955	2.073
114.7	1.955	2.033
114.8	1.955	2.019
114.9	2.083	2.024
115	2.083	2.036
115.1	2.083	2.047
115.2	1.954	2.054
115.3	2.083	2.063
115.4	2.083	2.075
115.5	2.083	2.092
115.6	2.083	2.111
115.7	2.163	2.129
115.8	2.163	2.144
115.9	2.163	2.154
116	2.163	2.159
116.1	2.16	2.161
116.2	2.16	2.161
116.3	2.16	2.16
116.4	2.16	2.161
116.5	2.16	2.163
116.6	2.16	2.168
116.7	2.16	2.177
116.8	2.16	2.188
116.9	2.23	2.202

Distance (m)	Box curve (g/cm3)	Filtered (g/cm3)
117	2.23	2.213
117.1	2.23	2.222
117.2	2.23	2.228
117.3	2.23	2.23
117.4	2.23	2.23
117.5	2.23	2.231
117.6	2.23	2.234
117.7	2.23	2.242
117.8	2.23	2.256
117.9	2.23	2.275
118	2.342	2.297
118.1	2.342	2.316
118.2	2.342	2.33
118.3	2.342	2.338
118.4	2.342	2.341
118.5	2.342	2.342
118.6	2.342	2.342
118.7	2.342	2.341
118.8	2.342	2.334
118.9	2.342	2.318
119	2.342	2.295
119.1	2.342	2.27
119.2	2.113	2.252
119.3	2.113	2.246
119.4	2.307	2.253
119.5	2.307	2.269
119.6	2.307	2.287
119.7	2.307	2.3
119.8	2.307	2.306
119.9	2.307	2.307
120	2.307	2.307
120.1	2.307	2.306
120.2	2.307	2.3
120.3	2.307	2.285
120.4	2.307	2.26
120.5	2.307	2.227
120.6	2.106	2.192
120.7	2.106	2.16
120.8	2.124	2.133
120.9	2.124	2.109
121	2.124	2.085
121.1	2.124	2.06
121.2	1.954	2.035
121.3	1.954	2.014
121.4	2.008	2.001
121.5	2.008	2.002
121.6	2.008	2.024
121.7	1.954	2.066
121.8	1.954	2.124
121.9	2.343	2.191
122	2.343	2.253
122.1	2.343	2.299
122.2	2.343	2.32
122.3	2.343	2.318
122.4	2.343	2.301
122.5	2.343	2.283
122.6	2.051	2.27
122.7	2.299	2.267
122.8	2.299	2.27
122.9	2.299	2.268
123	2.299	2.248
123.1	2.299	2.205
123.2	2.299	2.146
123.3	1.898	2.086
123.4	1.898	2.038
123.5	1.898	2.01
123.6	2.205	2.007
123.7	1.954	2.031
123.8	1.954	2.077
123.9	1.954	2.139
124	2.368	2.207
124.1	2.368	2.271
124.2	2.368	2.32
124.3	2.368	2.341
124.4	2.368	2.322
124.5	2.368	2.259
124.6	2.299	2.166
124.7	2.299	2.071

Distance (m)	Box curve (g/cm3)	Filtered (g/cm3)
124.8	1.52	2.005
124.9	1.52	1.991
125	2.124	2.031
125.1	2.299	2.103
125.2	2.299	2.175
125.3	2.259	2.22
125.4	2.259	2.227
125.5	2.259	2.208
125.6	2.127	2.182
125.7	2.127	2.16
125.8	2.127	2.152
125.9	2.127	2.165
126	2.127	2.2
126.1	2.127	2.252
126.2	2.435	2.31
126.3	2.435	2.362
126.4	2.435	2.401
126.5	2.435	2.424
126.6	2.435	2.433
126.7	2.435	2.436
126.8	2.435	2.444
126.9	2.435	2.463
127	2.435	2.495
127.1	2.435	2.538
127.2	2.689	2.584
127.3	2.689	2.615
127.4	2.689	2.619
127.5	2.689	2.588
127.6	2.689	2.529
127.7	2.299	2.458
127.8	2.299	2.389
127.9	2.299	2.328
128	2.299	2.272
128.1	2.299	2.223
128.2	2.299	2.183
128.3	1.905	2.16
128.4	1.905	2.162
128.5	2.309	2.188
128.6	2.309	2.228
128.7	2.309	2.268
128.8	2.309	2.295
128.9	2.309	2.307
129	2.309	2.309
129.1	2.309	2.309
129.2	2.309	2.309
129.3	2.309	2.309
129.4	2.309	2.309
129.5	2.309	2.309
129.6	2.309	2.309
129.7	2.309	2.309
129.8	2.309	2.309
129.9	2.309	2.309
130	2.309	2.309
130.1	2.309	2.309
130.2	2.309	2.309
130.3	2.309	2.309
130.4	2.309	2.309
130.5	2.309	2.309
130.6	2.309	2.309
130.7	2.309	2.309
130.8	2.309	2.309
130.9	2.309	2.309
131	2.309	2.309
131.1	2.309	2.309
131.2	2.309	2.309
131.3	2.309	2.309
131.4	2.309	2.309
131.5	2.309	2.309
131.6	2.309	2.309
131.7	2.309	2.309
131.8	2.309	2.311
131.9	2.309	2.322
132	2.309	2.349
132.1	2.309	2.394
132.2	2.309	2.454
132.3	2.67	2.517
132.4	2.67	2.571
132.5	2.67	2.607

Distance (m)	Box curve (g/cm3)	Filtered (g/cm3)
132.6	2.611	2.622
132.7	2.611	2.623
132.8	2.611	2.617
132.9	2.611	2.613
133	2.611	2.612
133.1	2.611	2.612
133.2	2.611	2.612
133.3	2.611	2.603
133.4	2.623	2.579
133.5	2.623	2.537
133.6	2.623	2.478
133.7	2.269	2.412
133.8	2.269	2.352
133.9	2.269	2.308
134	2.269	2.282
134.1	2.269	2.271
134.2	2.269	2.269
134.3	2.269	2.269
134.4	2.269	2.269
134.5	2.269	2.271
134.6	2.269	2.274
134.7	2.269	2.281
134.8	2.269	2.289
134.9	2.319	2.299
135	2.319	2.306
135.1	2.319	2.308
135.2	2.319	2.301
135.3	2.319	2.283
135.4	2.319	2.257
135.5	2.167	2.229
135.6	2.167	2.203
135.7	2.167	2.184
135.8	2.167	2.177
135.9	2.167	2.182
136	2.167	2.197
136.1	2.167	2.219
136.2	2.295	2.243
136.3	2.295	2.265
136.4	2.295	2.281
136.5	2.295	2.289
136.6	2.295	2.287
136.7	2.295	2.275
136.8	2.295	2.254
136.9	2.295	2.226
137	2.101	2.191
137.1	2.101	2.159
137.2	2.299	2.141
137.3	1.954	2.144
137.4	1.954	2.169
137.5	2.334	2.21
137.6	2.334	2.256
137.7	2.334	2.295
137.8	2.334	2.32
137.9	2.334	2.332
138	2.334	2.334
138.1	2.334	2.334
138.2	2.334	2.334
138.3	2.334	2.334
138.4	2.334	2.332
138.5	2.334	2.331
138.6	2.334	2.328
138.7	2.32	2.326
138.8	2.32	2.323
138.9	2.32	2.32
139	2.32	2.315
139.1	2.32	2.309
139.2	2.32	2.301
139.3	2.274	2.293
139.4	2.274	2.285
139.5	2.274	2.279
139.6	2.274	2.276
139.7	2.274	2.274
139.8	2.274	2.274
139.9	2.274	2.274
140	2.274	2.274
140.1	2.274	2.274
140.2	2.274	2.274
140.3	2.274	2.274

Distance (m)	Box curve (g/cm3)	Filtered (g/cm3)
140.4	2.274	2.274
140.5	2.274	2.274
140.6	2.274	2.274
140.7	2.274	2.274
140.8	2.274	2.273
140.9	2.274	2.266
141	2.274	2.249
141.1	2.274	2.224
141.2	2.274	2.196
141.3	2.04	2.172
141.4	2.04	2.159
141.5	2.197	2.159
141.6	2.197	2.168
141.7	2.197	2.181
141.8	2.197	2.191
141.9	2.197	2.196
142	2.197	2.197
142.1	2.197	2.197
142.2	2.197	2.197
142.3	2.197	2.197
142.4	2.197	2.197
142.5	2.197	2.197
142.6	2.197	2.197
142.7	2.197	2.197
142.8	2.197	2.199
142.9	2.197	2.204
143	2.197	2.212
143.1	2.197	2.223
143.2	2.26	2.234
143.3	2.26	2.245
143.4	2.26	2.253
143.5	2.26	2.258
143.6	2.26	2.259
143.7	2.26	2.256
143.8	2.26	2.249
143.9	2.26	2.235
144	2.26	2.215
144.1	2.133	2.194
144.2	2.259	2.179
144.3	1.954	2.175
144.4	2.232	2.182
144.5	2.232	2.196
144.6	2.232	2.212
144.7	2.232	2.224
144.8	2.232	2.23
144.9	2.232	2.232
145	2.232	2.232
145.1	2.232	2.232
145.2	2.232	2.232
145.3	2.232	2.232
145.4	2.232	2.23
145.5	2.232	2.223
145.6	2.232	2.209
145.7	2.232	2.188
145.8	2.232	2.165
145.9	1.954	2.146
146	2.15	2.135
146.1	2.15	2.131
146.2	2.15	2.131
146.3	2.15	2.132
146.4	2.119	2.13
146.5	2.119	2.127
146.6	2.119	2.129
146.7	2.119	2.141
146.8	2.119	2.164
146.9	2.119	2.197
147	2.311	2.233
147.1	2.311	2.266
147.2	2.311	2.29
147.3	2.311	2.301
147.4	2.311	2.301
147.5	2.311	2.293
147.6	2.311	2.28
147.7	2.234	2.265
147.8	2.234	2.252
147.9	2.234	2.242
148	2.234	2.237
148.1	2.234	2.234

Distance (m)	Box curve (g/cm3)	Filtered (g/cm3)
148.2	2.234	2.232
148.3	2.234	2.228
148.4	2.234	2.222
148.5	2.234	2.212
148.6	2.181	2.203
148.7	2.181	2.193
148.8	2.181	2.187
148.9	2.181	2.183
149	2.181	2.182
149.1	2.181	2.184
149.2	2.181	2.191
149.3	2.181	2.203
149.4	2.181	2.219
149.5	2.274	2.236
149.6	2.274	2.252
149.7	2.274	2.264
149.8	2.274	2.271
149.9	2.274	2.274
150	2.274	2.274
150.1	2.274	2.274
150.2	2.274	2.274
150.3	2.274	2.274
150.4	2.274	2.274
150.5	2.274	2.274
150.6	2.274	2.274
150.7	2.274	2.274
150.8	2.274	2.274
150.9	2.274	2.274
151	2.274	2.274
151.1	2.274	2.274
151.2	2.274	2.274
151.3	2.274	2.274
151.4	2.274	2.274
151.5	2.274	2.274
151.6	2.274	2.274
151.7	2.274	2.274
151.8	2.274	2.274
151.9	2.274	2.274
152	2.274	2.274
152.1	2.274	2.274
152.2	2.274	2.274
152.3	2.274	2.274
152.4	2.274	2.274
152.5	2.274	2.274
152.6	2.274	2.274
152.7	2.274	2.274
152.8	2.274	2.274
152.9	2.274	2.273
153	2.274	2.269
153.1	2.274	2.258
153.2	2.274	2.239
153.3	2.274	2.214
153.4	2.126	2.186
153.5	2.126	2.159
153.6	2.126	2.137
153.7	2.126	2.119
153.8	2.126	2.106
153.9	2.074	2.095
154	2.074	2.086
154.1	2.074	2.08
154.2	2.074	2.076
154.3	2.074	2.074
154.4	2.074	2.074
154.5	2.074	2.074
154.6	2.074	2.074
154.7	2.074	2.074
154.8	2.074	2.074
154.9	2.074	2.074
155	2.074	2.074
155.1	2.074	2.074
155.2	2.074	2.074
155.3	2.074	2.074
155.4	2.074	2.074
155.5	2.074	2.074
155.6	2.074	2.074
155.7	2.074	2.074
155.8	2.074	2.074
155.9	2.074	2.074

Distance (m)	Box curve (g/cm3)	Filtered (g/cm3)
156	2.074	2.074
156.1	2.074	2.074
156.2	2.074	2.074
156.3	2.074	2.074
156.4	2.074	2.074
156.5	2.074	2.074
156.6	2.074	2.074
156.7	2.074	2.076
156.8	2.074	2.087
156.9	2.074	2.111
157	2.074	2.147
157.1	2.074	2.187
157.2	2.427	2.219
157.3	2.427	2.232
157.4	2.152	2.225
157.5	2.152	2.204
157.6	2.152	2.18
157.7	2.152	2.164
157.8	2.152	2.169
157.9	2.152	2.197
158	2.152	2.242
158.1	2.152	2.294
158.2	2.579	2.338
158.3	2.579	2.362
158.4	2.292	2.362
158.5	2.292	2.344
158.6	2.292	2.321
158.7	2.292	2.302
158.8	2.292	2.294
158.9	2.292	2.294
159	2.292	2.305
159.1	2.292	2.329
159.2	2.292	2.364
159.3	2.292	2.401
159.4	2.649	2.426
159.5	2.649	2.43
159.6	2.317	2.413
159.7	2.317	2.382
159.8	2.317	2.35
159.9	2.317	2.326
160	2.317	2.315
160.1	2.306	2.314
160.2	2.306	2.321
160.3	2.306	2.334
160.4	2.306	2.352
160.5	2.419	2.373
160.6	2.419	2.392
160.7	2.419	2.406
160.8	2.419	2.415
160.9	2.419	2.418
161	2.419	2.419
161.1	2.419	2.419
161.2	2.419	2.419
161.3	2.419	2.419
161.4	2.419	2.419
161.5	2.419	2.419
161.6	2.419	2.419
161.7	2.419	2.419
161.8	2.419	2.419
161.9	2.419	2.419
162	2.419	2.419
162.1	2.419	2.419
162.2	2.419	2.419
162.3	2.419	2.419
162.4	2.419	2.419
162.5	2.419	2.419
162.6	2.419	2.419
162.7	2.419	2.419
162.8	2.419	2.419
162.9	2.419	2.419
163	2.419	2.419
163.1	2.419	2.419
163.2	2.419	2.419
163.3	2.419	2.419
163.4	2.419	2.419
163.5	2.419	2.418
163.6	2.419	2.416
163.7	2.419	2.41

Distance (m)	Box curve (g/cm3)	Filtered (g/cm3)
163.8	2.419	2.4
163.9	2.419	2.386
164	2.338	2.371
164.1	2.338	2.357
164.2	2.338	2.347
164.3	2.338	2.341
164.4	2.338	2.338
164.5	2.338	2.338
164.6	2.338	2.338
164.7	2.338	2.338
164.8	2.338	2.338
164.9	2.338	2.338
165	2.338	2.338
165.1	2.338	2.338
165.2	2.338	2.338
165.3	2.338	2.337
165.4	2.338	2.336
165.5	2.338	2.334
165.6	2.338	2.332
165.7	2.323	2.329
165.8	2.323	2.327
165.9	2.323	2.325
166	2.323	2.324
166.1	2.323	2.323
166.2	2.323	2.323
166.3	2.323	2.323
166.4	2.323	2.323
166.5	2.323	2.323
166.6	2.323	2.323
166.7	2.323	2.323
166.8	2.323	2.323
166.9	2.323	2.323
167	2.323	2.323
167.1	2.323	2.323
167.2	2.323	2.323
167.3	2.323	2.323
167.4	2.323	2.323
167.5	2.323	2.323
167.6	2.323	2.323
167.7	2.323	2.323
167.8	2.323	2.323
167.9	2.323	2.323
168	2.323	2.323
168.1	2.323	2.323
168.2	2.323	2.323
168.3	2.323	2.322
168.4	2.323	2.32
168.5	2.323	2.316
168.6	2.323	2.31
168.7	2.292	2.305
168.8	2.292	2.299
168.9	2.292	2.296
169	2.292	2.294
169.1	2.292	2.294
169.2	2.296	2.294
169.3	2.296	2.295
169.4	2.296	2.296
169.5	2.296	2.296
169.6	2.296	2.296
169.7	2.296	2.296
169.8	2.296	2.296
169.9	2.296	2.296
170	2.296	2.296
170.1	2.296	2.296
170.2	2.296	2.296
170.3	2.296	2.296
170.4	2.296	2.296
170.5	2.296	2.296
170.6	2.296	2.296
170.7	2.296	2.296
170.8	2.296	2.296
170.9	2.296	2.296
171	2.296	2.296
171.1	2.296	2.296
171.2	2.296	2.296
171.3	2.296	2.296
171.4	2.296	2.296
171.5	2.296	2.296

Distance (m)	Box curve (g/cm3)	Filtered (g/cm3)
171.6	2.296	2.296
171.7	2.296	2.296
171.8	2.296	2.296
171.9	2.296	2.296
172	2.296	2.296
172.1	2.296	2.296
172.2	2.296	2.296
172.3	2.296	2.296
172.4	2.296	2.296
172.5	2.296	2.296
172.6	2.296	2.296
172.7	2.296	2.296
172.8	2.296	2.296
172.9	2.296	2.296
173	2.296	2.296
173.1	2.296	2.296
173.2	2.296	2.297
173.3	2.296	2.3
173.4	2.296	2.304
173.5	2.296	2.309
173.6	2.332	2.314
173.7	2.332	2.316
173.8	2.332	2.314
173.9	2.299	2.311
174	2.299	2.306
174.1	2.299	2.302
174.2	2.299	2.3
174.3	2.299	2.299
174.4	2.299	2.299
174.5	2.299	2.299
174.6	2.299	2.299
174.7	2.299	2.299
174.8	2.299	2.299
174.9	2.299	2.299
175	2.299	2.299
175.1	2.299	2.299
175.2	2.299	2.299
175.3	2.299	2.299
175.4	2.299	2.299
175.5	2.299	2.299
175.6	2.299	2.299
175.7	2.299	2.299
175.8	2.299	2.299
175.9	2.299	2.299
176	2.299	2.299
176.1	2.299	2.299
176.2	2.299	2.299
176.3	2.299	2.299
176.4	2.299	2.299
176.5	2.299	2.299
176.6	2.299	2.299
176.7	2.299	2.299
176.8	2.299	2.299
176.9	2.299	2.299
177	2.299	2.299
177.1	2.299	2.299
177.2	2.299	2.299
177.3	2.299	2.299
177.4	2.299	2.299
177.5	2.299	2.299
177.6	2.299	2.299
177.7	2.299	2.299
177.8	2.299	2.299
177.9	2.299	2.299
178	2.299	2.299
178.1	2.299	2.299
178.2	2.299	2.299
178.3	2.299	2.299
178.4	2.299	2.299
178.5	2.299	2.299
178.6	2.299	2.299
178.7	2.299	2.299
178.8	2.299	2.299
178.9	2.299	2.299
179	2.299	2.299
179.1	2.299	2.299
179.2	2.299	2.299
179.3	2.299	2.299

Distance (m)	Box curve (g/cm3)	Filtered (g/cm3)
179.4	2.299	2.299
179.5	2.299	2.299
179.6	2.299	2.299
179.7	2.299	2.299
179.8	2.299	2.299
179.9	2.299	2.299
180	2.299	2.299
180.1	2.299	2.299
180.2	2.299	2.299
180.3	2.299	2.299
180.4	2.299	2.299
180.5	2.299	2.299
180.6	2.299	2.299
180.7	2.299	2.299
180.8	2.299	2.299
180.9	2.299	2.299
181	2.299	2.304
181.1	2.299	2.315
181.2	2.299	2.334
181.3	2.299	2.36
181.4	2.451	2.389
181.5	2.451	2.415
181.6	2.451	2.434
181.7	2.451	2.443
181.8	2.451	2.434
181.9	2.451	2.402
182	2.451	2.346
182.1	2.451	2.269
182.2	2.004	2.186
182.3	2.004	2.109
182.4	2.004	2.053
182.5	2.004	2.02
182.6	2.004	2.007
182.7	2.004	2.004
182.8	2.004	2.004
182.9	2.004	2.004
183	2.004	2.004
183.1	2.004	2.004
183.2	2.004	2.004
183.3	2.004	2.004
183.4	2.004	2.004
183.5	2.004	2.004
183.6	2.004	2.004
183.7	2.004	2.004
183.8	2.004	2.004
183.9	2.004	2.004
184	2.004	2.004
184.1	2.004	2.004
184.2	2.004	2.004
184.3	2.004	2.004
184.4	2.004	2.004
184.5	2.004	2.004
184.6	2.004	2.004
184.7	2.004	2.004
184.8	2.004	2.004
184.9	2.004	2.004
185	2.004	2.004
185.1	2.004	2.004
185.2	2.004	2.004
185.3	2.004	2.004
185.4	2.004	2.004
185.5	2.004	2.004
185.6	2.004	2.004
185.7	2.004	2.004
185.8	2.004	2.004
185.9	2.004	2.004
186	2.004	2.004
186.1	2.004	2.004
186.2	2.004	2.004
186.3	2.004	2.005
186.4	2.004	2.011
186.5	2.004	2.026
186.6	2.004	2.051
186.7	2.004	2.086
186.8	2.205	2.123
186.9	2.205	2.157
187	2.205	2.18
187.1	2.205	2.191

Distance (m)	Box curve (g/cm3)	Filtered (g/cm3)
187.2	2.205	2.193
187.3	2.177	2.19
187.4	2.177	2.188
187.5	2.177	2.189
187.6	2.177	2.193
187.7	2.215	2.2
187.8	2.215	2.206
187.9	2.215	2.21
188	2.215	2.209
188.1	2.215	2.2
188.2	2.215	2.185
188.3	2.215	2.169
188.4	2.083	2.16
188.5	2.083	2.165
188.6	2.083	2.186
188.7	2.301	2.217
188.8	2.301	2.25
188.9	2.301	2.277
189	2.301	2.293
189.1	2.301	2.3
189.2	2.301	2.301
189.3	2.301	2.301
189.4	2.301	2.301
189.5	2.301	2.301
189.6	2.301	2.301
189.7	2.301	2.301
189.8	2.301	2.301
189.9	2.301	2.301
190	2.301	2.301
190.1	2.301	2.301
190.2	2.301	2.301
190.3	2.301	2.301
190.4	2.301	2.301
190.5	2.301	2.301
190.6	2.301	2.301
190.7	2.301	2.301
190.8	2.301	2.301
190.9	2.301	2.301
191	2.301	2.301
191.1	2.301	2.301
191.2	2.301	2.301
191.3	2.301	2.301
191.4	2.301	2.301
191.5	2.301	2.301
191.6	2.301	2.301
191.7	2.301	2.301
191.8	2.301	2.303
191.9	2.301	2.305
192	2.301	2.31
192.1	2.301	2.314
192.2	2.352	2.318
192.3	2.32	2.321
192.4	2.32	2.322
192.5	2.32	2.322
192.6	2.32	2.321
192.7	2.32	2.32
192.8	2.32	2.32
192.9	2.32	2.32
193	2.32	2.32
193.1	2.32	2.32
193.2	2.32	2.32
193.3	2.32	2.32
193.4	2.32	2.32
193.5	2.32	2.32
193.6	2.32	2.32
193.7	2.32	2.32
193.8	2.32	2.32
193.9	2.32	2.319
194	2.32	2.318
194.1	2.32	2.315
194.2	2.32	2.312
194.3	2.299	2.308
194.4	2.299	2.304
194.5	2.299	2.301
194.6	2.299	2.3
194.7	2.299	2.299
194.8	2.299	2.3
194.9	2.299	2.301

Distance (m)	Box curve (g/cm3)	Filtered (g/cm3)
195	2.298	2.304
195.1	2.298	2.307
195.2	2.32	2.311
195.3	2.32	2.315
195.4	2.32	2.318
195.5	2.32	2.319
195.6	2.32	2.32
195.7	2.32	2.32
195.8	2.32	2.32
195.9	2.32	2.32
196	2.32	2.32
196.1	2.32	2.32
196.2	2.32	2.32
196.3	2.32	2.32
196.4	2.32	2.32
196.5	2.32	2.32
196.6	2.32	2.321
196.7	2.32	2.323
196.8	2.32	2.327
196.9	2.32	2.332
197	2.349	2.337
197.1	2.349	2.342
197.2	2.349	2.346
197.3	2.349	2.348
197.4	2.349	2.351
197.5	2.349	2.356
197.6	2.349	2.364
197.7	2.349	2.375
197.8	2.414	2.388
197.9	2.414	2.399
198	2.414	2.407
198.1	2.414	2.412
198.2	2.414	2.414
198.3	2.414	2.414
198.4	2.414	2.414
198.5	2.414	2.414
198.6	2.414	2.414
198.7	2.414	2.414
198.8	2.414	2.414
198.9	2.414	2.414
199	2.414	2.414
199.1	2.414	2.414
199.2	2.414	2.414
199.3	2.414	2.414
199.4	2.414	2.414
199.5	2.414	2.414
199.6	2.414	2.414
199.7	2.414	2.414
199.8	2.414	2.414
199.9	2.414	2.414
200	2.414	2.414
200.1	2.414	2.414
200.2	2.414	2.414
200.3	2.414	2.414
200.4	2.414	2.414
200.5	2.414	2.414
200.6	2.414	2.414
200.7	2.414	2.414
200.8	2.414	2.414
200.9	2.414	2.414
201	2.414	2.414
201.1	2.414	2.414
201.2	2.414	2.414
201.3	2.414	2.414
201.4	2.414	2.414
201.5	2.414	2.414
201.6	2.414	2.414
201.7	2.414	2.414
201.8	2.414	2.414
201.9	2.414	2.414
202	2.414	2.414
202.1	2.414	2.414
202.2	2.414	2.414
202.3	2.414	2.412
202.4	2.414	2.401
202.5	2.414	2.373
202.6	2.414	2.327
202.7	2.414	2.272

Distance (m)	Box curve (g/cm3)	Filtered (g/cm3)
202.8	2.038	2.225
202.9	2.038	2.2
203	2.038	2.205
203.1	2.349	2.236
203.2	2.349	2.278
203.3	2.349	2.315
203.4	2.349	2.338
203.5	2.349	2.347
203.6	2.349	2.349
203.7	2.349	2.348
203.8	2.349	2.342
203.9	2.349	2.331
204	2.349	2.315
204.1	2.349	2.299
204.2	2.124	2.287
204.3	2.299	2.281
204.4	2.299	2.28
204.5	2.299	2.282
204.6	2.299	2.283
204.7	2.299	2.281
204.8	2.226	2.278
204.9	2.28	2.276
205	2.28	2.276
205.1	2.28	2.277
205.2	2.28	2.279
205.3	2.28	2.28
205.4	2.28	2.279
205.5	2.28	2.275
205.6	2.28	2.27
205.7	2.28	2.264
205.8	2.234	2.26
205.9	2.234	2.26
206	2.234	2.266
206.1	2.299	2.273
206.2	2.299	2.278
206.3	2.299	2.273
206.4	2.299	2.257
206.5	2.299	2.238
206.6	2.124	2.226
206.7	2.124	2.232
206.8	2.124	2.259
206.9	2.409	2.299
207	2.409	2.343
207.1	2.409	2.378
207.2	2.409	2.399
207.3	2.409	2.407
207.4	2.409	2.409
207.5	2.409	2.409
207.6	2.409	2.409
207.7	2.409	2.409
207.8	2.409	2.409
207.9	2.409	2.408
208	2.409	2.403
208.1	2.409	2.39
208.2	2.409	2.368
208.3	2.409	2.338
208.4	2.235	2.306
208.5	2.235	2.276
208.6	2.235	2.254
208.7	2.235	2.241
208.8	2.235	2.232
208.9	2.235	2.222
209	2.235	2.203
209.1	2.235	2.171
209.2	2.124	2.131
209.3	2.124	2.093
209.4	1.954	2.073
209.5	1.954	2.079
209.6	1.954	2.113
209.7	2.299	2.165
209.8	2.299	2.219
209.9	2.299	2.265
210	2.299	2.298
210.1	2.299	2.321
210.2	2.299	2.341
210.3	2.402	2.36
210.4	2.402	2.378
210.5	2.402	2.391

Distance (m)	Box curve (g/cm3)	Filtered (g/cm3)
210.6	2.402	2.399
210.7	2.402	2.402
210.8	2.402	2.402
210.9	2.402	2.402
211	2.402	2.402
211.1	2.402	2.402
211.2	2.402	2.402
211.3	2.402	2.402
211.4	2.402	2.402
211.5	2.402	2.402
211.6	2.402	2.402
211.7	2.402	2.402
211.8	2.402	2.402
211.9	2.402	2.402
212	2.402	2.402
212.1	2.402	2.402
212.2	2.402	2.402
212.3	2.402	2.402
212.4	2.402	2.402
212.5	2.402	2.402
212.6	2.402	2.402
212.7	2.402	2.403
212.8	2.402	2.408
212.9	2.402	2.419
213	2.402	2.434
213.1	2.402	2.448
213.2	2.567	2.454
213.3	2.567	2.449
213.4	2.372	2.434
213.5	2.372	2.412
213.6	2.372	2.393
213.7	2.372	2.379
213.8	2.372	2.374
213.9	2.372	2.373
214	2.372	2.373
214.1	2.372	2.373
214.2	2.372	2.373
214.3	2.372	2.373
214.4	2.372	2.373
214.5	2.372	2.373
214.6	2.372	2.373
214.7	2.372	2.373
214.8	2.372	2.373
214.9	2.372	2.373
215	2.372	2.373
215.1	2.372	2.373
215.2	2.372	2.373
215.3	2.372	2.373
215.4	2.372	2.374
215.5	2.372	2.383
215.6	2.372	2.401
215.7	2.372	2.427
215.8	2.372	2.451
215.9	2.656	2.461
216	2.656	2.452
216.1	2.319	2.425
216.2	2.319	2.388
216.3	2.319	2.354
216.4	2.319	2.331
216.5	2.319	2.321
216.6	2.319	2.319
216.7	2.319	2.319
216.8	2.319	2.319
216.9	2.319	2.319
217	2.319	2.319
217.1	2.319	2.319
217.2	2.319	2.319
217.3	2.319	2.319
217.4	2.319	2.319
217.5	2.319	2.319
217.6	2.319	2.319
217.7	2.319	2.319
217.8	2.319	2.319
217.9	2.319	2.319
218	2.319	2.319
218.1	2.319	2.319
218.2	2.319	2.319
218.3	2.319	2.319

Distance (m)	Box curve (g/cm3)	Filtered (g/cm3)
218.4	2.319	2.319
218.5	2.319	2.319
218.6	2.319	2.319
218.7	2.319	2.319
218.8	2.319	2.319
218.9	2.319	2.319
219	2.319	2.319
219.1	2.319	2.319
219.2	2.319	2.319
219.3	2.319	2.319
219.4	2.319	2.319
219.5	2.319	2.319
219.6	2.319	2.319
219.7	2.319	2.319
219.8	2.319	2.319
219.9	2.319	2.319
220	2.319	2.319
220.1	2.319	2.319
220.2	2.319	2.319
220.3	2.319	2.319
220.4	2.319	2.319
220.5	2.319	2.319
220.6	2.319	2.319
220.7	2.319	2.319
220.8	2.319	2.319
220.9	2.319	2.319
221	2.319	2.319
221.1	2.319	2.319
221.2	2.319	2.319
221.3	2.319	2.319
221.4	2.319	2.319
221.5	2.319	2.319
221.6	2.319	2.319
221.7	2.319	2.319
221.8	2.319	2.319
221.9	2.319	2.319
222	2.319	2.319
222.1	2.319	2.319
222.2	2.319	2.319
222.3	2.319	2.319
222.4	2.319	2.319
222.5	2.319	2.319
222.6	2.319	2.319
222.7	2.319	2.319
222.8	2.319	2.319
222.9	2.319	2.319
223	2.319	2.319
223.1	2.319	2.319
223.2	2.319	2.319
223.3	2.319	2.319
223.4	2.319	2.319
223.5	2.319	2.319
223.6	2.319	2.319
223.7	2.319	2.319
223.8	2.319	2.319
223.9	2.319	2.319
224	2.319	2.319
224.1	2.319	2.319
224.2	2.319	2.319
224.3	2.319	2.319
224.4	2.319	2.319
224.5	2.319	2.319
224.6	2.319	2.319
224.7	2.319	2.319
224.8	2.319	2.319
224.9	2.319	2.319
225	2.319	2.319
225.1	2.319	2.319
225.2	2.319	2.319
225.3	2.319	2.319
225.4	2.319	2.319
225.5	2.319	2.319
225.6	2.319	2.319
225.7	2.319	2.319
225.8	2.319	2.319
225.9	2.319	2.319
226	2.319	2.319
226.1	2.319	2.319

Distance (m)	Box curve (g/cm3)	Filtered (g/cm3)
226.2	2.319	2.319
226.3	2.319	2.319
226.4	2.319	2.319
226.5	2.319	2.319
226.6	2.319	2.319
226.7	2.319	2.319
226.8	2.319	2.319
226.9	2.319	2.319
227	2.319	2.319
227.1	2.319	2.319
227.2	2.319	2.319
227.3	2.319	2.319
227.4	2.319	2.319
227.5	2.319	2.319
227.6	2.319	2.319
227.7	2.319	2.319
227.8	2.319	2.319
227.9	2.319	2.319
228	2.319	2.319
228.1	2.319	2.319
228.2	2.319	2.319
228.3	2.319	2.319
228.4	2.319	2.319
228.5	2.319	2.319
228.6	2.319	2.319
228.7	2.319	2.319
228.8	2.319	2.319
228.9	2.319	2.319
229	2.319	2.319
229.1	2.319	2.319
229.2	2.319	2.319
229.3	2.319	2.319
229.4	2.319	2.319
229.5	2.319	2.318
229.6	2.319	2.315
229.7	2.319	2.307
229.8	2.319	2.292
229.9	2.319	2.273
230	2.205	2.251
230.1	2.205	2.233
230.2	2.205	2.221
230.3	2.205	2.219
230.4	2.205	2.228
230.5	2.205	2.243
230.6	2.299	2.261
230.7	2.299	2.277
230.8	2.299	2.289
230.9	2.299	2.296
231	2.299	2.299
231.1	2.299	2.3
231.2	2.299	2.301
231.3	2.299	2.303
231.4	2.299	2.306
231.5	2.316	2.309
231.6	2.316	2.312
231.7	2.316	2.314
231.8	2.316	2.315
231.9	2.316	2.316
232	2.316	2.316
232.1	2.316	2.316
232.2	2.316	2.316
232.3	2.316	2.316
232.4	2.316	2.316
232.5	2.316	2.316
232.6	2.316	2.316
232.7	2.316	2.316
232.8	2.316	2.316
232.9	2.316	2.316
233	2.316	2.316
233.1	2.316	2.316
233.2	2.316	2.316
233.3	2.316	2.316
233.4	2.316	2.316
233.5	2.316	2.316
233.6	2.316	2.316
233.7	2.316	2.316
233.8	2.316	2.316
233.9	2.316	2.316

Distance (m)	Box curve (g/cm3)	Filtered (g/cm3)
234	2.316	2.316
234.1	2.316	2.316
234.2	2.316	2.316
234.3	2.316	2.316
234.4	2.316	2.316
234.5	2.316	2.316
234.6	2.316	2.315
234.7	2.316	2.314
234.8	2.316	2.312
234.9	2.316	2.308
235	2.298	2.305
235.1	2.298	2.302
235.2	2.298	2.299
235.3	2.298	2.291
235.4	2.298	2.275
235.5	2.298	2.247
235.6	2.298	2.212
235.7	2.083	2.181
235.8	2.083	2.167
235.9	2.083	2.178
236	2.083	2.214
236.1	2.388	2.265
236.2	2.388	2.316
236.3	2.388	2.355
236.4	2.388	2.377
236.5	2.388	2.386
236.6	2.388	2.388
236.7	2.388	2.388
236.8	2.388	2.388
236.9	2.388	2.388
237	2.388	2.388
237.1	2.388	2.388
237.2	2.388	2.388
237.3	2.388	2.388
237.4	2.388	2.388
237.5	2.388	2.388
237.6	2.388	2.388
237.7	2.388	2.388
237.8	2.388	2.388
237.9	2.388	2.388
238	2.388	2.388
238.1	2.388	2.388
238.2	2.388	2.388
238.3	2.388	2.388
238.4	2.388	2.388
238.5	2.388	2.388
238.6	2.388	2.388
238.7	2.388	2.388
238.8	2.388	2.388
238.9	2.388	2.388
239	2.388	2.388
239.1	2.388	2.388
239.2	2.388	2.388
239.3	2.388	2.388
239.4	2.388	2.388
239.5	2.388	2.388
239.6	2.388	2.388
239.7	2.388	2.388
239.8	2.388	2.388
239.9	2.388	2.387
240	2.388	2.385
240.1	2.388	2.381
240.2	2.388	2.376
240.3	2.358	2.37
240.4	2.358	2.363
240.5	2.358	2.357
240.6	2.358	2.351
240.7	2.339	2.347
240.8	2.339	2.344
240.9	2.339	2.341
241	2.339	2.34
241.1	2.34	2.34
241.2	2.34	2.343
241.3	2.34	2.35
241.4	2.34	2.361
241.5	2.34	2.375
241.6	2.426	2.39
241.7	2.426	2.4

Distance (m)	Box curve (g/cm3)	Filtered (g/cm3)
241.8	2.426	2.4
241.9	2.426	2.386
242	2.426	2.363
242.1	2.271	2.334
242.2	2.271	2.308
242.3	2.271	2.288
242.4	2.271	2.277
242.5	2.271	2.272
242.6	2.271	2.271
242.7	2.271	2.271
242.8	2.271	2.271
242.9	2.271	2.271
243	2.271	2.271
243.1	2.271	2.271
243.2	2.271	2.271
243.3	2.271	2.273
243.4	2.271	2.279
243.5	2.271	2.288
243.6	2.271	2.299
243.7	2.341	2.313
243.8	2.341	2.324
243.9	2.341	2.333
244	2.341	2.339
244.1	2.341	2.342
244.2	2.341	2.346
244.3	2.341	2.352
244.4	2.341	2.36
244.5	2.388	2.369
244.6	2.388	2.377
244.7	2.388	2.383
244.8	2.388	2.386
244.9	2.388	2.388
245	2.388	2.388
245.1	2.388	2.387
245.2	2.388	2.385
245.3	2.388	2.381
245.4	2.388	2.377
245.5	2.36	2.371
245.6	2.36	2.365
245.7	2.36	2.359
245.8	2.36	2.353
245.9	2.341	2.349
246	2.341	2.345
246.1	2.341	2.343
246.2	2.341	2.342
246.3	2.341	2.341
246.4	2.341	2.341
246.5	2.341	2.341
246.6	2.341	2.341
246.7	2.341	2.341
246.8	2.341	2.341
246.9	2.341	2.341
247	2.341	2.341
247.1	2.341	2.341
247.2	2.341	2.341
247.3	2.341	2.341
247.4	2.341	2.341
247.5	2.341	2.341
247.6	2.341	2.341
247.7	2.341	2.341
247.8	2.341	2.341
247.9	2.341	2.341
248	2.341	2.341
248.1	2.341	2.341
248.2	2.341	2.341
248.3	2.341	2.341
248.4	2.341	2.342
248.5	2.341	2.344
248.6	2.341	2.346
248.7	2.354	2.349
248.8	2.354	2.351
248.9	2.354	2.352
249	2.354	2.353
249.1	2.354	2.354
249.2	2.354	2.353
249.3	2.354	2.353
249.4	2.354	2.351
249.5	2.354	2.35

Distance (m)	Box curve (g/cm3)	Filtered (g/cm3)
249.6	2.344	2.348
249.7	2.344	2.346
249.8	2.344	2.345
249.9	2.344	2.344
250	2.344	2.344
250.1	2.344	2.344
250.2	2.344	2.344
250.3	2.344	2.344
250.4	2.344	2.344
250.5	2.344	2.344
250.6	2.344	2.344
250.7	2.344	2.342
250.8	2.344	2.339
250.9	2.344	2.333
251	2.344	2.324
251.1	2.295	2.315
251.2	2.295	2.307
251.3	2.295	2.301
251.4	2.295	2.297
251.5	2.295	2.296
251.6	2.295	2.295
251.7	2.295	2.295
251.8	2.295	2.295
251.9	2.295	2.295
252	2.295	2.295
252.1	2.295	2.295
252.2	2.295	2.295
252.3	2.295	2.295
252.4	2.295	2.295
252.5	2.295	2.295
252.6	2.295	2.295
252.7	2.295	2.295
252.8	2.295	2.295
252.9	2.295	2.295
253	2.295	2.295
253.1	2.295	2.295
253.2	2.295	2.295
253.3	2.295	2.295
253.4	2.295	2.295
253.5	2.295	2.295
253.6	2.295	2.295
253.7	2.295	2.295
253.8	2.295	2.295
253.9	2.295	2.295
254	2.295	2.295
254.1	2.295	2.295
254.2	2.295	2.295
254.3	2.295	2.295
254.4	2.295	2.295
254.5	2.295	2.295
254.6	2.295	2.295
254.7	2.295	2.295
254.8	2.295	2.295
254.9	2.295	2.295
255	2.295	2.295
255.1	2.295	2.295
255.2	2.295	2.295
255.3	2.295	2.295
255.4	2.295	2.295
255.5	2.295	2.295
255.6	2.295	2.295
255.7	2.295	2.295
255.8	2.295	2.295
255.9	2.295	2.295
256	2.295	2.295
256.1	2.295	2.295
256.2	2.295	2.295
256.3	2.295	2.295
256.4	2.295	2.295
256.5	2.295	2.295
256.6	2.295	2.295
256.7	2.295	2.295
256.8	2.295	2.295
256.9	2.295	2.295
257	2.295	2.295
257.1	2.295	2.295
257.2	2.295	2.295
257.3	2.295	2.294

Distance (m)	Box curve (g/cm3)	Filtered (g/cm3)
257.4	2.295	2.292
257.5	2.295	2.291
257.6	2.283	2.291
257.7	2.283	2.294
257.8	2.283	2.303
257.9	2.283	2.315
258	2.36	2.329
258.1	2.36	2.342
258.2	2.36	2.352
258.3	2.36	2.357
258.4	2.36	2.359
258.5	2.36	2.359
258.6	2.36	2.358
258.7	2.36	2.355
258.8	2.36	2.352
258.9	2.34	2.348
259	2.34	2.345
259.1	2.34	2.342
259.2	2.34	2.341
259.3	2.34	2.34
259.4	2.34	2.34
259.5	2.34	2.34
259.6	2.34	2.34
259.7	2.34	2.34
259.8	2.34	2.34
259.9	2.34	2.34
260	2.34	2.34
260.1	2.34	2.34
260.2	2.34	2.34
260.3	2.34	2.34
260.4	2.34	2.34
260.5	2.34	2.34
260.6	2.34	2.34
260.7	2.34	2.34
260.8	2.34	2.34
260.9	2.34	2.34
261	2.34	2.34
261.1	2.34	2.34
261.2	2.34	2.34
261.3	2.34	2.34
261.4	2.34	2.34
261.5	2.34	2.34
261.6	2.34	2.34
261.7	2.34	2.34
261.8	2.34	2.34
261.9	2.34	2.34
262	2.34	2.34
262.1	2.34	2.34
262.2	2.34	2.34
262.3	2.34	2.34
262.4	2.34	2.341
262.5	2.34	2.341
262.6	2.34	2.343
262.7	2.34	2.345
262.8	2.34	2.346
262.9	2.37	2.343
263	2.37	2.338
263.1	2.308	2.33
263.2	2.308	2.322
263.3	2.308	2.315
263.4	2.308	2.31
263.5	2.308	2.308
263.6	2.308	2.308
263.7	2.308	2.307
263.8	2.308	2.305
263.9	2.308	2.303
264	2.295	2.302
264.1	2.295	2.304
264.2	2.295	2.31
264.3	2.295	2.319
264.4	2.354	2.331
264.5	2.354	2.343
264.6	2.354	2.354
264.7	2.354	2.364
264.8	2.37	2.373
264.9	2.396	2.378
265	2.396	2.38
265.1	2.396	2.378

Distance (m)	Box curve (g/cm3)	Filtered (g/cm3)
265.2	2.37	2.373
265.3	2.354	2.367
265.4	2.354	2.362
265.5	2.354	2.36
265.6	2.354	2.359
265.7	2.37	2.36
265.8	2.37	2.36
265.9	2.354	2.36
266	2.354	2.36
266.1	2.354	2.361
266.2	2.354	2.364
266.3	2.378	2.368
266.4	2.378	2.372
266.5	2.378	2.375
266.6	2.378	2.377
266.7	2.378	2.377
266.8	2.378	2.375
266.9	2.378	2.371
267	2.378	2.367
267.1	2.35	2.361
267.2	2.35	2.357
267.3	2.35	2.353
267.4	2.35	2.351
267.5	2.35	2.35
267.6	2.35	2.35
267.7	2.35	2.35
267.8	2.35	2.352
267.9	2.35	2.357
268	2.35	2.365
268.1	2.35	2.376
268.2	2.413	2.387
268.3	2.413	2.396
268.4	2.413	2.401
268.5	2.413	2.399
268.6	2.413	2.393
268.7	2.365	2.384
268.8	2.365	2.376
268.9	2.365	2.37
269	2.365	2.366
269.1	2.365	2.365
269.2	2.365	2.365
269.3	2.365	2.365
269.4	2.365	2.37
269.5	2.365	2.382
269.6	2.365	2.397
269.7	2.365	2.413
269.8	2.531	2.421
269.9	2.531	2.419
270	2.352	2.407
270.1	2.352	2.388
270.2	2.352	2.371
270.3	2.352	2.358
270.4	2.352	2.353
270.5	2.352	2.35
270.6	2.352	2.347
270.7	2.352	2.342
270.8	2.352	2.335
270.9	2.309	2.329
271	2.309	2.327
271.1	2.309	2.332
271.2	2.307	2.343
271.3	2.386	2.358
271.4	2.386	2.371
271.5	2.405	2.379
271.6	2.405	2.383
271.7	2.37	2.387
271.8	2.354	2.393
271.9	2.354	2.403
272	2.458	2.415
272.1	2.458	2.423
272.2	2.458	2.422
272.3	2.458	2.413
272.4	2.354	2.398
272.5	2.354	2.383
272.6	2.354	2.374
272.7	2.375	2.369
272.8	2.375	2.369
272.9	2.375	2.369

Distance (m)	Box curve (g/cm3)	Filtered (g/cm3)
273	2.375	2.37
273.1	2.354	2.369
273.2	2.37	2.368
273.3	2.37	2.367
273.4	2.37	2.365
273.5	2.37	2.363
273.6	2.354	2.36
273.7	2.354	2.358
273.8	2.354	2.356
273.9	2.354	2.354
274	2.354	2.354
274.1	2.354	2.354
274.2	2.354	2.354
274.3	2.354	2.354
274.4	2.354	2.354
274.5	2.354	2.354
274.6	2.354	2.354
274.7	2.354	2.355
274.8	2.354	2.358
274.9	2.354	2.363
275	2.354	2.369
275.1	2.392	2.373
275.2	2.392	2.372
275.3	2.392	2.364
275.4	2.392	2.349
275.5	2.29	2.331
275.6	2.29	2.314
275.7	2.29	2.301
275.8	2.29	2.294
275.9	2.29	2.291
276	2.29	2.29
276.1	2.29	2.29
276.2	2.29	2.29
276.3	2.29	2.29
276.4	2.29	2.293
276.5	2.29	2.299
276.6	2.29	2.308
276.7	2.29	2.321
276.8	2.37	2.334
276.9	2.37	2.345
277	2.354	2.352
277.1	2.354	2.355
277.2	2.354	2.355
277.3	2.354	2.354
277.4	2.354	2.354
277.5	2.354	2.354
277.6	2.354	2.354
277.7	2.354	2.354
277.8	2.354	2.355
277.9	2.354	2.356
278	2.354	2.357
278.1	2.37	2.357
278.2	2.354	2.358
278.3	2.354	2.359
278.4	2.354	2.36
278.5	2.365	2.362
278.6	2.365	2.364
278.7	2.365	2.366
278.8	2.37	2.368
278.9	2.37	2.369
279	2.37	2.37
279.1	2.37	2.37
279.2	2.37	2.369
279.3	2.37	2.369
279.4	2.367	2.368
279.5	2.367	2.368
279.6	2.367	2.367
279.7	2.367	2.367
279.8	2.367	2.367
279.9	2.367	2.366
280	2.367	2.363
280.1	2.367	2.358
280.2	2.37	2.351
280.3	2.326	2.343
280.4	2.326	2.336
280.5	2.326	2.331
280.6	2.326	2.328
280.7	2.326	2.326

Distance (m)	Box curve (g/cm3)	Filtered (g/cm3)
280.8	2.326	2.326
280.9	2.326	2.328
281	2.326	2.331
281.1	2.326	2.338
281.2	2.326	2.346
281.3	2.375	2.353
281.4	2.375	2.357
281.5	2.375	2.356
281.6	2.375	2.349
281.7	2.316	2.34
281.8	2.316	2.33
281.9	2.316	2.322
282	2.316	2.318
282.1	2.316	2.316
282.2	2.316	2.316
282.3	2.316	2.316
282.4	2.316	2.316
282.5	2.316	2.316
282.6	2.316	2.316
282.7	2.316	2.316
282.8	2.316	2.316
282.9	2.316	2.316
283	2.316	2.316
283.1	2.316	2.316

APPENDIX C

'DEN' FORTRAN program

FORTRAN program which creates the density BOX curve which is then filtered to produce the field density log.

```
ccccccccccccccccccccccccccccccccccccccccccccccccccccccccccccccccccccccccccccc
c 'DEN' FORTRAN Program - The program creates a density BOX curve which is
c                         then filtered, to produce a field density log with similar
c                         character and resolution as a wireline density log.
ccccccccccccccccccccccccccccccccccccccccccccccccccccccccccccccccccccccccccccc
c234567890123456789012345678901234567890123456789012345678901234567890123456789
      program den
      real depth,density,lith(14),lithx(14),lithave(14),from,to,lithol,
     .lithden,froma(1000),toa(1000),lithdena(1000),fromt,tot,dent,
     .litholt,dena(1000),xd,xda,st,en,z
      integer j,ca,x

      character filea*20,fileb*20,filec*20
      m=iargc()
      if (m.lt.3) then
      write(*,'(a)') 'enter filename which contains the density data'
      read(*,'(a)') filea
      write(*,'(a)') 'enter filename which contains the lithology data'
      read(*,'(a)') fileb
      write(*,'(a)') 'enter output filename '
      read(*,'(a)') filec
      else
      call getarg(1,filea)
      call getarg(2,fileb)
      call getarg(3,filec)
      endif
      open(unit=1,file=filea)
      open(unit=2,file=fileb)
      open(unit=3,file=filec)
      open(unit=4,file="filetemp")
      open(unit=7,file="filetemp2")
      open(unit=8,file="box")
      write(*,'(a)') 'enter start depth '
      read(*,*) st
      write(*,'(a)') 'enter end depth '
      read(*,*) en
ccccccccccccccccccccccccccccccccccccccccccccccccccccccccccccccccccccccccccccc
c  Calculate average density values for each lithology
c   change do j=1,##     depending on number of lithologies
ccccccccccccccccccccccccccccccccccccccccccccccccccccccccccccccccccccccccccccc
      j=1
 10    read(1,*,end=100) depth,density,lithol
       do j=1,15
        if (lithol .eq. j) then
         lith(j)=lith(j)+density
         lithx(j)=lithx(j)+1
        endif
       enddo
       goto 10
```

```
100  continue

ccccccccccccccccccccccccccccccccccccccccccccccccccccccccccccccccccccccc
c  Allow user to input average density for lithologies which have
c  not been sampled
c   change do j=1,##      depending on number of lithologies
ccccccccccccccccccccccccccccccccccccccccccccccccccccccccccccccccccccccc
      do j=1,15
       if (lith(j) .gt. 0) then
       lithave(j)=lith(j)/lithx(j)
       write(3,'(a,i2,a,f8.5)') 'lithology',j,' ave. den. =',lithave(j)
      else
       write(6,'(a,i2)') ' enter a density for lithology ', j
       read(5,*) lithave(j)
       write(3,'(a,i2,a,f8.5)') 'lithology',j,' ave. den. =',lithave(j)
      endif
      enddo
c
ccccccccccccccccccccccccccccccccccccccccccccccccccccccccccccccccccccccc
c Assign each depth range a density value, density values are averaged
c if more than one sample is in one lithology type
c
ccccccccccccccccccccccccccccccccccccccccccccccccccccccccccccccccccccccc
      rewind(1)
 120  read(2,*,end=200) from,to,lithden
      x=0
      xd=0
 140  read(1,*,end=180) depth,density,lithol
      if((depth.ge.from).and.(depth.le.to).and.(lithden.eq.lithol).and.
     .(x.gt.0)) then
      x=x+1
      xd=density+xd
      xda=xd/x
      backspace 4
      write(4,'(f8.2,f8.2,f10.6,i4)') from,to,xda,int(lithol)
      endif
      if((depth.ge.from).and.(depth.le.to).and.(lithden.eq.lithol).and.
     .(x.eq.0)) then
       write(4,'(f8.2,f8.2,f10.6,i4)') from,to,density,int(lithol)
      xd=density
      x=x+1
      endif
      if((depth.ge.from).and.(depth.le.to).and.(lithden.ne.lithol))
     .then
       print *,'lithology clash at sample depth ', depth
      endif
      goto 140
 180  continue
      rewind(1)
```

```
      goto 120
200   continue
      rewind(2)
      ca=1
210   read(2,*,end=220) froma(ca),toa(ca),lithdena(ca)
      dena(ca)=lithave(int(lithdena(ca)))
      ca=ca+1
      goto 210
220   continue
      ca=ca-1
      j=1
      rewind(4)
      do j=1,ca
230   read(4,*,end=240) fromt,tot,dent,litholt
      if((fromt.eq.froma(j)).and.(tot.eq.toa(j)).and.
     .(litholt.eq.lithdena(j))) then
      dena(j)=dent
      endif
      goto 230
240   continue
      rewind(4)
      write(7,'(f8.2,f8.2,f10.6,i4)') froma(j),toa(j),dena(j),
     .int(lithdena(j))
      enddo
ccccccccccccccccccccccccccccccccccccccccccccccccccccccccccccccccc
c
c  assign every 0.1m a density value
c
ccccccccccccccccccccccccccccccccccccccccccccccccccccccccccccccccc
      rewind(7)
      do z=(st*10),(en*10),1
      x=0
300   read(7,*,end=320) fromt,tot,dent,litholt
      if(((z/10).ge.fromt).and.((z/10).le.tot).and.(x.gt.0)) then
      x=x+1
      backspace 8
      write(8,'(f8.1,f10.6,i4)') (z/10),dent,int(litholt)
      endif
      if(((z/10).ge.fromt).and.((z/10).le.tot).and.(x.eq.0)) then
      x=x+1
      write(8,'(f8.1,f10.6,i4)') (z/10),dent,int(litholt)
      endif
      goto 300
320   continue
      rewind(7)
      enddo
      end
```

APPENDIX D

GMT C-shell scripts

This appendix contains four examples of UNIX C-shell scripts written for the Generic Mapping Tools (GMT) computer program. These were written to generate the majority of the figures seen in this thesis. The FORTRAN programs written to generate the shell scripts for the shaded logs seen in Figures 3.12, 3.13 & 5.19 are also included in this appendix.

UNIX C-shell script : Example 1

```
#!/bin/csh
set data = ~/logs/south/ashdown1.dat.gz

gzcat $data | awk '{print $2, $1}' | psxy -R0/85/146/1100 -JX2.5/-20 -Ba20f10:"GR":
/a100f10:"DEPTH (m)":/:."ASHDOWN 1":WsN -X4 -Y3 -W1/0 -P -K > sqr.ps

gzcat $data | awk '{print ($2*$2), $1}' | psxy -R0/6800/146/1100 -JX2.5/-20
-Ba3000f1000:"GR^2":/a100f10sN -X3 -W1/0 -P -O -K >> sqr.ps

gzcat $data | awk '{print ($2*$2*$2*$2), $1}' | psxy -R10/50000000/146/1100 -JX2.5/-20
-Ba100000000f10000000:"GR^4":/a100f10sN -X3 -W1/0 -P -O -K >> sqr.ps

gzcat $data | awk '{print (sqrt($2)), $1}' | psxy -R3/9.5/146/1100 -JX2.5/-20
-Ba2f1:"GR sqrt":/a100f10sN -X3 -W1/0 -P -O -K >> sqr.ps

gzcat $data | awk '{print (sqrt(sqrt(sqrt(sqrt($2))))), $1}' | psxy -R1.15/1.33/146/1100
-JX2.5/-20 -Ba.1f.01:"GR sqrt4":/a100f10esN -X3 -W1/0 -P -O  >> sqr.ps
```

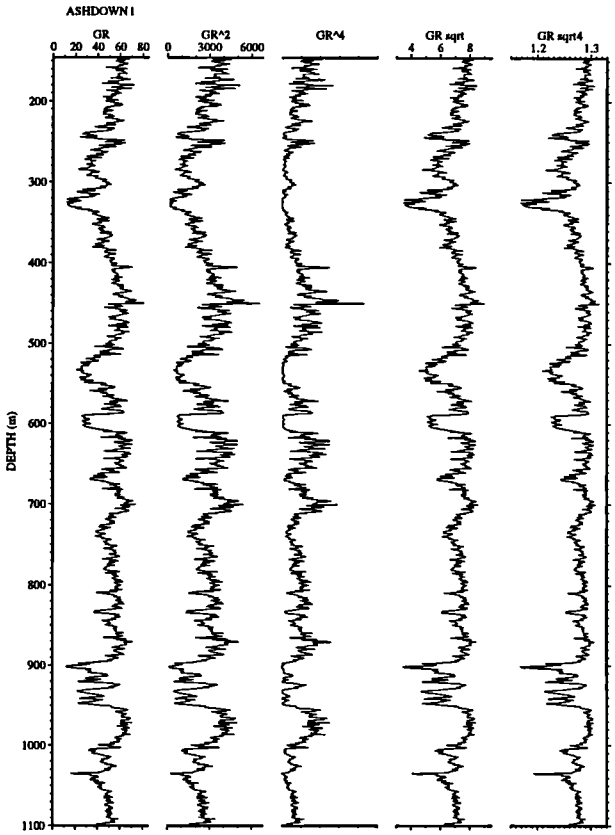

UNIX C-shell script : Example 2

```
#!/bin/csh
##################HENFIELD 1
gzcat ~/logs/south/henf.dat.gz | awk '{print $3, $1}' | psxy -R-30/75/820/1120 -JX2/-20
-Ba20f10:"SP":/a50f10:"DEPTH (m)":/:."HENFIELD 1":WsN -X3 -Y2 -W1/0 -P -K >
oldbio.ps

gzcat  ~/logs/south/henf.dat.gz | awk '{print $2, $1}' | psxy -R0.2/100/820/1120 -JX2l/-20
-Ba1f3:"RES":/a50f10esN -X2 -W1/0 -P -O -K>> oldbio.ps

##################COLLENDEAN FARM 1
gzcat ~/logs/south/collend.dat | awk '{print $3, $1}' | psxy -R0/120/1210/1510 -JX2/-20
-Ba50f10:"GR":/a50f10:"DEPTH (m)":WsN -X4 -W1/0 -P -K -O >> oldbio.ps

gzcat ~/logs/south/collend.dat | awk '{print $5, $1}' | psxy -R40/120/1210/1510 -JX-2/-20
-Ba50f10:"SONL":/a100f50sN -X2 -W1/0 -P -O -K >> oldbio.ps

gzcat ~/logs/south/collend.dat | awk '{print $6, $1}' | psxy -R-10/130/1210/1510 -JX2/-20
-Ba40f10:"SP":/a100f50/:."COLLENDEAN FARM 1 ":sN -X2 -W1/0 -P -O -K >>
oldbio.ps

gzcat ~/logs/south/collend.dat | awk '{print $2, $1}' | psxy -R2/200/1210/1510 -JX2l/-20
-Ba1f3:"RES":/a1000esN -X2 -W1/0 -P -O  >> oldbio.ps
```

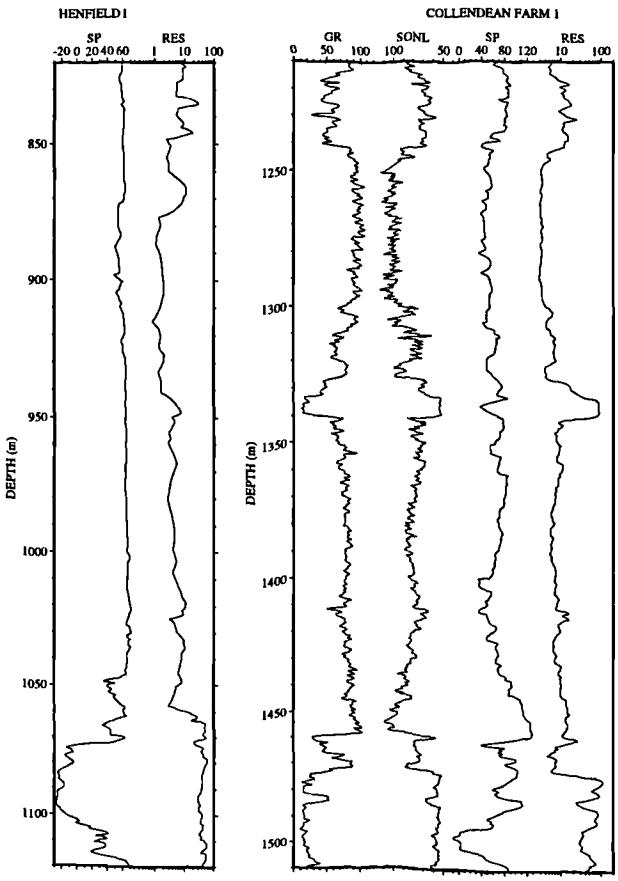

UNIX C-shell script : Example 3

```
#!/bin/csh
### change global x & y scale in .GMTDEFAULTS files
### Global X scale = .85
###       Y scale = .85
psbasemap -R0/4/160/585 -JX1/15.94 -Bwesn -X4 -Y-13 -K > fig2-19.ps

psxy -JX -R   -K -O -M << END >> fig2-19.ps
>
4 84.64
0 84.64
>
4 509.07
0 509.07
END

pstext -JX -R   -O -K << END >> fig2-19.ps
2.7 280 10 90 4 1 KIMMERIDGIAN (pars)
1.9 512 10 90 4 1 PORTLANDIAN
3.2 530 10 90 4 1 (pars)
END

### Ammonite zones ####
psbasemap -R0/4/160/585 -JX2.2/15.94 -Bwesn -X1 -O   -K >> fig2-19.ps

psxy -JX -R   -K -O -M << END >> fig2-19.ps
>
4 171.02
0 171.02
>
0 231.47
4 231.47
>
4 252.42
0 252.42
>
0 272.97
4 272.97
>
4 300.82
0 300.82
>
0 351.67
4 351.67
>
4 396.17
0 396.17
>
0 435.27
4 435.27
>
4 467.97
0 467.97
>
0 509.07
4 509.07
>
0 518.07
4 518.07
>
0 539.92
4 539.92
>
0 559.92
4 559.92
>
0 573.07
4 573.07
>
0 584.37
4 584.37
END
```

```
pstext -JX -R   -O -K << END >> fig2-19.ps
.2 163 10 0 6 1 eudoxus(pars)
.3 210 10 0 6 1 autissiodor-
.3 190 10 0 6 1 ensis
.3 241 10 0 6 1 elegans
.3 261 10 0 6 1 scitulus
.2 285 10 0 6 1 wheatleyensis
.3 326 10 0 6 1 hudlestoni
.3 375 10 0 6 1 pectinatus
.3 416 10 0 6 1 pallasioides
.3 451 10 0 6 1 rotunda
.3 486 10 0 6 1 fittoni
.3 511 10 0 6 1 albani
.3 524 10 0 6 1 glaucolithus
.3 545 10 0 6 1 okusensis
.3 565 10 0 6 1 kerberus
.3 577 10 0 6 1 anguiformis
END

#### field GR ####
awk '{print $2, $1}' < ~dgl3zma/fieldgr/kimm/contingr.txt | psxy -R0/60/160/585 -JX4.5/15.94
-Ba10f2:"GR (CPS)":/a50f10/:."geoMetrics GR310":N -X2.2 -W1/0  -M -O -K >> fig2-19.ps

psxy -JX -R0/4/160/585  -W1ta -K -O -M << END >> fig2-19.ps
>
4 171.02
0 171.02
>
0 231.47
4 231.47
>
4 252.42
0 252.42
>
0 272.97
4 272.97
>
4 300.82
0 300.82
>
0 351.67
4 351.67
>
4 396.17
0 396.17
>
0 435.27
4 435.27
>
4 467.97
0 467.97
>
0 509.07
4 509.07
>
END

##### tie lines
psxy -JX1.5/15.94 -R0/4/160/585 -X4.5 -K -O -M -W1ta << END >> fig2-19.ps
>
0 171.02
4 200.5
>
0 231.47
4 261.8
>
0 252.42
4 282
>
0 272.97
4 301.3
>
0 300.82
4 325.5
>
0 351.67
```

```
4 368.8
>
0 396.17
4 399
>
0 435.27
4 442
>
0 467.97
4 467.9
>
0 509.07
4 507.2
>
END

####### 98/11-4
gzcat /ts/global/dgl3zma/logs/offshore/98_11_4.dat.gz | awk '{print $2, $1/3.281}' | psxy -R20/150/550/975 -JX4.5/-15.94
-Ba20f10:"GR (API)":/a50f10:"DEPTH (M)":/:."98/11-4":N -X1.5 -W1/0 -P -O -K >> fig2-19.ps

psxy -JX -R0/4/550/975  -K -O -M  -W1ta << END >> fig2-19.ps
>
0 934.5
4 934.5
>
0 873.2
4 873.2
>
0 853
4 853
>
0 833.7
4 833.7
>
0 809.5
4 809.5
>
0 766.2
4 766.2
>
0 736
4 736
>
0 693
4 693
>
0 667.1
4 667.1
>
0 627.8
4 627.8
>
END

###### tie lines
psxy -JX1.5/-15.94 -R0/4/550/975 -X4.5 -K -O -M  -W1ta << END >> fig2-19.ps
>
0 934.5
4 908.3
>
0 873.2
4 858
>
0 853
4 841.3
>
0 833.7
4 823.7
>
0 809.5
4 794
>
0 766.2
4 726.5
>
0 736
```

```
4 693.2
>
0 693
4 653.6
>
0 667.1
2 653.6
>
0 627.8
0 653.6
>
END

### sine file for U/C
awk '{print $1, $2+653.6}' < ~/bin/sine | psxy -JX -R0/1/550/975 -K -O >> fig2-19.ps

################## Collendean farm
gzcat /ts/global/dgl3zma/logs/south/collend.dat | awk ' {print $3, $1}' | psxy -R10/120/620/1045 -JX4.5/-15.94
-Ba20f10:"GR (API)":/a50f10:"DEPTH":/:."COLLENDEAN FARM 1":N -X1.5 -W1/0   -K -O >> fig2-19.ps

psxy -JX -R0/4/620/1045   -K -O -M  -W1ta << END >> fig2-19.ps
>
0 978.3
4 978.3
>
0 928
4 928
>
0 911.3
4 911.3
>
0 893.7
4 893.7
>
0 864
4 864
>
0 796.5
4 796.5
>
0 763.2
4 763.2
>
END

### sine file for U/C
awk '{print $1, $2+723.6}' < ~/bin/sine | psxy -JX -R0/4/620/1045 -K -O >> fig2-19.ps

###### tie lines
psxy -JX1.5/-15.94 -R0/4/620/1045 -X4.5 -K -O -M  -W1ta << END >> fig2-19.ps
>
0 978.3
4 1016.1
>
0 928
4 963.7
>
0 911.3
4 943.4
>
0 893.7
4 926
>
0 864
4 897.5
>
0 796.5
4 826.4
>
0 763.2
4 791.8
>
0 723.6
4 760.5
>
2 723.6
```

```
4 730
>
4 723.6
4 680
>
END

### sine file for U/C
awk '{print $1, $2+723.6}' < ~/bin/sine | psxy -JX -R0/1/620/1045 -K -O >> fig2-19.ps

########## ashdown 1
gzcat /ts/global/dgl3zma/logs/south/ashdown1.dat.gz | awk '{print $2, $1}' | psxy -R0/100/300/725 -JX4.5/-15.94
-Ba20f10:"GR (API)":/a50f10:"DEPTH":/:."ASHDOWN 1":N -X1.5 -W1/0 -K  -O >> fig2-19.ps

psxy -JX -R0/4/300/725  -O -M -K  -W1ta << END >> fig2-19.ps
>
0 696.1
4 696.1
>
0 643.7
4 643.7
>
0 623.4
4 623.4
>
0 606
4 606
>
0 577.5
4 577.5
>
0 506.4
4 506.4
>
0 471.8
4 471.8
>
0 440.5
4 440.5
>
0 410
4 410
>
0 360
4 360
>
END

######## Scale & figure caption
psbasemap -R0/2/0/100 -JX.05/3.75 -B/a50f10:"Metres":wEsn -X5 -Y1 -K -O >> fig2-19.ps

psbasemap -R0/27.7/0/18 -JX27.7/18 -Bwesn -X-26.2 -Y-1 -O -K >> fig2-19.ps

pstext -R -JX -B -P -O -K << END >> fig2-19.ps
.5 16.1 9 45 4 1 Stage
1.5 16.1 9 45 4 1 Ammonite
2 16.1 9 45 4 1  Zones
END

pstext -JX28/18 -R0/28/0/18 -Y-2 -O  <<END>> fig2-19.ps
1.5 1.4 12 0 5 1 Fig. 2.19
3.2 1.4 12 0 4 1 Comparison of the field gamma-ray log produced using the geoMetrics GR310 spectrometer with wireline logs from three
boreholes
1.5 .9 12 0 4 1  from the Central Channel Sub-basin and the Weald Sub-basin of the Wessex Basin. See Fig. 2.1 for location of boreholes
and outcrop sections.
END
```

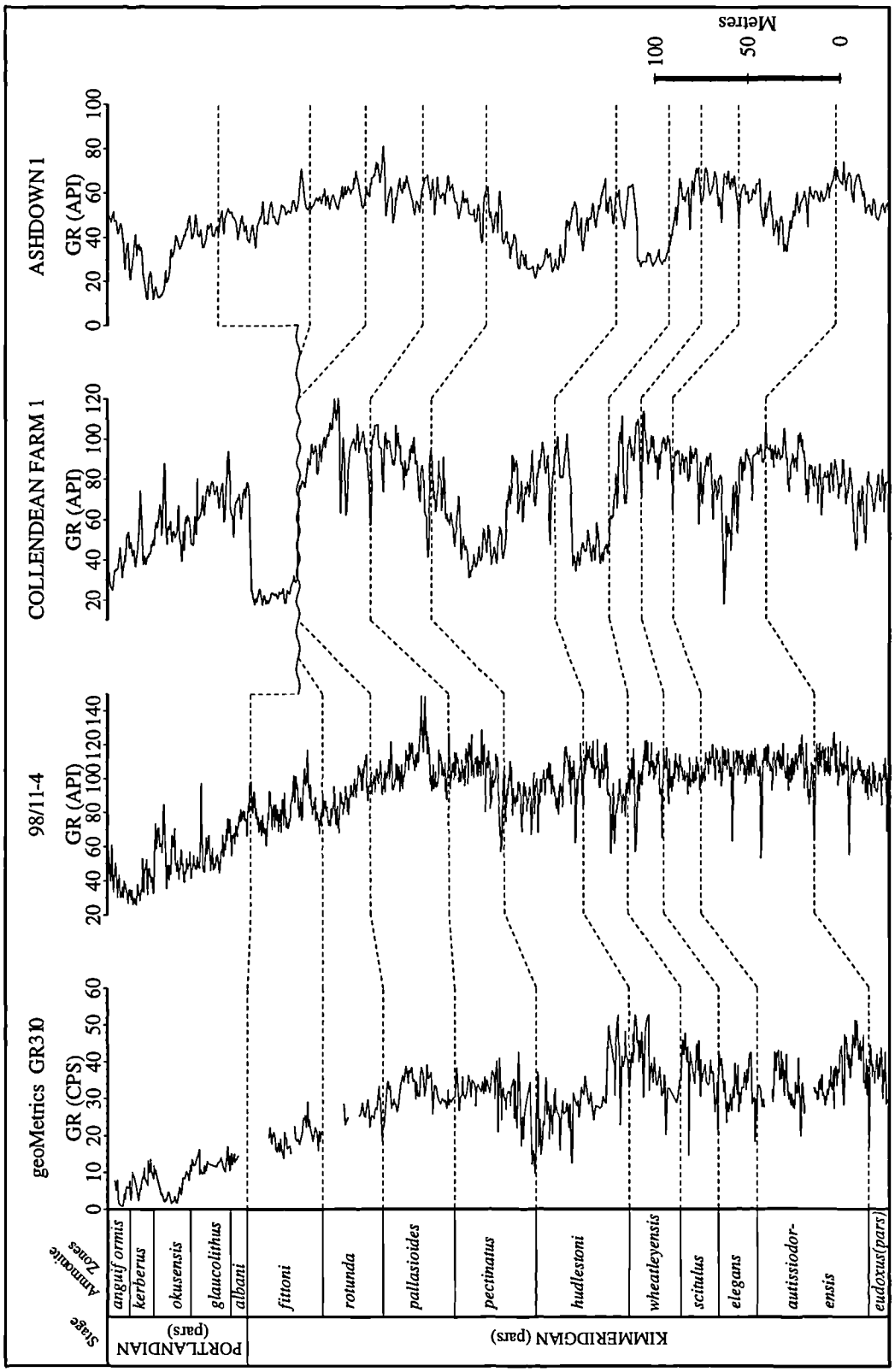

Fig. 2.19 Comparison of the field gamma-ray log produced using the geoMetrics GR310 spectrometer with wireline logs from three boreholes from the Central Channel Sub-basin and the Weald Sub-basin of the Wessex Basin. See Fig. 2.1 for location of boreholes and outcrop sections.

UNIX C-shell script : Example 4

```
#!/bin/csh

################## X-Y plot ammonite
psxy -R330.6/915.5/592.84/1078.14 -JX-5.849/-4.853 -Ba1000/a1000/:."Ammonite Zones":wens -X5 -Y3 -W1/0 -P -
K
<<END > gmtshel4.ps
330.6  592.84
379.1  633.32
409.8  658.87
440.5  701.51
474.2  730.9
548.09 774.89
574.3  799.68
593.39 818.57
614.5  838.74
669.9  900.13
813.7  997.09
866.6  1059.73
906.0  1072.53
915.5  1078.14
END

psxy -R330.6/915.5/592.84/1078.14 -JX-5.849/-4.853 -Bn -M -G0/0/0 -Sc.06 -P -K -O <<END >> gmtshel4.ps
330.6  592.84
379.1  633.32
409.8  658.87
440.5  701.51
474.2  730.9
548.09 774.89
574.3  799.68
593.39 818.57
614.5  838.74
669.9  900.13
813.7  997.09
866.6  1059.73
906.0  1072.53
915.5  1078.14
END

pstext -JX -R -P -O -K <<END >>  gmtshel4.ps
379.1  633.32  4 0 6 9  fittoni
409.8  658.87  4 0 6 9  rotunda
440.5  701.51  4 0 6 9  pallasioides
474.2  730.9  4 0 6 9  pectinatus
548.09 774.89  4 0 6 9  hudlestoni
574.3  799.68  4 0 6 9  wheatleyensis
593.39 818.57  4 0 6 9  scitulus
614.5  838.74  4 0 6 9  elegans
669.9  900.13  4 0 6 9  autissiodorensis
813.7  997.09  4 0 6 9  eudoxus
866.6  1059.73  4 0 6 1  mutabilis
906.0  1072.53  4 0 6 1  cymodoce
END

################## Y axis
gzcat ~/logs/offshore/98_11_4.dat.gz lawk '{print $2, ($1/3.281)-34.44}' | psxy -R40/140/592.84/1078.14 -JX1/-4.853
-Ba50f25:"GR":/a100f50:"98/11-4 (m)":WsN -X-1  -W1/0 -P -O -K >>  gmtshel4.ps

psxy -R0/1/592.84/1078.14 -JX -M  -W1ta -P -O -K << END >>  gmtshel4.ps
>
1  592.84
0  592.84
```

```
>
1  633.32
0  633.32
>
1  658.87
0  658.87
>
1  701.51
0  701.51
>
1  730.9
0  730.9
>
1  774.89
0  774.89
>
1  799.68
0  799.68
>
1  818.57
0  818.57
>
1  838.74
0  838.74
>
1  900.13
0  900.13
>
1  997.09
0  997.09
>
1  1059.73
0  1059.73
>
1  1072.53
0  1072.53
>
1  1078.14
0  1078.14
>
END

################## X axis
gzcat ~/logs/south/cowden.dat.gz | awk '$1-125.5>0 {print $1-125.5, $4}' | psxy -R330.6/915.5/10/120 -JX-5.849/-1
-Ba100f50:"Cowden (m)":/a50f25:"GR":wES -X1 -Y-1 -W1/0 -P -O  -K >>  gmtshel4.ps

psxy -R330.6/915.5/0/1 -JX -M  -W1ta -P -O  << END >>  gmtshel4.ps
>
330.6  0
330.6  1
>
379.1  0
379.1  1
>
409.8  0
409.8  1
>
440.5  0
440.5  1
>
474.2  0
474.2  1
>
548.09  0
```

548.09 1
>
574.3 0
574.3 1
>
593.39 0
593.39 1
>
614.5 0
614.5 1
>
669.9 0
669.9 1
>
813.7 0
813.7 1
>
866.6 0
866.6 1
>
906.0 0
906.0 1
>
915.5 0
915.5 1
>
END

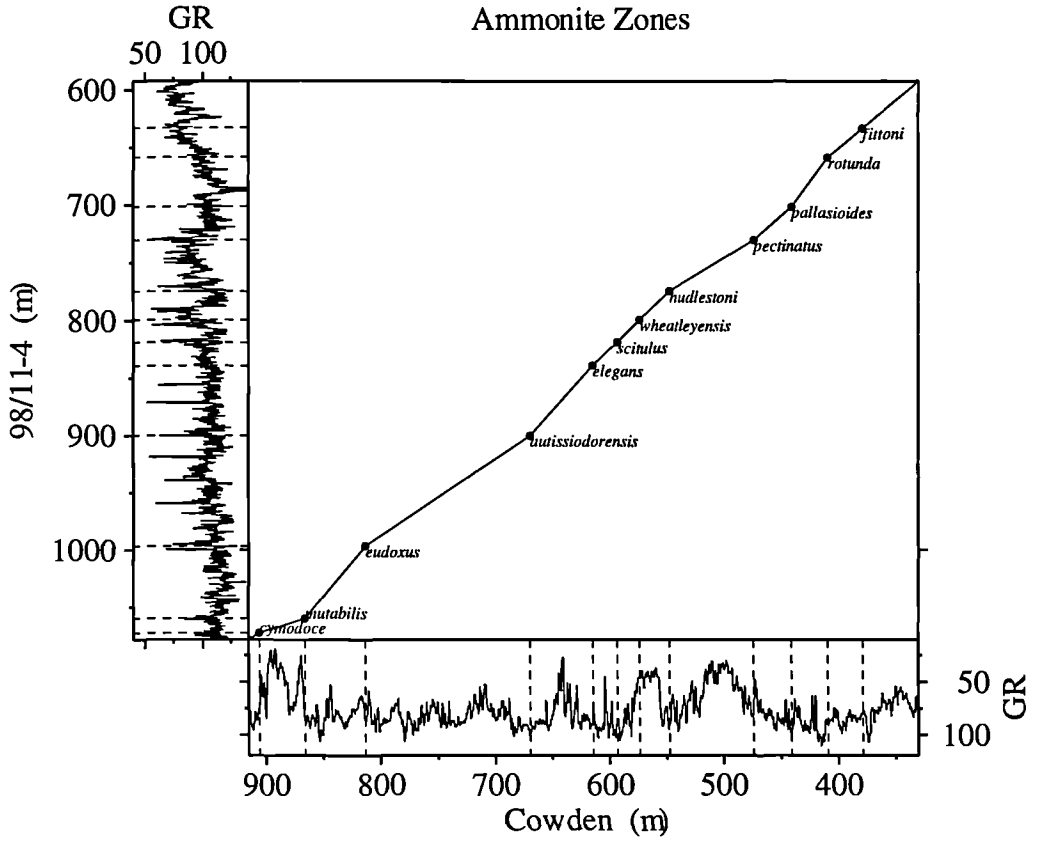

FORTRAN Program 1

This program generates the C-shell script for GMT, which shades between the gamma-ray and sonic logs. The shading is based on the gamma-ray curve. This shell script was produced to generate the shaded logs seen in Figures 3.12 & 5.19.

```
c234567890123456789012345678901234567890123456789012345678901234567890123456789012345
ccccccccccccccccccccccccccccccccccccccccccccccccccccccccccccccccccccccccccccccccccccc
      program ewc
      real depth, min, max, gr, gra(20000), deptha(20000), fact,
     .grgmt(20000), sonl, sonla(20000), mixa(20000)

      integer j, x, q, gm

c     character filea*20

c     write(*,'(a)') 'enter filename'
c     read(*,'(a)') filea
      open(unit=10,file="ewcol.dat")
      open(unit=11,file="ewbl.dat")
      open(unit=12,file="ewcow.dat")
      open(unit=13,file="ewash.dat")
      open(unit=14,file="ewdet.dat")
      open(unit=4,file="ewout")

      write(4, *) '#!/bin/csh'

      q = 0

      do q = 10, 14
ccccccccccccccccccccccccccccccccccccccccccccccccccccccccccccccccccccccccccccccccccccc
c  Calculate min & max GR values and put depth and GR in arrays
ccccccccccccccccccccccccccccccccccccccccccccccccccccccccccccccccccccccccccccccccccccc
      gm = 0
      x = 0
      max = 0
      min = 500
10    read(q,*,end=20) gr, sonl, depth
      x = x + 1
      mixa(x) = gr+sonl
      sonla(x) = sonl
      gra(x) = gr
      deptha(x) = depth
      if ((gr+sonl).le.min) then
      min = (gr+sonl)
      endif
      if ((gr+sonl).gt.max) then
      max = (gr+sonl)
      endif
     goto 10
20    continue

ccccccccccccccccccccccccccccccccccccccccccccccccccccccccccccccccccccccccccccccccccccc
c  Write psbasemap for the GR log depending on which well is in the loop
ccccccccccccccccccccccccccccccccccccccccccccccccccccccccccccccccccccccccccccccccccccc
     if (q.eq.10) then
```

```
      write(4, *) 'psbasemap -R0/120/1100/1450 -JX2/-12.347 -Ba50f10:"G
     .R":/a50f10:"Depth":/:."COLLENDEAN FARM":WN -X2 -Y-10 -K > e-w.ps'
      gm = 120
     endif

     if (q.eq.11) then
      write(4, *) 'psbasemap -R40/140/900/1250 -JX2/-12.347 -Ba50f10:"G
     .R":/a50f10:"Depth":/:."BLETCHINGLEY 1":N -X3 -K -O >> e-w.ps'
      gm = 140
     endif

     if (q.eq.12) then
      write(4, *) 'psbasemap -R0/120/920/1270 -JX2/-12.347 -Ba50f10:"GR
     .":/a50f10:"Depth":/:."COWDEN 1":N -X3 -K -O >> e-w.ps'
      gm = 120
     endif

     if (q.eq.13) then
      write(4, *) 'psbasemap -R0/120/650/1000 -JX2/-12.347 -Ba50f10:"GR
     .":/a50f10:"Depth":/:."ASHOUR 1":N -X3 -K -O >> e-w.ps'
      gm = 120
     endif

     if (q.eq.14) then
      write(4, *) 'psbasemap -R0/120/350/700 -JX2/-12.347 -Ba50f10:"GR"
     .:/a50f10:"Depth":/:."DETENTION 1":N -X3 -K -O >> e-w.ps'
      gm = 120
     endif


ccccccccccccccccccccccccccccccccccccccccccccccccccccccccccccccccccccc
c  Calculate GR values on a scale of 0-255 (with only 30 values)
ccccccccccccccccccccccccccccccccccccccccccccccccccccccccccccccccccccc

     fact = 30/(max-min)
     do j = 1, x
      grgmt(j) = int((mixa(j)-max)*fact)*(-8.5)
     enddo

     write (4, 40) int(grgmt(1)), int(grgmt(1))
40    format('psxy -JX -R -K -O -W0.2/'i3.3'tp -L -G'i3.3' << END >> e-w
    ..ps')
      write (4, '(i3, f8.2)') gm, deptha(1)

     grgmt(0)=grgmt(1)
     do j = 1, x

      if (j.eq.x) then
       write (4, '(f6.2, f8.2)') gra(j), deptha(j)
       write (4, '(i3, f8.2)') gm, deptha(j)
       write (4, *) 'END'
       goto 70
      endif

     if ((grgmt(j).eq.grgmt(j+1)).and.(grgmt(j).eq.grgmt(j-1))) then
      write (4, '(f6.2, f8.2)') gra(j), deptha(j)
     endif
```

```
      if ((grgmt(j).eq.grgmt(j+1)).and.(grgmt(j).ne.grgmt(j-1))) then
       write (4, '(f6.2, f8.2)') gra(j), deptha(j)
      endif


      if ((grgmt(j).ne.grgmt(j+1)).and.(grgmt(j).eq.grgmt(j-1))) then
       write (4, '(f6.2, f8.2)') gra(j), deptha(j)
       write (4, '(i3, f8.2)') gm, deptha(j)
       write (4, *) 'END'
       write (4, 50) int(grgmt(j+1)), int(grgmt(j+1))
       write (4, '(i3, f8.2)') gm, (deptha(j)+0.05)
      endif

      if ((grgmt(j).ne.grgmt(j+1)).and.(grgmt(j).ne.grgmt(j-1))) then
       write (4, '(f6.2, f8.2)') gra(j), deptha(j)
       write (4, '(i5, f8.2)') 120, deptha(j)
       write (4, *) 'END'
       write (4, 50) int(grgmt(j+1)), int(grgmt(j+1))
       write (4, '(i3, f8.2)') gm, (deptha(j)+0.05)
      endif

50    format('psxy -JX -R -K -O -W0.2/'i3.3'tp -L -G'i3.3'<< END >> e-w.
     .ps')

      enddo
70    continue


ccccccccccccccccccccccccccccccccccccccccccccccccccccccccccccccccccccc
c  Write psbasemap for the Sonic log depending on which well is in the loop
ccccccccccccccccccccccccccccccccccccccccccccccccccccccccccccccccccccc
      if (q.eq.10) then
       write (4, *) "gzcat ~/logs/south/collend.dat.gz | awk '{print $3,
     .$1}' | psxy -R -JX -Ba500/a10000n -W1/0 -O -K >>  e-w.ps"
       write(4, *) 'psbasemap -R40/140/1100/1450 -JX-2/-12.347 -Ba50f10:
     ."SONL":/a50f10:"Depth":N -X2 -K -O >> e-w.ps'
      endif

      if (q.eq.11) then
       write (4, *) "gzcat ~/logs/south/bletch.dat.gz | awk '{print $3,
     .$1}' | psxy -R -JX -Ba500/a10000n -W1/0 -O -K >>  e-w.ps"
       write(4, *) 'psbasemap -R40/140/900/1250 -JX-2/-12.347 -Ba50f10:"
     .SONL":/a50f10:"Depth":N -X2 -K -O >> e-w.ps'
      endif

      if (q.eq.12) then
       write (4, *) "gzcat ~/logs/south/cowden.dat.gz | awk '{print $4,
     .$1}' | psxy -R -JX -Ba500/a10000n -W1/0 -O -K >>  e-w.ps"
       write(4, *) 'psbasemap -R40/140/920/1270 -JX-2/-12.347 -Ba50f10:"
     .SONL":/a50f10:"Depth":N -X2 -K -O >> e-w.ps'
      endif

      if (q.eq.13) then
       write (4, *) "gzcat ~/logs/south/ashour.dat.gz | awk '{print $3,
     .$1}' | psxy -R -JX -Ba500/a10000n -W1/0 -O -K >>  e-w.ps"
       write(4, *) 'psbasemap -R40/140/650/1000 -JX-2/-12.347 -Ba50f10:"
     .SONL":/a50f10:"Depth":N -X2 -K -O >> e-w.ps'
      endif
```

```
      if (q.eq.14) then
       write (4, *) "gzcat ~/logs/south/detent.dat.gz | awk '{print $2,
     .$1}' | psxy -R -JX -Ba500/a10000n -W1/0 -O -K >>  e-w.ps"
       write(4, *) 'psbasemap -R40/140/350/700 -JX-2/-12.347 -Ba50f10:"S
     .ONL":/a50f10:"Depth":EN -X2 -K -O >> e-w.ps'
      endif


      write (4, 90) int(grgmt(1)), int(grgmt(1))
90    format('psxy -JX -R -K -O -W0.2/'i3.3'tp -L -G'i3.3' << END >> e-w
     ..ps')
      write (4, '(i5, f8.2)') 140, deptha(1)

      do j = 1, x

      if (j.eq.x) then
       write (4, '(f6.2, f8.2)') gra(j), deptha(j)
       write (4, '(i5, f8.2)') 140, deptha(j)
       write (4, *) 'END'
       goto 97
      endif

      if ((grgmt(j).eq.grgmt(j+1)).and.(grgmt(j).eq.grgmt(j-1))) then
       write (4, '(f6.2, f8.2)') sonla(j), deptha(j)
      endif

      if ((grgmt(j).eq.grgmt(j+1)).and.(grgmt(j).ne.grgmt(j-1))) then
       write (4, '(f6.2, f8.2)') sonla(j), deptha(j)
      endif


      if ((grgmt(j).ne.grgmt(j+1)).and.(grgmt(j).eq.grgmt(j-1))) then
       write (4, '(f6.2, f8.2)') sonla(j), deptha(j)
       write (4, '(i5, f8.2)') 140, deptha(j)
       write (4, *) 'END'
       write (4, 95) int(grgmt(j+1)), int(grgmt(j+1))
       write (4, '(i5, f8.2)') 140, (deptha(j)+0.05)
      endif

      if ((grgmt(j).ne.grgmt(j+1)).and.(grgmt(j).ne.grgmt(j-1))) then
       write (4, '(f6.2, f8.2)') sonla(j), deptha(j)
       write (4, '(i5, f8.2)') 140, deptha(j)
       write (4, *) 'END'
       write (4, 95) int(grgmt(j+1)), int(grgmt(j+1))
       write (4, '(i5, f8.2)') 140, (deptha(j)+0.05)
      endif
95    format('psxy -JX -R -K -O -W0.2/'i3.3'tp -L -G'i3.3' << END >> e-w
     ..ps')

      enddo
97    continue

      if (q.eq.10) then
       write (4, *) "gzcat ~/logs/south/collend.dat.gz | awk '{print $5,
     .$1}' | psxy -R -JX -Ba500/a10000n -W1/0 -O -K >>  e-w.ps"
      endif
```

```
if (q.eq.11) then
 write (4, *) "gzcat ~/logs/south/bletch.dat.gz | awk '{print $4,
.$1}' | psxy -R -JX -Ba500/a10000n -W1/0 -O -K >> e-w.ps"
endif

if (q.eq.12) then
 write (4, *) "gzcat ~/logs/south/cowden.dat.gz | awk '{print $2,
.$1}' | psxy -R -JX -Ba500/a10000n -W1/0 -O -K >> e-w.ps"
endif

if (q.eq.13) then
 write (4, *) "gzcat ~/logs/south/ashour.dat.gz | awk '{print $4,
.$1}' | psxy -R -JX -Ba500/a10000n -W1/0 -O -K >> e-w.ps"
endif

if (q.eq.14) then
 write (4, *) "gzcat ~/logs/south/detent.dat.gz | awk '{print $3,
.$1}' | psxy -R -JX -Ba500/a10000n -W1/0 -O >> e-w.ps"
endif

write (4, *) 'echo there should be 5 of these messages'
enddo

end
```

FORTRAN Program 2

This program generates the C-shell script for GMT, which shades between the gamma-ray and sonic logs. The shading is based on the gamma-ray and sonic curves. This shell script was used to generate Figure 3.13b.

```
c234567890123456789012345678901234567890123456789012345678901234567890123456789012
ccccccccccccccccccccccccccccccccccccccccccccccccccccccccccccccccccccccccccccccccc
      program mix
      real depth, min, max, gr, gra(20000), deptha(20000), fact,
     .grgmt(20000), sonl, sonla(20000), mixa(20000)

      integer j, x

      character filea*20

      write(*,'(a)') 'enter filename'
      read(*,'(a)') filea
      open(unit=1,file=filea)
      open(unit=4,file="mixout")

ccccccccccccccccccccccccccccccccccccccccccccccccccccccccccccccccccccccccccccccccc
c  Calculate min & max GR values and put depth and GR in arrays
ccccccccccccccccccccccccccccccccccccccccccccccccccccccccccccccccccccccccccccccccc
      x = 0
      max = 0
      min = 500
10    read(1,*,end=20) gr, sonl, depth
       x = x + 1
       mixa(x) = gr+sonl
       sonla(x) = sonl
       gra(x) = gr
       deptha(x) = depth
       if ((gr+sonl).le.min) then
       min = (gr+sonl)
       endif
       if ((gr+sonl).gt.max) then
       max = (gr+sonl)
       endif
      goto 10
20    continue

ccccccccccccccccccccccccccccccccccccccccccccccccccccccccccccccccccccccccccccccccc
c  Calculate GR values on a scale of 0-255 (with only 30 values)
ccccccccccccccccccccccccccccccccccccccccccccccccccccccccccccccccccccccccccccccccc
      write(4, *) '#!/bin/csh'
      write(4, 30) deptha(1), deptha(x)
30    format ('psbasemap -R0/120/'f5.1'/'f6.1' -JX4/-24.69 -Ba20f10:"GR"
     .:/a50f10:"Depth":WsN -X2 -Y2 -P -K > mix.ps')

      fact = 30/(max-min)
      do j = 1, x
       grgmt(j) = int((mixa(j)-max)*fact)*(-8.5)
      enddo
```

```
      write (4, 40) int(grgmt(1)), int(grgmt(1))
40     format('psxy -JX -R -P -K -O -W0.2/'i3.3'tp -L -G'i3.3'<< END >> m
     .ix.ps')
      write (4, '(i5, f8.2)') 120, deptha(1)

      grgmt(0)=grgmt(1)
      do j = 1, x

      if (j.eq.x) then
       write (4, '(f6.2, f8.2)') gra(j), deptha(j)
       write (4, '(i5, f8.2)') 120, deptha(j)
       write (4, *) 'END'
       write (4, *) "gzcat ~/logs/south/cowden.dat.gz | awk '{print $4,
     . $1}' | psxy -R -JX -Ba500/a10000wsn -W1/0 -P -O -K >>  mix.ps"
       goto 70
      endif

      if ((grgmt(j).eq.grgmt(j+1)).and.(grgmt(j).eq.grgmt(j-1))) then
       write (4, '(f6.2, f8.2)') gra(j), deptha(j)
      endif

      if ((grgmt(j).eq.grgmt(j+1)).and.(grgmt(j).ne.grgmt(j-1))) then
       write (4, '(f6.2, f8.2)') gra(j), deptha(j)
      endif


      if ((grgmt(j).ne.grgmt(j+1)).and.(grgmt(j).eq.grgmt(j-1))) then
       write (4, '(f6.2, f8.2)') gra(j), deptha(j)
       write (4, '(i5, f8.2)') 120, deptha(j)
       write (4, *) 'END'
       write (4, 50) int(grgmt(j+1)), int(grgmt(j+1))
c       write (4, '(i5, f8.2)') 0, deptha(j+1)
       write (4, '(i5, f8.2)') 120, (deptha(j)+0.05)
      endif

      if ((grgmt(j).ne.grgmt(j+1)).and.(grgmt(j).ne.grgmt(j-1))) then
       write (4, '(f6.2, f8.2)') gra(j), deptha(j)
       write (4, '(i5, f8.2)') 120, deptha(j)
       write (4, *) 'END'
       write (4, 50) int(grgmt(j+1)), int(grgmt(j+1))
c       write (4, '(i5, f8.2)') 0, deptha(j+1)
       write (4, '(i5, f8.2)') 120, (deptha(j)+0.05)
      endif

50     format('psxy -JX -R -P -K -O -W0.2/'i3.3'tp -L -G'i3.3'<< END >> m
     .ix.ps')

      enddo
70     continue

ccccccccccccccccccccccccccccccccccccccc

      write(4, 80) deptha(1), deptha(x)
80     format ('psbasemap -R40/140/'f5.1'/'f6.1' -JX-4/-24.69 -Ba20f10:"S
     .onl":/a50f10:"Depth":esN -X4 -P -K -O >> mix.ps')

      write (4, 90) int(grgmt(1)), int(grgmt(1))
90     format('psxy -JX -R -P -K -O -W0.2/'i3.3'tp -L -G'i3.3'<< END >> m
```

```
     .ix.ps')
      write (4, '(i5, f8.2)') 140, deptha(1)

      do j = 1, x

      if (j.eq.x) then
       write (4, '(f6.2, f8.2)') gra(j), deptha(j)
       write (4, '(i5, f8.2)') 140, deptha(j)
       write (4, *) 'END'
       write (4, *) "gzcat ~/logs/south/cowden.dat.gz | awk '{print $2,
     . $1}' | psxy -R -JX -Ba500/a10000esn -W1/0 -P -O >> mix.ps"
       goto 97
      endif

      if ((grgmt(j).eq.grgmt(j+1)).and.(grgmt(j).eq.grgmt(j-1))) then
       write (4, '(f6.2, f8.2)') sonla(j), deptha(j)
      endif

      if ((grgmt(j).eq.grgmt(j+1)).and.(grgmt(j).ne.grgmt(j-1))) then
       write (4, '(f6.2, f8.2)') sonla(j), deptha(j)
      endif


      if ((grgmt(j).ne.grgmt(j+1)).and.(grgmt(j).eq.grgmt(j-1))) then
       write (4, '(f6.2, f8.2)') sonla(j), deptha(j)
       write (4, '(i5, f8.2)') 140, deptha(j)
       write (4, *) 'END'
       write (4, 50) int(grgmt(j+1)), int(grgmt(j+1))
       write (4, '(i5, f8.2)') 140, (deptha(j)+0.05)
      endif

      if ((grgmt(j).ne.grgmt(j+1)).and.(grgmt(j).ne.grgmt(j-1))) then
       write (4, '(f6.2, f8.2)') sonla(j), deptha(j)
       write (4, '(i5, f8.2)') 140, deptha(j)
       write (4, *) 'END'
       write (4, 95) int(grgmt(j+1)), int(grgmt(j+1))
       write (4, '(i5, f8.2)') 140, (deptha(j)+0.05)
      endif
95    format('psxy -JX -R -P -K -O -W0.2/'i3.3'tp -L -G'i3.3'<< END >> m
     .ix.ps')

      enddo
97    continue

      end
```